FZM-4637
31 May 1966
CR-10 2226

DEVELOPMENT OF HEAVY GAGE BONDED HONEYCOMB

GENERAL DYNAMICS
Fort Worth Division

N69-76676
(ACCESSION NUMBER) 422 (PAGES)
(THRU) NONE (CODE)
CR-102226 (NASA CR OR TMX OR AD NUMBER)
(CATEGORY)
FACILITY FORM 602

SEP 1969
RECEIVED
NASA STI FACILITY
INPUT BRANCH

DOCUMENT REQUEST

NASA Scientific and Technical Information Facility
operated for the National Aeronautics and Space Administration by Documentation Incorporated
Post Office Box 33 College Park, Maryland 20740

DOCUMENT REQUESTED

A. NASA ACCESSION NUMBER: N69-76676

B. NACA/NASA REPORT NUMBER:

OR

MAY WE HAVE LOAN OF CASE FILE COPY OR A REPRODUCTION

C. (PLEASE DO NOT WRITE IN THIS SPACE)

D. COPY TYPE REQUESTED: ☐ MICROFICHE ☒ FULL SIZE

OTHER BIBLIOGRAPHIC INFORMATION

H. DOCUMENT TITLE:

I. DATE OF REPORT:

J. AUTHOR(S):

K. CORPORATE SOURCE:

L. CORPORATE REPORT NO.:

M. CONTRACT NO.:

REQUESTER IDENTIFICATION

E. REQUESTER'S FACILITY IDENT. NO.: 10

F. REQUESTER'S CONTRACT NO.:

G. AUTHORIZED SIGNATURE AND DATE: Lois Robertson

N. MAILING LABEL (must be imprinted on all copies; include zip code)

NASA
Marshall Space Flight Center
ATTN: MS-IL
Marshall Space Flight Center,
Alabama 35812

FF NO. 492 REV. OCT. 67

SERIES	MULTI-REQUEST UNITS	MULTI-REQUEST TITLES	REPR METH
09			

DAY IN	REQUESTER PROFILE CLASS	TYPE	LEVEL	DOCUMENT TYPE	SECURITY	NON STD. REQUEST	ASSIGNMENT IDENT.	ACQ.	STOCK	REPRO.	HOLD	REJECT	DAY OUT
113				0					113				

5. PROCESSING COPY

16 JUN 1971

INSTRUCTIONS FOR COMPLETION OF FORM

THE FOLLOWING MUST BE TYPED ON ALL REQUESTS:

1. ITEM "A", or ITEM "B", or ITEMS "H" through "M".
2. ITEMS "D" through "G".
3. ITEM "N".

UPON COMPLETION OF THE FORM, DETACH COPY 3, REQUESTER'S RETENTION COPY, AND FORWARD THE REMAINING SET, INTACT, TO THE NASA SCIENTIFIC AND TECHNICAL INFORMATION FACILITY.

ITEM—BY—ITEM INSTRUCTION

Item A: Give the NASA document accession number, e.g., N65-12345, as announced in the NASA abstract journal (*TPA, STAR,* Etc.)

Item B: If the accession number is not available, give the NACA/NASA report number, e.g., NACA RM E53H59a or NASA TM X-102.

Item C: Please leave this space blank.

Item D: Indicate type of copy preferred.

Item E: If your organization has been assigned a Facility Identification Number, give that Number.

Item F: Give the contract number under which this document is being requested. Indicate "EXCHANGE" or "DEPOSITORY", if applicable.

Item G: This request must be signed by an authorized person within your organization.

Items H through L: If neither the NASA document accession number nor the NACA/NASA report number is available, it is essential that complete bibliographic information be given, as itemized H through M.

Item N: Give complete return mailing address, including zip code. If stamped, this address must appear on all copies of the form. The document will be sent to you using this label.

PROMPT ATTENTION WILL BE GIVEN TO YOUR REQUEST. IN THE EVENT OF A DELAY IN OBTAINING THE DOCUMENT, YOU WILL BE NOTIFIED.

FZM-4637

DEVELOPMENT OF HEAVY GAGE BONDED HONEYCOMB

TECHNICAL DOCUMENTARY REPORT

MAY 1966

Prepared For

George C. Marshall Space Flight Center

National Aeronautics and Space Administration

Huntsville, Alabama

Prepared Under Contract Number NAS 8-11943

Request Number 1-5-53-01150

GENERAL DYNAMICS

Fort Worth Division

Fort Worth, Texas

F O R E W O R D

This report was prepared by General Dynamics Corporation, Fort Worth Division, Fort Worth, Texas, under contract number NAS 8-11943, request number 1-5-53-01150.

The work was administered under the direction of the Advanced Design Section of Advanced Programs Department of Engineering. Mr. C. F. Herndon, Project Design Engineer, was the Project Manager. The time period covered by the contract was 4 May 1965 to 4 June 1966.

This General Dynamics program was performed for the George C. Marshall Space Flight Center, National Aeronautics and Space Administration, Huntsville, Alabama. The MSFC Project Engineer was Mr. M. D. Mims.

The testing and analysis work was conducted under the direction of Mr. T. S. Love, Senior Test Engineer, Engineering Test Laboratory, and Mr. P. D. Shockey, Structures Engineer, Structural Materials and Processes. The design and analysis work was conducted under the direction of Mr. T. B. Hollar, Senior Design Engineer and Mr. V. J. Studer, Project Structures Engineer, of the Structural Materials and Processes Group.

Development of digital analysis and computer solution procedures were accomplished by Mr. J. R. Blacklock, Senior Structures Engineer and Mr. M. G. Allen, Senior Structures Engineer, and the acoustics analysis work was performed by Mr. J. D. Anderson, Senior Structures Engineer, all of the Advanced Structural Dynamics Section.

The sample Manufacturing and Quality Control Plans were prepared by Mr. W. L. J. Williams, Manufacturing Research Engineer, Manufacturing Research and Development Section, and Mr. V. L. Neece, Process Engineer, Quality Control Department, respectively.

Others who contributed significantly to this technical development program from General Dynamics were:

Mr. C. W. Rogers, Structural Materials and Processes
Mr. M. E. Waddoups, Structural Materials and Processes
Mr. A. A. Stiles, Manufacturing Research and Development
Mr. J. W. Cogburn, Special Projects
Mr. J. L. Leonhardt, Special Projects
Mr. C. H. Walker, Advanced Design

A B S T R A C T

A hypothetical large diameter booster skirt has been designed of heavy gage bonded honeycomb based on Small Deflection Theory. The primary design is for a bolted skirt assembly; however, a welded sandwich skirt design and assembly was evaluated as well.

This initial development program showed sandwich composite to be technically feasible for primary load bearing structure by test analysis and by digital computer stress and buckling analysis.

The investigation emphasis was on shear lag, sandwich and cylinder behavior, and bonded joints. Extensive analytical and empirical evaluations were made of the effects of initial imperfections on the face wrinkling characteristics of heavy gage sandwich. Sufficient empirical data were obtained from various types of bonded overlap joints to indicate that tensile and compressive tests of identical double overlap joints yield significantly different results. A computer procedure which uses a stiffness matrix approach to the buckling analysis was developed.

An acoustic and flutter analysis was made of the final design, and sample Manufacturing and Quality Control Plans are included. A weight summary is given comparing the heavy gage bonded honeycomb skirt designs to conventional plate-ring-stringer construction. A budgetary cost analysis is also provided for quantities of one and ten production units.

TABLE OF CONTENTS

	Page
SUMMARY	vi
INTRODUCTION	ix
SECTION	
1. LITERATURE SURVEY AND MATERIALS SELECTION	1-1
1.1 Literature and Industry Survey	1-1
1.2 Materials Selection	1-1
2. THEORETICAL INVESTIGATIONS	2-1
2.1 Preliminary Sizing Analysis	2-1
2.2 Internal Loads Distribution	2-22
2.3 Digital Buckling	2-25
2.4 Sonic Fatigue	2-28
3. DESIGN AND MANUFACTURING STUDIES	3-1
3.1 Preliminary Structural Design	3-1
3.2 Joint Analysis and Secondary Testing	3-31
3.3 Manufacturing Study for Weld Joining	3-39
4. STRUCTURAL TESTING	4-1
4.1 Test Program	4-1
4.2 Specimen Fabrication and Quality Control	4-7
4.3 Discussion of Results	4-8
4.4 Structural Testing Conclusions	4-45

TABLE OF CONTENTS (Cont'd)

	Page
5. FINAL DESIGN DEFINITION AND ANALYSIS	5-1
5.1 Internal Load Distribution	5-1
5.2 Cylinder Buckling Analysis	5-7
5.3 Thrust Structure Design	5-13
5.4 Alternate Design	5-48
5.5 Thermal Analysis	5-50
5.6 Flutter Analysis	5-55
5.7 Acoustic Analysis	5-58
6. DESIGN EVALUATIONS	6-1
6.1 Weight Comparison Study	6-1
6.2 Cost Analysis Estimate	6-7
6.3 Manufacturing Considerations	6-9
7. PROGRAM CONCLUSIONS	7-1
8. RECOMMENDATIONS	8-1

APPENDIXES

A. Secondary Testing	A-1
B. Structural Testing	B-1
C. Preliminary Sizing Analysis	C-1
D. Digital Analysis	D-1
E. Sample Manufacturing Plan	E-1
F. Sample Quality Control Plan	F-1

LIST OF FIGURES

LIST OF TABLES

(References follow each section)

S U M M A R Y

The objective of this program was to develop heavy gage bonded honeycomb sandwich for use as primary load bearing structures in large diameter boosters. The program was defined by three overlapping phases:

(I) Literature Survey with major emphasis on recent design and analytical work related to heavy gage honeycomb techniques, which resulted in an annotated bibliography published under the document number FZM-4445.

(II) Theoretical Investigations based on Small Deflection Theory required to formulate and develop an analytical approach for prediction of stress fields and buckling loads. These investigations included the development of a simplified computer program and resulted in a preliminary design for the specified hypothetical booster skirt. Design and analytical emphasis was on the problems of shear lag, sandwich and cylinder behavior, and bonded joints. Investigations yielded these specific solutions:

- The maximum skin thickness necessary is .375 inch
- External thickness steps can be used
- A constant core thickness of 1.50 inches is satisfactory
- A conventional lightweight aluminum honeycomb core is adequate - 4.4 lbs./ft^3, 1/8-inch cell diameter, 5052 alloy
- The configuration is tolerant to normal minor imperfections
- Lightweight joint design with short high strength bond overlaps are reliable
- Sandwich composite is technically feasible for booster applications

Significant technical accomplishments were made in support of the development program. For example:

- Extensive analytical and experimental evaluations were made of the effects of initial imperfections on the face wrinkling characteristics of heavy gage sandwich. Initial imperfections in the form of waviness in one facing were fabricated into sandwich column compression specimens. Analytical evaluations were made of the critical face wrinkling stresses of the specimens utilizing the theories of Forest Products Laboratory and Syed Uysuff and the critical face wrinkling stresses were determined experimentally.

- Sufficient empirical data were obtained from various types of bonded overlap joints to indicate that tensile and compressive tests of identical double overlap joints yield significantly different results. The compression overlap specimens produce higher values for the apparent adhesive shear strength because of the sensitivity of the adhesives to tensile forces which are normal to the bond in tests of tension overlap specimens.

- A computer procedure which uses a stiffness matrix approach to the buckling analysis has been developed. This procedure uses the internal loads distribution plus the structural geometry to develop a correction to the stiffness matrix. Sample problems solved for buckling indicate that the computer analysis is always conservative. This procedure has been used in analyzing the skirt structure and the results indicate a reasonable margin of safety.

(III) Skirt Definitions for the two different designs of heavy gage bonded honeycomb were made. One design was a bolted joint assembly concept. The other was planned as a welded joint assembly concept, utilizing weldable aluminum facings. Design and analysis determined that the lightest weight weld-joined design was with bonded-on weldable edgemembers. Accordingly, the weight penalty

for making the thrust and rebound fittings of a weldable aluminum alloy was prohibitive. Therefore, in the weld-joined design concept, the application for weld-joining was limited to butt splices of adjacent panels, making the two parallel designs in final definition very similar despite intensive investigation and testing.

A budgetary cost analysis was made covering tooling and fabrication for quantities of one and ten final designed units. Results are as follows:

Bolted Panel Splices		Welded Panel Splices	
One Unit	Ten Units	One Unit	Ten Units
$969,000	$5,770,000	$1,419,000	$8,295,000

The above figures are for comparison purposes only and do not constitute a commitment by General Dynamics.

A weight summary comparing heavy gage bonded honeycomb skirt design with conventional plate-ring-stringer design indicated a 1600 pound weight savings for the bonded honeycomb structure.

An acoustic and flutter analysis showed a sonic fatigue life far in excess of the single flight requirements, and that panel flutter of the skirt structure would not occur within a reasonable flight envelope.

INTRODUCTION

Heavy gage sandwich applications are rare. Seldom have skin gages over one-tenth of an inch been required. We are now at the threshold of an era, however, when sandwich in extremely heavy forms is becoming attractive. This is especially true for the future generations of skirt and intertank structures.

The main attraction of heavy sandwich lies in the potential weight savings for compression load-critical components. In these components a sandwich construction can provide efficient resistance to instability failures as well as to accommodate the other attendant loading conditions.

The objective of this program was to develop heavy gage bonded honeycomb sandwich for use as primary load bearing structure in large diameter boosters. This objective was to be accomplished by analytical investigations and structural testing and to result in two different designs carried to a state of completion whereby weight and cost comparisons of each design could be made. Design was to be based on Small Deflection Theory. The basic requirement was for a hypothetical simplified version of the S-IC thrust skirt, for which each of three loadings were to be applied:

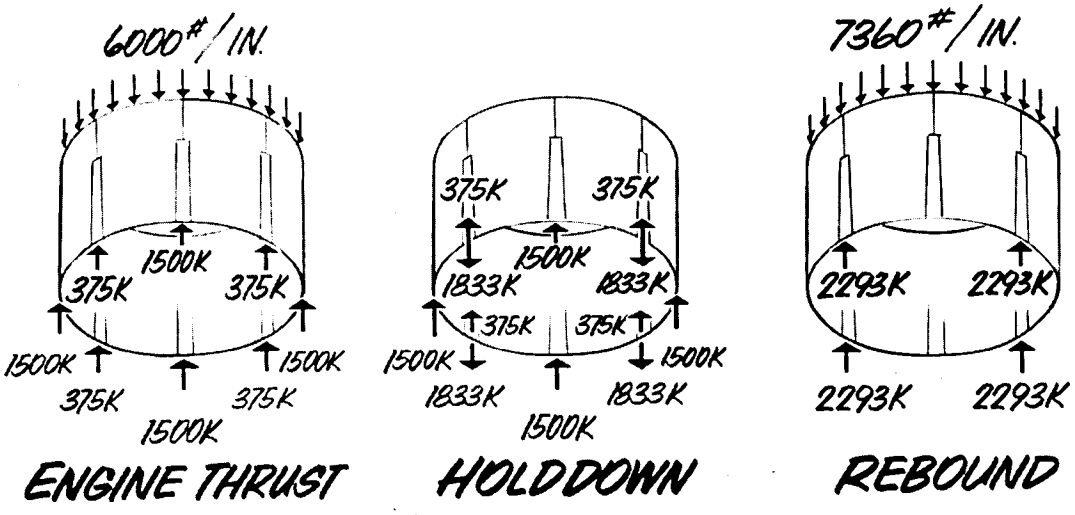

Loads were to be considered as applied in-plane, and the load at the forward boundary was to be a maximum 15,000 pounds per inch.

The technical approach to this program used by General Dynamics Corporation is illustrated simply as follows:

- MATERIAL SELECTION
  - ADHESIVES - MB329 AND FM96
  - SKINS - 7075T6 ALUMINUM ALLOY
- THEORETICAL INVESTIGATIONS
  - SHEAR LAG
  - CYLINDER BUCKLING
  - SANDWICH BEHAVIOR
  - BONDED JOINT STRESS DISTRIBUTION
- DESIGN STUDIES
  - WELDED JOINTS
  - BOLTED JOINTS
  - BONDED JOINTS
- STRUCTURAL TESTS (158 SMALL SPECIMENS AND PANELS)
  - SKIN THICKNESS EFFECTS
  - PANEL THICKNESS EFFECTS
- DEFINITION OF COMPLETE HYPOTHETICAL SKIRT

SECTION 1

LITERATURE SURVEY AND MATERIALS SELECTION

1.1 LITERATURE AND INDUSTRY SURVEY

A survey was performed of the literature pertinent to the design and analysis of a large bonded honeycomb skirt. The survey was conducted at the Fort Worth Division of General Dynamics Corporation principally through the services of the Division Research Library and the Manufacturing Research and Development Library. Specific searches on analytical methods were run on a digital computer using the AIAA and NASA STAR reference back to 1962 and the ASTIA back to 1960. Aluminum welding sources were provided by DMIC.

Numerous direct personal communications were held with authoritative individuals to supplant the formal documents. The personal approach was particularly useful in gathering the latest developmental information in the industry on adhesive materials. Results of the survey were compiled in report form under the headings of Materials and Processes, Structural Analysis Techniques, and Digital Procedures. The report which composed the annotated bibliography required by the contract (Article I - NAS 8-11943) was prepared and submitted to NASA/MSFC. The report is identified as follows:

Title: Phase I Report Annotated Bibliography for Development of Heavy Gage Bonded Honeycomb

No.: FZM - 4445

Date: 28 July 1965

Numerous documents were examined which do not appear in the report. Only those documents of specific value were included.

1.2 MATERIALS SELECTION

After the literature and industry survey was completed selections were made for the particular materials which were to be utilized during the performance of the contract.

1.2.1 Facing Materials

Because of the requirement for two designs of the thrust structure, one welded and one non-welded, two facing materials were selected. Aluminum alloy 7075T6 was selected for use with the non-welded design and aluminum alloy 2219T87 was selected for use with the welded design. The 7075T6 alloy was chosen because of its proven reliability under the applicable environments and its superior bonding characteristics which have been demonstrated in past programs. The 2219T87 alloy was chosen because of its superior welding characteristics when compared to the other weldable aluminum alloys and because it has also demonstrated acceptable bondability.

1.2.2 Core Materials

The core material selected was a hexagonal cell shape 5052 aluminum alloy which is qualified to a General Dynamics F-111 specification for high temperature resistant aluminum honeycomb core. Extensive background and experience is reflected in the requirements of this specification and while some of the requirements are more stringent than was necessary for this program, relaxing the requirements was not necessary because of the availability of an adequate supply of qualified material.

1.2.3 Adhesives and Potting Materials

In addition to Narmco's Metlbond 329, which was selected as the prime adhesive candidate in this program, Bloomingdale's FM96 and Minnesota Mining's AF30 were also selected for preliminary evaluation. MB329 is an epoxy novolac, FM96 is a modified epoxy and AF30 is a nitrile phenolic. MB329 is qualified to MIL-A-5090D Type II and FM96 is qualified to MIL-A-25463 Type II. Both adhesives are considered reliable for metal-to-core and metal-to-metal bonds. AF30 does not have the long time 300°F temperature resistance required of Type II adhesives in either specification. AF30 was considered as a back-up adhesive in the event that the adhesives with higher temperature capabilities were unable to transfer the high loads in the thick gages because of their high shear moduli.

Several types of potting materials were evaluated during this program. For splicing sections of core, the primary candidates were Minnesota Mining's AF3002 and Furane's Epocast 1310. AF3002 is a syntactic foam in a film form and Epocast 1310 is a thixotropic paste-type material. In addition to these potting materials there was also a requirement for a pourable compound for which an available syntactic foam pastetype material was selected, based on previous General Dynamics sandwich specimen test programs.

1.2.4 Preliminary Testing

The adhesives and core materials tentatively selected as a result of the literature survey were subjected to preliminary testing as small specimens. The purpose was to determine acceptable test configurations for the theoretical investigations to follow and to demonstrate that the selected materials were compatible for heavy gage bonded sandwich.

Figure 1-1 shows the manner in which the specimens were loaded and the dimensions of the specimens which had .100 inch thick facings. The sandwich compression shear specimens with .312 inch facings were 10 inches long, 1.5 inches wide, and 2.65 inches thick, and were tested in a manner similar to that shown in Figure 1-1b.

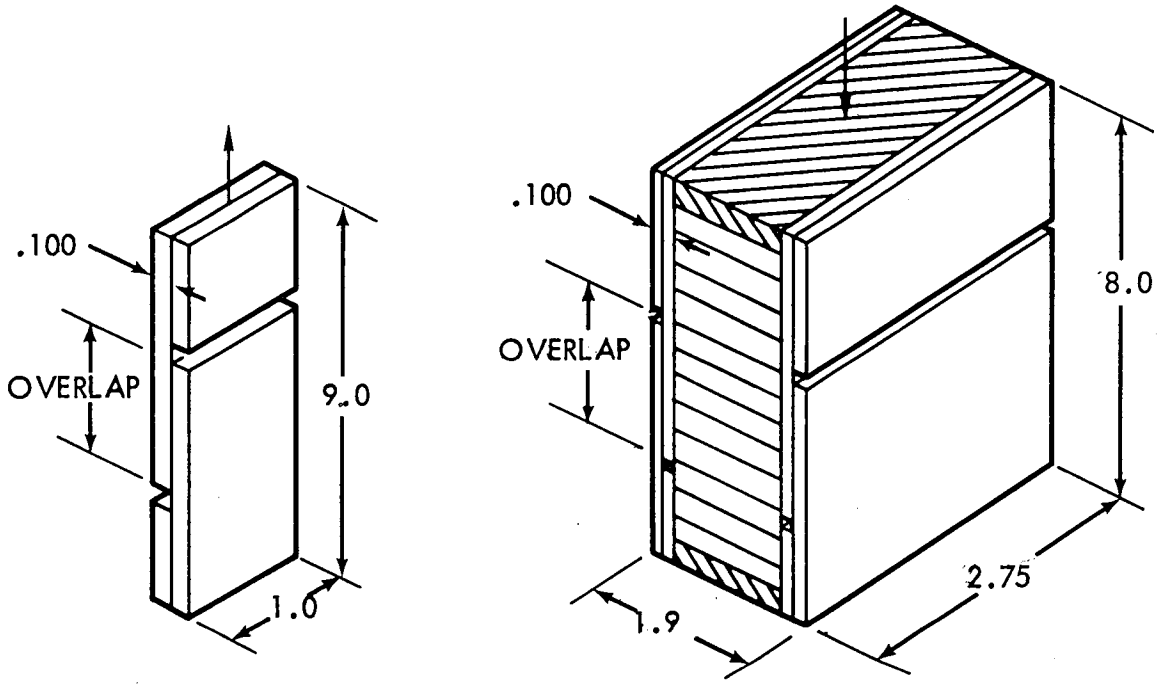

(A) SINGLE OVERLAP TENSILE SHEAR (B) SANDWICH COMPRESSION SHEAR

Figure 1-1 TEST SPECIMEN CONFIGURATIONS

The single overlap tensile shear specimens were tested first. These tests were run to produce information of a qualitative nature on comparisons of long and short overlaps. They also provided a comparison with similar tests run previously at General Dynamics. The appearance and general load capacity of the specimens provided a basis for the more expensive but more meaningful symmetrical specimens which followed.

Because of the eccentricities and the peeling forces inherent in tests of the single overlap specimen, it was felt necessary to test overlaps in a symmetrical test specimen. The double overlap tensile shear specimen fits this requirement as does the sandwich compression shear specimen. The sandwich specimen allows a compression loading condition similar to the actual loading condition that the cylinder will experience especially at the forward ring area. Although available analysis methods do not distinguish between compression and tension loadings on bonded overlaps, it was felt that the sandwich compression shear tests would be more meaningful at this stage than tests of double overlap specimens in tension.

Typical failed specimens of each type of test method are shown in Figures 1-2 and 1-3.

All results obtained during this testing are shown in Table 1-1.

The sandwich test results indicate that heavy gage bonded lap joints in sandwich are practical. Also, these tests served to provide a basis for the configurations of the secondary testing specimens. These preliminary tests also tentatively showed that MB329 is compatible with the heavy gages and high loads.

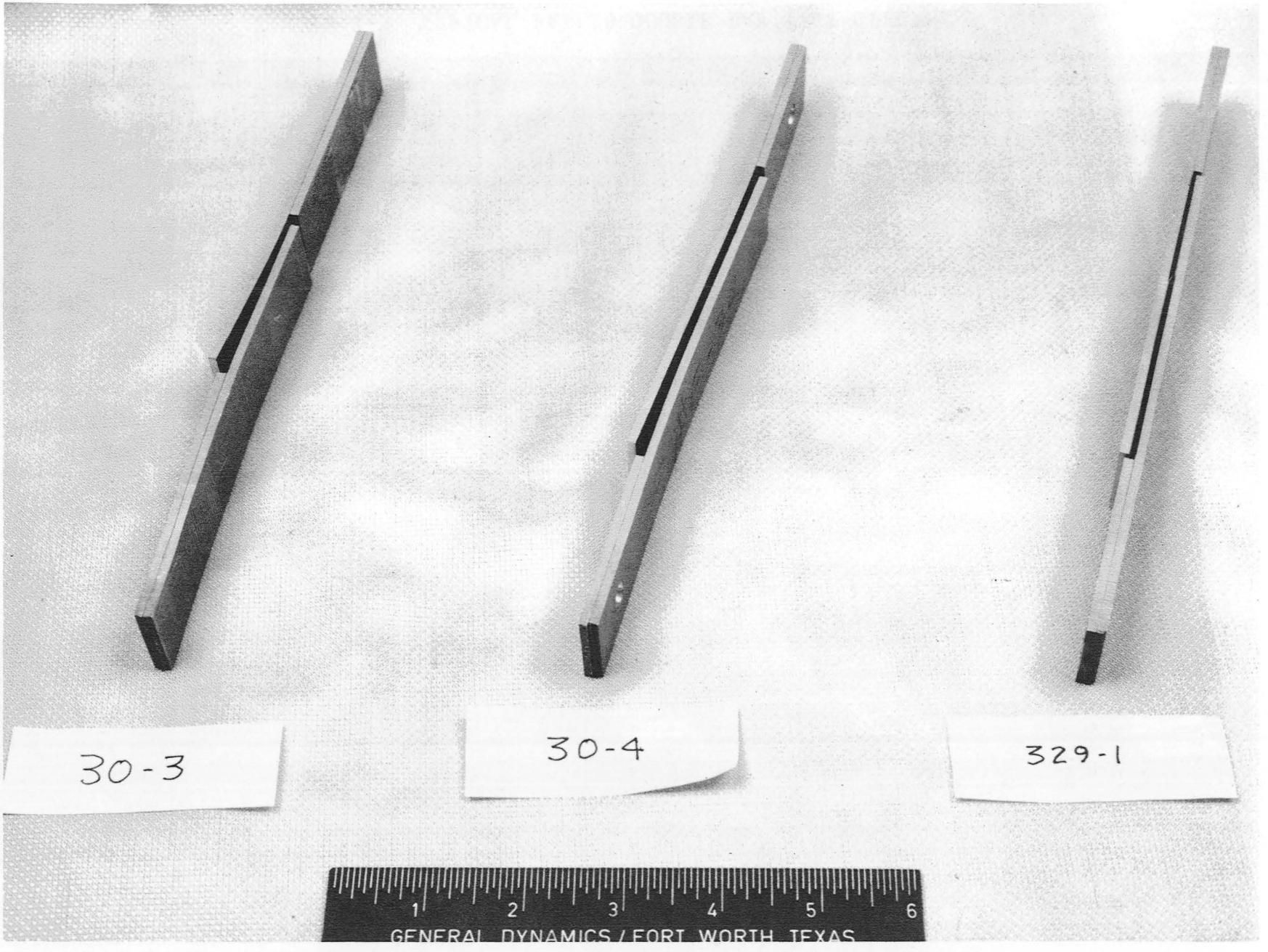

Figure 1-2 TYPICAL FAILED SINGLE LAP TEST SPECIMENS

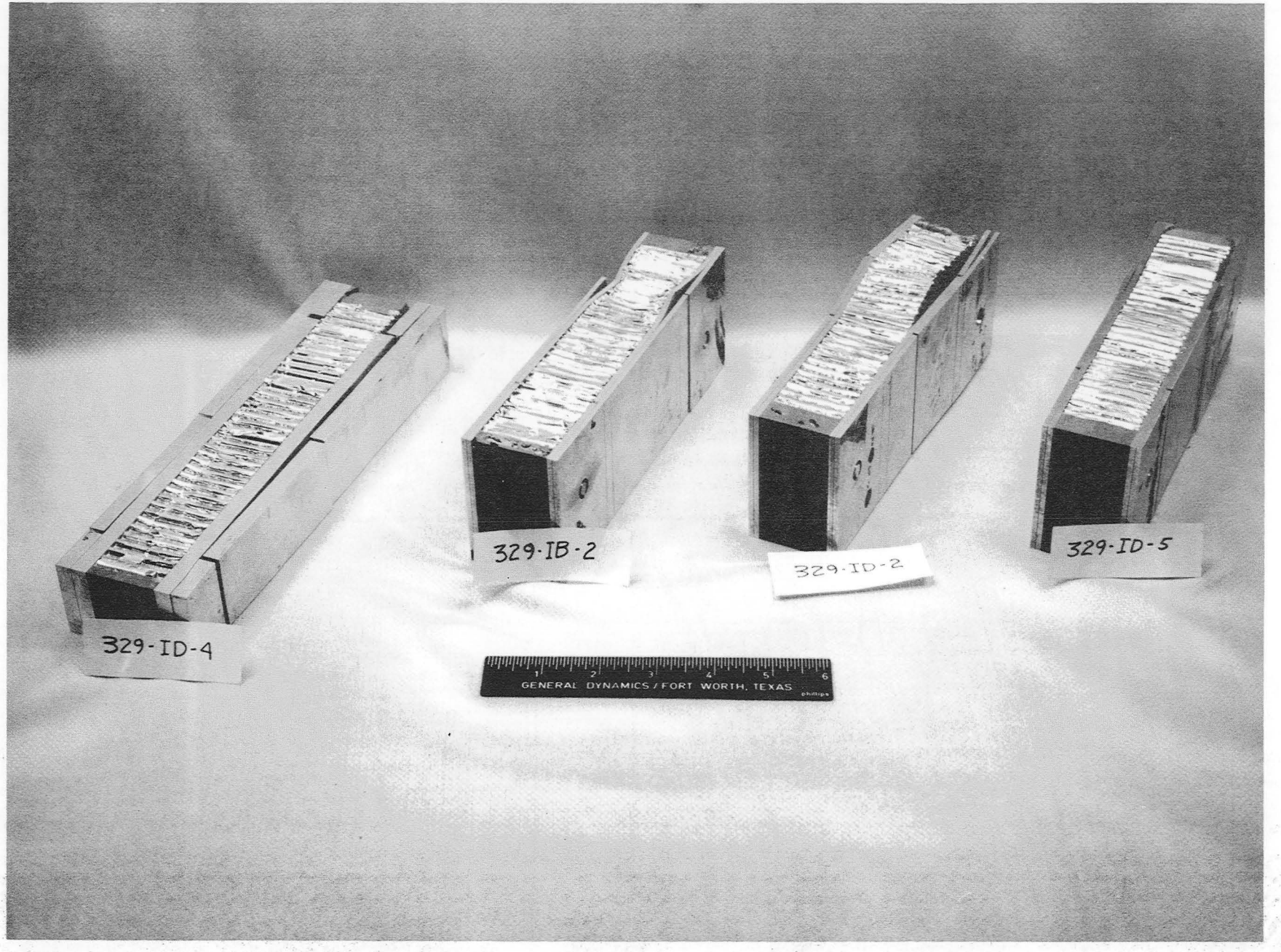

Figure 1-3 TYPICAL FAILED DOUBLE LAP TEST SPECIMENS

Table 1-1 PRELIMINARY TEST RESULTS

SPECIMEN	ADHESIVE	OVERLAP	SKIN GAGE	L/T	WIDTH	LOAD	STRESS AT FAILURE		TYPE OF FAILURE
							BOND	SKIN	
				SINGLE OVERLAP TENSILE SHEAR					
329-1	MB329	4.35	.100	43.5	1.00	3,650	840	36,500	ADHESIVE PEEL AND SHEAR
329-2	MB329	4.35	.100	43.5	1.00	4,450	1,030	44,500	ADHESIVE PEEL AND SHEAR
329-3	MB329	4.35	.100	43.5	1.00	4,740	1,090	47,400	ADHESIVE PEEL AND SHEAR
329-4	MB329	3.00	.100	30.0	1.00	3,400	1,140	34,000	ADHESIVE PEEL AND SHEAR
329-5	MB329	3.00	.100	30.0	1.00	2,830	950	28,300	ADHESIVE PEEL AND SHEAR
329-6	MB329	3.00	.100	30.0	1.00	3,720	1,250	37,200	ADHESIVE PEEL AND SHEAR
30-1	AF30	4.35	.100	43.5	1.00	7,350	1,690	73,500	METAL IN TENSION
30-2	AF30	4.35	.100	43.5	1.00	7,390	1,700	73,900	METAL IN TENSION
30-3	AF30	2.25	.100	22.5	1.00	6,730	2,920	67,000	ADHESIVE PEEL AND SHEAR
30-4	AF30	4.35	.100	43.5	1.00	5,940	1,370	59,500	ADHESIVE PEEL AND SHEAR
30-5	AF30	4.35	.100	43.5	1.00	5,820	1,340	58,200	METAL IN BEARING
				SANDWICH COMPRESSION SHEAR					
329-IB-1	MB329	4.03	.100	40.3	2.75	31,500	1,420	57,300	BUCKLING-FACE WRINKLING
329-IB-2	MB329	2.25	.100	22.5	2.75	29,700	2,400	54,000	BUCKLING-FACE WRINKLING
329-ID-1	MB329	3.95	.100	39.5	2.75	35,650	1,640	64,800	BUCKLING-FACE WRINKLING
329-ID-2	MB329	2.25	.100	22.5	2.75	34,800	2,810	63,300	BUCKLING-FACE WRINKLING
329-ID-3	MB329	7.50	.312	24.0	1.50	60,000+	2,670	64,200	NO FAILURE
329-ID-3R	MB329	3.75	.312	12.0	1.50	53,750	4,770	57,300	ADHESIVE SHEAR
329-ID-4	MB329	3.75	.312	12.0	1.50	52,500	4,670	56,200	ADHESIVE SHEAR
329-ID-5	MB329	1.00	.100	10.0	2.75	30,250	5,530	55,300	ADHESIVE SHEAR
329-ID-6	MB329	1.25	.100	12.5	2.75	35,400	5,150	63,400	BUCKLING-FACE WRINKLING
329-ID-7	MB329	2.50	.312	8.0	1.50	48,600	6,480	51,900	ADHESIVE SHEAR
329-ID-8	MB329	2.50	.312	8.0	1.50	45,800	6,110	48,900	ADHESIVE SHEAR
96-ID-1	FM96	1.00	.100	10.0	2.75	38,000	6,910	69,100	ADHESIVE SHEAR
96-ID-2	FM96	1.00	.100	10.0	2.75	32,950	5,970	59,700	ADHESIVE SHEAR
96-ID-3	FM96	0.40	.100	4.0	2.75	20,900	9,740	38,000	ADHESIVE SHEAR
96-ID-4	FM96	0.40	.100	4.0	2.75	28,800	13,090	52,400	ADHESIVE SHEAR

1. ALL FACINGS WERE 2024 T81.
2. SPECIMENS XX-IB-X HAD 1.50 INCH THICK 4.5 LB/FT^3 CORE.
   SPECIMENS XX-ID-X HAD 1.38 INCH THICK 8.1 LB/FT^3 CORE.

SECTION 2

THEORETICAL INVESTIGATIONS

Theoretical investigations were conducted as required in order to develop basic design and analysis procedures and formulate rigorous analytical techniques. Methods were developed for the analyses of shear lag, internal loads distribution, cylinder buckling, and sonic fatigue.

2.1 SHEAR LAG

The purpose of the shear lag analysis was to determine the initial skin gage and longeron area requirements for the diffusion of load from the longerons to skin panels in the thrust structure. The techniques which were to be used had to meet two specific requirements. First, the analysis had to be simple enough to allow the comparison of a broad spectrum of concepts, and second, the results were to be of sufficient accuracy to require little refinement when the comprehensive finite element analysis of internal loads distribution was undertaken.

In order to meet these requirements, two separate analytical techniques were employed. The first was a closed form series solution for the load diffusion from a longeron to a uniform panel in which both uniform and exponentially-tapered longerons were considered. The second technique was a simplified one-dimensional numerical shear lag model.

2.1.1 Closed Form Series Solution

The closed form series solution which was utilized during the program was similar to that described by Riparbelli in Reference 2-1. Two structural configurations were chosen. The first configuration was an infinite length panel with a constant area longeron, and the second was an infinite length panel with an exponentially-tapered longeron.

While these two geometries did not satisfy the boundary conditions on the upper edge of the structure, they did indicate the load diffusion rates which, in turn, allowed the panel sizing. The requirements for the tank-thrust structure interface dictated that the axial stress resultant be less than 15,000 pounds per inch. This load requirement then indicated that the longeron area must fade out, hence the solution for the constant thickness panel with a tapered longeron proved to be the most helpful.

If a typical quadrant is taken from between two of the loaded longerons and developed into a flat panel as shown in Figure 2-1, then the load diffusion into the web of the flat panel will serve as the model for the load diffusion into the sandwich panels.

The longeron area is represented by a function of the form

$$A_s = A_{so} \; e^{-cy} \qquad C>0 \tag{2-1}$$

The solution is achieved by first assuming that the structure quadrant (Figure 2-1) is infinitely rigid in shear. The stress distribution then is as shown in Figure 2-2a. An Eigen load, with a zero resultant as shown in Figure 2-2b, is then computed. The resulting loads, Figures 2-2a and 2-2b, are then superimposed as shown in Figure 2-2c.

As $y \rightarrow \infty$ the longeron area approaches zero, hence, the load on the longeron also approaches zero. This indicates that the entire load P is available for redistribution.

The panel displacement is assumed to be one dimensional in the y direction and of the form

$$v\,(x,y) = \sum a_n e^{-r_n y} - \sum b_n \left[\sin \frac{n\pi x}{b}\right]\left[e^{-(r_n+c)y}\right] \tag{2-2}$$

$$u\,(x,y) = 0 \tag{2-3}$$

the strain in the axial direction then becomes

$$\frac{\partial v}{\partial y} = \epsilon_y = - \sum a_n r_n e^{-r_n y} + \sum b_n\,(r_n+c)\left[\sin \frac{n\pi x}{b}\right]\left[e^{-(r_n+c)y}\right] \tag{2-4}$$

$$\frac{\partial v}{\partial x} = \gamma_{xy} = - \frac{\pi}{b} \sum n b_n \left[\cos \frac{n\pi x}{b}\right]\left[e^{-(r_n+c)y}\right] \tag{2-5}$$

The following conditions must then be satisfied for the Eigen load:

1. The load in the longeron at y=0, x=0 must balance the applied load.

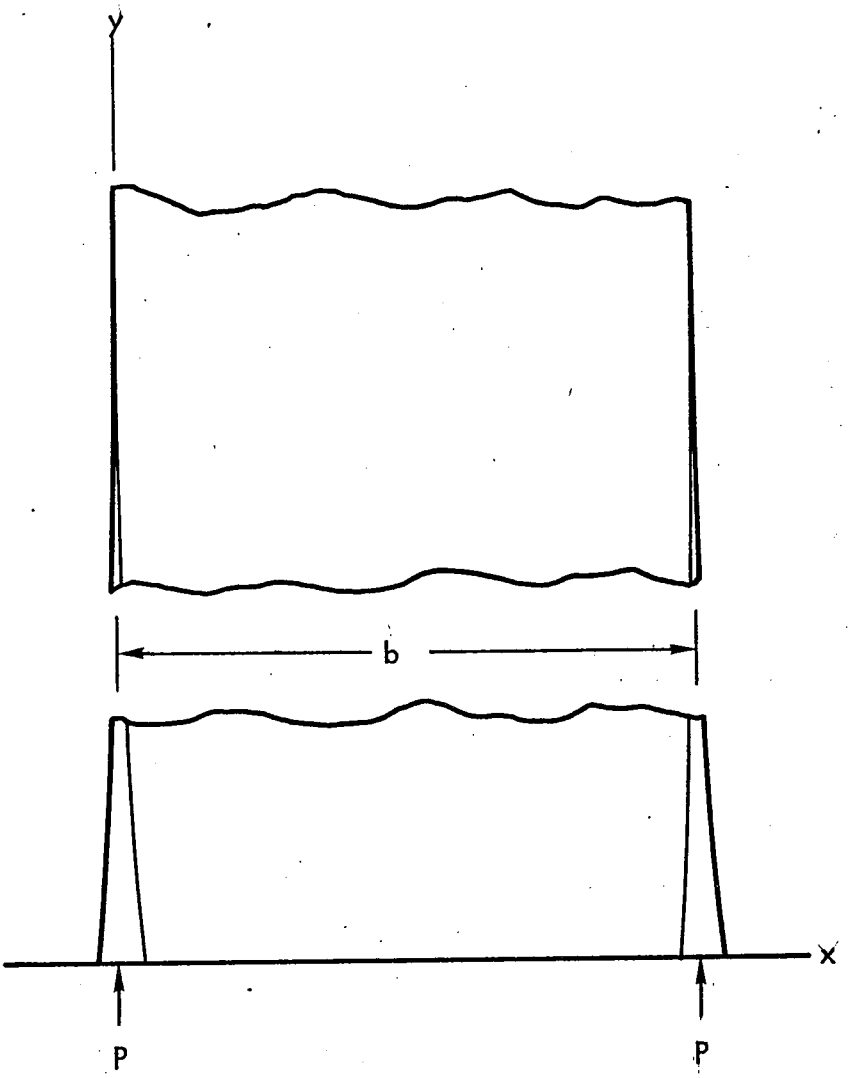

Figure 2-1 ASSUMED PANEL AND LONGERON GEOMETRY

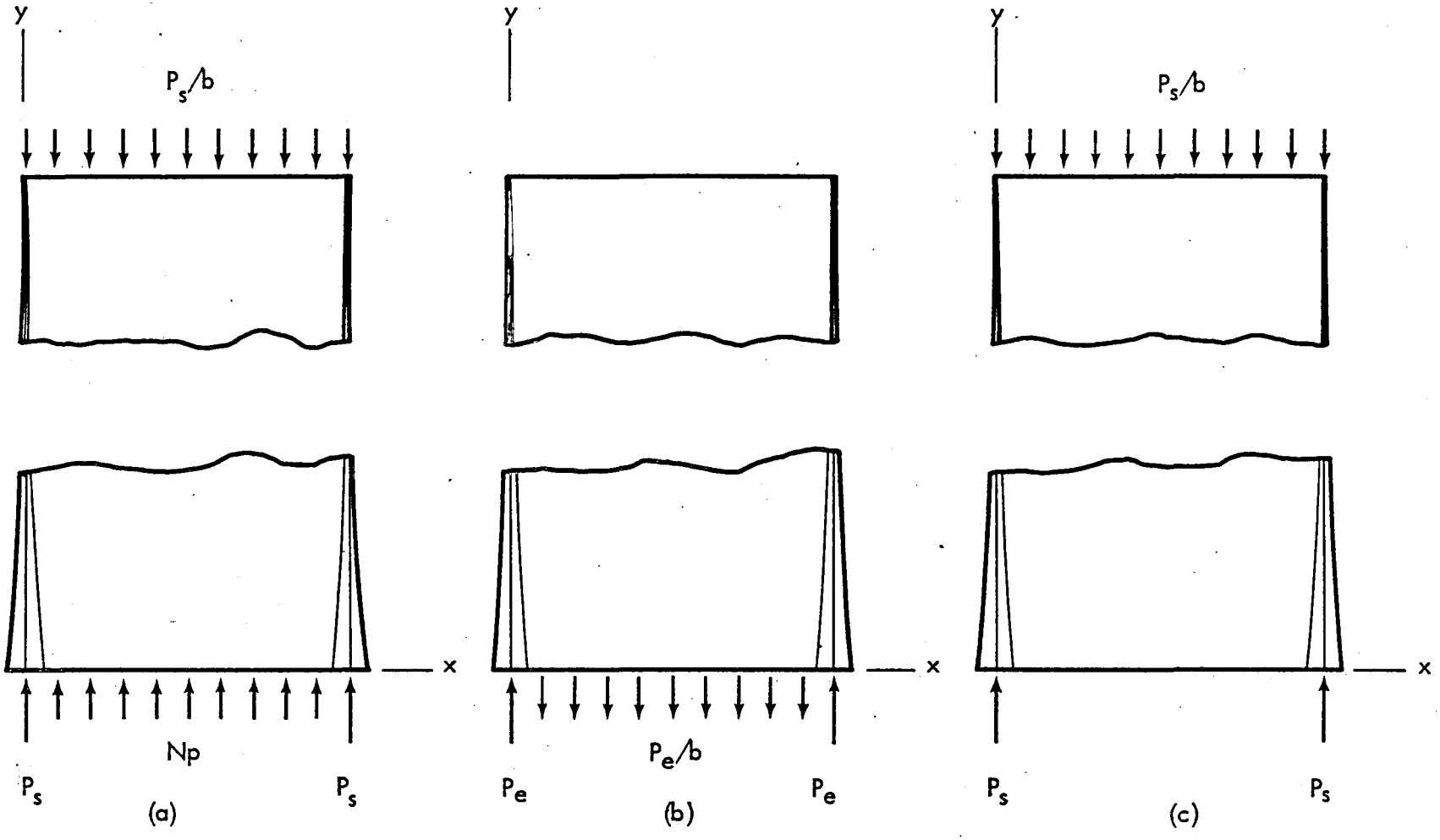

Figure 2-2 SUPERPOSITION OF LOADS

2. The gradient in axial load in the longeron must balance the shear flow to the panel.

3. The panel surface along the line y=0 must be stress free.

Since the longeron area, A_s, approaches zero as $y \rightarrow \infty$ the total load P is available for redistribution. Hence:

$$P_e = P \tag{2-6}$$

The first condition is satisfied by the relation

$$E \left(\epsilon y \cdot A_s\right)_{\substack{y=0 \\ x=0}} = P \tag{2-7}$$

hence,

$$P_e = -EA_{so} \sum a_n r_n$$

and

$$\sum a_n r_n = \frac{|P_e|}{EA_{so}} \tag{2-8}$$

The second condition is satisfied if

$$-\frac{Pe}{btE} = -\sum a_n r_n + \sum b_n (r_n+c) \sin \frac{n\pi x}{b} \tag{2-9}$$

from which

$$\sum b_n(r_n+c) \sin \frac{n\pi x}{b} = \frac{Pe}{E} \left(\frac{1}{A_{so}} + \frac{1}{bt}\right) \tag{2-10}$$

which may be satisfied by

$$b_n(r_n+c) = \frac{4\beta}{n\pi} \tag{2-11}$$

where,

$$\beta = \frac{F}{E} \left(\frac{1}{A_{so}} + \frac{1}{bt}\right)$$

$$b_n (r_n+c) = \frac{4F}{n\pi E} \left(\frac{1}{A_{so}} + \frac{1}{bt}\right)$$

The third and final condition may be satisfied by considering the gradient of the axial load in the longeron and the shear flow along the line x = 0.

$$\frac{dN}{dy} = EA_{so}\sum a_n r_n \quad (r_n+c)e^{-(r_n+c)y} \tag{2-12}$$

$$qo = -\frac{Gt\pi}{b} \sum n\, b_n\, e^{-(rn+c)y} \tag{2-13}$$

and equilibrium yields

$$EA_{so}\ a_n r_n\ (r_n+c) = \frac{2\pi Gt}{b}\ n\ bn$$

or

$$\frac{a_n r_n\ (r_n+c)}{nbn} = \frac{2\pi Gt}{bEA_{so}} \tag{2-14}$$

Recapitulating, the relations among the coefficients are

$$\sum a_n r_n = \frac{F}{EA_{so}} \tag{2-15}$$

$$nbn\ (r_n+c) = \frac{4F}{\pi E}\left(\frac{1}{A_{so}} + \frac{1}{bt}\right) \tag{2-16}$$

$$\frac{a_n r_n (r_n+c)}{nbn} = \frac{2\pi Gt}{bEA_{so}} \tag{2-17}$$

assuming that

$$r_n = ne \qquad e = \text{const} > 0$$

$$a_n = \frac{\alpha}{n^3} \qquad d = \text{const} > 0$$

$$b_n = \frac{\beta}{n^2} \qquad \beta = \text{const} > 0$$

The final equations may be tabulated as follows

$$\rho = \pi \sqrt{\frac{Gt}{bE}\left(\frac{1}{A_{so}} + \frac{1}{bt}\right)} - \frac{c}{n} \tag{2-18}$$

$$\alpha = \frac{8F}{\pi^2 EA_{so}\rho} \tag{2-19}$$

and

$$a_n r_n = \frac{8F}{\pi^2 EA_{so} n^2} \tag{2-20}$$

$$b_n(r_n+c) = \frac{4F}{n\pi E}\left(\frac{1}{A_{so}} + \frac{1}{bt}\right) \tag{2-21}$$

It should be noted that a taper rate of

$$c = \pi \sqrt{\frac{Gt}{bE}\left(\frac{1}{A_{so}} + \frac{1}{bt}\right)}$$

violates some of the initial assumptions and the solution will not apply.

The pertinent equations may now be tabulated as follows:

(1) Axial load in the longeron

$$N = \frac{8Pe}{\pi^2} \sum \frac{e^{-ny}}{n^2} \tag{2-22}$$

$$Y = \left\{\pi \sqrt{\frac{Gt}{bE}\left(\frac{1}{A_{so}} + \frac{1}{bt}\right)}\right\} y \tag{2-23}$$

(2) Shear flow at the longeron

$$q = -\frac{4Pe}{\pi} \sqrt{\frac{Gt}{bE}\left(\frac{1}{A_{so}} + \frac{1}{bt}\right)} \sum \frac{e^{-nY}}{n} \tag{2-24}$$

(3) Axial load in the panel

$$\sigma = -\frac{Pe}{bt} - \frac{8Pe\ e^{cy}}{\pi^2 A_{so}} \sum \frac{e^{-n\gamma}}{n^2} + \frac{4Pe}{\pi}\left(\frac{1}{A_{so}} + \frac{1}{bt}\right) \quad (2\text{-}25)$$

$$\sum \sin \frac{n\pi x}{b} \frac{e^{-n\gamma}}{n}$$

The final equations may then be simplified by writing them as follows:

(1) Axial load in the longeron

let,

$$A_1 = \frac{8Pe}{\pi^2}$$

$$\gamma = \left\{ \pi \sqrt{\frac{Gt}{be}\left(\frac{1}{A_{so}} + \frac{1}{bt}\right)} \right\} y$$

$$\phi_1 = \sqrt{\frac{Gt}{be}\left(\frac{1}{A_{so}} + \frac{1}{bt}\right)}$$

$$f_1(x,y) = \sum \frac{e^{-n\gamma}}{n^2}$$

then,

$$N = A_1 \cdot f_1(x,y) \quad (2\text{-}26)$$

(2) Shear flow at the longeron:

let,

$$A_2 = -\frac{4Pe}{\pi} \sqrt{\frac{Gt}{bE}\left(\frac{1}{A_{so}} + \frac{1}{bt}\right)}$$

$$f_2(x,\gamma)_{x=0} = \sum \frac{e^{-n\gamma}}{n}$$

then,

$$q = A_2 \cdot f_2(x,y) \qquad (2\text{-}27$$

(3) Axial load in the panel:

$$A_3 = -\frac{Pe}{bt}$$

$$f_3(x,y) = \frac{e^{cy}}{A_{so}}$$

$$A_4 = \frac{4Pe}{\pi}\left(\frac{1}{A_{so}} + \frac{1}{bt}\right)$$

$$f_4(x,y) = \sum \sin \frac{n\pi x}{b} \frac{e^{-nY}}{n}$$

then,

$$\sigma = A_3 + A_1 \cdot f_3(x,y) \cdot f_1(x,y) + A_4 \cdot f_4(x,y) \qquad (2\text{-}28)$$

The functions,

$f_1(x,y)$

$f_2(x,y)$

$f_4(x,y)$

may be found in Figures 2-3, 2-4, and 2-5.

Further investigation of the solution determined that once the geometric and material parameters, i.e., panel width, initial longeron area, E, and G, are determined then the required panel length for load damping from the longeron may be found in terms of the variable panel thickness. Figure 2-6 shows the relationship of the damping parameter ϕ_1 and the panel thickness.

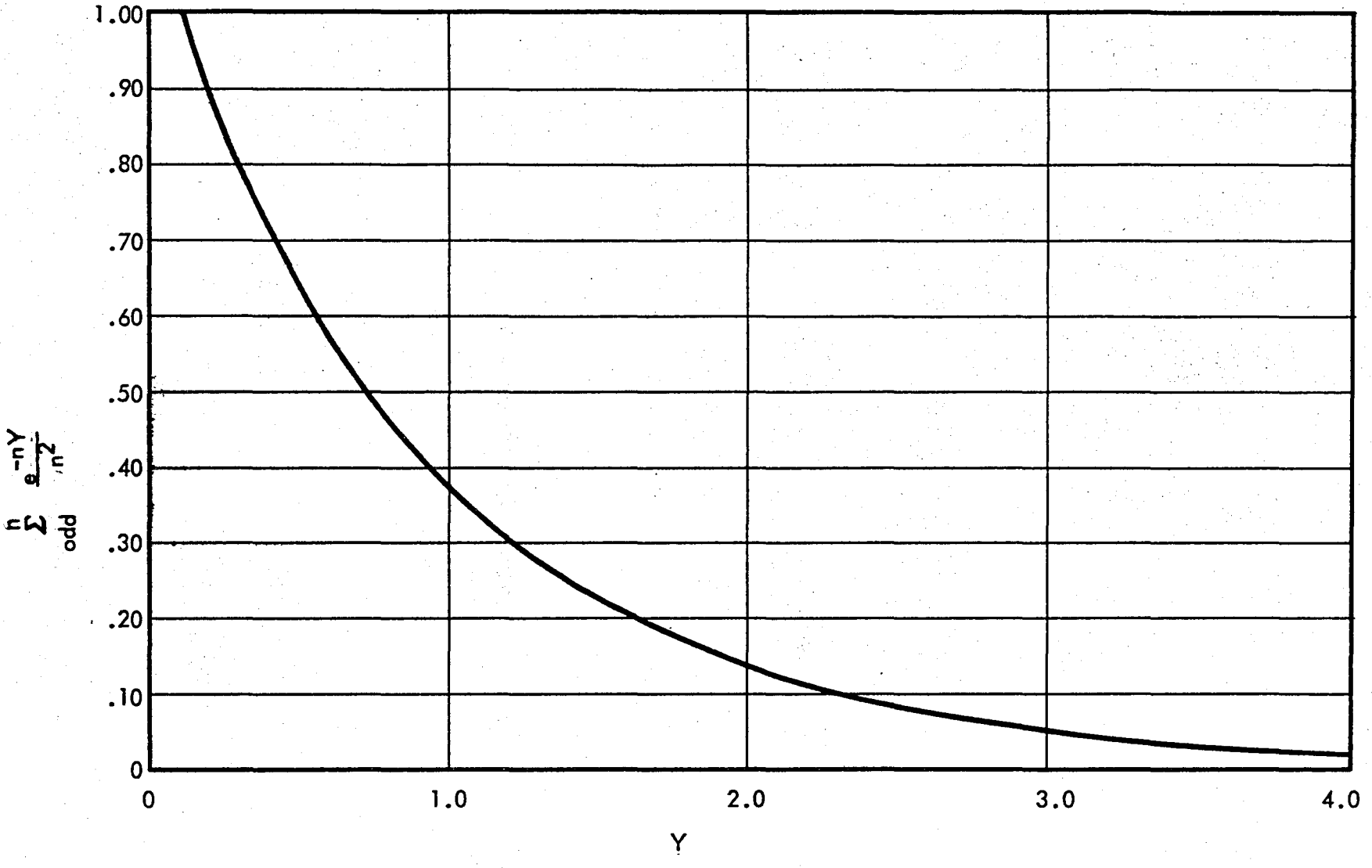

Figure 2-3 $f_1(x,y)$ vs Y

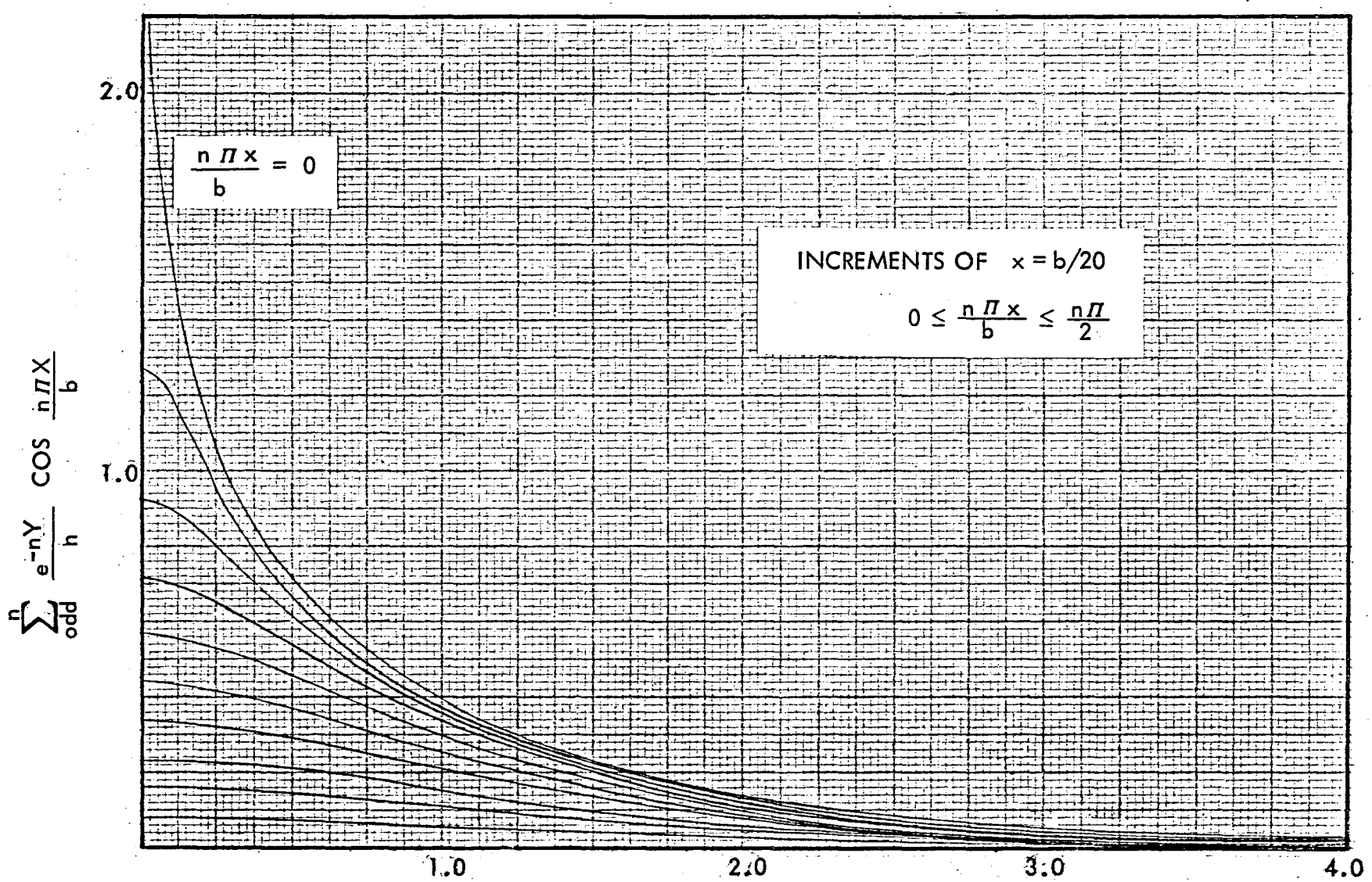

Figure 2-4 $f_2(x,y)$ vs Y

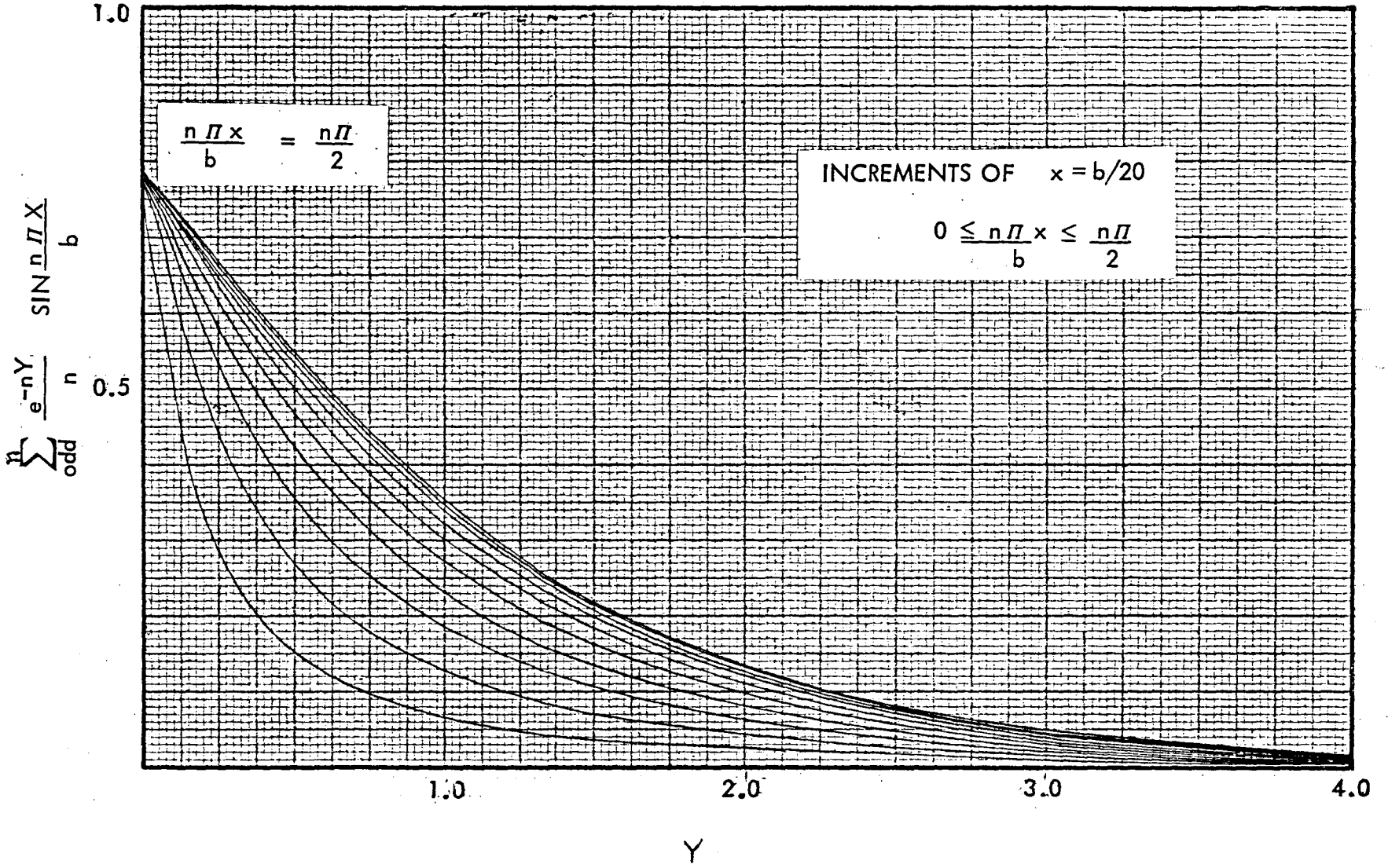

Figure 2-5 $f_4(x,y)$ vs Y

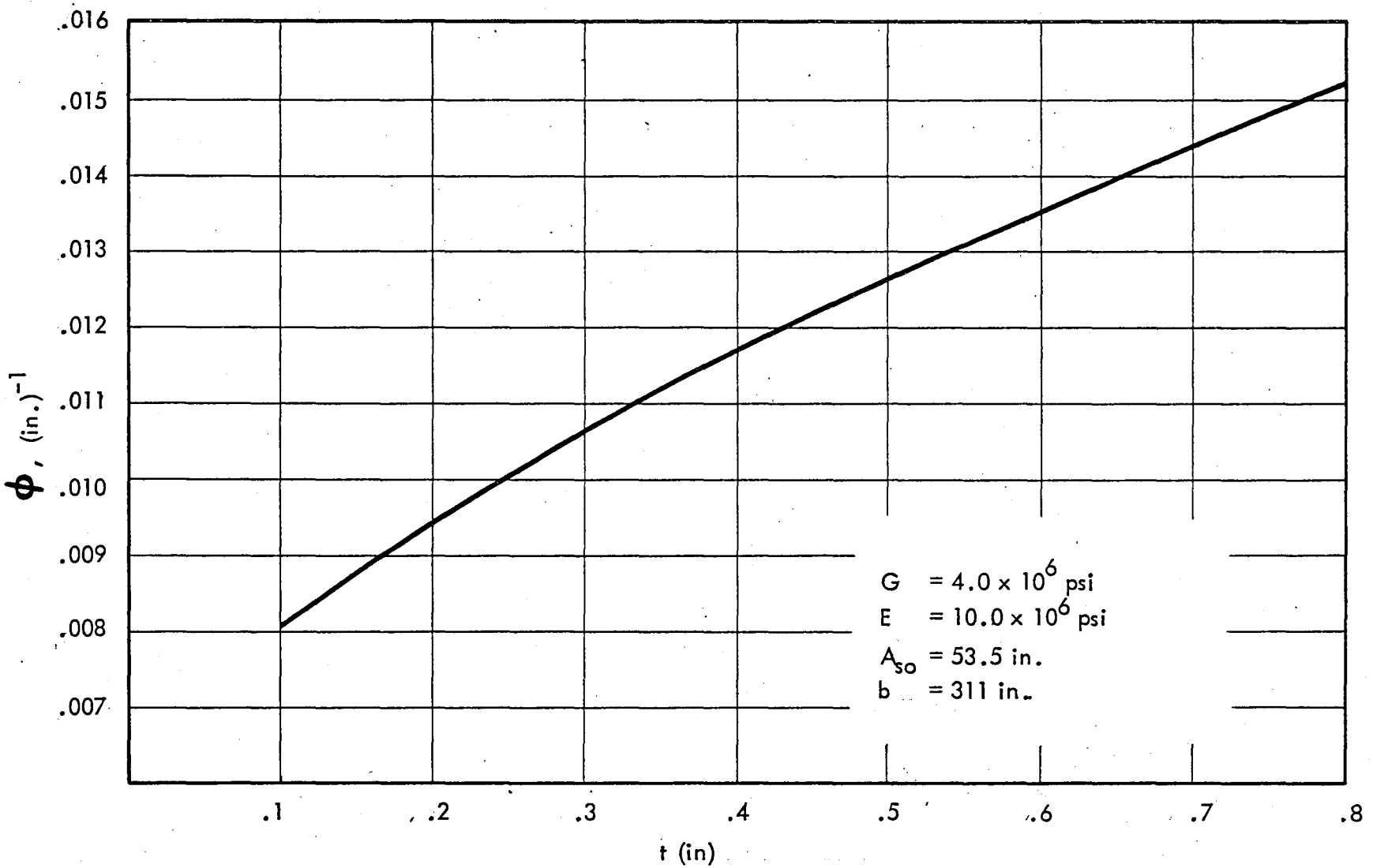

Figure 2-6 ϕ_1 vs t - REBOUND LONGERON

Final utilization of a panel of constant thickness would not be optimum. Hence, the final step in the analysis was to stress-size the longerons and panel, assuming a thickness variation in the panel in the y direction to satisfy the longeron-panel interface requirements. A plot of these thickness requirements are shown in Figure 2-7.

2.1.2 One-Dimensional Numerical Solution

The second technique used in the preliminary shear lag analysis was a one-dimensional, numerical solution. This analysis provided for tapered panels and tapered longerons and considered the effects of taking the loads into a rigid foundation. The flexibility of the analysis allowed the completion of the initial sizing phase of work.

The structure was simulated by dividing a half quadrant into 90 coordinates and writing force displacement relations as described in Reference 2-2 at each of the 90 points. A half quadrant was chosen because the loads were of equal value and were placed at 90° intervals, hence each quadrant had symmetric forces and displacements about its centerline. The geometry of a typical half quadrant is shown in Figure 2-8.

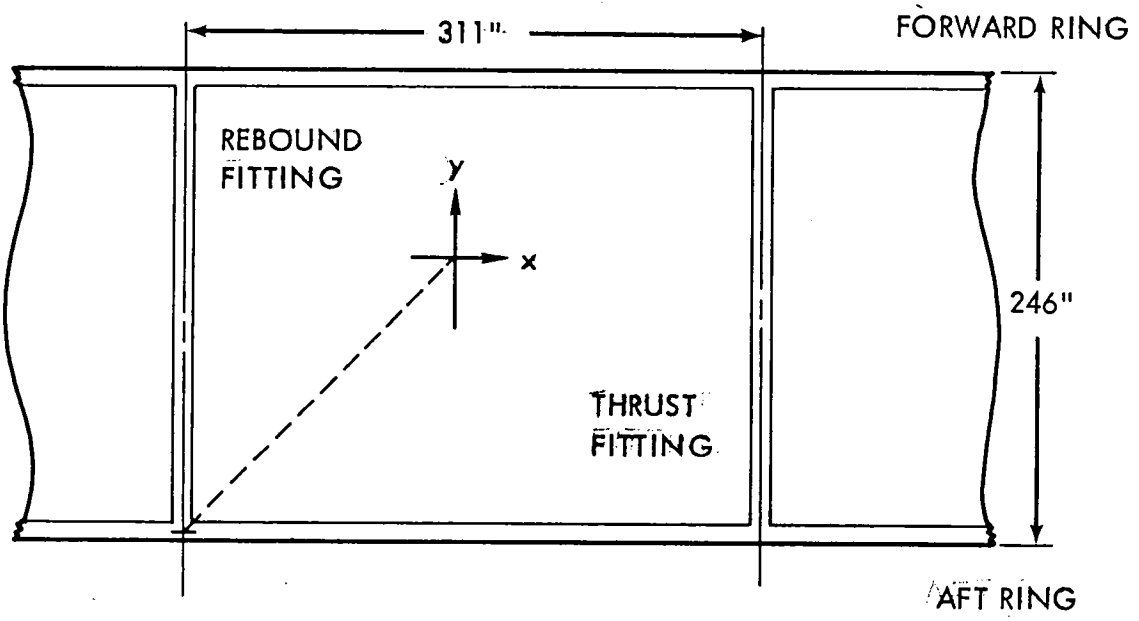

Figure 2-8 HALF QUADRANT GEOMETRY

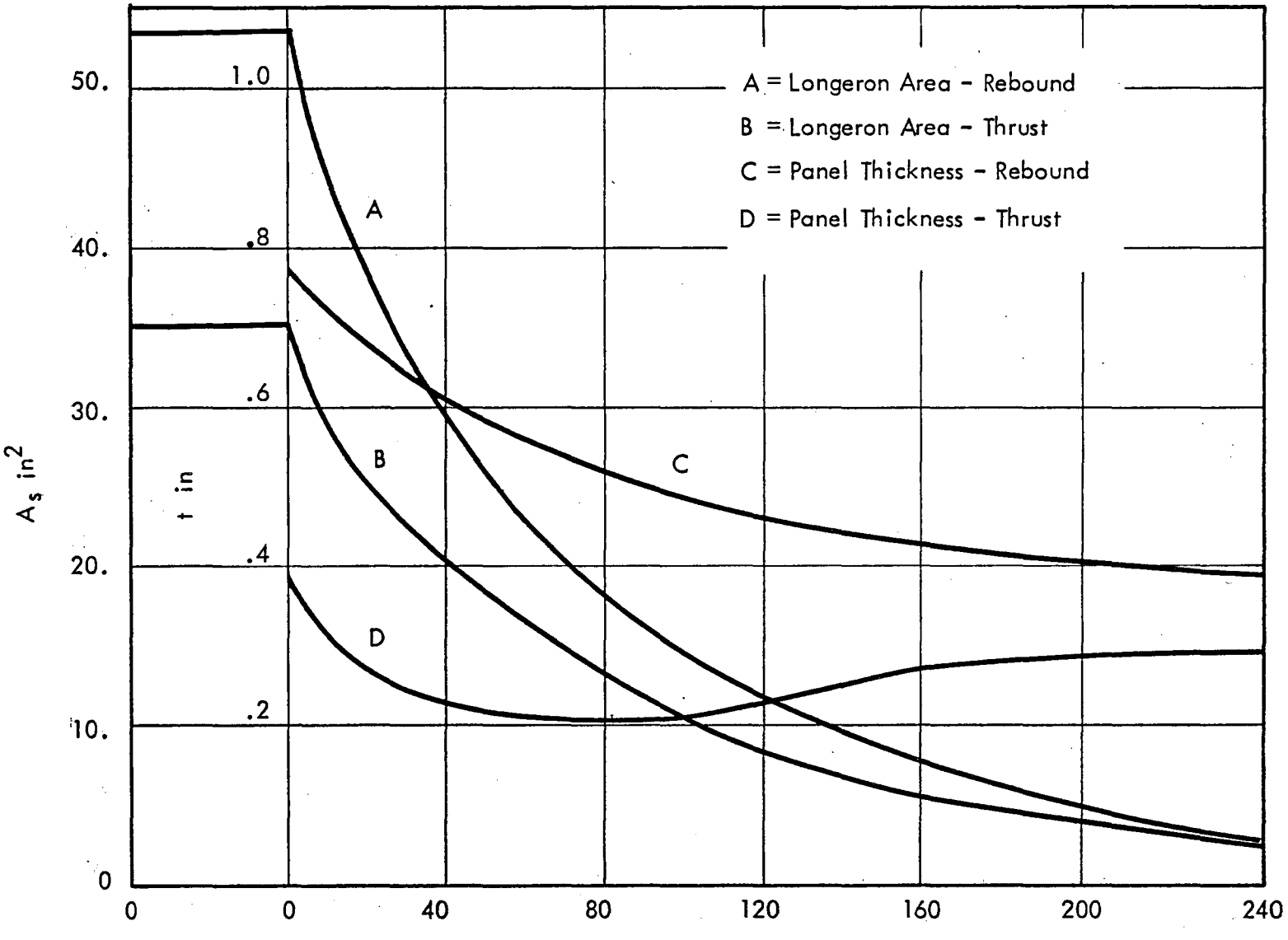

Figure 2-7 INITIAL STRUCTURE REQUIREMENTS

The structure half quadrant was subjected to the following assumptions:

1. The structure will be stable and unbuckled over the load ranges specified.

2. The loads and strains in the x direction are small compared to the loads and strains in the y direction.

3. All axial load carrying material is concentrated at the centerlines of idealized longerons.

4. All of the shear loads are carried by idealized shear panels.

5. Across a single element the axial loads and shear flows are constant.

6. The structural material is Hookian and the deflections are small.

Assumptions 1 and 2 justified a one-dimensional model for which the curvature was neglected. Assumptions 3 and 4 allowed the simulation of the structure by a finite number of structural elements. Assumption 5 permitted consideration of constant loads on each element and assumption 6 allowed linear force displacement equations.

The analysis was divided into four parts

1. The development of force displacement equations for the interior of the panel.

2. The development of force displacement equations for the aft boundary points.

3. The development of force displacement equations for the forward boundary points.

4. The development of the computer program and checkout procedures.

The panel coordinate system used is shown in Figure 2-9.

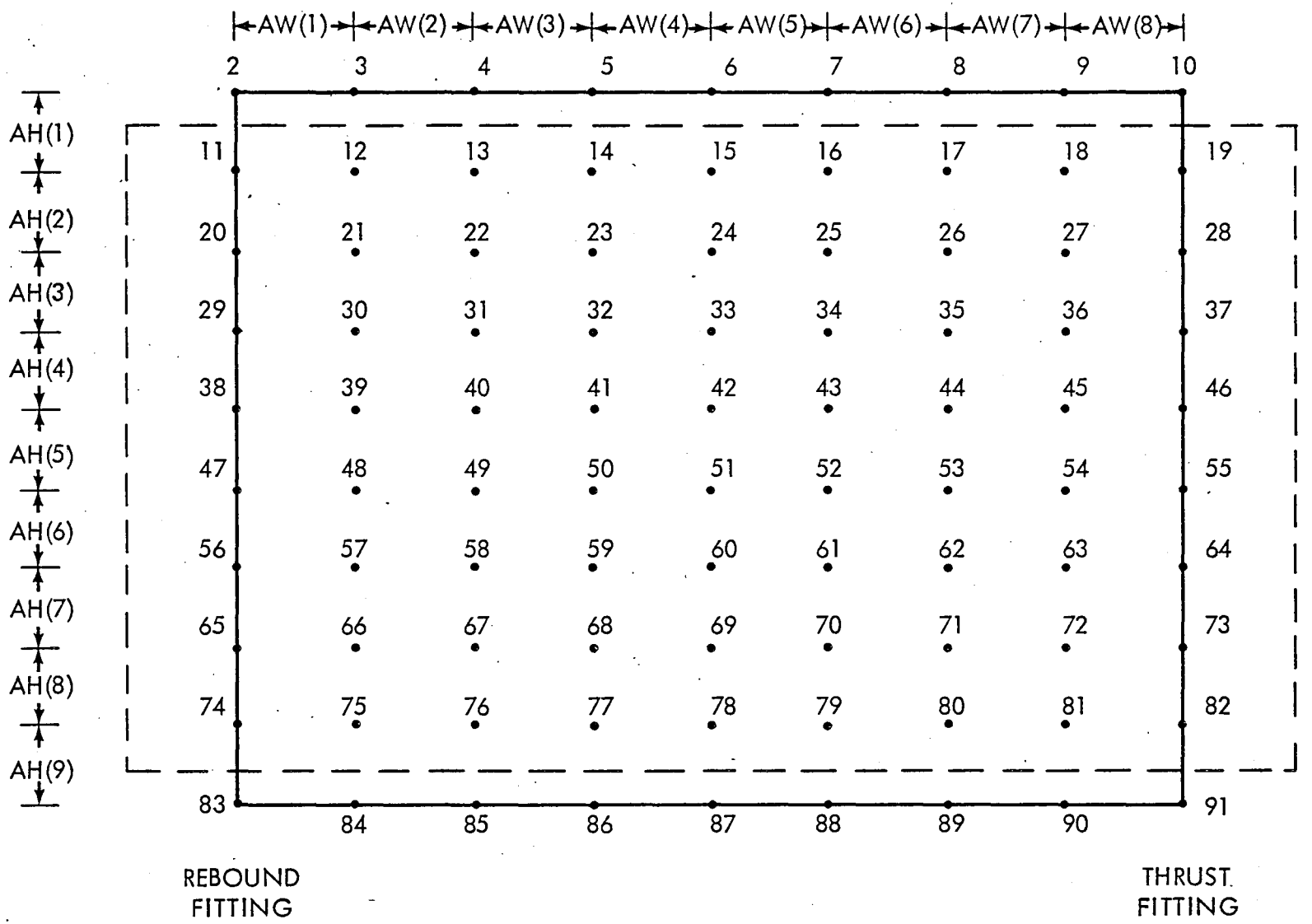

Figure 2-9 COORDINATE SYSTEM

Figure 2-10 shows the force equilibrium diagram at each interior point. The panel thickness and longeron area, if any is present, are given at each of the coordinate points. Hence, the idealized longeron area and the idealized shear panel area must be computed at each point.

The average shear panel areas are

$$TA\ (n) = \left[T\ (n) + T\ (n+1)\right]/2 \qquad (2\text{-}29)$$

The idealized longeron areas are computed from the areas as outlined in the dashed portion of Figure 2-10.

For interior points the idealized longeron area is

$$AA\ (n) = \left[TA\ (n-10) + TA\ (n-1)\right] \cdot AW\ (j)\ /4 + \left[TA\ (n-9) + TA\ (n)\right] \cdot AW\ (j+1)\ /4 \qquad (2\text{-}30)$$

For the boundary points (2 + K9) the idealized longeron area is

$$AA\ (2 + K9) = \left[TA\ (2 + K9) + TA\ (2 + K9 - 9)\right] .\ AW\ (1)\ /4 \qquad (2\text{-}31)$$

and for the boundary points (10 + K9)

$$AA\ (10 + K9) = \left[TA\ (10 + K9 - 1) + TA\ (10 + K9 - 10) \cdot AW\ (8)\right]/4 \qquad (2\text{-}32)$$

With the area relations known the displacements may be written in terms of the coordinates and the forces in terms of the displacements.

The force displacement relations for the interior points are

$$F\ (n) = \left[AA\ (n) .\ EM/AH\ (k)\right]\left[U\ (n-9) - U\ (n)\right] \qquad (2\text{-}33)$$

$$F\ (n+9) = \left[AA\ (n+9) .\ EM/AH\ (k+1)\right]\left[U\ (n) - U\ (n+9)\right]$$

$$AQ\ (n) = \left[TA\ (n) .\ GM/AW\ (j+1)\right]\left[U\ (n+1) - U\ (n)\right]$$

$$AQ\ (n-1) = \left[TA\ (n-1) .\ GM/AW\ (j)\right]\left[U\ (n) - U\ (n-1)\right]$$

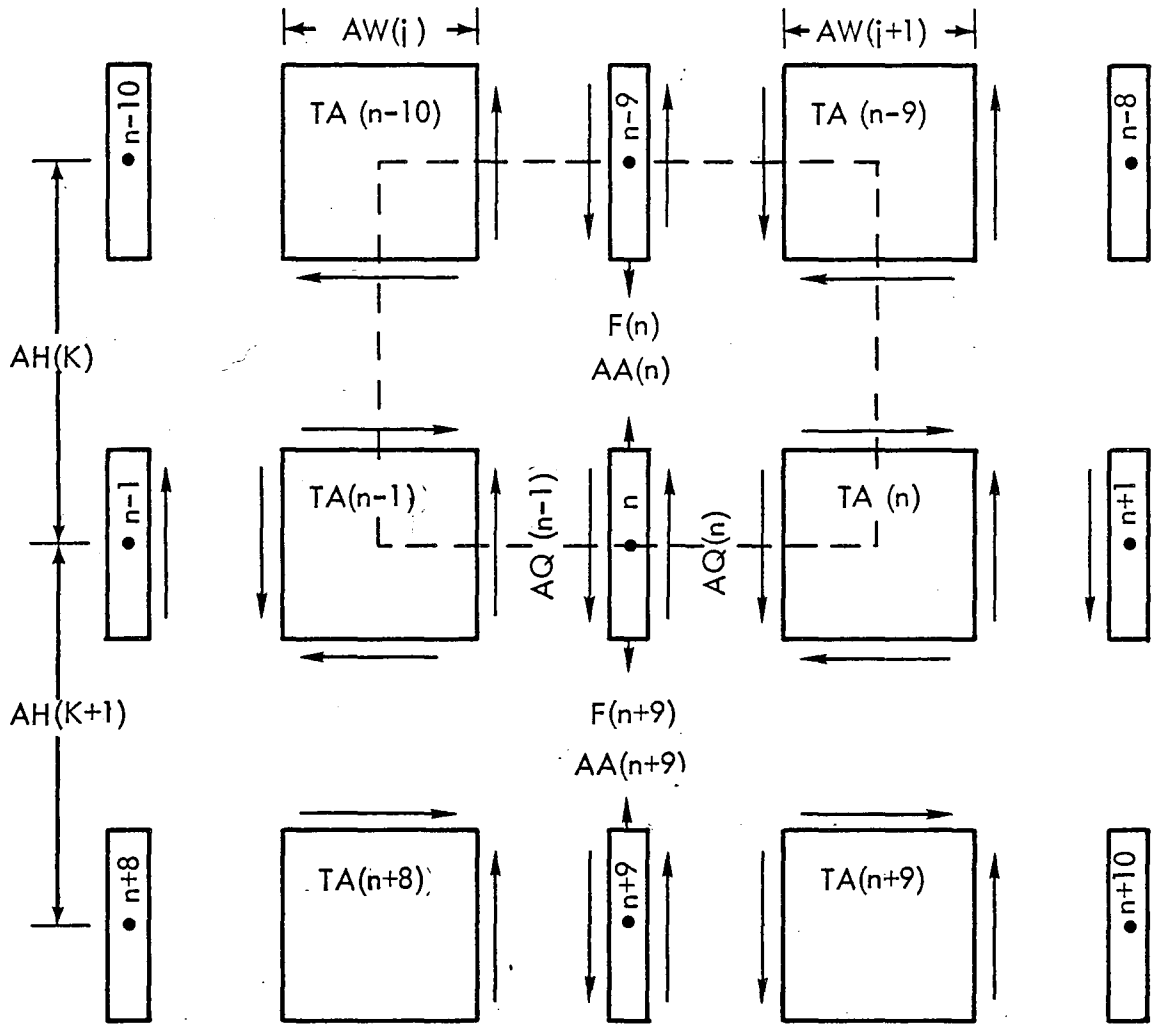

Figure 2-10 INTERIOR POINT EQUILIBRIUM

Let the following coefficients be defined

$$K1 = AA\ (n) \cdot EM/AH\ (k) \tag{2-34}$$

$$K2 = AA\ (n+9) \cdot EM/AH\ (k+1)$$

$$K3 = TA\ (n) \cdot GM/AW\ (j+1)$$

$$K4 = TA\ (n-1) \cdot GM/AW\ (j)$$

In absence of external forces equilibrium conditions about the point (n) require

$$F\ (n) + AQ\ (n) - AQ\ (n-1) - F\ (n+9) = 0 \tag{2-35}$$

hence

$$K1\left[U\ (n-9) - U\ (n)\right] + K3\left[U\ (n+1) - U\ (n)\right] - K4\left[U\ (n) - U\ (n-1)\right] - K2\left[U\ (n) - U\ (n+9)\right] = 0 \tag{2-36}$$

$$K1\left[U\ (n-9)\right] + K4\left[U\ (n-1)\right] + K3\left[U\ (n+1)\right] + K2\left[U\ (n+9)\right] - \left[K1 + K2 + K3 + K4\right]\left[U\ (n)\right] = 0$$

On the boundary points (2 + K.9) (K = 1,2,··,9) the force AQ (n-1) is absence. Hence

$$K1\left[U\ (n-9)\right] + K3\left[U\ (n+1)\right] + K2\left[U\ (n+9)\right] - \left[K1 + K2 + K3\right]\left[U\ (n)\right] = 0 \tag{2-37}$$

On the boundary (10 + K.9) the force AQ (n) is absent. Hence,

$$K1\left[U\ (n-9)\right] + K2\left[U\ (n+9)\right] + K4\left[U\ (n-1)\right] - \left[K1 + K2 + K4\right]\left[U\ (n)\right] = 0 \tag{2-38}$$

This completes the force deflection relations for the interior points. Next, the force deflection relations must be developed for the boundary points.

On the forward boundary points the deflection U must disappear. This boundary condition may be enforced by zeroing out the rows and columns containing the boundary displacements. On the aft edge the force conditions F (n+9) disappear.

The mathematical expressions were then programmed and the structure refined using the digital analysis. The program written is U42. A write-up and customer utilization is presented in Appendix C.

2.2 INTERNAL LOADS DISTRIBUTION

A stiffness matrix approach was used for the internal loads analysis. This approach involves a synthetic model (or simulation) of the structure and a set of equations for the simulation in the form of a stiffness matrix. A stiffness matrix is a linear expression relating loads and deflections, such as

$$\left[S \right] \left\{ \Delta \right\} = \left\{ P \right\} \qquad (2\text{-}39)$$

where

$\left[S \right]$ = stiffness matrix

$\left\{ \Delta \right\}$ = deflections

$\left\{ P \right\}$ = externally applied loads.

The simulation of the structure is obtained by considering the structure as being composed of a finite number of discrete elements. These elements are then used as building blocks to "build up" or simulate the actual structure.

The math model (or stiffness matrix) is formed by first developing the stiffness matrix for the discrete elements and then assembling these elemental matrices into the matrix for the composite structure. This is accomplished by adding stiffnesses (parallel or superposition method) at common coordinates (points) in the simulation. Each coordinate defines a translation or rotation in an assigned direction and location on the simulated structure.

If the stiffness matrix is non singular, the unknown deflections are readily obtained from

$$\left\{ \Delta \right\} = \left[S \right]^{-1} \left\{ P \right\} \qquad (2\text{-}40)$$

These deflections are then used to obtain the loading for the structural elements, using the elemental stiffness matrix in an equation of the same form as (2-39) above. These applied loads, considered external to the discrete element, are actually internal to the composite structure.

Only two types of discrete elements were used in the simulation for the Saturn Skirt. These were the beam segment and the general quadrilateral plate. The development of these elemental stiffness matrices are presented in Appendix D.

The simulation used took full advantage of the structural symmetry and the axially symmetric static applied loads. If the structure is divided into four parts, with each part being defined as a 90 degree arc length of the circumference and extending the full skirt length, then each of the four parts are identical. Furthermore, if the 90 degree arc length is taken either from rebound column to rebound column or thrust column to thrust column, then each of the four parts are also symmetric about the 45 degree centerline.

This being the case, only 1/8 of the structure is required for simulation. This is illustrated in Figure 2-11.

The grid work or density of panels used is also shown in Figure 2-11. Five panels were used for the circumferential span; each panel represented a 9 degree arc length. This was done for two reasons: (1) The quadrilateral plates are flat, and therefore a fine grid is necessary to properly simulate the curved surface with straight segments. (2) Because each discrete element is assumed to carry shear of a parabolic (2nd order) nature, the combination of fine grid and high ordered shear distribution on each element should give an excellent approximation to the shear distribution on the skirt.

The skirt length was composed of eight panel layers to allow for proper redistribution of load and also to form a discrete panel of almost square shape (causing the panel stiffness matrix to be well ordered).

Because the panels used in the simulation carry in-plane loads only, beams were used to carry the out of plane (radial) loads. Beam segments border the panels shown in the simulation (i.e., extend both circumferentially and longitudinally) and approximate the lateral stiffness of the honeycomb structure. Of course, the beams which extend longitudinally on each edge of the simulated (1/8) structure also possess (1/2) the stiffness of the thrust or rebound columns.

With the beams furnishing out-of-plane stiffnesses which the plates do not possess, the edge forces on the plates may now "turn-the-corners" in traveling circumferentially and switching planes as they do so.

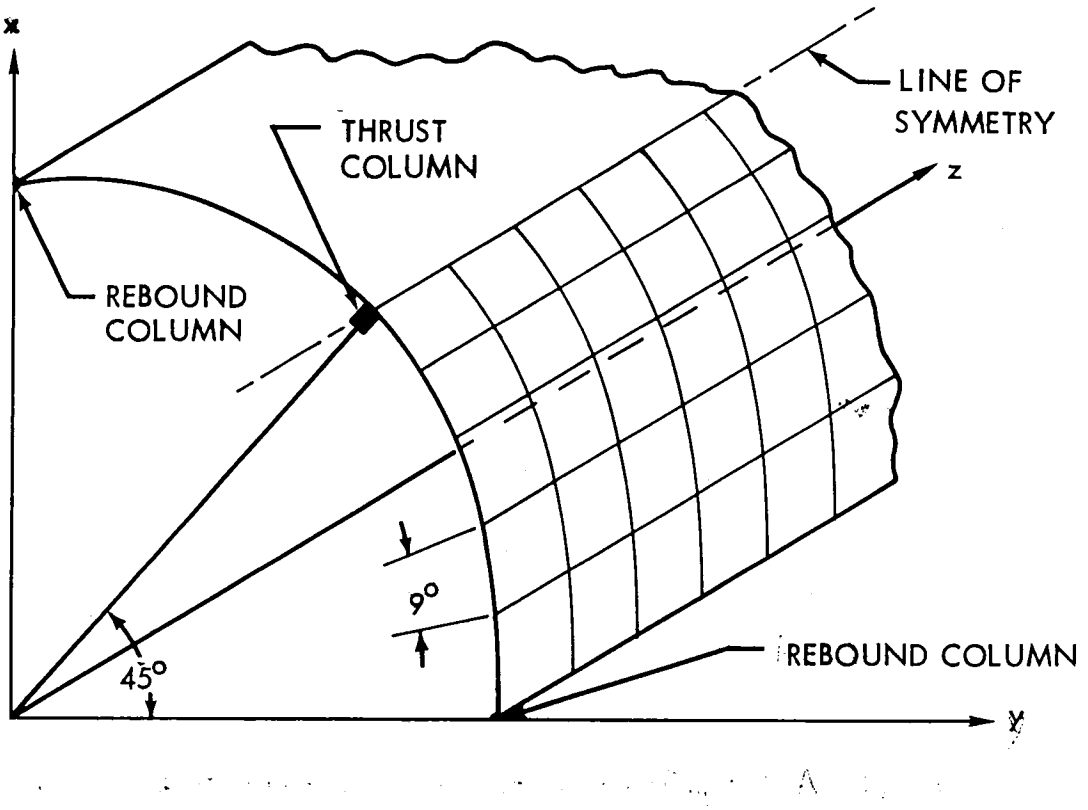

Figure 2-11 SKIRT STRUCTURE SIMULATION FOR DIGITAL ANALYSIS

2.3 DIGITAL BUCKLING

In Section 2.2 the stiffness matrix approach for static analysis was expressed as

$$\left[S \right] \left\{ \Delta \right\} = \left\{ P \right\} \tag{2-39}$$

The assumptions made in the above static analysis are (a) small deflections are obtained within the linear theory and because of this (b) the internal loads do not change direction as the structure deforms.

Generally speaking, buckling occurs because the internal loads change direction as the structure deforms. A classical example is the Euler column. Hence, to perform a buckling analysis using the stiffness matrix approach, it is necessary to correct the internal loading as a function of the state of deformation.

An example of how this is accomplished is indicated in Figure 2-12. If a simple bar element in compression is laterally deflected as shown, the element is no longer in a state of equilibrium.

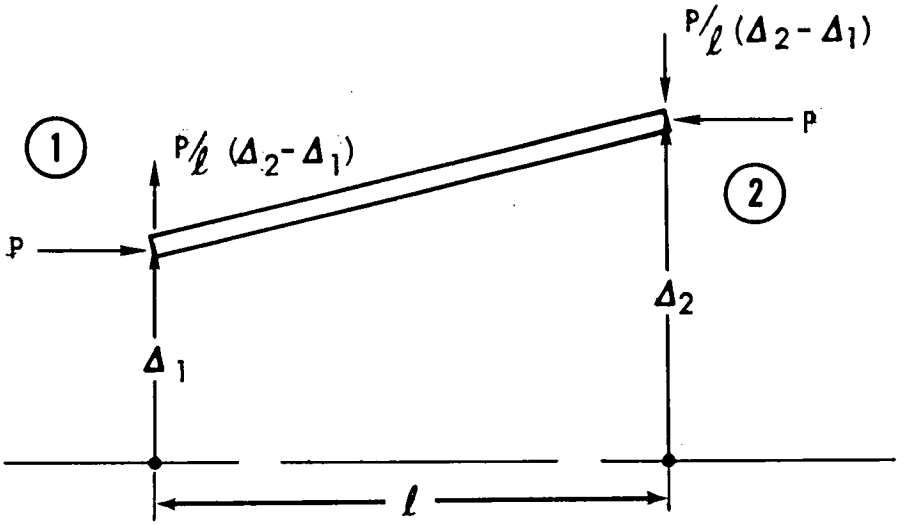

Figure 2-12 LATERALLY DEFLECTED BAR IN COMPRESSION

However, it may be placed in equilibrium by applying the lateral loads as shown. Note that the balancing lateral loads are a function of the state of deformation and the applied loads within the linear theory.

Using this approach, a correction to the stiffness matrix (denoted a perturbed or Δ S matrix) is obtained for each element used in the simulation of the structure. The correction term for the above bar element would appear as

$$\left[\Delta S\right] = \frac{1}{\ell} \begin{bmatrix} P_1 & 0 \\ 0 & P_2 \end{bmatrix} \begin{bmatrix} -1 & +1 \\ +1 & -1 \end{bmatrix} \qquad (2\text{-}41)$$

Another example of required correction is that for the general quadrilateral complex plate element. This plate element is considered as carrying only in-plane loads in a linear analysis and the effects on these loads of the lateral deformation of the plate are ignored. When the plate is laterally warped extensively, the directions of the in-plane loads change and they then possess components lateral to the unwarped plate. The consideration of these lateral components constitutes a correction to the analytical technique and must be considered for a buckling analysis.

These components are calculated as follows:

1. A new plane is considered as defined by the mid-points of the laterally deflected corners.

2. This new plane carries the in-plane loads only and is in balance.

3. The components of the in-plane loads, lateral to the unwarped plate, constitute the desired corrections and appear in matrix form as

$$S = \begin{bmatrix} s_{11} & s_{12} & s_{13} & s_{14} \\ s_{21} & s_{22} & s_{23} & s_{24} \\ s_{31} & s_{32} & s_{33} & s_{34} \\ s_{41} & s_{42} & s_{43} & s_{44} \end{bmatrix} = \begin{bmatrix} \frac{1}{2} & & & \\ \frac{1}{2} & \frac{1}{2} & & \\ & \frac{1}{2} & \frac{1}{2} & \\ & & \frac{1}{2} & \frac{1}{2} \end{bmatrix} \begin{bmatrix} \frac{1}{2} & & & \\ & \frac{1}{2} & & \\ & & \frac{1}{2} & \\ & & & \frac{1}{2} \end{bmatrix} \left\{ \begin{bmatrix} V_{12} & & & \\ & V_{23} & & \\ & & V_{34} & \\ & & & V_{41} \end{bmatrix} \begin{bmatrix} -\ell_{12}^{-1} \\ \ell_{23}^{-1} \\ -\ell_{34}^{-1} \\ \ell_{41}^{-1} \end{bmatrix} \right.$$

$$\left. (-k_3\ k_4\ -k_1\ k_2) \right\} + \quad \text{cont'd next page}$$

$$+ \begin{bmatrix} F_{12} & & & \\ & F_{23} & & \\ & & F_{34} & \\ & & & F_{41} \end{bmatrix} \begin{bmatrix} 0 & -1 \\ \cos\alpha_1 & \sin\alpha_1 \\ \cos\alpha_2 & \sin\alpha_2 \\ \cos\alpha_3 & \sin\alpha_3 \end{bmatrix} \begin{bmatrix} x_1^{-1} & \\ & y_3^{-1} \end{bmatrix} \left[\begin{array}{cc|cc} k_1 & & -k_2 & \\ k_1\left(1-\frac{x_3}{x_1}\right)-1 & & -k_2\left(1-\frac{x_3}{x_1}\right) & \\ -k_1 & & k_2 & \\ 1-k_1\left(1-\frac{x_3}{x_1}\right) & & k_2\left(1-\frac{x_3}{x_1}\right) & \end{array}\right]$$

The symbols used are defined in Figure 2-13.

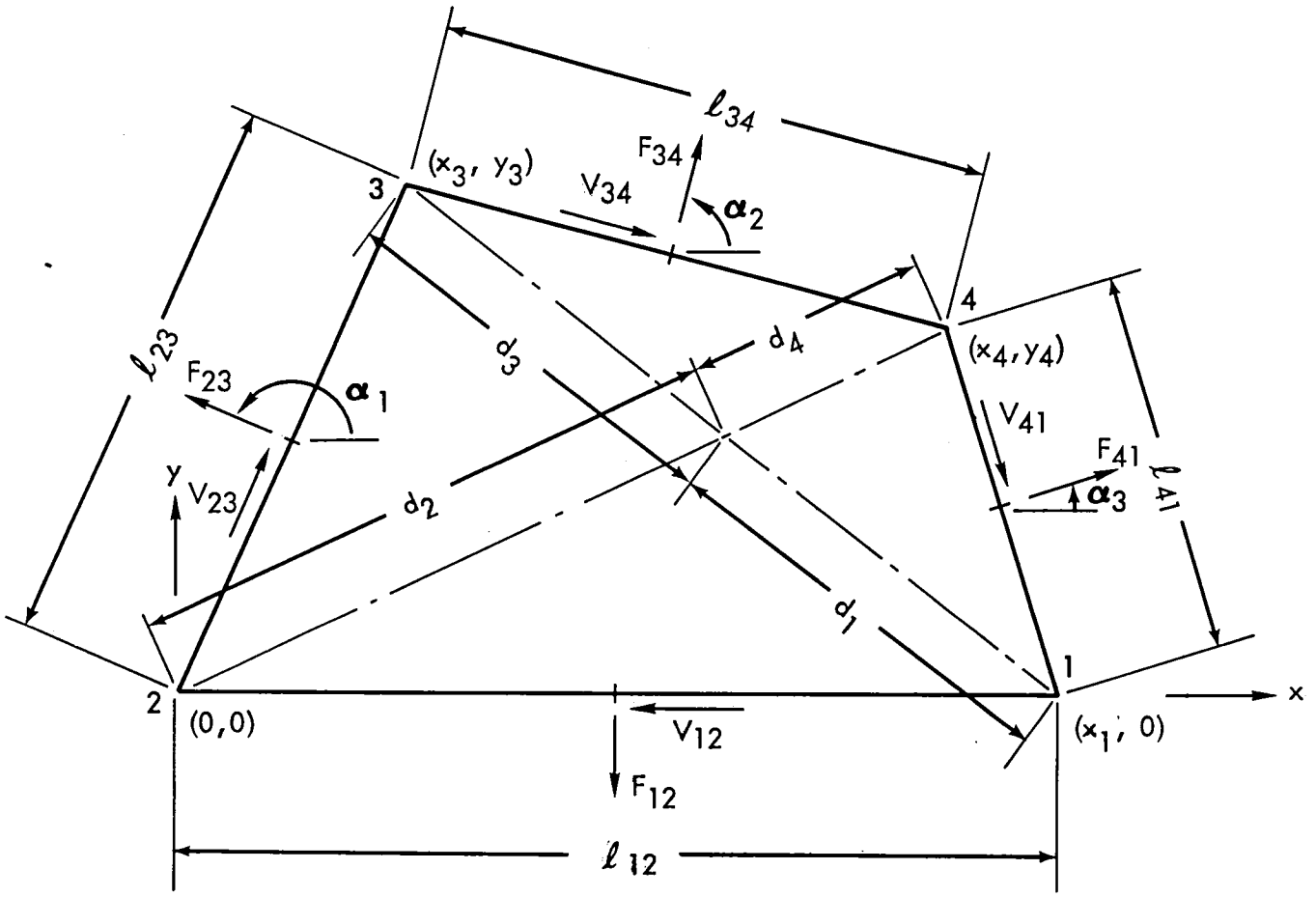

NOTE: $K_1 = \frac{d_1}{d_1+d_3}$; $K_2 = \frac{d_2}{d_2+d_4}$; $K_3 = \frac{d_3}{d_1+d_3}$; $K_4 = \frac{d_4}{d_2+d_4}$

Figure 2-13 GENERAL QUADRILATERAL PLATE LAYOUT

After all the corrective terms are formed (i.e., all beams and plates used in simulating the structure) they are assembled into a master matrix by superposition. Equation (2-39) then becomes

$$\left(\left[S \right] + \left[\Delta S \right] \right) \left\{ \Delta \right\} = \left\{ P \right\} \qquad (2\text{-}39a)$$

and the new state of deformation obtained, provided that the matrix is nonsingular. This process of analysis may be recycled, adding a corrective term to the matrix with each cycle, until the rate of change in the matrix becomes so small that continuation is unnecessary. At this point the problem of buckling analysis has been solved. However, it is expensive in computing time as well as laborious.

A good approximation to the buckling load and mode shape may be obtained by modifying (2-39a) so that iteration may be performed. The buckling load is defined as that load at which deformation continues to increase while the load is maintained constant. Hence, the matrix becomes singular at buckling, and cannot be inverted. This may be expressed as

$$\left(\left[S \right] + K \left[\Delta S \right] \right) \left\{ \Delta \right\} = 0 \qquad (2\text{-}39b)$$

where K is a perturbation parameter. Equation (2-39b) may be written as

$$-\frac{1}{K} \left\{ \Delta \right\} = \left[S \right]^{-1} \left[\Delta S \right] \left\{ \Delta \right\} \qquad (2\text{-}40a)$$

which when iterated, yields the lowest buckling load factor K and the normalized buckling shape.

2.4 SONIC FATIGUE

At present the most useful method of predicting the fatigue life of structures excited by random inputs is that of considering the complex response analogous to the response of a linear single-degree-of-freedom system. It is theoretically possible that a infinite number of modes may be excited, but strain gauge measurements indicate that on certain parts of the structure such as the skin, only a few modes are excited, and usually the predominant response is that associated with the fundamental mode.

The analysis method will begin with an estimate of the fundamental resonant frequency of the structure. The part of the sound spectrum corresponding to that frequency is then defined. The maximum stress produced in the structure by that magnitude of sound pressure loading is then calculated. At this point the analysis resorts to Miner's law of cumulative fatigue damage which substitutes for the rms stress an equivalent stress defined as a constant amplitude stress which would cause the same fatigue damage in the total number of cycles as is caused by the probable number of cycles at all stress levels. The number of cycles which will cause failure can then be read from a conventional S-N curve for the material of the structure.

2.4.1 Natural Frequency Analysis

The fundamental frequench of honeycomb panels can be calculated using the following formula:

$$f = 0.01\sqrt{\frac{K}{M}} \qquad (2\text{-}42)$$

where: K = spring constant = $\dfrac{D}{K_1 + VrD\ K_2}$

M = mass = $a \times b \times \rho$

.01 = an empirical constant which includes the conversion from radians to cps.

a = short dimension of panel, inches

b = long dimension of panel, inches

$D = \dfrac{E_F}{12\ (1-\mu^2)} \left[t^3 - t_c^3 - 3t_c\ (t_{F_1} - t_{F_2})^2 \right]$

E = Modulus of elasticity

G = Modulus of rigidity

K_1 & K_2 = Empirical constants related to shear

t = thickness, inches

u = transverse shear stiffness = $\frac{(t + t_c)^2}{4t_c} G_c$

V = dimensionless parameter = $\frac{\pi D}{a^2 U}$

μ = Poisson's ratio

$\rho = \frac{(\gamma F_1 \; t_{F1}) + (\gamma F_2 \; t_{F2}) + (\gamma c \; t_c)}{386}$

γ = weight, lb/in^3

subscripts: F = face, used with 1 and 2 to denote particular face, c = core

2.4.2 Response of a Simple Oscillator

We begin with some of the mathematics involved in analyzing the linear single-degree-of-freedom system shown in Figure 2-14.

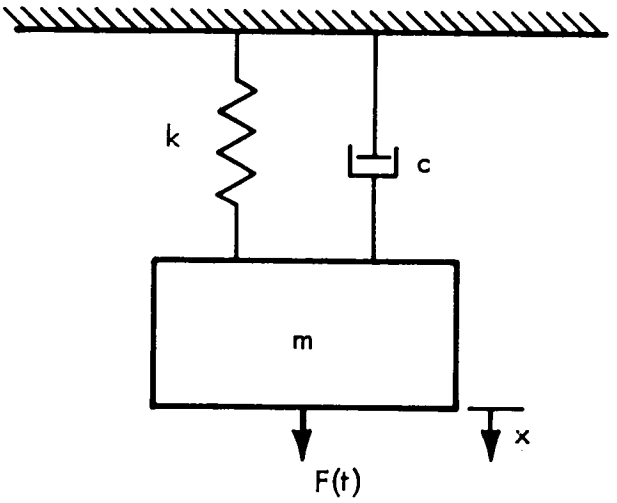

Figure 2-14 LINEAR SINGLE-DEGREE-OF-FREEDOM SYSTEM

The differential equation of motion for forced vibration of a linear single-degree-of-freedom system is

$$m\ddot{x} + c\dot{x} + kx = F(t) \tag{2-43}$$

where m is the mass of the system

c is the damping of the system

k is the spring constant of the system

F(t) is the input forcing function

x is the displacement from equilibrium

Using the physical relationships

$$M = \frac{k}{\omega_n^2} \tag{2-44}$$

$$k = \frac{F_n}{x_n} \tag{2-45}$$

$$c = 2m\eta\ \omega_n \tag{2-46}$$

where ω_n is the natural angular frequency of the system

F_n is a static force which would produce the displacement, x_n

η is the ratio of damping to critical damping, $\frac{c}{c_c}$

Equation (2-43) can be rearranged to the form

$$\ddot{x} + 2\eta\ \omega_n \dot{x} + \omega_n^2\ x = \frac{1}{m} F(t) \quad . \tag{2-47}$$

Letting F(t) be a unit impulse $\delta(t)$, with all initial conditions zero, the impulse response function will be

$$h(t) = \left(\frac{e^{\eta\ \omega_n t}}{m\ \omega_n \sqrt{1 - \eta^2}} \right) \sin \left| \omega_n \sqrt{1 - \eta^2}\ t \right| \quad . \tag{2-48}$$

The frequency response function is given by

$$H(j\omega) = \int_0^\infty h(t)(m\, e^{-j\omega_n t})dt, \tag{2-49}$$

and substituting (2-48) into (2-49)

$$H(j\omega) = \frac{1/m}{(\omega_n^2 - \omega^2) + jz\,\eta\omega\omega_n} \tag{2-50}$$

It can be shown that

$$S_x(\omega) = \left|H(j\omega)\right|^2 S_f(\omega) \tag{2-51}$$

where $S_x(\omega)$ is the output spectral density function

$\left|H(j\omega)\right|^2$ is the square of the magnitude of the frequency response function

$S_f(\omega)$ is the input spectral density function.

The mean square value of the response is given by

$$\overline{x^2(t)} = \frac{1}{2\pi} \int_0^\infty \left|H(j\omega)\right|^2 S_f(\omega)d\omega \tag{2-52}$$

where $\overline{x^2(t)}$ is the mean square displacement, the bar indicating the mean value.

To this point no simplifying assumptions have been made. The development presented consists of listing the major steps in obtaining the mean square displacement of a simple oscillator when forced by a function f(t) which has not yet been defined. The details involved in obtaining these steps are readily available and are therefore not presented. However, to find the value of $\overline{x^2(t)}$, the function $S_f(\omega)$ must be known.

Experimental investigations with actual aircraft structures show that when excited by random pressure fluctuations from jet engines, the structure acts as a filter. This means that the structure accepts energy only at or near certain frequencies, these frequencies being near one of the many natural frequencies of the complex structure. Also, experiments show that the maximum amplitude of the response is usually near the fundamental or lowest natural frequency (see Figure 2-15).

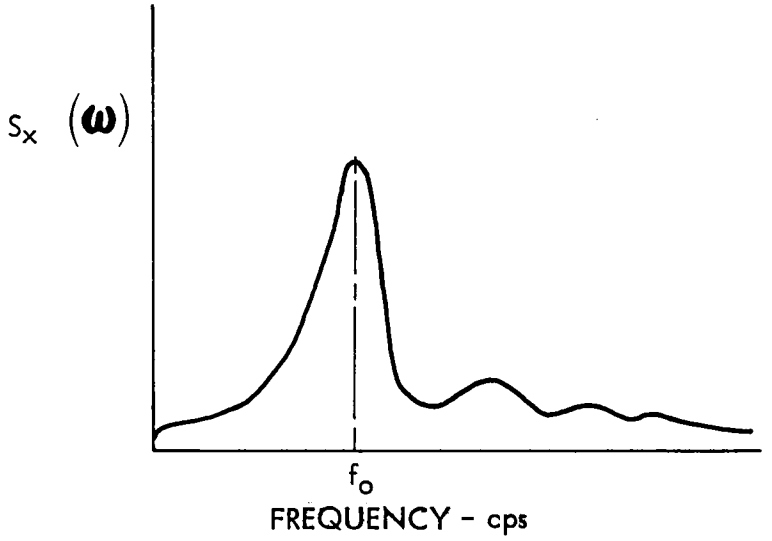

Figure 2-15 RESPONSE OF STRUCTURE TO RANDOM NOISE

The spectral density function of the random input jet engine and boundary layer pressure fluctuations is relatively flat and may be considered constant over the narrow frequency range of the maximum response. By using these observations we greatly facilitate the integration in Equation (2-52) while losing very little accuracy. Performing the integration leads to

$$\overline{x^2(t)} = \left(\frac{x_n}{F_n}\right)^2 \frac{S_f(\omega)\omega_n}{4\eta} \approx \left(\frac{x_n}{F_n}\right)^2 \frac{S_f(f) f_n}{4\eta} \qquad (2\text{-}53)$$

for the mean square response where

$S_f(f)$ is the spectral density function in lb^2/cps

f_n is the natural frequency of the system in cps.

The analysis thus far has dealt with a force acting on a mass. The same concepts can be applied to continuously elastic structure whose significant response is only at its resonant frequency.

To make the analysis useful for the response of a structure to acoustic loading, it is necessary to convert force to pressure.

$$\frac{F_n}{A} = P_n \text{ and } \frac{S_f(f)}{A^2} = \phi_n \qquad (2\text{-}54)$$

The pressure is assumed to be uniform over the surface of the structure. This assumption of uniform acoustic pressure tacitly assumes unit correlation of pressure over the entire surface of the structure. Experimental investigations tend to justify this assumption for the fundamental frequency. If the actual situation does not have unit correlation of pressure, the analysis will be conservative. Substituting equations (2-54) into equation (2-53) and rearranging

$$\frac{\overline{x(t)^2}}{x^2_n} = \frac{\pi \phi_n f_n}{4\eta} \cdot \frac{1}{P_n^2} \cdot \qquad (2\text{-}55)$$

For a linear system the stress produced is proportional to the deflection which is in turn proportional to the pressure causing the deflection.

$$\overline{\sigma_r^2} = c_1 \overline{x(t)^2} = c_2 \overline{P_r^2} \qquad (2\text{-}56)$$

and $$\sigma_n = c_1 x_n = c_2 P_n \qquad (2\text{-}57)$$

where σ_r^2 is the mean square stress produced by the mean square delfection, $\overline{x_{(t)}^2}$, produced by the mean square pressure, P_r^2

σ_n is the stress produced by the deflection, x_n, produced by the static pressure P_n

c_1 and c_2 are undefined constants.

Then

$$\frac{\overline{\sigma_r^2}}{\sigma_n^2} = \frac{\overline{x(t)^2}}{x_n^2} = \frac{\overline{P_r^2}}{P_n^2} \qquad (2\text{-}58)$$

Therefore, from equations (2-55) and (2-58)

$$P_r = \sqrt{\frac{\pi}{4\eta}} \sqrt{\phi_n f_n} \qquad (2\text{-}59)$$

and

$$\sigma_r = \sqrt{\frac{\pi}{4\eta}} \sqrt{\phi_n f_n} \left(\frac{\sigma_n}{P_n}\right) \qquad (2\text{-}60)$$

In this form the parts of equation (2-60) can be identified as: the damping of the structure

$$\left(\sqrt{\frac{\pi}{4\eta}}\right),$$

the sound pressure impinging on the structure $\left(\sqrt{\phi_n f_n}\right)$, and the static ratio

$$\left(\frac{\sigma_n}{P_n}\right).$$

These terms are evaluated in the following sections.

2.4.2.1 Evaluation of the Damping

Of all the parameters involved in the fatigue life of a structure, there is probably more room for improvement in the damping properties than in any other parameter. Though damping is of great importance in the acoustical fatigue phenomenon, theory is not presently available for maximizing this parameter, and therefore the significant improvements possible have not yet been fully exploited by design engineers.

For purposes of the analysis a value for the damping ratio must be assumed. Some typical values are given below.

Type of Structure	η
Aluminum or magnesium plate stringer	0.01 to 0.02
Honeycomb bonded	0.04

2.4.2.2 Evaluation of $\sqrt{\phi_n f_n}$

The term $\sqrt{\phi_n f_n}$ can be evaluated from the sound pressure level impinging on the structure being analyzed. The mean squared pressure density corresponding to the decibels measured for the band-width Δf is

$$\phi_n = \frac{(\overline{P_r}/P_o)^2}{\Delta f} \cdot P_o^2 \qquad (2\text{-}61)$$

where P_o is the reference sound pressure.

Multiplying both sides of Equation (2-61) by f_n and taking the square root,

$$\frac{\sqrt{\phi_n f_n}}{P_o} = \sqrt{\frac{f_n}{f}} \left(\frac{\overline{P_r}}{P_o} \right). \qquad (2\text{-}62)$$

Taking the log of both sides of Equation (2-62) and multiplying both sides by 20,

$$20 \log_{10} \frac{\sqrt{\phi_n f_n}}{P_o} = 10 \log_{10} \frac{f_n}{\Delta f} + 20 \log_{10} \left(\frac{\overline{P_r}}{P_o} \right). \qquad (2\text{-}63)$$

Since the sound pressure levels found in the octave band, 1/3 octave band, etc., represent energy levels contained within a band-width, $f_n \cong f_{av}$. Equation (2-63) can be written as

$$20 \log_{10} \frac{\sqrt{\phi_n f_n}}{P_o} = 10 \log_{10} \frac{f_{av}}{\Delta f} + 20 \log_{10} \left(\frac{\overline{P_r}}{P_o} \right). \qquad (2\text{-}64)$$

or $$20 \log_{10} \frac{\sqrt{\phi_n f_n}}{P_o} = c + 20 \log_{10} \left(\frac{\overline{P_r}}{P_o} \right) \qquad (2\text{-}65)$$

where f_{av} = average frequency in bandwidth Δf

c = 1.78 db for full octave band

c = 4.65 db for one-half octave band

c = 6.38 db for one-third octave band.

From the preceding it can be seen that $\sqrt{\phi_n f_n}$ is found by adding c to the sound pressure level at the surface of the structure and converting to $\pm$ rms pressure units.

2.4.2.3 Static Stress Per Unit Constant Pressure Loading

The term $\left(\frac{\sigma_n}{P_n}\right)$ from Equation (2-60) is the ratio of stress to pressure loading under static conditions. Its value can be found experimentally at any point on the structure by measuring the stress at that point while loading the structure with a uniform constant pressure.

The stresses produced in an elastic structure by uniform pressure loading will vary over the parts of the structure because of its deformation. The maximum stress, σ_{max}, will be located by the geometry and boundary conditions of the structure.

The equation for the maximum stress σ_{max} in a flat, rectangular, isotropic plate due to a constant pressure loading P_n is

$$\sigma_{max} = \frac{\beta a^2}{h^2} \cdot P_n \qquad (2\text{-}66)$$

where β is a constant depending on the boundary conditions and geometry of the plots,

a is the length of the short side of the plate in inches,

h is the thickness of the plate in inches.

For a unit pressure loading, P_n - 1, Equation (2-66) becomes

$$\sigma_m = \frac{\beta a^2}{h^2} \cdot \qquad (2\text{-}67)$$

For flat, rectangular, honeycomb sandwich panels, thickness (h) in Equation (2-64) is replaced by the equivalent thickness, h_e.

$$h_e = 2\sqrt{3\ \lambda_F \frac{D}{H}} \qquad (2\text{-}68)$$

where $\lambda_F = 1 - \nu_1 \nu_2$

$$D = \frac{E_F}{12\lambda_F}\left[3t_{F_1}t_{F_2}\ \frac{(t + tc)^2}{t - t_c} + t_{F_1}{}^3 + t_{F_2}{}^3\right]$$

$$H = E_F\ (t - t_c)$$

and subscript F denotes "facing"

subscript 1 and 2 denote particular "facings"

subscript c denotes core

ν is Piosson's ratio

E is Young's modulus

t is sandwich thickness, subscripts denote thickness of either facing or core.

2.4.3 Law of Fatigue Damage

There exist a number of hypotheses that state researchers' opinions on what causes cyclic fatigue failure. Some of these are quite convincing in their explanations of the fundamental mechanisms associated with the fatigue phenomenon, but none has been completely verified, and few have more than a small amount of experimental data to support any one of them. In this report, the hypothesis of fatigue damage chosen is one that is quite simple, relatively easy to use, and verified within limits by much experimental data. The hypothesis is called Miner's Law of linear cumulative damage in fatigue.

For a particular structure it is assumed that the total number of cycles at failure is a constant and therefore independent of the variables--frequency and time. Experimental data indicates that this assumption is not always a good one but that for most structures it is a reasonable one. The law then states that

$$D_1 = \frac{n_1}{N_1}, \quad D_2 = \frac{n_2}{N_2}, \quad \ldots \quad D_k = \frac{n_k}{N_k} \tag{2-69}$$

where D_1 = damage done by n_1 cycles of strain at a constant amplitude, P_i.

N_i = number of cycles to cause failure at a constant amplitude, P_i.

The damage at failure, D, is then given by

$$D = D_1 + D_2 + \ldots + D_k = \sum_{i=1}^{k} \frac{n_i}{N_i} = 1. \tag{2-70}$$

Experimental data show that when the stress amplitudes begin at large values and decrease steadily, $D < 1$ at failure, and when the loading sequence is the opposite, i.e., when the stress amplitudes begin with small amplitudes and increase steadily to large amplitudes, $D > 1$. But for random loading D tends to approach the value of 1. However, Equation (2-70) must be modified to account for the relatively greater damage that results from cycles of large stress amplitudes which occur when the response is random. The modification is made by finding a sinusoidal constant amplitude stress that is equivalent to the random stress.

An approximation of fatigue data plotted as σ vs N is

$$N(\sigma) = (\sigma_1 / \sigma)^{\alpha} \tag{2-71}$$

where

$N(\sigma)$ is the number of cycles to failure at stress level σ and σ_1 is the hypothetical stress at which failure occurs in one cycle.

α is a constant determined from experimental data. It is the inverse slope of the σ-N curve when plotted on log-log graph paper. Obtain the value of α as follows: using Equation (2-71)

$$\alpha = \frac{\log(N_b) - \log(N_a)}{\log \sigma_a - \log \sigma_b} \qquad (2\text{-}72)$$

where

N_a is the number of cycles to failure at stress σ_a

N_b is the number of cycles to failure at stress σ_b.

Figure 2-16 illustrates this concept.

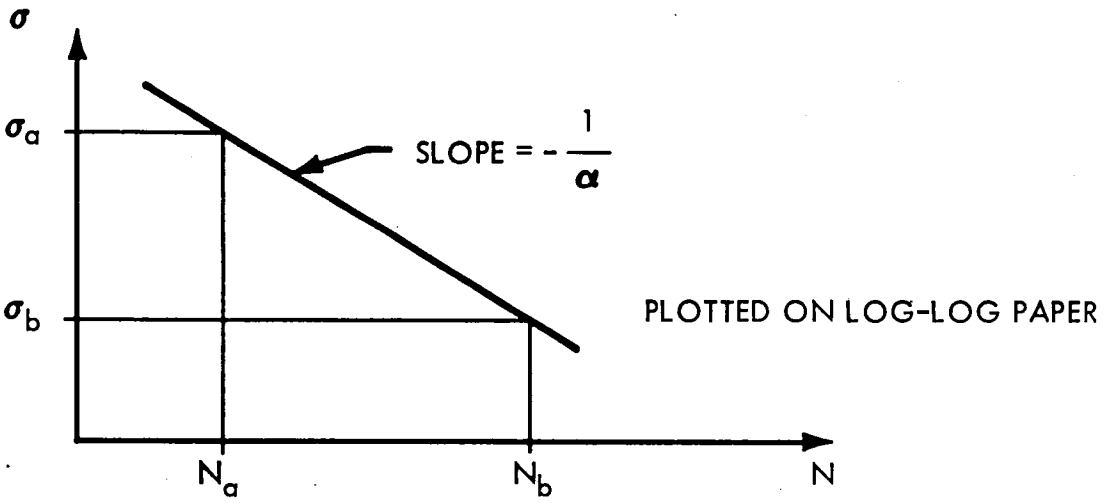

Figure 2-16 IDEALIZED σ-N CURVE

Note that finding the value of α is somewhat simplified if we let the interval N_b-N_a = Δ N be an integral multiple of one octave since the numerator then becomes 1, 2, 3, etc., if we let Δ N be 1, 2, 3, etc., octaves.

Then substituting (2-71) into (2-70) we obtain

$$D = \sum_{i=1}^{k} n_i \left(\frac{\sigma_i}{\sigma_1} \right)^{\alpha} . \qquad (2\text{-}73)$$

We now assume that the damage could be caused by a constant amplitude stress, σ_e, acting for $\sum_{i=1}^{k} n_i$ cycles.

Then

$$D = (\sigma_e)^{\alpha} \sum_{i=1}^{k} n_i (1/\sigma_1)^{\alpha} \quad . \tag{2-74}$$

Solving (2-73) and (2-74) for σ_e, we obtain

$$\sigma_e = \left[\frac{\sum_{i=1}^{k} n_i (\sigma_i)^{\alpha}}{\sum_{i=1}^{k} n_i} \right]^{1/\alpha} \tag{2-75}$$

If we introduce the rms stress σ_r and substitute $c\alpha$ for α (to more closely fit experimental data for various materials, $1 \leq c \leq 2$) we obtain

$$\frac{\sigma_e}{\sigma_r} = \left[\frac{\sum_{i=1}^{k} n_i (\sigma_i/\sigma_r)^{c\alpha}}{\sum_{i=1}^{k} n_i} \right]^{\frac{1}{c\alpha}} \tag{2-76}$$

As stated previously, the structure acts as a filter and when excited by a broadband random input, the stress response will be narrow-band random. The time history of the stress response then, has the appearance of a sinusoidal function whose frequency varies slightly about a mean value corresponding to the natural frequency of the structure and whose amplitude varies slowly and irregularly between small and large values. The distribution of the peak values must be predicted statistically. A usual choice is to assume that the system is excited by a broadband Gaussian random vibration. Then the peaks are distributed according to the Raleigh distribution given by

$$P\left(\frac{\sigma_p}{\sigma_r}\right) = \exp\left[\frac{-\sigma_p^2}{2\sigma_r^2}\right] \tag{2-77}$$

where

σ_p is the peak stress and

σ_r is the rms stress.

P is the Raleigh probability distribution function. The probability density $p(\frac{\sigma_p}{\sigma_r})$ is given by

$$p(\frac{\sigma_p}{\sigma_r}) = \frac{\sigma_p}{\sigma_r} \exp\left[\frac{-\sigma_p^2}{2\sigma_r^2}\right] \qquad (2\text{-}78)$$

or

$$p(\frac{\sigma_p}{\sigma_r})d(\frac{\sigma_p}{\sigma_r}) = \frac{\sigma_p}{\sigma_r} \exp\left[\frac{-\sigma_p^2}{2\sigma_r^2}\right] d(\frac{\sigma_p}{\sigma_r}) \quad . \qquad (2\text{-}79)$$

Equation (2-79) represents the probability of stress cycles that have stress amplitudes between σ_p and $\sigma_p + d\sigma_p$ and thus may be taken as a limiting form of the ratio

$$\frac{n_i}{\sum_{i=1}^{k} n_i} \quad .$$

For a random response the summation may be replaced by an integral in Equation (2-76) and using Equation (2-79) we have

$$\frac{\sigma_e}{\sigma_r} = \left[\int_0^\infty (\frac{\sigma_p}{\sigma_r})^{c\propto} \exp\left[\frac{-\sigma_p^2}{2\sigma_r^2}\right] d(\frac{\sigma_p}{\sigma_r})\right]^{\frac{1}{c\propto}} \quad . \qquad (2\text{-}80)$$

Substituting a change of variable, using the gamma function (Stirling's formula) and simplifying, we obtain for the equivalent stress

$$\sigma_e \cong \left(\frac{c\propto \sigma_r^2}{e}\right)^{1/2} \quad \propto >> 1 \qquad (2\text{-}81)$$

Then Equation (2-81) may be used to determine the number of cycles of narrowband random amplitude to failure from known σ-N curves. The time to failure T may then be determined by

$$T = \frac{N}{f_n(3600)} \tag{2-82}$$

where N is the number of cycles to failure found from a conventional σ-N curve

f_n is the natural frequency of the system for the mode of maximum response (usually the fundamental natural frequency)

T is the time to failure in hours.

2.5 REFERENCES

2-1 Riparbelli, C., Shear Lag in a Panel with Uniform or Tapered Stringers, General Dynamics/Astronautics Report, ZS7102, 6 February 1956.

2-2 Stern, M., "Numerical Procedures for Calculation of Stress Distribution in Sheet-Stringer Frame Combinations," Journal of Aeronautical Sciences, August 1947, p. 481.

SECTION 3

DESIGN AND MANUFACTURING STUDIES

Design and manufacturing studies were initiated in order to support the development of candidate design and manufacturing concepts for the thrust structure. A preliminary general configuration drawing was made and various design problems were evaluated relative to their effect on the anticipated final design. The panel joining concepts which were studied during this effort lead directly into the definition of specimens for test and the evaluation of sandwich panel welding techniques.

3.1 PRELIMINARY STRUCTURAL DESIGN

The general configuration drawing reflected the results of the preliminary sizing analyses and illustrated preliminary design concepts for the sandwich structure.

3.1.1 Preliminary Sizing Analysis

The initial panel facing thicknesses and longeron cross-sectional areas were established from the results of the shear lag analyses described in Section 2.1. General panel geometries were checked and the initial core thickness was established from the results of preliminary sandwich behavior analyses.

3.1.1.1 Shear Lag

The results of the closed form series solution and the computer solution may be compared for the case of a constant area stringer and a constant area web with the loads reacted into a rigid foundation. Two results are desired from this comparison; first, a cross check on both types of analyses and second, verification of whether or not the closed form series solution will provide an accurate starting point for computer analyzing the bi-directionally tapered panel and tapered stringers.

For the case of constant area stringers and a constant thickness web the amount of Eigen-load available for distribution to the web may be defined by the load conditions at infinity. First the load distribution at infinity is defined and then the panel is clamped at some section y = L. A reverse Eigen-load necessary to satisfy the condition of zero displacement is determined and thus completes the analysis.

The load at infinity is defined by:

$$\lim_{y \to \infty} \sigma_y = K \tag{3-1}$$

hence,

$$N_s = \frac{N A_s}{A_s + bt} \tag{3-2}$$

$$N_p = \frac{bt\ N}{A_s + bt} \tag{3-3}$$

The amount of Eigen-load available is N_p. The displacement function for the case of the clamped edge panel is:

$$u = \sum_{odd}^{\infty} (a_n - b_n \sin \frac{n\pi x}{b}) \quad (e^{-rny} - e^{-r_n L}) + \frac{H}{2} \quad (y^2 - L^2) \tag{3-4}$$

The coefficients are:

$$a_n = \frac{8\ Np}{\pi^3 n^3 E A_s} \sqrt{\frac{bE}{Gt} \frac{1}{(A_s} + \frac{1}{bt)}} \tag{3-5}$$

$$b_n = \frac{4\ Np}{\pi^2 n^2 E} \sqrt{\frac{bE}{Gt} \frac{1}{(A_s} + \frac{1}{bt)}} \tag{3-6}$$

$$r_n = \pi n \sqrt{\frac{Gt}{bE} \frac{1}{(A_s} + \frac{1}{bt)}} \tag{3-7}$$

$$H = \frac{2\ \pi\ Gt}{bEA_s} \sum_{odd}^{\infty} n\ b_n\ e^{-r_n L} \tag{3-8}$$

The axial load on the stringer is:

$$N = N_s + \left[- \frac{8\ Np}{\pi^2} \sum_{odd}^{\infty} \frac{e^{-n\gamma}}{n^2} - y \frac{8\ N_p}{\pi} \sqrt{\frac{Gt}{bE} \frac{1}{(A_s} + \frac{1}{bt)}} \sum_{odd}^{\infty} \frac{e^{-nL'}}{n} \right] \tag{3-9}$$

let,

$$A_3 = \frac{8\ N_p}{\pi^2} \tag{3-10}$$

$$A_4 = \frac{8\ N_p}{\pi} \sqrt{\frac{Gt}{bE} \left(\frac{1}{A_s} + \frac{1}{bt}\right)} \tag{3-11}$$

$$Y = K \cdot y \tag{3-12}$$

$$L' = K \cdot L \tag{3-13}$$

where

$$K = \pi \sqrt{\frac{Gt}{bE} \left(\frac{1}{A_s} + \frac{1}{bt}\right)} \tag{3-14}$$

and the axial load in the stringer becomes: (3-15)

$$N = N_s - A_3 \cdot f_1\ (x,y) - A_4 \cdot y \cdot f_2\ (0,L)$$

The shear flow along the edges x = 0,b is:

$$q_{0,b} = - A_1 \cdot f_2\ (0,y) + A_1 \cdot f_2\ (0,L) \tag{3-16}$$

where,

$$A_1 = \frac{4\ N_p}{\pi} \sqrt{\frac{Gt}{bE} \left(\frac{1}{A_s} + \frac{1}{bt}\right)} \tag{3-17}$$

The axial stress resultant along the edge y = L is:

$$N_y = t \left[- A_5 \cdot f_1\ (x,L) + A_2 \cdot f_4\ (x,L) + A_6 \cdot L \cdot f_2\ (0,L) \right] - N_p \tag{3-18}$$

where,

$$A_2 = \frac{4\ N_p}{\pi} \left(\frac{1}{A_s} + \frac{1}{bt}\right) \tag{3-19}$$

$$A_5 = \frac{8\ N_p}{A_s \pi^2} \tag{3-20}$$

$$A_6 = \frac{8\ N_p}{\pi A_s} \sqrt{\frac{GT}{bE} \left(\frac{1}{A_s} + \frac{1}{bt}\right)} \tag{3-21}$$

Figures 2-3, 2-4, and 2-5 are plots of $f_1(x,y)$, $f_2(x,y)$ and $f_4(x,y)$ vs Y respectively.

Figures 3-1,3-2, and 3-3 are plots of stringer axial load vs y, shear flow at x = 0, b vs y, and the axial stress resultant along y = L vs x. Also superimposed on Figures 3-1, 3-2, and 3-3 are the results obtained by considering the same problem utilizing computer program U42 which is the one dimensional shear lag program written especially for this problem. The spatial dimensions and stiffnesses considered for this evaluation are:

L = 246 in. (Length of Stringer)

b = 311 in. (Width of 90° segment of shell)

t = 0.3 in. (Total Skin Thickness, average, along stringer length)

A_s = 53.5 in^2 (Total cross- sectional area of stringer at aft end)

E = 10.0 x 10^6 lbs/in^2

G = 4.35 x 10^6 lbs/in^2

The function coefficients are:

$A_1 = .00456 \times 10^6$

$A_2 = .0382 \times 10^6$

$A_3 = .828 \times 10^6$

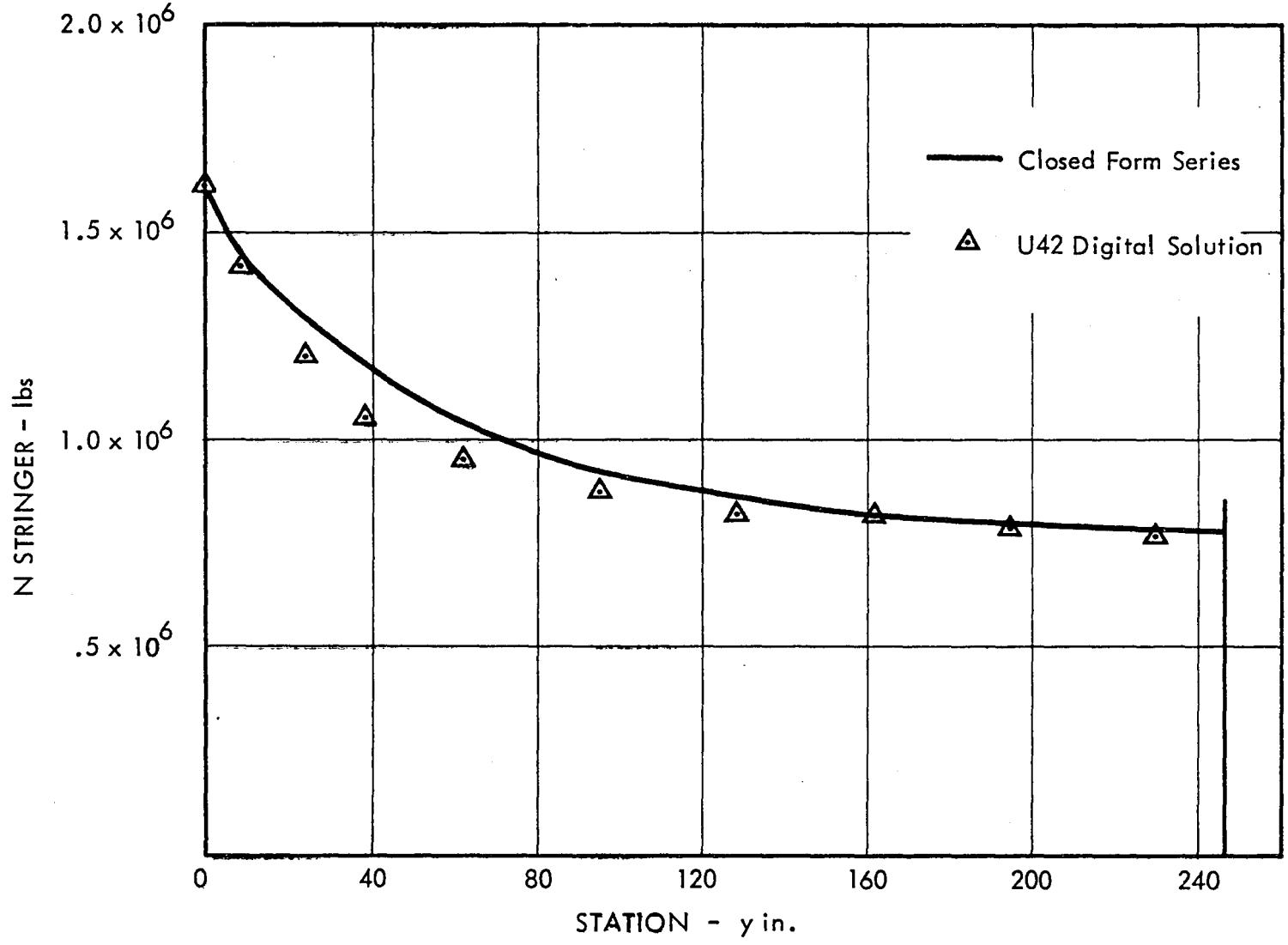

Figure 3-1 STRINGER AXIAL LOAD VS y

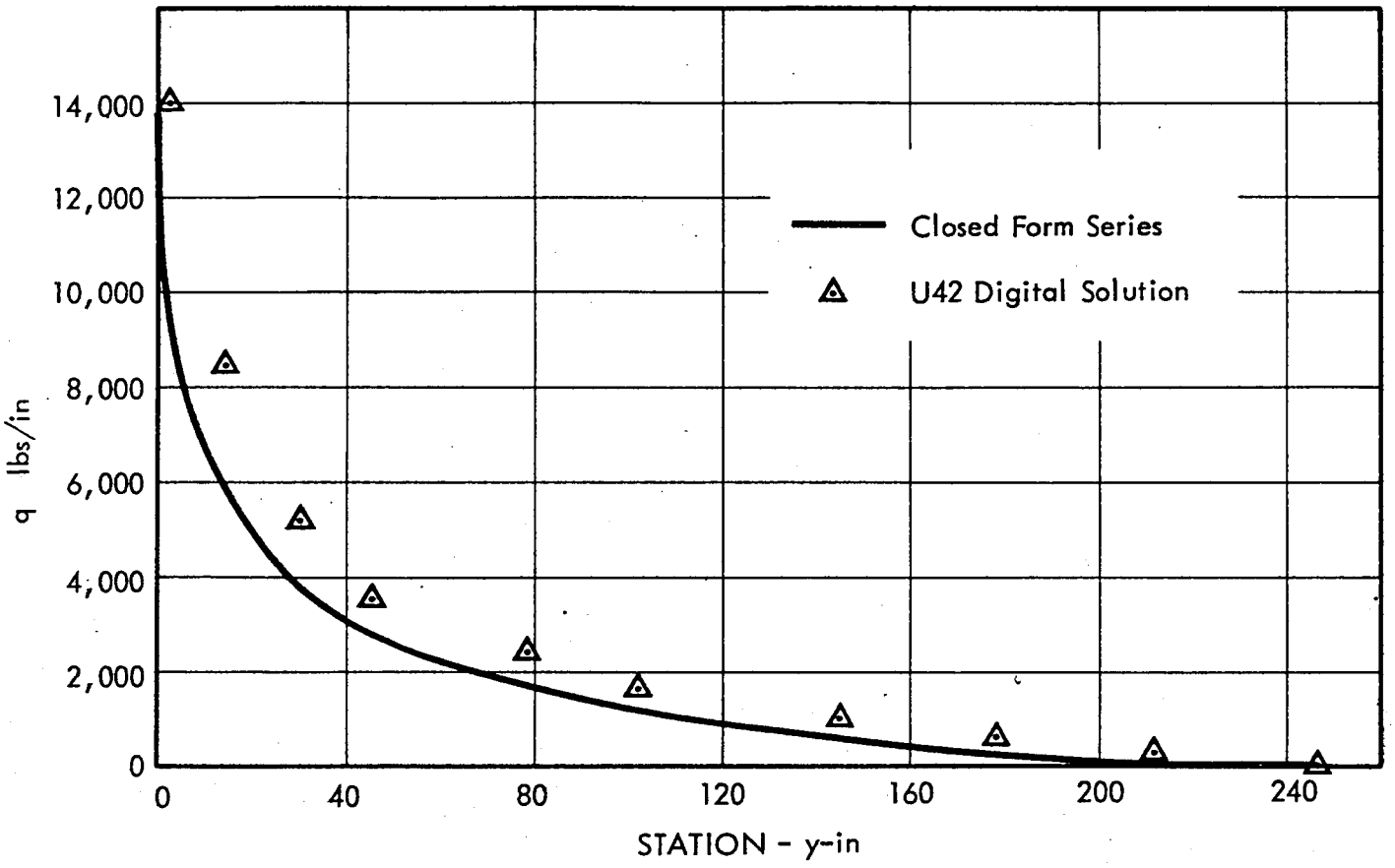

Figure 3-2 SHEAR FLOW VS y

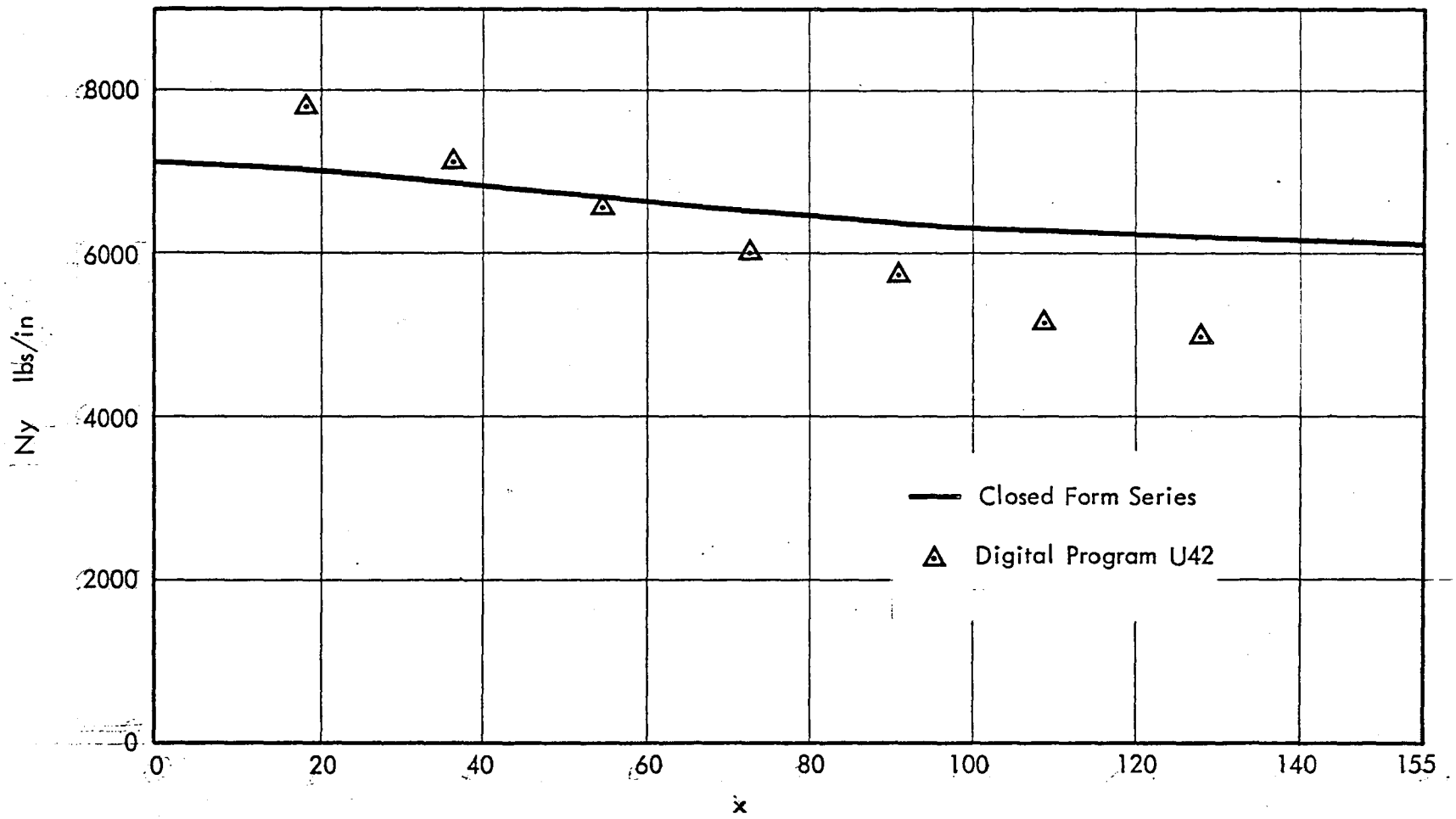

Figure 3-3 AXIAL STRESS RESULTANT VS x

$A_4 = .00913 \times 10^6$

$A_5 = .01546 \times 10^6$

$A_6 = .0001705 \times 10^6$

The correlation between the Fourier Series Analysis and the digital analysis is good except in the region of the thrust structure - tank interface.

In determining the reason for the discrepancy between the digital and fourier series analysis, it was determined that the series analysis is in error unless the longeron area A is equal to the panel area bt. This discrepancy is from the failure of the Eigen load resultant to be zero except under the special geometric case. The error may be estimated from the term which is not zero.

Adding the Eigen load in the longeron to the panel Eigen load the following result is obtained:

$$P_e(x,y) = P_e(x,y)\ \text{Longeron} + P_e(x,y)\ \text{Panel} =$$

$$-\frac{8\,Pe}{\pi^2}\sum\frac{e^{-r_n y}}{n^2} - y\,\frac{8\,Pe}{\pi}\sqrt{\frac{Gt}{bE}\left(\frac{1}{A_s}+\frac{1}{bt}\right)}\sum\frac{e^{-r_n L}}{n} + \frac{8\,Pe}{\pi^2}\sum\frac{e^{-r_n y}}{n^2} + y\left(\frac{bt}{A_s}\right)\frac{8\,Pe}{\pi}\sqrt{\frac{Gt}{bE}\left(\frac{1}{A_s}+\frac{1}{bt}\right)}\sum\frac{e^{-r_n L}}{n} = -\frac{bt}{(1-A_s)} \qquad (3\text{-}22)$$

$$\frac{8\,P_e y}{\pi}\sqrt{\frac{Gt}{bE}\left(\frac{1}{A_s}+\frac{1}{bt}\right)}\sum\frac{e^{-r_n L}}{n}$$

which will disappear if $bt = A_s$.

The actual magnitude of the error will be small if the load is nearly damped, since $\sum\frac{e^{-r_n L}}{n}$ will be small.

The bi-directionally tapered panels adjacent to the vertical longeron fittings were first sized using the closed form series analysis for an infinite panel with exponentially-tapered longerons. The panels were then analyzed with the numerical computer solution and the resulting load distributions were used to re-size the panels. Several iterations were performed with the computer analysis to refine panel and longeron geometries and load levels. The object of this phase of investigation was to determine panel gages such that the panel was approximately uniformly stressed near yield and the axial stress resultant at the upper edge was kept below 15,000 pounds per inch.

The initial sizing attempts were made assuming that the skin material requirement is established by the sum total of the shear and compression forces. This was done to facilitate rapid processing of the computer results. It was decided that for the current period a more efficient technique would be used. The interaction formula given in the N.A.S.A. Astronautic Structures Manual, Section A3, page 11 was used. The formula is

$$R_f^2 + R_s^2 = 1 \tag{3-23}$$

where,

$$R_f = \frac{f_a}{F} + \frac{f_b}{F} \tag{3-24}$$

$$R_s = \frac{f_s}{F_s} \tag{3-25}$$

and,

f_a, f_b = applied normal stresses

This failure theory is the maximum shear theory and is valid when

$$0.5 \leq \frac{F_s}{F} \leq 0.7$$

This criterion is met by the candidate aluminum alloys considered for this structure.

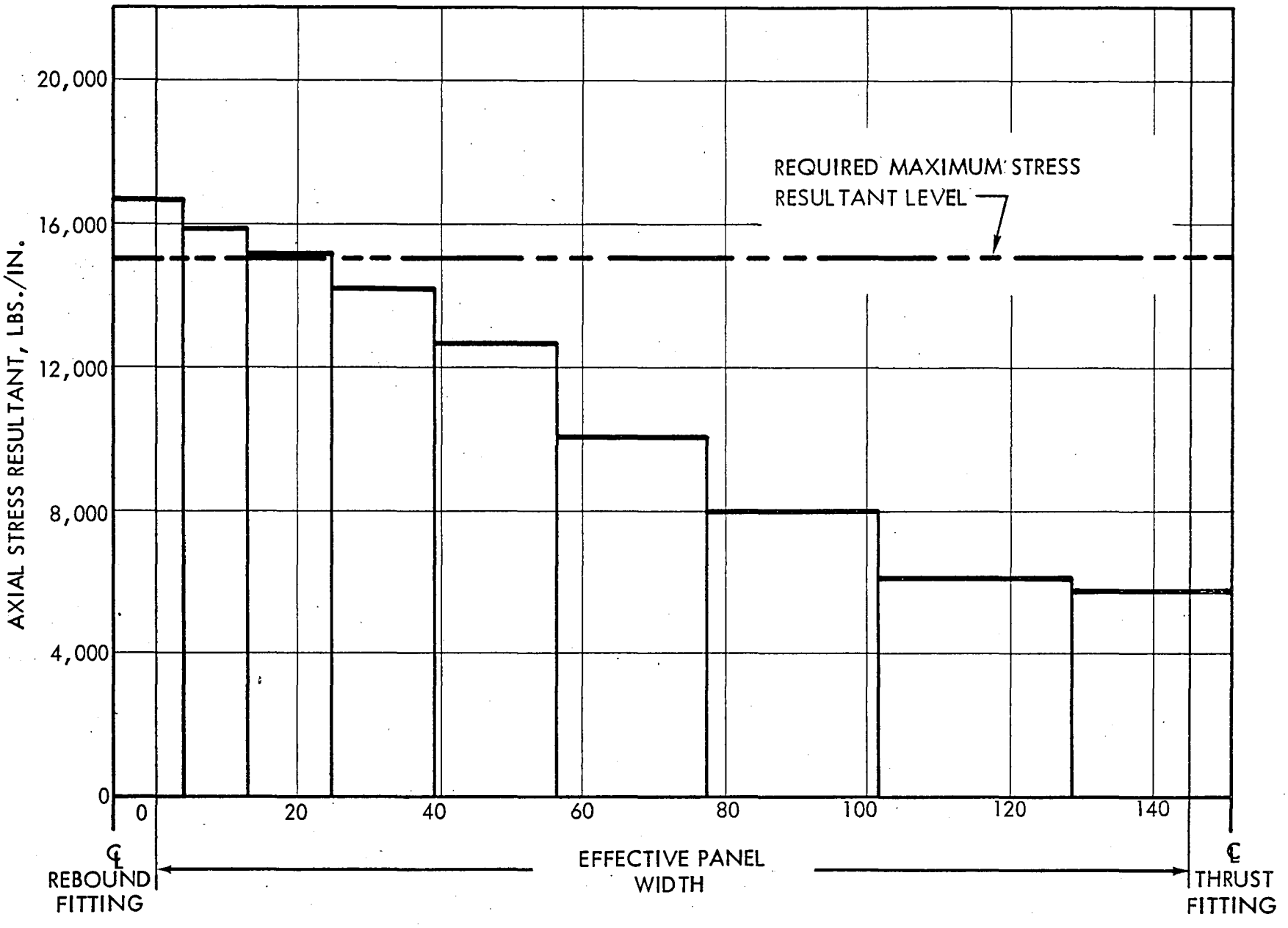

Figure 3-4 AXIAL STRESS RESULTANT VS DISTANCE FROM FITTING

This analytical technique yielded the axial stress resultants at the tank-thrust structure interface as shown in Figure 3-4. This particular solution assumed an infinitely rigid tank. It may be observed that the peak axial stress resultant is at 16,600 pounds per inch instead of the 15,000 pounds per inch maximum. It was decided that this load level was satisfactory for the preliminary sizing analysis because further refinements in assumptions on the rigidity of the tank and load levels in the thrust structure were to be a product of the analysis of internal load distribution.

3.1.1.2 Heavy Gage Sandwich Behavior

The size relation of facing gage and honeycomb core thickness for sandwich structure varies with requirements of load capability, unsupported panel dimensions, flat or contoured shape, and desired failure mode. For this thrust cylinder study preliminary buckling analyses were performed for both local and cylinder buckling.

a. Local Buckling

The theoretical relationships and practical considerations used in sandwich design are presented below for each local buckling mode of failure for the expected size range of interest.

Shear Instability - A sandwich panel will fail in the shear instability mode when the core is not stiff enough in shear to make the two faces work together in resisting buckling. A failure of this type is easily identified because the skins will still be parallel even though severely buckled and the core will be failed in shear. See Figure 3-5.

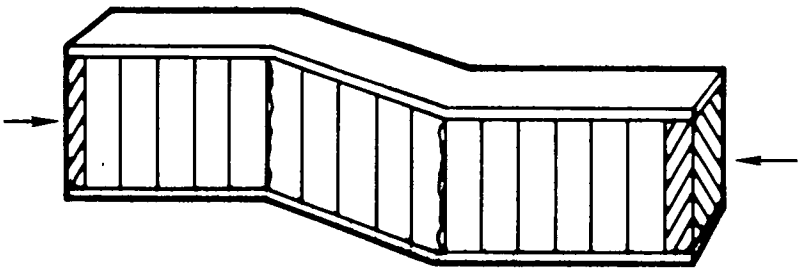

Figure 3-5 TYPICAL CORE SHEAR INSTABILITY FAILURE

The relationships between the core shear modulus, skin gage and core thickness for this mode of failure are shown in Figure 3-6 and Figure 3-7. It can be seen that this mode of failure is not critical as long as the shear modulus, G_c, is above 25,000 psi for 1.5 inch thick core or the core thickness is not less than one inch for the 67,000 psi modulus core. It can also be seen that for the nominal case, where the skin gage does not exceed .125 inches and the core shear moduli are 67,000 psi with the ribbon and 26,000 psi transverse to the ribbon, this mode of failure is not critical. However, it does serve to point out that where the gages increase due to local load introduction and the core thickness is reduced because of internal doublers or some other design peculiarity, a marginal condition may exist, particularly in the weak direction of the core.

Intracellular Dimpling - This mode of failure is the result of buckling of the skin within the boundaries of an individual core cell. The critical stress is given by:

$$\sigma_{1D} = 0.9 \cdot n \cdot E \cdot \left(\frac{t_f}{d}\right)^{3/2} \qquad (3\text{-}26)$$

where 'd' is the diameter of a circle that will fit within a core cell.

For the skin gages and core cell sizes considered here, this mode of failure is not critical. Recognizing that greater core strength and efficiency are achieved through larger cells with thicker foil gages while maintaining the same density, it is necessary to justify the core cell selection on a basis other than intracellular dimpling. This justification appears in the latter part of the discussion on face wrinkling below.

Face Wrinkling - The most common local failure mode is face wrinkling. A brief examination of the parameters for shear instability and intracellular dimping modes reveals that these failure modes may be easily and efficiently maintained non-critical by proper selection of core density, cell size, and thickness. This is not the case with face wrinkling. The general analytical approach is to treat the core material as an elastic spring and treat the face as a beam on an elastic foundation subject to buckling from an axial load. This relationship is given as

$$N_{cr} = 2\sqrt{K \quad EI} \qquad (3\text{-}27)$$

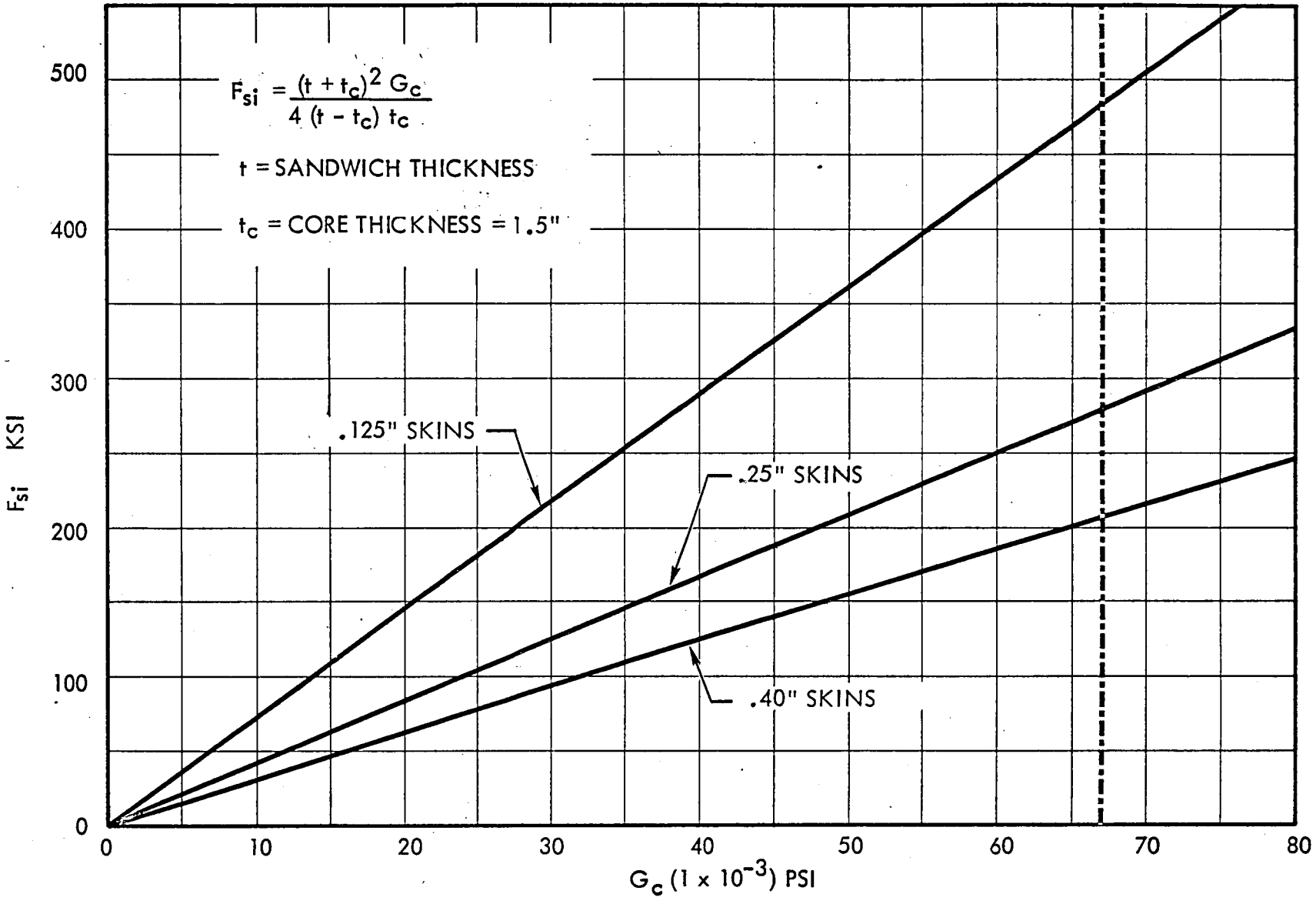

Figure 3-6 CORE SHEAR INSTABILITY VS CORE MODULUS

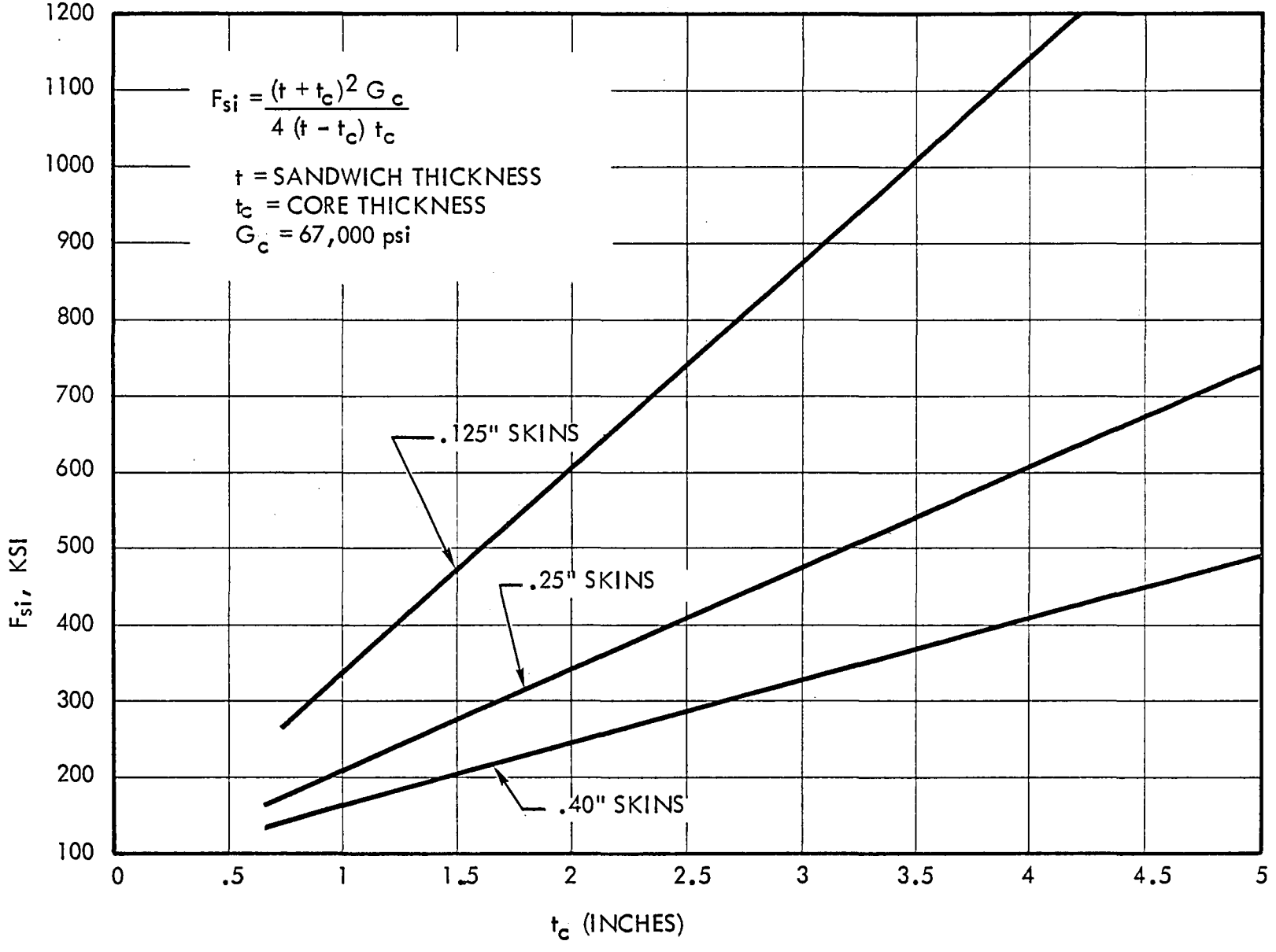

Figure 3-7 CORE SHEAR INSTABILITY VS CORE THICKNESS

where K is the spring constant of the foundation. Using this basic approach, Yusuff developed the relationships presented in Figures 3-8 and 3-9. (Reference 3-1)

Figures 3-8 and 3-9 show the expression for W, a term defining whether the sandwich is "thick" or "thin". A thin sandwich, $t_c < 2W$, is one where the core is assumed to act like a number of individual springs. A thick sandwich, $tc > 2W$, is one where the stiffness of the foundation results from both the flatwise and shear stiffnesses of the core. The critical buckling stress for the individual faces of a thick sandwich, therefore, are not related to the core thickness.

Examination of the curves presented in Figure 3-8 show that for sandwich segments loaded in the "L" direction of the core the .125 inch skin is in the "thick" core region and the .250 inch skin is marginal between "thick" and "thin". Similar examination of the curves presented in Figure 3-9 show that for sandwich segments loaded in the "W" direction of the core the .125 inch skin is marginal between "thick" and "thin".

Since the sandwich configuration considered here is borderline between thick and thin sandwich, Figures 3-10 and 3-11 are presented showing the critical buckling stress vs surface waviness, A_o, and the tangent modulus, E_f, for the faces of thick and thin sandwich respectively. A_o represents the amplitude of a surface wave, or imperfection, over a critical half wave length. This relationship will be discussed below. Both of these curves show that surface waviness of .004 inches can be tolerated providing the core ribbon is oriented in the direction of the load, and the bond strength is equal to or greater than 410 psi. The flatwise compression strength of the core, 410 psi, was used for these curves.

Figures 3-12 and 3-13 show what happens if F_c, the flatwise compression strength of the core (or the flatwise tension strength of the bond), change with an assumed Ao of .004. Note that when Fc drops to 200 psi, the critical face wrinkling stress is in the range of 50,000 psi.

Insufficient empirical data are available to support the accuracies of the theories of face wrinkling. Therefore, it is suggested that considerable margin be allowed by assuming a conservative A_o. A second recommendation is to maintain a high bond strength relative to the minimum requirement in order to permit some reduction in bond strength typical of factory production. Since bond strength is a function of the

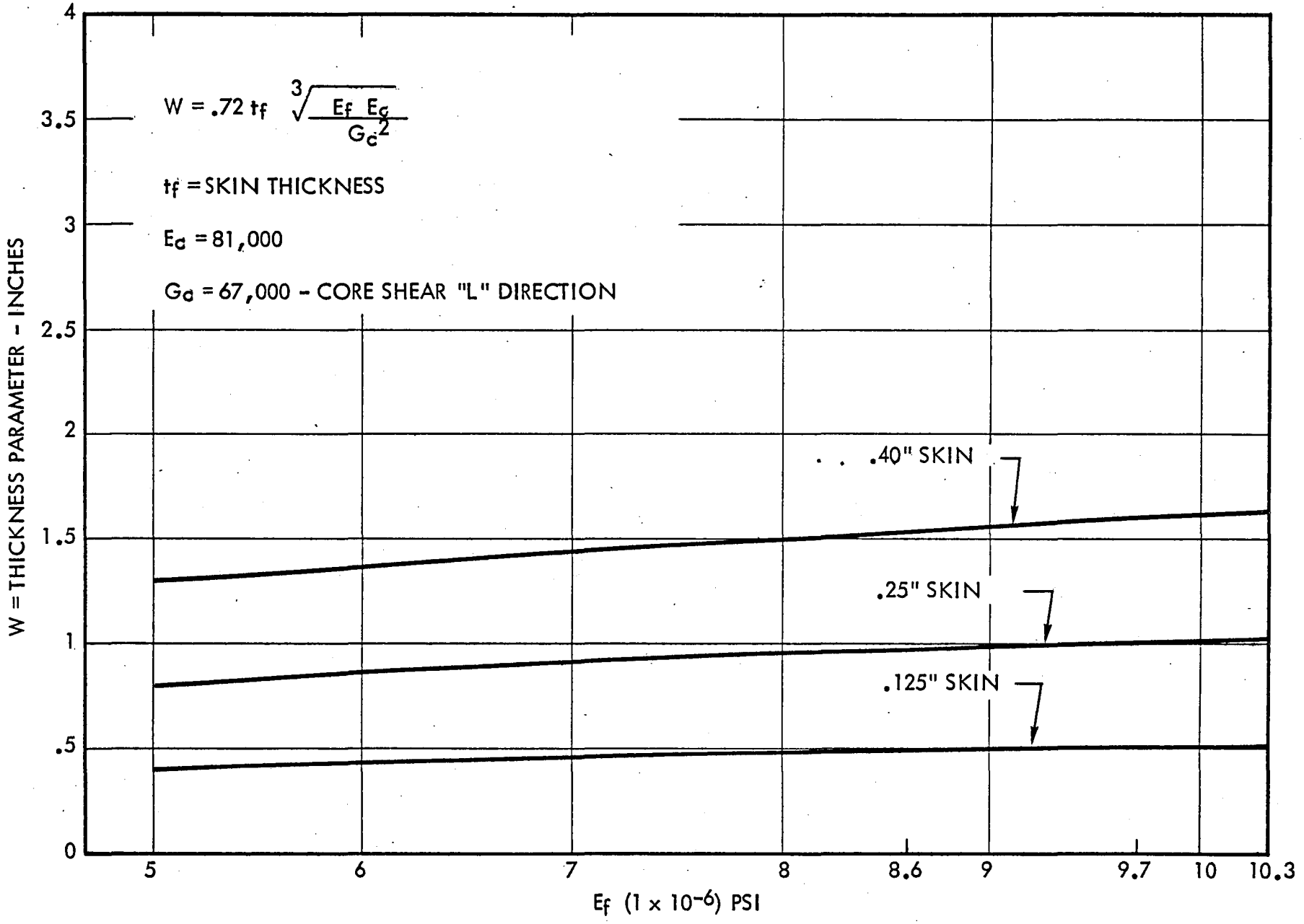

Figure 3-8 THICKNESS PARAMETER - CORE IN "L" DIRECTION

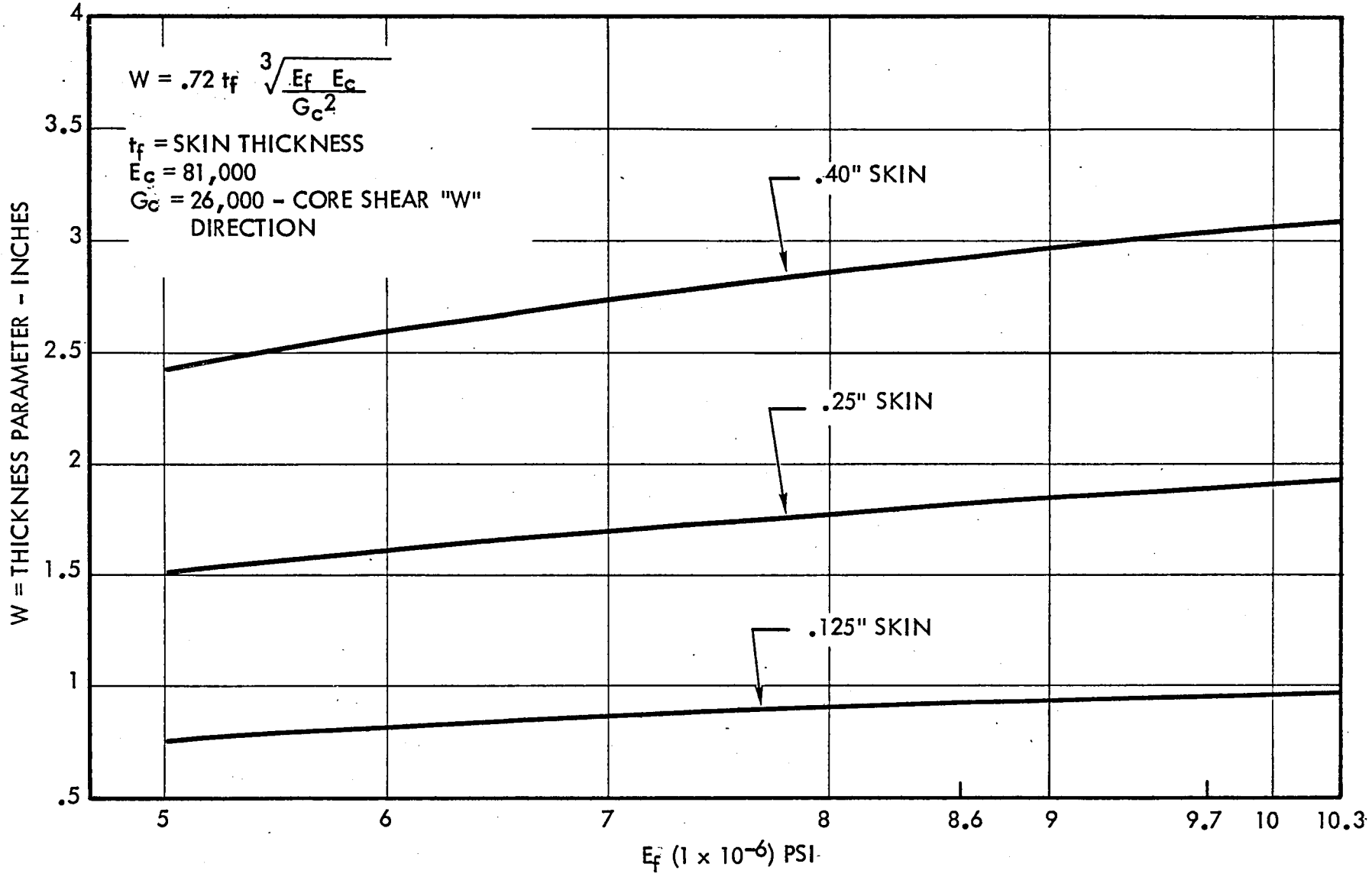

Figure 3-9 THICKNESS PARAMETER - CORE IN "W" DIRECTION

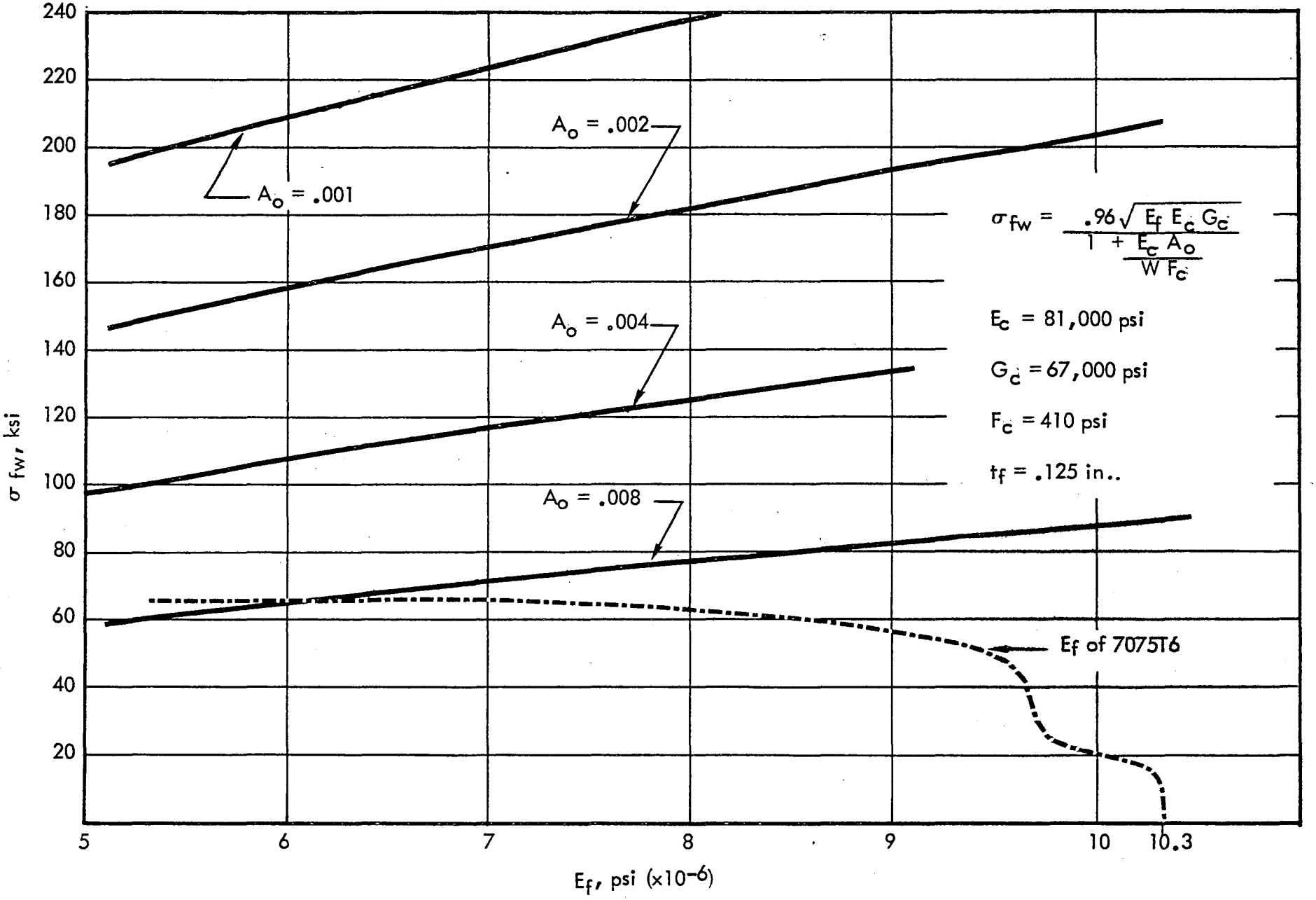

Figure 3-10 FACE WRINKLING VS EFFECTIVE MODULUS AND A_o (THICK CORE)

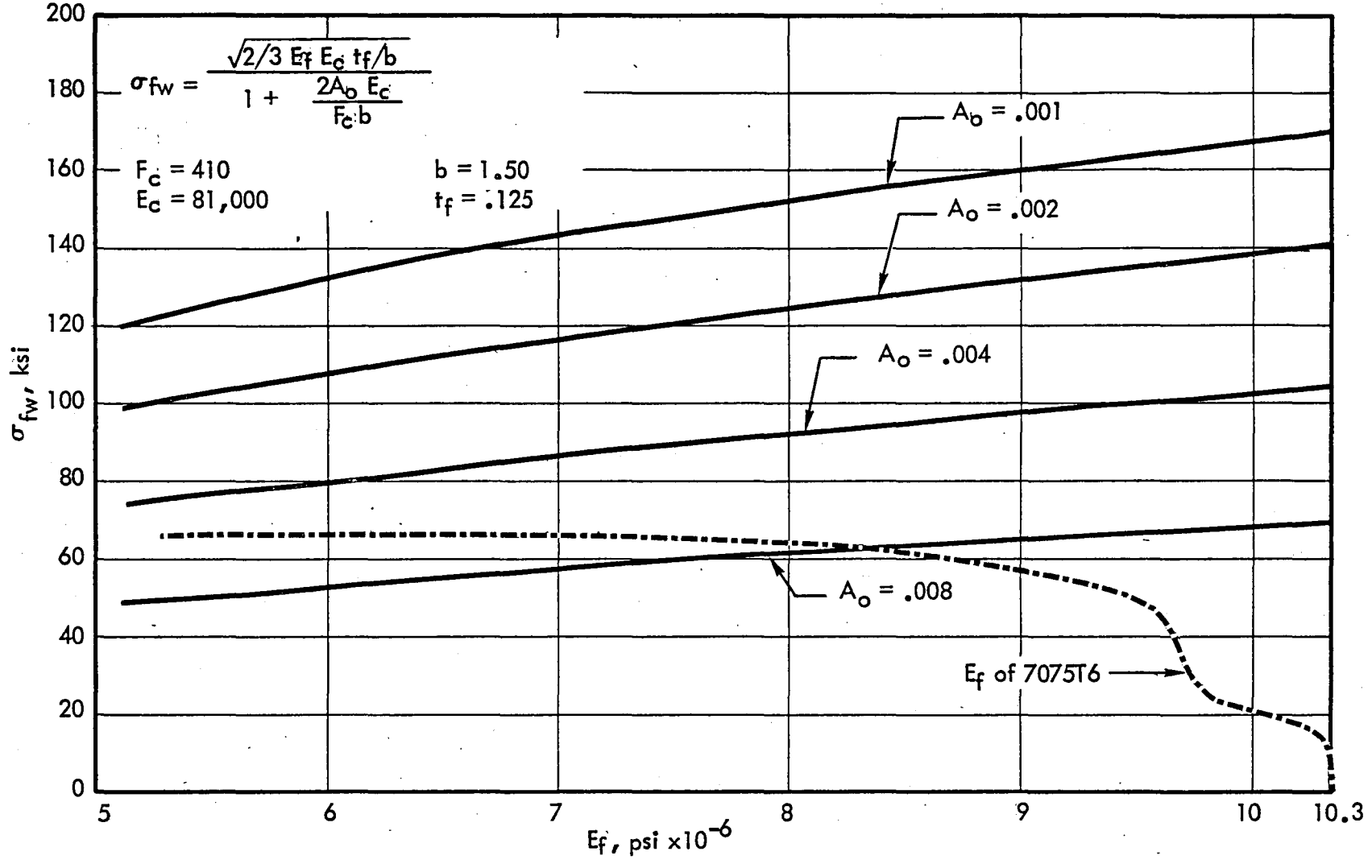

Figure 3-11 FACE WRINKLING VS EFFECTIVE MODULUS AND A_o (THIN CORE)

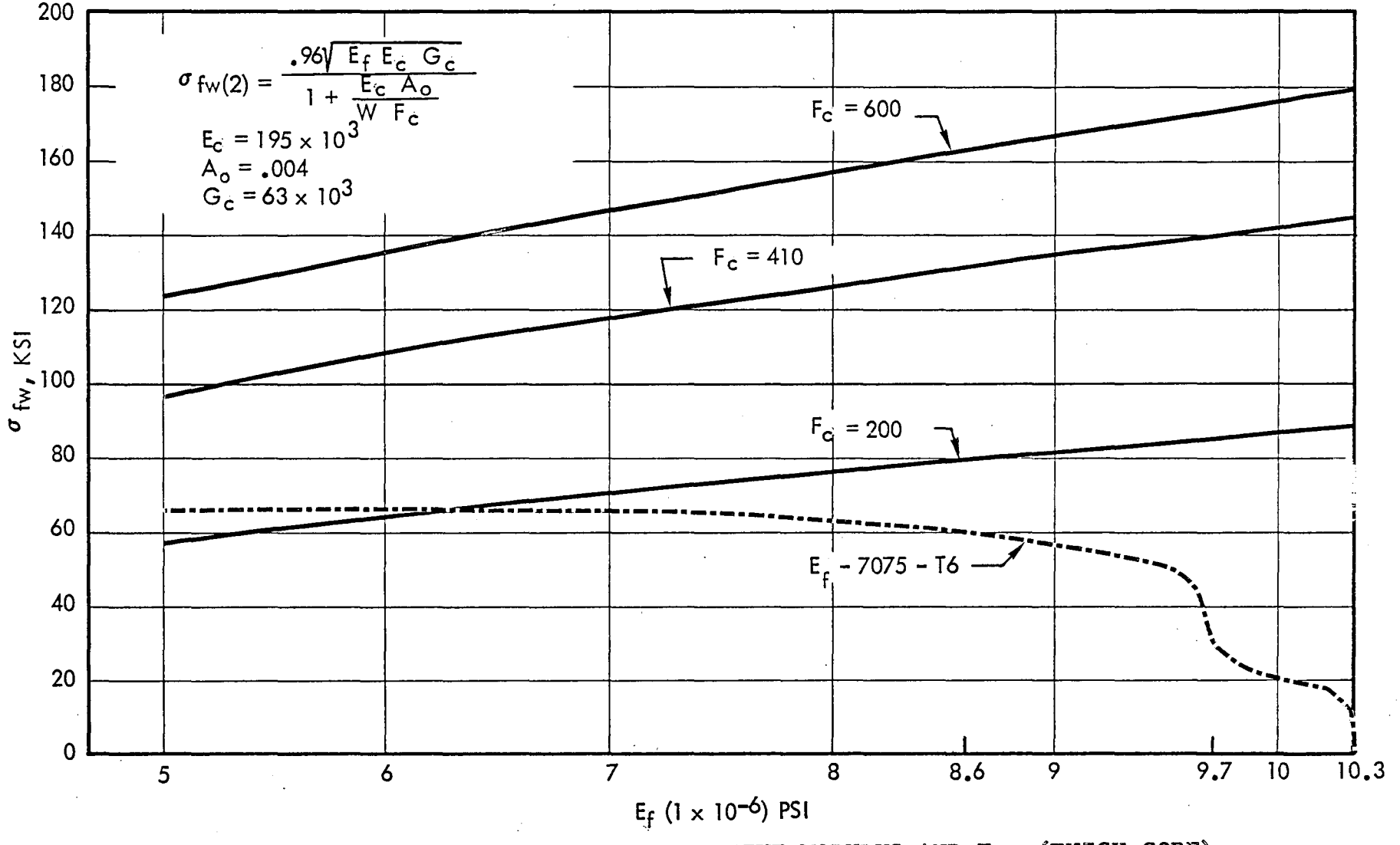

Figure 3-12 FACE WRINKLING VS EFFECTIVE MODULUS AND F_c (THICK CORE)

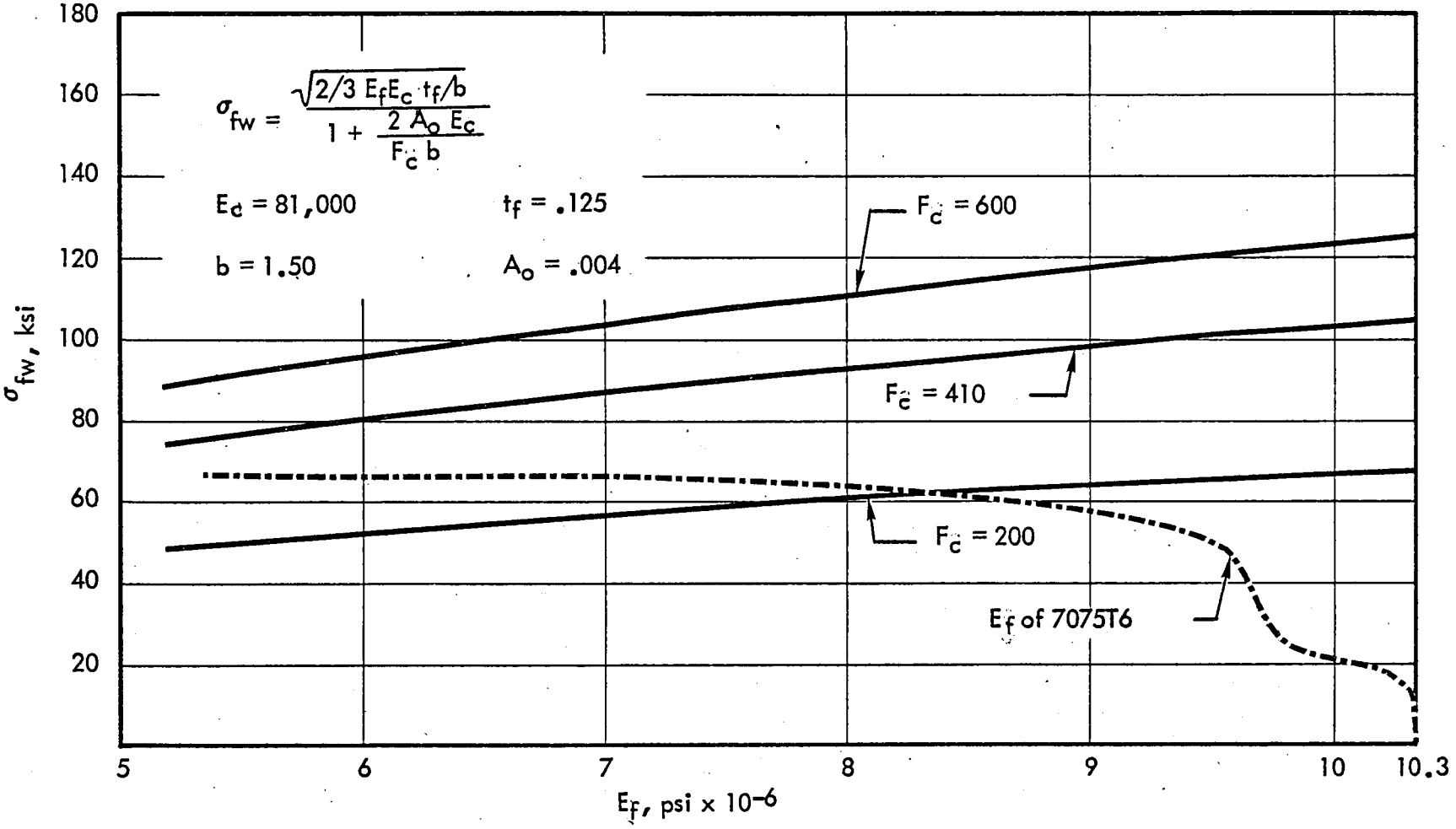

Figure 3-13 FACE WRINKLING VS EFFECTIVE MODULUS AND F_c (THIN CORE)

adhesive properties and core cell size, a small cell core is desired with the best core bonding type of adhesive available. It should be noted that this is a tension requirement and is directly related to peel strength.

The surface waviness parameter, Ao, is not easily predetermined during the design stage or even by direct measurement after fabrication of the part. This term is generally an assumed value based on past experience with a manufacturing process and a tooling concept. In order to translate the assumed waviness, for example, Ao = .004, into an allowable imperfection it is necessary to calculate the critical half wave length as shown in Figures 3-14, 3-15, and 3-16. It may be seen that the range of critical half wave lengths is from .75 inch to 2.75 inches. Therefore, imperfections which fall into this range of critical lengths and do not exceed a depth of .004 inch would be acceptable. A comparison of this assumed waviness with normal production bonding tolerances will show it to be quite liberal.

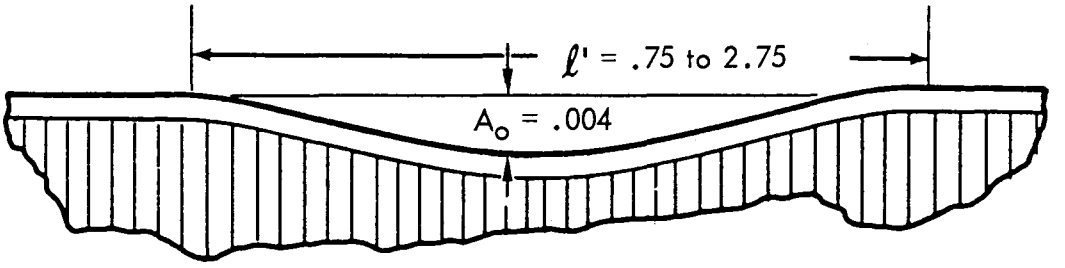

Figure 3-14 INITIAL IMPERFECTION

b. Cylinder Buckling

The most significant problem associated with the design of a cylinder subjected to an axial load is the determination of the buckling stress. Since the sandwich designer has a certain working stress in mind, the problem is one of selecting the required core thickness to maintain cylinder stability up to that stress.

There are, however, two theoretical approaches to cylinder buckling that yield widely different results. From Reference 3-2 Small Deflection Theory sometimes called classical theory, yields

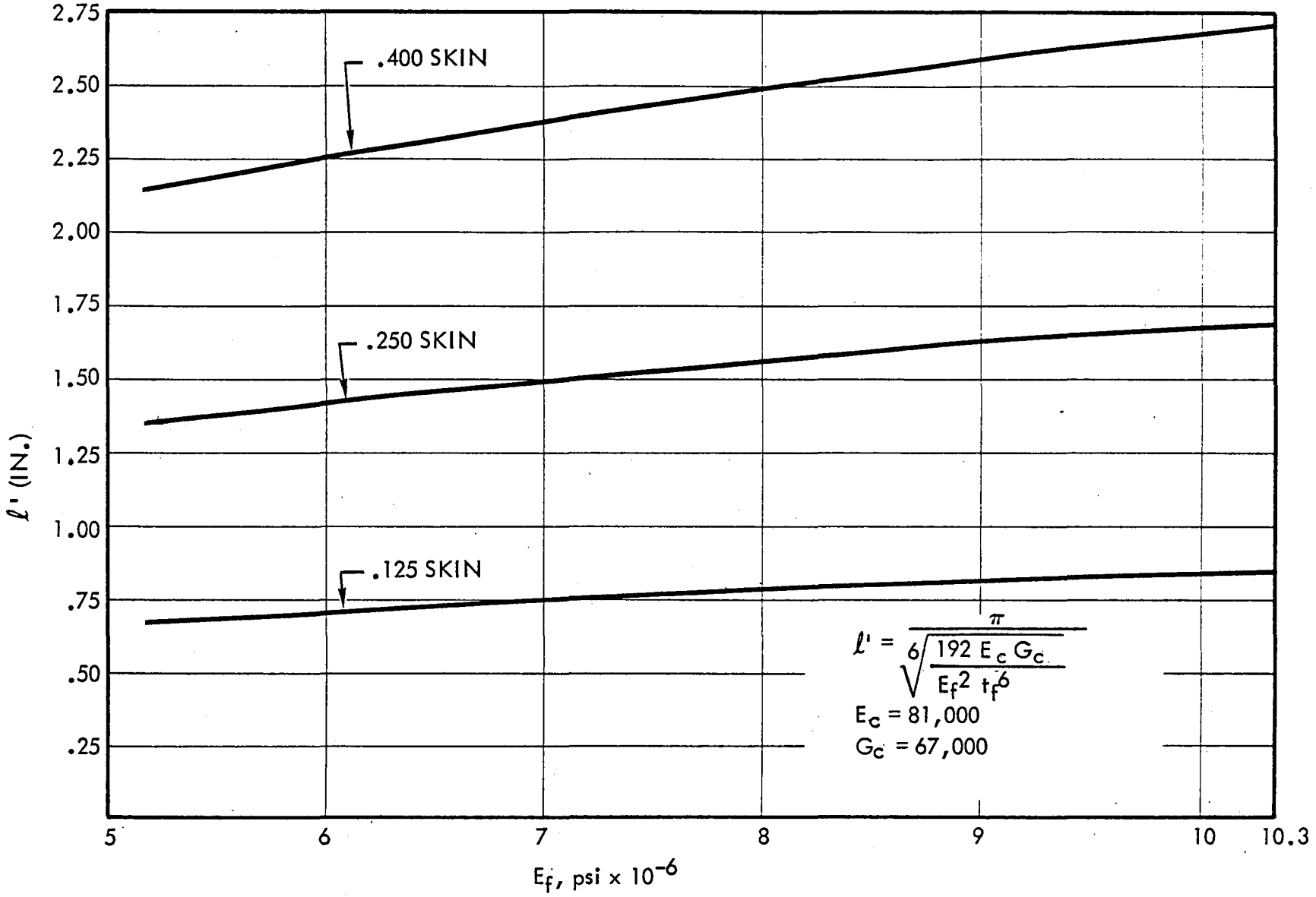

Figure 3-15 CRITICAL HALF WAVE LENGTH (THICK CORE)

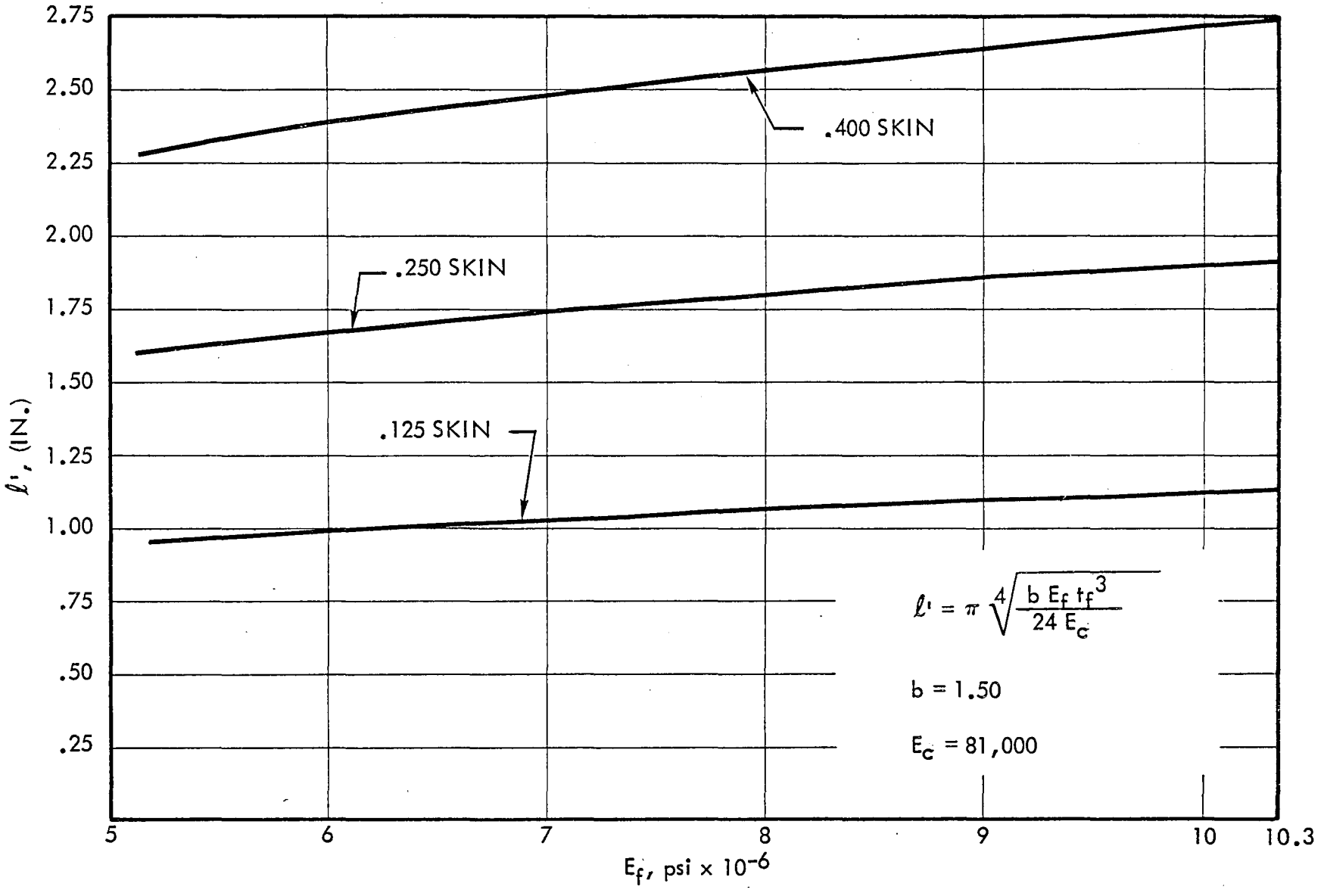

Figure 3-16 CRITICAL HALF WAVE LENGTH (THIN CORE)

$$\sigma_{cr} = \frac{Ncr}{2t_f} = \frac{nEt_c}{R}\left[1.05 - \frac{nEt_f}{1.8\ RG_c}\right] \qquad (3\text{-}28)$$

when

$$Gc \geq \frac{Et_f}{R} \qquad (3\text{-}29)$$

and

$$n = \sqrt{\frac{Et\ Esec}{E}} \qquad (3\text{-}30)$$

It should be noted that Equation (3-29) places the sandwich in the rigid core region.

Equation (3-28) is shown in Figure 3-17 in relation to the expression for cylinder buckling using Large Deflection Theory as described in Reference 3-3. Large Deflection Theory assumes that imperfections exist in the curvature of the cylinder and that buckling deformation starts to form immediately upon loading. The calculated critical buckling stress is the stress corresponding to a minimum energy solution of a diamond pattern buckle mode. Data reported in Reference 3-3 supports this approach; however, it should be noted that these data are well in the soft core region and are from curved panels rather than full cylinders.

Recent full cylinder data described in Reference 3-4 show the calculated large and small deflection theoretical stress versus actual failure stress for five cylinders. All five supported the small deflection theory. Specimen #1 was a 36 inch diameter cylinder with .010 inch thick 7075T6 aluminum faces and .125 inch thick, 3/16 cell 5052 aluminum core of 3.1 pound per cubic foot density. This is a reasonable scale model of the proposed thrust cylinder. The failure stress for this cylinder was 61,000 psi.

As shown in Figure 3-17 analysis of the thrust structure for general instability using Small Deflection Theory indicated that a core thickness of 1.5 inch provides adequate stiffness to insure general stability to a stress level near the yield strength of the facing material. For the thinnest expected facings on the thrust structure $t_f = .100$ and Equation 3-28 yields

$$\sigma_{cr} = \frac{nE\ (1.5)}{198}\left[1.05 - \frac{nE\ (.10)}{1.8 \cdot 198 \cdot 67{,}000}\right]$$

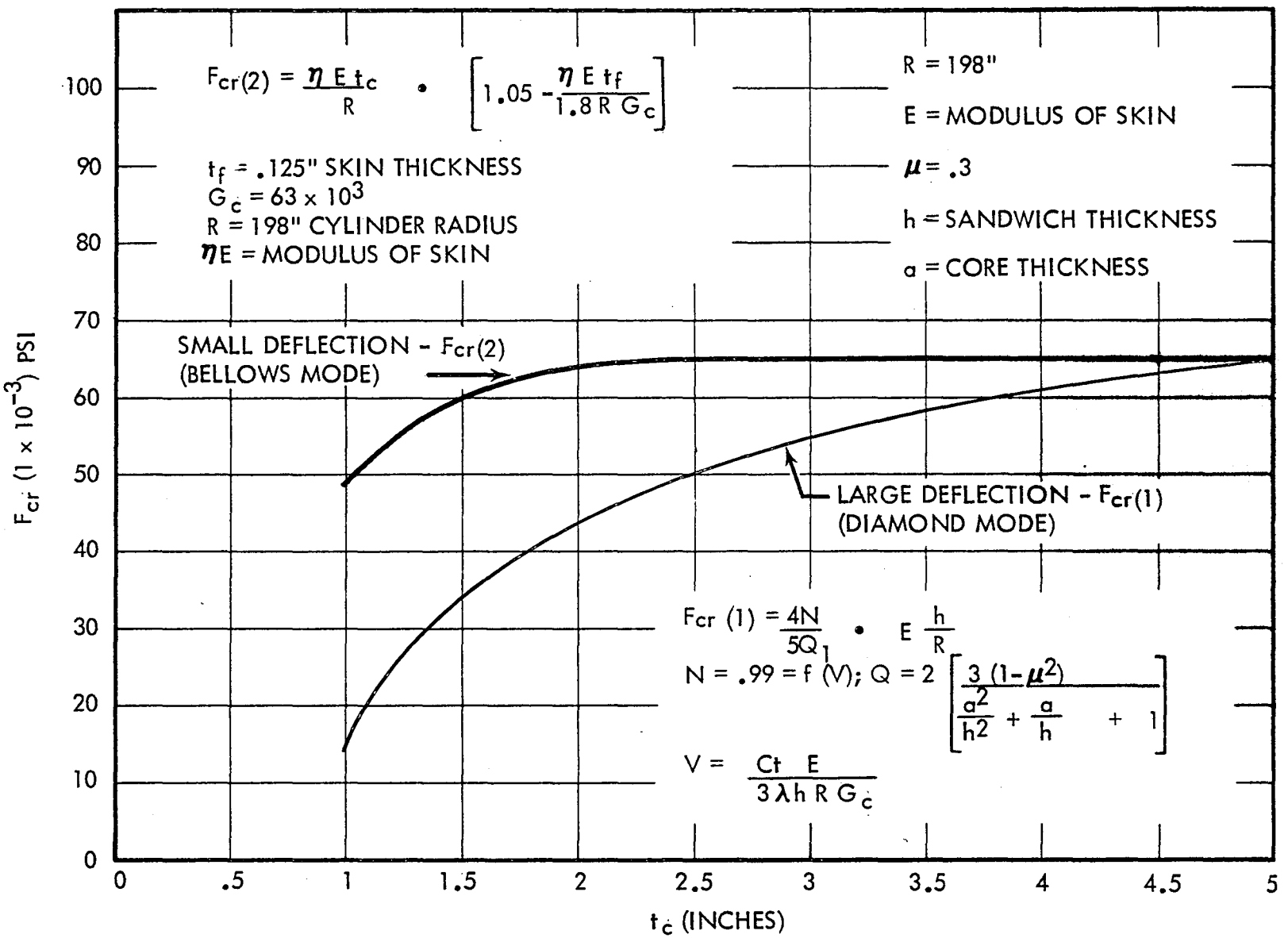

Figure 3-17 CYLINDER BUCKLING VS CORE THICKNESS

or

$$\sigma_{cr} \approx 59{,}000 \text{ psi}$$

where

$$\eta E \approx 8.0 \times 10^6 \text{ psi}$$

$$t_c = 1.5 \text{ inches}$$

$$G_c = 67{,}000 \text{ psi}$$

For thicker facings, say $t_f = .30$, computing the critical stress gives

$$\sigma_{cr} \approx 59{,}500 \text{ psi}$$

where

$$\eta E \approx 7.8 \times 10^6 \text{ psi}$$

It can be seen that the cylinder axial buckling stress remains at about 59,000 psi throughout the range of facing thicknesses likely to be used.

Reference 3-4 contains a discussion of the role of imperfections in small deflection theory and states that a factor of the form $1/\sqrt{1 + K \frac{R}{T} \frac{Wo}{T}}$ accounts for the effect of the imperfection. A more detailed treatment of this effect is presented in Reference 3-5. There, the equation for critical buckling load is given as:

$$N_{cr} = \frac{2E\, t_f\, T}{R} \sqrt{\frac{1}{1 + \frac{4}{3} \frac{R}{T} \frac{W_o}{T}}} \qquad (3\text{-}31)$$

where W_o = amplitude of imperfection

T = sandwich thickness

In terms of facing stress

$$F_{cr} = \frac{N_{cr}}{2t_f} = \frac{ET}{R} \sqrt{\frac{1}{1 + \frac{4}{3} \frac{R}{T} \frac{W_o}{T}}} \qquad (3\text{-}32)$$

The value of $\frac{4}{3}$ for K is derived for a buckling mode consisting of flattening of the cylinder resulting in four mode points in the circumference where no radial deflection occurs. For the thrust cylinder of this study, the presence of stiff longitudinal stringers at eight equidistant positions around the circumference effectively precludes sandwich imperfections at these locations. The analysis of imperfection effects should logically be based on an eight node circumferential buckle pattern. This results in a value of K of $\frac{4}{15}$. Then the equation for buckling stress is

$$F_{cr} = \frac{ET}{R} \sqrt{\frac{1}{1 + \frac{4}{15} \frac{R}{T} \frac{W_o}{T}}} \qquad (3\text{-}33)$$

To be applicable above the facing elastic range this equation should include the plasticity factor, η :

$$F_{cr} = \frac{\eta ET}{R} \sqrt{\frac{1}{1 + \frac{4}{15} \frac{R}{T} \frac{W_o}{T}}} \qquad (3\text{-}34)$$

This equation is used to calculate values from which the curves in Figure 3-18 are constructed. These curves indicate a substantial loss of strength in sandwich with 1.5 in. core if the imperfection amplitude is large. As would be expected, an increase in core thickness reduces the strength loss. To assess this effect on choice of sandwich core thickness, an estimate of probable imperfections must be made.

The large metal sandwich panels previously manufactured at GD/FW have been observed to be well within .10 inch of true vehicle contour when installed and usually within half that amount. A half quadrant of the presently considered structure would be attached to rigid structure on all edges, thus limiting installed imperfections to a bulge or flattening in the central area of a panel. If an imperfection amplitude of .10 is taken as the maximum expected or allowed, strength loss may amount to 20 percent for the thinnest facings considered.

3.1.2 Preliminary Thrust Structure Design

The preliminary general configuration drawing is presented as Figure 3-19. This drawing represented a major early milestone in the program in that it provided a base line for a number of activities which followed.

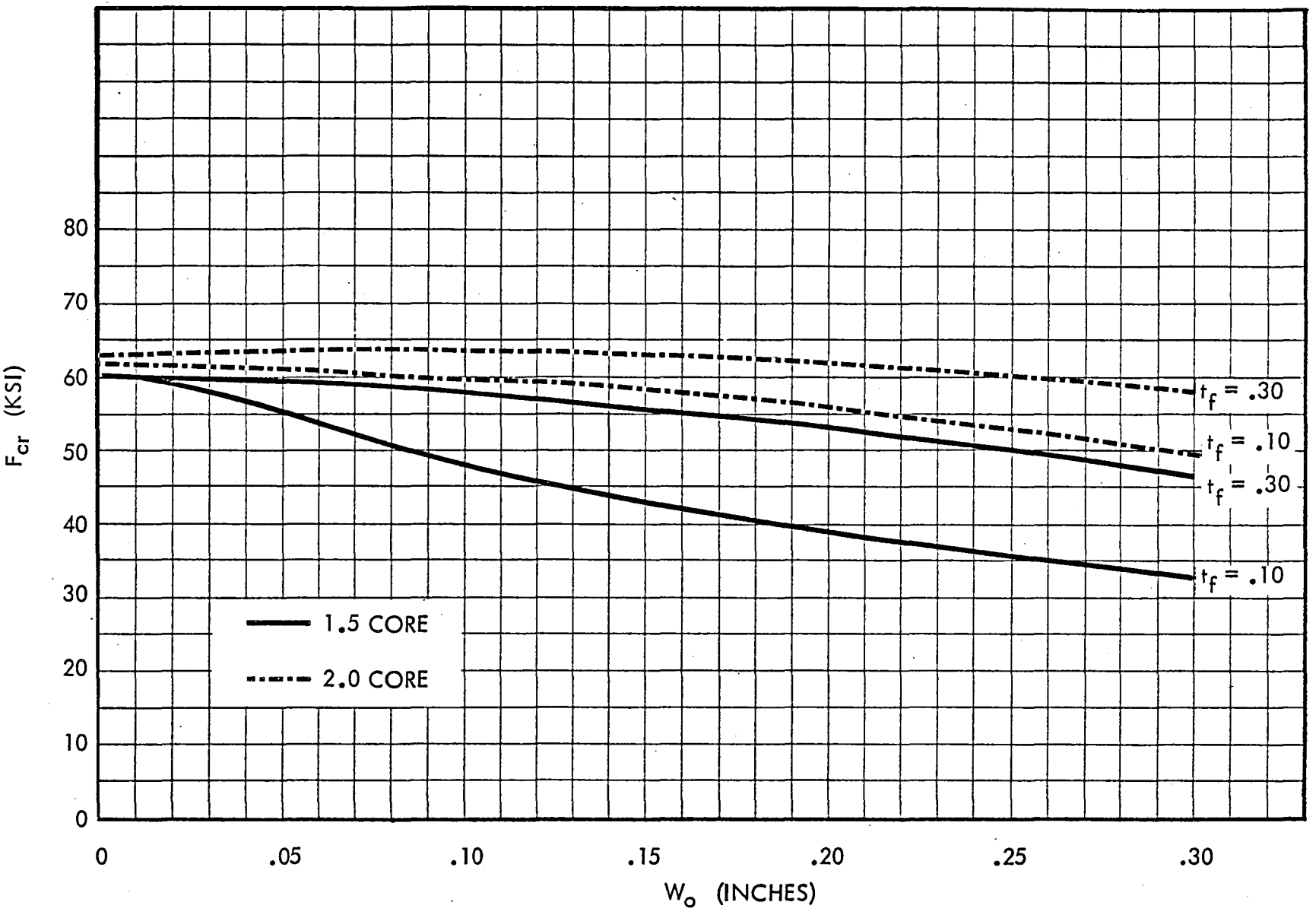

Figure 3-18 CRITICAL BUCKLING STRESS VS IMPERFECTION AMPLITUDE (SMALL DEFLECTION THEORY)

3.1.2.1 Skin and Panel Geometry

Figure 3-19 shows a series of steps in the thrust structure sandwich facings. These steps were defined by evaluating the requirements suggested by the preliminary sizing analysis discussed in Subsection 3.1.1, compression load requirements, and manufacturing considerations. The inner and outer facings were equal in thickness at all points and the steps in thickness occurred on the outer surface of each facings. It may be noted that the preliminary configuration drawing showed a maximum facing gage of .375 inch and a minimum skin gage of .100 inch.

As shown in Figure 3-19 the panel thicknesses vary with skin thickness variations while the core thickness remains constant at 1.50 inches. This core thickness was derived from the preliminary analyses of sandwich behavior as presented in Subsection 3.1.1.2.

3.1.2.2 Boundaries and Splices

Figure 3-19 also shows a preliminary concept for panel boundaries. An integral bonded slug edgemember formed a continuous insert around each panel and a similar member was used around each access hole. At the longeron locations the internal slug edgemember was designed to be a part of the total required longeron area as determined by the preliminary sizing analysis discussed in Subsection 3.1.1. The internal edgemember was designed so that it could be effectively tapered by variation of width and by internal machining.

3.1.2.3 Access Holes

Two possible locations are shown for the access holes. One was considered less desirable than the other and was called an alternate. The significance of the two locations was to show that a slight compromise in lateral location would simplify the detail design requirements.

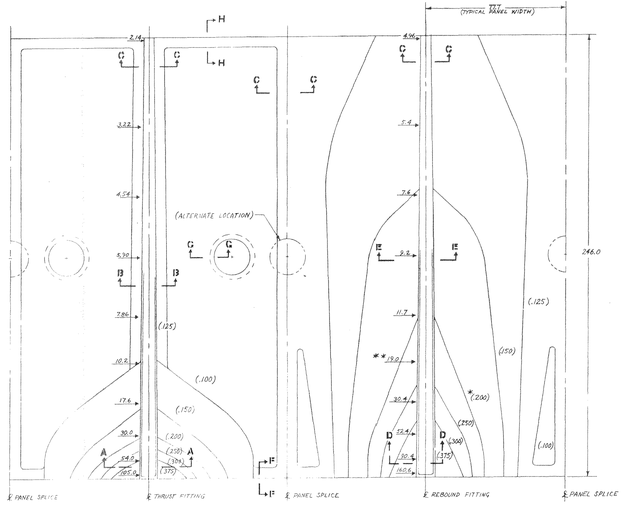

90° SEGMENT OF SHIRT FOLDED OUT FLAT
(4 IDENTICAL SEGMENTS REQD.)
1/10 SCALE

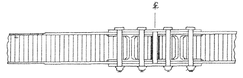

SECTION C-C
FULL SIZE

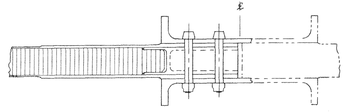

SECTION B-B
FULL SIZE

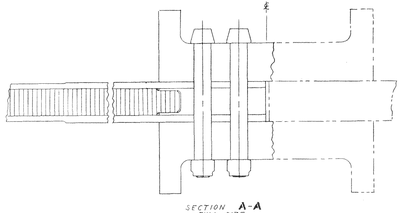

SECTION A-A
FULL SIZE

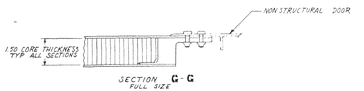

SECTION G-G
FULL SIZE

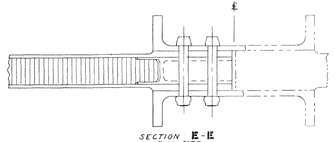

SECTION E-E
FULL SIZE

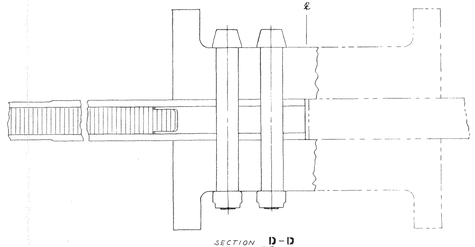

SECTION D-D
FULL SIZE

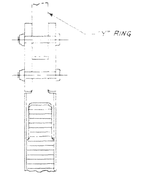

SECTION H-H
FULL SIZE

SECTION F-F
FULL SIZE

REVISED SKIN GA. AND JOINING X-SECT. AREA
9-11-65

PRELIMINARY DESIGN DRAWING

PRELIMINARY STRUCTURAL CONFIGURATION
HEAVY GAGE HONEYCOMB SANDWICH
(NAS 9-11943)

GENERAL DYNAMICS | FORT WORTH

FW65280003A

3.2 JOINT ANALYSIS AND SECONDARY TESTING

A secondary test program was initiated to provide design and analysis data for bonded overlap joints and to study the effects of surface waviness on sandwich sections. In addition, the capabilities of welded joints and bonded-bolted joints were to be determined.

3.2.1 Test Program

The test specimen configurations for this phase of testing are shown in Figure 3-20. Specific tasks required in the fabrication of panels and preparation of test specimens received detail shop planning similar to that provided for production hardware. All fabrication tasks were performed in production fabrication departments except for the panel welding which was accomplished in Manufacturing Research and Development Pilot Shop facilities. The panel welding and support studies are discussed in Subsection 3.3.

A discussion of each of the joint concepts investigated in this phase of testing is provided below:

3.2.1.1 Bonded Joint

There were two types of specimens used in evaluating the metal-to-metal bonded overlap. The evolution of the sandwich compression shear specimen was described in Subsection 1.2.4. The double overlap tensile shear specimens were included because they are more readily tested at the extreme temperatures -320°F and +300°F. These extreme temperature tests were provided in order to demonstrate structural integrity of the bonded joint over the inclusive temperature range.

Of secondary concern during this portion of the test program was a determination of correlation between adhesive shear strengths produced by tension and compression tests. This correlation was required because a large majority of the values for adhesive shear strength were to be generated by the double overlap tensile tests but, in application, the joints would normally be loaded in compression. Available analysis methods do not distinguish between compression and tension loadings on bonded overlap. In order to assure that no difference existed, it was felt necessary to test a typical skin gage and overlap by both methods and then compare results.

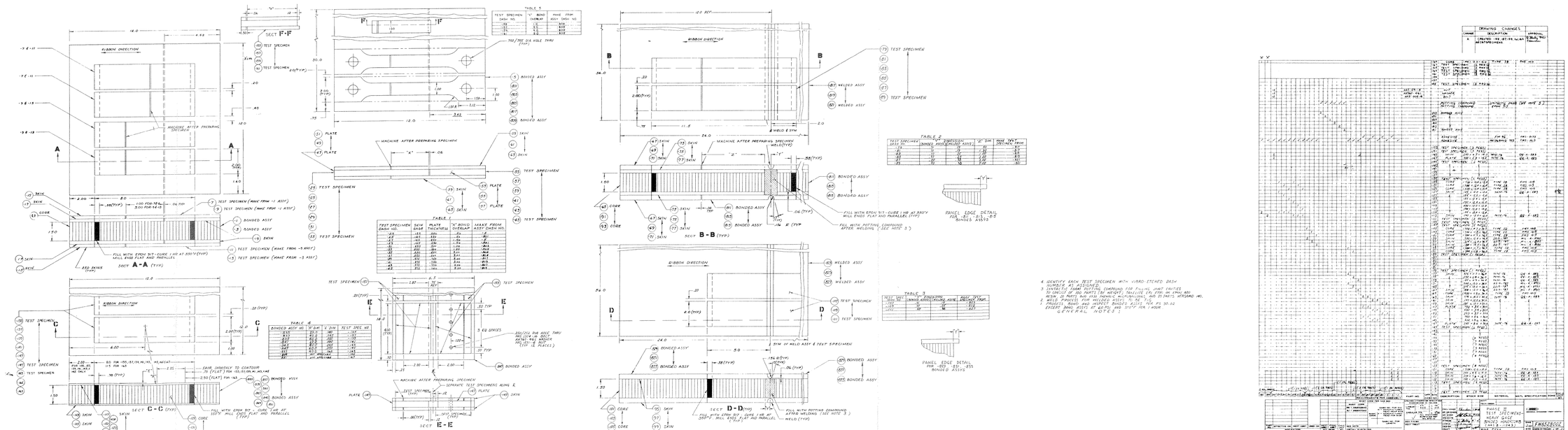

DRAWING CHANGES		
CHANGE	DESCRIPTION	APPROVAL
A	CREATED -98, -87, -99, -94, -97 TEST SPECIMENS	2-26-74

3.2.1.2 Welded Joint

There were two types of welded joints tested. One of the types allowed evaluation of the integrity of an adhesive bond between 2219 and 7075 alloys after the 2219 alloy had been welded. The second type allowed evaluation of the integrity of an adhesive bond between 2219 alloy facing material and 5052 alloy honeycomb core after the 2219 alloy had been welded. The panels from which the specimens were removed were larger than required for specimens alone so that the effect of weld heating on specimen geometry could also be evaluated.

3.2.1.3 Bonded-Bolted Joint

This portion of the test program was designed to determine whether a bonded-bolted joint concept was feasible with the selected materials. Tests with the control specimens, those without bolts, established the load-carrying ability of the adhesive bond, and then tests of the bonded specimens which also contained bolts established the load carrying ability of the bond with the bolts. Compression specimens were utilized because of the resulting simplicity in specimen fabrication and testing.

3.2.1.4 Core and Core Bond Requirements

The intent of this portion of the test program was to determine the effects of surface waviness on the face wrinkling characteristics of the typical sandwich sections. The broad range of surface waviness characteristics evaluated allowed a determination of the applicability of the Forest Products Laboratory and Syed Yusuff theories of face wrinkling. The 4.5 lb/ft^3 core density was typical of most of the sandwich area which appeared in the preliminary configuration drawing as shown in Figure 3-19.

Figures 3-21 through 3-24 show typical failure of each type of test specimen. Test results with pertinent discussions are provided in Appendix A.

3.2.2 Conclusions

In general conclusions of the test program may be stated as follows:

1) Allowable adhesive shear strengths were established from the test data for use in the design of the specimens for the structural test program.

2) Welding and the associated residual stresses had only minor effects on the joint strengths of the welded sandwich test specimens.

3) The addition of bolts to the bonded joint did not substantially improve the total joint shear strength.

4) Face wrinkling is not critical as a mode of buckling failure for the particular structure being considered.

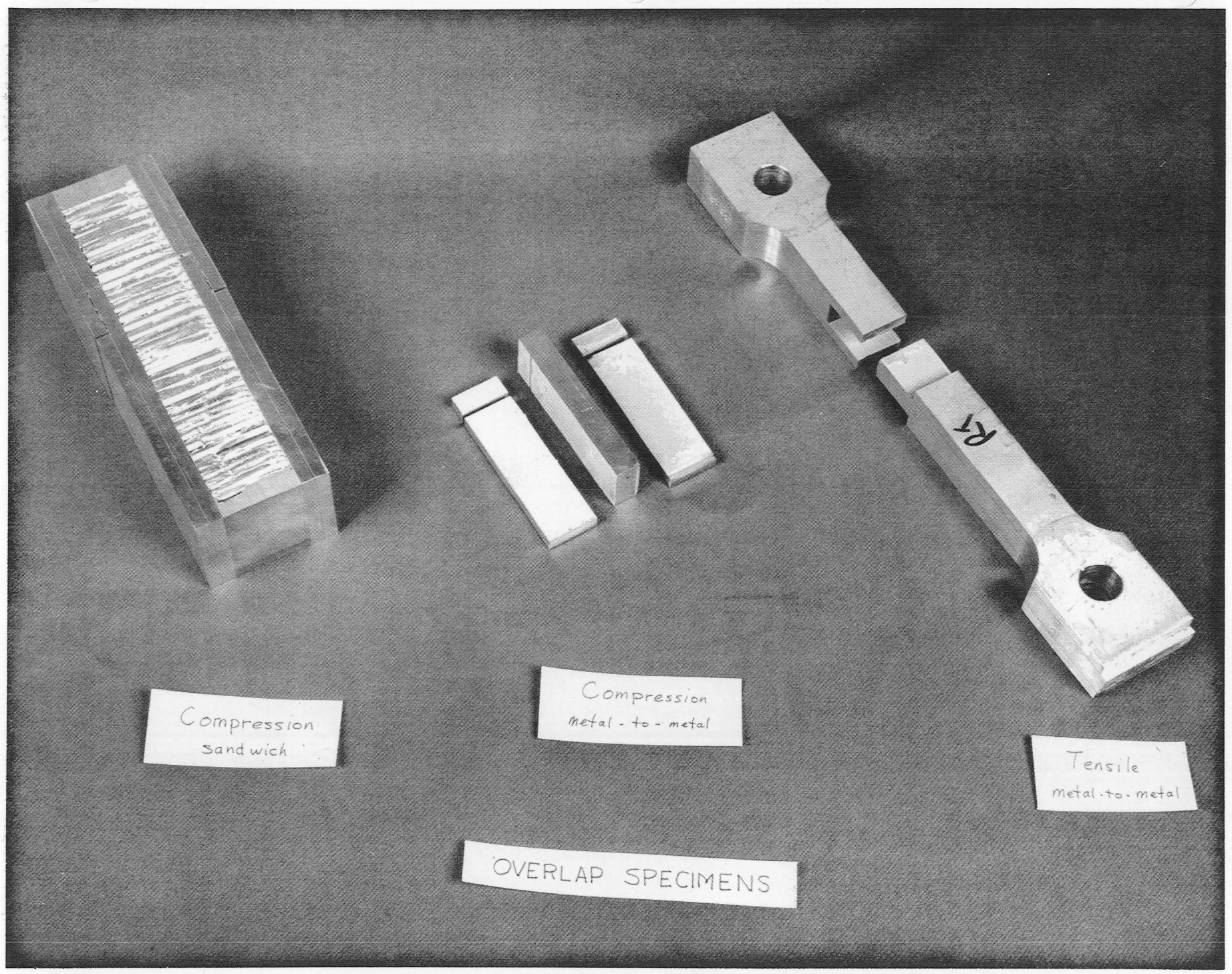

Figure 3-21 TYPICAL OVERLAP TEST SPECIMENS

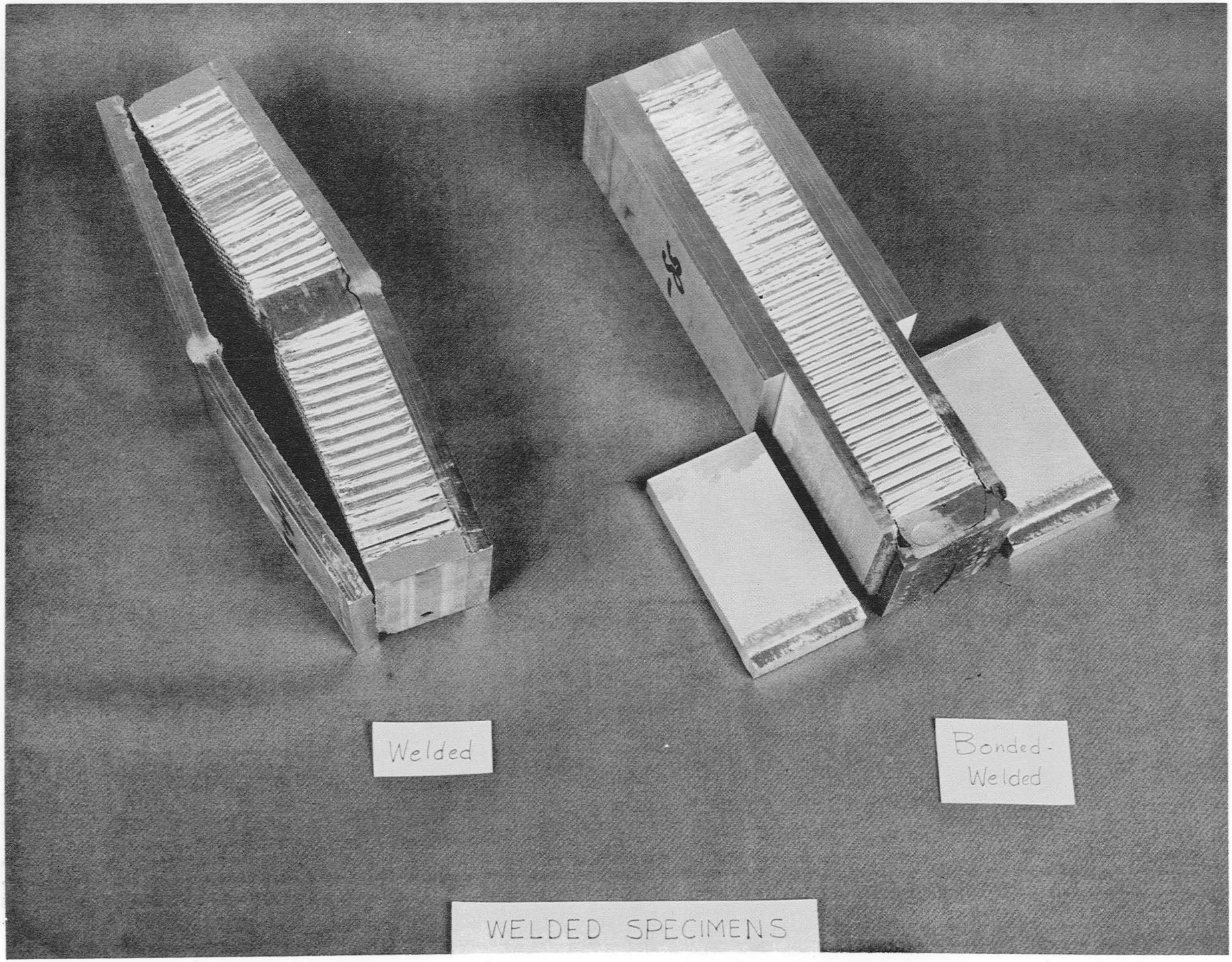

Figure 3-22 TYPICAL WELDED TEST SPECIMENS

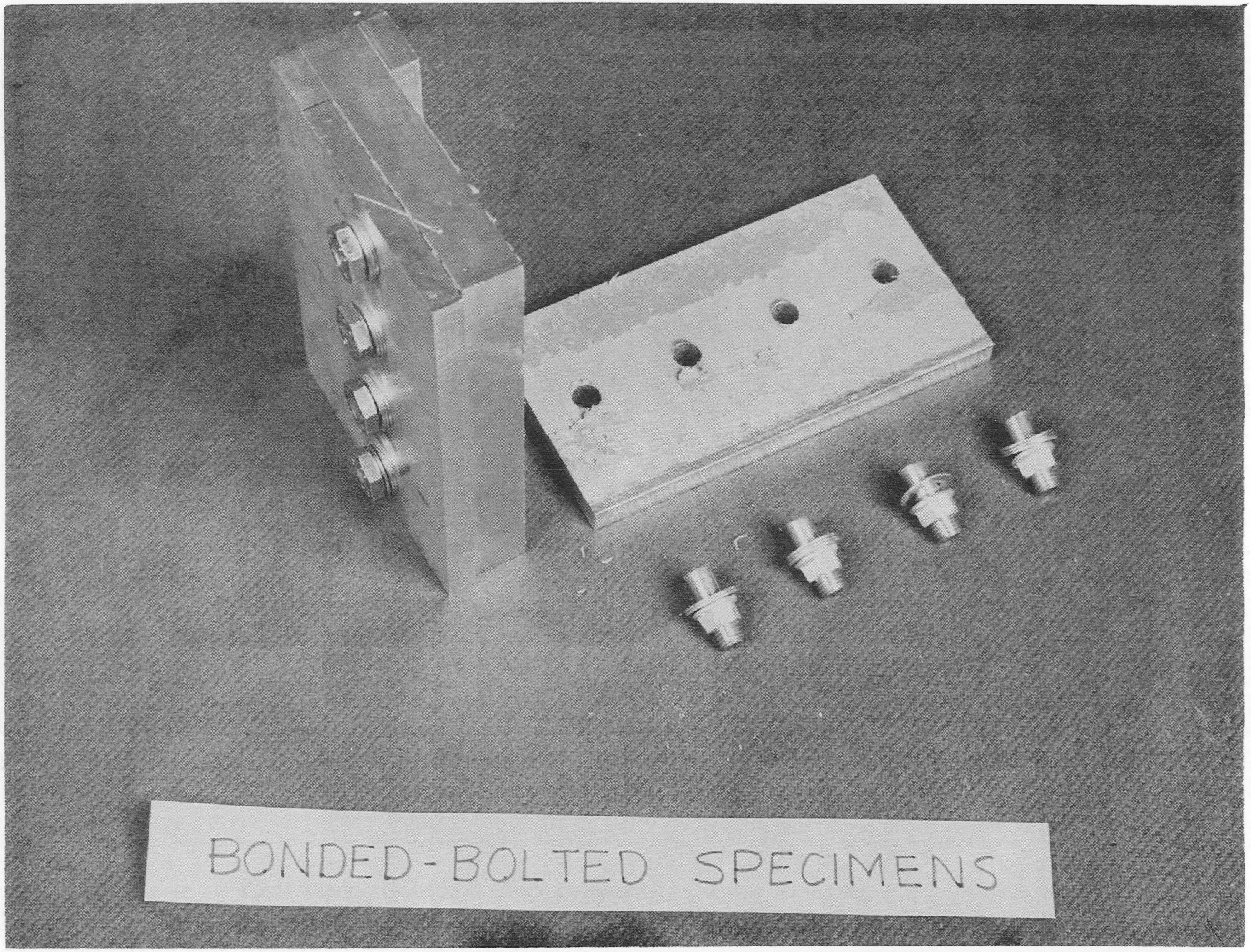

Figure 3-23 TYPICAL BONDED-BOLTED TEST SPECIMENS

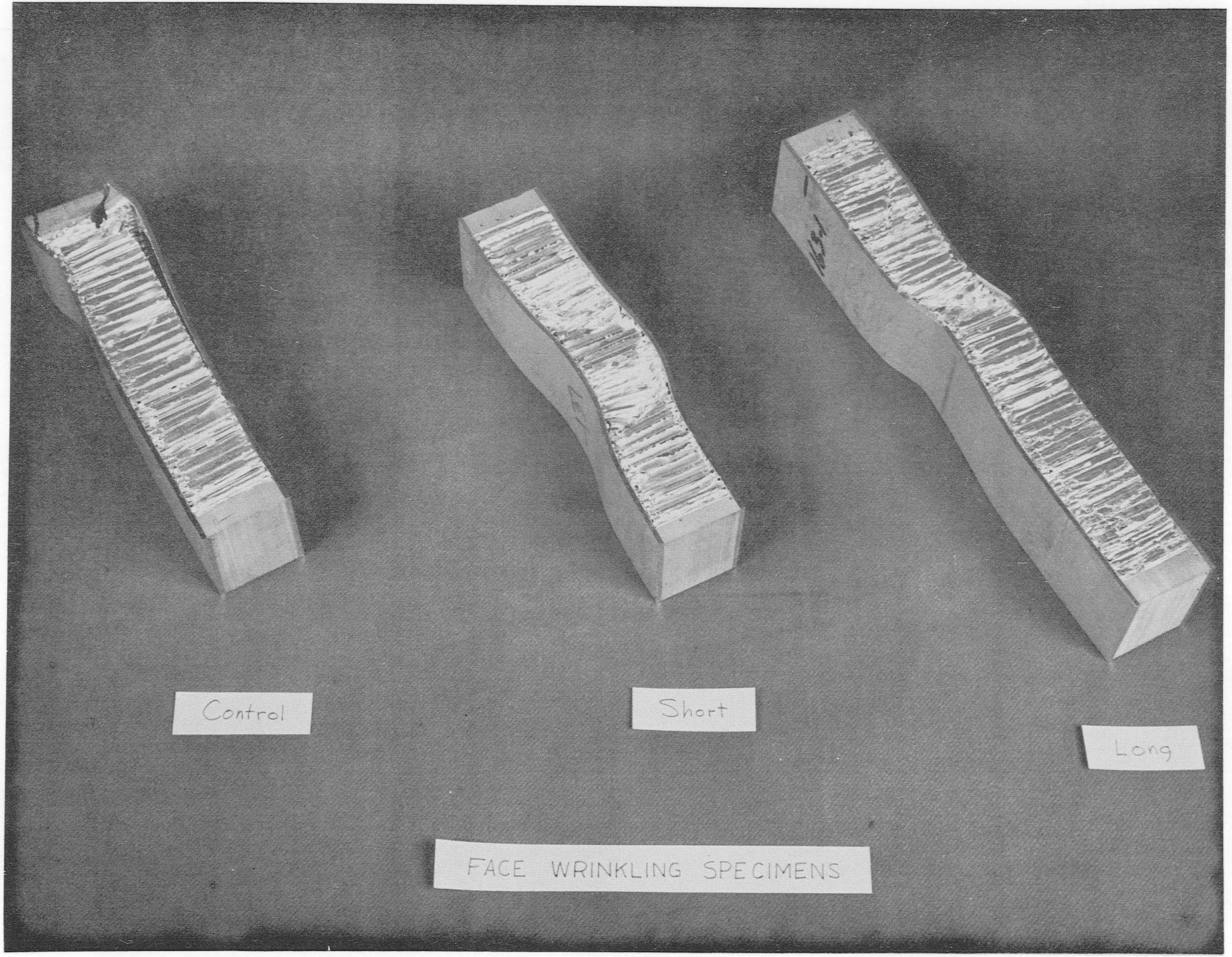

Figure 3-24 TYPICAL FACE WRINKLING TEST SPECIMENS

3.3 MANUFACTURING STUDY FOR WELD JOINING

Joining bonded panels by welding presents certain requirements which normally are not involved in welding procedures. These requirements are:

1. The heat from welding must not be permitted to cause a temperature rise at the bond line of a magnitude and time interval which would cause a loss in bond joint strength.

2. Tooling for locating and clamping the part must not cause crushing or crippling of the core.

Although only small test specimens were required in the Secondary Testing program it was considered that the welding approach and procedures developed there should also be applicable for the Structural Testing program. With this in mind, the following additional factors were considered:

3. Panels welded in the Secondary Testing program should be large enough to reflect conditions for large panel assemblies from both a welding and tooling standpoint.

4. Although the test specimens were made to represent the individual thicknesses of stepped skin gages, the welding procedures developed should be applicable for welding skins with stepped thicknesses.

5. Design of the edge preparation for the various skin gages should permit making the edge preparation on a stepped skin with a single rotary form-tool in one machining pass.

6. Welding shrinkage for the various gages should be as near equal as possible in order to facilitate dimensional control in the final weldment.

3.3.1 Approach

Based upon the above considerations, the following weld planning was developed:

1. Water cooled copper chill tubes bonded to heavy aluminum plates, with cooling water flow opposite to direction of welding should be used for weld heat control.

2. Vacuum clamping to be applied for part location and holding, and for holding the water chill plates.

3. Panel sizes of 14 x 36 inches to produce 36-inch long welds and a 28 x 36-inch weld assembly.

4. Skin steps should be located on the external surfaces of panels to facilitate core machining, weld joint edge preparation, and welding.

5. Weld joint edge preparation was based upon a single rotary cutter form as shown in Figure 3-25. The thickness of the land for all gages was made constant so that one depth setting and one machine pass completes the edge preparation for all thicknesses. This facilitates welding all gages at a constant speed and a minimum change in welding current for the root pass weld.

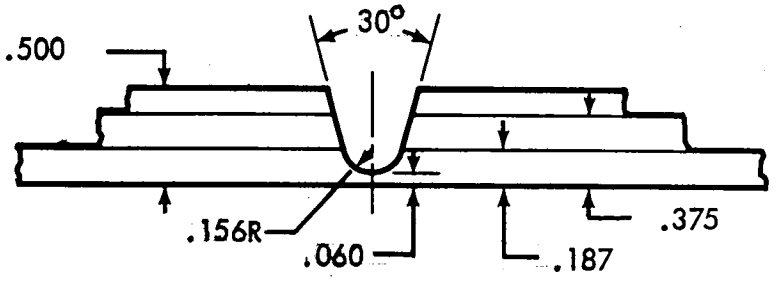

Figure 3-25 CUTTER FORM CONFIGURATION

6. The magnitude of the shrinkage in a butt weld joint is a function of and is proportional to material thickness, width of the fused area, and the number of weld passes. The joint preparation method selected provides some compensation for difference in shrinkage in thin and thick sections since the ratio of width of fused metal to material thickness is considerably greater for the thin section.

Welding was accomplished on the vacuum chuck butt weld fixture shown in Figure 3-26. The welding equipment consisted of a HWM-3 Linde automatic TIG head and controls on a boom-mounted side beam. A Vickers 300 ampere DC power supply with a weld programmer was used. The Linde HW13 torch was mounted on a Linde cross-seam torch oscillator.

3.3.2 Development of Welding Parameters

The welding parameters for flat position welds were developed for the joint configuration shown in Figure 3-25. All test weld joints were 36 inches long. The test plates were 14 inches wide and were held on a vacuum chuck fixture base having a 1 5/8 inch clearance space at the root of the weld. This fixture is shown in Figure 3-27, and was designed for butt welding sheet material. The space under the weld joint was provided for by removal of one of the 3/8 x 1 1/2 inch back-up bars. Water cooled chill plates were used on the top of the test plates to simulate thermal conditions for bonded panel welding. A welding speed of 14 inches per minute was selected for all gages and all weld passes in order to minimize the number of welding parameters that would require changing in welding step gage skins. The use of preliminary curves for welding parameters facilitates maintenance of proper balance of the parameters from one gage to another. The final parameter curves are most useful when additional gages within the range of the curves must be welded; additional weld tests are not required for the intermediate gages. Multi-pass welding was used for all gages in order to keep welding heat flow to the bond line to a minimum. The welding parameters data are shown in Tables 3-1, 3-2, and 3-3 and the temperatures recorded are shown in Table 3-4.

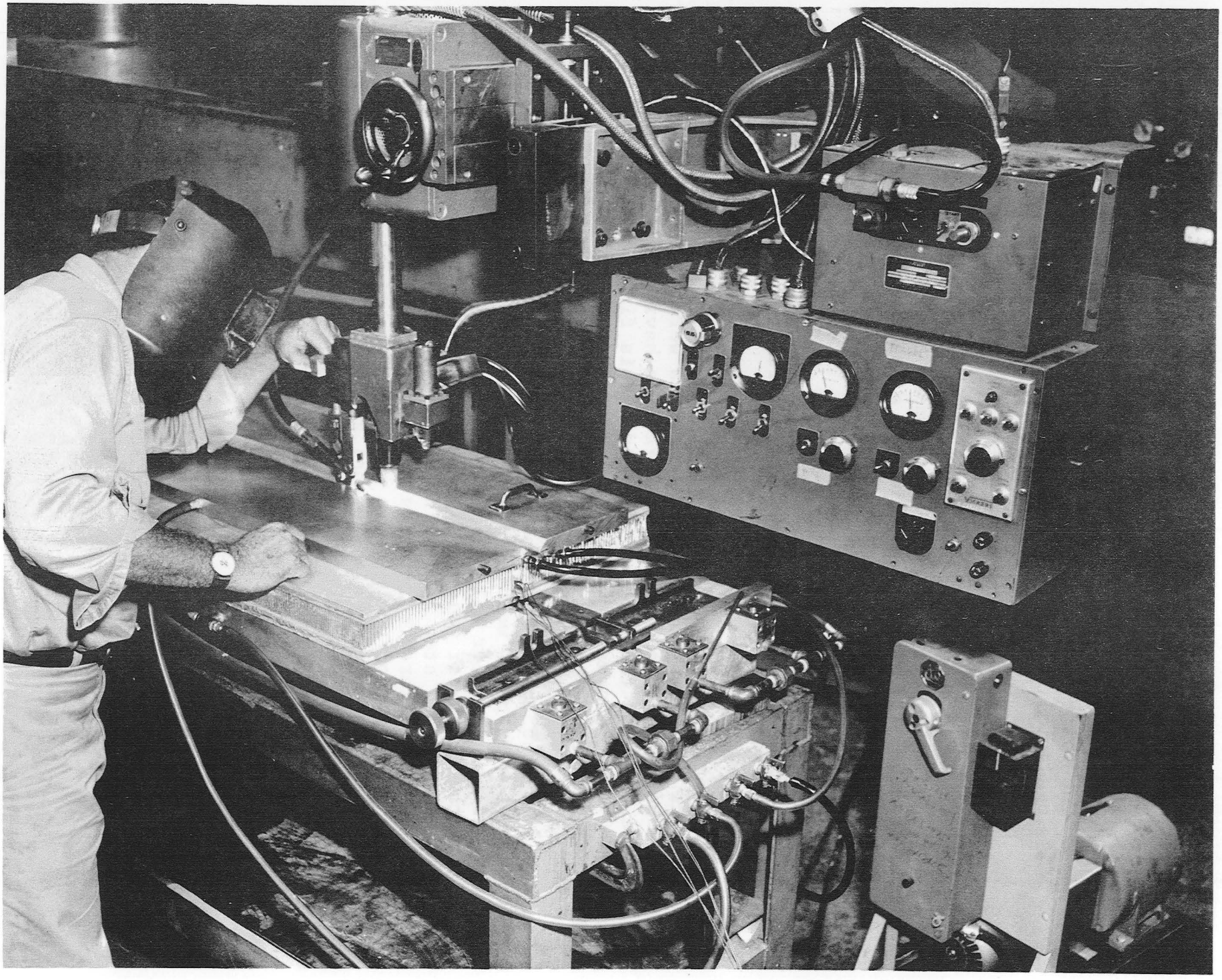

Figure 3-26 SANDWICH BUTT-WELDING IN PROCESS

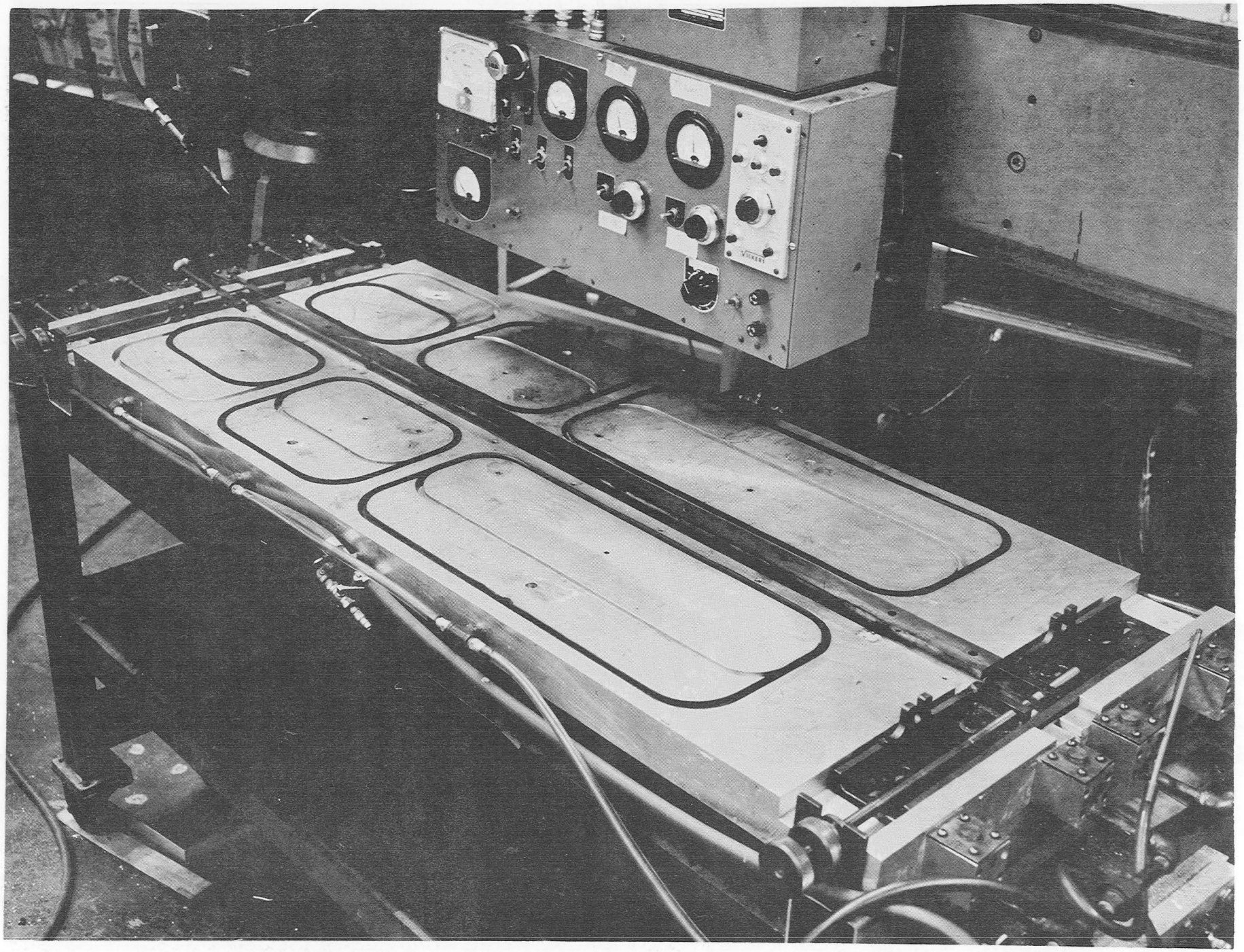

Figure 3-27 VACUUM CHUCK FIXTURE

Table 3-1 WELDING PARAMETERS DATA ON 2219, .188 GAGE, FLAT POSITION

WELD PASS	1	2	3
VOLTS - D.C.	13 1/2	15	15 1/2
AMPERES (D.C. ST. POL.)	110	95	120
WIRE FEED - IPM (.045 DIA.)	30	45	55
TORCH SPEED - IPM	14	14	14
TORCH GAS - CFH HELIUM	70	70	70
BACKUP GAS - CFH HELIUM	40	40	-
ELECTRODE - DIA. & POINT ANG.	3/32 - 60°	3/32 - 60°	3/32 - 60°
GAS CUP SIZE - LINDE	#8	#8	#8
ELECTRODE EXTENSION - IN.	1 1/8	1 1/8	1.0
OSCILATOR - AMPLITUDE - IN.	-	.045	.093
COOLING WATER - GAS/MIN	2 (EST.)	2	2
TOP CLAMP SPACING - IN.	.62	.62	.75

Table 3-2 WELDING PARAMETERS DATA ON 2219, .375 GAGE, FLAT POSITION

WELD PASS	1	2	3	4	5
VOLTS - D.C.	14 3/4	15	15	15	16
AMPERES - D.C.	140	130	150	160	160
WIRE FEED - IN/MIN (.045 DIA.)	45	55	60	65	40
TORCH SPEED - IN/MIN	14	14	14	14	14
TORCH GAS - CFH HELIUM	70	70	70	70	70
BACKUP GAS - CFH HELIUM	40	40	-	-	-
ELECTRODE - DIA. & POINT ANG.	3/32 - 60°	3/32 - 60°	3/32 - 60°	3/32 - 60°	3/32 - 60°
GAS CUP SIZE - LINDE	#8	#8	#8	#8	#8
ELECTRODE EXTENSION - IN.	1 1/8	1 1/8	1.0	13/16	3/4
OSCILLATOR AMPLITUDE - IN.	-	.045	.093	.125	.140
COOLING WATER - GAL/MIN	2 (EST.)	2	2	2	2
TOP CLAMP SPACING - IN.	.62	.62	.75	.87	1.00

Table 3-3 WELDING PARAMETERS DATA ON 2219, .500 GAGE, FLAT POSITION

WELD PASS	1	2	3	4	5	6
VOLTS - D.C.	16	16	16	17	18	18
AMPERES (D.C. ST. POL.)	170	160	170	190	200	210
WIRE FEED - IPM (.045D)	48	63	65	80	80	90
TORCH SPEED - IPM	14	14	14	14	14	14
TORCH GAS - CFH HELIUM	70	70	70	70	70	70
BACKUP GAS - CFH HELIUM	40	40	--	--	--	--
ELECTRODE - DIA. & POINT ANG.	3/32 - 60°	3/32 - 60°	3/32 - 60°	3/32 - 60°	3/32 - 60°	3/32 - 60°
GAS CUP SIZE - LINDE	#8	#8	#8	#8	#8	#8
ELECTRODE EXTENSION - IN.	1 1/8	1 1/8	1	13/16	3/4	11/16
OSCILATOR - AMPLITUDE IN.	--	.045	.093	.125	.140	.170
COOLING WATER - GAL/MIN	2 (EST.)	2	2	2	2	2
TOP CLAMP SPACING - IN.	.62	.62	.75	.75	.87	1.00

Table 3-4 SKIN TEMPERATURES ADJACENT TO WELD ZONE

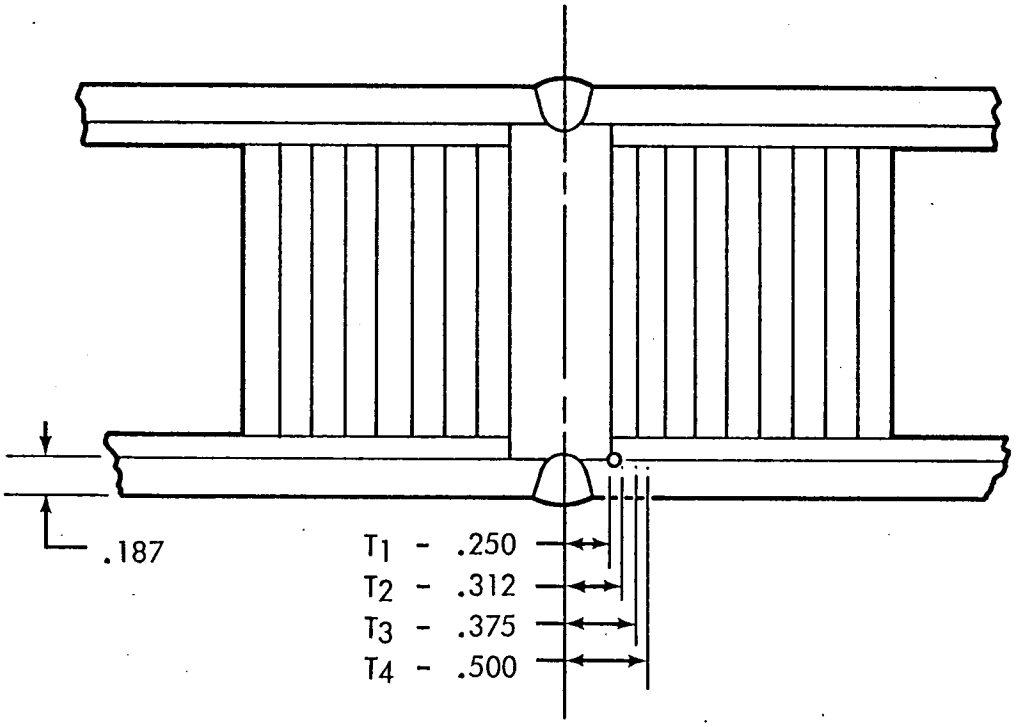

WELD PASS	GAGE	T_1 = .250	T_2 = .312	T_3 = .375	T_4 = .500
NO. 1	.187				
NO. 2	.187	245	230	215	185
NO. 3	.187	265	240	225	210

WELD PASS	GAGE	T_1 = .312	T_2 = .375	T_3 = .437	T_4 = .512
NO. 1	.375	245	215	205	160
NO. 2	.375	210	215	195	165
NO. 3	.375				

3.3.3 Test Panel Welding

The test panels to be welded were all 14 inches wide by 36 inches long; the weld being made along the 36-inch edges. The external skin surfaces were wiped clean with MEK. The adhesive on the underside of skins was removed by hand scraping. The curved portion of the machined edges was hand scraped using a hardened round rod scraper. The flat portion of the machined edge and the top edges of the panels were then hand scraped. A rotary powered stainless steel wire brush was used for cleaning before each weld pass. The .187 gage weld joints were made in three weld passes on each side, the .375 gage in five each side, and the .500 gage in six each side. In order to maintain a balance of weld stresses in the two welds, the welding sequences shown in Figure 3-28 were employed. A cross-seam torch oscillator was used on all weld passes except the root pass for each gage.

The residual weld stress pattern for butt joints in flat plates is illustrated in Figure 3-29 which shows..500 inch plates in the "as welded condition." The root side of the joint is up in this photo. The bow in the 28-inch width measured about .400 inch. The amount of bow in the unrestrained welded plate is an indication of the magnitude of residual stresses in the welds. Also, sections were sawed from each bonded sandwich panel. The core was then sawed on one side of the joint as shown in Figure 3-30. It may be observed that the amount of bow was considerably less in the bonded panels than in the unrestrained flat welded skins. The lesser distortion in the welded bonded panels may be attributed to the added stiffness afforded by the honeycomb core. After welding, and before sawing as shown in Figure 3-30, the panels were relatively flat.

The effect of weld peening was investigated in making a butt joint on .500 inch 2219 aluminum plate. Each weld pass (after the root pass) was peened using a rivet gun with throttled air flow and a blunt (.125 radius) polished chisel. Measurement of bow in the 27-inch wide panel was .050 inch at one end of the joint and .025 at the other end. It is possible that peening the welds could be very useful for reducing residual stresses, strengthening weld by cold working, and reduction of weld shrinkage in the thicker sections so that a more uniform weld shrinkage can be attained for thick and thin skins. Figure 3-31 illustrates the configuration of the peening tool.

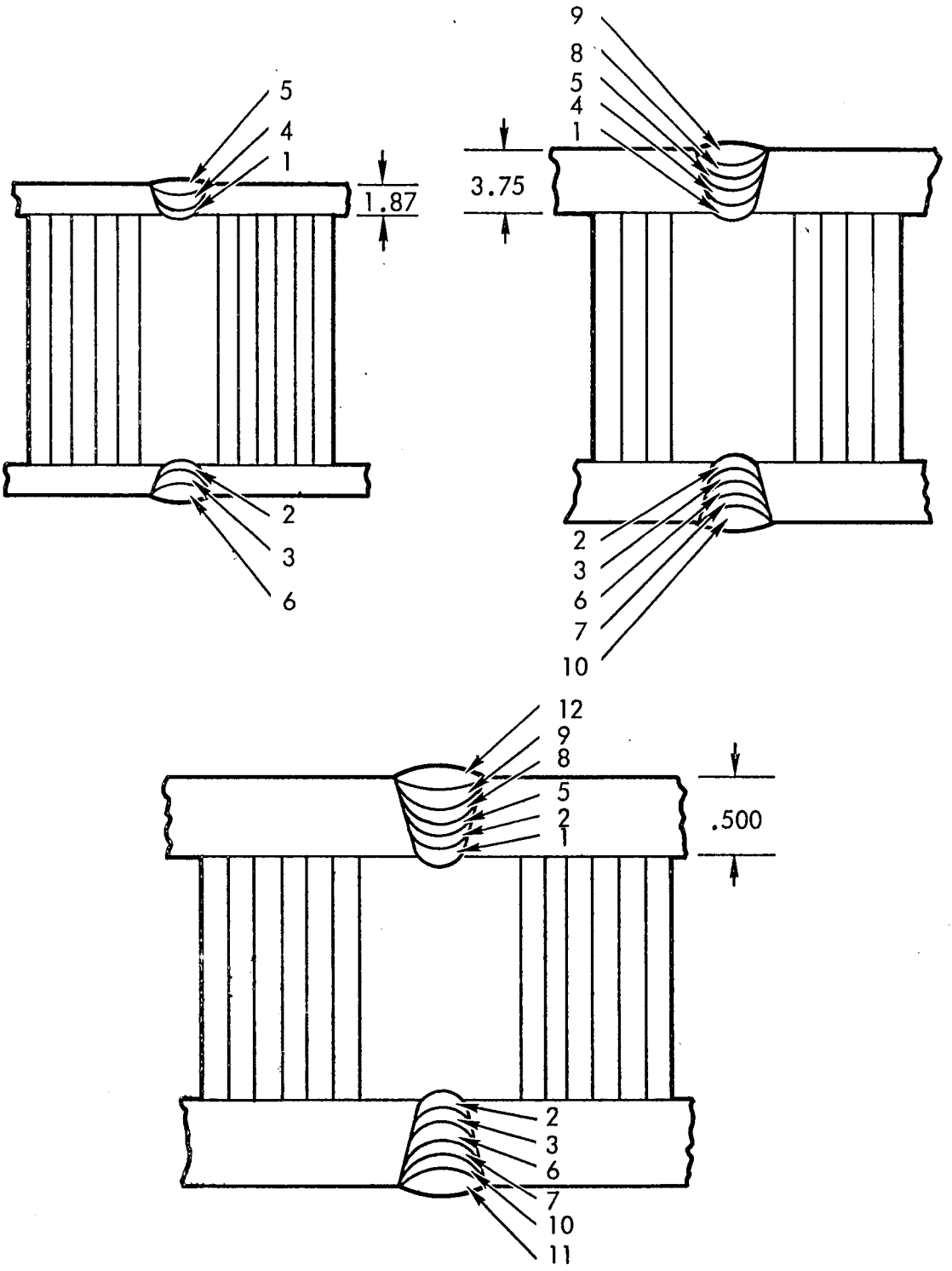

Figure 3-28 WELDING PASS SEQUENCE

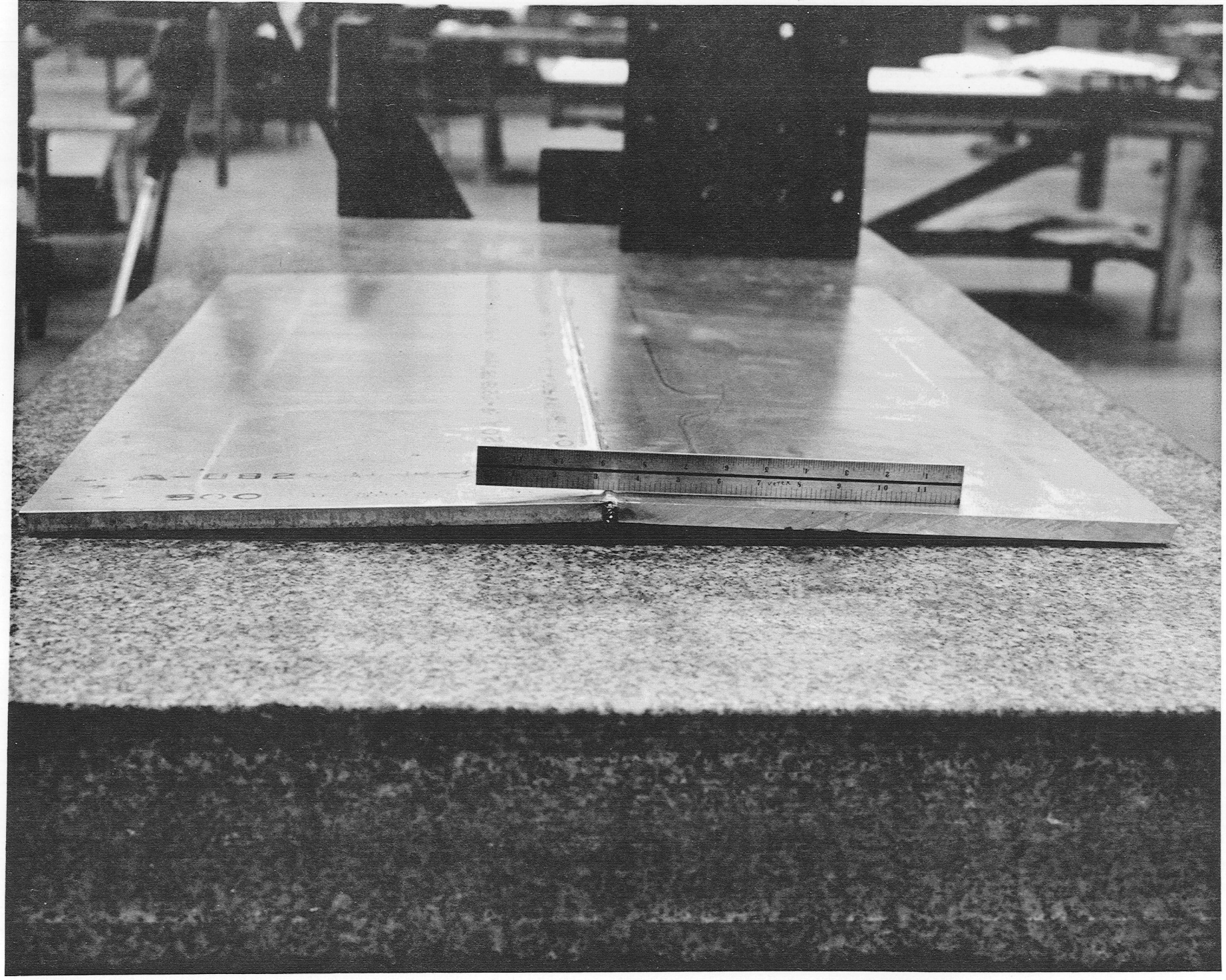

Figure 3-29 WELD DISTORTION ON .500 INCH 2219 PLATE

Figure 3-30 WELDED SANDWICH SPECIMENS

One 36-inch weld on .500 plate was x-rayed. The weld was free of defects with the exception of a local area of porosity about 1.50 inches long near the middle of the weld.

3.3.4 Post-Weld Potting of Cavity

After the panels were welded the cavities in the core beneath the welds were filled with a syntactic foam potting compound. Realizing that the procedure used in filling the cavity should be representative of a practical method of filling a similar cavity in a full size production part, several methods were considered. It was decided that the introduction of the potting compound at a point below the surface of the compound would minimize the formation of voids in the cured potting compound. The procedure selected involved drilling a .250 hole through one end of the weld into the cavity, plugging the end of the cavity adjacent to the hole, and injecting the potting compound through the hole under pressure with the weld in a vertical position until the potting compound emerged at the top of the panel. The total length of cavity that could safely be filled in this manner was undetermined but these panels which were 36 inches long were successfully filled with no apparent problem.

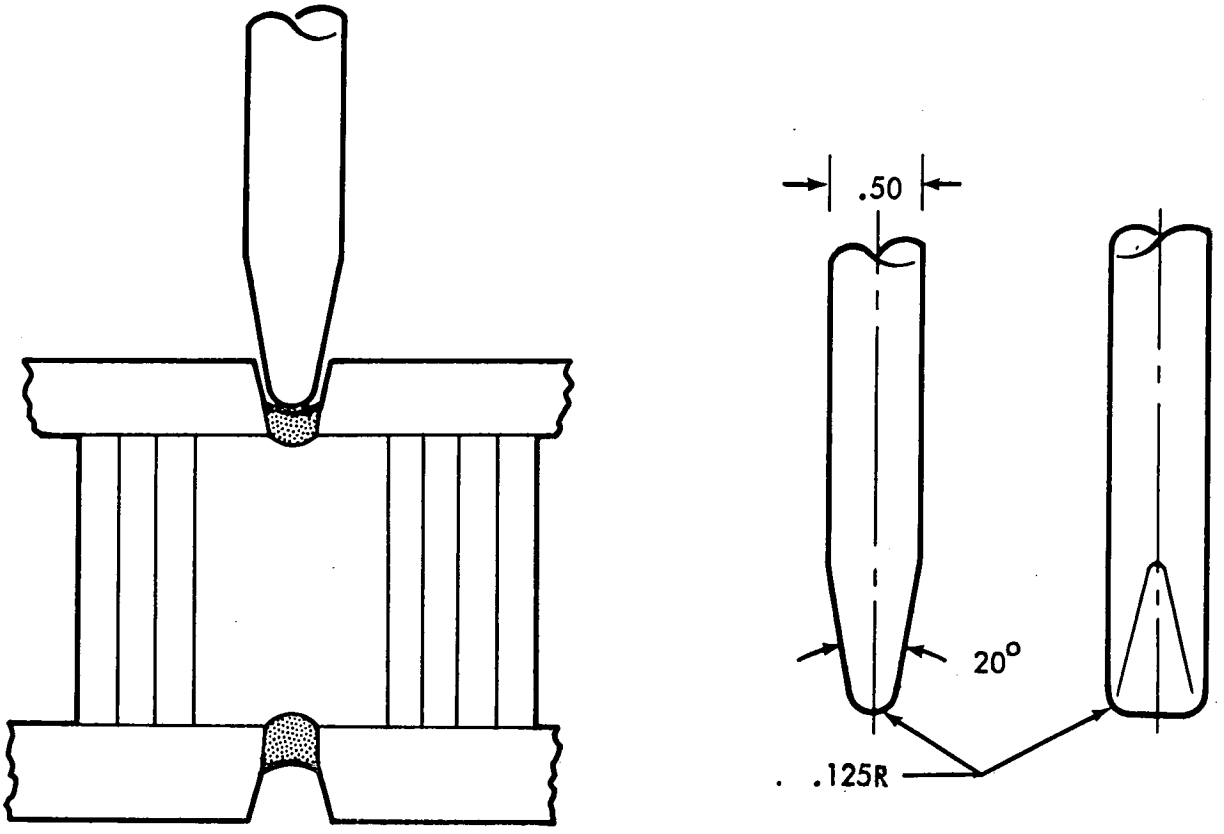

Figure 3-31 POST-WELD PEEN TOOL AND PEEN TOOL SETUP

3.4 REFERENCES

3-1 Yusuff, S., "Face Wrinkling and Core Strength in Sandwich Construction", Journal of the Royal Aeronautical Society, March 1960.

3-2 Stein, M. and Mayers, J., Compressive Buckling Stress of Simply Supported Curved Plates and Cylinders of Sandwich Construction, NACA TN 2601, January 1952.

3-3 Kuenzi, E. W. and March, H. W., Buckling of Cylinders of Sandwich Construction in Axial Compression, Forest Products Laboratory Report No. 1830, Revised December 1957.

3-4 Cunningham, J. H. and Jacobsen, M. J., "Design and Testing of Honeycomb Sandwich Cylinders Under Axial Compression", Collected Papers on Instability of Shell Structures - 1962, NASA TN D-1510, December 1962.

3-5 Cunningham, J. H., "Instability and Buckling of Shells," Lecture No. 8 of Course X414PQ Analysis and Design of Modern Pressure Vessels, UCLA Short Course, 1962.

SECTION 4

STRUCTURAL TESTING

The phase of structural testing was initiated in order to evaluate candidate design configurations and to detect and evaluate fabrication variables associated with methods applicable to the fabrication of heavy gage sandwich structures.

4.1 TEST PROGRAM

The test specimen configurations are shown in Figure 4-1, General Dynamics Engineering drawing FW6528004A and also in Figure 4-2. These configurations represented specific areas of the preliminary designs for the thrust cylinder. The specimens can be classified according to the particular loading situation - compression or shear.

4.1.1 Compression

There were two types of compression specimens tested - bonded edgemember and bolted joint.

4.1.1.1 Bonded Edgemember

The bonded edgemember specimen represented a typical section of the circumferential forward interface. The design variables which were evaluated in these tests are

1. Core thicknesses of 1.5 and 3.0 inches

2. Adhesive thicknesses of .014 and .018 inch.

The tests of two thicknesses of core were to demonstrate that the edgemember concept utilized with the 1.5 inch core could be adapted with minimum modifications to thicker sandwich sections in case that the thicker sections were required by later analyses of the structure. The tape adhesive which is thicker, and therefore heavier, was evaluated in case that manufacturing fitting tolerances on the later full-size structure required a thicker bond line. Figure A-5 in Appendix A presents the design allowables for Metlbond 329 adhesive when used in compression shear loadings. The decision was made during the design

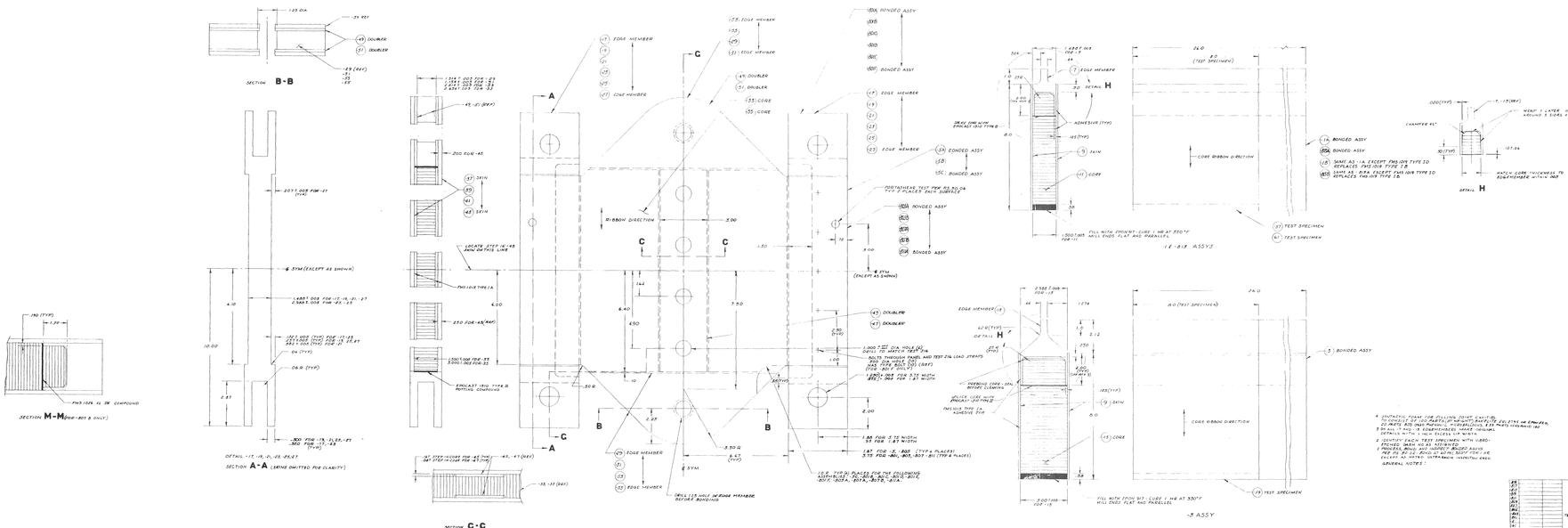

Figure 4-1 Page 4-2

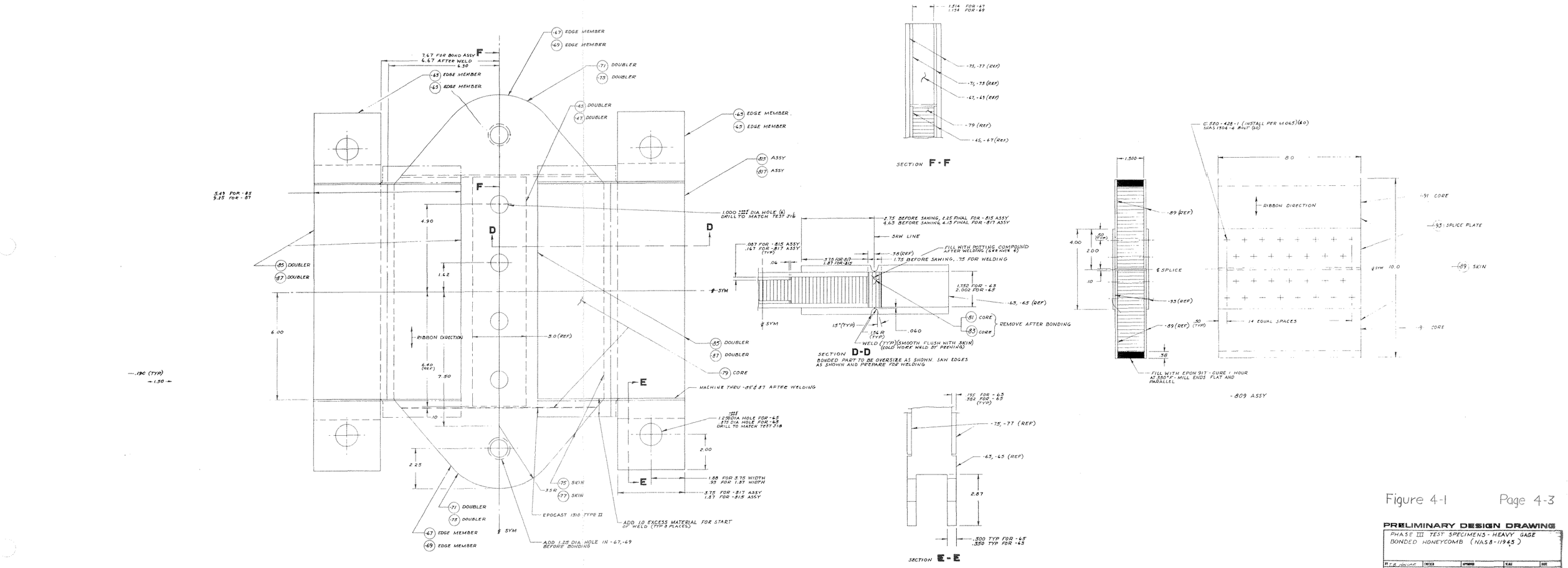

Figure 4-1 Page 4-3

PRELIMINARY DESIGN DRAWING

PHASE III TEST SPECIMENS - HEAVY GAGE BONDED HONEYCOMB (NAS8-11945)

BY	DATE	APPROVED	SCALE	SIZE
R.B. HOUSE				

GENERAL DYNAMICS | FORT WORTH

FW6528004
SHEET 2

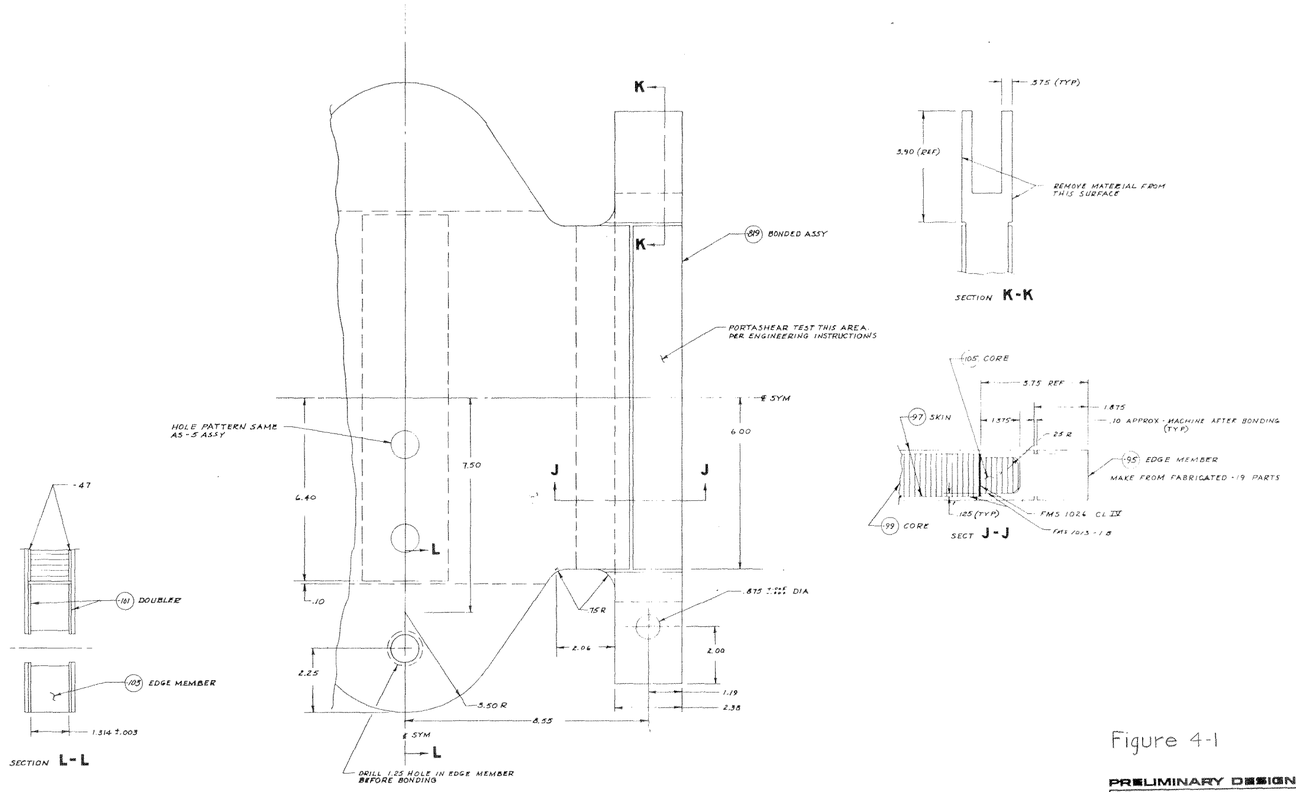

Figure 4-1 Page 4-4

PRELIMINARY DESIGN DRAWING

PHASE III TEST SPECIMENS - HEAVY GAGE BONDED HONEYCOMB (NAS8-11943)

GENERAL DYNAMICS | FORT WORTH

FW6528004
SHEET 3

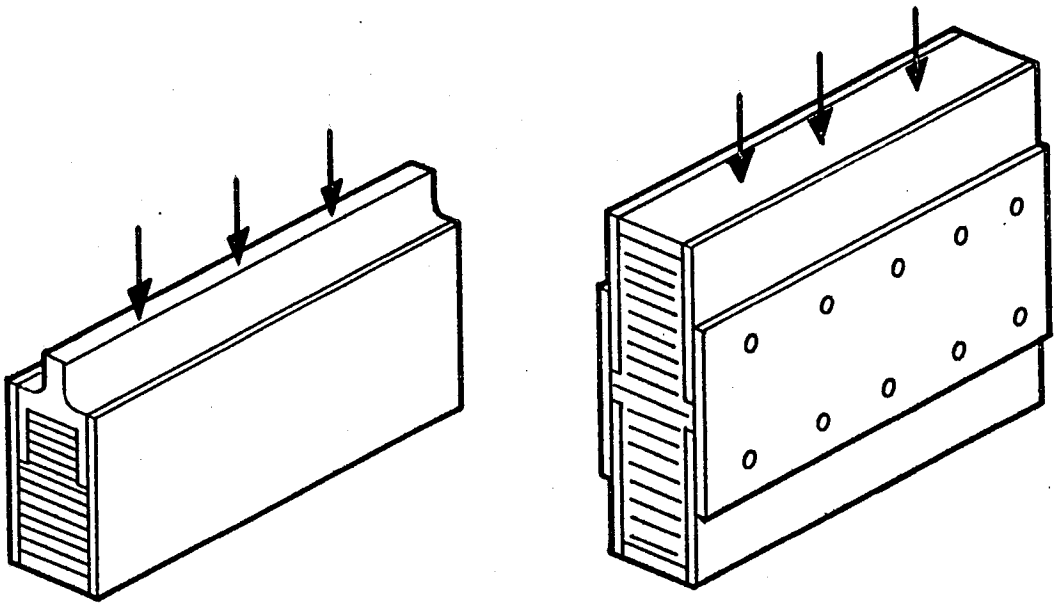

BONDED EDGEMEMBER

BOLTED JOINT

COMPRESSION TESTS

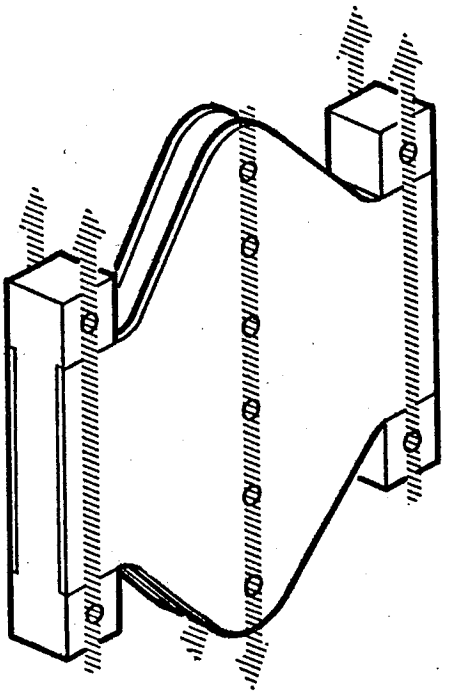

SHEAR TEST

Figure 4-2 TEST SPECIMENS AND LOADING CONDITIONS

of the specimens for the Structural Test Program to use the optimistic values for the compression specimens; that is, the overlap lengths were based on the actual test data average curve. For the .125 gage specimens, this assumption corresponded with an L/t of 16 and a shear stress of 4260 psi. The initial specimens were bonded and tested with edgemember overlap lengths based on that stress level. For .125 thickness skin and L/t = 16, the overlap is equal to 2.00 inches. In the event that the specimens were critical to overlap length and appeared to require longer overlaps, additional tests were to be run using a reduced stress value based on the design allowable curve. To prepare for that contingency, extra detail edgemembers were machined with 3.00 inch legs. That dimension corresponds with an L/t of 24 and a stress of 3,000 psi.

4.1.1.2 Bolted Joint

The bolted joint specimen represented a possible method of joining adjacent panels along the vertical splice. The purpose of the test was to evaluate the ramifications of attaching splice plates to sandwich panel joints with blind fasteners. The use of blind fasteners was thought to be desirable from a weight savings standpoint because, theoretically, potting compounds and spacers are not required as reinforcement in the local area of the core around the fasteners.

4.1.2 Shear

The particular design requirement of this type of specimen was to transfer loads from an edgemember to sandwich skins through an adhesive bond in a manner which simulates a possible load transfer method in the area of the vertical longerons and splices. The variables which were to be evaluated in this type of test included

1. 7075T6 skin gages of .125, .250, and .375 each on 1.5 inch thick core
2. 7075T6 skin gages of .125 and .250 each on 3.0 inch thick core
3. Step in 7075T6 skin thickness from .200 to .250 inch on 1.5 inch thick core
4. 2219T87 skin gages of .188 and .375 bonded to 7075T6 skins on 1.5 inch thick core and welded at the joint.

The bond overlaps for the shear specimens were designed with a higher degree of conservatism than that reflected in the design of the compression specimens because of the increased complexity and cost of the specimens. The adhesive bond requirement for these specimens was based on the design allowable stress of 3,000 psi as shown in Figure A-5.

4.2 SPECIMEN FABRICATION AND QUALITY CONTROL

Specific tasks required in the fabrication and inspection of panels and preparation of test specimens received detail shop planning similar to that provided for production hardware. All fabrication tasks were performed in production fabrication departments except for the panel welding which was accomplished in Manufacturing Research and Development Pilot Shop facilities. Standard shop procedures which might be utilized for fabrication of full-scale heavy gage bonded structures were observed wherever practicable.

All hardware was inspected with a through-transmission ultrasonic tester to check for adhesive voids or unusual bond conditions. It was determined that the stubmeter normally used at the Fort Worth Division of General Dynamics needed modifications to transmit through the heavy skin gages. Also, it is felt that with the manufacture of large size bonded structures the through-tramsmission equipment lends itself to mechanization, which can lead to much faster inspection rates than possible with the stubmeter. Plans were also made to modify the Portashear adhesive test unit so that the unit could be utilized in further nondestructive inspection of adhesive bonds in the test panels. Modification was required to the existing Portashear design in order to give the unit the capability of testing adhesive bonds of thick skins.

The fabrication of the structural test specimens was closely monitored by both structural and manufacturing engineers. The primary purpose of the close follow-up was to detect and evaluate any problems which might have appeared that were peculiar to the fabrication of heavy gage, thick honeycomb sandwich.

4.3 DISCUSSION OF RESULTS

Discussions of both test results and the evaluations of fabrication variables are presented in this section.

4.3.1 Test Results

The test configurations, procedures, and data obtained are described in General Dynamics Engineering Test Report Number FSG-600, Appendix B. The test data is reduced and discussed below for each type of specimen tested.

4.3.1.1 Compression

Bonded Edgemember - The results for the bonded edgemember tests are shown in Table 4-1. The basic specimen configurations with the 1.50 and 3.0 inch thick core sections are shown in Figures 4-3 and 4-4 respectively. Particular evaluations were made of the significance of the core strength, core installation methods, and adhesive thickness.

Specimens -57 a, b, and c contained the lightweight core and the thinner adhesive and -61 a, b, and c contained the lightweight core and the thicker adhesive as shown in Table 4-1. These specimens all failed prematurely and the failures were characterized by a tension failure in the core as shown in Figure 4-5.

The core was installed in specimens -57 d and e in a manner which was different from that utilized in the other bonded edgemember compression specimens. These installation procedures and test data are discussed in Section 4.3.2.2.

Specimens -57 f, g, and h contained the heavier core and the thinner adhesive as shown in Table 4-1. The primary mode of failure for each of these specimens was adhesive shear in the bond line between the edgemember lip and the skin. The specimens failed a little prematurely because of a slight imperfection in the panels. The bond lines were tapered in thickness across their length and the panels were slightly bowed. These defects were caused by a minor error in the procedure of specimen lay-up in the bond form which allowed the edgemember to rotate slightly during bonding. In spite of this problem the failing loads weresatisfactory. The mode of failure is shown in Figure 4-6. The failed specimens are shown in Figure 4-7.

Table 4-1 BONDED EDGEMEMBER TEST DATA

SPECIMEN	CORE DENSITY (LB/FT^3)	CORE THICKNESS (INCH)	ADHESIVE THICKNESS (INCH)	FAILING LOAD LB/INCH WIDTH	BOND STRESS DEVELOPED (PSI)	SKIN STRESS DEVELOPED (PSI)
-57 a	4.5	1.5	.014	10,800	2,700	43,200
b	4.5	1.5	.014	9,800	2,500	39,800
c	4.5	1.5	.014	11,800	2,960	47,300
d	8.1	1.5	.014	10,700	2,670	42,600
e	8.1	1.5	.014	12,200	3,060	48,900
f	8.1	1.5	.014	15,600	3,900	62,300
g	8.1	1.5	.014	15,700	3,920	62,600
h	8.1	1.5	.014	16,000	4,010	64,000
-59 a	8.1	3.0	.014	17,500	4,370	69,900
b	8.1	3.0	.014	16,300	4,090	65,300
c	8.1	3.0	.014	15,300	3,780	61,300
-61 a	4.5	1.5	.018	11,500	2,870	45,800
b	4.5	1.5	.018	13,200	3,300	52,700
c	4.5	1.5	.018	11,500	2,880	46,000
d	8.1	1.5	.018	20,000	5,000	80,000
e	8.1	1.5	.018	19,600	4,900	78,400
f	8.1	1.5	.018	19,200	4,830	77,000

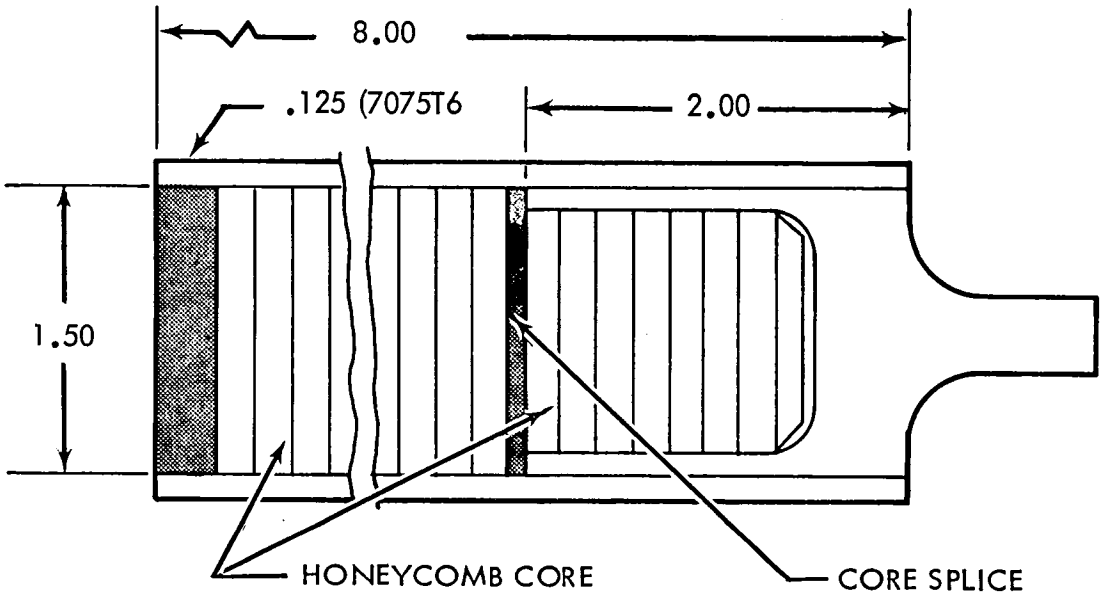

Figure 4-3 BONDED EDGEMEMBER COMPRESSION TEST SPECIMENS (1.50 INCH CORE)

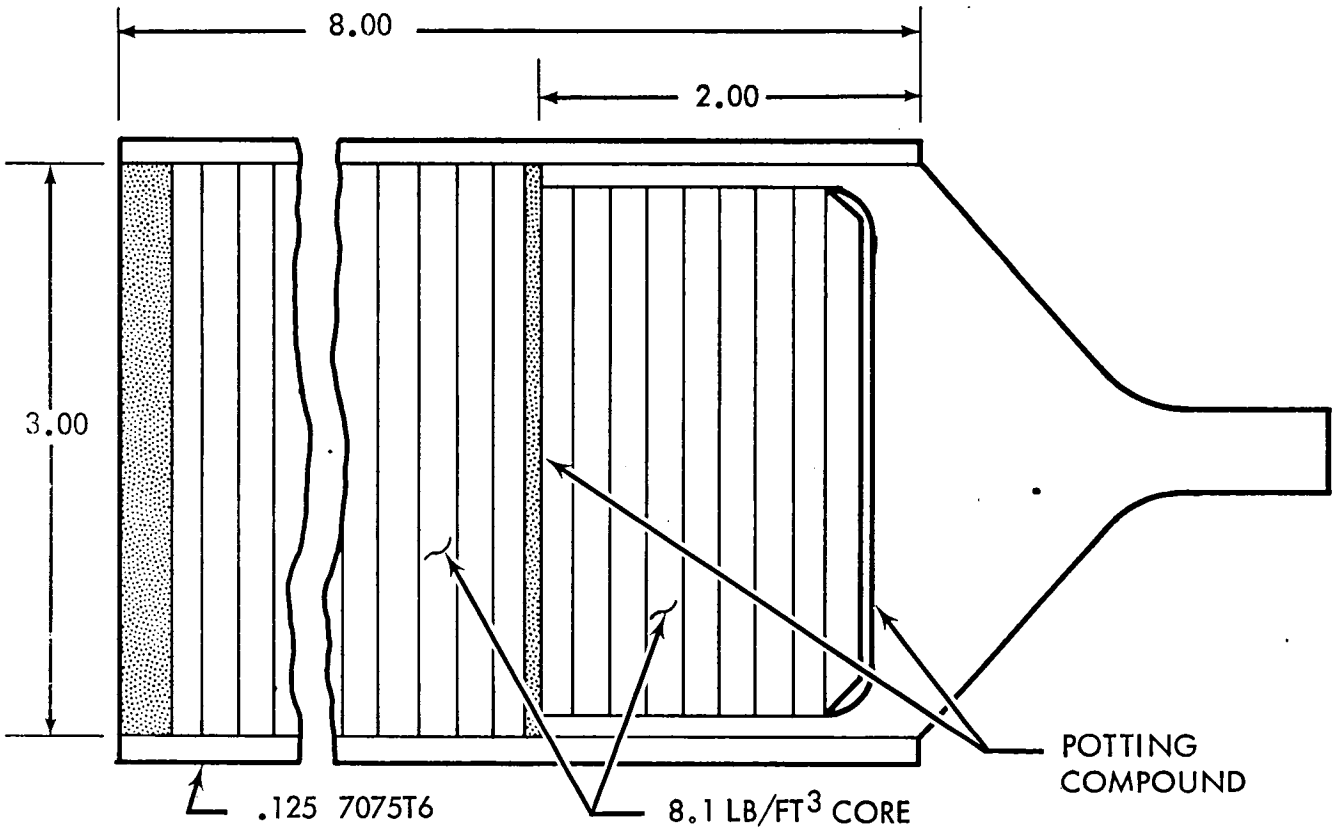

Figure 4-4 BONDED EDGEMEMBER COMPRESSION TEST SPECIMEN (3.00 INCH CORE)

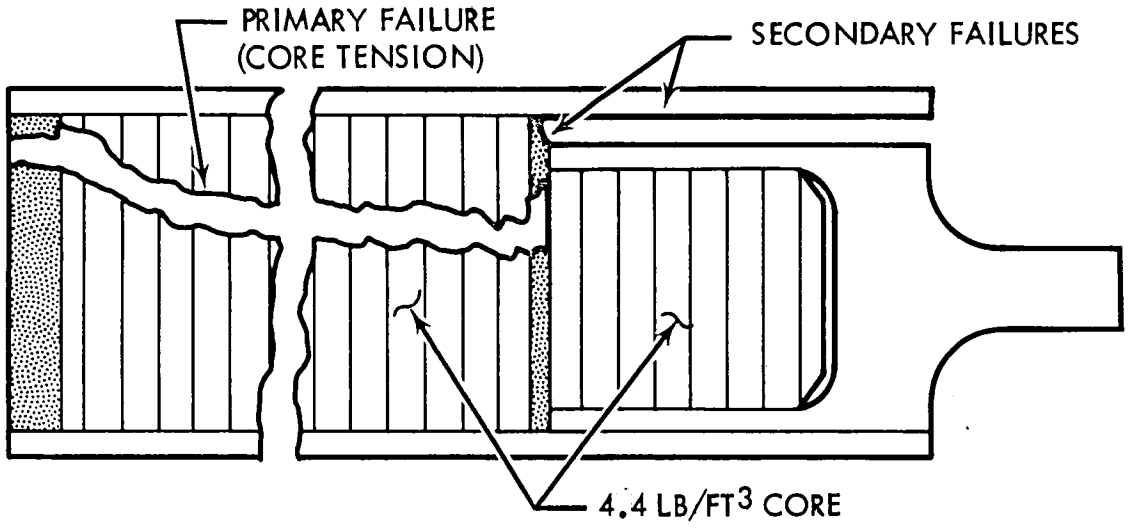

Figure 4-5 MODE OF FAILURE FOR 4.4 LB/FT^3 CORE SPECIMENS

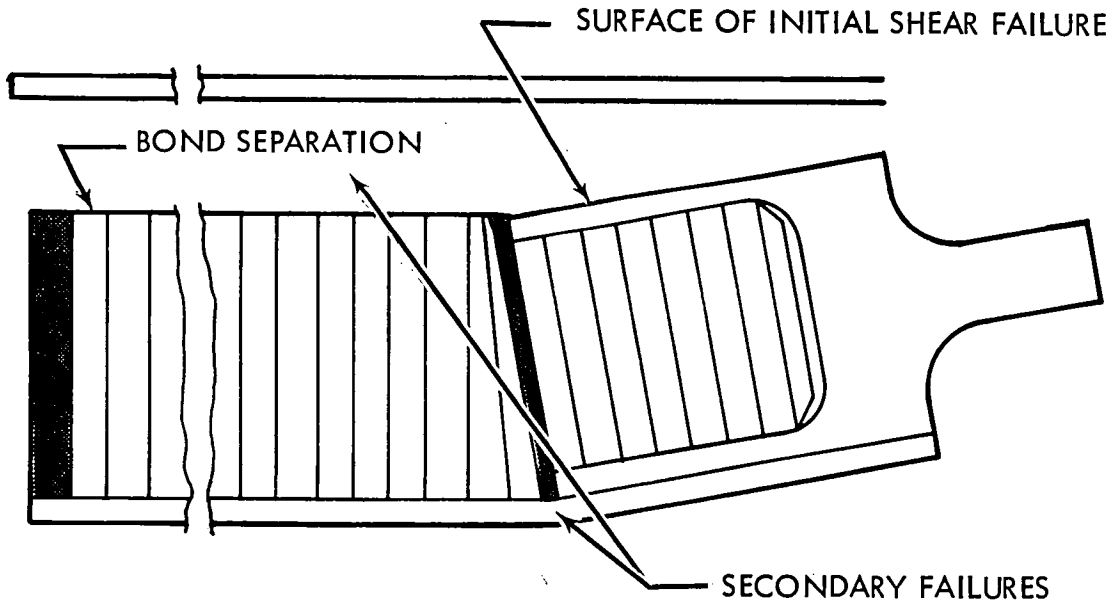

Figure 4-6 MODE OF FAILURE FOR BASIC 1.50 INCH CORE SPECIMENS

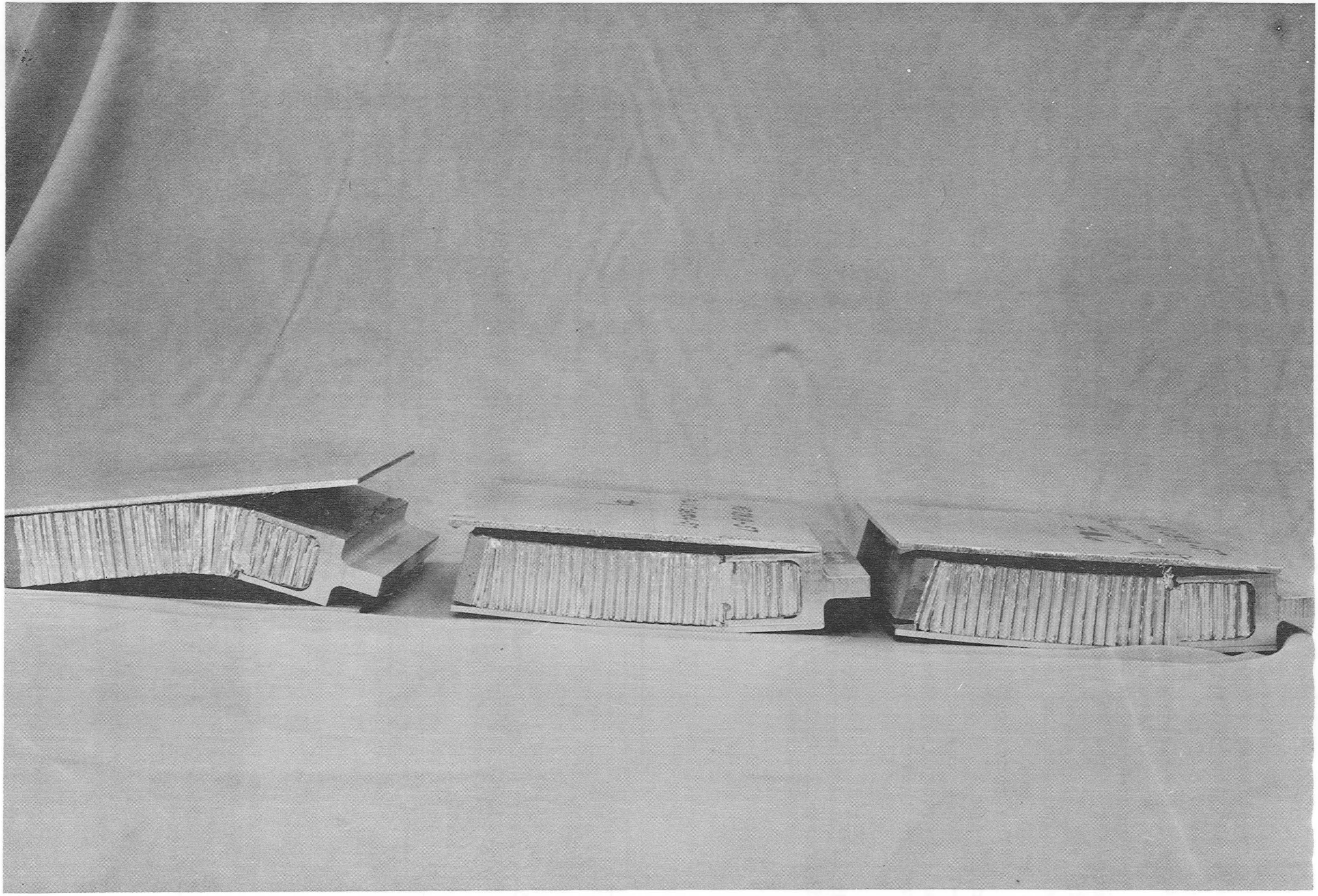

Figure 4-7 FAILED EDGEMEMBER TEST SPECIMENS, 1.50 INCH CORE, .125 SKINS

Specimens -59 a, b, and c contained the heavier and thicker core and the thinner adhesive as noted in Table 4-1. The failed specimens had the same appearance as that of the -57 f, g, and h specimens as shown in Figure 4-8.

Specimens -61 d, e, and f had the heavier core and the thicker adhesive. The failed specimens had the same appearance as that of the -57 f, g, and h except for one specimen in which the edgemember failed in tension as shown in Figure 4-9.

The range of the acceptable test data from Table 4-1 is shown in Figure 4-10 plotted on the L/t curve from Figure A-5. Figure 4-10 shows that the edgemember design is capable of developing the full strength of the adhesive for these particular skin gages, overlap lengths, and panel thicknesses.

Bolted Joint - The results for the bolted joint tests are shown in Table 4-2. The basic specimen configuration is shown in Figure 4-11.

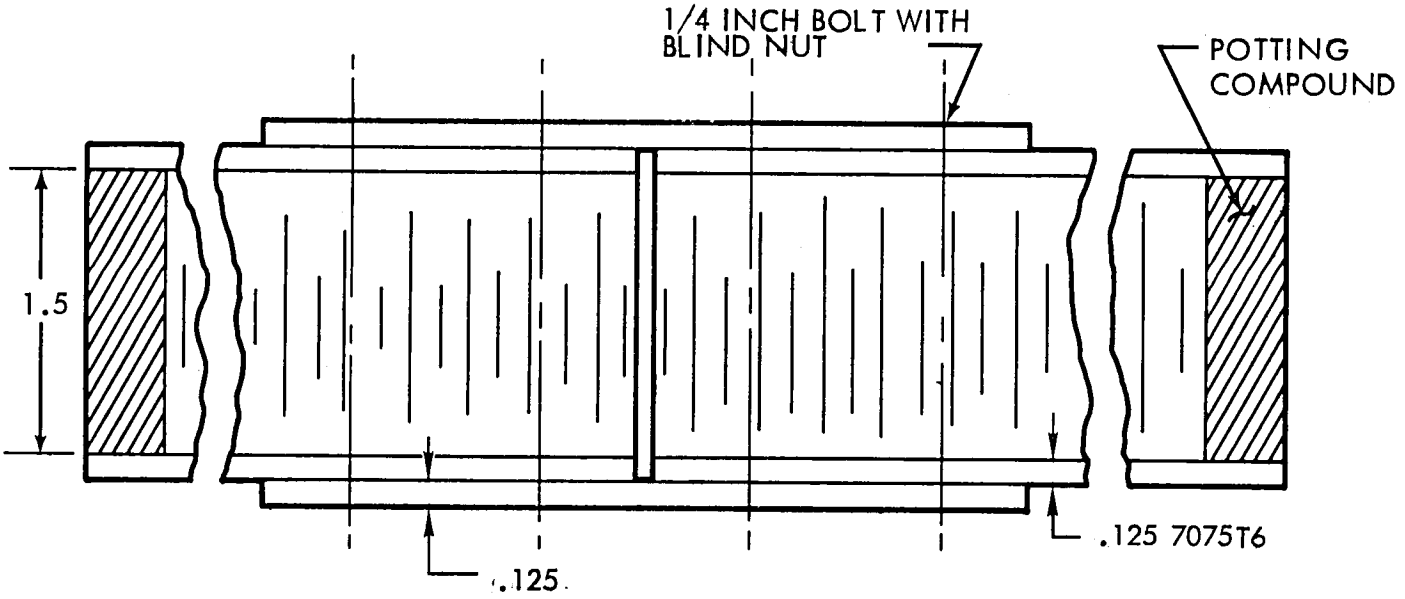

Figure 4-11 BOLTED SPLICE JOINT SPECIMEN

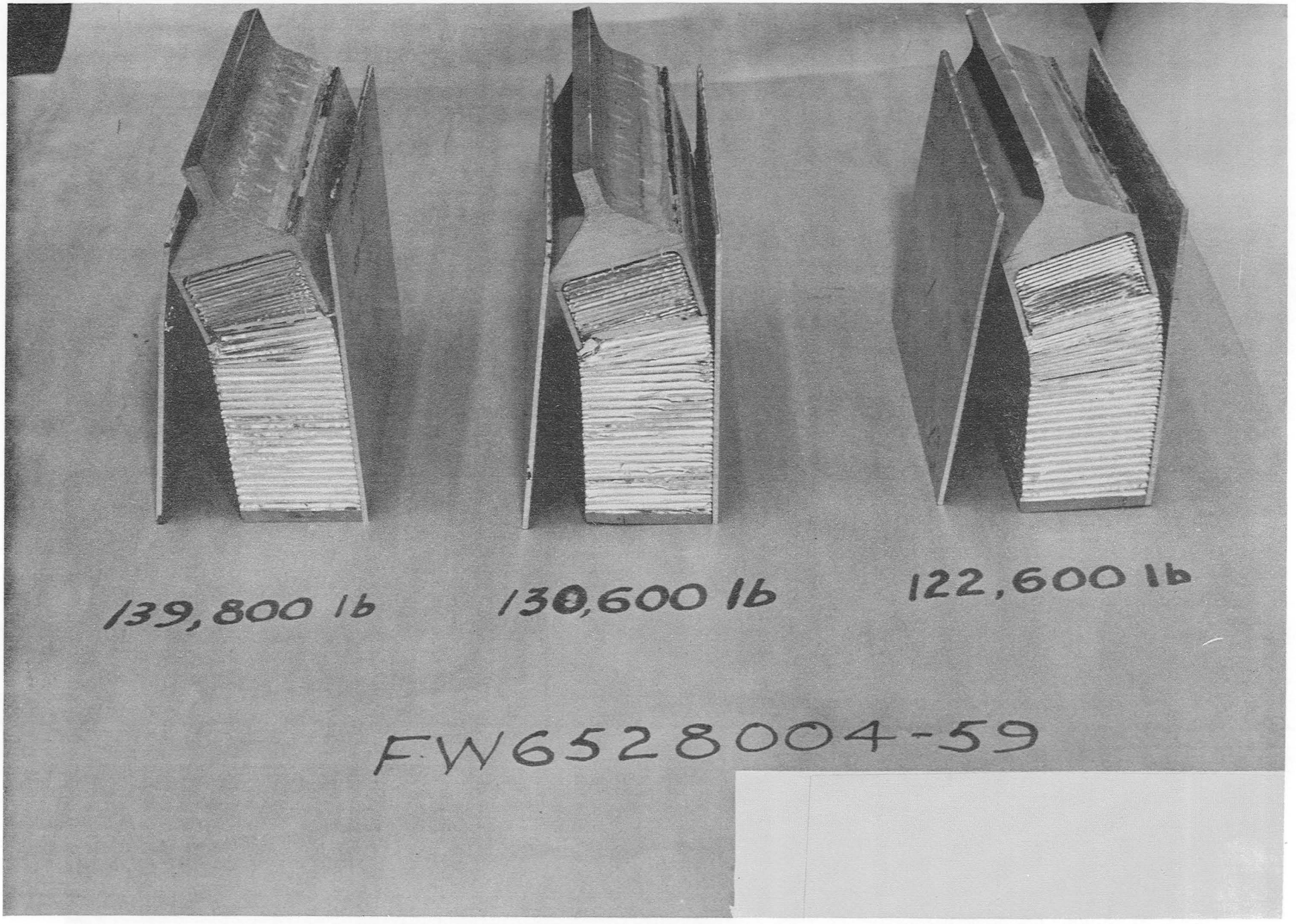

Figure 4-8 FAILED EDGEMEMBER TEST SPECIMENS, 3.00 INCH CORE, .125 SKINS

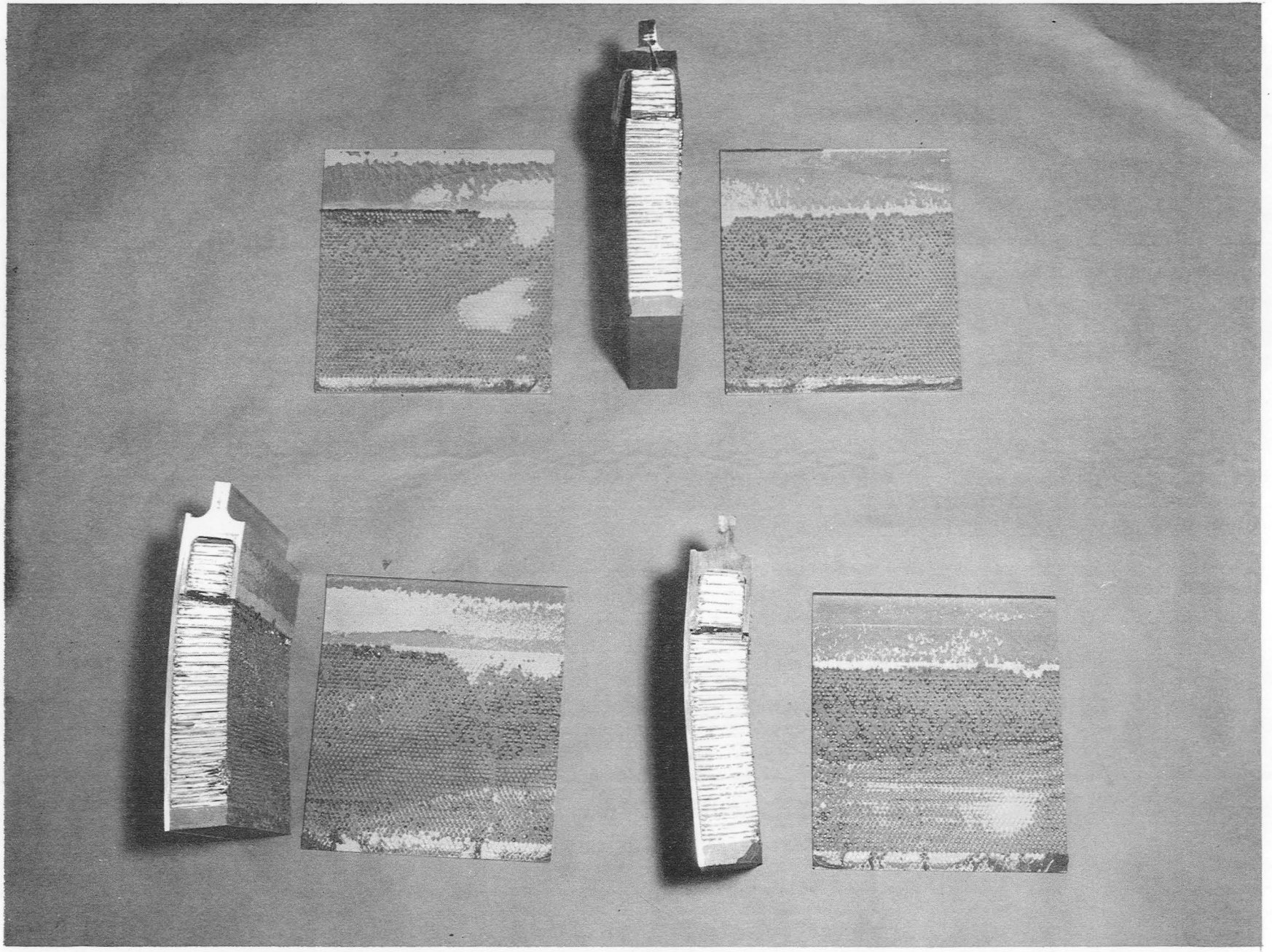

Figure 4-9 FAILED EDGEMEMBER TEST SPECIMENS, 1.50 INCH HEAVY CORE, THICK ADHESIVE

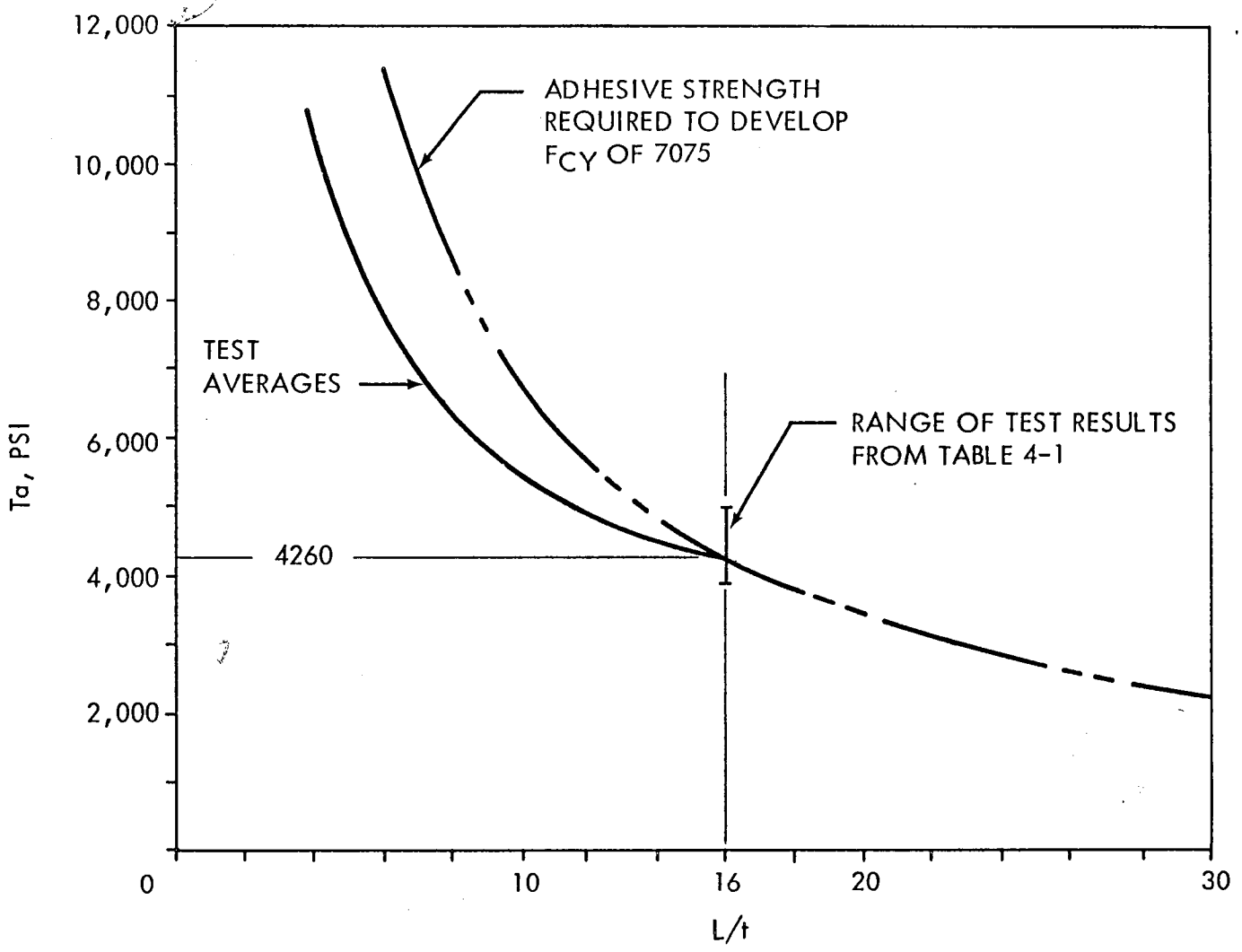

Figure 4-10 BONDED EDGEMEMBER COMPRESSION TEST DATA

Table 4-2 BOLTED SPLICE JOINT TEST DATA

SPECIMEN	CORE DENSITY (LB/FT^3)	BOLT CONFIGURATION	FAILING LOAD (LB/INCH WIDTH)	SKIN STRESS (PSI)	FAILURE
809a	4.4	STANDARD	11,000	44,000	CORE TENSION
b	4.4	STANDARD	11,500	46,000	CORE TENSION
c	8.1	STANDARD	10,100	40,400	CORE-TO-SKIN BOND
d	8.1	STANDARD	11,900	47,500	CORE-TO-SKIN BOND
e	23.0	STANDARD	14,800	59,000	CORE-TO-SKIN BOND
f	8.1	STANDARD EXCEPT EIGHT WERE THRU BOLTS	19,600	78,300	SKIN BUCKLE
g	8.1	STANDARD EXCEPT EIGHT WERE THRU BOLTS	21,000	84,000	SKIN BUCKLE
h	4.4	STANDARD EXCEPT THREE THRU BOLTS ADDED	16,000	64,000	SKIN BUCKLE

Differences in configurations between specimens are described in Table 4-2 along with the test results. The standard bolt configuration consisted of a total of sixty 1/4 inch bolts with blind nuts arranged as shown in Figure 4-1, Sheet 2. The test results show that reinforcing the core in the area of bolted splice joints will be required. This reinforcement could be in the form of heavier density core in the local areas of the splice or a relatively small number of thru bolts spaced advantageously along the splice.

4.3.1.2 Shear

All of the specimen configurations and test data are described in Table 4-3. A typical shear test specimen which has been sectioned in order to show internal details is shown in Figure 4-12. All of the shear test specimens are shown in Figure 4-16 after testing and Figures 4-17 through 4-21 show particular failed test specimens. The majority of the specimens were disassembled in the metal-to-metal bond area after failure by sawing the edgemembers free of the specimens. All specimens, except for -801 f, failed in the facing-to-edgemember bond and the sawcut after failure allowed the bond area to be visually inspected as shown in Figures 4-17 through 4-21.

The first .125 inch skin gage panel which was instrumented and tested is shown in Figure 4-22 after failure. The photoelastic material and strain gage locations are evident and the points at which readings were made of the photoelastic material are also shown.

Observations of the photoelastic material during this particular test indicated the presence of high stress concentrations in the skins at each of the four corners near the corner radius as shown in Figure 4-23. The concentration of stress in this area was objectionable because of the close proximity of the bond area under evaluation. Complete removal of the stress concentrations from tests of specimens which had already been fabricated appeared to be impractical; therefore, in order to move the area of stress concentration away from the facing-to-edgemember bond, the specimens were modified on all four corners as shown in Figure 4-24.

Table 4-3 SHEAR TEST RESULTS

SPECIMEN CONFIGURATION					TEST RESULTS		
DASH NO.	THICKNESS FACING	THICKNESS CORE	CORNER(2) MOD.	CONFIGURATION DESCRIPTION	FAILING LOAD - LB	SKIN SHEAR STRESS - PSI	BOND STRESS - PSI
5a	.125	1.5	NO	SEE FW6528004(1)	184,000	30,600	2,040
5b	.125	1.5	NO	SEE FW6528004	178,000	29,700	1,980
5c	.125	1.5	YES	SEE FW6528004	215,000	35,800	2,390
801a	.250	1.5	NO	SEE FW6528004	306,000	25,500	1,700
801b	.250	1.5	YES	SEE FW6528004	300,000	25,000	1,670
801c	.250	1.5	YES	SEE FW6528004	309,000	25,700	1,720
801d	.250	1.5	YES	SEE FW6528004	316,000	26,300	1,760
801e	.250	1.5	YES	SEE FW6528004	336,000	28,000	1,870
801f	.250	1.5	YES	SEE FIGURE 4-13	500,000	41,700	-
803a	.375	1.5	YES	SEE FW6528004	367,000	20,400	2,040
803b	.375	1.5	NO	SEE FW6528004	401,000	22,200	2,220
807a	2.50	3.0	YES	SEE FW6528004	359,000	30,000	2,000
807b	2.50	3.0	YES	SEE FIGURE 4-14	342,000	28,500	1,900
811a	.200/.250	1.5	YES	SEE FW6528004	313,000	32,600	1,740
815a	.125/.188	1.5	NO	SEE FW6528004(4)	215,000	23,900	2,390
815b	.125/.188	1.5	NO	SEE FW6528004	190,000	21,100	2,110
817a	.250/.375	1.5	NO	SEE FW6528004(3)	249,000(5)	-	-
817b	.250/.375	1.5	NO	SEE FW6528004	352,000	19,600	1,960
819a	.125	1.5	YES	SEE FIGURE 4-15	240,000	40,000	2,670
819b	.125	1.5	YES	SEE FIGURE 4-15	251,000	41,800	2,790

NOTES:
(1) Drawing FW6528004 is presented as Figure 4-1 in this report.
(2) The corner modification is described in a later paragraph.
(3) The 817 specimens were modified with the addition of 3/8 diameter bolts in the doubler area as shown in Figure 4-20.
(4) The 815 specimens were modified with the addition of 5/16 diameter bolts in the doubler area.
(5) The 817a specimen had a damaged bond prior the test.

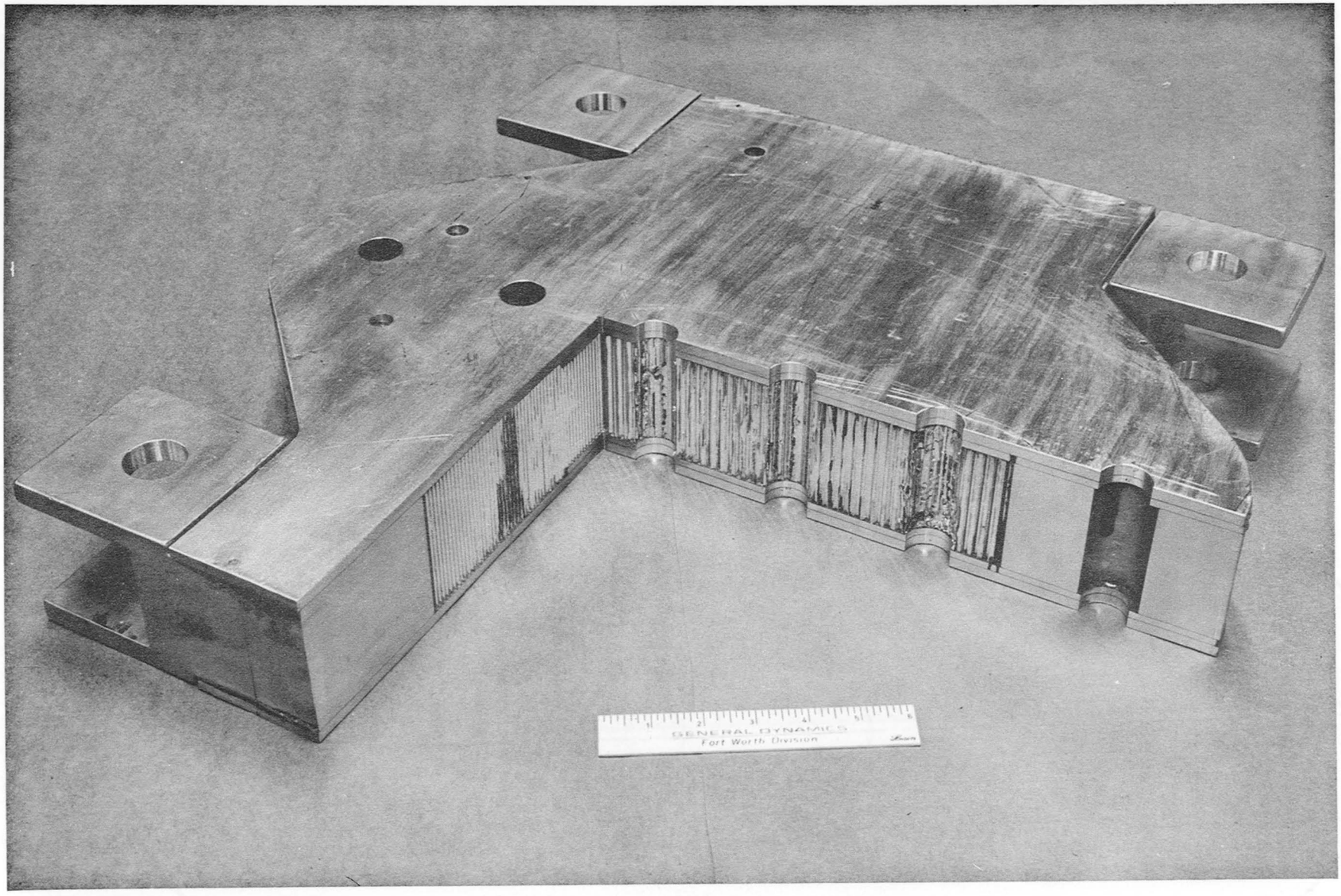

Figure 4-12 SHEAR TEST SPECIMEN

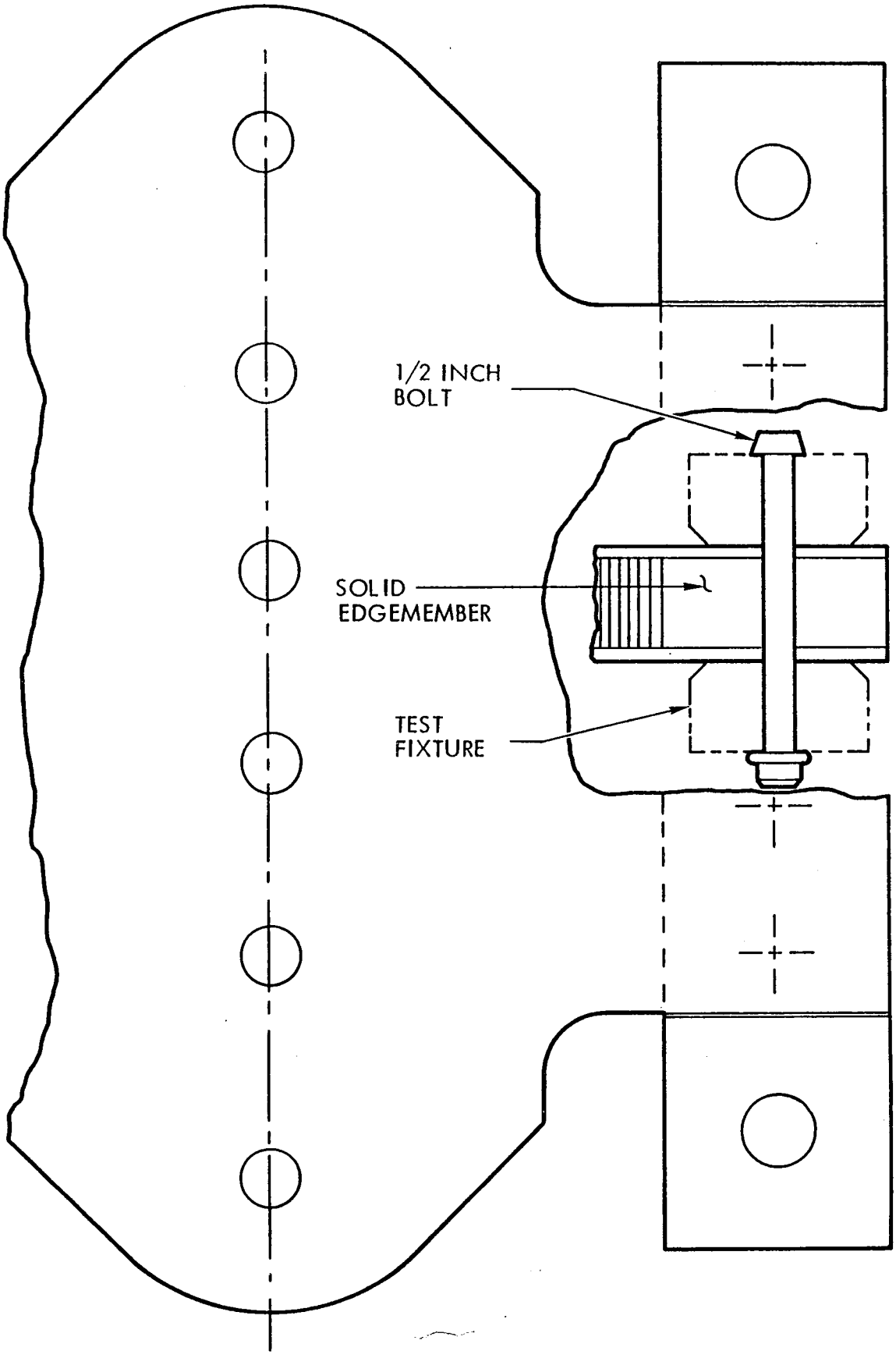

Figure 4-13 BONDED-BOLTED SPECIMEN CONFIGURATION

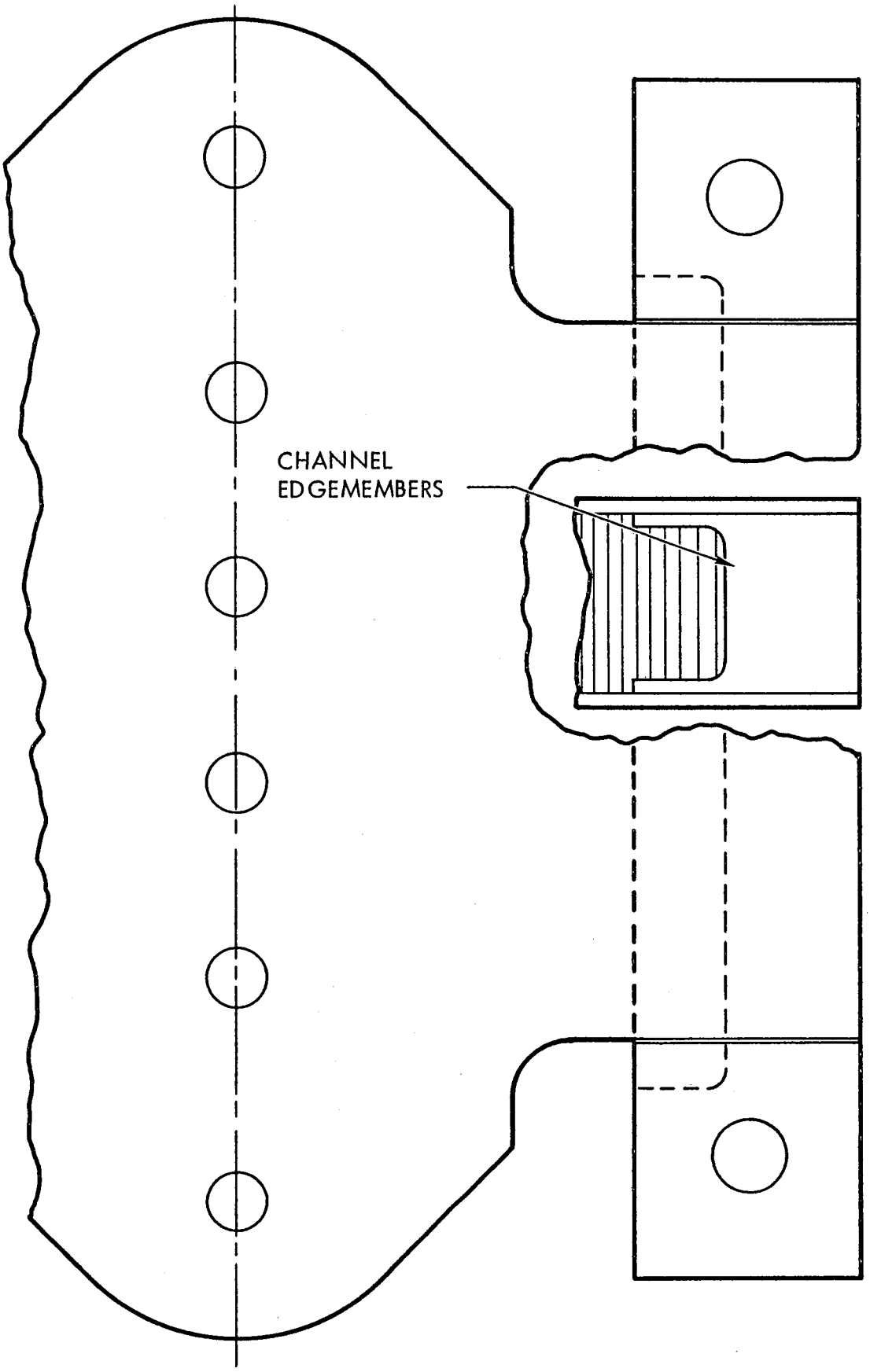

Figure 4-14 SPECIMEN CONFIGURATION - CHANNEL EDGEMEMBERS

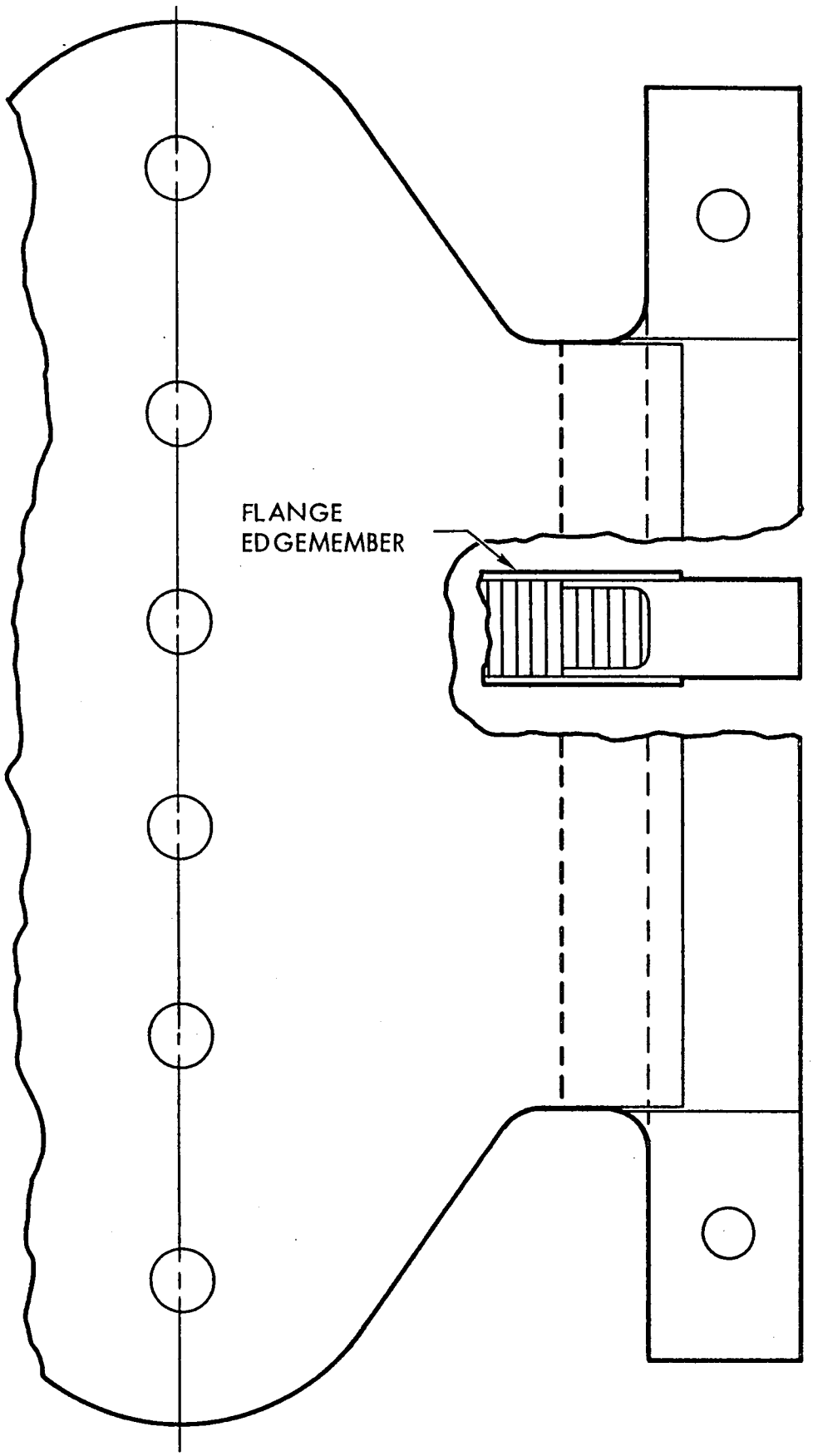

Figure 4-15 SPECIMEN CONFIGURATION - FLANGE EDGEMEMBERS

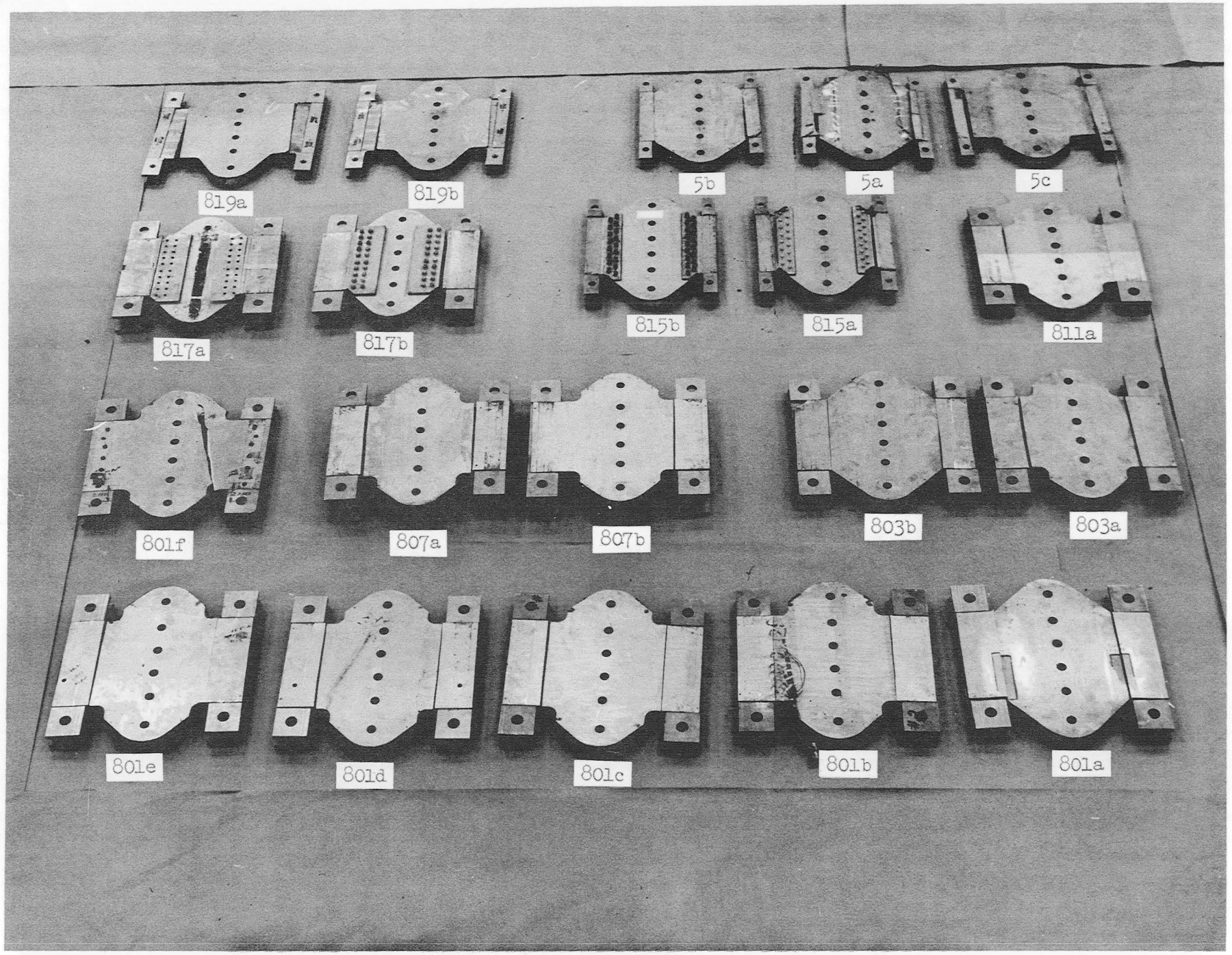

Figure 4-16 SHEAR TEST SPECIMENS AFTER TESTING

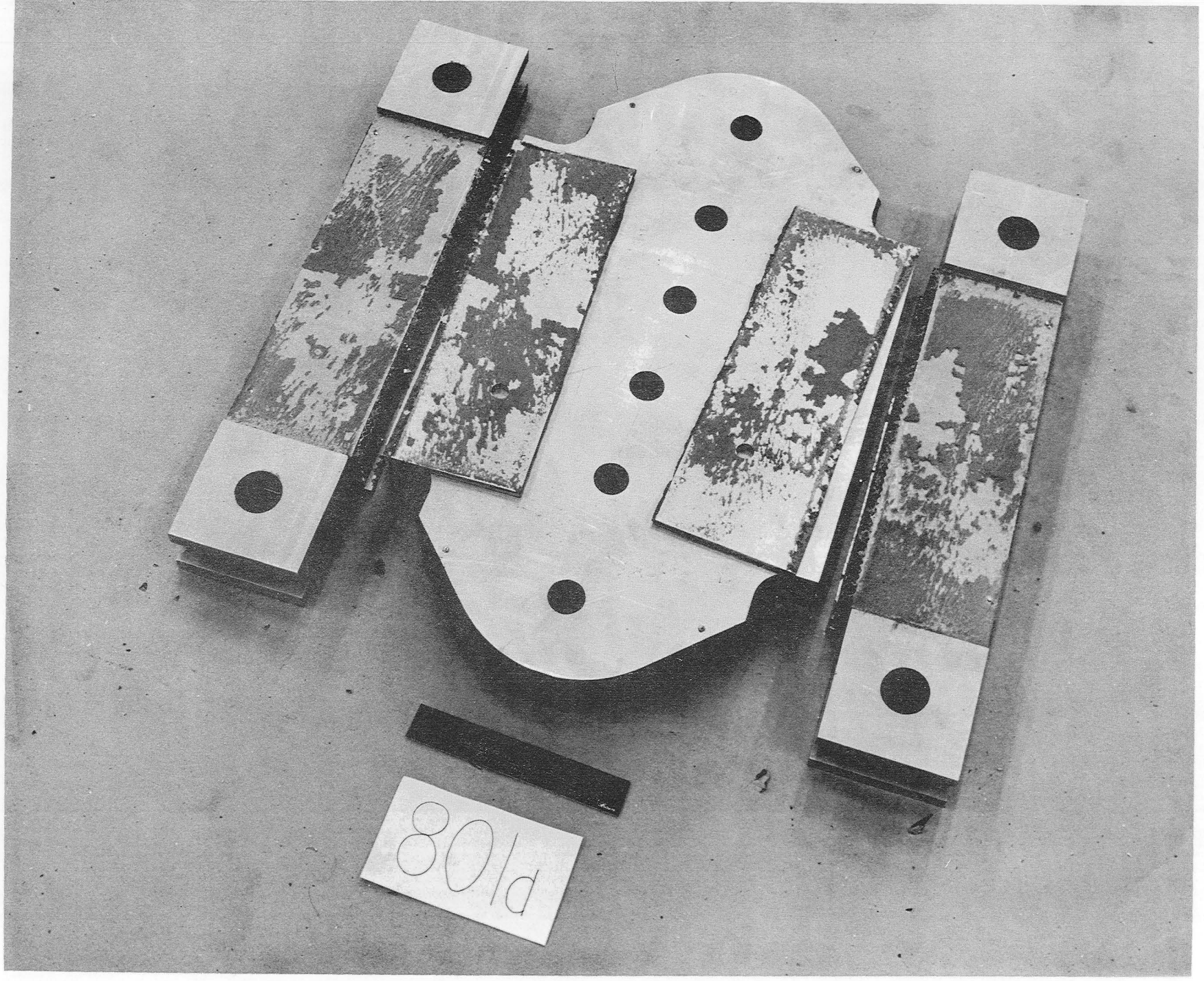

Figure 4-17 TYPICAL SHEAR TEST SPECIMEN - .250 FACINGS

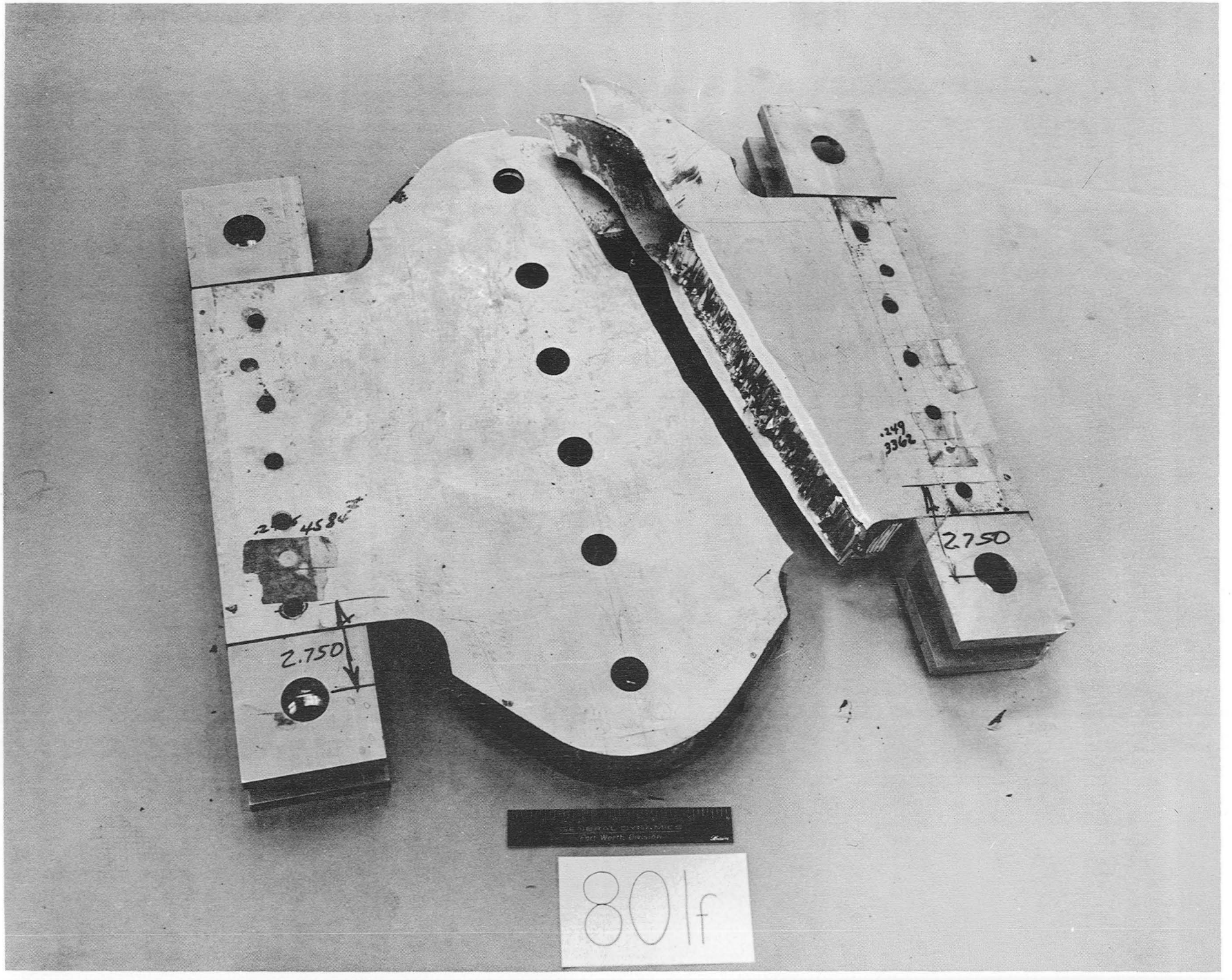

Figure 4-18 BONDED-BOLTED SHEAR TEST SPECIMEN

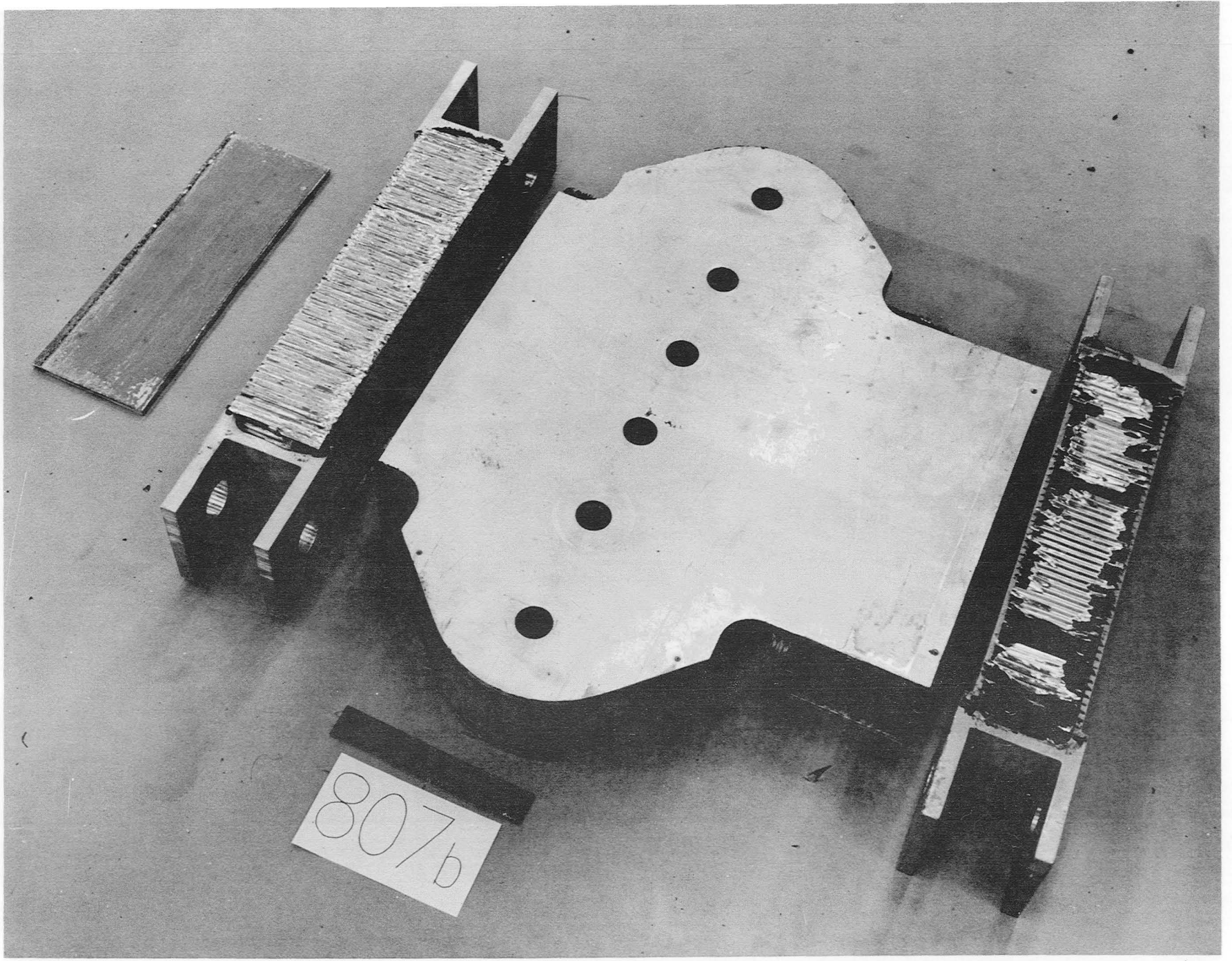

Figure 4-19 MODIFIED SHEAR TEST SPECIMEN - .25 FACINGS, 3.0 INCH SANDWICH, CHANNEL EDGEMEMBERS

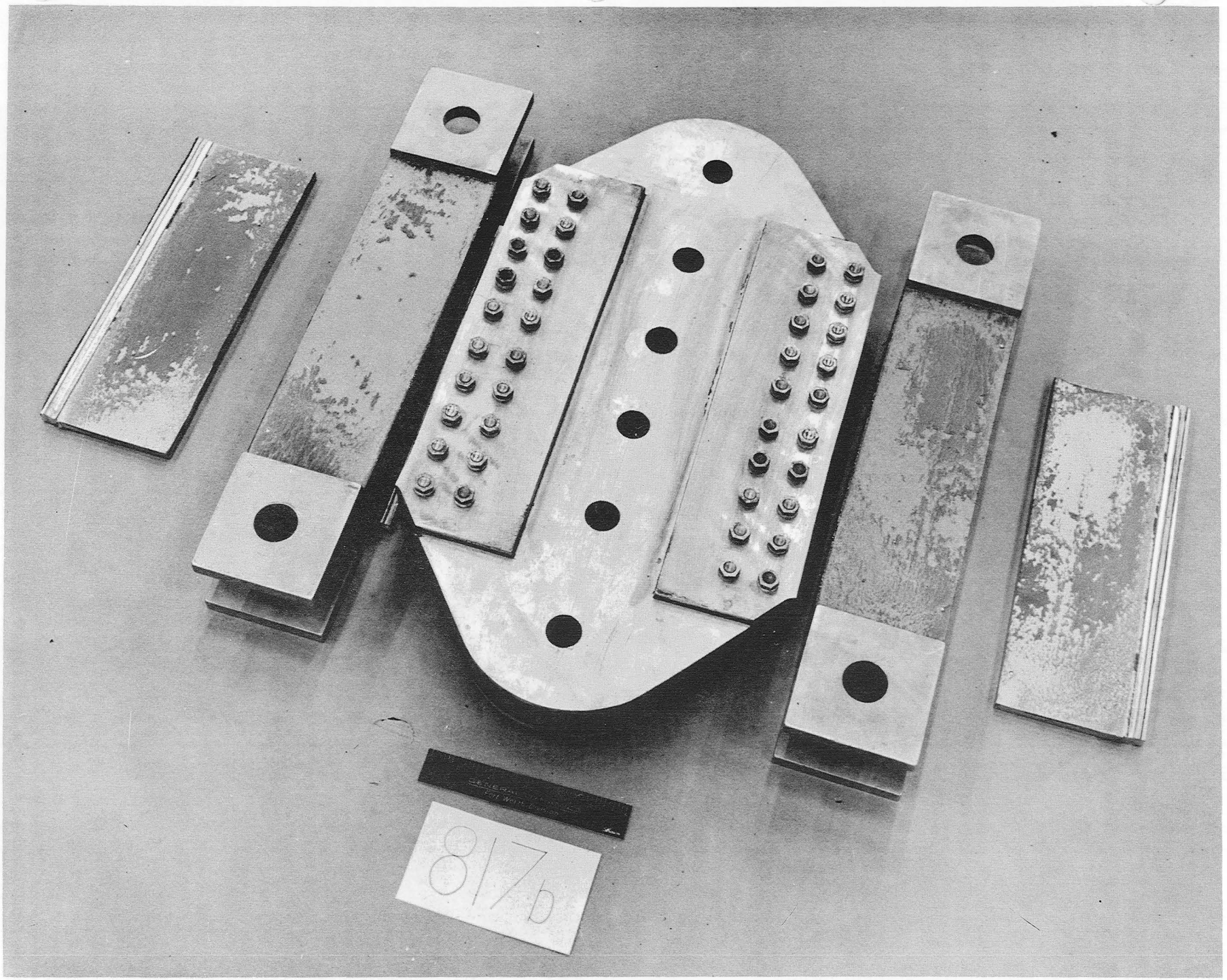

Figure 4-20 WELDED SHEAR TEST SPECIMEN - .250-.375 FACINGS

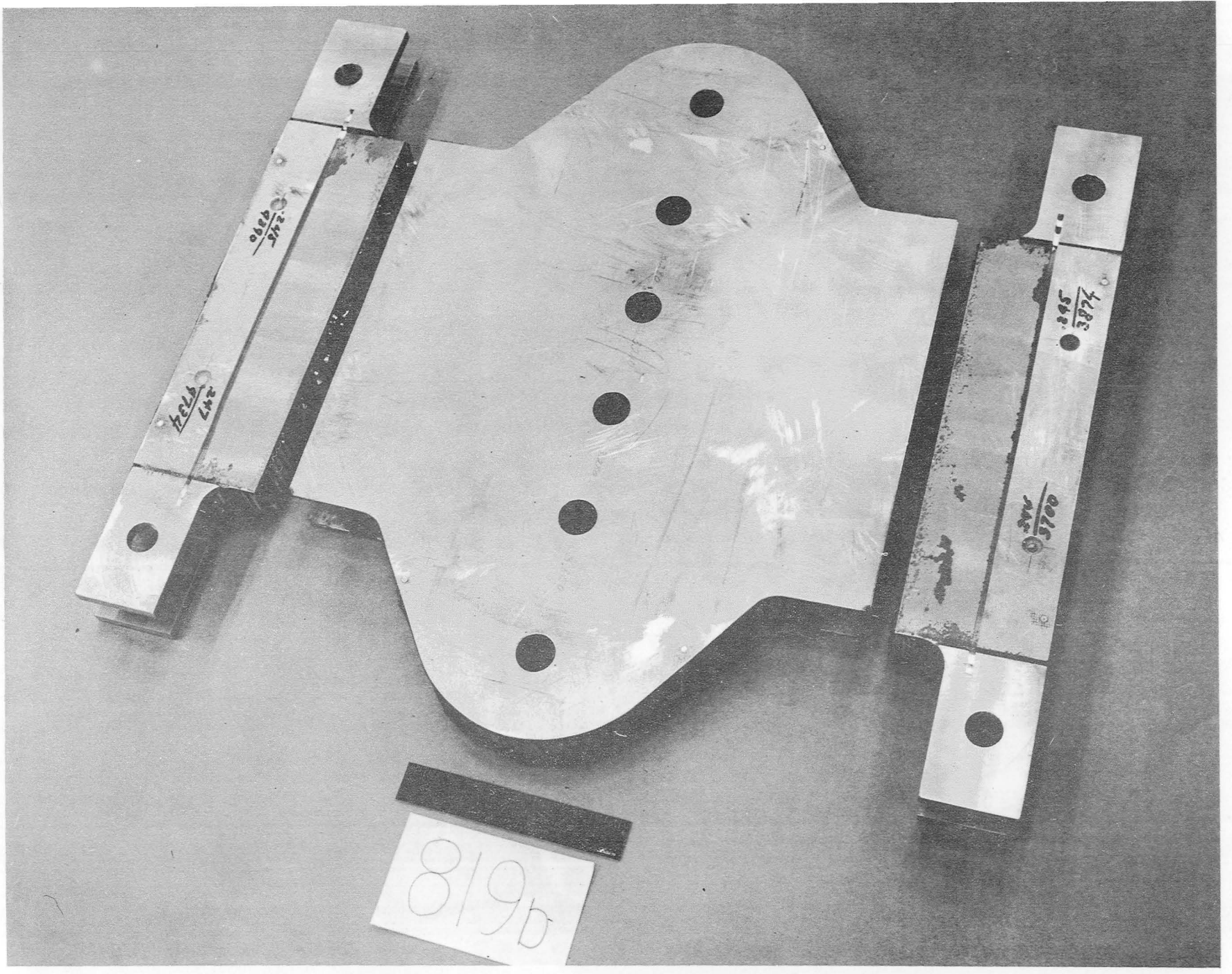

Figure 4-21 MODIFIED SHEAR TEST SPECIMEN - .125 FACINGS, FLANGE EDGEMEMBERS

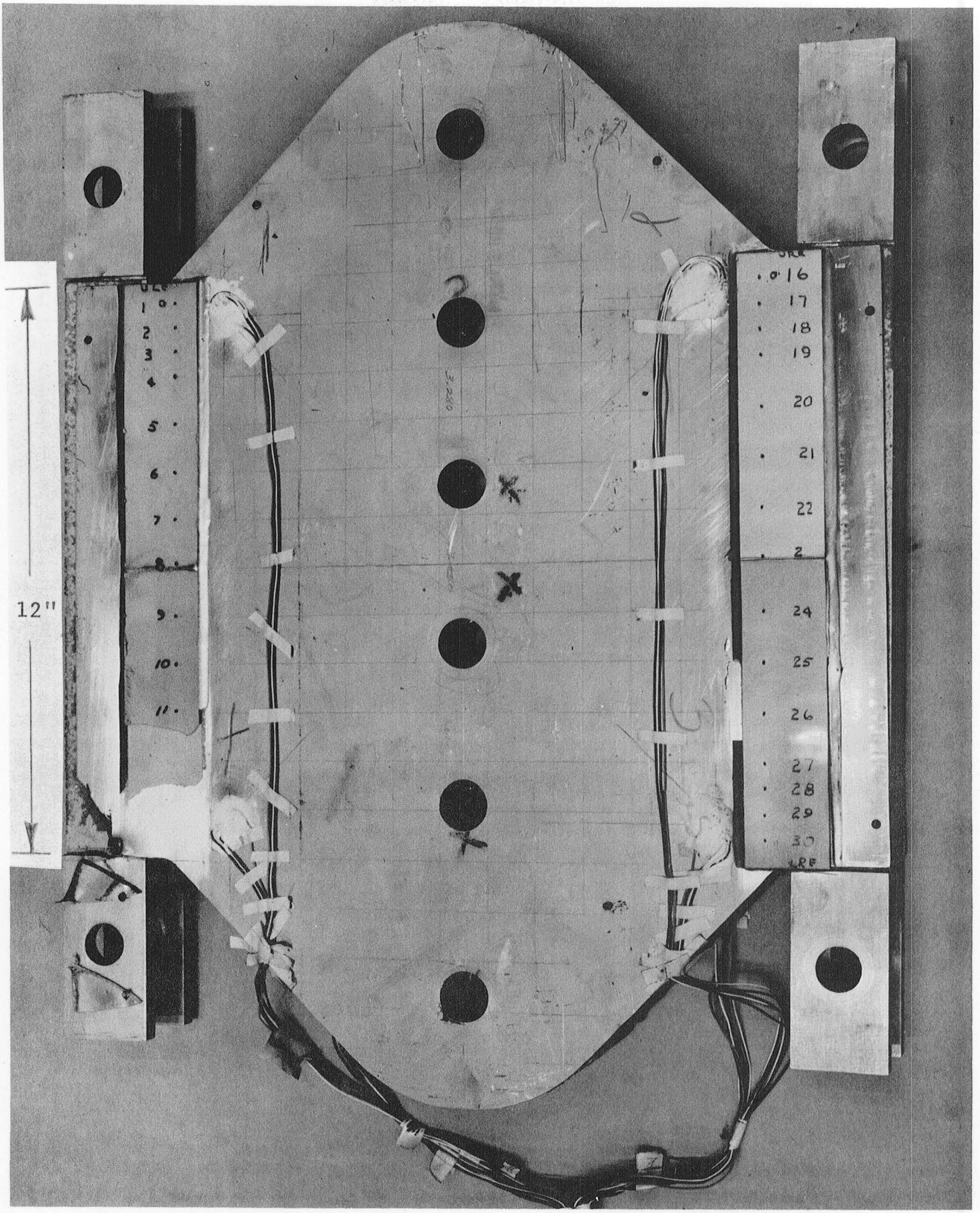

Figure 4-22 SHEAR TEST SPECIMEN WITH INSTRUMENTATION

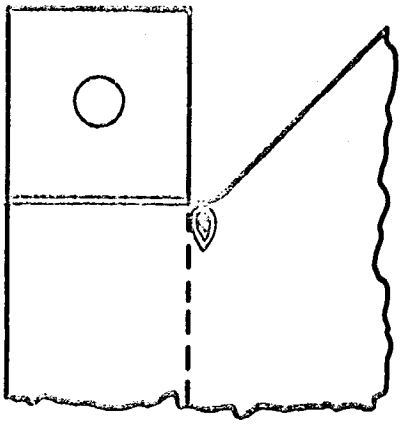

Figure 4-23 STRESS CONCENTRATIONS IN SHEAR SPECIMENS

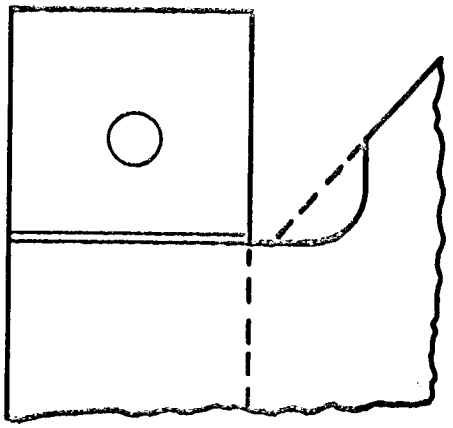

Figure 4-24 MODIFICATION OF CORNERS OF SHEAR SPECIMENS

A .250 skin gage shear specimen, modified as shown in Figure 4-24, was instrumented in the same manner as earlier specimens except that eight strain gages were applied in a line along one edge. Observations of the photoelastic material indicated that the stress concentrations had moved away from the skin-to-edgemember bond.

Locations of strain gages and distributions of horizontal normal and vertical shear stresses in the skin at 50 percent maximum expected load are shown in Figure 4-25. It should be noted that the normal stress distribution in the skin resembled a bending stress distribution and that the vertical shear stress in the skin was approximately uniform for 83 percent of the bond length. This type of distribution of stresses was considered to be typical of all corners and all other shear specimens.

These shear tests have established the significance of the shape of the sandwich panel edgemember cross-section. The particular design requirement of the shear specimens was to transfer loads from an edgemember to sandwich facings through an adhesive bond in manners which simulate possible load transfer methods in the areas of vertical longerons and splices. The design configuration which received the most emphasis during this test program consisted of solid edgemembers bonded to the sandwich facings. Observations of the photoelastic materials during the initial tests indicated the presence of very high stress gradients in the facings, and resulting high shear stresses in the bonds, over the innermost edge of the solid edgemembers. Analyses, which have been developed and are presented in Appendix B, later indicated that a peak in the adhesive shear stress of a magnitude approximately eight times the calculated average shear stress was present as shown in Figure 4-26. The peak in the adhesive stress was created by the inability of the solid edgemember to deform locally with the shear deformation of the sandwich facings. This peak in the adhesive shear stress appeared to govern the load capability of the bonded joint and rendered a portion of the edgemember width ineffective for load transfer. Two approaches were utilized in attempting to transfer additional load from the edgemembers to the sandwich sections.

The first approach was to reduce the effective edgemember thickness bonded to the sandwich facings so that the edgemember could deform with the sandwich facings along the innermost edge of the edgemember. The 807b specimen was modified as shown in Figure 4-14 by removing edgemember material to form a channel with legs of approximately the same thickness as the sandwich facings. The test of this specimen did not show improvement because the ends of the channel legs were restrained from deforming in the areas where the edgemember again assumed a solid cross section. Two 819 specimens

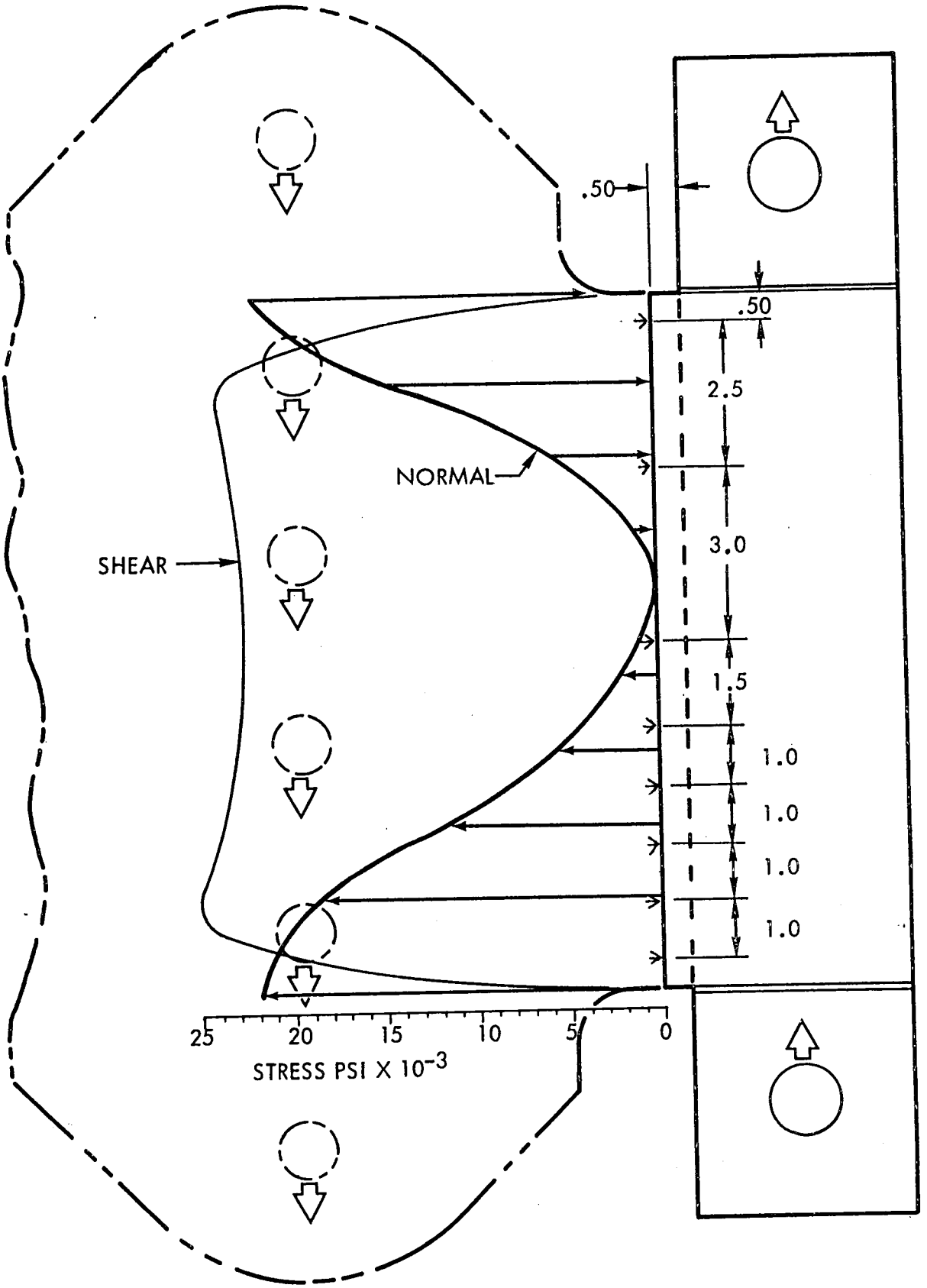

Figure 4-25 SKIN STRESS DISTRIBUTIONS ON SHEAR SPECIMENS

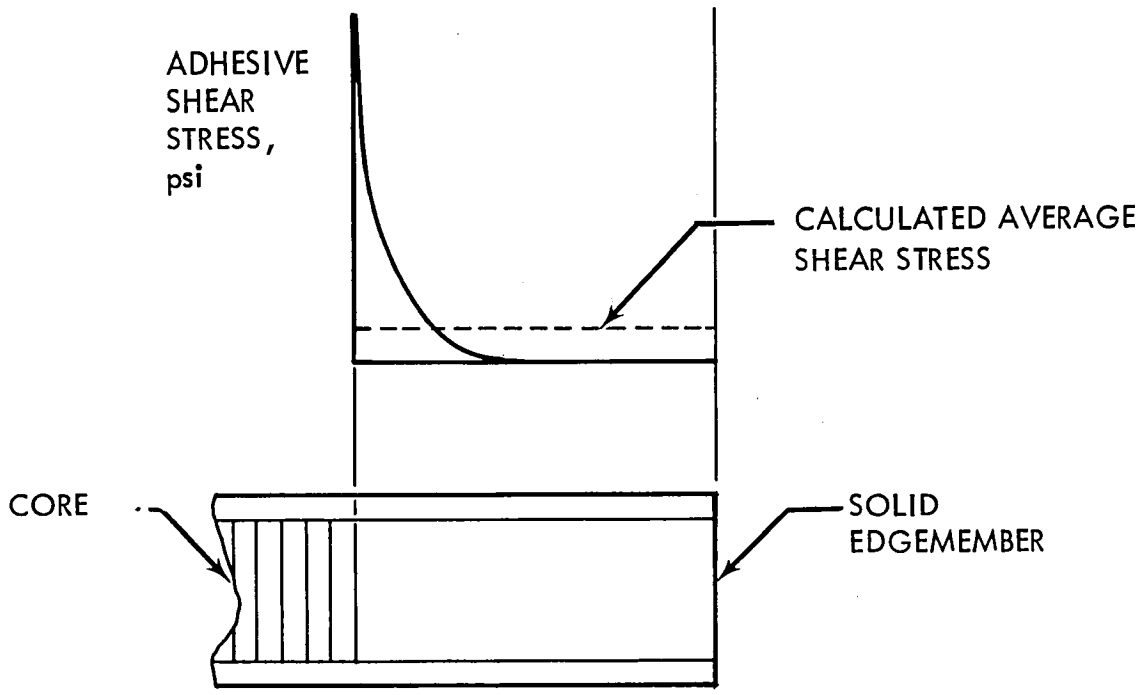

Figure 4-26 ADHESIVE SHEAR STRESS DISTRIBUTION

were then designed and fabricated as shown in Figure 4-15. For these specimens the ends of the flanges were not restrained and were allowed to deform with the sandwich facing. The test data shown an improvement in the load transfer capability of this type of edgemember.

The second approach was to add bolts through the test fixture, sandwich facings, and edgemembers as shown in Figure 4-13 so that load could be transferred from the edgemember to the facings by an adhesive bond and also from the test fixture to the facings by bolts in bearing. In this configuration the test fixture represented external longerons which are required in the areas of hold-down and rebound loads. The test of this specimen failed the sandwich facings as shown in Figure 4-18.

4.3.2 Fabrication Evaluations

Because of the utilization of standard methods of fabricating the test specimens of this test program, several observations have been made of variables which will be present in the fabrication of full scale hardware. Discussions are provided below of the general theory of bonding variables and then the influences of the variables which were observed during fabrication of the test specimens are discussed.

4.3.2.1 Prefit

The most influential single contributor to the introduction of fabrication variables is an inadequate prefit of details prior to bonding. Prefit is required in order to assure that the thicknesses of slugs and edgemembers relative to the surrounding core are such that nominal adhesive thicknesses are obtained in the skin-to-slug bond areas. For example, if the core is much higher then the adjacent slug as shown in Figure 4-27, the core will support the skin

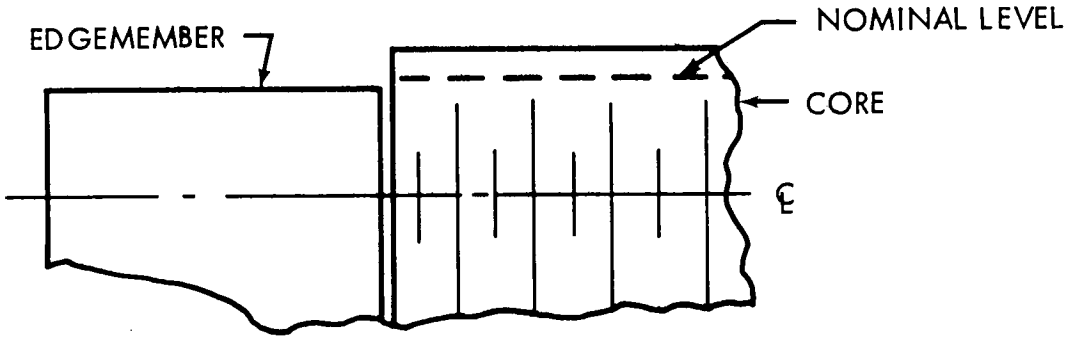

Figure 4-27 PREFIT OF SKIN TO SLUG AND CORE

during bonding. This condition can result in either thick bond lines, tapered bond lines, or local areas of insufficient bond pressures. Improper prefit can also permit bond contamination by allowing foreign materials, such as core splice potting compounds, to enter the adhesive during cure. Any of the conditions can result in lower average bond shear strengths. Prefit of details is especially important in heavy gage structure because of the inherent greater bending stiffnesses of heavier gage skins and the resulting tendency on the part of these skins to retain their own contours and not conform with the other details under bonding pressures.

Although these variables have been observed in previous programs to be critical, their presence in selected shear specimens of this program apparently did not affect the shear test results to much extent. Possible reasons for the test results not being affected are discussed below:

1. The shear stress distribution in a bonded joint tends to peak higher as adhesive shear modulus increases or bond line thickness decreases. The load capability of that joint depends on the magnitude of the peak stress and the shear strength of the adhesive. The core splicing material (potting compound) which squeezed out into the adhesive between the edgemember and facing on some specimens is thought to have lower shear strength and modulus than the MB329 adhesive. Then, for the type of joint where the edgemember is a solid section, the elastic and strength properties of different adhesives can compensate and as a result the bonded joint can have approximately the same load carrying capability for several different adhesives. In a similar manner, thick or tapered bond lines and insufficient bond pressure can be related to lower adhesive shear strength and the resulting compensation can also act to produce bonded joints with similar load carrying capabilities. Adhesive shear strength as used in this discussion is the actual maximum stress that the adhesive can sustain and not the calculated average shear strength.

2. Past experience has shown that these variables are critical in the load carrying capability of bonded joints tested in either tensile or compressive shear such as the tests described in Section 3.2. Axial tests of these types produce tensile forces normal to the plane of the bond while

the tests of the type performed on the shear specimens do not produce these normal forces. Then, if the variables described above are more susceptible to normal forces than to shear forces, the shear tests will not be affected by the variables as will the axial tests.

4.3.2.2 Cure Cycle

Another important variable which must generally be considered is the insufficient cure of the adhesive system. Several massive members which are joined together for bonding can have local areas where the heat-up rate during bonding is not uniform. If the bond cycle is not paced by the last area to reach bonding temperature, then some areas will have an insufficient dure and a possible lower average bond shear strength. Normally the heat-up rates of hardware and associated tooling is checked prior to bonding.

Some of the shear test specimens experienced variations in the cure cycle. A few specimens were brought to cure temperature, which was 350°F, in 20 minutes and others in 40 minutes as determined by thermocouples in the bond lines. In most cases, the one hour cure at bonding temperatures was measured after the bonding press reached 350°F, which was about 20 minutes after the press was closed. Figure 4-28 shows that the bond areas which are slow to heat-up may not receive the complete one hour cure at 350°. Past experience has shown that time at temperature is very critical with some adhesives but the test data generated with the shear specimens has shown that MB329 may not be susceptible to variations in cure time as long as the specimen was cured at 350° for at least 30 to 40 minutes.

4.3.2.3 Core Installation

Three methods of installing the core sections into the edgemembers for the bonded edgemember specimens were evaluated.

1. The technique that was employed for all 1.50 inch core specimens, except -57 d and e, appears to be satisfactory and lends itself to scaling up to large parts. It consists of a single stage bond which achieves surface bonds and core bonds simultaneously. The pertinent installation steps are described in Figure 4-29.

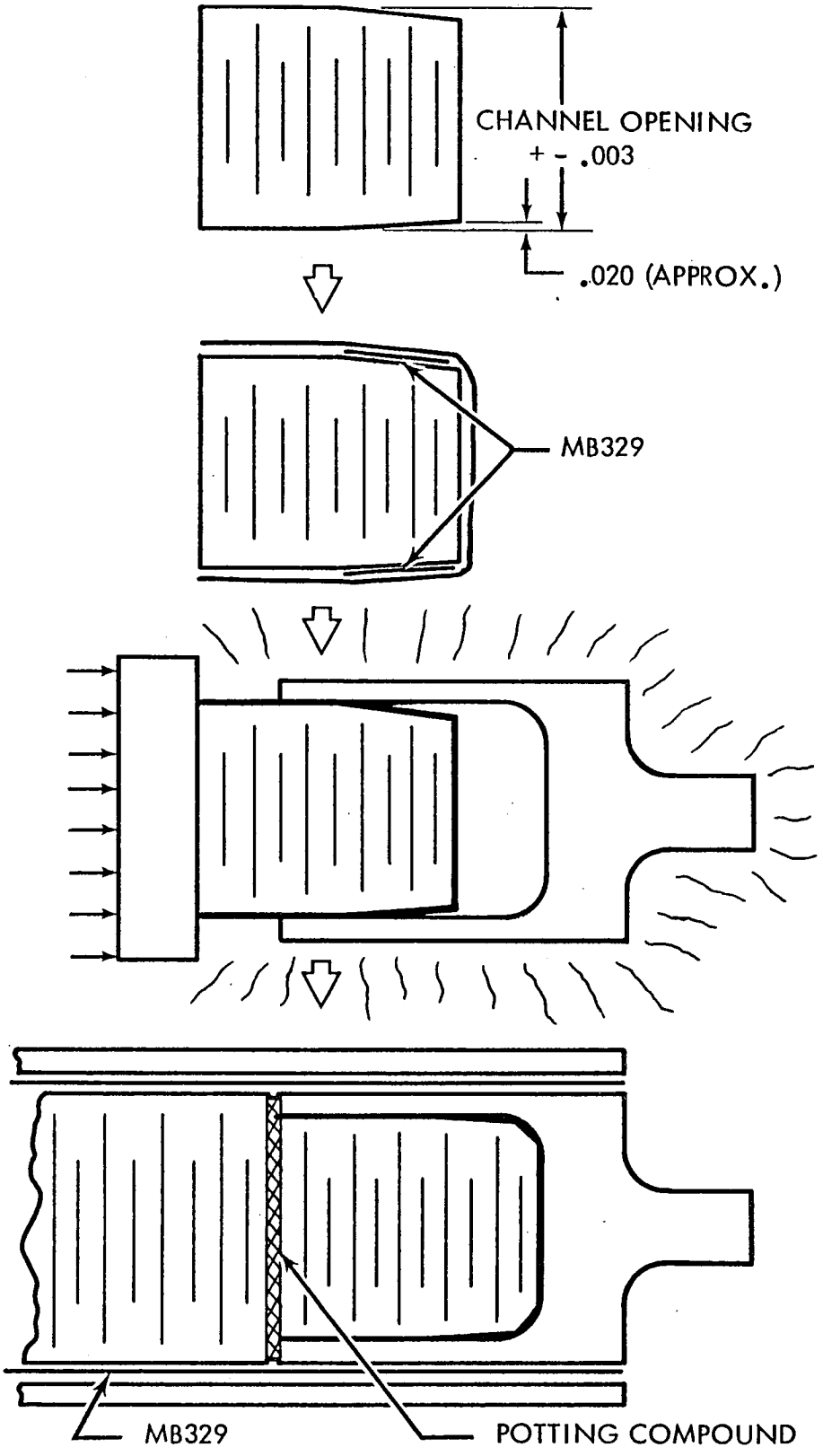

MACHINE CORE THICKNESS TO MATCH OPENING OF CHANNEL

PROVIDE A SLIGHT LEAD-IN TAPER

WRAP MB329 ADHESIVE TAPE AROUND CORE

HEAT EDGEMEMBER AND CORE INSERT (ADHESIVE SOFTENS AND BECOMES SLIPPERY)

PRESS CORE INSERT INTO CHANNEL

APPLY POTTING COMPOUND TO VERTICAL FACE OF CORE

COMPLETE LAYUP OF OTHER DETAILS

Figure 4-29 CORE INSERT INSTALLATION PROCEDURE

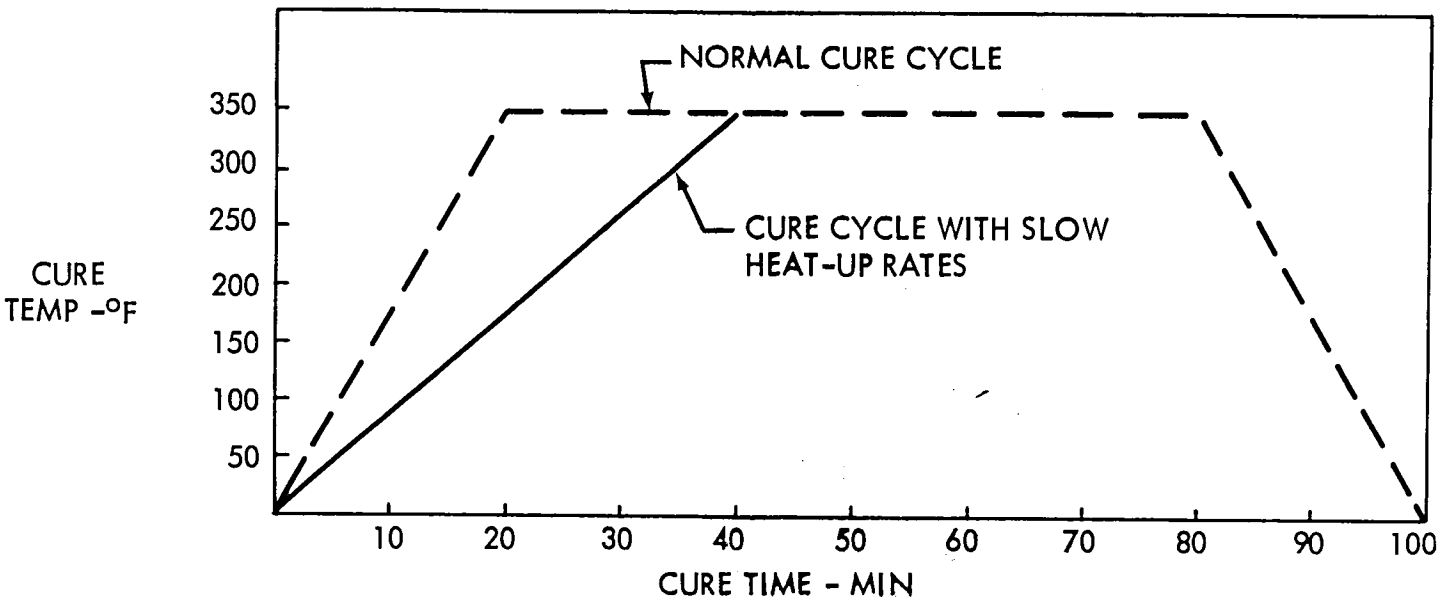

Figure 4-28 SHEAR SPECIMEN CURE CYCLES

2. A preliminary stage of prebonding the core insert does have merit in that the edgemember dimensions and the bond quality can be checked before advancing to a final stage bond. This method was used for the 3.00 inch core bonded edgemember specimens. The major disadvantage of this approach is that it is difficult to seal the part adequately (by plastic maskant) to allow it to be immersed in the acid cleaning solution. Since proper cleaning with acid is vital for good adhesion qualities, it was felt that this procedure has not been developed for use with large panels.

3. The -57 d and e specimens were fabricated with a core insert that was made to a thickness dimension which was reduced from the channel opening dimension by the total initial adhesive tape thickness, as shown in Figure 4-30.

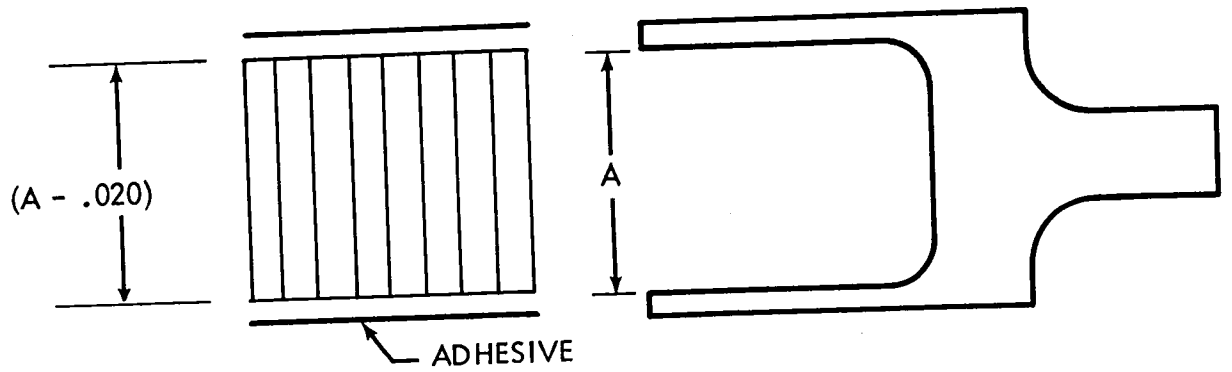

Figure 4-30 CORE INSERT WITH LOOSE FIT

Tests of these specimens failed prematurely by a bond tensile failure between the core insert and the edgemember channel. This provided sufficient evidence to support the need for a well bonded core insert.

4.3.2.4 Quality Control

All bonded panels were inspected with the through transmission ultrasonic tester to check for adhesive voids. No voids were discovered by the ultrasonic technique and none were discovered in the disassembly of each of the specimens in the critical bond area.

The Portashear adhesive test unit was modified in time to be used during the later stages of this test phase. Several of the shear panels were checked with the Portashear unit and Portashear tests were also performed on several remnants of earlier test panels. Figure 4-12 also shows the locations of a few of the Portashear tests which were performed on this panel. These tests have demonstrated the compatibility of the Portashear unit with heavy gage structure, but an additional modification of the shear tip insert as shown in Figure 4-31 will be required before the unit can be considered reliable for skin gages up through 0.25 inch. The Portashear unit is functionally illustrated in Figures 4-32 and 4-33.

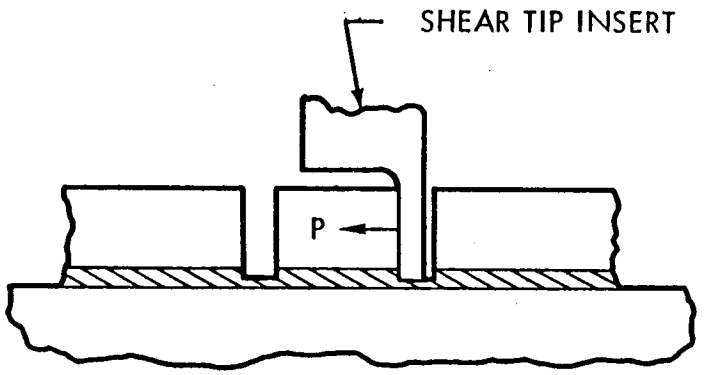

APPLIED FORCE P MAY ALSO INDUCE AN OVERTURNING MOMENT OF INDETERMINATE MAGNITUDE.

(A) PRESENT CONFIGURATION

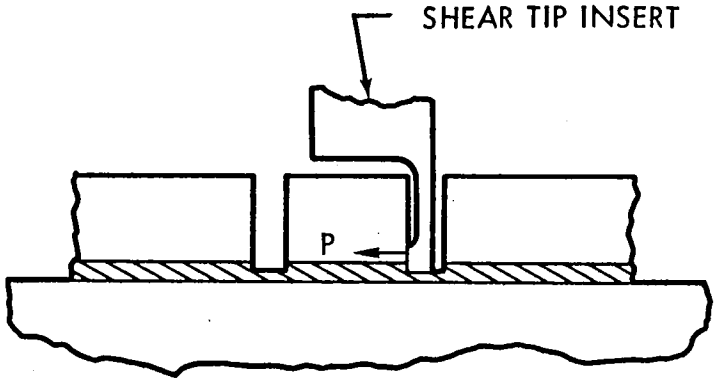

REDUCE THE MAGNITUDE OF THE OVERTURNING MOMENT.

(B) PROPOSED CONFIGURATION

Figure 4-31 PROPOSED MODIFICATION TO THE SHEAR TIP INSERT FOR PORTASHEAR

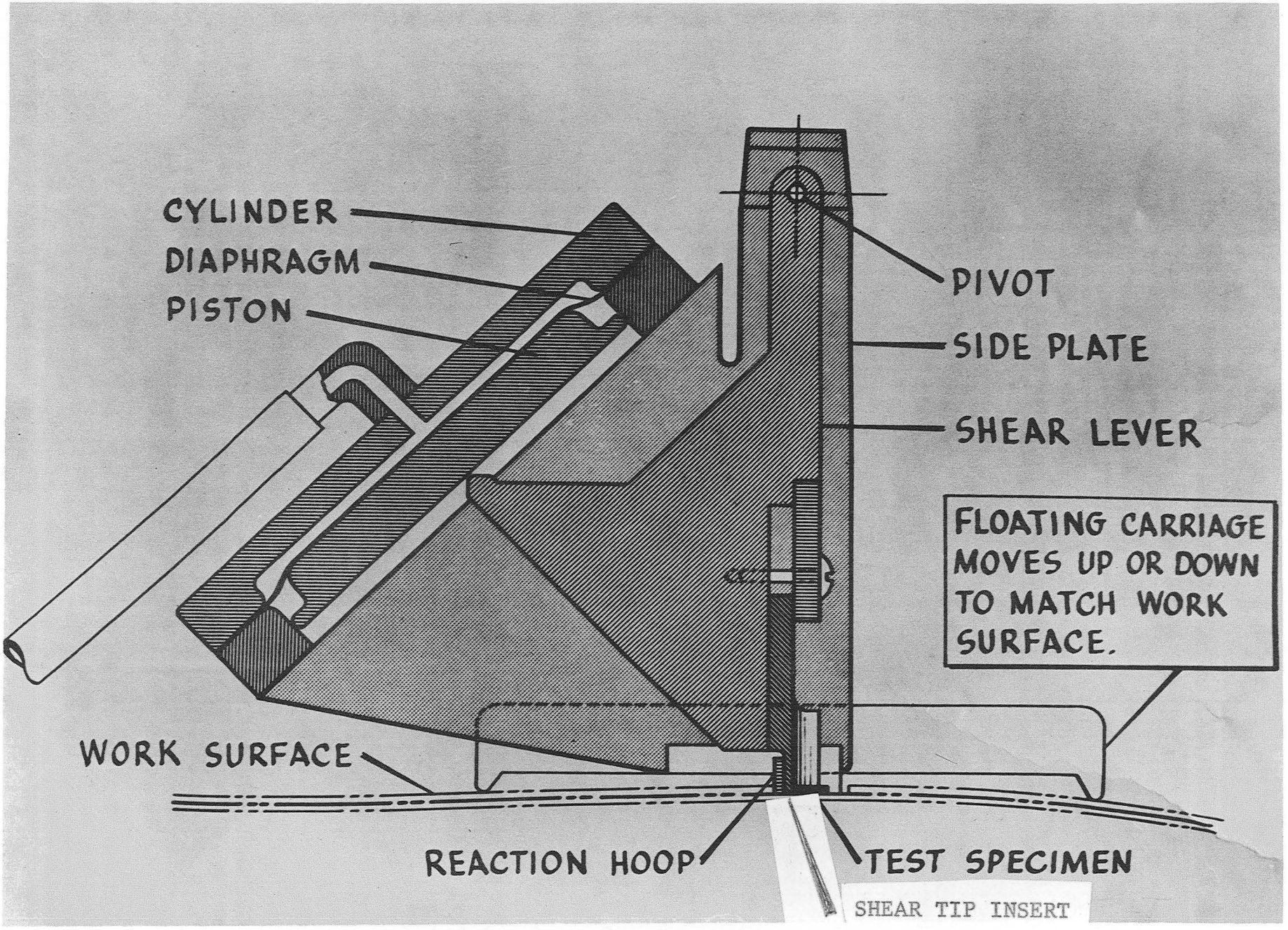

Figure 4-32 SCHEMATISM OF PORTASHEAR TESTING COMPONENT

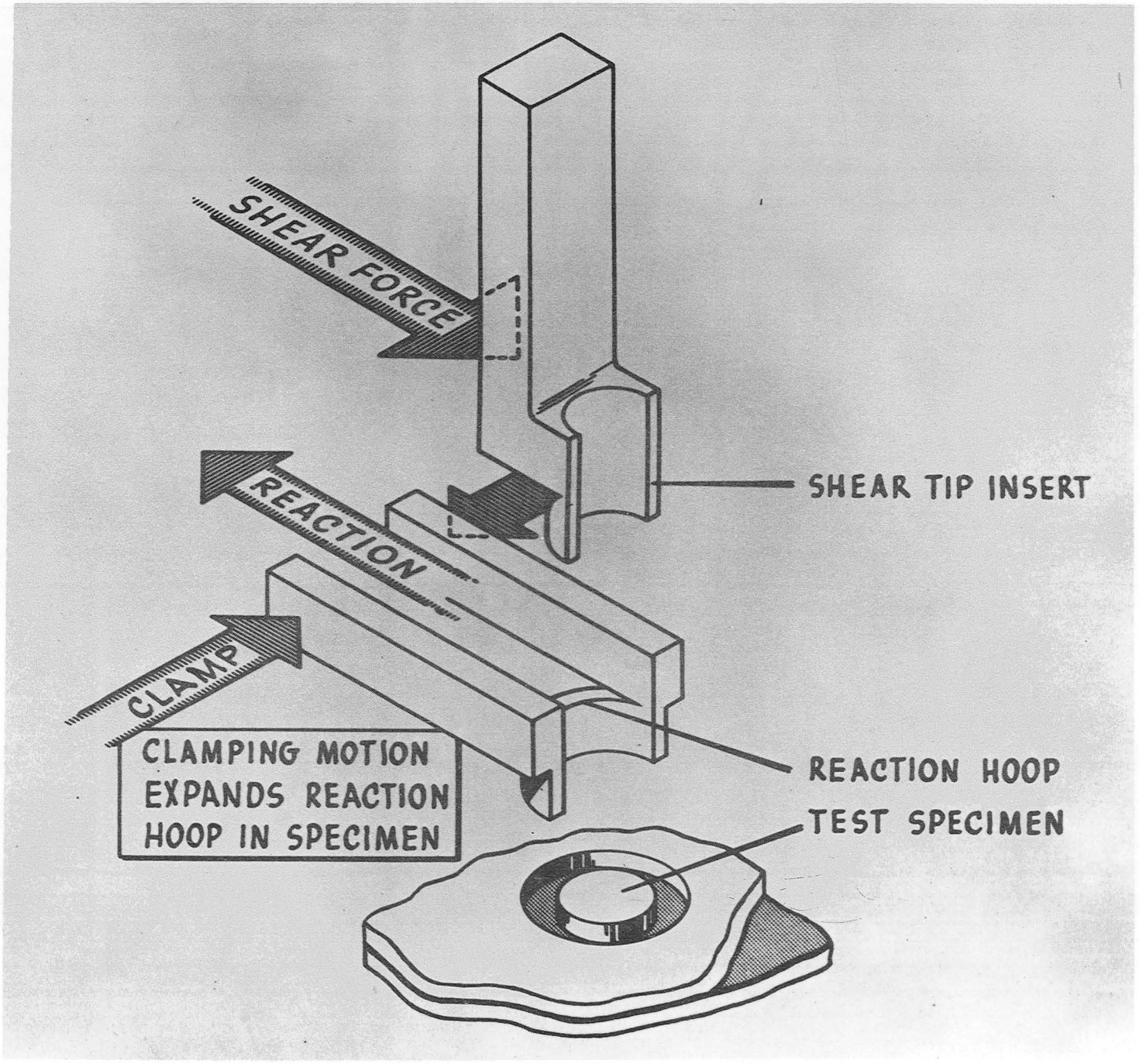

Figure 4-33 SCHEMATISM OF PORTASHEAR SHEAR MECHANISM

4.4 STRUCTURAL TESTING CONCLUSIONS

The structural test program and the resulting test data have permitted the following conclusions:

1. The bonded edgemember tests have demonstrated the structural integrity of the proposed edgemember configuration for the circumferential forward interface in panel thicknesses through three inches.

2. The bolted splice joint tests have shown that this type of joint will develop the necessary load transfer capability of the vertical splices, but local core reinforcement will be required.

3. The shear tests have shown that

   a. Solid edgemember slugs will not develop the necessary load transfer through a bonded interface when subjected to edgewise shear loads unless bolts are added to the joint.

   b. Channel type edgemembers will develop the necessary load transfer through a bonded interface when subjected to edgewise shear loads.

SECTION 5

FINAL DESIGN DEFINITION AND ANALYSIS

The final design of the thrust structure was initiated as results from the analysis of internal load distribution became available. The digital buckling analysis and secondary test program also provided inputs to the design effort which considered both welded and non-welded design concepts. Thermal, flutter, and acoustic analysis were also performed in support of the design task.

5.1 INTERNAL LOAD DISTRIBUTION

The thrust structure was idealized using a discrete stiffness element representation as discussed in Subsection 2.2. The total structure considered was composed of the following substructures:

(a) Sandwich cylinder
(b) Four (4) rebound longerons
(c) Four (4) thrust longerons
(d) Lower adaptor ring
(e) Upper Y-ring
(f) Upper elastic foundation

Full advantage was taken of the axial symmetry of the skirt, hence only one-eighth (1/8) of the structure was treated in the discrete stiffness element simulation. This one-eighth of the structure represents a forty-five degree arc bounded on the left by a rebound longeron and on the right by a thrust longeron. The skirt length was divided into eight equal layers and five (5) panels were used in the circumferential direction to represent a forty-five degree arc. Thus a total of forty panels were used for this one-eighth structure. Each longeron was composed of eight segments and each ring was composed of five segments. Basic properties such as cross-sectional areas, moments of inertia, thicknesses, etc. were allowed to vary linearly in each element and to be discontinuous across the synthetic joints as required to effect as nearly as possible the exact stiffness representation.

The honeycomb sandwich cylinder was simulated using two types of discrete elements, the quadrilateral complex plate and the tapered beam both of which are described in detail in Appendix D. A good simulation of the curved surface of the shell was obtained with the flat plates by limiting the arc of each plate to nine degrees as shown in Figures 5-1 and 5-2. The total stiffness of the honeycomb shell was divided between the plates and beams. The plates which can carry only in-plane loads were used to represent all of the in-plane stiffness. The capability of the honeycomb shell to carry out-of-plane loads was represented by including circumferential and longitudinal beams bounding each plate. This simulation of the honeycomb shell is illustrated in Figure 5-3.

The longerons and rings were represented by tapered bar elements placed end to end. This produced members with moment, shear and axial load carrying continuity along their length. They were tied to the adjacent plates of the honeycomb shell at each regular and dual node and in addition, the rings were tied to the boundary at each end. This is illustrated in Figure 5-4.

The elastic foundation was assumed to consist of a uniform cylindrical shell 0.30 inches thick and 150 inches long fully constrained at its upper end. It was represented by a layer of five (5) quadrilateral plates bounded by tapered bars on the longitudinal sides. Figures 5-4 illustrates a portion of the elastic foundation, the Y-ring, rebound longeron and the honeycomb shell.

Boundary conditions were applied to the one-eighth of the structure so that the upper boundary of the sandwich skirt, the Y-ring and the lower boundary of the elastic foundation were fixed against radial motion at each regular node. In addition, the side boundaries at the longerons were constrained to have zero tangential motion and zero rotation about the axes of the longerons. These boundary conditions are illustrated for a portion of the skirt in Figure 5-4.

The idealization thus far outlined is composed of 194 individual discrete elements requiring approximately 1000 displacement coordinates to join them together. The stiffness matrices for these elements were generated in a General Dynamics digital computer program designated P-42. Once the element matrices are generated they can either be assembled directly into a master stiffness matrix or they can first be subassembled into several

The regular nodes are located at each corner of the P-42 substructures. The regular node coordinate directions are as shown below. There are as many as six coordinates possible at each regular node; two in each of the directions shown and two that are vertical. Only those actually used in the stiffness model are shown on the force distribution drawing.

(View Looking Down on the Model)

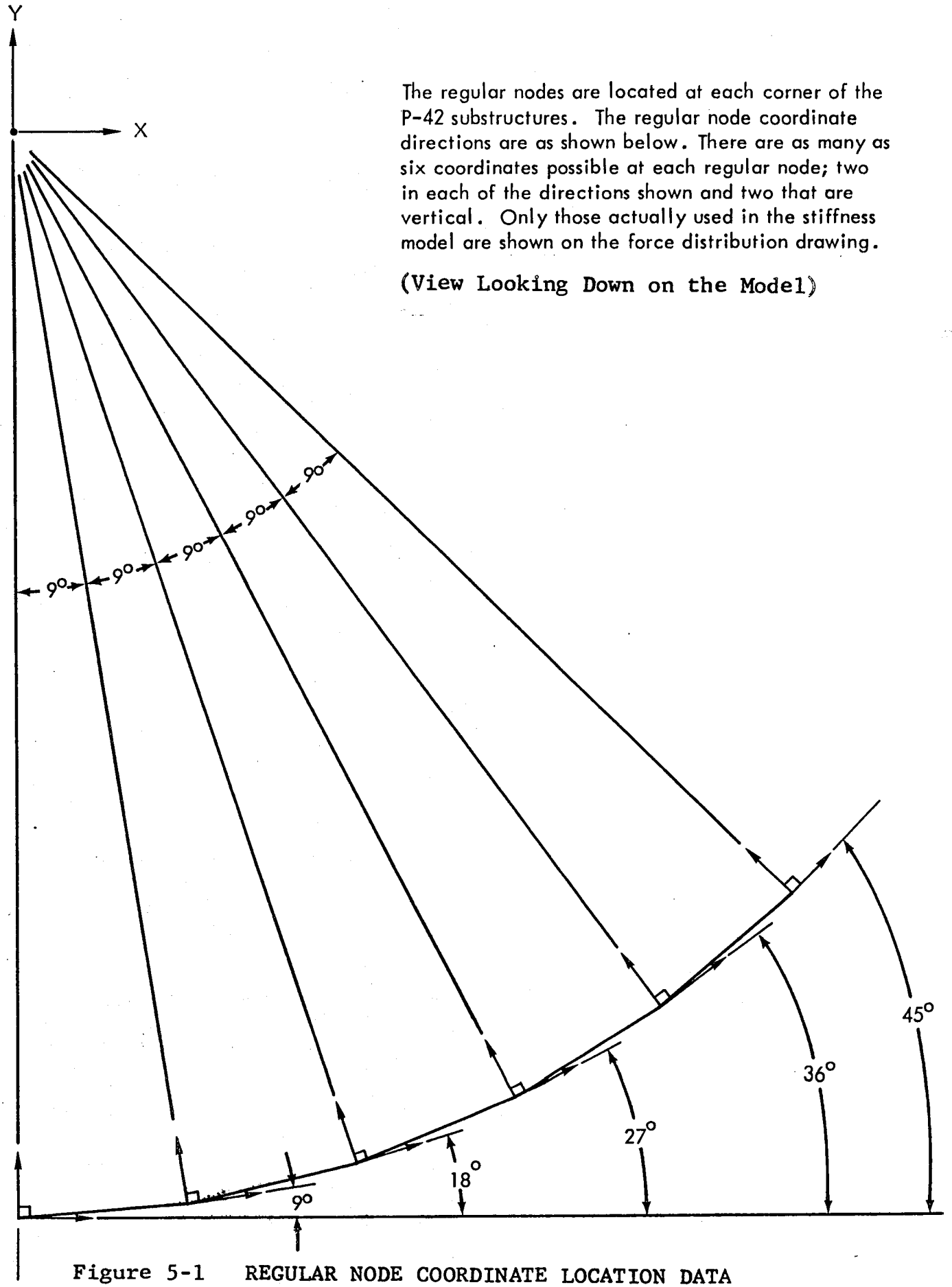

Figure 5-1 REGULAR NODE COORDINATE LOCATION DATA

The dual nodes are located midpoint between the regular nodes or corner nodes on both the horizontal and the vertical sides of the P-42 substructures. The coordinates shown are representative of those found at the dual nodes. There are as many as six possible coordinates at each node location; two in each of the directions shown and two that are vertical. Only those used in the stiffness model are shown on the force distribution drawing.

(View Looking Down on the Model)

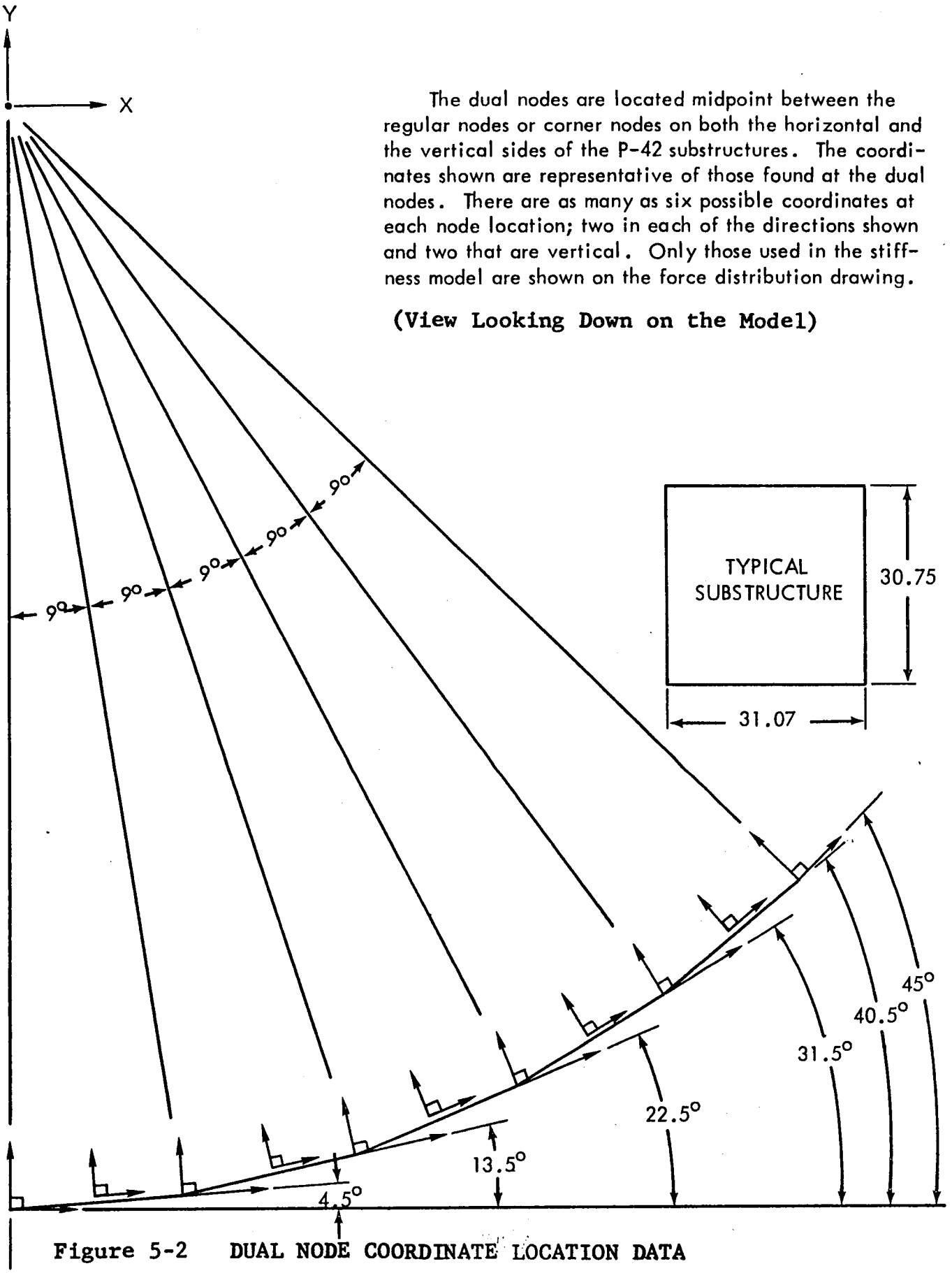

Figure 5-2 DUAL NODE COORDINATE LOCATION DATA

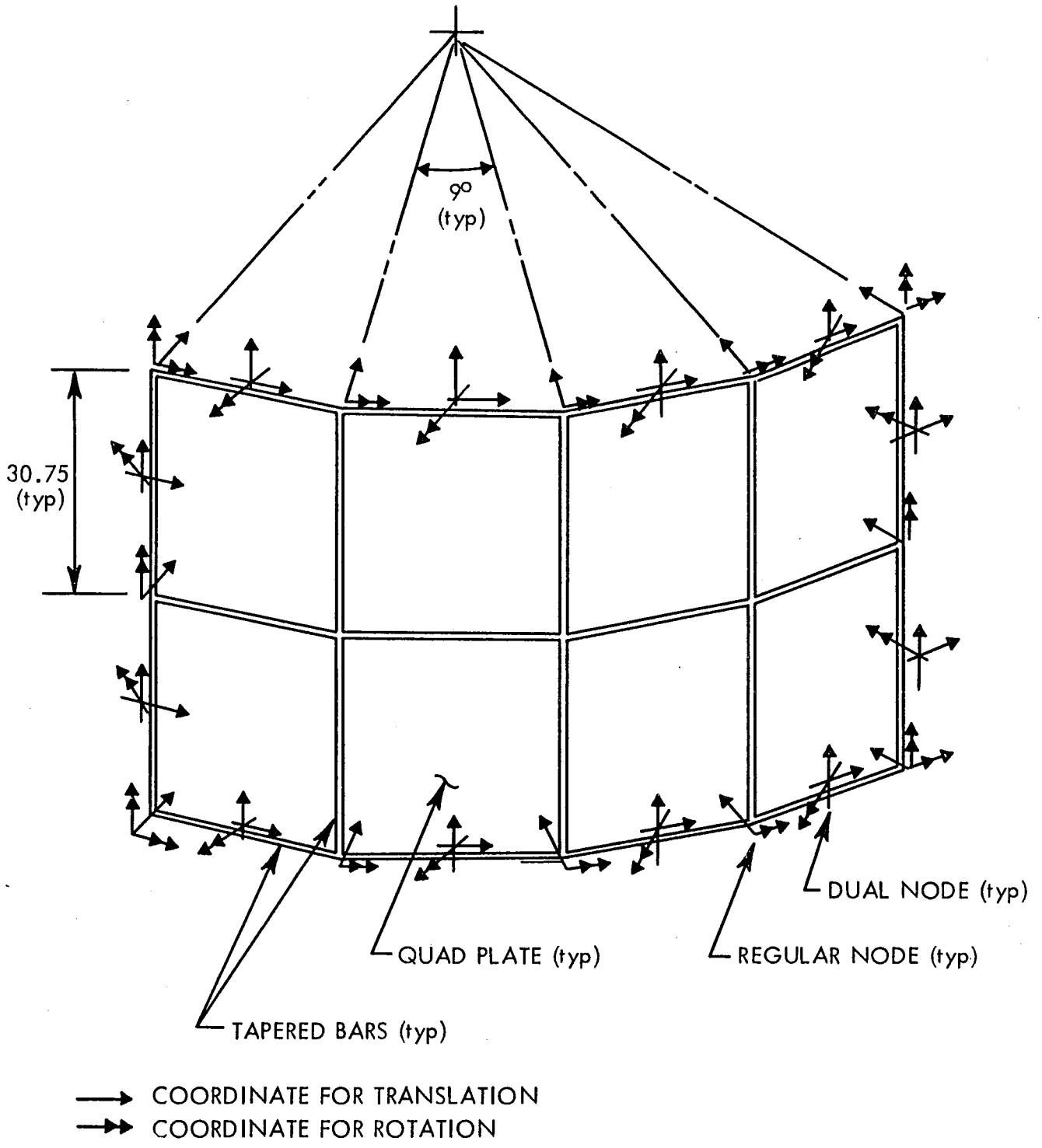

Figure 5-3 TYPICAL SECTION OF SANDWICH SHELL SIMULATION

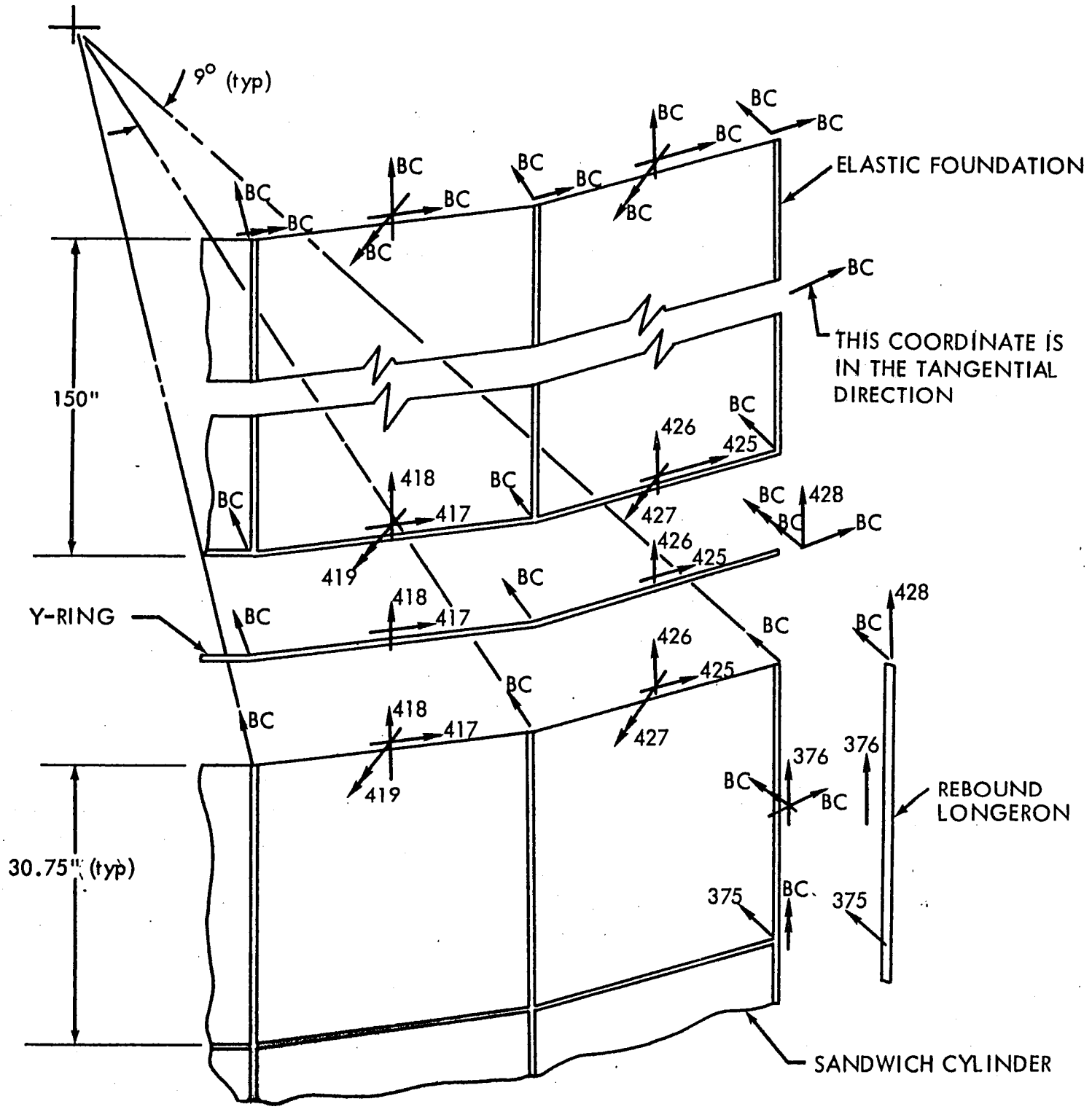

NOTE: "BC" indicates that a particular degree of freedom is tied to the boundary; i.e., that it has zero deflection. Two coordinates with the same number are connected, i.e. that degree of freedom is used to help tie two discrete elements together.

Figure 5-4 SIMULATION OF SANDWICH SHELL AND ELASTIC FOUNDATION

substructure stiffness matrices of a smaller number of coordinates. The latter procedure was used in this program with the advantage that the size of the substructure stiffness matrices could be reduced through beaming together of similar coordinates and through elimination of those coordinates which were not required to maintain continuity between the substructures. In Figure 5-5 a typical P-42 substructure is illustrated. The size of the substructure was reduced through beaming and elimination from 47 coordinates to 19 coordinates. The thrust skirt element stiffness matrices were subassembled into 52 P-42 substructures. These were then assembled into a master stiffness matrix of only 440 coordinates. The forces and boundary conditions associated with these remaining coordinates were only those necessary to define the internal stress distribution of the thrust skirt.

The output of this computer program was the load distribution for each of the 52 substructures for the three loading conditions- rebound, hold-down, and thrust - as shown in Figures 5-6, 5-7 and 5-8 respectively.

5.2 CYLINDER BUCKLING ANALYSIS

The philosophy pursued in performing the buckling analysis is discussed in Subsection 2.3. The internal loads, resulting from the analysis described in Subsection 5.1, were supplied as input to the digital buckling procedure along with the necessary discrete element geometry. (Said digital procedure is identified as code V39 and was developed under this contract).

The simulation was extended to one-fourth from one-eighth of the structure for the buckling analysis. This was done to prohibit the inadvertant stabilization of the structure when applying the boundary conditions necessary for one-eighth.

The analysis results indicate that the rebound load, the most critical of the three load conditions considered, must be escalated by a factor of 2.8 to cause buckling. The pre-buckling shape for the rebound load is shown in Figure 5-9. This analysis disregards all fabrication imperfections and material impurities.

NOTE: The coordinates designated with the letter "b" have their stiffness added to that of an adjacent coordinate which is in the same direction. The coordinate designated "e" are eliminated. The remaining coordinates determine the size of the P-42 stiffness matrix.

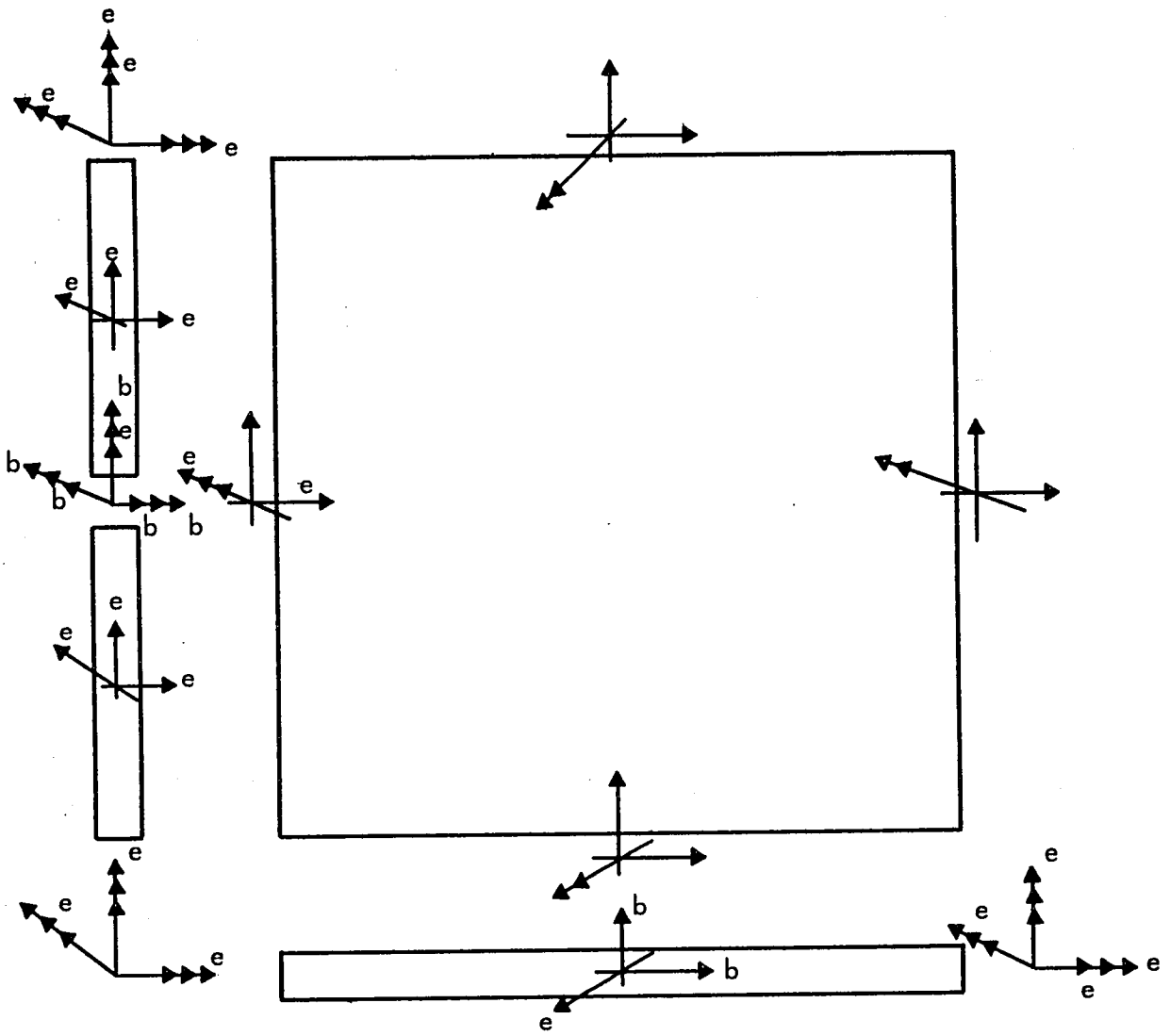

Figure 5-5 TYPICAL P-42 SUBSTRUCTURE

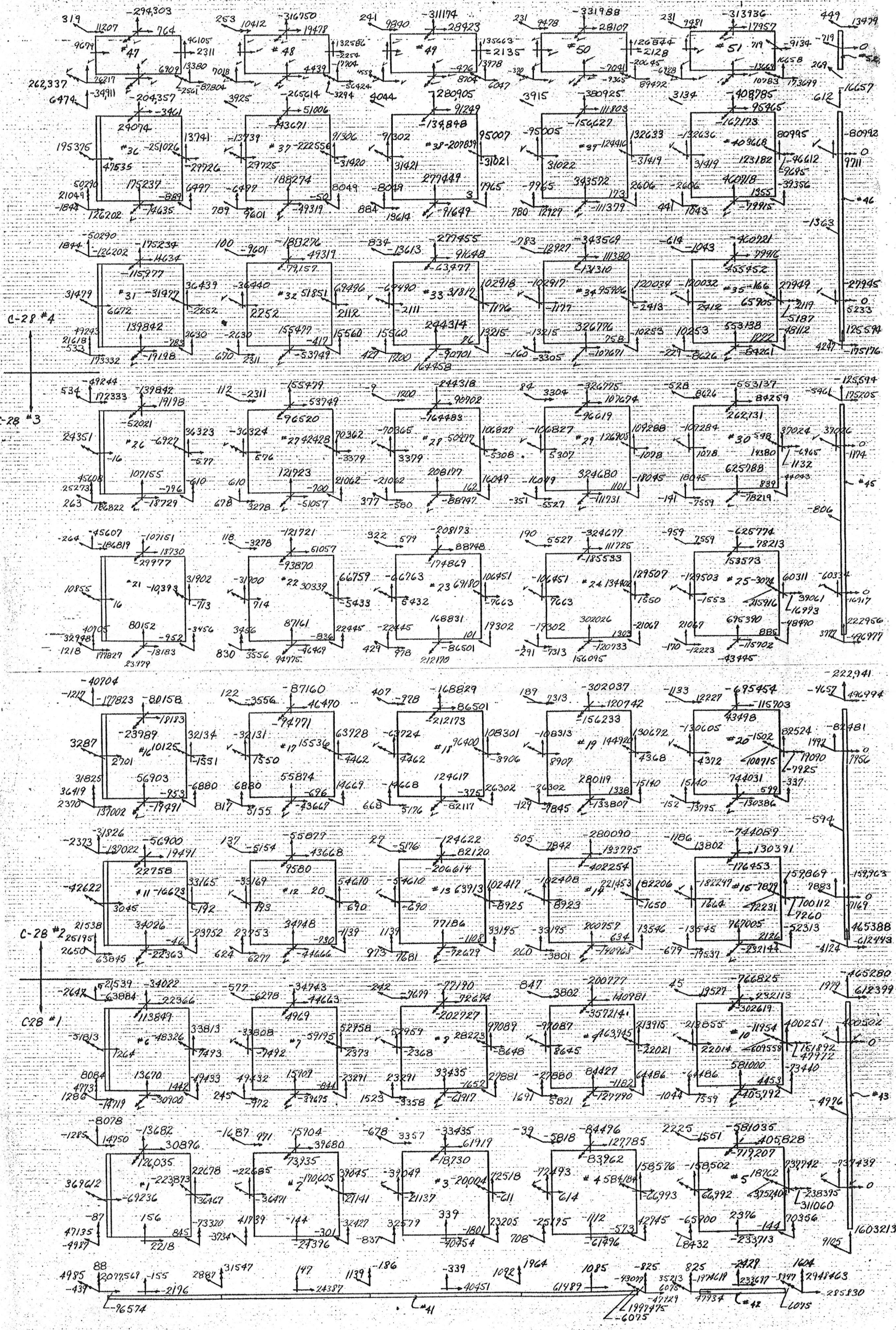

Figure 5-6 TYPE V - REBOUND

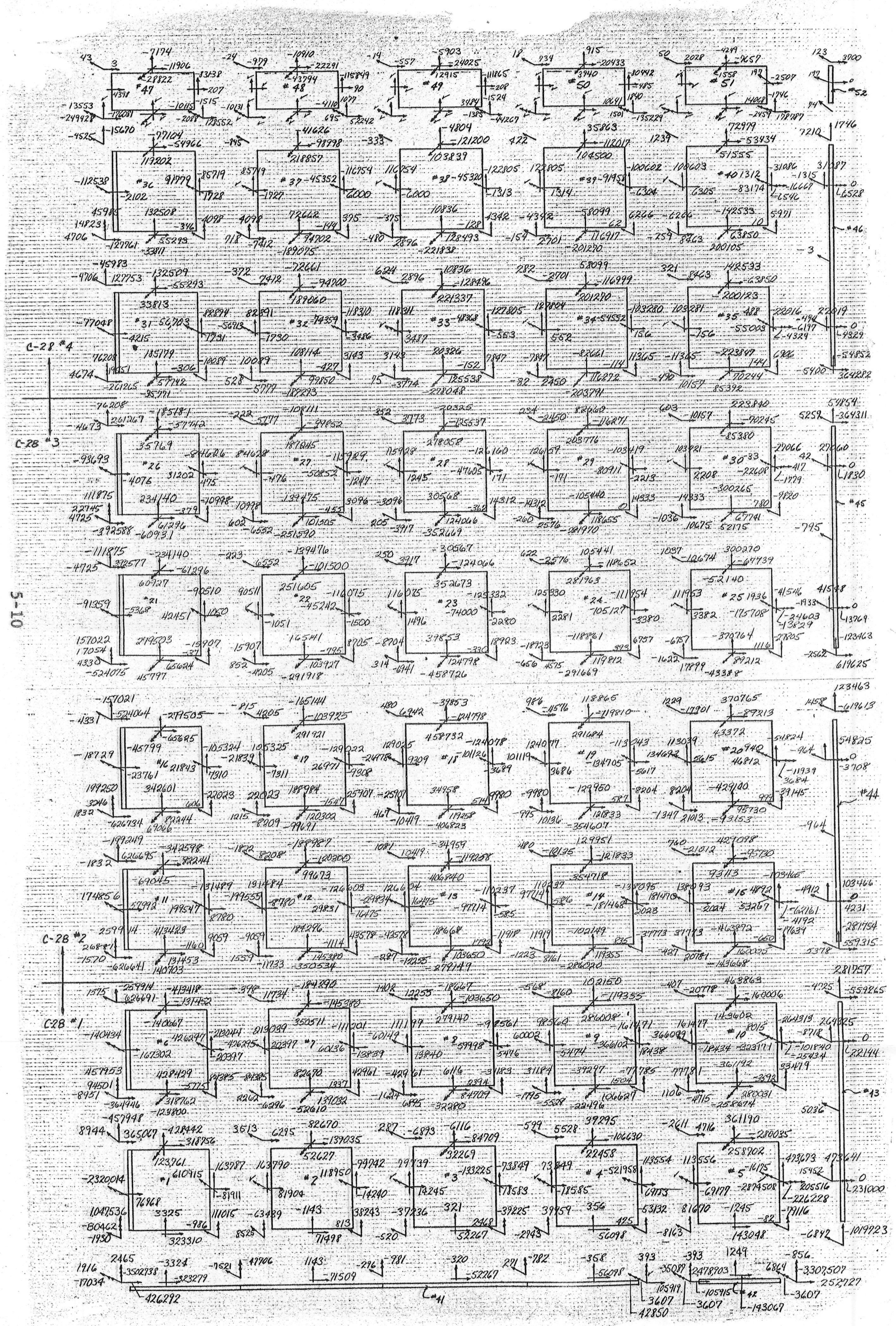

Figure 5-7 TYPE V HOLD-DOWN

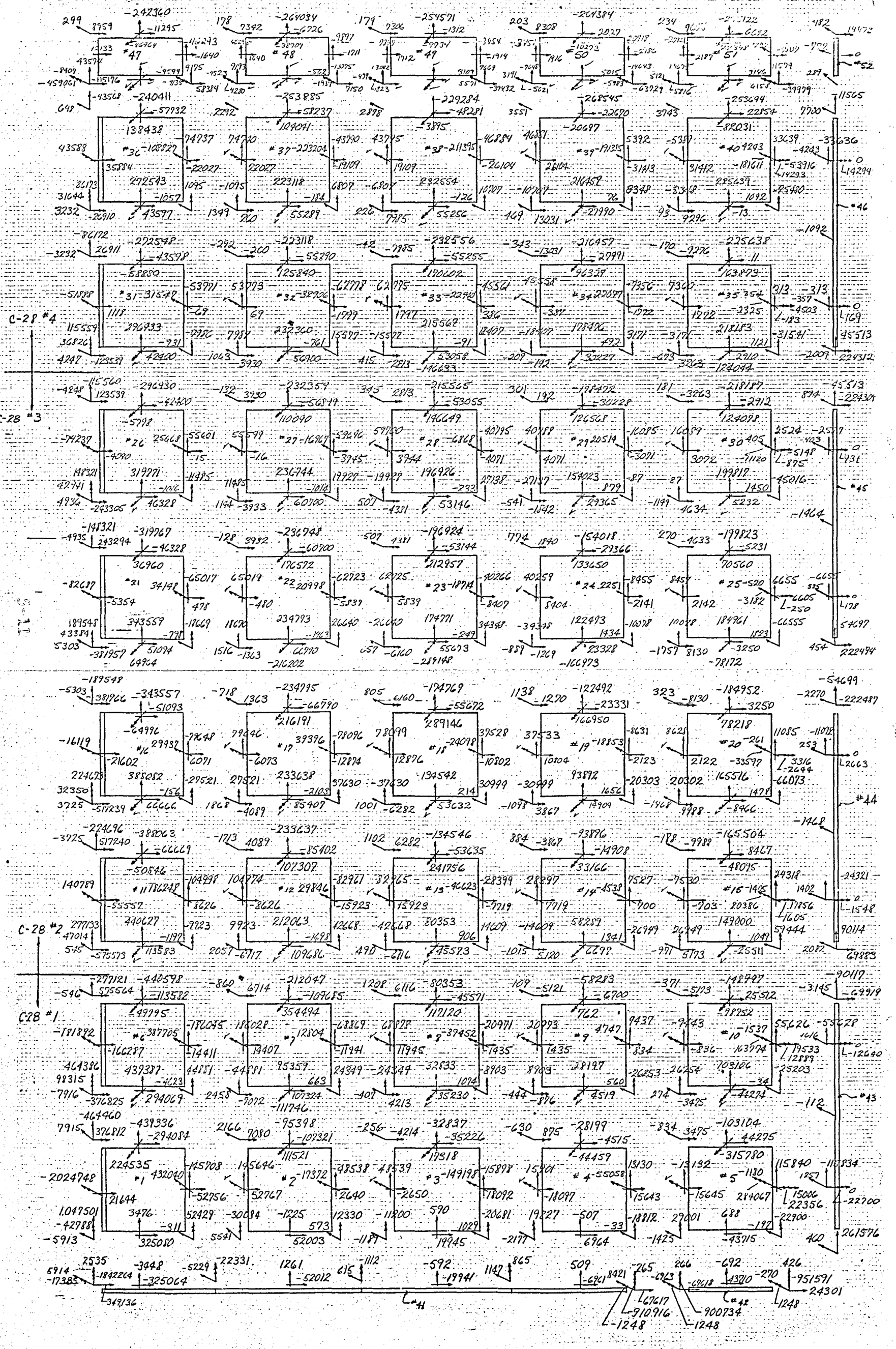

Figure 5-8 TYPE V - THRUST

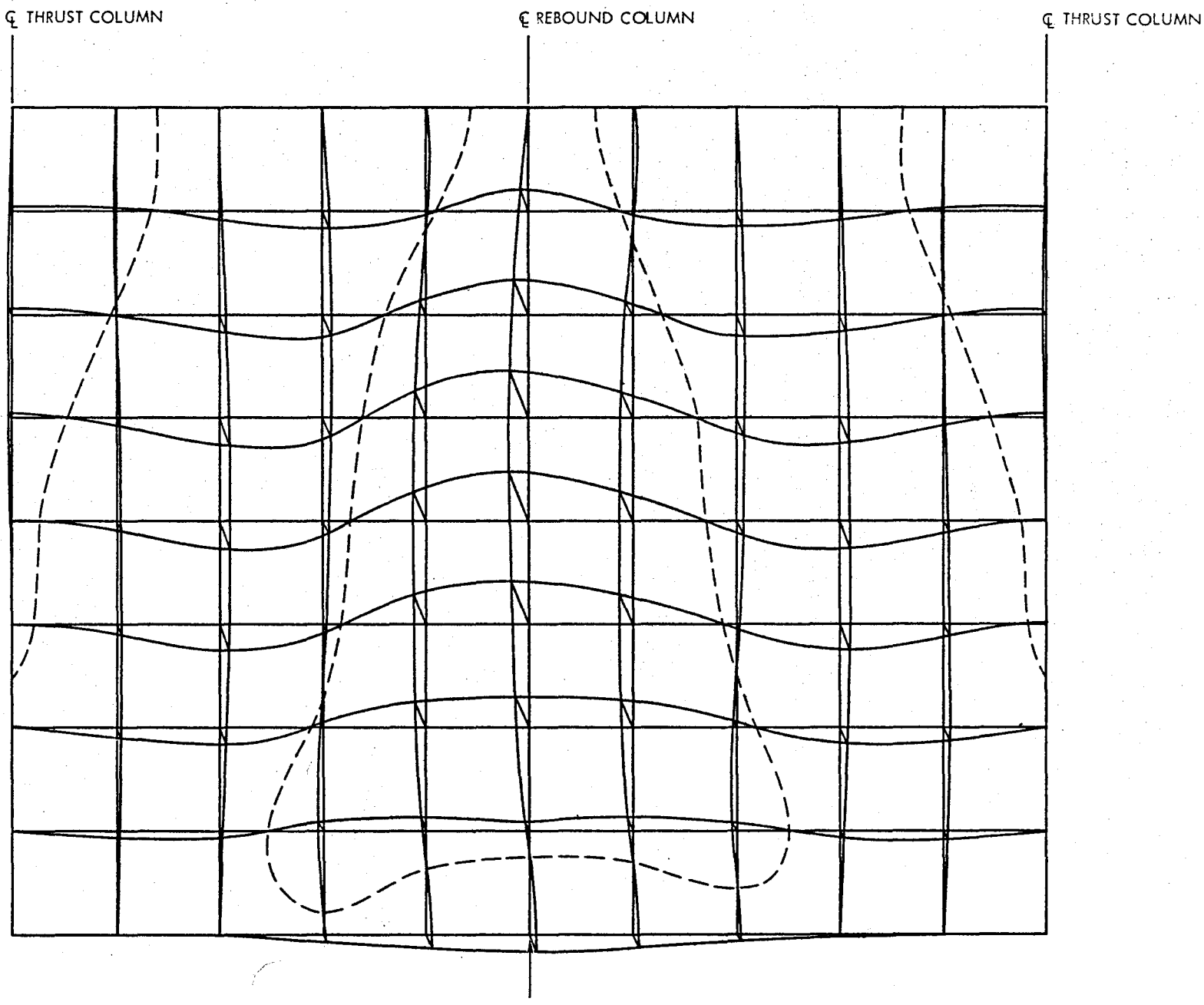

Figure 5-9 1st MODE $P_{cr} = 2.83P$

5.3 THRUST STRUCTURE DESIGN

The final assembly of thrust structure details is shown in Figure 5-10. It should be noted that for the non-welded design the assembly of details, such as panel-to-panel and longeron-to-panel, is accomplished with mechanical fasteners.

5.3.1 Thrust and Rebound Longerons

Final design definition for the thrust and rebound longerons are given in Figures 5-11, 5-12, 5-13, and 5-14. The cross-sectional area requirements for the longeron fittings was based on data previously obtained and confirmed by the analysis of internal load distribution described in Subsection 5.1. The distribution of the area for stiffness (EI) was made according to information obtained from the cylinder buckling analysis discussed in Subsection 5.2.

Because of the extremely high load concentration in the aft portion of each longeron fitting, the decision was made to utilize a one piece fitting separate from the forward longeron sections. The aft fitting serves to react engine thrust force in the case of the thrust fitting and the rebound forces or the holddown forces (through a pin joint) in the case of the rebound fitting, and also to provide a means of splicing the bonded sandwich panels and the lower ring. The panel splice provision consists of integral machined tabs on the edges of the fitting.

The forward longerons are two-piece machined parts. The two details are attached to the vertical edges of adjacent honeycomb panels by bolts. They are designed for buckling stability and as a panel splice. The forward longeron details are spliced to the aft fitting by bolts through matching "bathtub" provisions on the mating ends.

The longitudinal variation of longeron cross section area that was used in the digital computer analysis is shown in Figures 5-15 and 5-16. It may be noted that the aft end areas are very large but that the gradient in area with progression forward is very steep. At approximately one-fourth of the height the area is about 15% of that at the aft extreme end. The forward three-fourths has a gradual area taper.

These area profile characteristics then require severely-tapered elements in the lower fittings. The forward segments are designed to follow the theoretical area profile as closely as

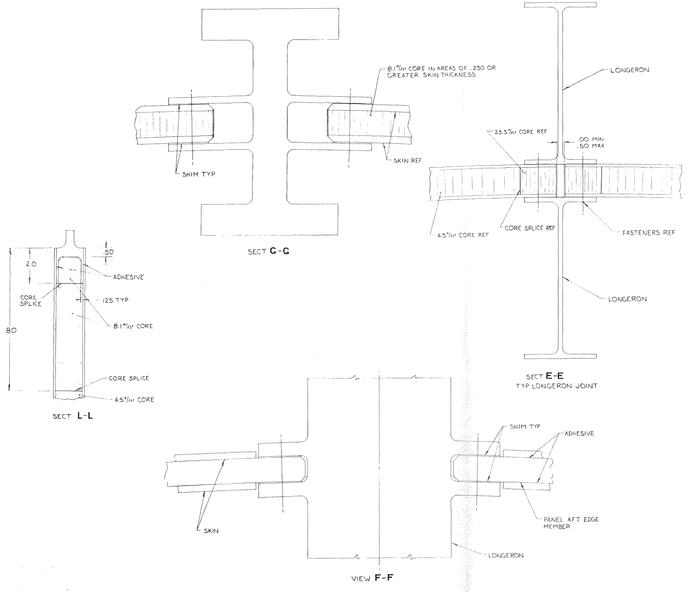

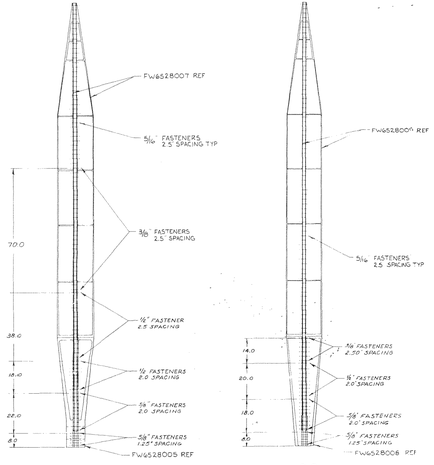

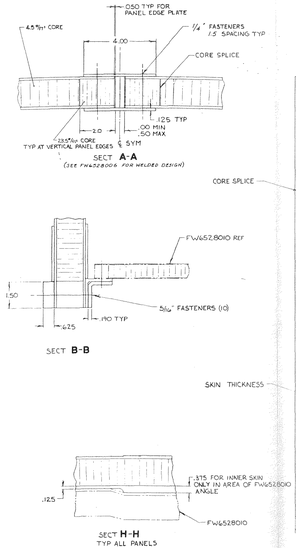

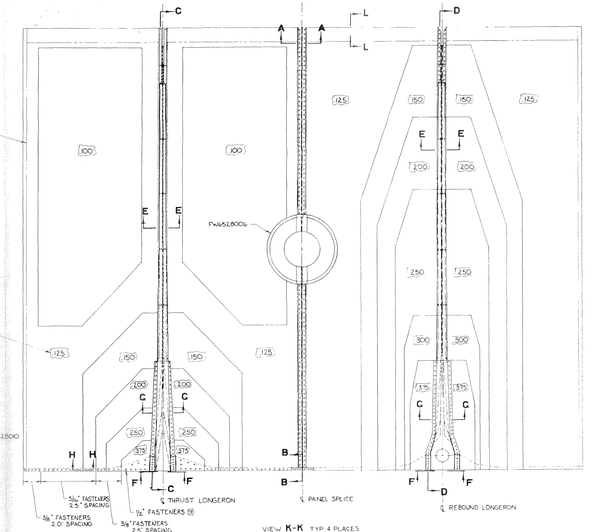

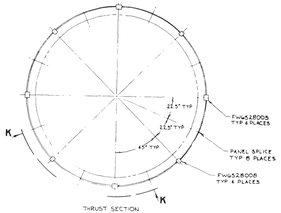

PRELIMINARY DESIGN DRAWING

HEAVY GAGE BONDED HONEYCOMB-THRUST PANEL ASSY NAS8-11943

A							
SIZE	CODE IDENT. NO.	DRAWING NO.					SCALE 1/10 SHEET
							FW6528011

GENERAL DYNAMICS | FORT WORTH

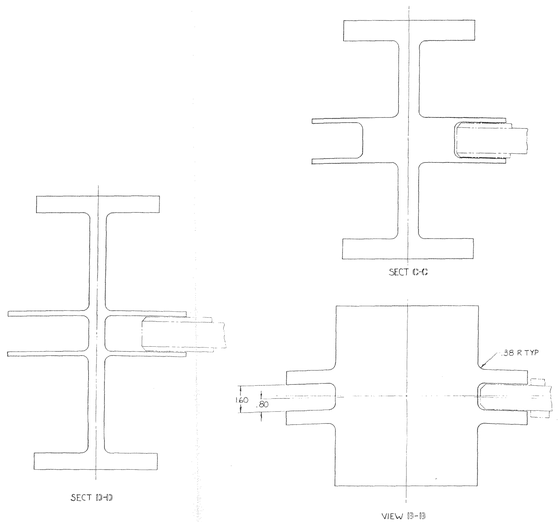

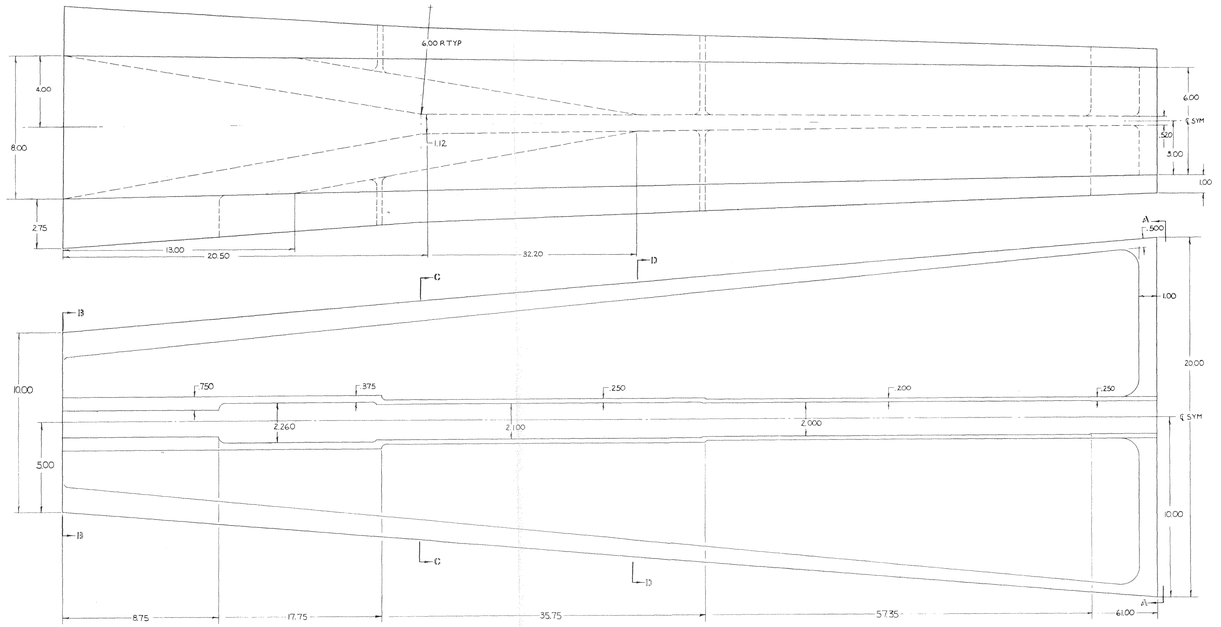

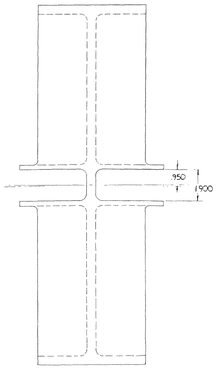

PRELIMINARY DESIGN DRAWING

HEAVY GAGE BONDED HONEYCOMB THRUST LONGERON FITTING, LOWER (NASB-1948)

GENERAL DYNAMICS | FORT WORTH

FW6528008 A

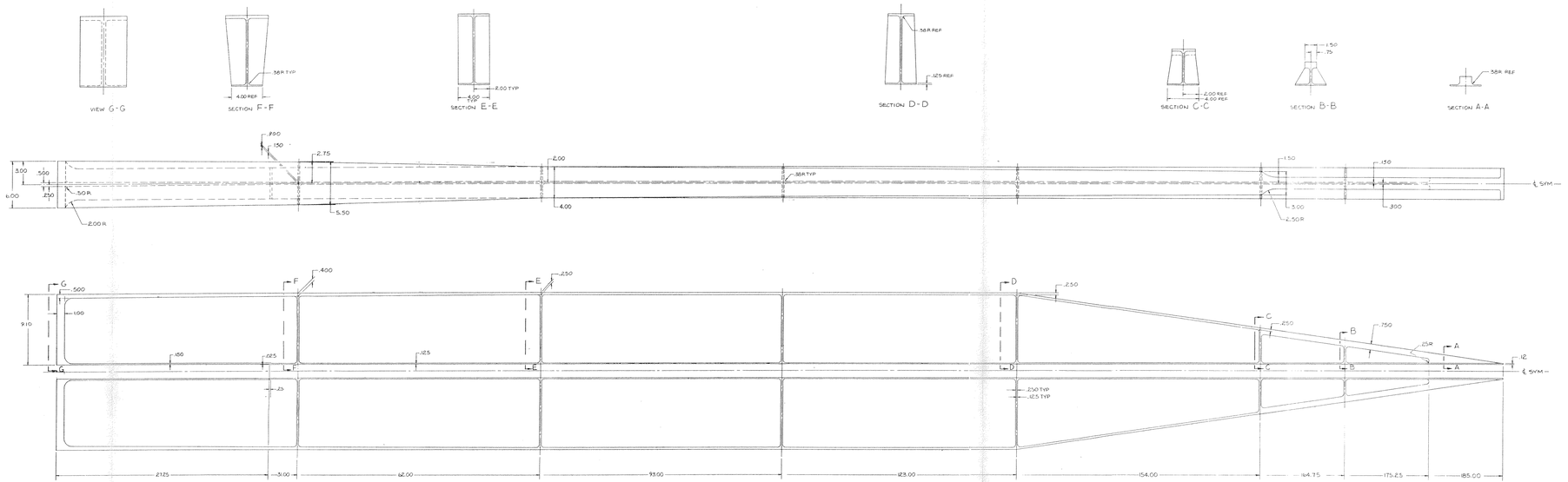

1. MATERIAL TO BE 7079 AL ALY MACHINED FORGING.

NOTES:

Figure 5-12

PRELIMINARY DESIGN DRAWING

HEAVY GAGE BONDED HONEYCOMB THRUST LONGERON (NAS 8-11943)

Designed	Drawn	Traced	Stress	Weights	Sht. No.

GENERAL DYNAMICS | FORT WORTH

FW65-8009

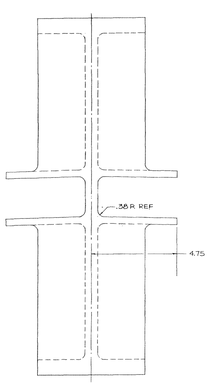

VIEW A-A

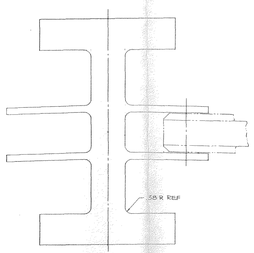

SECTION B-B

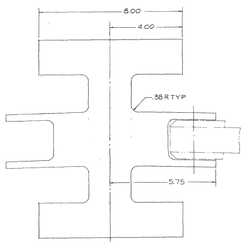

SECTION C-C

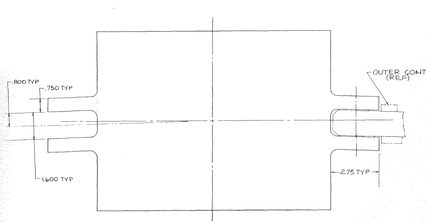

VIEW D-D

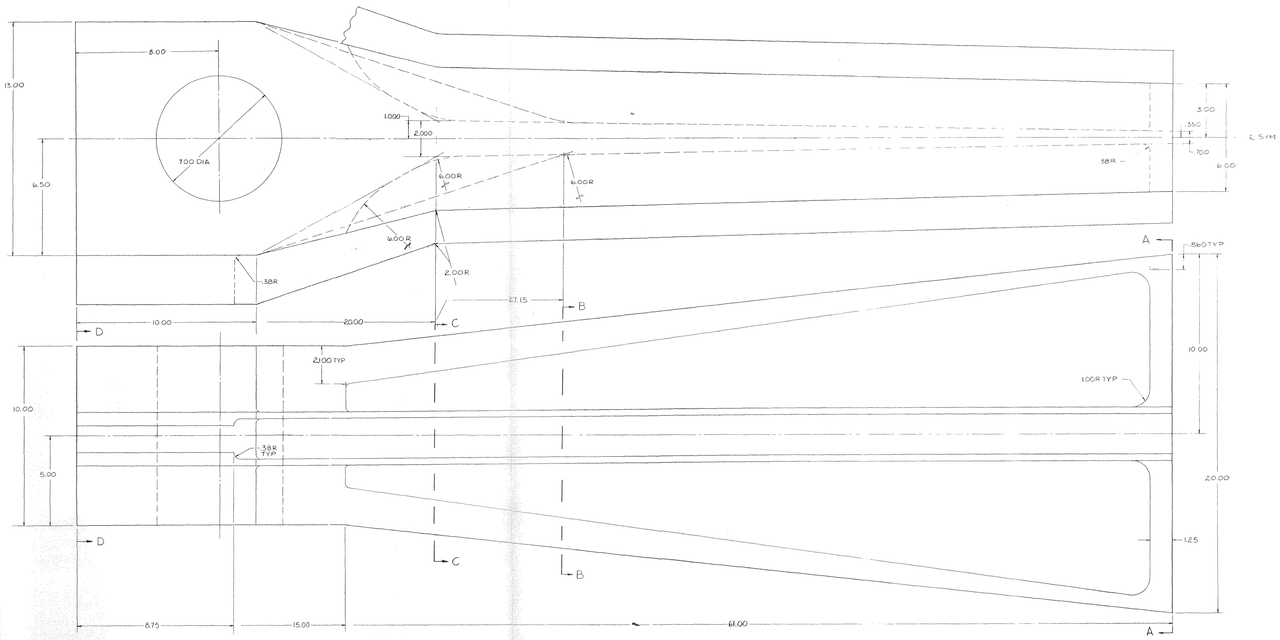

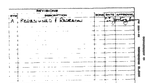

NOTES

1. MATERIAL TO BE 7079 AL ALY MACHINED FORGING.

Figure 5-13 Page 5-17

PRELIMINARY DESIGN DRAWING

HEAVY GAGE, BONDED HONEYCOMB — REBOUND, LONGERON FITTING, LOWER (NAS 8-11943)

Engineer		Date	Checked		Date	

GENERAL DYNAMICS | FORT WORTH

FWK528005 A

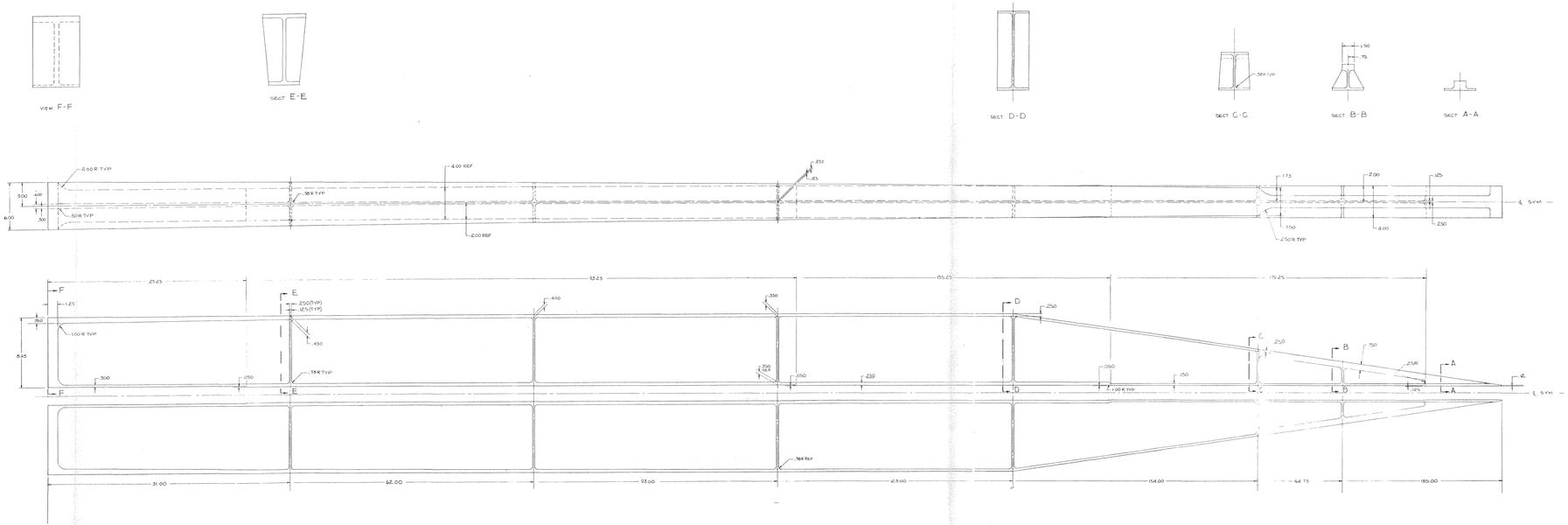

MATERIAL TO BE TOTALLY MACHINED FROM PLATE

NOTES:

Figure 5-14

PRELIMINARY DESIGN DRAWING

HEAVY GAGE BONDED HONEYCOMB — REBOUND LONGERON (NAS8-11943)

Prep'd by	Date	Appd	Date	Appd	Date

GENERAL DYNAMICS | FORT WORTH

FW628007

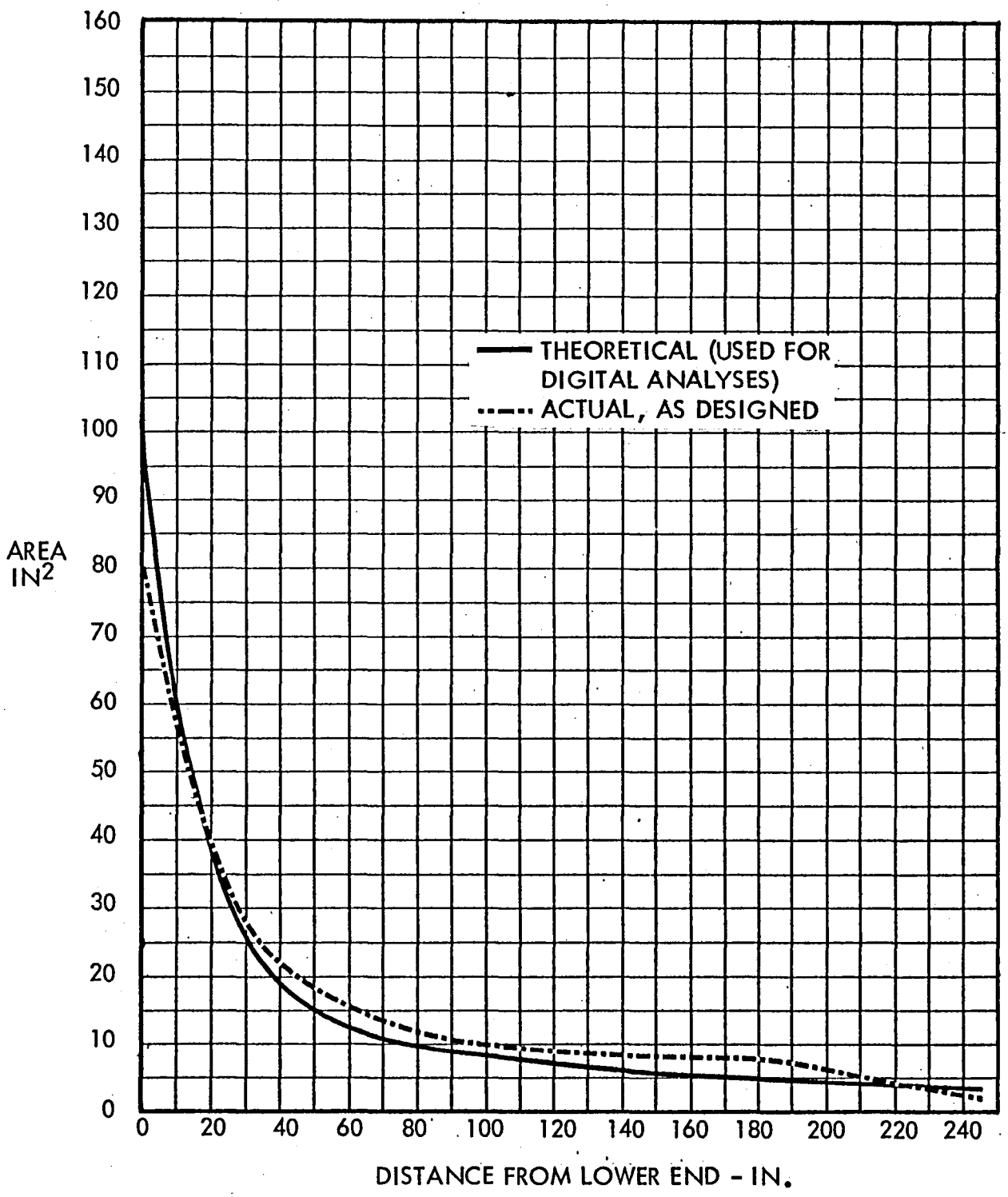

Figure 5-15 THRUST LONGERON AREA PROFILE

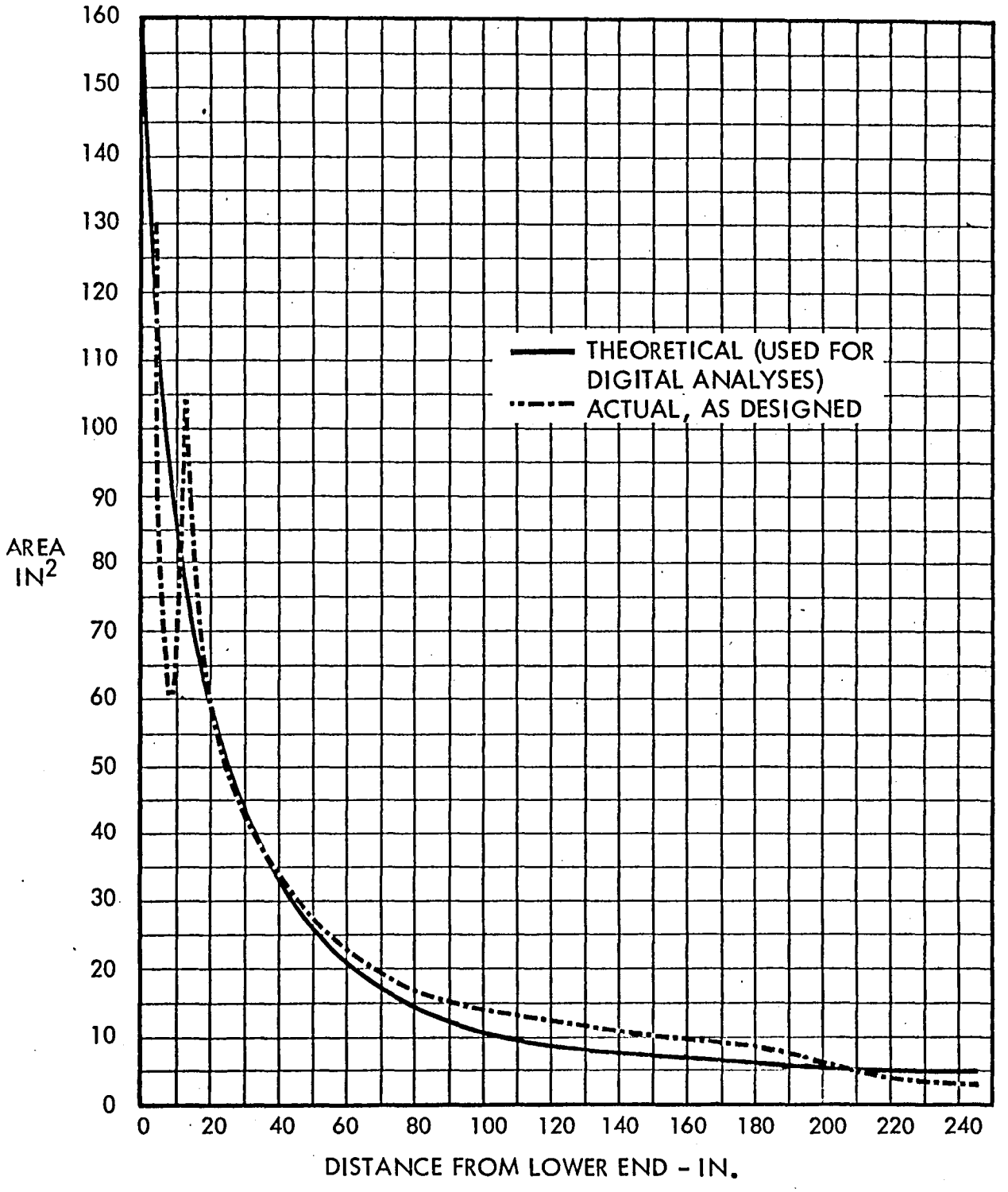

Figure 5-16 REBOUND LONGERON AREA PROFILE

possible while maintaining the radial depth of section indicated necessary by the digital buckling analysis. In addition, web and flange thicknesses and widths must be balanced and support ribs added to insure local stability.

Longeron depth over the middle height region is maintained at 20 inches overall. This depth provides the desired column stiffness (EI) for general stability in the computer buckling analysis of the composite thrust structure.

Profiles of the stress levels in the longerons for the three applied load conditions are shown in Figures 5-17 and 5-18.

Because the forward regions of the longeron have small areas for the depth required, local instability considerations become important. Apportioning of available areas in flange and web elements along with use of integral ribs allows local stability to be achieved, as shown by the following analyses:

a) Rebound Longeron

1. Outstanding flange lateral stability:

$$F_{c\ cr} = \frac{2E}{(L'/\rho)^2}$$

where L' = rib spacing

and ρ = .289 x (flange width)

to insure lateral stability up to 60,000 psi

$$\frac{L'}{\rho} \leq \left(\frac{\pi^2 E}{F}\right)^{.5} \leq (1710)^{.5} \leq 41.3$$

then, $L' \leq 41.3\ (.289\ w)$ (w = flange width)

or, $L' \leq 11.95\ w$

In the most forward bay of full depth section;

$$\text{Maximum } \frac{L'}{w} = \frac{31}{3.50} = 8.9$$

Therefore, flange lateral buckling is precluded.

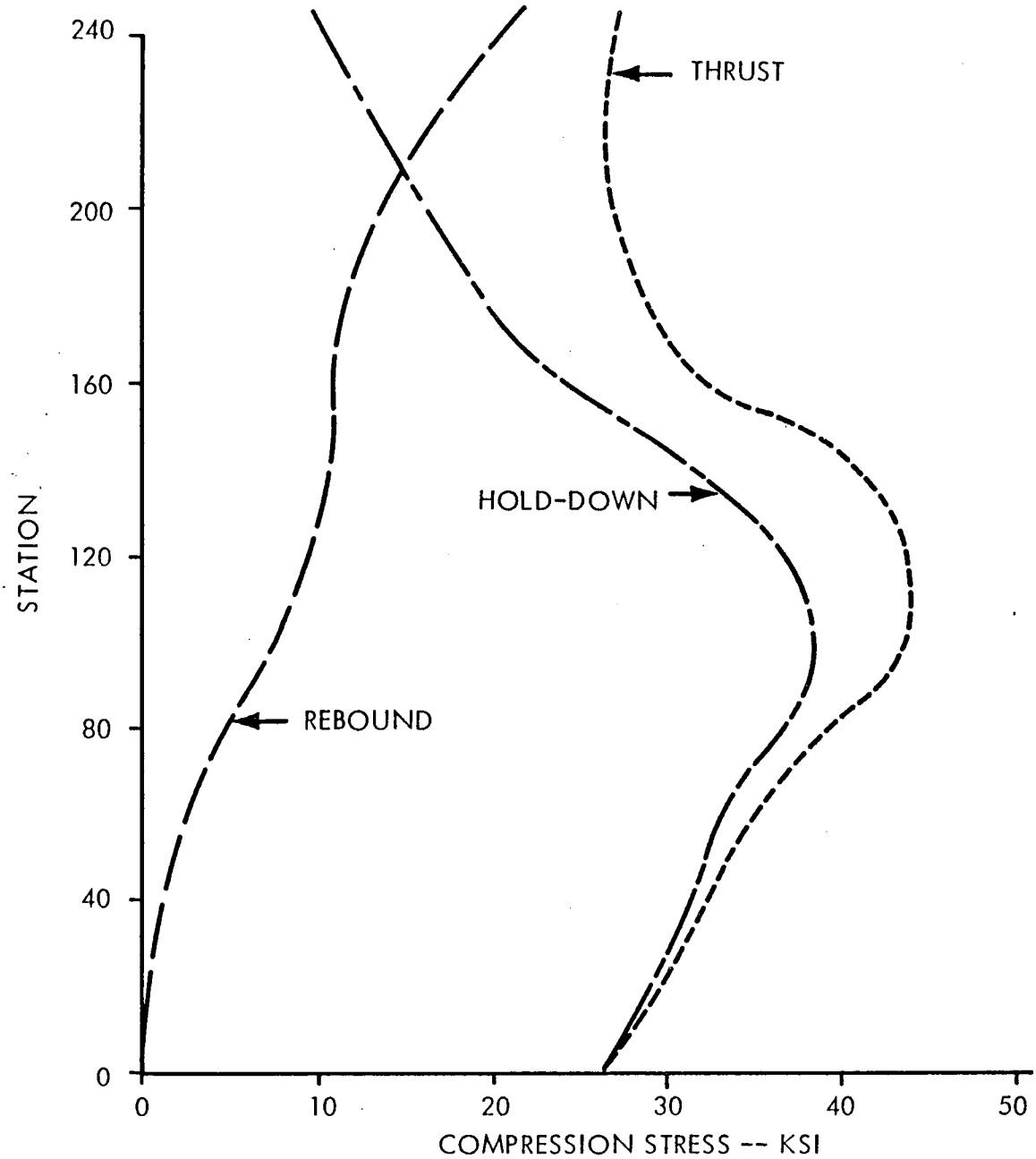

Figure 5-17 THRUST LONGERON APPLIED STRESS PROFILE

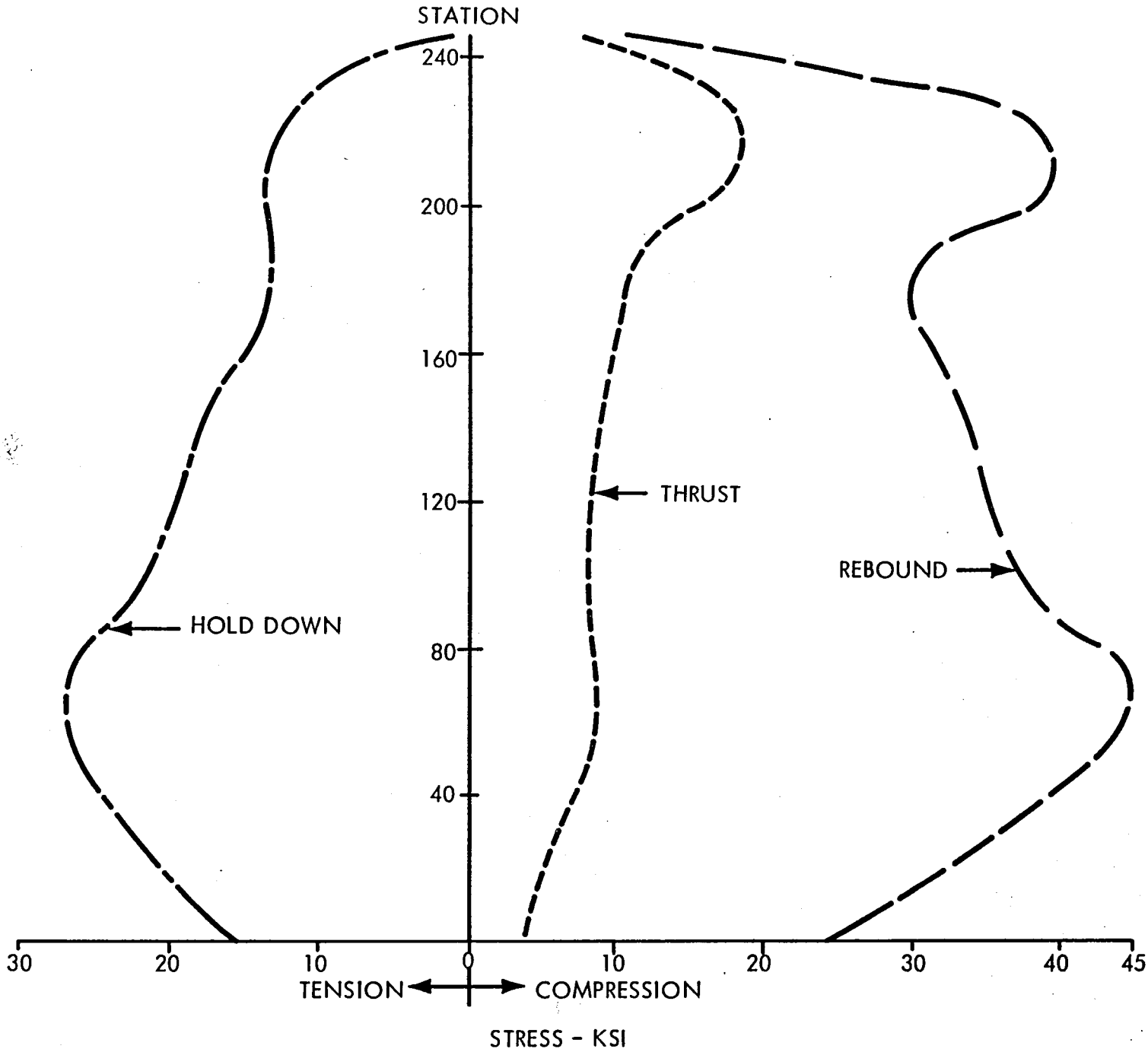

Figure 5-18 REBOUND LONGERON APPLIED STRESS PROFILE

2. Flange leg crippling:

The leg may be treated as an infinitely long flat plate simply supported on one side, free on the other side. Critical stress is given by,

$$F_{c\ cr} = \frac{K_c\ Et^2}{b^2}$$

Where b is taken as width from the web center to the edge of part, and $K_c = .38$ for given edge condition. To insure leg local stability up to 60,000 psi,

$$\frac{b}{t} \leq \left(\frac{K_c E}{F_c}\right)^{.5} - \left(\frac{.38 \times 10.4 \times 10^6}{60,000}\right)^{.5}$$

$$\leq (66)^{.5} \leq 8.1$$

At longeron midpoint, where b/t is maximum, where $w = 4.7$.

$$\frac{b}{t} = \frac{4.7 \times .5}{.40} = 5.8$$

Therefore, flange local cripping is precluded.

3. Web Crippling:

The web acts as a long plate simply supported on the edge at the outstanding flange and fixed at the flange which attaches to the sandwich panel.

$$F_{c\ cr} = \frac{K_c\ Et^2}{b^2},$$

where b = web depth between flanges and $Kc = 5.02$ for the given edge conditions.
To insure web stability up to 60,000 psi,

$$\frac{b}{t} \leq \left(\frac{K_c E}{f_c}\right)^{.5} \leq \left(\frac{5.02 \times 10.4 \times 10^6}{60,000}\right)^{.5}$$

$$\leq (870)^{.5} \leq 29.5$$

In the forward bay of full depth section,

$$b = 8.5,$$

$$\frac{b}{t} = \frac{8.5}{.25} = 34.$$

This bay will buckle below 60,000 psi

$$F_{c\ cr} = \frac{5.02 \times 10.4 \times 10^6}{34^2} = 48{,}000 \text{ psi}$$

Since maximum longeron compression stress in this area is less than 40,000 psi, web crippling will not occur below design load.

b) Thrust Longeron

1. Outstanding flange lateral stability:

$$f_{c\ cr} = \frac{\pi^2 E}{(L/\rho)^2}$$

Lateral stability up to 60,000 psi flange compressive stress is assured if $L'/w \leq 11.95$ (Ref. p 5-21)
Maximum L'/w occurs in the bay between 31 and 62 inches from the upper end of the longeron there

$$L' = 31$$

$$w = 3.0$$

$$L'/w = 10.3$$

therefore flange lateral buckling is precluded.

2. Flange leg crippling:

Flange is stable against crippling if $b/t = 8.1$ (Ref. p 5-24) Max b/t occurs at mid-height of the longeron where flange width is 4.0 in.

then $b = w/2 = 4.0/2 = 2.0$

$t = .25$

$b/t = \frac{2.0}{.25} = 8.0$

therefore flange leg crippling will not occur below 60,000 psi compressive stress.

3. Web Crippling:

$$f_{c\ cr} = \frac{K_c\ Et^2}{b^2}$$

where K_c = 5.02 for a plate with one long edge fixed, the other simply supported

b = web depth between flanges

t = web thickness

Maximum web depth = 9.0 in.

Minimum thickness = .30 in.

$$F_{c\ cr} = \frac{5.02 \times 10.4 \times 10^6 \times .30^2}{9.0^2} = 58{,}000 \text{ psi}$$

Since maximum longeron compression stress in this area is less than 45,000 psi, web crippling will not occur below design load.

Information received from one of the forging producers indicates that the longeron fittings are practical with regard to manufacturing method, cost, section mechanical properties, and delivery span time. These estimates for a typical fitting are as follows:

a) Manufacturing Method - The rough hand forging received from the vendor in the 7079 (F) condition would be machined to within one-half inch of net size. The part would then be heat treated and quenched to the 7079 (W) condition. Final machining would be accomplished and the part would be straightened if required. Finally, the part would be heat treated and aged to the 7079 (T6) condition.

b) Cost

(1) Part - $2085

(2) Parts - $1950 Each

(5-9) Parts - $1575 Each

c) Section Mechanical Properties

Approximate Minimum Properties 7079 (T6)

	Tensile Ultimate	Tensile Yield	% Elong.
Longitudinal	60 ksi	50 ksi	6
Long Transverse	58 ksi	46 ksi	4
Short Transverse	55 ksi	44 ksi	3

d) Delivery Span Time - Eleven (11) Weeks

5.3.2 Sandwich Panels

Sandwich panel internal loads as obtained for the three design loading conditions by digital computer are shown in Figures 5-6 through 5-8. From these plate element loads, skin stresses were calculated at numerous points in the panels. These stresses are shown in Figures 5-19 through 5-21. Zones of skin in various ranges of axial and shear stress are shown in Figures 5-22 and 5-23. It is seen that regions of high stress change location as the applied load conditions vary. All regions of skin except the lower area midway between longerons have high axial compression, high shear stress, or a combination of these under at least one condition. The lower middle area, although not highly stressed, provides the shear stiffness required to transfer a significant fraction of applied rebound load over to the thrust longeron region. It thus helps spread the upper boundary distributed load enough to avoid exceeding the 15,000 lb. per inch ultimate load limitation at the boundary. Skin failure at or below design ultimate load will not occur due to any stability deficiency. Local instability failure modes were checked and found to be non critical. Cylinder general stability was found to be adequate by a large margin in the digital cylinder buckling analysis. The remaining possible failure mode, facing shear rupture, is avoided by providing enough facing thickness to keep total shear stress at

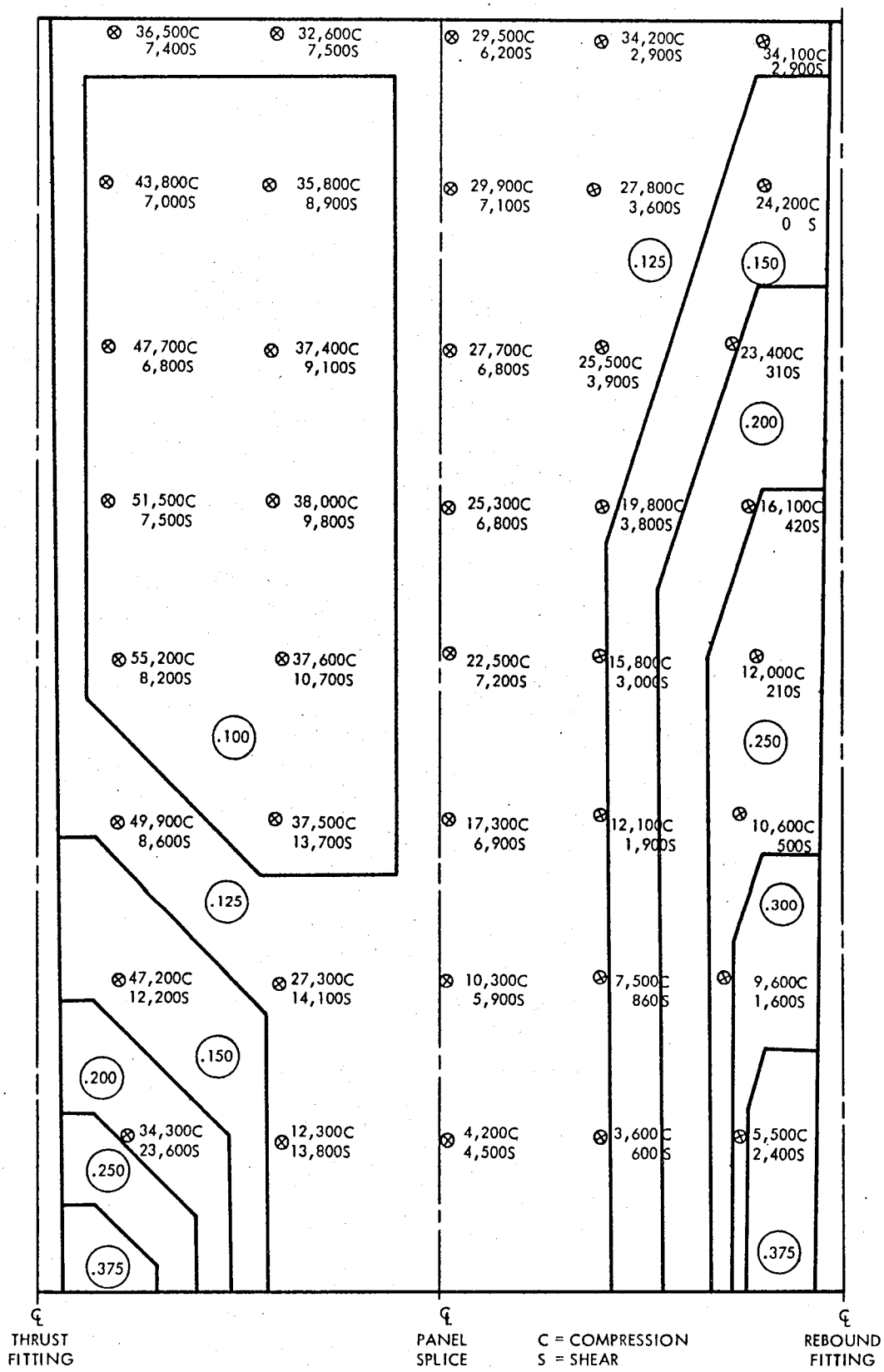

Figure 5-19 SKIN STRESSES, THRUST CONDITION FINAL COMPUTER RUN

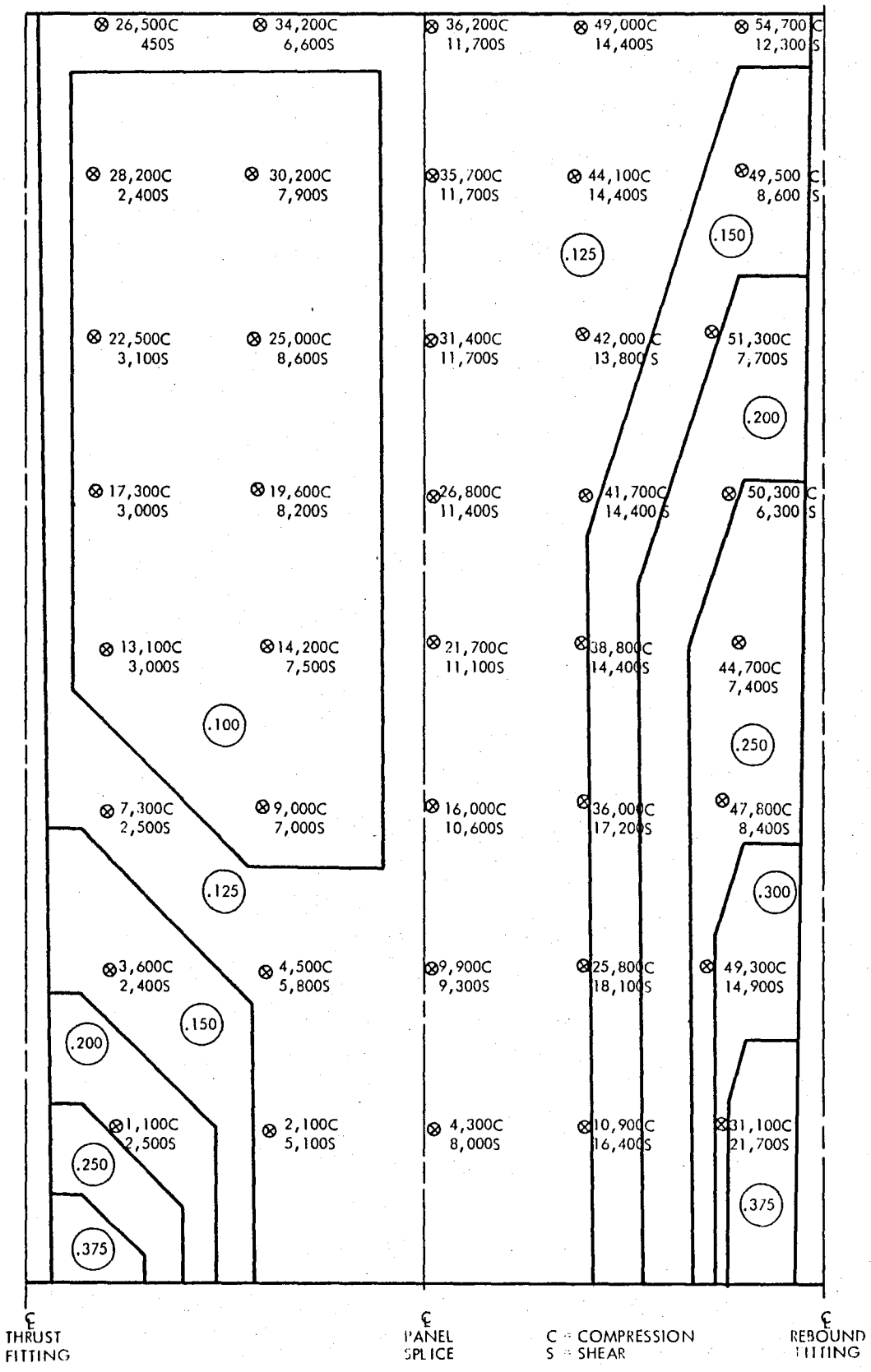

Figure 5-20 SKIN STRESSES, REBOUND CONDITION FINAL COMPUTER RUN

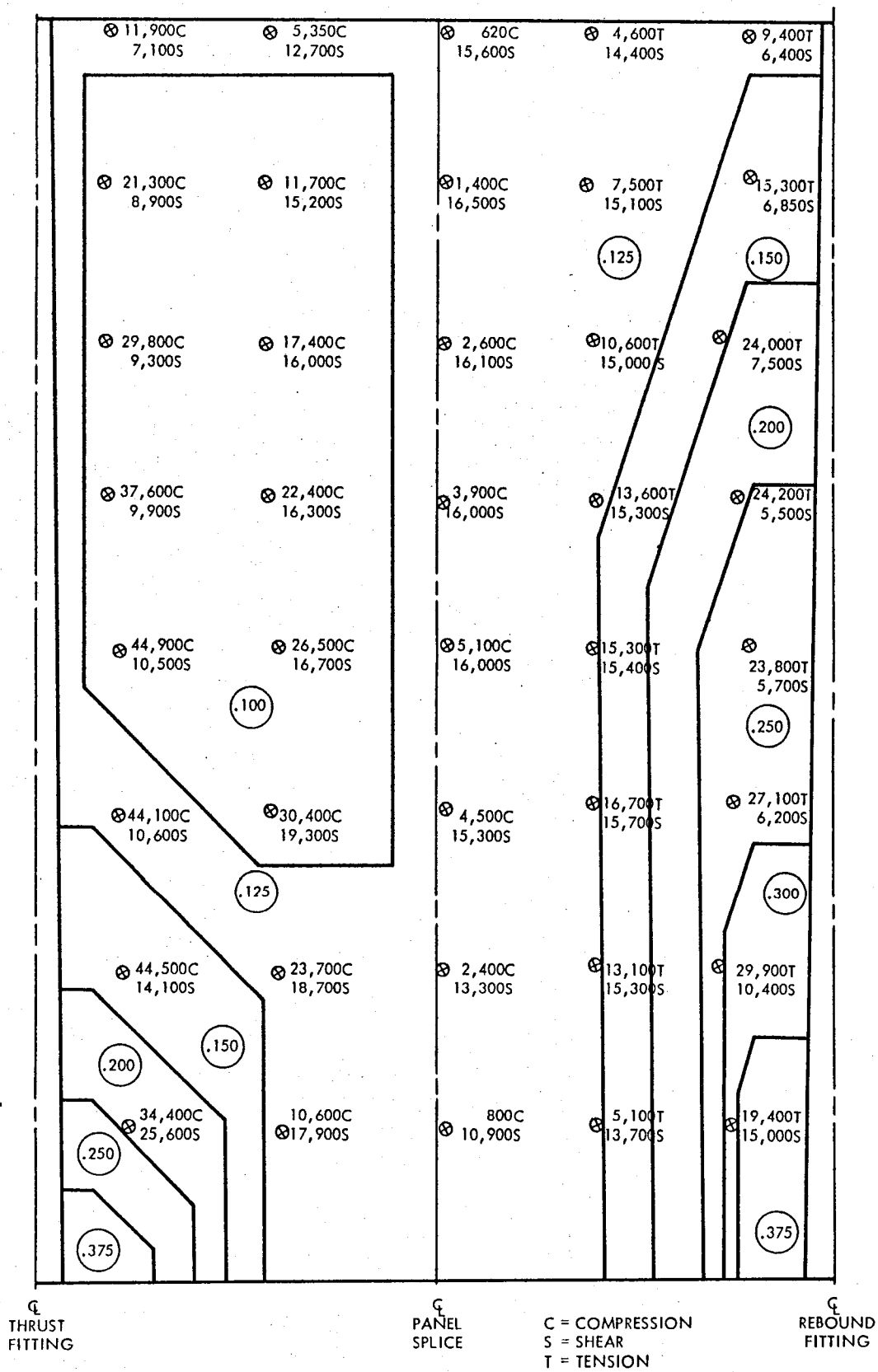

Figure 5-21 SKIN STRESSES, HOLD-DOWN CONDITION FINAL COMPUTER RUN

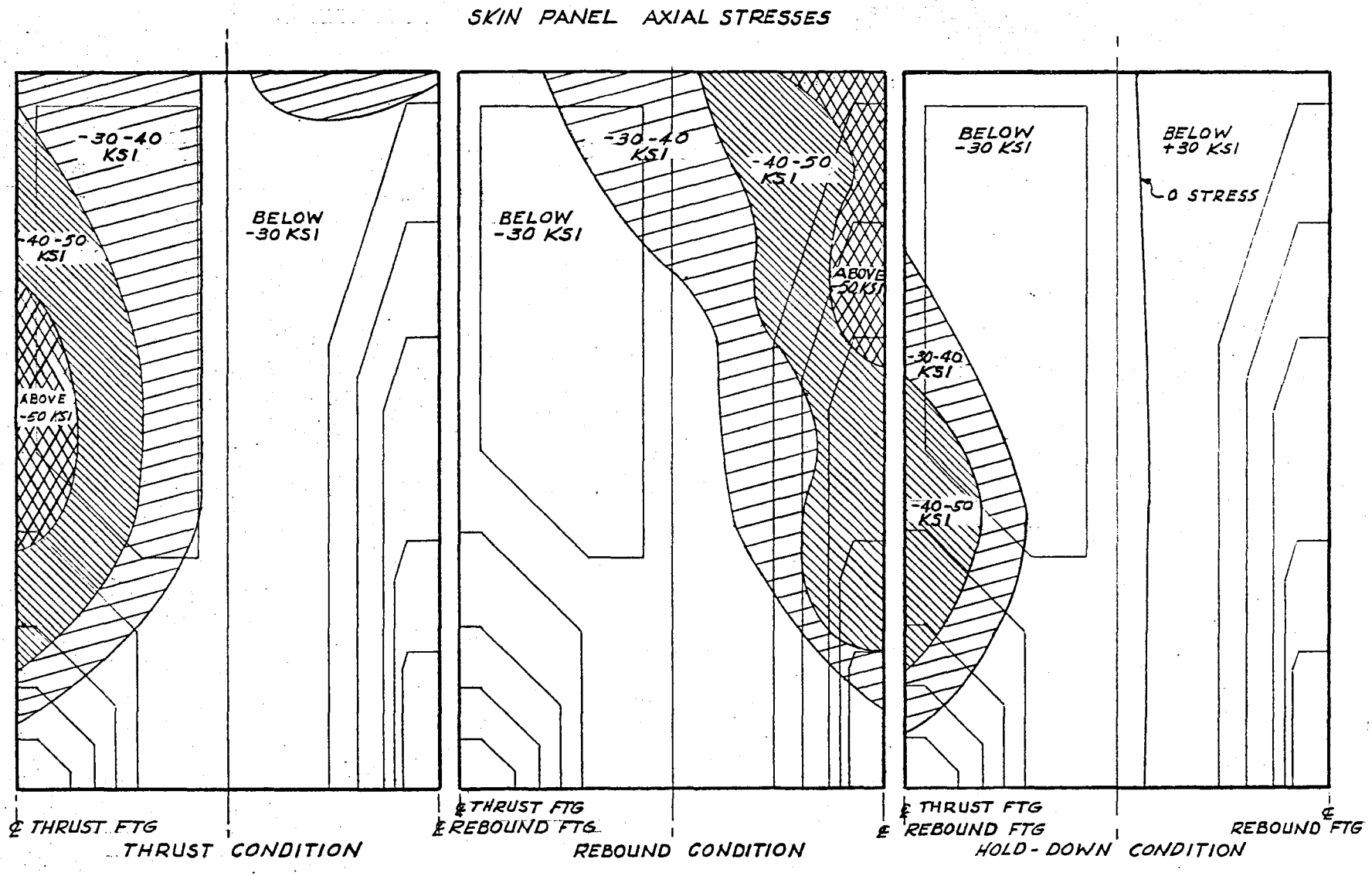

Figure 5-22 SKIN PANEL AXIAL STRESS ZONES

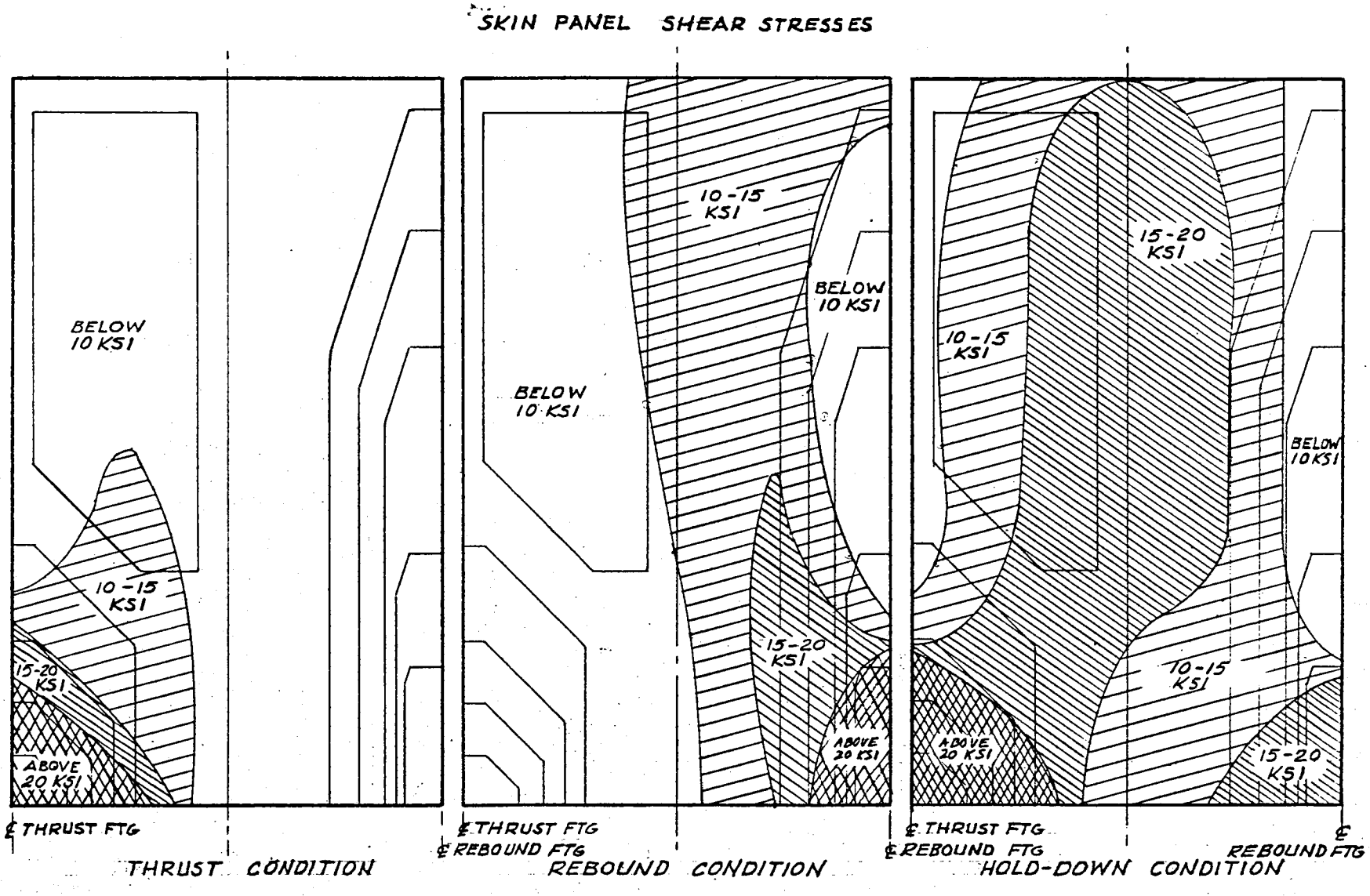

Figure 5-23 SKIN PANEL SHEAR STRESS ZONES

ultimate load below the ultimate shear strength of the facing sheet. It is seen in Figures 5-22 and 5-23 that maximum shear stresses are in moderate axial stress regions, and that high axial stresses are in areas of low shear stress.

The bonded sandwich panels are loaded along their upper edges through adhesive bonded attachment to a channel edgemember. The edgemember has a forward extension for mechanical attachment to adjacent forward structure. Applied axial distributed loads and joint allowable strength are plotted in Figure 5-24. The allowable was obtained from Figure A-5 (Appendix A). The panel lower edge contains a solid aluminum edgemember bonded into the sandwich assembly. Since edgewise shear is the primary applied load and edgemember cross-section is highly variable, a line of bolts is used to serve the dual purpose of transferring skin shear into the edgemember and of attachment of the lower ring frame to the sandwich panels. Applied shear load and allowable strength are plotted in Figure 5-25. Allowable strength is based on the more critical of skin bearing strength or standard bolt shear strength.

Attachment of panel vertical edges to the longeron utilizes steel bolts in a single row pattern. Bolt size and spacing are adjusted to insure adequate strength over the length of the pattern even though loads vary considerably. Plots of critical applied loads and of joint allowable load are presented in Figures 5-26 and 5-27. The panel edge is reinforced against crushing under bolt installation loads by the inclusion of a strip of high density core material in place of the regular 4.5 or 8.1 lb core (Reference Section E-E, Figure 5-10).

Splicing of sandwich panels at the line midway between longerons is accomplished by use of bolted-on splice plates. Figure 5-28 shows the applied load curves for the three design conditions as well as the allowable joint strength. This splice edge of each panel also contains the strip of high density core (23.5 lb/ft^3) to resist crushing under bolt installation loads. Access holes at mid-height on this splice line are treated in Subsection 5.3.4.

5.3.3 Lower Ring

The lower ring was designed as a 20 inch wide horizontal beam with heavy edgemembers and a bonded honeycomb web. The ring edgemembers attach at the ends to the thrust and rebound fittings and splice at the skirt panel splices. The ring sandwich webs are continuous from thrust to rebound fittings, at which points the webs are spliced. The design details are shown in Figure 5-29.

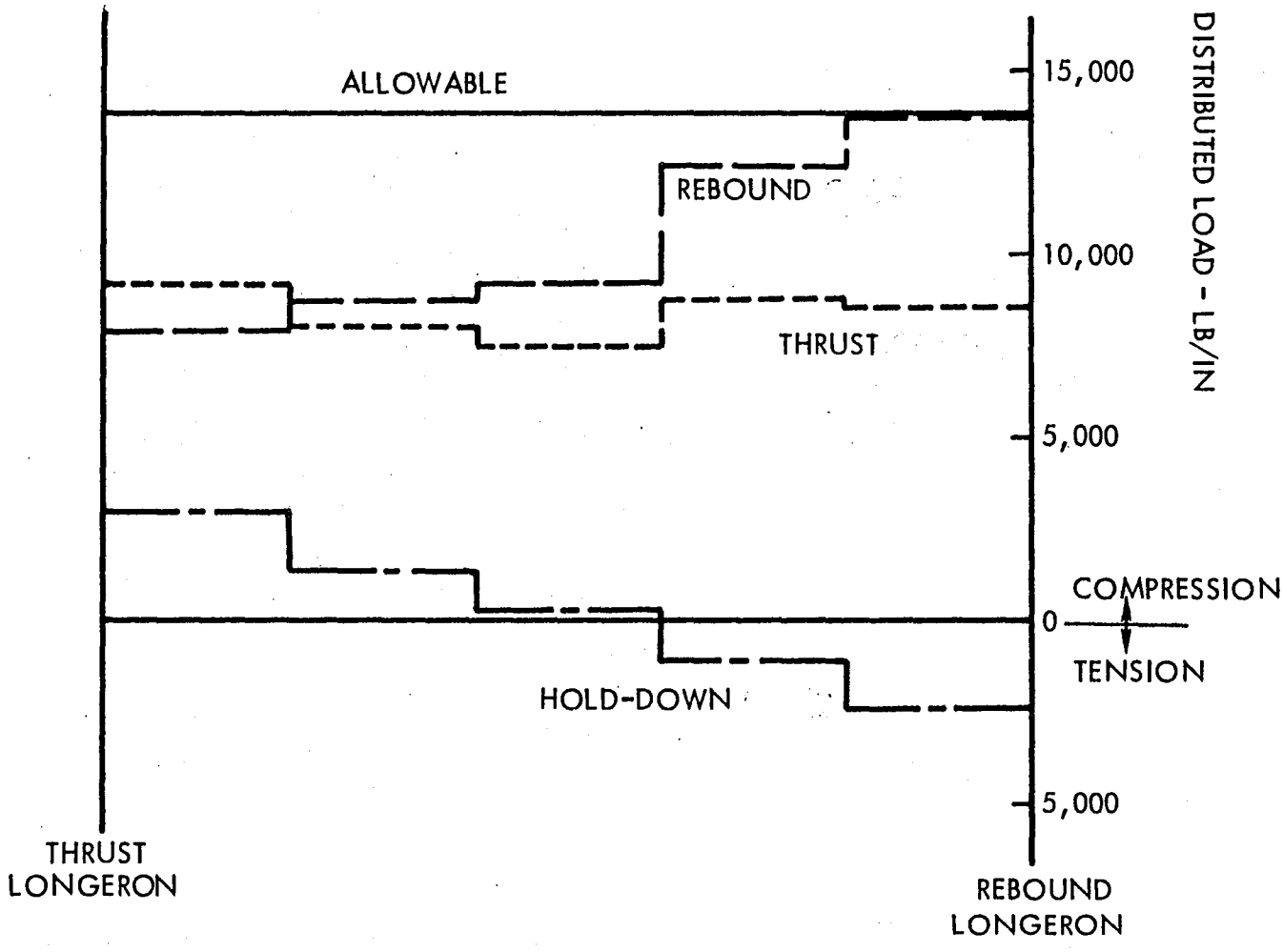

Figure 5-24 PANEL UPPER EDGE JOINT LOADING AND STRENGTH

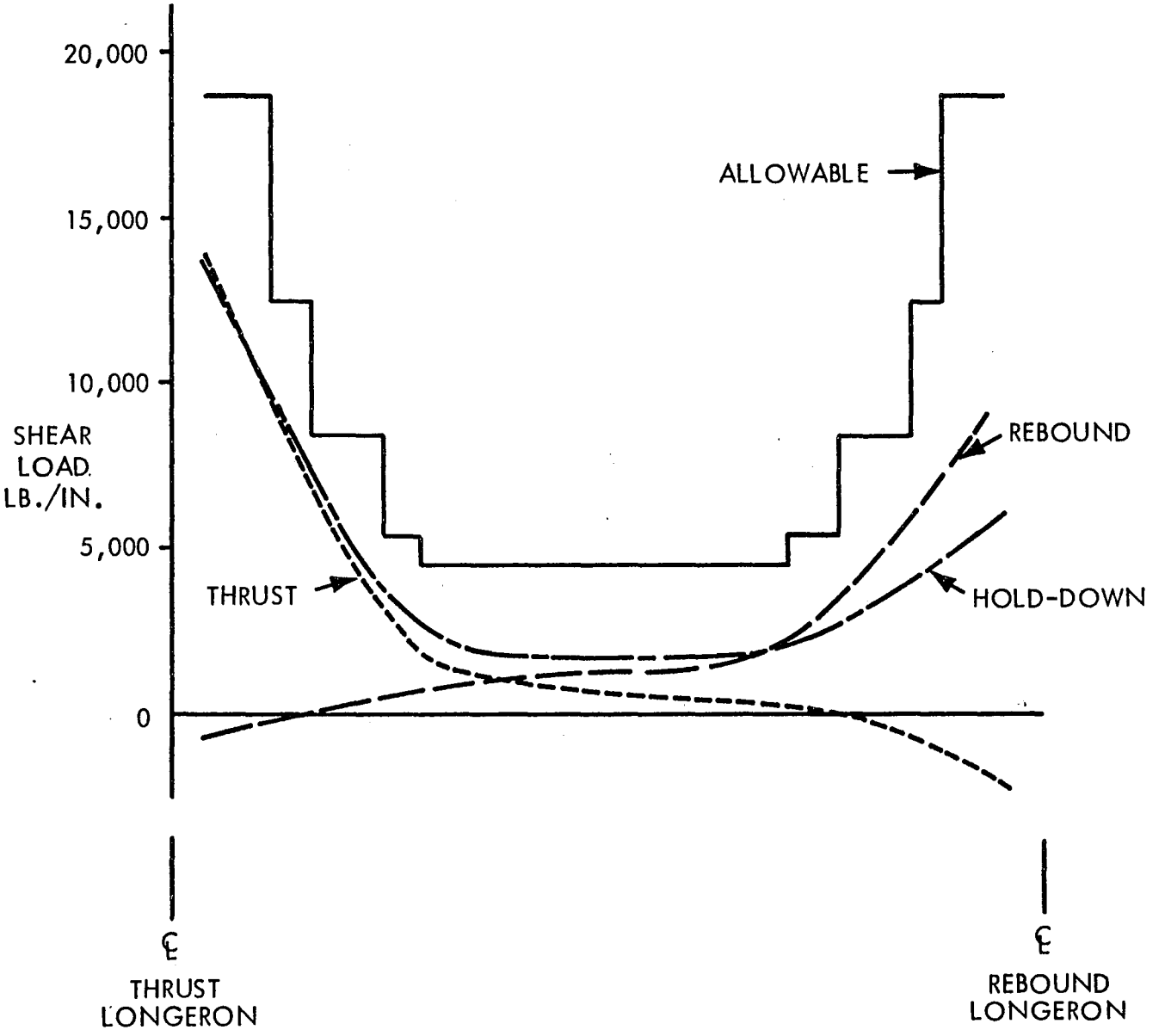

Figure 5-25 PANEL LOWER EDGE JOINT LOADING AND STRENGTH

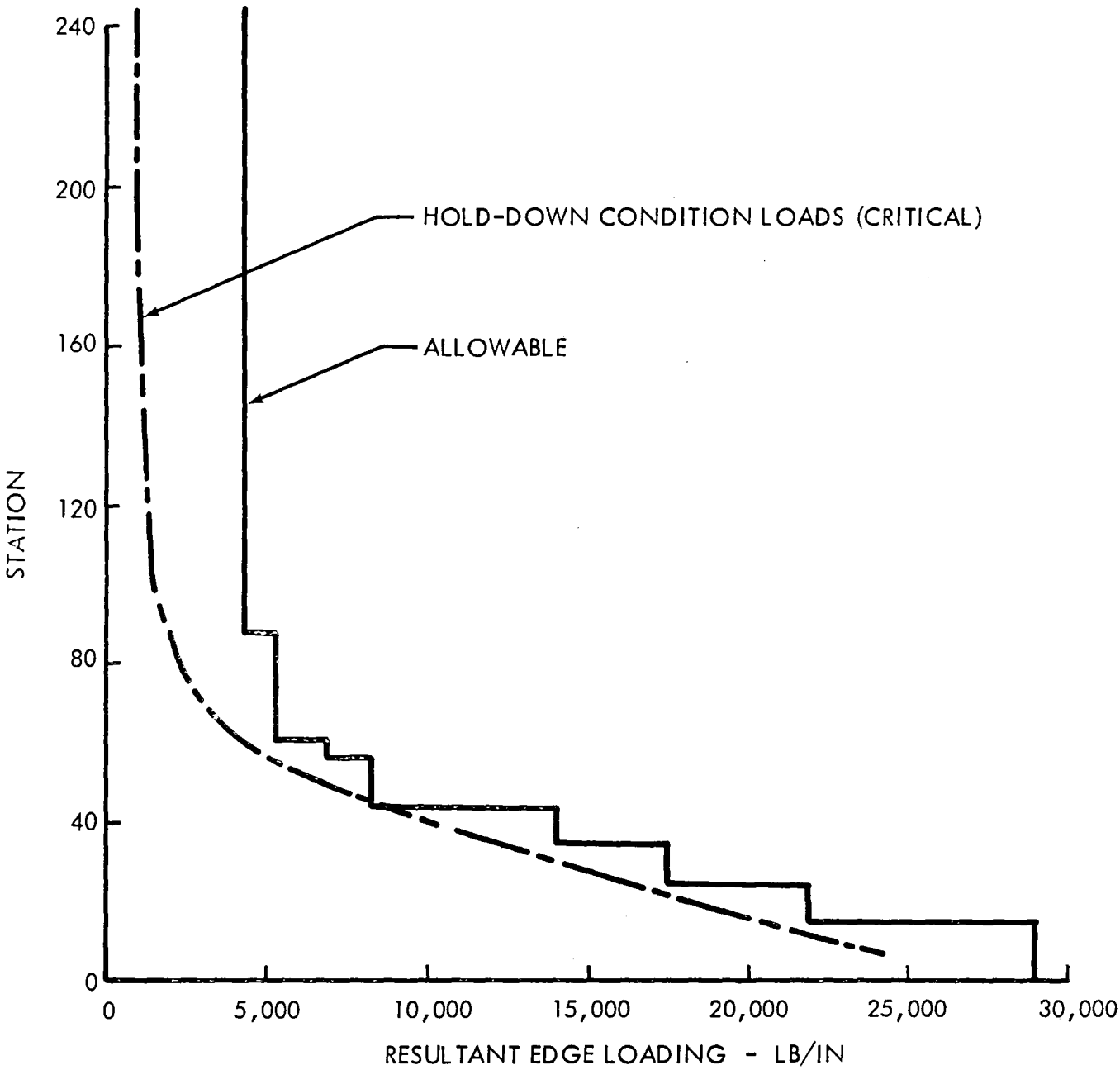

Figure 5-26 THRUST LONGERON ATTACHMENT LOADING AND STRENGTH

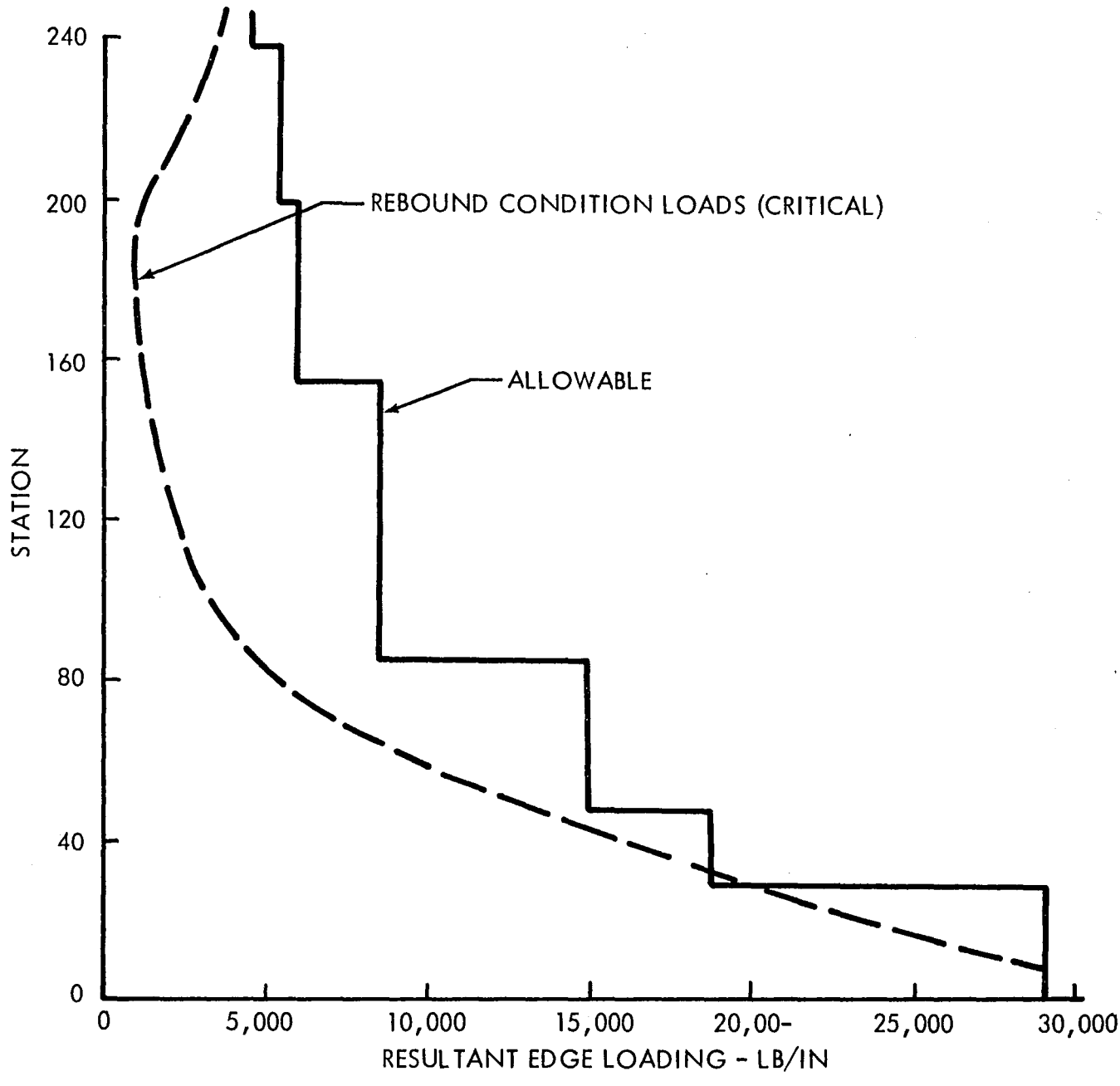

Figure 5-27 **REBOUND LONGERON ATTACHMENT LOADING AND STRENGTH**

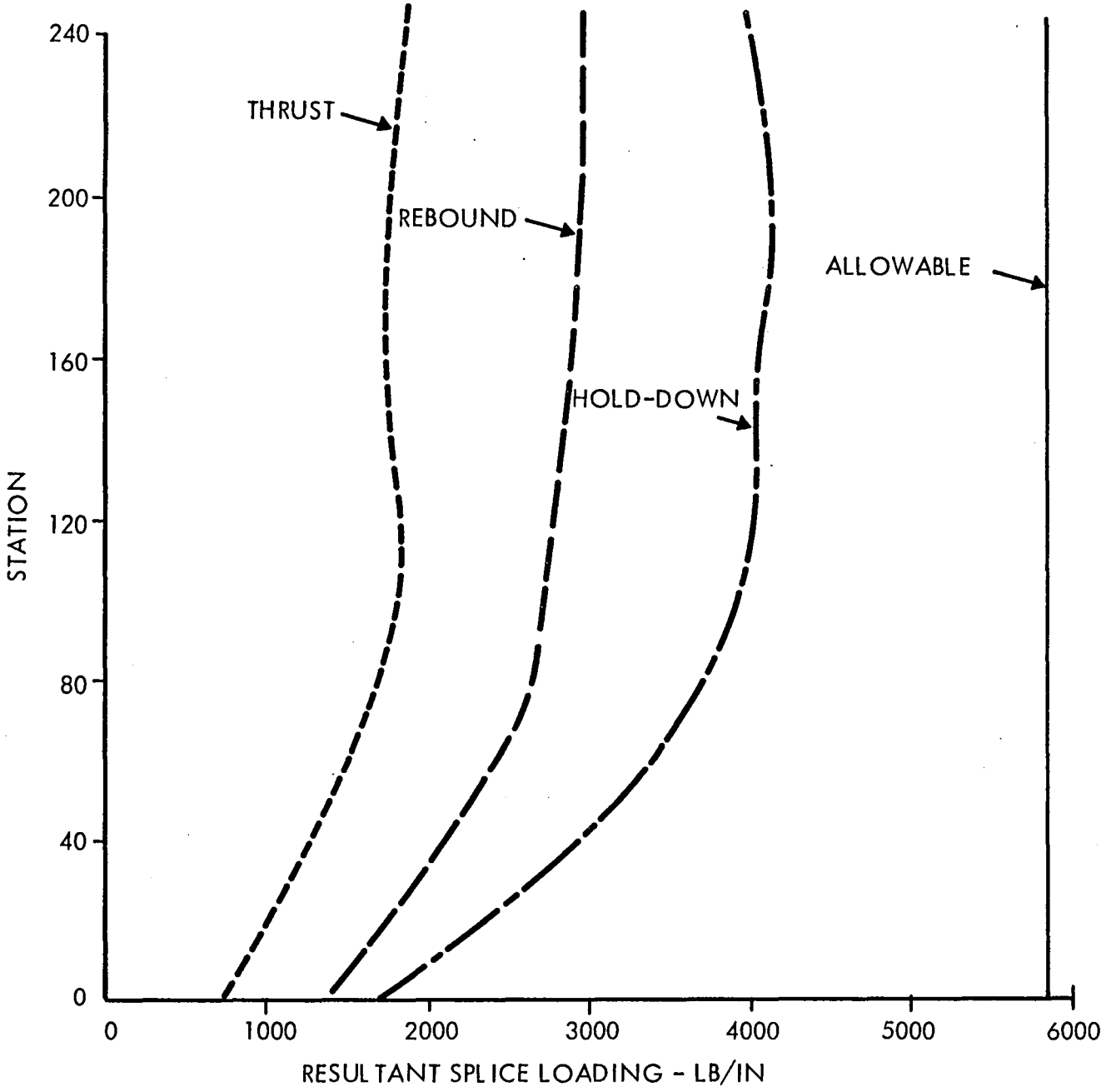

Figure 5-28 PANEL SPLICE ATTACHMENT LOADING AND STRENGTH

Loads in the lower ring are obtained from computer outputs for the three conditions of applied load. These loads establish requirements for flange area, web thickness, and attachment pattern.

Ring Load	At Thrust Longeron		At Rebound Longeron	
	Load	Condition	Load	Condition
Axial Tension	96,547	Rebound	252,727	Hold-down
Axial Comp. (lbs)	426,292	Hold-down	285,830	Rebound
+ Bending Mom	2,077,569	Rebound	3,307,507	Hold-down
- Bending Mom (in-lbs)	3,502,738	Hold-down	2,948,463	Rebound
Shear (lbs)	5,419	Thrust	8,947	Rebound

(+ Bending Moment is tension inboard)

Maximum shear at a section between longerons is 43,077 lbs, rebound condition

Geometry of the ring and position of its elements induce the following distribution of ring internal forces:

a) All transverse shear is carried by the web.
b) All axial force is carried by the outer flange. Where bending moment produces an outer flange load which relieves the direct axial force, only half of the relief is considered effective.
c) The inner flange load is produced by full bending moment.

These considerations result in a design summarized below:

a) Ring depth: 20 in. overall
b) Web: Sandwich, .040 faces, .75 core
c) Inner Flange: 3.5 in^2 at longerons taper to 1.75 in^2 mid-way between longerons
d) Outer Flange: 6.0 in^2 net at longerons, 2.5 in^2 mid-way between longerons.

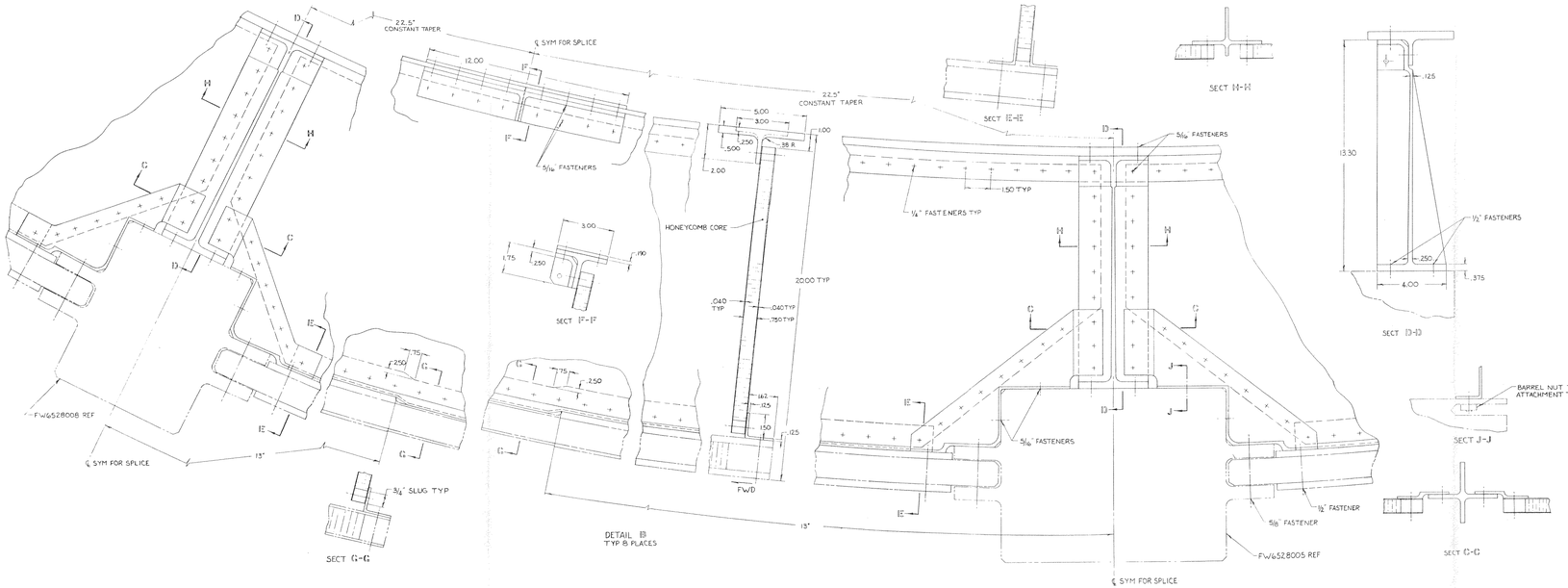

1. MATERIAL FOR MACHINED FITTINGS TO BE 7079 AL ALY.

NOTES.

Figure 5-29 Page 5-90

PRELIMINARY DESIGN DRAWING

HEAVY GAGE BONDED HONEYCOMB AFT RING INSTL (NAS8-11943)

(GRUMMAN) GENERAL DYNAMICS | FORT WORTH				FW628010

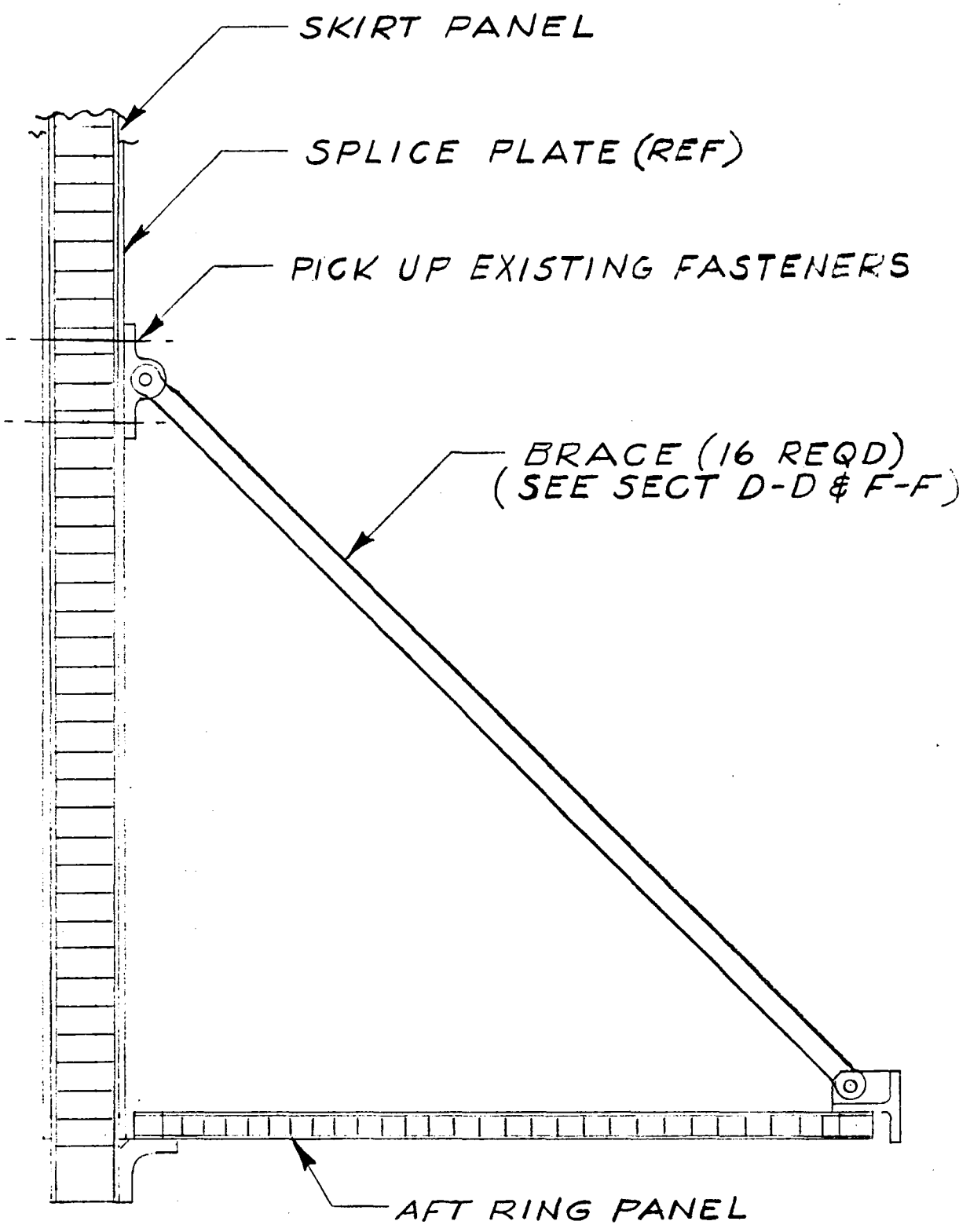

Figure 5-29 HEAVY GAGE BONDED HONEYCOMB
AFT RING INSTL (Sh. 2)

Note: Outer flange of ring includes lower edge slug in cylinder sandwich.

Maximum stresses induced in ring elements are as follows:

a) Web sandwich skin: 30,000 psi shear
b) Flange compression: 55,000 psi
c) Flange tension: 42,000 psi

5.3.4 Access Holes

A study was made of the splicing and reinforcement requirements at a typical access hole, and the resulting design is detailed in Figure 5-30, based on the analytical approach which follows, and on the results of several splice tests which are discussed in Subsection 4.3.1.1. Both bolted and welded concepts are illustrated.

Although door details are not shown, this design can represent either an open hole or a hole to be covered by a non-loaded access door. The door would be attached either by hinges or quick release mechanical fasteners.

The 20 inch diameter access holes required in the thrust cylinder are considered to be located at mid-height and midway between rebound and thrust longerons. This is a region of comparatively low skin stresses. Since resultant forces in the skin vary in direction with change in loading condition, a constant section reinforcement ring around the hole is required. During any specific loading condition, some portions of the ring are highly stressed while other portions are not.

If a uniformly stressed membrane has a hole which must be reinforced with like material in a manner allowing no increase in membrane stress around the reinforcement, the volume of ring material is double the volume of membrane removed. This is illustrated in the sketches below.

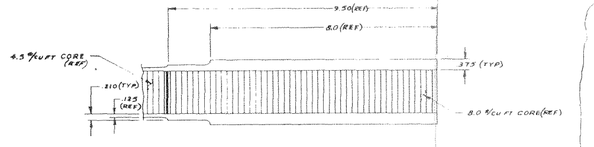

SECTION **C-C** FULL SCALE

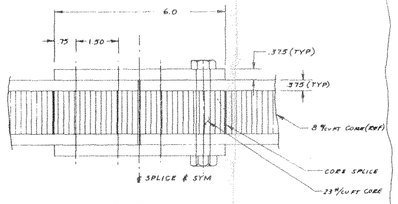

SECTION **B-B** FULL SCALE
(TYP BOLTED AND WELDED DESIGN)

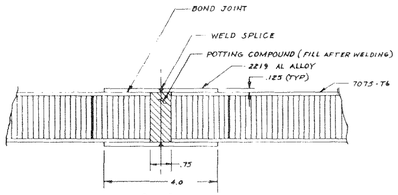

SECTION **A-A** (WELDED DESIGN)(FULL SCALE)

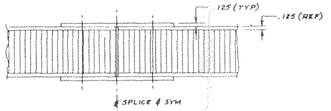

SECTION **A-A** FULL SCALE
(BOLTED DESIGN)

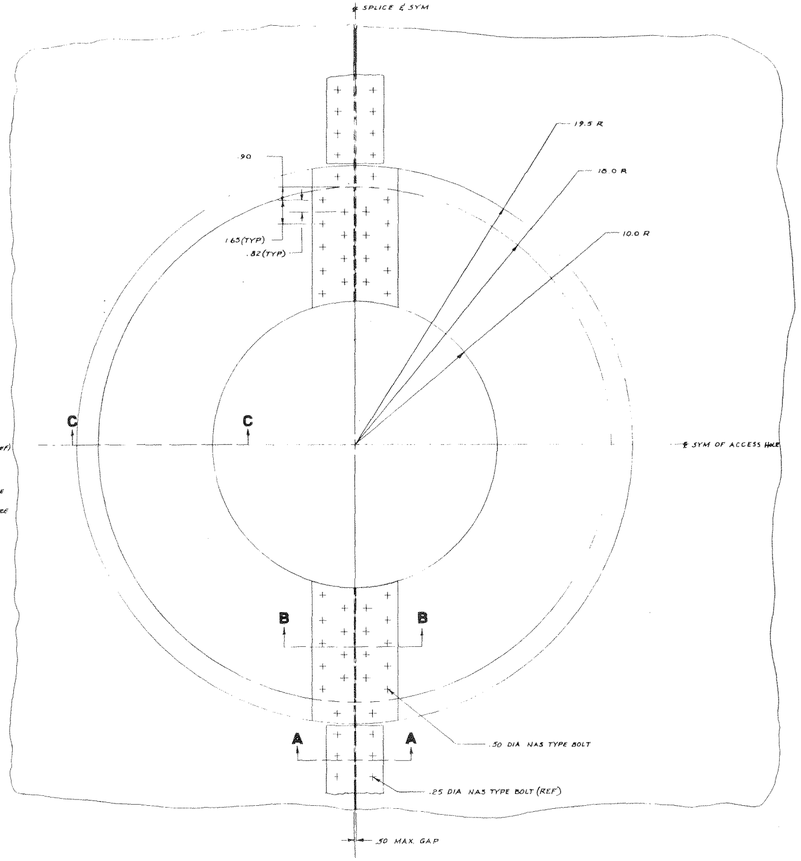

2. MATERIAL FOR WELDED SPLICE: 2219
1. MATERIAL FOR SPLICE PLATES & SKINS: 7075-T6
NOTES:

Figure 5-30 Page 5-43

PRELIMINARY DESIGN DRAWING

ACCESS HOLE - HEAVY GAGE BONDED HONEYCOMB (NAS 8-11949)

W. T. HOLLAR	CHECKED	APPROVED	DATE	DATE 8-8-66

GENERAL DYNAMICS | FORT WORTH

FW6328006

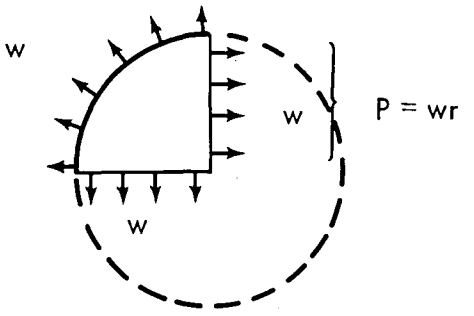

WEIGHT OF FULL DISC = $\pi r^2 t\omega$

w = distributed loading in membrane, lb/in.

r = hole radius, in

t = membrane thickness, in

ω = membrane material density, lb/in^3

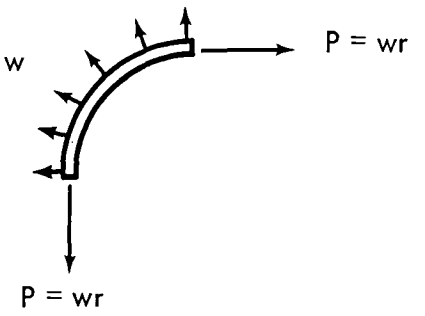

Note: To work at the same stress and therefore the same strain as membrane, ring crosssection area, A = tr
Weight of full ring = W_r

$$W_r = (A)\ (2\pi r)\ (\omega)$$

$$= (tr)\ (2\pi r)\ (\omega)$$

$$= 2\pi r^2\ t\omega$$

A directionally stressed membrane or skin with a hole will load a reinforcing ring much less favorably than the uniform stress case since ring internal bending moments are induced as well as the axial force. Then, a ring capable of supporting adjacent skin with approximately the stiffness of continuous skin must have a weight of several times that of the removed skin.

In the region chosen, rebound condition loads are critical, although thrust loads are nearly as high. These loads are:

Axial compression - 5120 lb./in.

Hoop compression - 302 lb./in.

Shear - 2950 lb./in.

These resolve into principal plane loads of 6200 lb/in. compression and 800 lb./in. tension. This loading can be treated as a uniaxial compression of 7000 lb./in.

As a rigid ring under plane loading, the reinforcement experiences the following internal loading at the critical section normal to the applied loading:

Axial load $P = w\ r$

Bending Moment $M = K_m\ Pr$

where $K_m = .19944$

Then $M = .19944\ w\ r^2$

An efficient reinforcement ring is obtained by increasing sandwich skin thickness locally. Since .375 gage skins are required elsewhere on the panels, this thickness is available in the skin for use around the access holes. By trial, a ring width of 8 inches was found to be adequate. With a hole radius of 10 inches, ring outer radius is 18 inches, and centroid radius is 14 inches. Applied load radius is taken as ring centroid radius, 14 inches.

Stresses induced at critical section of ring:

$f_b = 38,200$ psi (compression inside)

$f_c = 16,300$ psi

(total) $f_c = 54,500$ psi

Curved beam effect increases bending stresses at inner edge of ring and decreases them at the outer fibers.

r/c = 14/4 = 3.5

K_{inside} = 1.2

$K_{outside}$ = .83

f_b (inside) = 1.2 x 38,200 - 45,800 psi (comp.)

f_b (outside) = .83 x 38,200 = 31,700 psi (tens)

Net stresses:

f_c (inside) = 45,800 + 16,300 = 62,100 psi

f_t (outside) = 31,700 - 16,300 = 15,400 psi

Calculated deflections:

Ring deflection across mean dia. = .0998 inch

Adjacent skin deflection in 28 in. = .0785 inch

The close compatibility of deflections indicates that "rigid ring" analysis is applicable to this case and that adjacent skin stress distribution is not seriously affected by the reinforced access hole.

Calculated weight of reinforcement per hole is about 40 pounds. Weight of skin removed for hole is about 8 pounds. The net weight penalty is therefore approximately 32 pounds per access hole, excluding a door.

Splice of hole reinforcement occurs at the vertical center line where ring loads are somewhat lower than the maximum occuring near the horizontal line.

Axial load = K_a w r

where K_a = axial load coefficient

= .637 at a point 90° from max P

Splice axial load = .637 x 7000 x 14 = 62,400 lb.

Bending Moment = K_m Pr - K_m w r^2

where K_m = moment coefficient

= .174 at a point 90° from max P

Splice B.M. = .174 x 7000 x 14^2 = 238,000 in -lb

f_b = 29,800 psi

Due to curved beam effect,

f_b (inside) = 1.2 x 29,800 = 35,700 psi (tension)

f_b (outside) = .83 x 29,800 = 24,700 psi (compression)

f_c (direct axial) = 10,400 psi

Net stresses:

f_t (inside) = 35,700 - 10,400 = 25,300 psi

f_c (outside) = 24,700 + 10,400 = 35,100 psi

Maximum loading per facing

= 35,100 x .375 = 13,150 lb/in.

Splice bolts:

Bolt Spacing = .86 in.

Bolt Shear = .86 x 13,150 = 11,350 lb.

.50 dia. NAS bolt shear strength = 18,650 lb

7075T6 bearing strength = 17,500 lb

5.4 ALTERNATE DESIGN

The basic or primary design of the thrust skirt consists of sandwich panels of nonweldable materials which are attached to the thrust and rebound longerons by the use of bolts. The intermediate splices, panel to panel, are accomplished with bolted splice plates.

An alternate parallel design study was made for a welded structure. The initial investigation into the welded design began with a literature search of applicable aluminum welding techniques and candidate weldable alloys. The emphasis of the search was on TIG and electron beam procedures and how they applied to the selected skin gages. The candidate weldable aluminum alloys were 2219, 7106 and 7139. The 2219 alloy and TIG welding procedures were selected for use in the joint development phase of testing as a result of the literature search (see Subsection 1.1 and Report No. FZM-4445).

Manufacturing studies were made to determine the optimum design for the various skin gages and steps (see Subsection 3.3). Sandwich panels were fabricated using 1.5 inch thick aluminum 5052 core and .187, .375 and .500 2219 skins. All secondary and structural testing which involved welded specimens was done in support of the alternate weld joined design concept (see Subsections 3.2 and 4.1).

Mechanical and physical properties of nonweldable aluminums are commonly superior to the weldable alloys. Therefore, design of sandwich facings for weld joining to adjacent structure requires necessarily thicker material for a given load requirement, when the lower strength weldable alloys are used. Since the densities are virtually the same a weight penalty would result from use of weldable facings. For example, if the F_{ty} of nonweldable 7075-T6 alloy is taken as 73,000 psi from a materials handbook and the F_{ty} of weldable 2219-T87 is taken as 57,000 psi then the material requirement, and therefore weight, for a given load is 28 percent higher using the weldable alloy. For a complete structure as defined in this program, a 28 percent weight increase for weldable facings would add a weight penalty estimated at 2500 pounds.

The obvious alternative for weld joining panels to adjacent structure was to maintain the higher strength nonweldable facings for the alternate design and to bond-on weldable edgemember strips only. The welded attachment of adjacent panels was thus satisfied for the alternative design.

Welded attachment to longerons presented a similar problem. To use longeron forgings of a lower strength and weldable material made the weight penalty prohibitive, requiring over 1000 pounds of additional material. The alternative again was to use weldable edgemembers only, for panels and longerons; however, for the primary design, thrust and rebound loads are distributed directly to the panel facings by bolt patterns, not relying on adhesive shear strength. Therefore, to make use of weldable edgemembers, each edgemember would be bolted to the respective part and then weld joined. The obvious answer was simply to use bolts to join the panels directly to the longerons, which was the identical solution for the primary design.

The alternate weld joined design then, despite intensive investigation and testing, limited the actual use of weld joining to butt splices of adjacent panels only. Thus the parallel study alternate design became very similar in the final definition to the primary design.

The welding studies for the alternate design provided interesting information for possible application to other structures, such as:

1. No significant sandwich strength deterioration resulted from the weld joining process in either compression or shear tests.

2. The temperature in the facing could readily be controlled to avoid damaging the adjacent adhesive. Moderate temperatures were observed during welding within .10 to .15 inch from the edge.

Weld joining of sandwich is a practical assembly method and might well be feasible and used to better advantage for other applications.

5.5 THERMAL ANALYSIS

Cold Tank Effect at Upper Boundary

The attachment of a room temperature (+70°F) sandwich thrust cylinder to a cryogenic (-250°F) tank induces discontinuity stresses in the juncture area. These stresses in the sandwich are evaluated for the simple case of an abrupt step from warm to cold occurring at the sandwich edge. This is conservative in that an actual temperature gradient at the juncture would occur over a length of several inches.

The stresses obtained would combine with those existing in the structure as a result of primary loading. Since they are calculated for a structure not designed for use with a cryogenic tank, the combined loads would require additional structural material in the upper boundary region of the thrust cylinder. The thermal effects analysis for the skirt structure as designed only for primary loads is as follows:

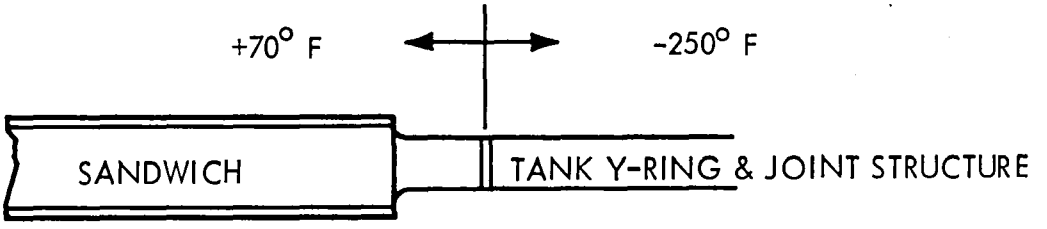

Tank unrestrained radial shrinkage

$$= \alpha \Delta T R = (11.0 \times 10^{-6})\ (320)\ (198) = .697 \text{ in.}$$

Forces induced at the joint are shears and moments large enough to force equal radial position and edge rotation of the two joined cylinders.

Let ϕ = joint rotation

ΔR = radial displacement from free position

then ϕ (tank) = ϕ (Sandwich)

and ΔR (tank) + ΔR (Sandwich) = .697 in.

$$\phi_T = \frac{M}{D_T \lambda_T} + \frac{V}{2 D_T \lambda_T^2}$$ Reference 5-1

$$\phi_S = -\frac{M}{D_S \lambda_S} + \frac{V}{2 D_S \lambda_S^2}$$

$$\Delta R_T = \frac{M}{2 D_T \lambda_T^2} + \frac{V}{2 D_T \lambda_T^3}$$

$$\Delta R_S = -\frac{M}{2 D_S \lambda_S^2} + \frac{V}{2 D_S \lambda_S^3}$$

where $D_T = \frac{E t^3}{12 (1-\mu^2)}$ (homogeneous plate)

$D_S = \frac{E h^2 t_f}{2 (1-\mu^2)}$ (sandwich)

$\lambda_T = \sqrt[4]{\frac{3(1-\mu^2)}{R^2 t^2}}$ (homogeneous plate)

$\lambda_S = \sqrt[4]{\frac{E (2tf)}{4 R^2 D}}$ (sandwich)

Using tank Y-ring properties

$E = 11.3 \times 10^6$ psi (-250^oF)

$t = 1.0$ in.

$\mu = .30$

$D_T = 1.035 \times 10^6$

$\lambda_T = .0913$

and sandwich properties

$E = 10.4 \times 10^6$ psi

$t_f = .125$ in.

$h = 1.625$ in.

$\mu = .30$

$D_S = 1.887 \times 10^6$

$\lambda_S = .0545$

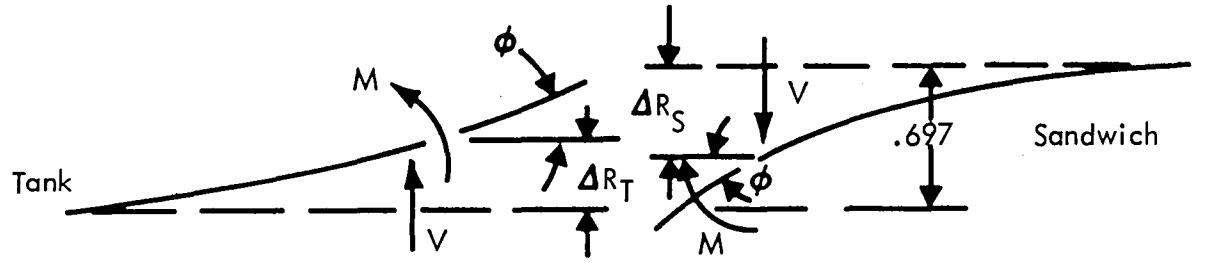

Solution of the equations of rotation and displacements for the distributed discontinuity loads V and M yields:

$V_o = 314$ lb/in.

$M_o = 485$ in.-lb/in.

Radial displacements at joint:

$\triangle R_T = .227$ in. outward from free position

$\triangle R_S = .470$ in. inward

Joint rotation:

$\phi = .02333$ radian or 1.337 degrees

Bending moment is maximum at a point away from the edge due to the predominant effect of edge radial shear.

$$M_V \text{ (max.)} = .322 \frac{V}{\lambda} \quad \text{at } x = \frac{\pi}{4\lambda}$$

M_V = 1860 in. - lb/in. at 14.4 in. from end

Discontinuity moment M_o has diminished at this point to

$$M = M_o \quad e^{-\lambda x} \quad (\cos \lambda x + \sin \lambda x)$$

M = 315 in.-lb/in. opposite in direction from M_V

Maximum net moment:

M_{max} = 1860 - 315 = 1545 in.-lb/in. (compression inside)

Stresses produced by thermally induced discontinuity loads:

Sandwich edge member bond joint:

Overlap length L = 2.0 in.

Core thickness t_c = 1.5 in.

$$f_s = \frac{Mo}{t_c L} = \frac{485}{1.5 \times 2} = 162 \text{ psi}$$

Sandwich core:

Facing centroid spacing h = 1.50 + .125 = 1.625 in.

$$f_s = \frac{V}{h} = \frac{314}{1.625} = 193 \text{ psi}$$

Facings:

Take the general case where facing thickness is .125 in.,

$$f_b \text{ (longitudinal)} = \frac{M}{ht_f} = \frac{1545}{1.625 \times .125} = 7600 \text{ psi compression inside}$$

Hoop compression:

$$f_c = \frac{2 V \lambda R}{2 t_f} - \frac{2 M_o \lambda^2 R}{2 t_f} = 24{,}920 \text{ psi}$$

Thermally induced dimensional changes provide additional stresses in the upper end of the sandwich cylinder. These stresses along with the discontinuity stresses calculated above combine to require additional sandwich strength in the upper end region. Approximately 50% increase in the inner facing thickness extending down about 24 inches would be required to retain a safe stress level. Also, the upper edge member bond joint to the sandwich skin would require some additional overlap length. No change in core thickness or density would be required. Additional weight in upper end of sandwich is estimated to be about 200 lbs.

5.6 FLUTTER ANALYSIS

Reference 5-2 presents experimental flutter data for various types of panels. These results are presented in Figure 5-31. The two curves shown are bounds separating the three regions of Flutter, Flutter Questionable, and No Flutter. The length/width ratio is plotted versus the standard flutter parameter. This parameter is

$$\left(\frac{BE}{q}\right)^{1/3} \frac{t}{L} \quad ,$$

where

$B = \sqrt{M^2-1}$

M = Mach Number

E = Young's Modulus

q = dynamic pressure

t = panel gage

L = panel length

These parameters have been applied to the thrust structure with the objective of substantiating a more detailed flutter analysis. Four data points have been prepared, and are shown superposed on the figure.

The presented data are for a single panel which comprises one-eighth (1/8) of the skirt). Its length is the full skirt length and it is bounded on each side by the thrust and rebound columns. Said data also considers the honeycomb panel to have constant gage skins of the indicated value (t). The actual skirt gages vary throughout the structure, with minimum of 0.100 inch.

The skin gage (t), along with the core depth, was used in arriving at an effective thickness (t_{eff}) for a flat plate which possesses the same bending stiffness. This value was needed as a substitute for the honeycomb in the flutter parameter. The t_{eff} was then reduced to account for the prestressed condition caused by the thrust loading. This reduction amounted to a straight

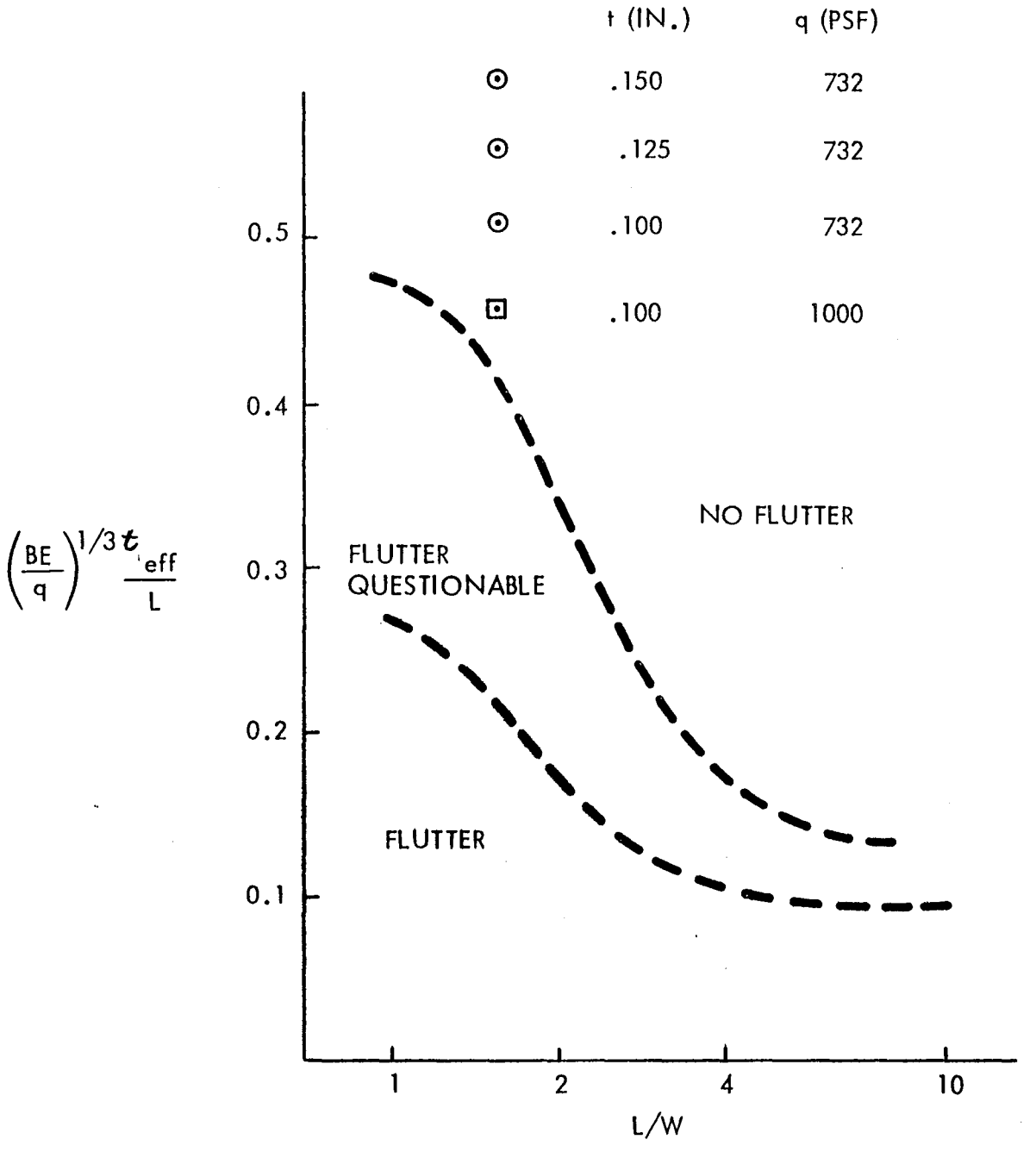

Figure 5-31 PANEL FLUTTER PREDICTION

fifteen percent in bending stiffness even though the analysis indicated a fifteen percent as maximum which appeared in one local area and was much less elsewhere.

The dynamic pressure used (732PSF) was obtained from a Saturn I B maximum dynamic pressure trajectory. Realizing that there shall be some variation in dynamic pressure in changing to a Saturn V trajectory, an extra data point for the minimum honeycomb skin gage (0.1") and an enlarged pressure (1000) has been included.

It was concluded from this analysis that panel flutter of the thrust structure shall not occur within a reasonable flight envelope and a more detailed analysis was therefore unnecessary.

5.7 ACOUSTIC ANALYSIS

Honeycomb sandwich panel construction is by nature highly resistant to fatigue damage by acoustical noise loading. However, because of the extremely high noise levels produced by the Saturn engines, an approximate analysis was conducted to demonstrate that the proposed heavy gage honeycomb structure has a more than adequate sonic fatigue life in this environment.

The panel analyzed extends from thrust fitting to rebound fitting. This is actually made up of two panels joined together by a welded joint or a mechanically fastened joint. It was assumed that the joint will approximate the stiffness of the panel. Also for analysis purposes the panel was assumed to be flat. This simplification is necessary because of lack of knowledge of the response of curved panels. It has been shown to add conservatism to the analysis.

The fundamental frequency was calculated using the following formula:

$$f = 0.01 \sqrt{\frac{K}{M}}$$

where: K = spring constant $= \dfrac{D}{K_1 + VrD\ K_2}$

M = mass $= a \times b \times \rho$

.01 - an empirical constant which includes the conversion from radians to cps.

a = short dimension of panel, inches

b = long dimension of panel, inches

$$D = \frac{E_F}{12\ (1-\mu^2)} \left| t^3 - t^3_c - 3\ t_c\ (t_{F_1} - t_{F_2})^2 \right|$$

E = Modulus of elasticity

G = Modulus of rigidity

K_1 & K_2 = Empirical constants related to shear

t = thickness, inches

u = transverse shear stiffness = $\frac{(t + t_c)^2}{4t_c} Gc$

v = dimensionless parameter = $\frac{D}{a^2U}$

μ = Poisson's ratio

$$\rho = \frac{(\gamma_{F_1} t_{F_1}) + (\gamma_{F_2} t_{F_2}) + (\gamma_c t_c)}{386}$$

γ = weight, lb/in^3

subscripts: F = face, used with 1 and 2 to denote particular face, c = core

The fundamental frequency was calculated first assuming a constant skin thickness of 0.10 inch, then again assuming a constant skin thickness of 0.375 inch. These thicknesses represent the lower and upper limits of skin gages used on the panels. The frequencies calculated were 79 cps and 107 cps. The fundamental frequency should lie somewhere between these two limits and, because of frequency rising due to panel curvature, probably toward the upper frequency. A frequency of 100 cps was used in further analysis.

The sonic fatigue life was calculated using a method based on the works described in References 5-3 and 5-4. Experimental investigations have shown that a structure will accept energy from the random pressure fluctuations only at or near its natural frequencies. Furthermore, the maximum amplitude of the response is usually at the lowest natural frequency. The spectral density function of the random noise from the booster engines is relatively flat and may be considered constant over the narrow frequency range of the maximum response.

The rms stress corresponding to the acoustic loading σ_r was calculated by:

$$\sigma_r = \sqrt{\frac{\pi}{4\eta}} \times \sqrt{\phi_n f_n} \times \sigma_m$$

which is derived from the differential equation of motion for forced vibration of a linear single-degree-of-freedom system using the assumptions given in the paragraph above. In this

form the term $\sqrt{\frac{\pi}{4\eta}}$ accounts for the damping of the structure, the term $\sqrt{\phi_n f_n}$ accounts for the sound pressure impinging on it and σ_m is the maximum stress produced by a unit loading.

The damping of honeycomb structure is characteristically high, so for this case the damping factor η is assumed to be .04.

The maximum stress due to a unit static load was calculated by:

$$\sigma_m = \frac{\beta a^2}{h_e^2}$$

h_e = equivalent thickness = $2\sqrt{3 \lambda F \frac{D}{H}}$

a = short side of panel

β = empirical constant accounting for edge fixity.

$H = E_F (t - t_c)$

The acoustic loading ($\sqrt{\phi_n f_n}$) was evaluated by adding $10 \log_{10} f_n/\Delta f$ to the sound pressure level predicted for the 1/3 octave band containing the fundamental frequency, f_n, and converting to psi. For 1/3 octave bands $10 \log_{10} \frac{fn}{\Delta f} = 6.28$ db.

$$\sqrt{\phi_n f_n} = 154.5 \text{ db} + 6.28 \text{ db} = 160.78 \text{ db}$$

$$160.78 \text{ db} \approx .33 \text{ lb/in}^2$$

The rms stress corresponding to the acoustic loading is then:

$$\sigma_r = \sqrt{\frac{\pi}{4\eta}} \times \sqrt{\phi_n f_n} \times \sigma_m = 7.050 \text{ psi}$$

The equivalent constant amplitude stress which would cause the same damage as the rms stress is calculated by:

$$\sigma_e \approx \sqrt{\frac{a \sigma_r^2}{e}} \approx 14{,}200 \text{ psi}$$

where: a = the inverse slope of the idealized σ-n curve for the material

e = the base of natural logarithms.

From the σ-n curve the cycles of life corresponding to 14,200 psi stress is:

$$N = 1 \times 10^9 \text{ cycles}$$

Then the sonic fatigue life in hours,

$$T = \frac{N}{f_n\ (3600)} = 2{,}780 \text{ hours}$$

This is several orders of magnitude greater than the required life of the honeycomb structure. However, this life is highly sensitive to the stress amplitude. To illustrate this, consider the life if the equivalent stress should actually be as much as twice that predicted, or 28,400 psi.

$$\text{then } N = 9 \times 10^5$$

$$\text{and } T = 2.5 \text{ hours}$$

This is still many times the planned duration of the high intensity noise environment.

5.8 REFERENCES

5-1 Roark, R. J., Formulas for Stress and Strain, McGraw - Hill Book Company, Inc., New York, 1954, Third Edition.

5-2 Kordes, E. E., Tuorilla, W. J., and Guy, L. D., Flutter Research on Skin Panels, NASA, TND-451.

5-3 Miles, J. W., "On Structural Fatigue Under Random Loading," Journal of the Aeronautical Sciences, November 1954.

5-4 Miner, M. A., "Cumulative Damage in Fatigue," Journal of Applied Mechanics, September 1945.

SECTION 6

DESIGN EVALUATIONS

6.1 WEIGHT COMPARISON STUDY

The total weights of the major structural categories of the sandwich thrust skirt design are presented in Table 6-1. The corresponding circular segment chart of Figure 6-1 shows the relative importance of the various components in the total weight.

A more detailed tabulation of component weights appears in Tables 6-2 and 6-3, and a comparison of the sandwich skirt weight with a plate-ring-stringer designed skirt weight is shown in Table 6-4. Structural components other than the cylindrical shell structure and intermediate stabilizing elements, such as attach edgemembers, forward attach ring, and aft stabilizing ring, though of different configuration, would be of equal weight for both design concepts. The thrust and rebound longerons would also be of equal weight for either design.

Table 6-1 TOTAL WEIGHTS OF MAJOR STRUCTURAL CATEGORIES

Weight Summary – Sandwich thrust cylinder assembly

Item		Weight (Lbs)
Honeycomb Sandwich		
Skin	9059	
Core	1570	
Adhesive	670	
		11,299
Panel Splices and Edge Members		1,591
Longeron Fittings		4,050
Fasteners		502
Total		17,442

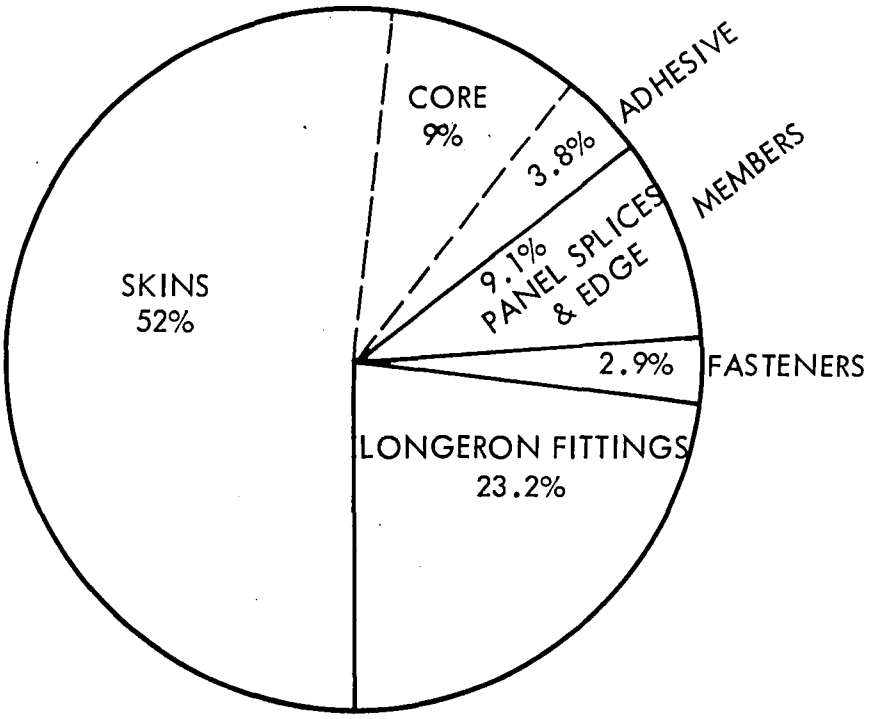

Figure 6-1 RELATIVE WEIGHTS OF MAJOR STRUCTURAL CATEGORIES

Table 6-2 DETAILED WEIGHT TABULATION FOR SANDWICH CYLINDER

Item		Weight (Lbs)
Bonded Sandwich Assemblies (Excluding edgemembers)		
Facing Sheets (Including access hole reinforcement)		
Thickness Regions (in.)	.100	1385
	.125	3137
	.150	1104
	.200	1072
	.250	1008
	.300	317
	.375	1036

9059

Table 6-2 (Cont.)

Item			Weight (Lbs)
Honeycomb Core			
Density (lb/ft^3)	4.5	976	
	8.1	304	
	23.5	290	
			1570
Adhesive (.15 lb/ft^2)			
			670
		Total	11,299

Table 6-3 DETAILED WEIGHT TABULATION FOR AUXILIARY STRUCTURE

Item		Weight (Lbs)
Longeron Assemblies		
Rebound, Hold-down		
Upper longerons	916	
Lower fittings	1490	
		2406
Thrust		
Upper longerons	676	
Lower fittings	968	
		1644
		4050

Table 6-3 (Cont.)

Item		Weight (Lbs)	
Edge Members and Splices			
Top edge ring		240	
Panel Splice Plates		197	
Lower ring frame			
Cylinder lower edge slugs	394		
Frame Sandwich Web	386		
Inner Flange	256		
Splice Angles & Fittings	118		
		1154	
			1591
Fasteners (bolts, lock-bolts)			502
		Total	6143

Table 6-4 WEIGHT COMPARISON — SANDWICH VERSUS PLATE STRINGER

		Weight (Lbs.)
1. Sandwich Skirt:		
Honeycomb Sandwich		
Skin (including access hole reinforcement)	9059	
Honeycomb core	1570	
Adhesive	670	
		11,299
Auxiliary Structure (Splices, end rings, bolts, fittings)		6143
	Total	17,442
2. Plate-Stringer Skirt:		
Cylinder Covering		
Skin	8576	
Stringers	2864	
Intermediate Rings	1128	
Access Hole Frames	329	
		12,897
Auxiliary Structure		6143
	Total	19,040

Weight Savings for Bonded Honeycomb Structure = 1598 pounds

The weight comparison study with a conventional plate-ring-stringer design was not meant to be more than a preliminary estimate to indicate approximately the weight difference of the two designs. Weight savings for a heavy gage bonded honeycomb design was not a primary objective of the program. The weight comparison calculations show an approximate 1600 pounds savings for bonded honeycomb structure and are based on conservative estimations such that an accurate weight comparison of two final designs would be expected to show a minimum ten percent savings for the bonded honeycomb skirt.

A weight comparison of the primary sandwich skirt design with the parallel study alternate sandwich design would show a negligible weight difference between the two because of the high commonality of the two final designs.

6.2 COST ANALYSIS ESTIMATE

An analysis was made to estimate costs of bonded honeycomb sandwich thrust skirts. The two designs for which costs were compared were the primary design utilizing bolted panel splice joints, and the alternate design with the panels spliced by weld joining.

The costs were based on certain arbitrarily selected criteria which, however, were set in an attempt to provide realistic answers. Engineering costs were not included in order to limit estimates to cost comparisons of the structure.

Pertinent criteria influencing costs were selected as follows:

1. Estimate to be budgetary
2. Assumed go-ahead of 1 January 1967
3. Workweek - 5 days of 8 hours with spot overtime as required
4. Costs not to include cost of required welding facilities which are not currently available at the Fort Worth plant.
5. For quantities of 10 units, costs to assume a production rate of one complete unit every two months
6. Tooling to be based on the assumption that there will be a total of only ten units.

The results of the cost analysis as follows are for comparison purposes and does not constitute a commitment by General Dynamics:

	Bolted		Welded	
	One Unit	Ten Units	One Unit	Ten Units
Tooling	$ 82,000	$123,000	$126,000	$173,000
Quality Control	103,000	627,000	155,000	941,000
Manufacturing	629,000	3,973,000	944,000	5,960,000
Material	94,000	756,000	101,000	799,000
Tool Material	15,000	16,000	25,000	27,000
Gen'l. and Adm. Exp.	46,000	275,000	68,000	395,000
Total Cost	$ 969,000	$5,770,000	$1,419,000	$8,295,000

The welded design cost estimate is shown to be considerably greater than that for the bolted design because of additional tooling requirements and limited cost experience with welded fabrication of large

honeycomb structures. Welding requires additional expense for preparation of the material and edges, and inspection of the welded joints would be difficult and expensive. Also, the repair and scrappage rate would be higher for welded assemblies.

6.3 MANUFACTURING CONSIDERATIONS

6.3.1 Manufacturing Plan

Production of a sandwich booster skirt would require a Manufacturing Plan to insure fabrication of flight hardware of the highest quality, lowest cost, and to the necessary production schedule requirements. The manufacturing plan would describe operational sequences and provide illustrations for the structural fabrication of the details and subassemblies for the thrust skirt, longeron-fittings, aft ring, and the final assembly of all components. Tooling requirements to implement the fabrication and assembly procedures would also be included.

A sample Manufacturing Plan is illustrated in Appendix E for the concept of a heavy gage bonded honeycomb thrust skirt as derived in this program. The plan illustrates what would be required to serve as a guide for the preparation of manufacturing and process specifications appropriate for producing a full scale thrust structure skirt.

6.3.2 Quality Control Plan

Attendant with a manufacturing plan for production of a bonded honeycomb thrust skirt would also be a Quality Control Plan. The quality control requirements and objectives peculiar to specific contracts are planned, coordinated, and administered in accordance with the applicable work statement or contract. The quality control plan would be prepared to establish sound quality control practices and policies and to provide high quality workmanship in the production of all assemblies, subassemblies and detail parts. The practices and policies would be applicable at all times with respect to materials, parts and assemblies, as well as to the procedures related to material handling, from incoming raw stock and purchased parts to the final shipment of finished items.

A quality control outline of requirements for manufacture of heavy gage bonded panel assemblies is given in Appendix F. Similar quality control requirements would also be made for all other detail parts of the thrust skirt. This sample document illustrates the policy that would be used in establishing procedures for use in controlling the incoming materials to assure that they comply with specifications, and in controlling and monitoring the manufacturing processes.

SECTION 7

PROGRAM CONCLUSIONS

The performance of this program has provided the opportunity for valuable insight and information through research into previously unexplored areas of heavy gage bonded honeycomb structure. As a direct result of this contract such relationships were established as, (a) joint peak stress and adhesive shear modulus, (b) joint load capability as a function of peak stress, (c) the significance of sandwich panel edgemember cross-section shape on load transfer through adhesive shear strength, and (d) combined bonded-bolted joint performance versus theory. In addition, certain fabrication variables previously thought to be critical to the strength of structural sandwich was found to be of less importance.

The basic conclusions, then, of the performance of this program are:

1. Heavy gage bonded honeycomb is feasible for primary load carrying structure as determined by intensive investigations and test programs.

2. Heavy gage bonded honeycomb does offer valuable weight savings.

SECTION 8

RECOMMENDATIONS

The necessary experimental background to support the use of heavy gage bonded honeycomb should have as a minimum two programs:

1. Fabrication of a sandwich cylinder of scaled-down proportions not less than 10 feet in diameter and with scaled-down sandwich dimensions from the present development program but with uniform facing gages. This cylinder would be tested under a uniform compression load to failure. This test would verify the basic Small Deflection Theory approach to sandwich cylinder stability upon which the present program final design has been predicated and which results in maximum weight savings advantages.

2. A full scale sandwich cylinder incorporating the final design of the present development program should be tested under the design loading conditions to failure. This test would prove the ability of honeycomb core to stabilize heavy gage facings to stresses approaching the facing yield strengths. Also, it would provide additional confidence in the current capability for fabrication of large heavy gage sandwich cylinders.

A P P E N D I X A

S E C O N D A R Y T E S T I N G

This appendix contains the data generated in the phase of secondary testing and discussions of the data. The test equipment and procedures utilized are discussed and the test data is presented in General Dynamics Engineering Test Laboratory Report Number FTDM-3549 which follows.

TEST: Phase II, Test Program - Heavy Gage Bonded Honeycomb

OBJECT: This program was designed to obtain the sandwich edgewise compression strengths and double-lap shear strengths of bonded joints at room, elevated, and cryogenic temperatures using specially designed specimens which were loaded in tension or compression.

PROGRAM:

TEST SPECIMENS

The test specimens were delivered to the Engineering Test Laboratory ready to be measured and tested. The details of the specimen designs, a list of materials, and the method of fabrication are recorded in GD/FW Drawing Number FW6528002. Sketches of the basic configurations are shown by Figures 1, 2, and 3.

TEST EQUIPMENT AND PROCEDURE

The tension and compression loads were applied to the various specimen configurations with either a 60,000-pound or a 120,000-pound capacity Baldwin Universal Test Machine. The compression specimens were positioned between standard compression plates centered in the test machine with their faces parallel. The arrangements for the room, elevated, and cryogenic temperature tensile tests are shown by Figures 4, 5, and 6, respectively. The clevises were designed to accommodate the three specimen thicknesses by interchangeable bushings. All of the parts were fabricated from 18 Ni Maraging steel and heat treated to the 250-ksi minimum strength level.

The elevated temperature tests were conducted in a General Dynamics designed circulating air furnace and the temperature was monitored with a clip-on thermocouple connected to an appropriate recorder.

The cryogenic tests were run in a General Dynamics cryostat which was fabricated from stainless steel and welded to the lower extension rod below the clevis grip. The double walled chamber was designed for evacuation and was coated with 1½ inches of foamed insulation. The lower grip was submerged in the liquid nitrogen and attached to the lower extension rod by a self-centering coarse thread.

The liquid nitrogen was transferred from the 50-liter flask by air pressure (5 psi max., non-rigid connection). It was not necessary to drain the cryostat to remove the broken specimen and grip. This was done with a special wrench.

The specimens for the elevated temperature tests were allowed to soak between 20 and 30 minutes at 300°F. Similarly, the cryogenic soak was 5 minutes for the 1/2-inch thick specimens, 10 minutes for the 1-inch, and 15 minutes for the 1½-inch. Time was measured from the complete coverage of the specimen and quiescent boil of the liquid nitrogen.

The contour of the deformed skin specimens was measured on a surface plate with a dial gage. The nondeformed surface was deburred with fine emery paper before placing the specimen on the plate. The dial gage was zeroed at a point one inch from the end and one-half inch from the edge of the specimen. Sliding the dial gage stand across the surface plate permitted the gage to render a continuous profile. Readings were made at appropriate intervals.

RESULTS

1. Data for the tensile tests at room, elevated and cryogenic temperatures are recorded in Tables I, II, and III, respectively.

2. Table IV contains the data for all the deformed skin compression specimens. The contour profile as measurements of the specimen thickness are recorded for each specimen in Tables V and VI.

3. Tables VII and VIII contain the data for all the remaining compression type specimens.

CONCLUSION

The results of this test program are presented as empirical data.

Prepared by

John F. Hildebrand

J. F. Hildebrand
Project Engineering Metallurgist

Approved by

F. C. Nordquist

F. C. Nordquist
Chief Engineering Metallurgist

TABLE I

BONDED JOINT STRENGTH IN HEAVY GAGE ALUMINUM,
TENSION TYPE SPECIMEN, ROOM TEMP. TEST

Specimen Type & Number	Lap ins.	Load Rate lb/min.	Load lb	Bond Str. psi	Skin Gage in.	Skin Stress ksi	Remarks*
23-1	.50	1300	7040	7000	.126	27.9	
23-2	.49	1300	6560	6700	.126	26.0	
25-1	.49	1300	9000	9200	.127	35.4	
25-2	.50	1300	8950	9000	.127	35.2	
27-1	1.55	3900	10700	3500	.126	42.4	
27-2	1.55	3900	10540	3400	.126	41.8	
29-1	1.50	3900	18360	6100	.127	72.3	
29-2	1.49	3900	17280	5800	.127	68.0	
31-1	1.0	2600	11040	5500	.256	21.6	
31-2	1.0	2600	9720	4900	.256	19.0	
31-3	1.0	2600	11680	5800	.256	22.8	
33-1	1.0	2600	16720	8400	.255	32.8	pop at 5300 lb.
33-2	1.0	2600	16260	8100	.255	31.9	pop at 3200 lb.
33-3	1.0	2600	16880	8400	.255	33.1	pop at 3800 lb.
35-1	3.0	7800	11700	2000	.256	22.9	
35-2	3.0	7800	12550	2100	.256	24.5	
35-3	3.0	7800	11350	1900	.256	22.2	
37-1	3.05	7800	23800	3900	.255	46.7	
37-2	3.05	7800	21350	3500	.255	41.9	
37-3	3.05	7800	22150	3630	.255	43.4	pop at 5500 lb.
39-1	3.0	7800	15650	2600	.374	20.9	pop at 5500 lb.
39-2	3.0	7800	19350	3200	.374	25.9	pop at 5500 lb.
41-1	3.0	7800	26900	4500	.374	36.0	pop at 9000 lb.
41-2	3.0	7800	27700	4600	.374	37.0	pop at 7100 lb.
43-1	5.0	13000	21950	2200	.374	29.3	pops at 5500 lb. & 20000 lb.
43-2	5.0	13000	19300	1900	.374	25.8	pops at 6200 lb. & 17300 lb.
45-1	5.0	13000	28100	2800	.374	37.6	pop at 10000 lb.
45-2	5.0	13000	27500	2800	.374	36.8	pop at 9000 lb.

* Pop - an instantaneous, minute load drop.

TABLE II

BONDED JOINT STRENGTH IN HEAVY GAGE ALUMINUM,
TENSION TYPE SPECIMEN, 300°F TEST TEMP.

Specimen Type & Number	Lap ins	Load Rate lb/min	Load lb	Bond Str. psi	Skin Gage in	Skin Stress ksi	Remarks*
23-3	.50	1300	3150	3200	.126	12.5	
23-4	.50	1300	3300	3300	.126	13.1	
25-3	.50	1300	3640	3600	.127	14.3	
25-4	.50	1300	1600	1600	.127	6.3	
27-3	1.55	3900	10350	3300	.126	41.1	
27-4	1.55	3900	10160	3300	.126	40.3	
29-3	1.50	3900	9530	3200	.127	37.5	
29-4	1.50	3900	8930	3000	.127	35.2	
31-4	1.00	2600	7150	3600	.256	14.0	
31-5	1.00	2600	7170	3500	.256	14.0	pop at 3950 lb.
35-4	3.0	7800	15270	2500	.256	29.8	
35-5	3.0	7800	14950	2500	.256	29.2	
39-3	3.0	7800	18900	3200	.374	26.1	pop at 5050 lb.
39-4	3.0	7800	17200	2900	.374	23.8	pop at 3500 lb.
41-3	3.0	7800	13500	2200	.374	18.6	
41-4	3.0	7800	13300	2200	.374	18.3	
43-3	5.0	13000	18800	1900	.374	26.0	
43-4	4.97	13000	18300	1800	.374	25.2	pop at 6500 lb.
45-3	5.0	13000	18800	1900	.374	26.0	
45-4	5.0	13000	19000	1900	.374	26.2	

*Pop - an instantaneous, minute load drop.

TABLE III

BONDED JOINT STRENGTH IN HEAVY GAGE ALUMINUM, TENSION TYPE SPECIMEN, - 320° TEST TEMP.

Specimen Type & Number	Lap ins.	Load Rate lb/min.	Load lb	Bond Str. psi	Skin Gage in.	Skin Stress ksi	Remarks*
23-5	.50	1300	4500	4500	.126	17.9	
23-6	.50	1300	6600	6600	.126	26.2	
25-5	.50	1300	5700	5700	.127	22.4	
25-6	.50	1300	5000	5000	.127	19.7	
27-5	1.55	3900	9400	3000	.126	37.3	
27-6	1.55	3900	9400	3000	.126	37.3	pop at 7600 lb.
29-5	1.50	3900	8600	2900	.127	33.9	pop at 5700 & 7500 lbs.
29-6	1.50	3900	7900	2600	.127	31.1	pop at 5600 & 6400 lbs(1)
31-6	1.00	2600	10400	5200	.256	20.3	pop at 8800 lb
31-7	1.00	2600	12800	6400	.256	25.0	
35-6	3.0	7800	12800	2100	.256	25.0	
35-7	3.0	7800	11100	1800	.256	21.7	
39-5	3.0	7800	8800	1500	.374	11.8	pop at 1800 & 6000 lbs.
39-6	3.0	7800	14100	2400	.374	18.9	
41-5	3.0	7800	13500	2200	.374	18.0	
41-6	3.0	7800	13400	2200	.374	17.9	
43-5	5.0	13000	15000	1500	.374	20.0	pop at 12500 lb,
43-6	5.0	13000	16000	1600	.374	21.4	pop at 14500 lb.
45-5	5.0	13000	13300	1300	.374	17.8	

*Pop - an instantaneous, minute load drop.
(1) Load dropped several hundred pounds.

TABLE IV

BONDED JOINT STRENGTH IN HEAVY GAGE ALUMINUM, DEFORMED SKIN, COMPRESSION TYPE SPECIMEN, ROOM TEMP. TEST

Specimen Type & Number	Skin Gage in	Load Rate lb/min	Load lb	Skin Stress ksi	Remarks
135-1	.088	10000	26400	75	
-2	.088	10000	27000	77	
137-1	.088	10000	28100	80	
137M	.088	10000	13300	76	One skin load-backup block.
139-1	.088	10000	29100	83	
-2	.088	10000	28700	82	
141-1	.127	10000	30000	59	
-2	.127	10000	30300	60	
143-1	.128	10000	37400	73	
-2	.128	10000	37000	72	
145-1	.127	10000	40900	80	
-2	.127	10000	41200	81	
163-1	.088	10000	26600	76	
-2	.088	10000	27000	77	
-3	.088	10000	27000	77	

TABLE V

CONTOUR PROFILE AS MEASUREMENTS OF SPECIMEN
THICKNESS-DEFORMED SKIN, COMPRESSION TYPE SPECIMEN

Distance from end (ins)	1.0	1.5	2.0	2.5	3.0	3.5	4.0	4.5	5.0	5.5	6.0	6.5	7.0
Specimen Type and Number													
135-1	1.681	81	74	55	35	19	15	24	46	69	84	85	1.685
-2	1.677	76	70	52	32	14	09	17	39	63	79	81	1.680
137-1	1.685	82	71	58	44	33	32	35	47	60	71	77	1.680
137M	1.675	71	62	48	34	26	25	31	45	61	74	81	1.683
139-1	1.680	74	65	56	49	46	48	52	60	70	81	89	1.691
-2	1.675	68	56	45	37	33	33	35	43	55	64	75	1.679
141-1	1.758	57	67	26	1.702	1.685	1.682	1.692	1.713	38	53	56	1.757
141-2	1.759	60	50	31	1.711	1.692	1.687	1.695	1.715	37	53	57	1.759
Repeat #1 -2	1.759	60	51	31	1.709	1.691	1.687	1.697	1.717	39	55	58	1.759
Repeat #1 -2	1.759	60	50	31	1.709	1.691	1.687	1.696	1.716	39	55	58	1.759
143-1	1.755	51	40	26	24	08	08	13	23	39	52	58	1.758
-2	1.758	55	46	29	26	09	08	12	23	38	53	60	1.760
145-1	1.759	49	41	33	25	19	20	24	31	40	50	56	1.773
-2	1.755	52	44	38	30	24	24	29	37	46	55	62	1.765

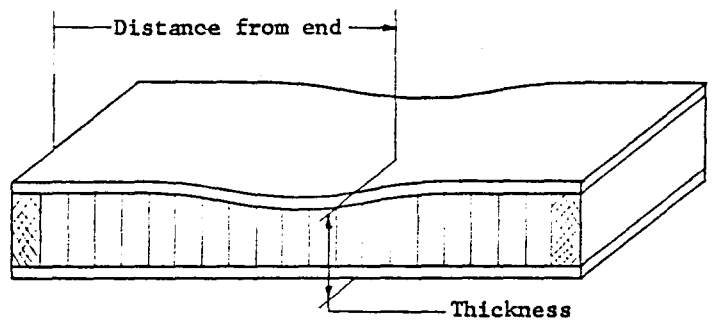

TABLE VI

CONTOUR PROFILE AS MEASUREMENTS OF SPECIMEN
THICKNESS-DEFORMED SKIN, COMPRESSION TYPE SPECIMENS

Distance from end (ins)		1.0	2.0	2.5	3.0	3.5	4.0	4.5	5.0	5.5	6.0	6.5	7.0	8.0	9.0
Specimen Type and Number															
163-1	dg	1.682	83	81	79	71	55	38	26	1.624	31	44	61	73	77
	m	1.682								1.618					
163-2	dg	1.681	81	81	76	67	52	36	27	1.626	34	48	64	77	84
	m	1.681								1.623					
163-3	dg	1.680	79	78	74	62	47	30	19	17	25	39	57	69	76
	m	1.680								1.618					

dg - dial gage reading converted to thickness in inches
m - micrometer measurements at starting point and thinnest point

Note - see sketch in Table V

TABLE VII

BONDED JOINT STRENGTH IN HEAVY GAGE ALUMINUM, COMPRESSION TYPE SPECIMENS, ROOM TEMP. TEST

Specimen Type & Number	Lap ins	Load Rate lb/min	Load lb	Bond Str. psi	Skin Gage in	Skin Stress ksi	Remarks
151-1	2.0	30000	105300	6600	.255	53	
-2	2.0	30000	100200	6300	.255	50	
-3	2.0	30000	107500	6700	.255	54	
153-1	2.0	30000	107000	6700	.255	54	
-2	2.0	30000	112600	7000	.255	56	
-3	2.0	30000	118500	7400	.255	59	
107-1		20000	41800		.191	55	
-2		20000	40600		.191	53	
109-1		20000	77900		.374	52	
-2		20000	78500		.374	52	
111-1		20000	119800		.514	58	No failure
-2		20000	120000		.514	58	No failure
79	0.5	2600	18000	9000	.129* / .191	35 / 24	
81	1.55	7800	31700	5100	.129 / .191	63 / 42	
83	1.0	5200	35300	8800	.255 / .374	35 / 23	
85	3.05	15600	51500	4200	.255 / .374	52 / 35	
87	3.0	15600	64100	5300	.374 / .515	43 / 30	pop at 60000 lbs.**
89	5.0	26000	72000	3600	.374 / .515	48 / 34	

* Skin gages $\frac{.XXX}{.YYY}$ for $\frac{7075}{2219}$ - likewise for skin stress.

** Pop - an instantaneous, minute load drop.

TABLE VIII

BONDED JOINT STRENGTH IN HEAVY GAGE ALUMINUM, COMPRESSION TYPE SPECIMENS, ROOM TEMP. TEST.

Specimen Type & Number	Lap ins	Load Rate lb/min	Load lb	Bond Str. psi	Skin Gage in	Skin Stress ksi	Remarks*
155-1	1.0	2600	19400	9700	.255	38	
155-2	1.0	2600	20400	10200	.255	41	
155-3	1.0	2600	19700	9800	.255	39	
157-1	3.0	7800	37500	6200	.255	74	
157-2	3.0	7800	39000	6500	.255	76	
157-3	3.0	7800	38500	6400	.255	75	
159-1	4.0	10400	38300	4800	.255	75	
159-2	4.0	10400	38300	4800	.255	75	pop at 24000 lb*
159-3	4.0	10400	38000	4800	.255	74	
161-1	5.0	13000	37000	3700	.255	73	
161-2	5.0	13000	35500	3600	.255	70	
161-3	5.0	13000	38200	3800	.255	75	
165-1		10000	28800		.090	80	
165-2		10000	28500		.090	79	
167-1		10000	41400		.125	83	
167-2		10000	41500		.125	83	
7-1	.99	80000	39700	10000	.255	39	
7-2	.96	80000	38800	10000	.255	38	
7-3	.94	20000	46600	12000	.255	45	pop at 25400 lb
9-1	3.0	20000	52300	4400	.255	51	
11-1	1.0	20000	55100	14000	.255	54	
11-2	1.0	20000	51400	13000	.255	50	pop at 4400 & 48800 lb
13-1	3.0	80000	55000	4600	.255	54	
13-2	3.0	20000	67400	5600	.255	66	pop at 62000 & 67000 lb

*Pop - an instantaneous load drop.

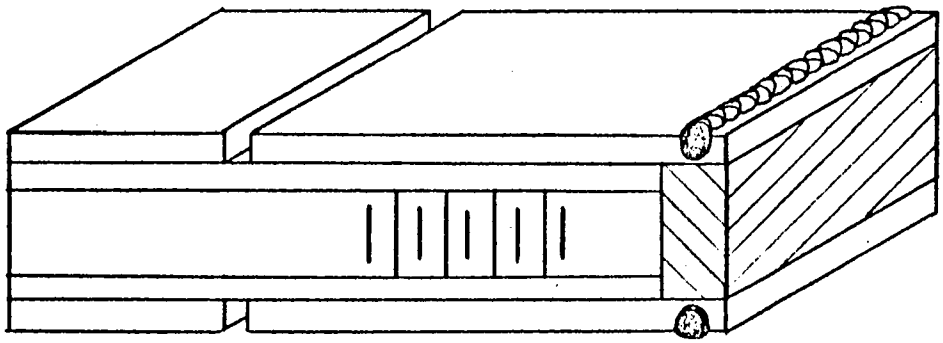

Welded Skin, Double Lap Compression
-79 thru -89

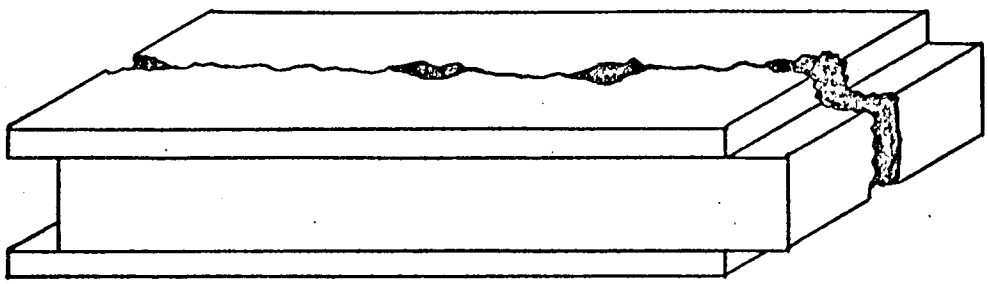

Double Lap Compression
wide -151, -153(with bolts)
long -155 thru -161

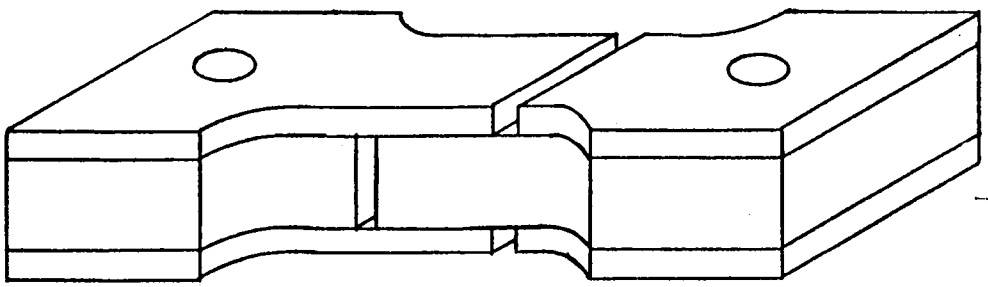

Double Lap Tension
-23 thru -45

TEST SPECIMEN CONFIGURATION.

FIGURE 1

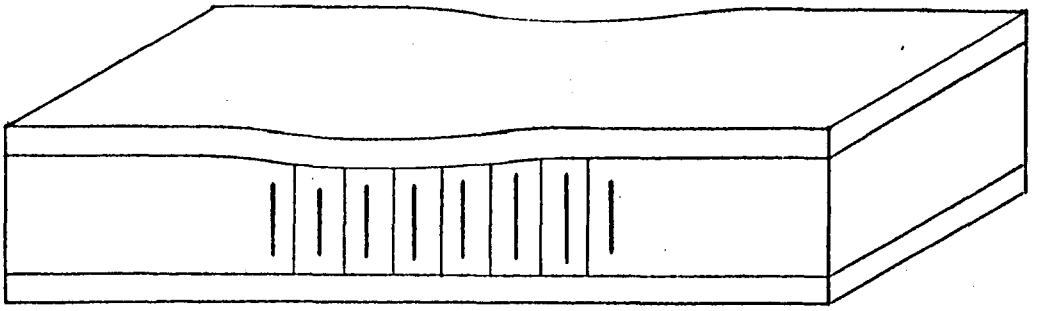

Deformed Skin Compression
-135 thru -145 and -163

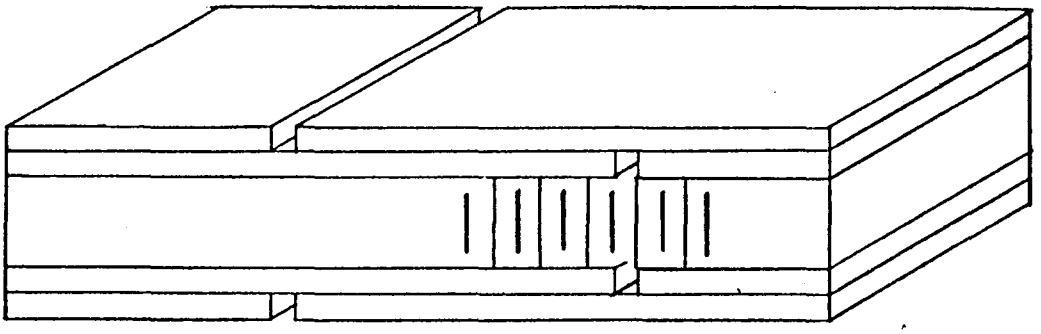

Double Lap Compression
-7 thru -13

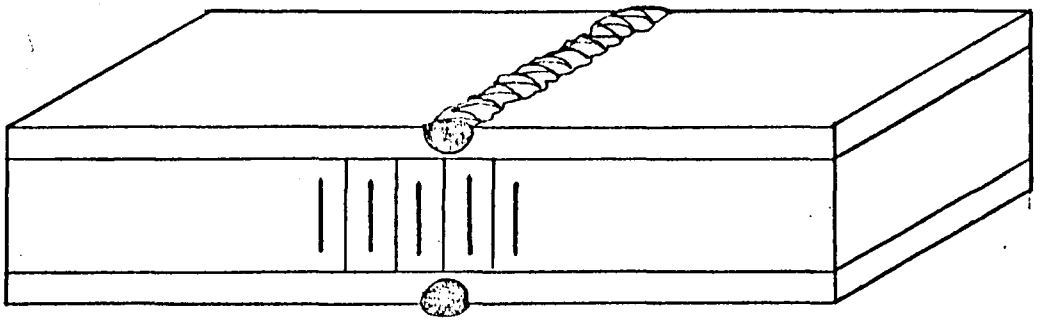

Welded Skin Compression
-107, -109, and -111

TEST SPECIMEN CONFIGURATIONS

FIGURE 2

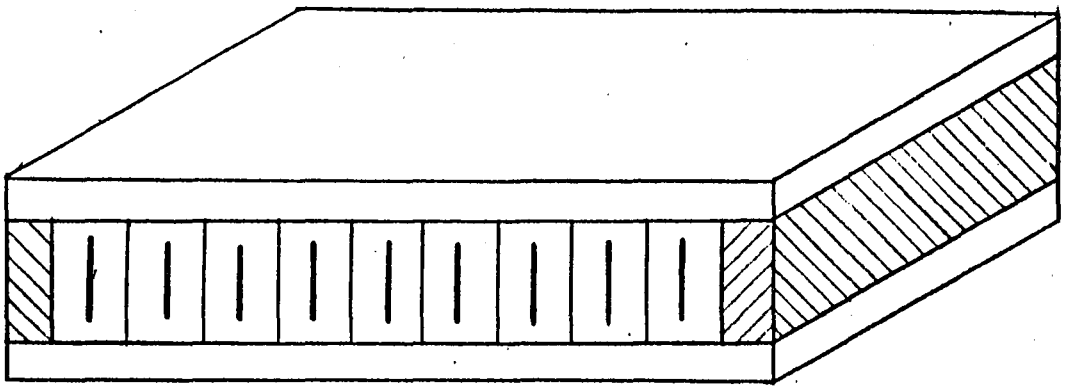

Edge Compression
-165 and -167

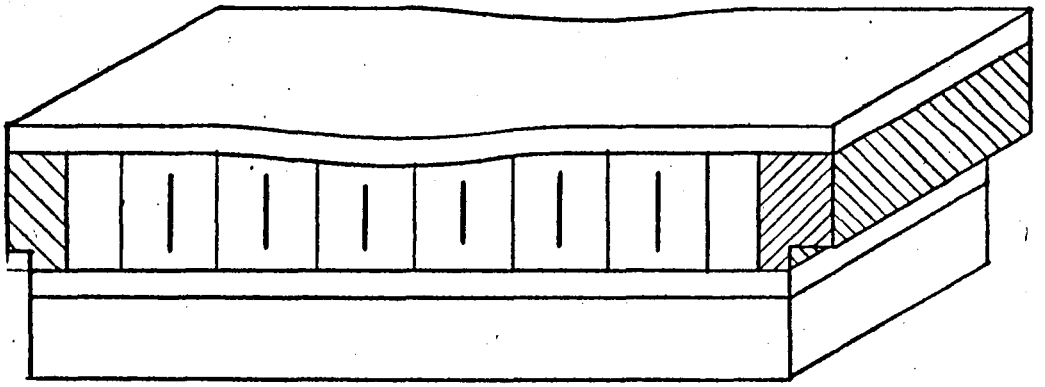

Deformed Skin Compression
-137 modified

TEST SPECIMEN CONFIGURATION

FIGURE 3

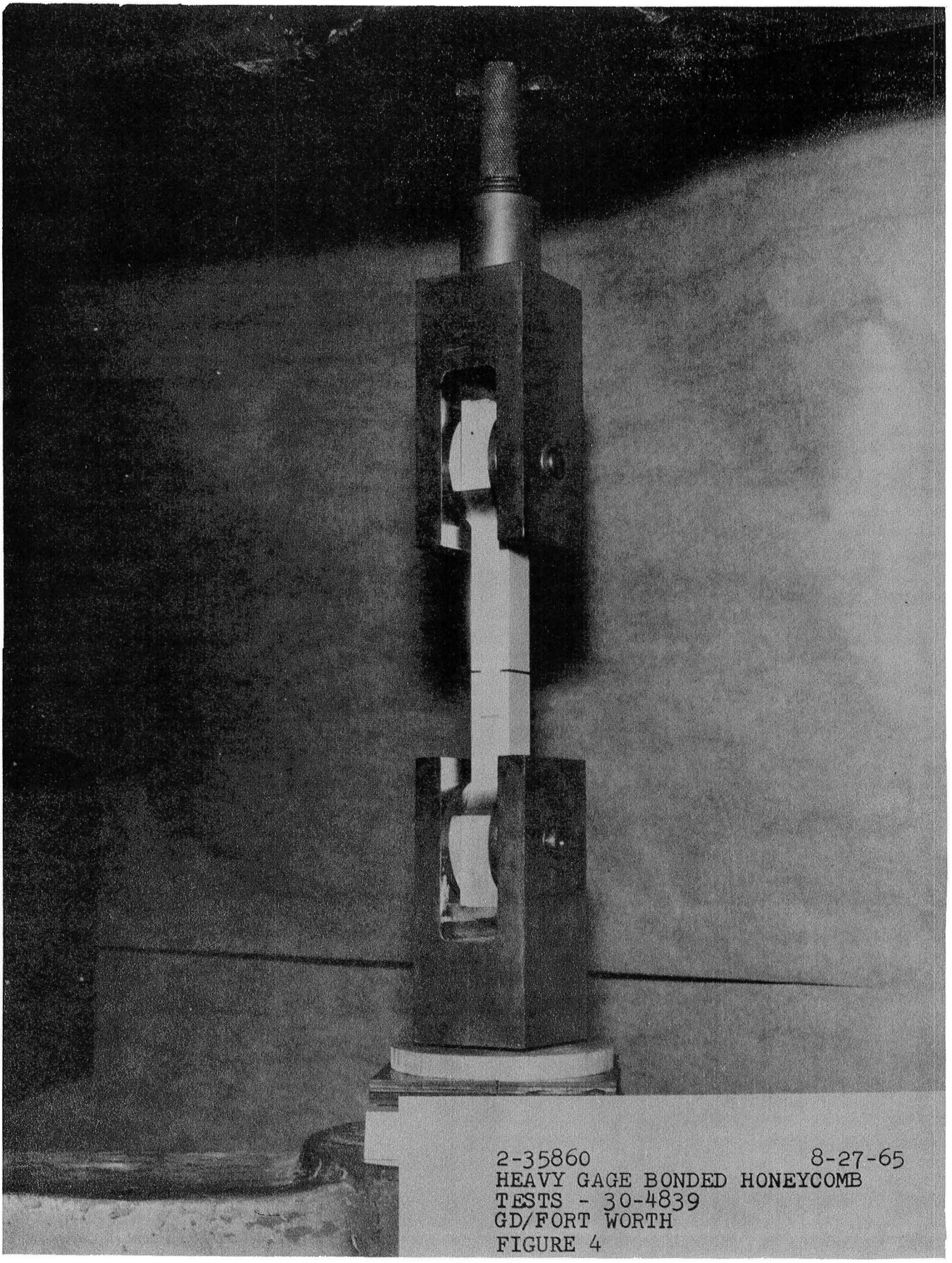

2-35860 8-27-65
HEAVY GAGE BONDED HONEYCOMB
TESTS - 30-4839
GD/FORT WORTH
FIGURE 4

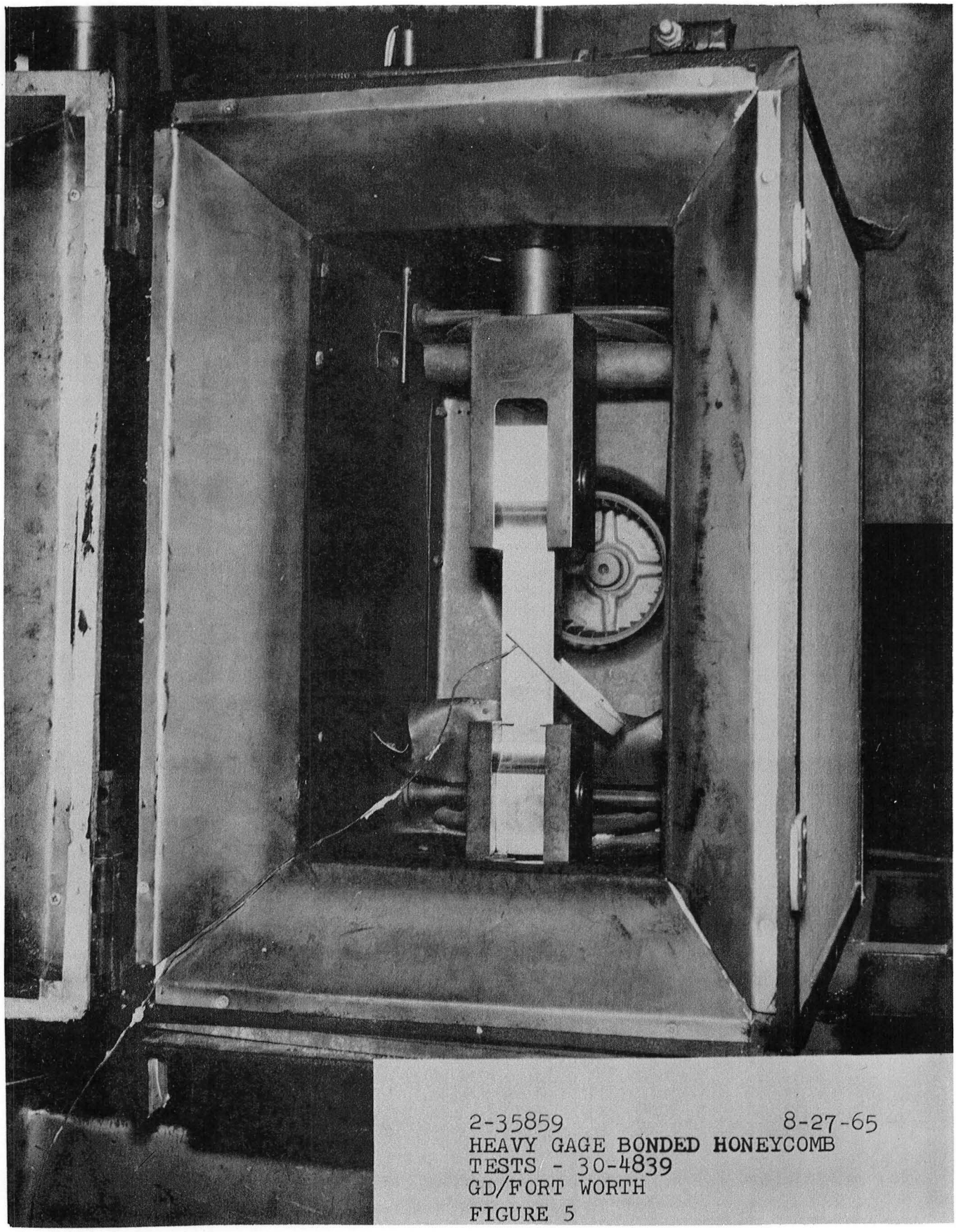

2-35859 8-27-65
HEAVY GAGE BONDED HONEYCOMB
TESTS - 30-4839
GD/FORT WORTH
FIGURE 5

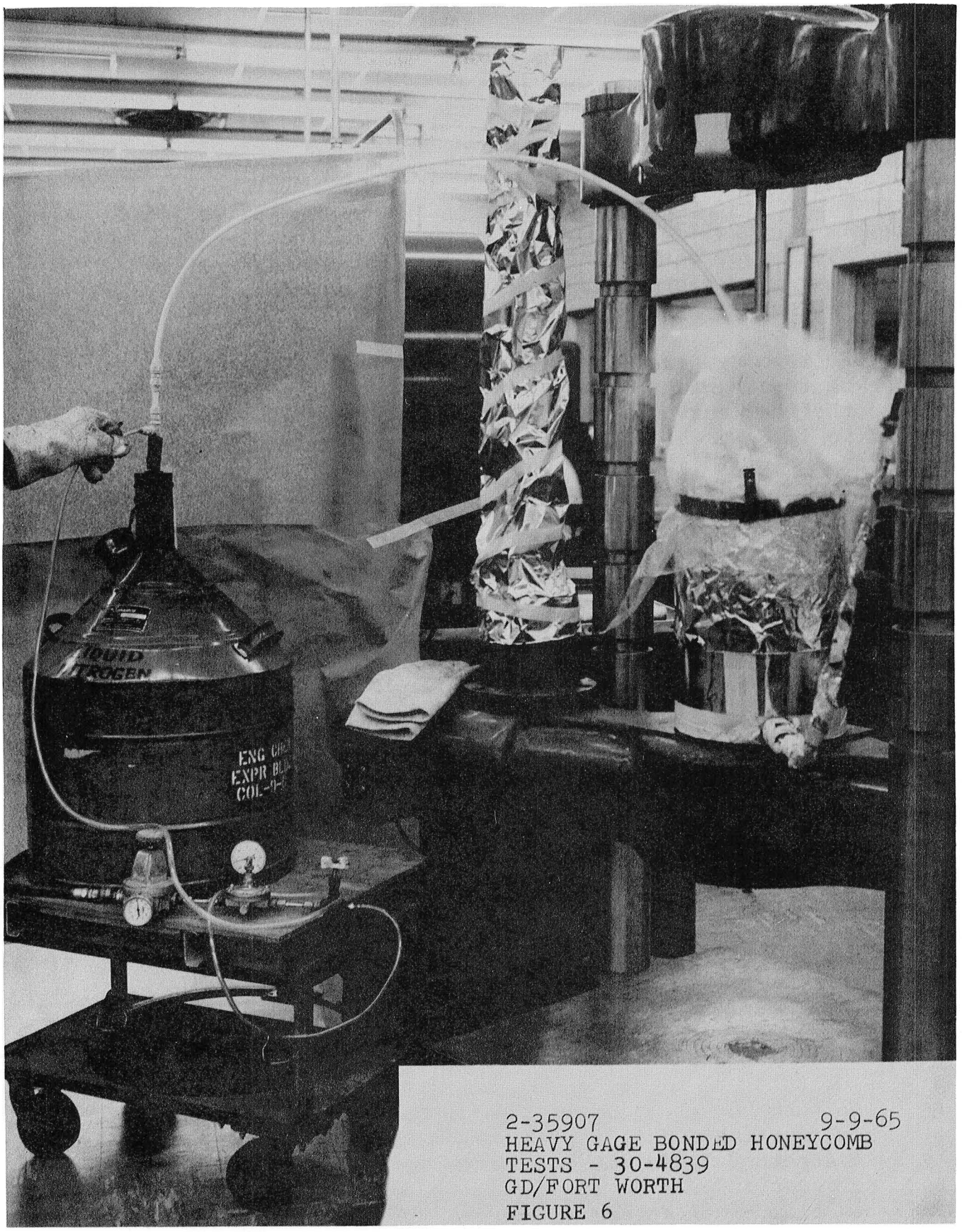

2-35907 9-9-65
HEAVY GAGE BONDED HONEYCOMB
TESTS - 30-4839
GD/FORT WORTH
FIGURE 6

Discussions of the significance of the data is provided below:

Bonded Joint

The sandwich compression shear test data from Table 1-1 is shown in Figure A-1 in relation to a hypothetical curve which describes the adhesive shear strengths which would be required in order to develop the minimum guaranteed compressive yield strength of 2024T81, the material from which the specimens were made. This type of hypothetical curve is used as a reference because it represents an approximate upper bound on the capability of a specimen made from the material.

The room temperature test data generated in the secondary phase of testing is shown in Figures A-2 and A-3 in relation to a hypothetical curve which describes the adhesive shear strengths which would be required in order to develop the minimum guaranteed compressive yield strengths of 7075T6. Several interesting observations may be made from the data in these figures:

1. There is no common L/t effect for the three skin thicknesses tested in tension.

2. The data obtained in sandwich compression shear tests is not of the same family as that obtained in tensile shear tests.

3. The data obtained from test specimens which have identical dimensions in the overlap area form different families of data for tension and compression tests.

4. The data obtained in sandwich compression shear tests are not of the same family as that obtained in double overlap compression tests.

Figure A-4 shows, in a simplified manner, the loading conditions of these three types of specimens and may, in part, explain the differences in the three test types. In each case the axial load P creates a moment about Point 0 which must be reacted by an opposite moment. Discounting the relative stiffnesses of Adherend I, forces normal to the overlap are required to constitute the reactive moment. Generally, the normal stresses at Point A are of less concern than those at Point B because Adherend I has either continuity and inherent stiffness, such as shown in a. and c., or a frictional force μP which relieves the normal stress at Point A such as shown in b.

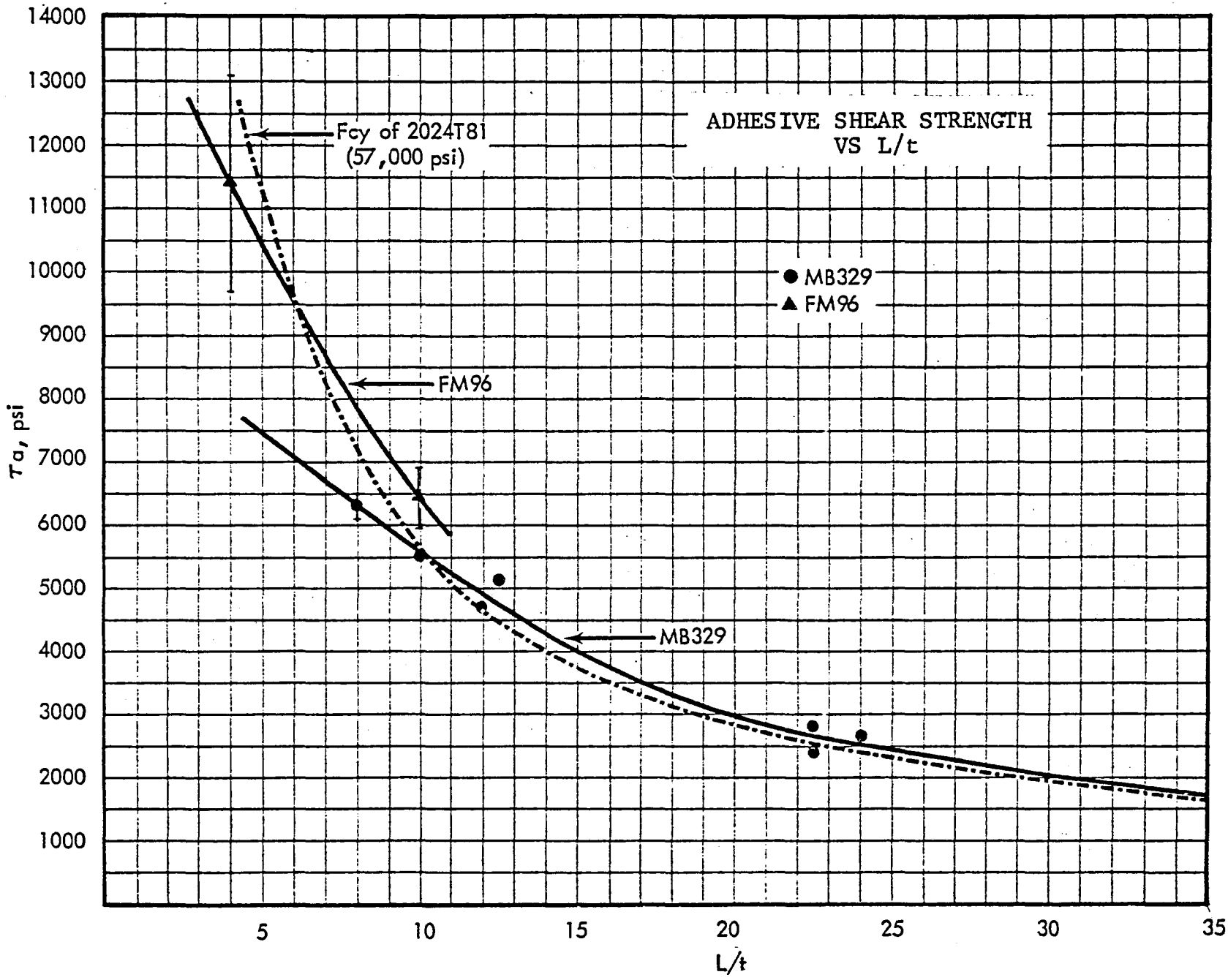

Figure A-1 ADHESIVE SHEAR STRENGTHS FROM PRELIMINARY TEST PROGRAM

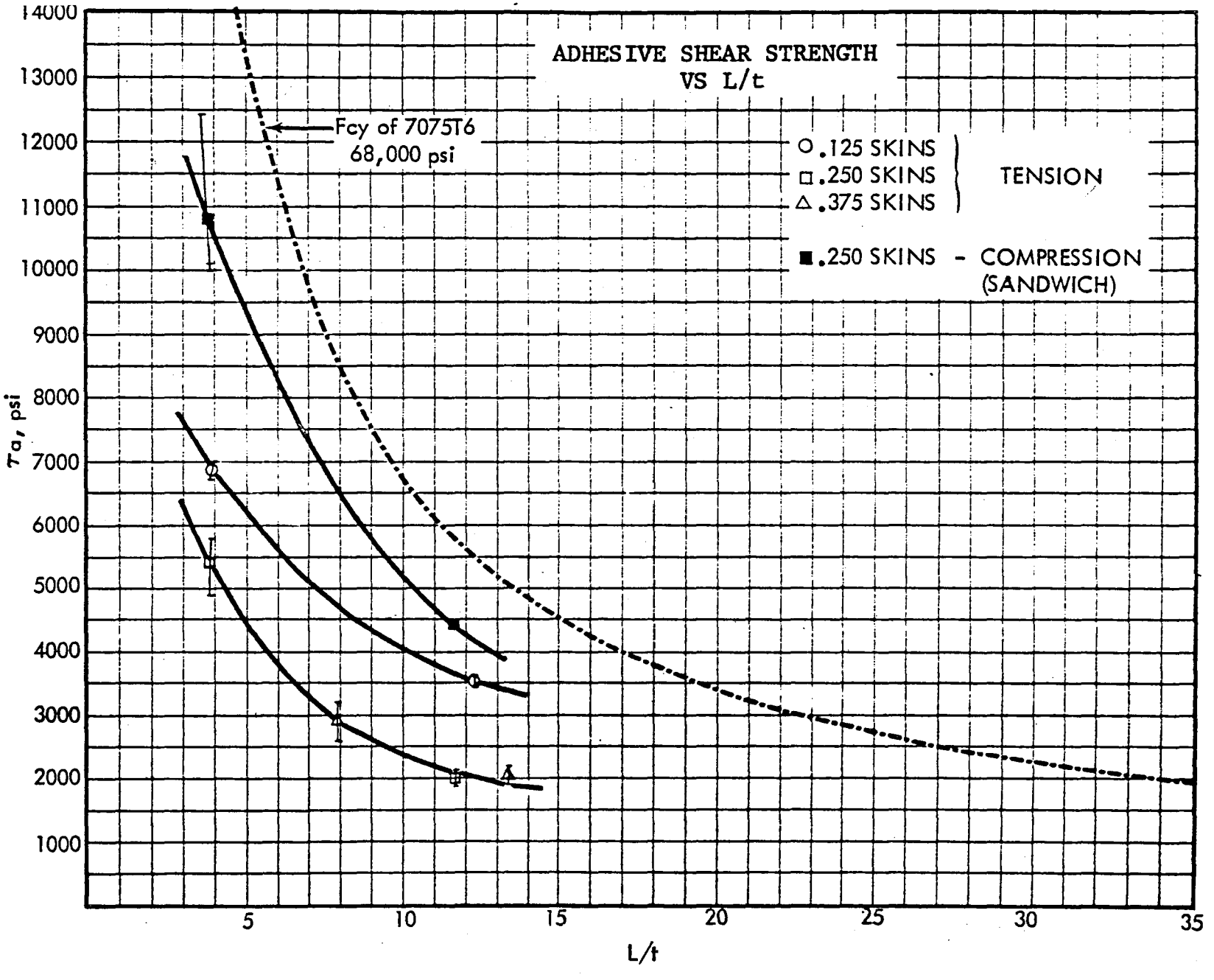

Figure A-2 ADHESIVE SHEAR STRENGTHS OF MB329 - TENSION AND COMPRESSION TESTS

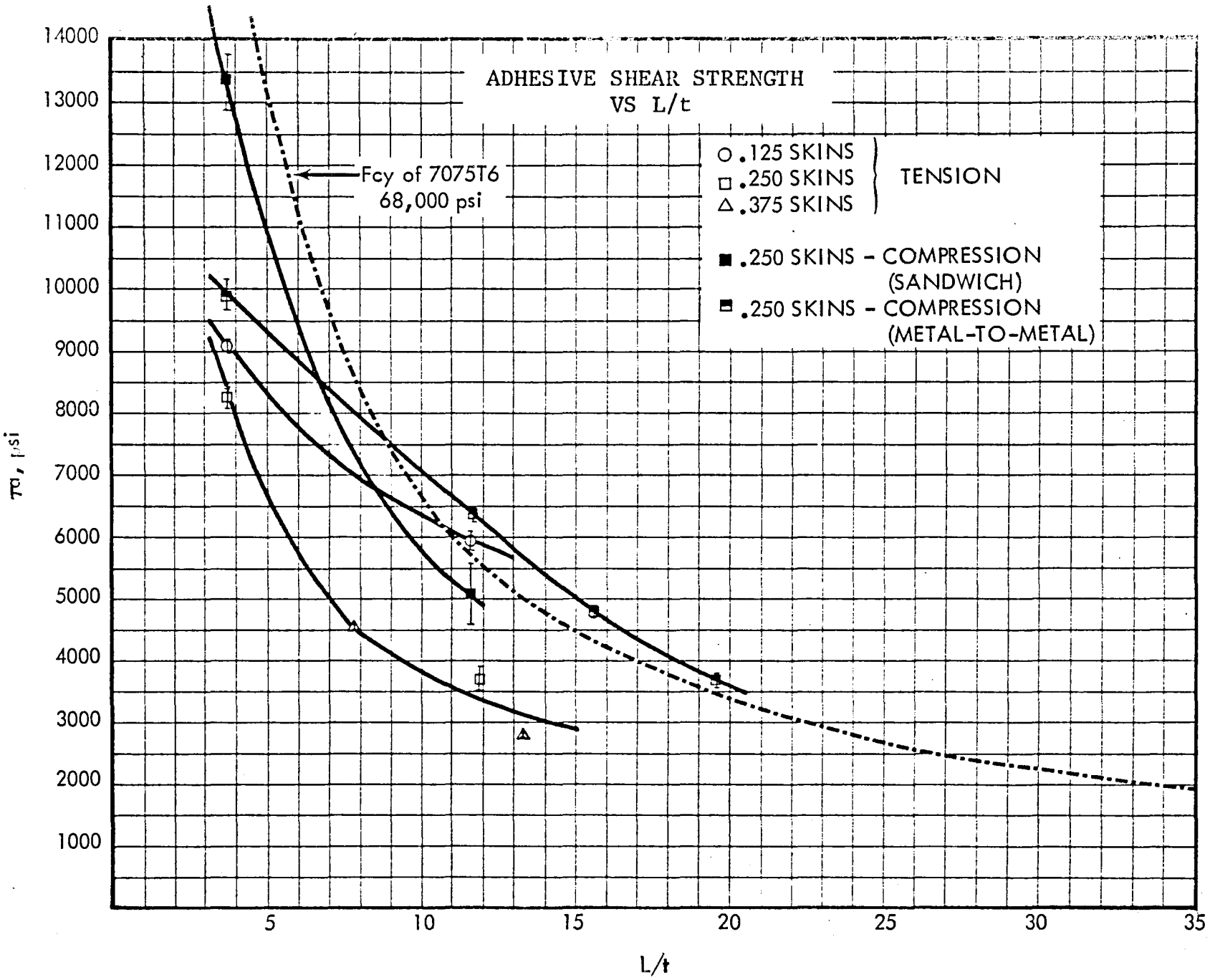

Figure A-3 ADHESIVE SHEAR STRENGTHS OF FM96 - TENSION AND COMPRESSION TESTS

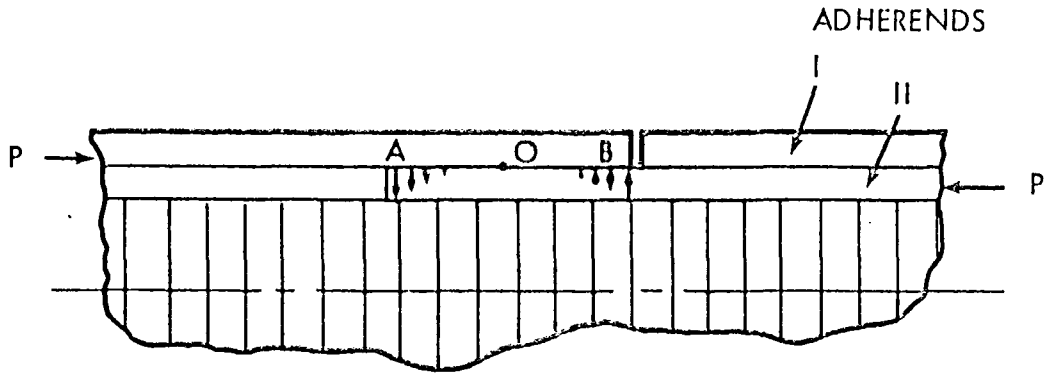

(A) SANDWICH COMPRESSION SHEAR

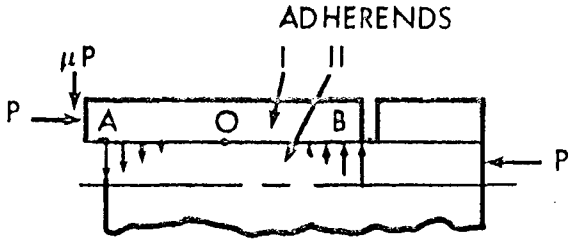

(B) DOUBLE OVERLAP COMPRESSION

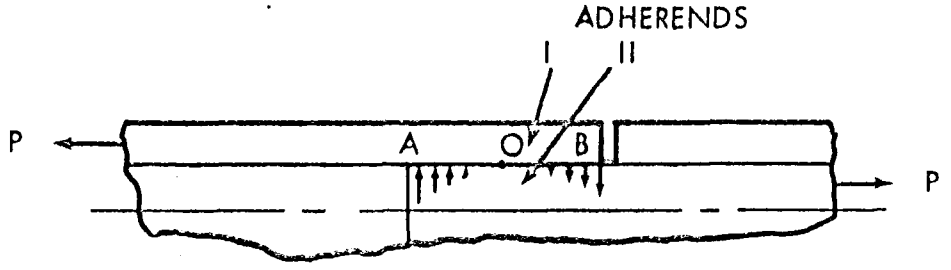

(C) DOUBLE OVERLAP TENSION

Figure A-4 FORCES PRESENT IN BONDED JOINTS

Both compression tests create normal compressive stresses in the adhesive at Point B in addition to the shear stresses. On the other hand, the tension test creates normal tensile stresses in the adhesive at Point B in addition to the shear stresses. Since most structural adhesives are more susceptible to tensile stresses then to compression stresses in this type of situation, it might be expected that the tension test would fail at a lower total load than a similar compression test as noted in 2. and 3.

Considering the two types of compression specimens it can be seen that the rigidity of Adherend II in the direction of the stresses at Points A and B is much greater for the double overlap specimen than for the sandwich compression specimen. Then bending deformations are lower in the double overlap specimen and adhesive stress concentrations, which are dependent upon both the differential axial strain and the bending strain of the adherends, are also lower and as a result the failing loads should be higher. This theory is verified by the test results as noted in 4.

Figures A-5 and A-6 show the averages of compression shear tests data and resulting allowables for both MB329 and FM96 adhesives. The "allowables" curve represents a line drawn at 80% of the test data average curve. Based on previous overlap test experience, this reduction represents a good guide for selecting overlap lengths with limited test data points.

Figures A-7 and A-8 show the double overlap tensile test data for the three test temperatures - -320°, R. T, and +300°F. The data for MB329 demonstrates inconsistencies between skin gages but also shows that MB329 is affected by temperature extremes to a lesser extent than is FM96.

Welded Joint

The minimum guaranteed compressive yield strengths for 2219T87 plate are 50,000 and 53,000 psi for L and T directions respectively from MIL-HDBK-5. The welded sandwich specimens tested during this phase demonstrated a minimum of 52,000 psi in the 2219T87 facings as welded at specimen failure. It may be concluded then that welding the sandwich facings had little effect on the adhesive bond between the facings and the core.

The test data for the specimens in which the 2219T87 doublers were bonded to 7075T6 facings and then welded is shown in Figure A-9. It should be noted that shear strengths for the bond between welded 2219 and 7075 are slightly reduced from those for the bond between two plates of 7075.

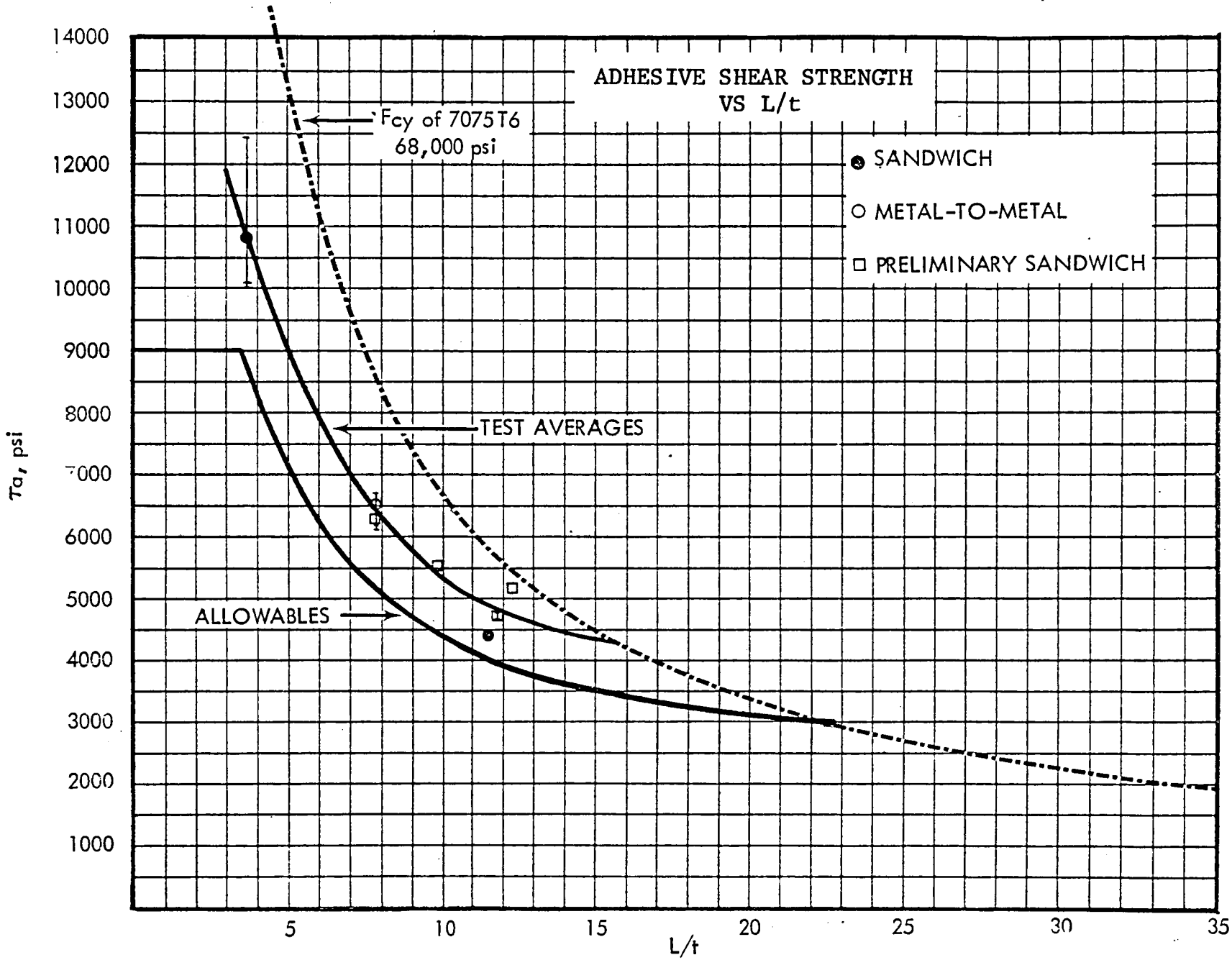

Figure A-5 TEST AVERAGES AND ALLOWABLES FOR MB329 IN COMPRESSION

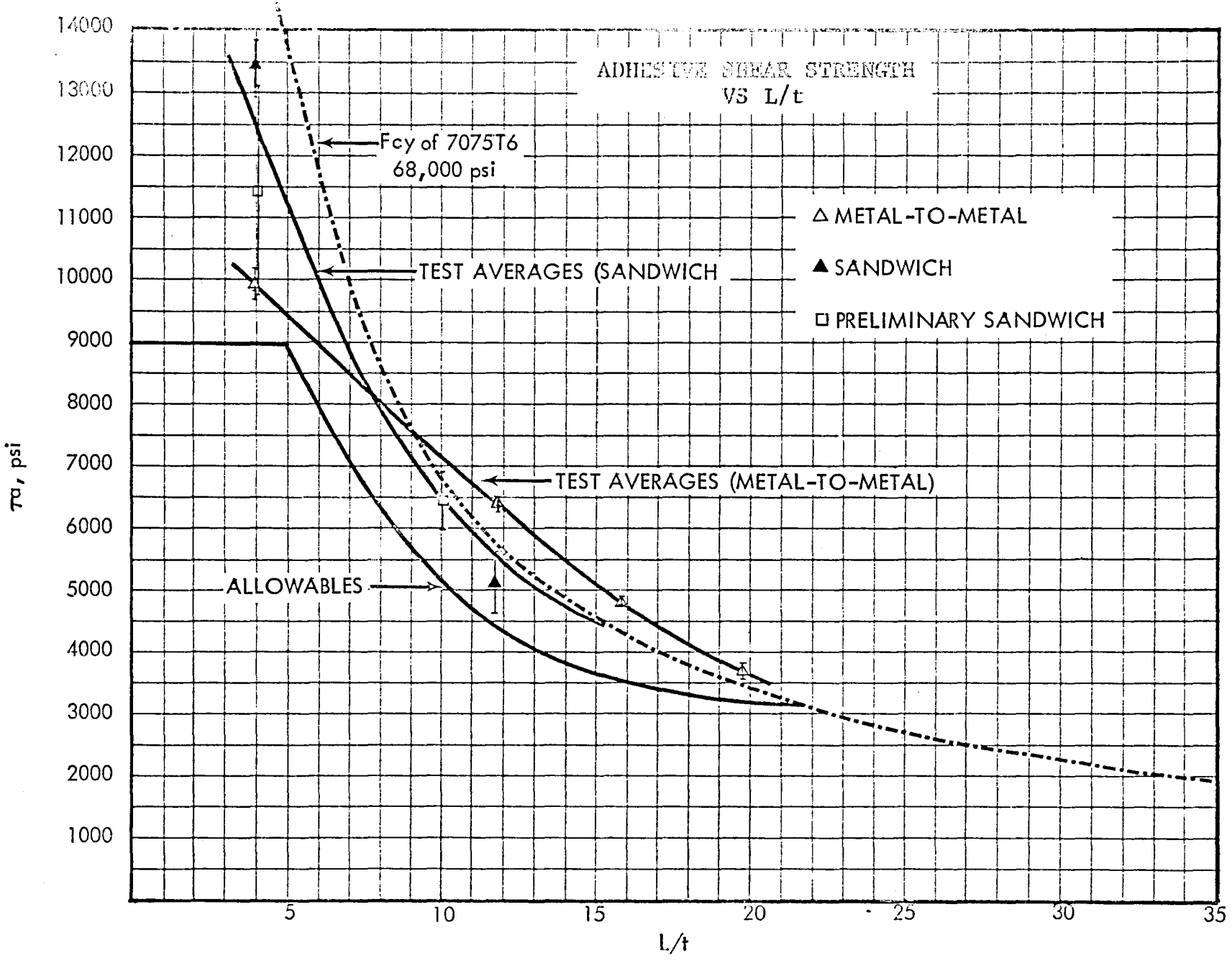

Figure A-6 TEST AVERAGES AND ALLOWABLES FOR FM96 IN COMPRESSION

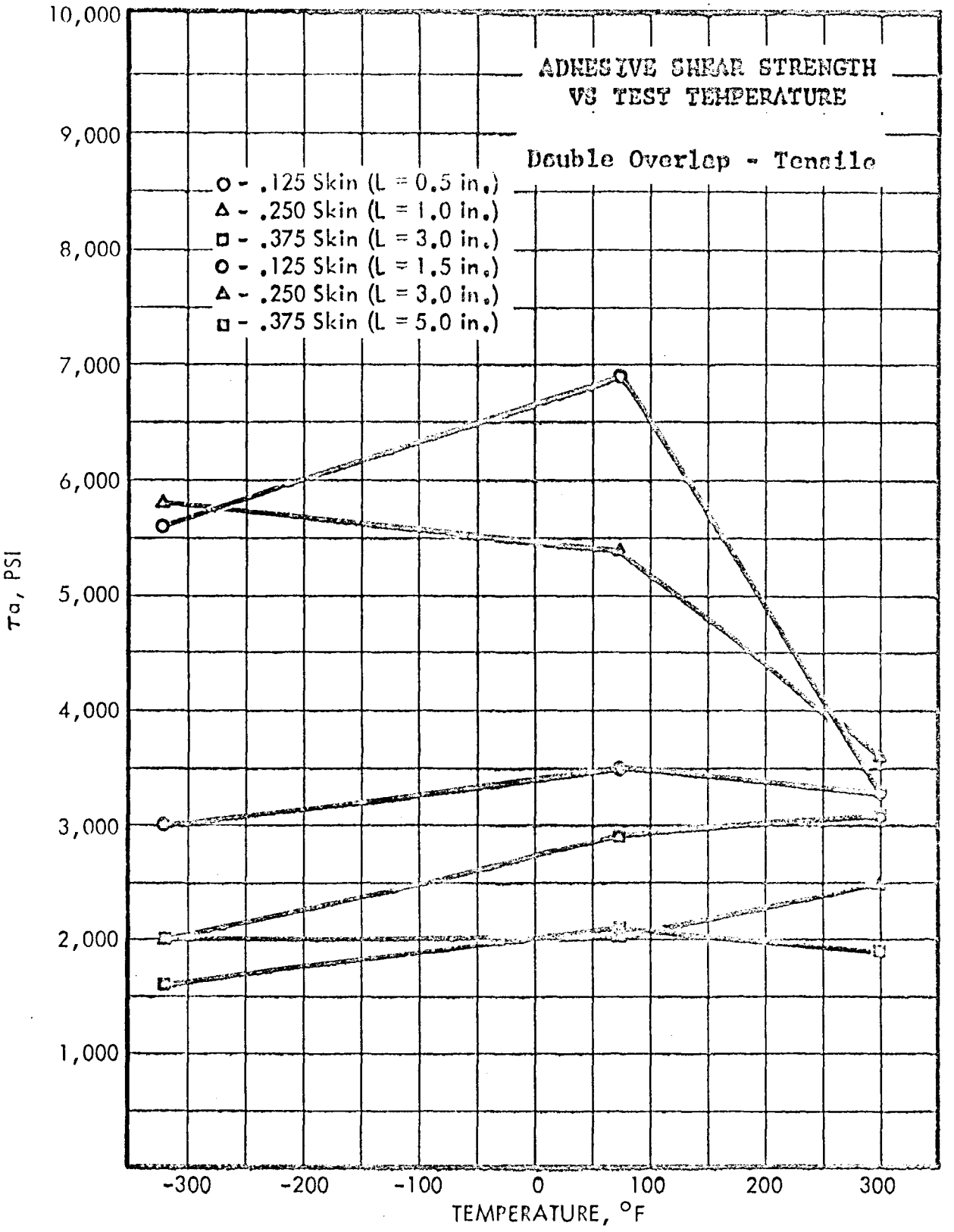

Figure A-7 EFFECT OF TEMPERATURE ON MB329 SHEAR STRENGTHS

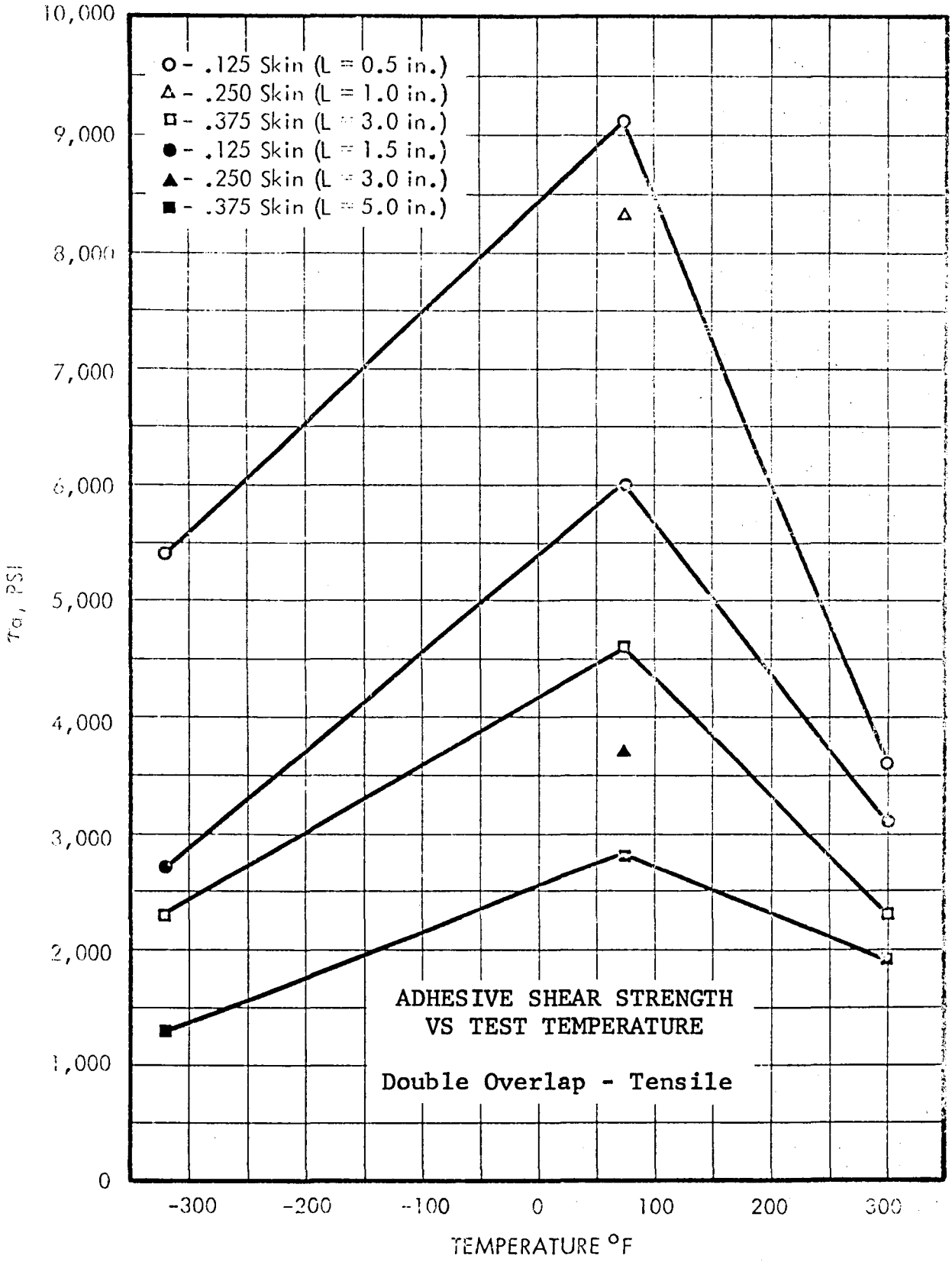

Figure A-8 EFFECT OF TEMPERATURE ON FM96 SHEAR STRENGTHS

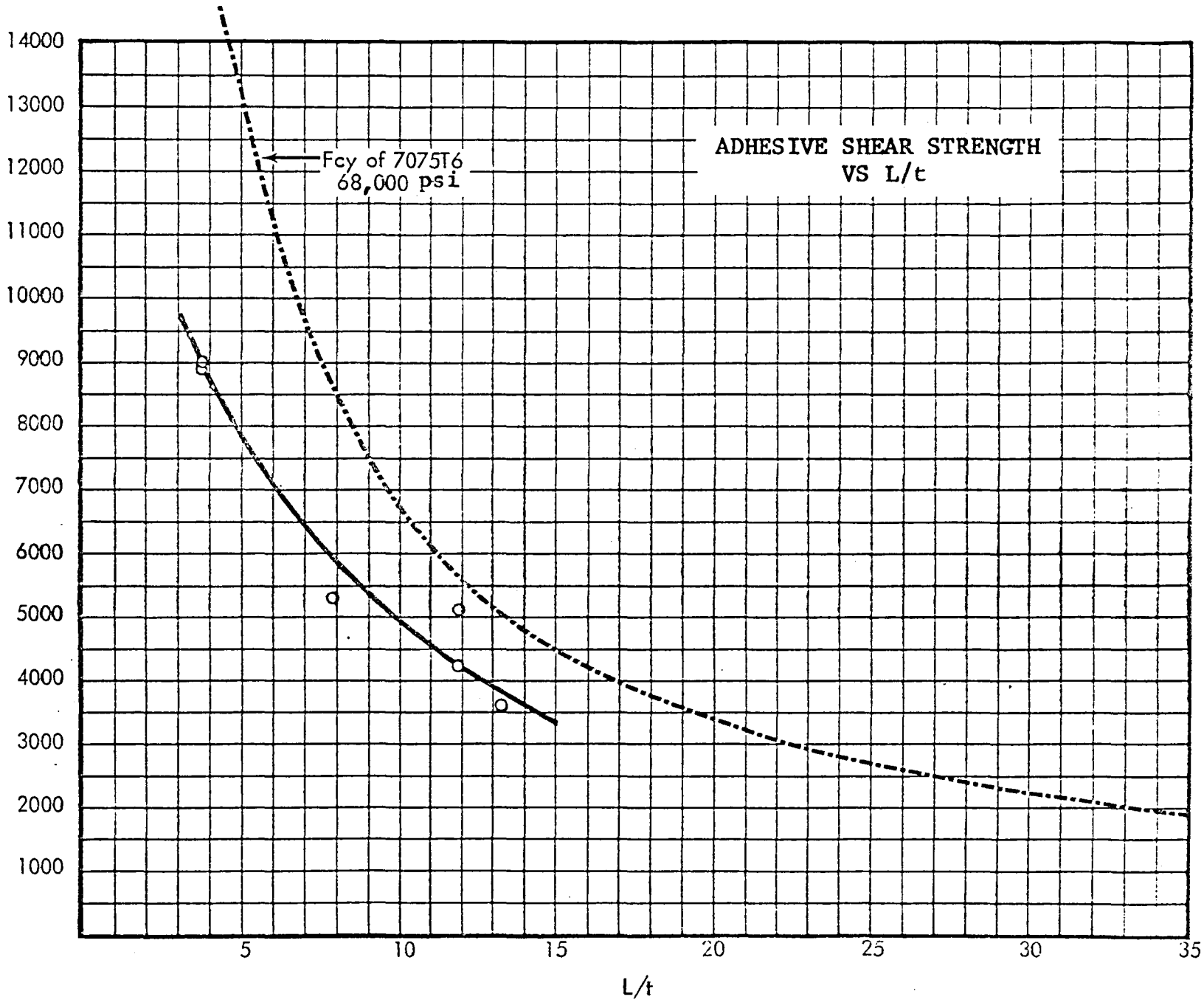

Figure A-9 ADHESIVE SHEAR STRENGTHS FOR 7075T6 BONDED TO 2219T87

Bonded-Bolted Joint

The tests of the bonded-bolted specimens demonstrated an average of 8% greater load carrying ability than the bonded specimens of the same configuration. It was concluded that this 8% increase is not substantial enough to warrant further consideration of this particular type of bonded-bolted joint.

Core and Core Bond Requirements

The theories of two prominent contributors to the analysis of face wrinkling were utilized and will be discussed briefly. Both theories require some knowledge of the imperfections of the type shown in Figure A-10 which are present in specimens prior to loading.

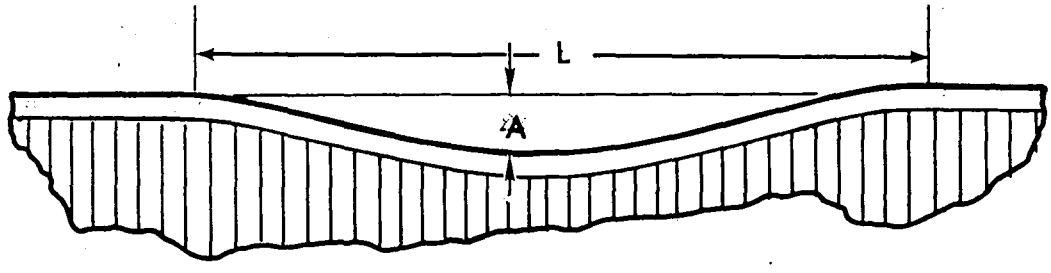

Figure A-10 INITIAL IMPERFECTIONS

Forest Products Laboratory

Reference A-1 presents the equation for σ_{cr}, the facing stress at wrinkling, for these particular specimens to be

$$\sigma_{cr} = \frac{\pi^2 t_f^2 E_f}{12 L_{cr} \lambda} \cdot \frac{1 + \frac{24 E_c \lambda L_{cr}^4}{\pi^4 E_f t_f^3 t_c}}{1 + \frac{2 E_c A_o}{\pi F_c t_c}}$$

where:

t_f is facing thickness

t_c is core thickness

E_f is facing compression modulus at stress level σ_{cr}

E_c is core compression modulus at a core stress level F_c

F_c is core compressive or tensile strength whichever is lower

L_{cr} is the critical half wavelength of the initial imperfection

A_o is the maximum amplitude of the initial imperfection contained in the length L_{cr}

$\lambda = 1 - \mu^2$ where μ is Poisson's ratio for the facing.

In order to determine a value for A_o then L_{cr} must be known and is given to be

$$L_{cr} = \pi \sqrt{\frac{t_f}{2}} \sqrt[4]{\frac{E_f t_f t_c}{6E_c}}$$

For these test specimens the value of L_{cr} was in the range 0.5 to 0.7 inch and the corresponding values of A_o ranged from .001 to .003 inch.

Syed Yusuff

Reference A-2 presents two relationships for face wrinkling stress which differ in the manner in which the core properties influence the face wrinkling stress. Yusuff theory requires the determination of the thickness, W, of a zone of core adjacent to each facing and to which all displacements in the core are restricted. This zone thickness is given by

$$W = 0.72\ t_f \sqrt[3]{\frac{E_f\ E_c}{(G_c)^2}}$$

where:

G_c is core shear modulus

The core is said to be thin if

$$t_c < 2W$$

and thick if

$$t_c > 2W$$

Then, the differences in thin and thick cores create the requirement for two relationships for face wrinkling stress. The configuration of the test specimens indicated that the theory for thick core was applicable; however, analyses were made with both theories and both theories are presented here for discussion:

THIN CORE

For this case Yusuff presents the equation for the facing stress at wrinkling to be

$$\sigma_{cr} = \frac{\sqrt{\frac{2\ E_t\ E_c\ t_5}{3\ t_c}}}{1 + \frac{2\ A_o\ E_c}{F_c\ t_c}}$$

As before A_o can be determined if L_{cr} is known and L_{cr} for this case is given to be

$$L_{cr} = \frac{\pi\ t_f}{2} \sqrt[4]{\frac{2\ E_f\ t_c}{3\ E_c\ t_f}}$$

For the test specimens the value of L_{cr} ranged from .5 to .77 and the corresponding values of A_o ranged from .001 to .004.

THICK CORE

For this case Yusuff presents the equation for the facing stress at wrinkling to be

$$\sigma_{cr} = \frac{0.96\ \sqrt{E_f\ E_c\ G_c}}{1 + \frac{A_o\ E_c}{W\ F_c}}$$

where tensile or compressive core strengths are critical and

$$\sigma_{cr} = \frac{0.96 \sqrt[3]{E_f \, E_c \, G_c}}{1 + \frac{A_o \, G_c}{T_c \, L_{cr}}}$$

where core shear strengths are critical and

T_c is core shear strength

The critical half wave length for this case is

$$L_{cr} = 1.307 \, t_f \sqrt[6]{\frac{E_f^2}{E_c G_c}}$$

For the test specimens the values of L_{cr} ranged from .3 to .36 and the corresponding values of A_o ranged from .0002 to .0009.

Actual measured values of A and L, which were determined from recorded profiles of each specimen, are shown in Table A-1 along with the predicted results of the several theories discussed earlier and the test results. Table A-1 shows that even with the severe imperfections fabricated into the specimens only one of the specimens failed below the minimum guaranteed compression yield strength of the 7075T6 and that at a stress level in excess of the maximum anticipated working stress levels in the thrust structure. Table A-1 also shows that the test results correlate better with the Forest Products Laboratory theory than with the Yusuff theories.

Table A-1 FACE WRINKLING RESULTS

SPECIMEN	SURFACE WAVINESS		PREDICTED FACE WRINKLING RESULTS				TEST RESULTS
			FPL	YUSUFF			
				THICK		THIN	
	A	L	TENSION OR COMPRESSION	TENSION OR COMPRESSION	SHEAR	TENSION OR COMPRESSION	
135	.0698	5.5	69,300	100,000+	67,000+	62,000	75,900
137	.0564	6.25	72,000	100,000+	90,000+	67,300	79,900
137M	.0564	6.25	72,000	100,000+	90,000+	67,300	75,600
163	.0564	6.25	72,000	100,000+	90,000+	67,300	76,300
139	.0420	6.25	73,000	100,000+	100,000+	69,000	81,800
165	0	-	-	-	-	-	79,600
141	.0745	5.5	73,300	100,000+	70,000	63,300	59,400
143	.0510	5.80	76,200	100,000+	87,000	69,000	72,700
145	.0365	6.0	77,000	100,000+	100,000+	70,700	81,100
167	0	-	-	-	-	-	83,000

References

A-1 Jenkinson, P. M. and Kuenzi, E. W., Wrinkling of the Facings of Aluminum and Stainless Steel Sandwich Subjected to Edgewise Compression, FPL Report No. 2171 December 1959

A-2 Yusuff, S., "Face Wrinkling and Core Strength in Sandwich Construction", Journal of the Royal Aeronautical Society, Vol. 64, March 1960, P. 164

A P P E N D I X B

S T R U C T U R A L T E S T I N G

This appendix contains General Dynamics Engineering Test Laboratory Report Number FSG-600, which presents the test data from the structural test program. An analysis of the adhesive shear stress distribution over the solid edgemember of the shear test specimens is also provided.

GENERAL DYNAMICS | FORT WORTH

TEST NO. 10-4920

REPORT FSG-600

MODEL NASA

DATE 4-15-66

TITLE

RESEARCH - HEAVY GAGE BONDED HONEYCOMB - PHASE III TEST PROGRAM

The tests described in this report were conducted between 10-27-65 and 2-16-66.

SUBMITTED UNDER
CONTRACT NUMBER

NAS 8-11943

PREPARED BY: C. E. Archer

GROUP STRUCTURES ENGINEERING TEST LABORATORY

REFERENCE

CHECKED BY: T. S. Love

APPROVED BY G. W. Robinson

NO. OF PAGES iii & 25

NO. OF DIAGRAMS 14

TABLE OF CONTENTS

		PAGE NUMBER
1.0	PURPOSE	1
2.0	SUMMARY	1
3.0	DESCRIPTION OF TEST SPECIMENS	2
4.0	SETUP AND PROCEDURE	2
5.0	RESULTS	4
6.0	CONCLUSION	5

FIGURE INDEX

FIGURE NO.		PAGE NO.
1	Shear Test Setup Negative No. 2-36312	6
2	Data Point Locations -801 Panel Heavy Gage Bonded Panel Test Program	7
3	Data Point Locations -5 Panel Heavy Gage Bonded Panel Test Program	8
4	Shear Panel -5a, After Testing Negative No. 2-36319	9
5	Shear Panel -801b, After Testing Negative No. 2-36525	10
6	Test Results -61 Compression Panels Negative No. 2-36469	11
7	Test Results -809 Compression Panels Negative No. 2-36470	12
8	Test Results -809 Compression Panel Negative No. 2-36241	13
9	Test Results -807b Shear Panel Negative No. 2-36524	14
10	Test Results -811a Shear Panel Negative No. 2-36520	15
11	Test Results -817b Shear Panel Negative No. 2-36521	16
12	Test Results -819b Shear Panel Negative No. 2-36518	17
13	Test Results -801f Shear Panel Negative No. 2-36522	18
14	Test Results Shear Test Panels Negative No. 2-36516	19

TABLE INDEX

TABLE NO.		PAGE NO.
I	Summary of Test Results Heavy Gage Bonded Honeycomb Panel Test Program	20
II	Strain Gage Data Panel Number FW6528004-5a Heavy Gage Bonded Honeycomb Test Program	21
III	Strain Gage Data Panel Number FW6528004-801b Heavy Gage Bonded Honeycomb Test Program	22
IV	Photoelastic Data Recorded During Tests on Panels FW6528004-5a and -801b	23

1.0 PURPOSE:

The purpose of these tests was to determine the ultimate load carrying capacity, in compression or shear, of a series of experimental heavy gage bonded aluminum honeycomb panels. This data is necessary for the determination of the shear stresses in the panel faces and bonding adhesives.

2.0 SUMMARY:

Tests were performed on aluminum honeycomb adhesive bonded panel specimens having various facing and core thicknesses. Compression test panels were approximately 8 inches square. Panels for shear tests were approximately 18 inches square. All test parts are described in drawing number FW6528004.

A total of 25 compression tests and 20 shear tests were conducted. The compression specimens were setup in the 200,000 pound BLH test machine and loaded to failure at a constant rate of 41,600 pounds per minute.

The shear specimens were tested in a fixture designed to apply uniform loads along two edges of the panel and to react the load uniformly along the specimen centerline. Three of the shear specimens were instrumented with photo-elastic plastic and/or electric resistance strain gages. These specimens were loaded in data increments. The remaining shear specimens were loaded to failure at a uniform rate of increasing load. The shear tests were conducted in the 1,000,000 pound Tinius Olsen test machine. Test results are presented in Table I.

3.0 DESCRIPTION OF TEST SPECIMENS:

The specimens for these tests were fabricated with an aluminum honeycomb core, 1.5 inches or 3.0 inches thick, bonded between aluminum facings varying from .125 to .375 inch thick.

Compression specimens represented panels with bonded aluminum channel edge members or bolted splices between panels without the channel edge members. Several variations of bolt patterns and bolt hole preparation were tested. The loaded edges of the compression panels were all reinforced with either the channel edge member or a buildup of potting compound. The compression test panels were approximately 8 inches square.

Shear test specimens were approximately 18 inches square. Solid aluminum edge members were used to reinforce two edges for load introduction. The skins were reinforced by doublers at the other two edges to help react the test loads. All but four of the shear specimens were initially an all-bonded construction. The four exceptions, -815a and b and -817a and b, had bolted connections between panel facings and skin doublers which were in turn bonded to the solid edge members. The final panel tested, -801f, was reinforced in the panel facing to edge member bond joint by a pattern of half inch diameter bolts.

Details of all the test specimens tested are given in Drawing FW6528004.

4.0 SETUP AND PROCEDURE:

The loaded edges of the compression test specimens were machined flat and parallel to insure a uniform load introduction. Testing was accomplished in the 200,000 pound BLH test machine.

The specimens were placed between parallel heads of the test machine and loaded to failure. The rate of load

application for all compression tests was a constant 41,600 pounds per minute. Twenty-five compression specimens were tested.

The shear test panels were mounted in a special fixture designed to apply load through the edge reinforcing members and react load through a pattern of six, one inch diameter holes along the centerline of the specimen parallel to the loaded edge members. The test fixture is detailed in drawing 12FTJ18279 and illustrated in the test setup photo, Figure 1. The shear tests were conducted in the 1,000,000 pound Tinius Olsen test machine. Twenty shear specimens were tested.

Two of the shear test panels, numbers FW6528004-5a and -801b, were instrumented with electric resistance strain gages for the purpose of determining the load distribution into the specimens. These two panels plus panel -801a, were also instrumented with photoelastic plastic to aid in the determination of magnitude and distribution of in-plane shear stresses in the test panel facings. Panel 801a was instrumented with photoelastic plastic for a qualitative indication of the shear concentration in the area of the edge slug. No stress data was recorded. All photoelastic data obtained in the test program utilized the reflective polariscope set-up. The locations of the strain gages and photoelastic data points are shown in Figures 2, 3, 4 and 5. The light shield utilized in taking photographs for the photoelastic data acquisition is also shown in the test setup photograph, Figure 1.

The first shear panel tested, -801a, was installed in the test machine and given an initial load of 87,000 pounds to condition the specimen and loading apparatus. The load was then returned to zero. The specimen was then loaded to 90,000 pounds and photoelastic stress patterns were observed. The load was then increased until specimen failure occurred.

The second shear specimen, -5a, was loaded three times to 20% of the expected failing load of 270,000 pounds to condition the fixture and strain gages. After returning to zero load the specimen was loaded in 10% increments to 60% of 270,000 pounds with an extra stop at 45%. At each increment the load was held constant while strain gages were read and a photo of the photoelastic plastic was made. In this panel test, stress data, obtained from the photoelastic material was recorded at the 30% load level.

After the data had been recorded 60%, the specimen load was increased at 116,700 pounds per minute until failure occurred.

The third shear panel tested, -801b, was loaded twice to 40% of the expected failing load of 540,000 pounds before any data was taken from the strain gages installed. Data was then recorded for each 10% increment of load through 40% and each 5% increment thru 55%. Photoelastic stress data was recorded at the 30% load level. The part was then loaded to failure at a constant rate of 234,000 pounds per minute.

Strain gage data is presented in Tables II and III. Photoelastic data is presented in Table IV.

The remaining shear test specimens had no instrumentation installed. Each panel was mounted in the test machine and loaded to failure at a constant rate of 116,700 pounds per minute for the -5 and -815 specimens, and 234,000 pounds per minute for all the remaining panels.

5.0 RESULTS:

Test results are summarized in Table I. In all but one shear test panel, failure occurred in the facing to edge member bond. The one exception was the last panel tested, -801f. This specimen had been reinforced in the bonded area by a bolt pattern and failure occurred as skin shear.

Failure of fifteen of the compression specimen also occurred in the bond line. Eight failed by core tension due to buckling of the facings. The two remaining specimens failed in core crushing, also due to skin buckling.

All the shear test specimens were cut open after testing to expose the facing-to-edge-member bond for examination.

Typical specimen failures are shown in Figures 4 thru 12. Figure 13 is a failure photograph of specimen number -801f and Figure 14 shows all tested shear specimens.

6.0 CONCLUSION:

The data requested has been compiled and is presented in this report.

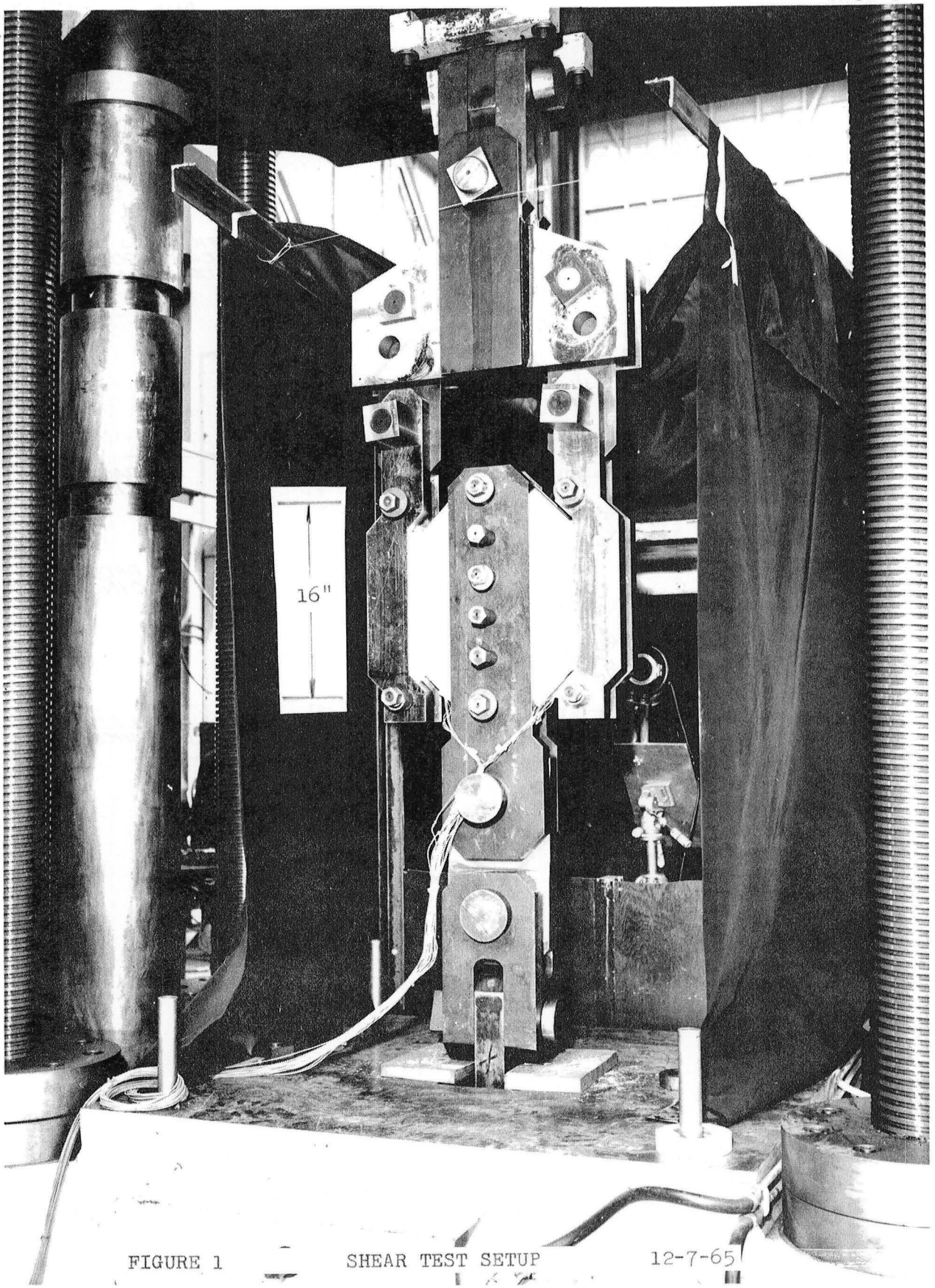

FIGURE 1 SHEAR TEST SETUP 12-7-65

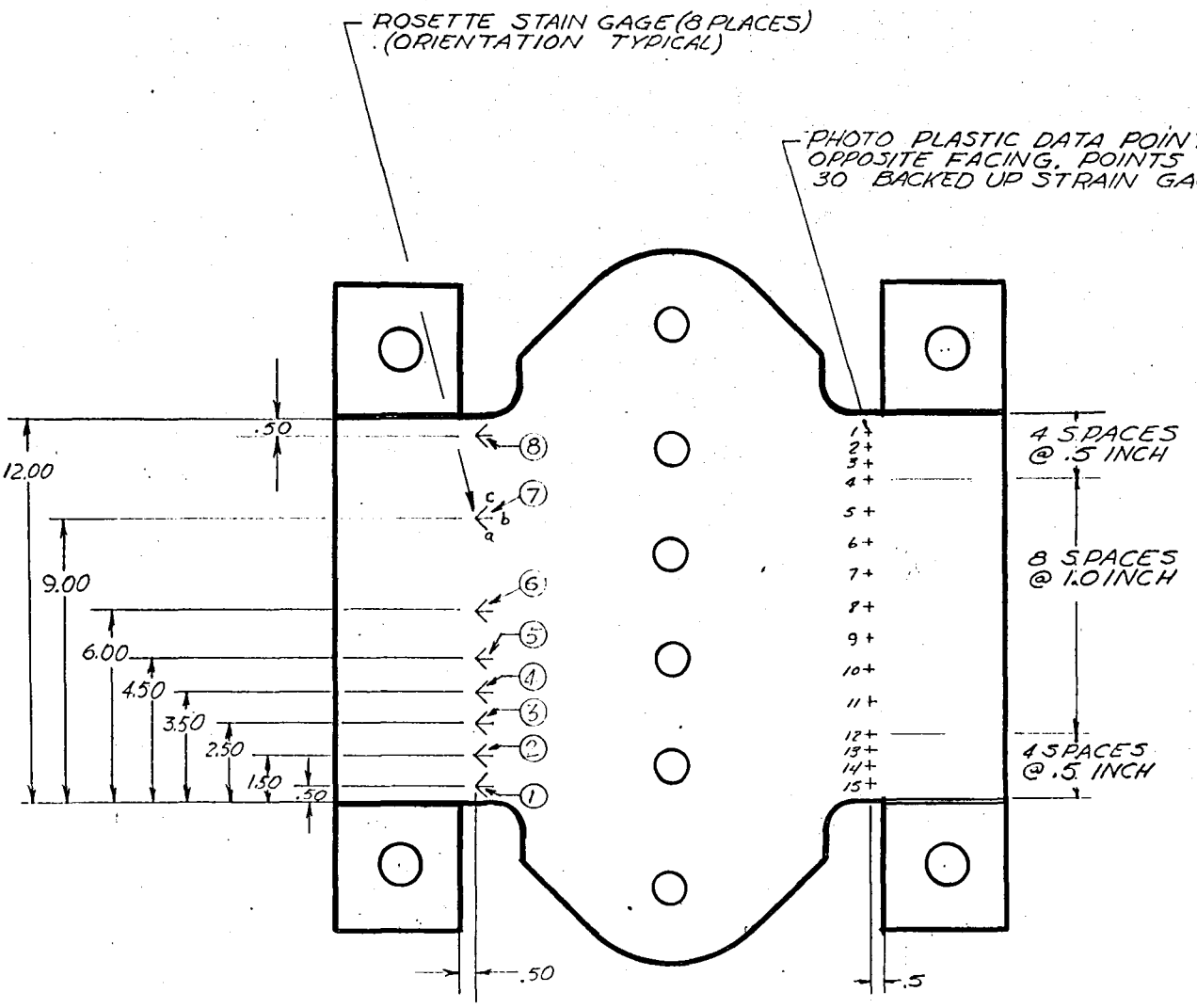

FIGURE 2

DATA POINT LOCATIONS -801 PANEL
HEAVY GAGE BONDED PANEL TEST PROGRAM
10-4920

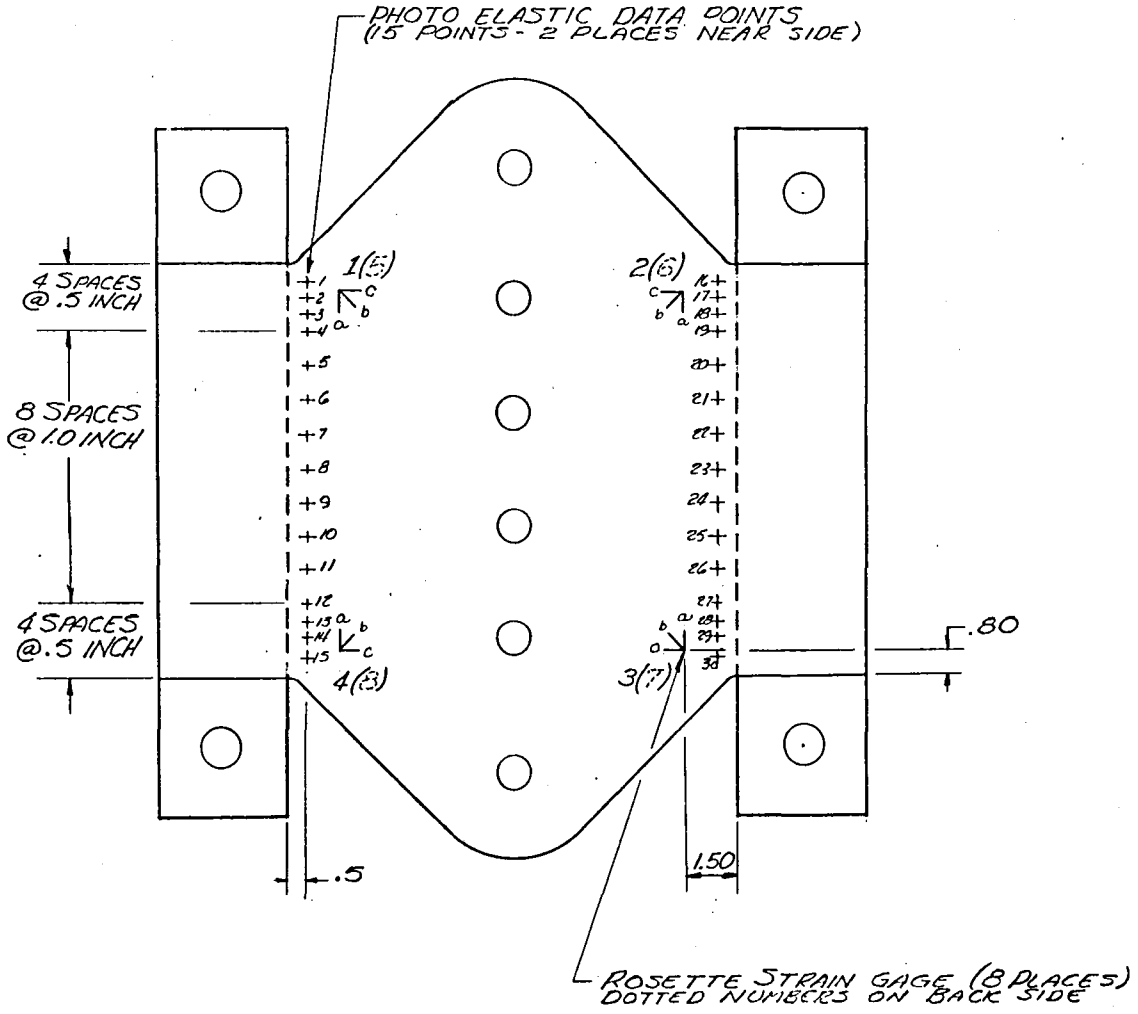

FIGURE 3

DATA POINT LOCATIONS -5 PANEL
HEAVY GAGE BONDED PANEL TEST PROGRAM
10-4920

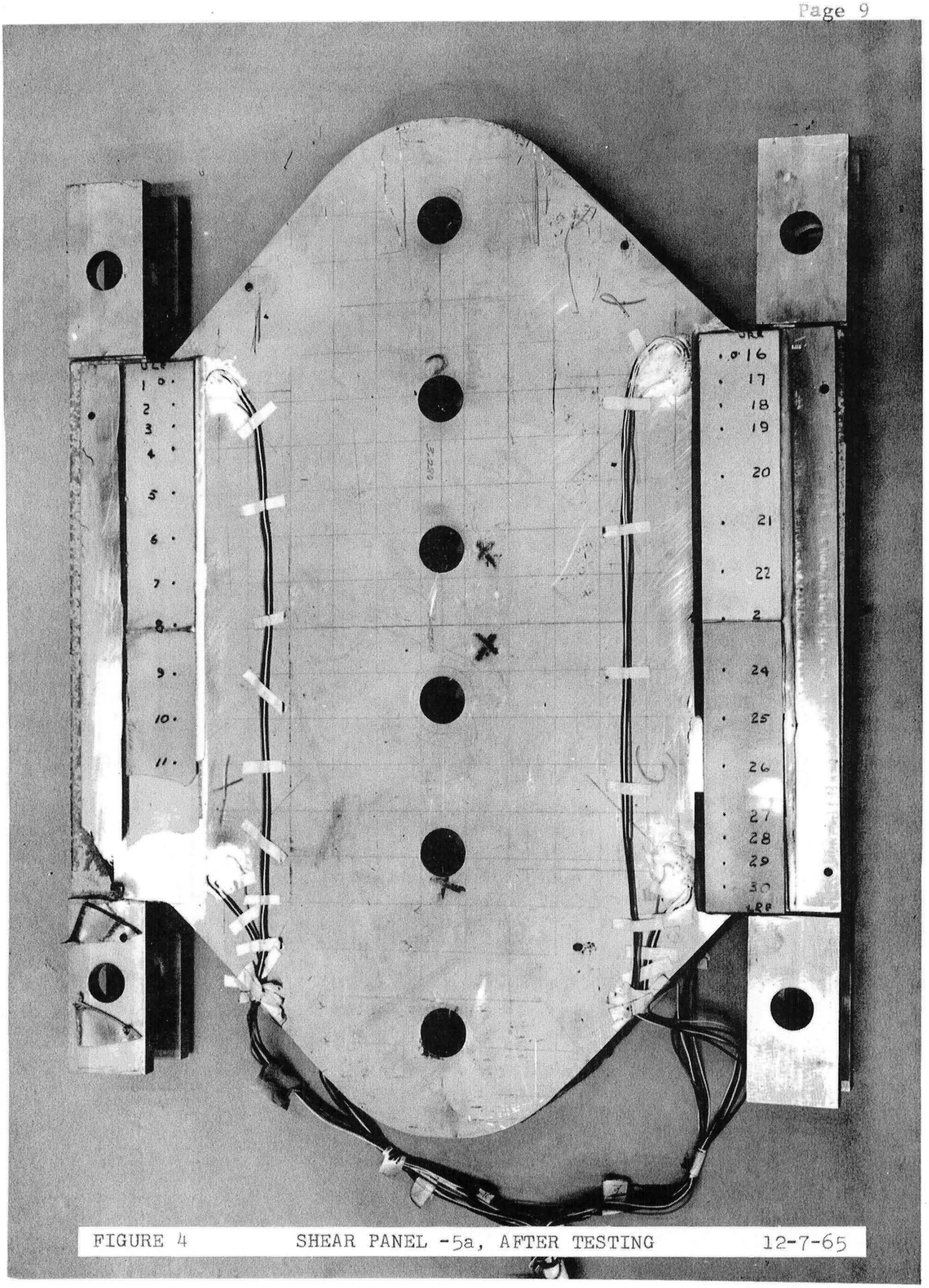

FIGURE 4 SHEAR PANEL -5a, AFTER TESTING 12-7-65

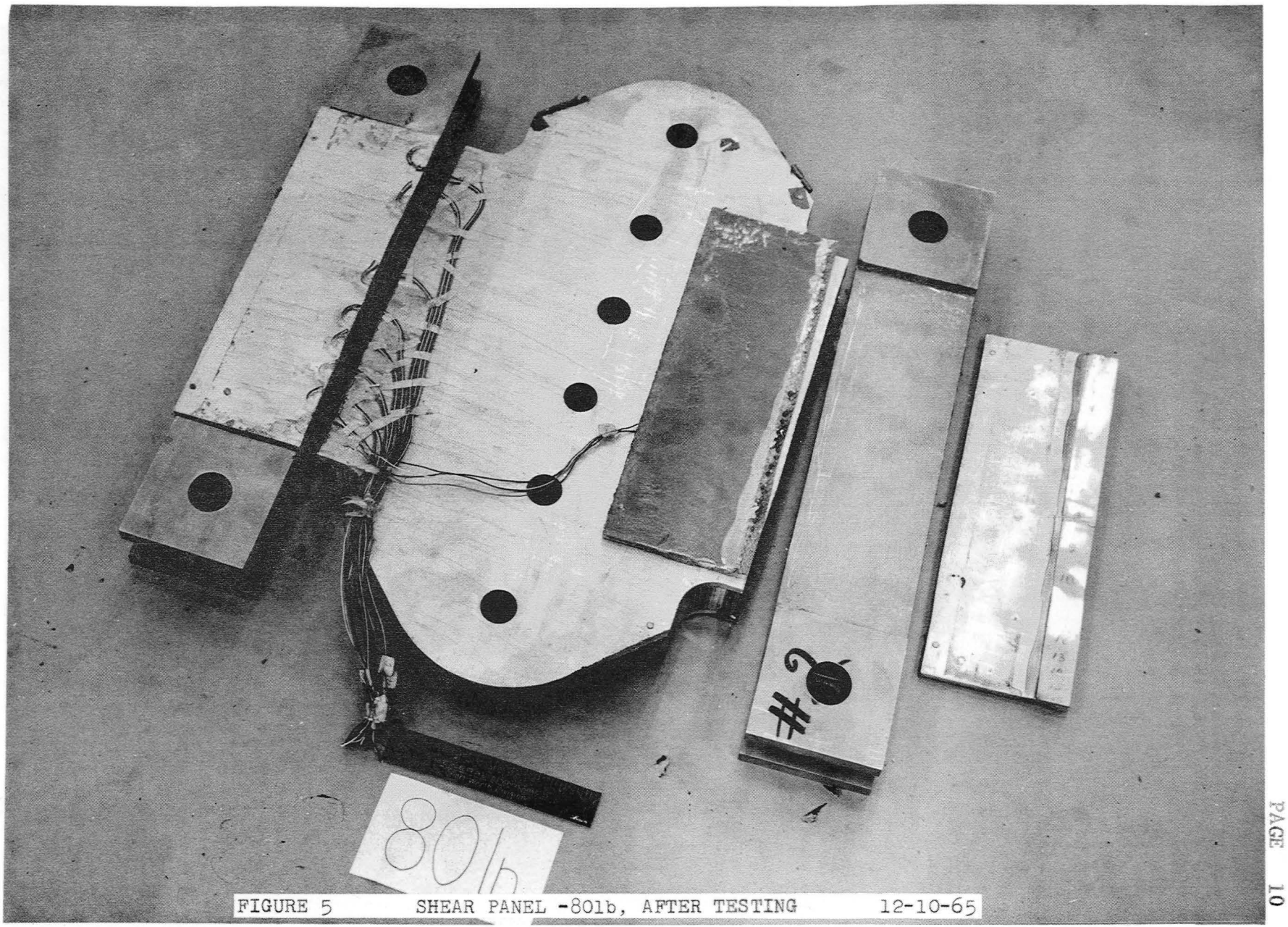

FIGURE 5 SHEAR PANEL -801b, AFTER TESTING 12-10-65

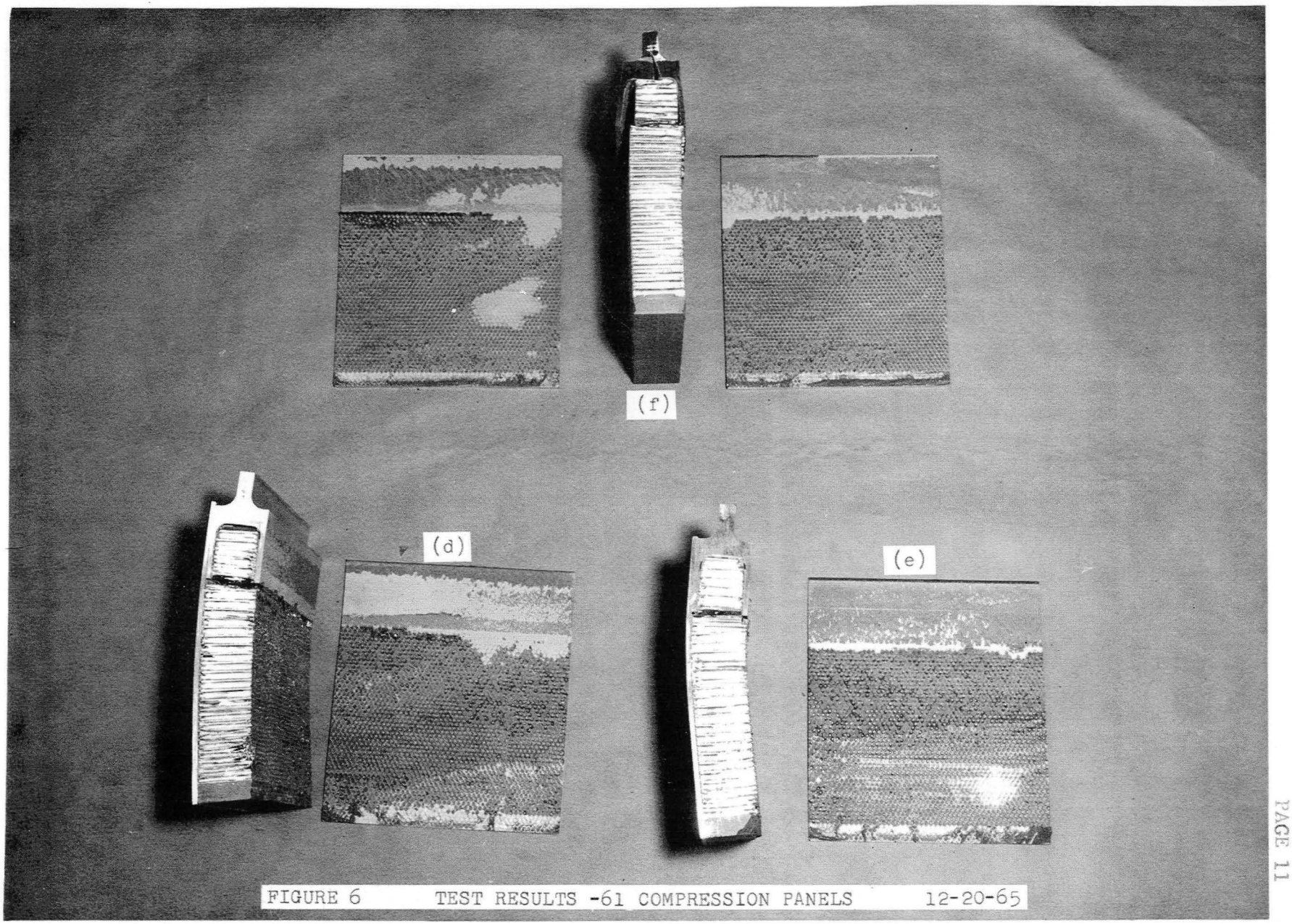

FIGURE 6 TEST RESULTS -61 COMPRESSION PANELS 12-20-65

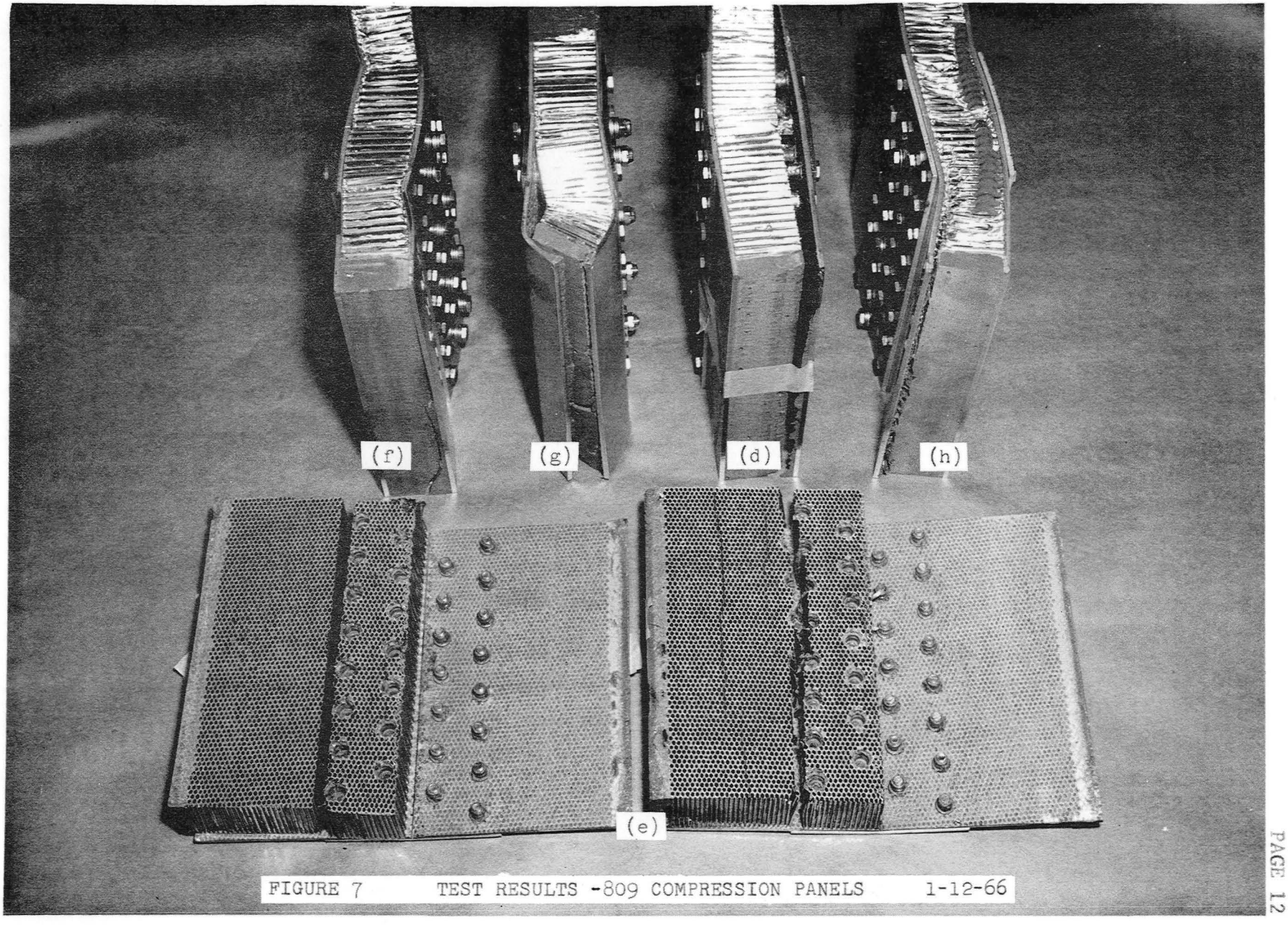

FIGURE 7 TEST RESULTS -809 COMPRESSION PANELS 1-12-66

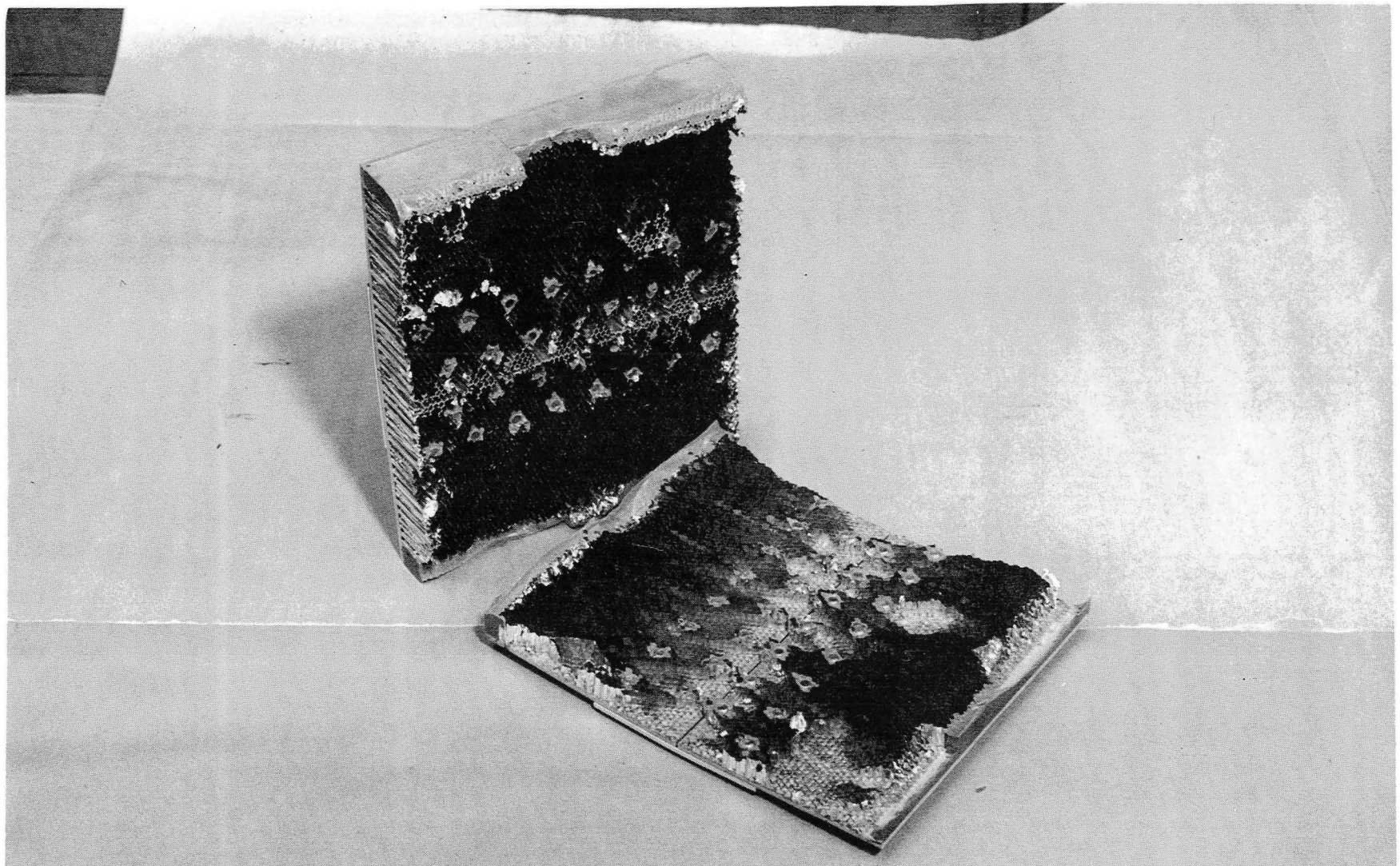

FIGURE 8 TEST RESULTS -809 COMPRESSION PANEL 11-3-65

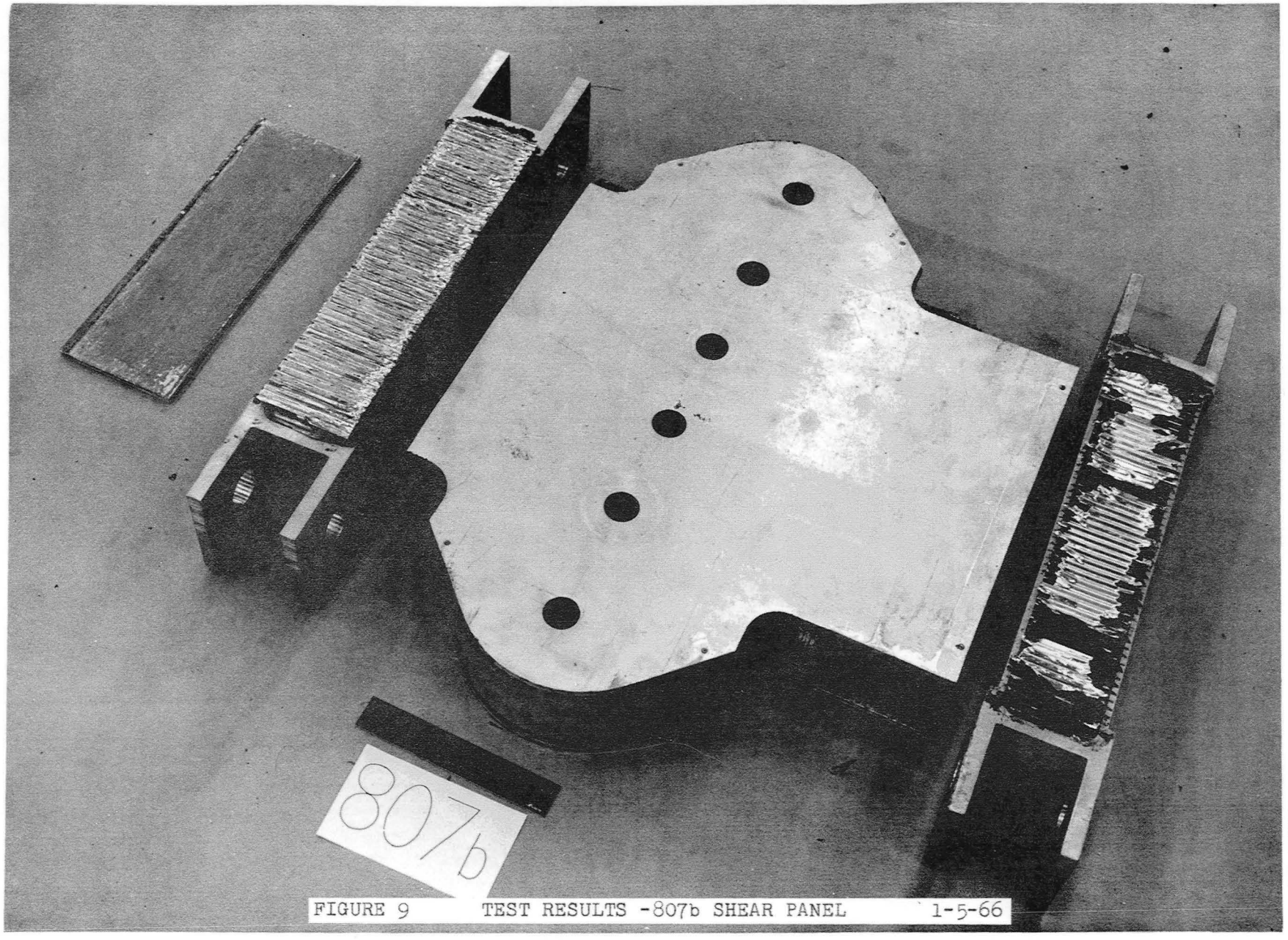

FIGURE 9 TEST RESULTS -807b SHEAR PANEL 1-5-66

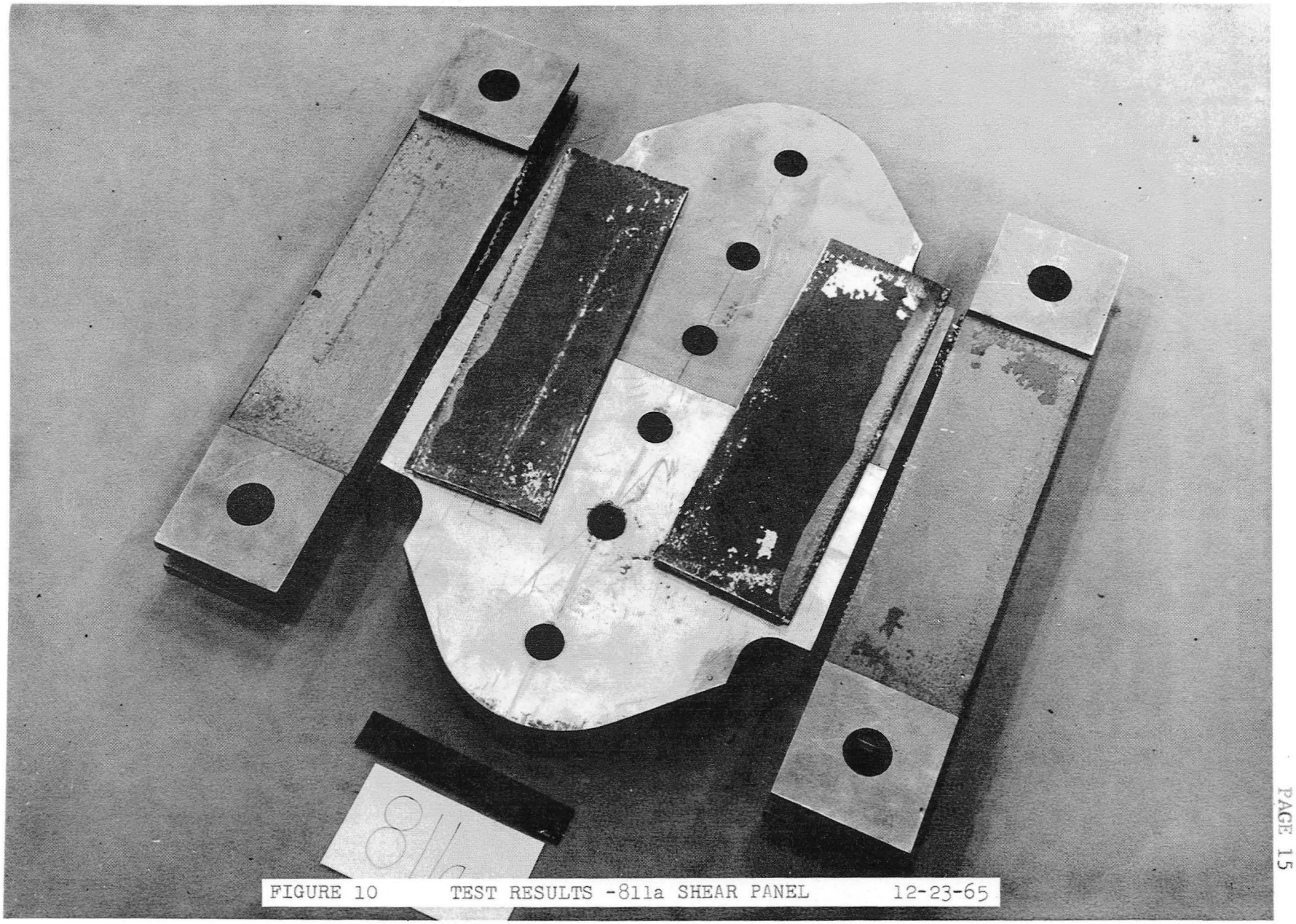

FIGURE 10 TEST RESULTS -811a SHEAR PANEL 12-23-65

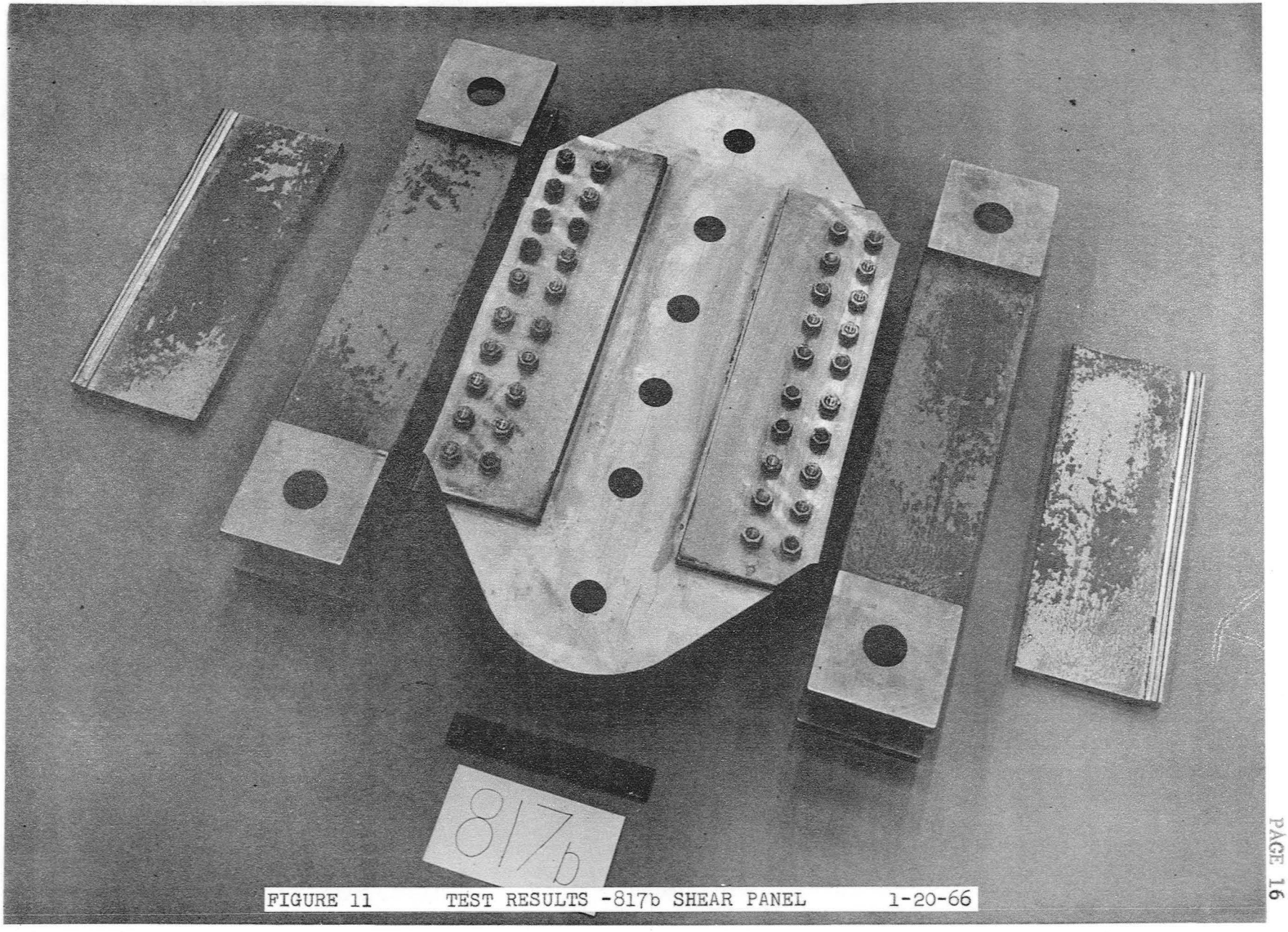

FIGURE 11 TEST RESULTS -817b SHEAR PANEL 1-20-66

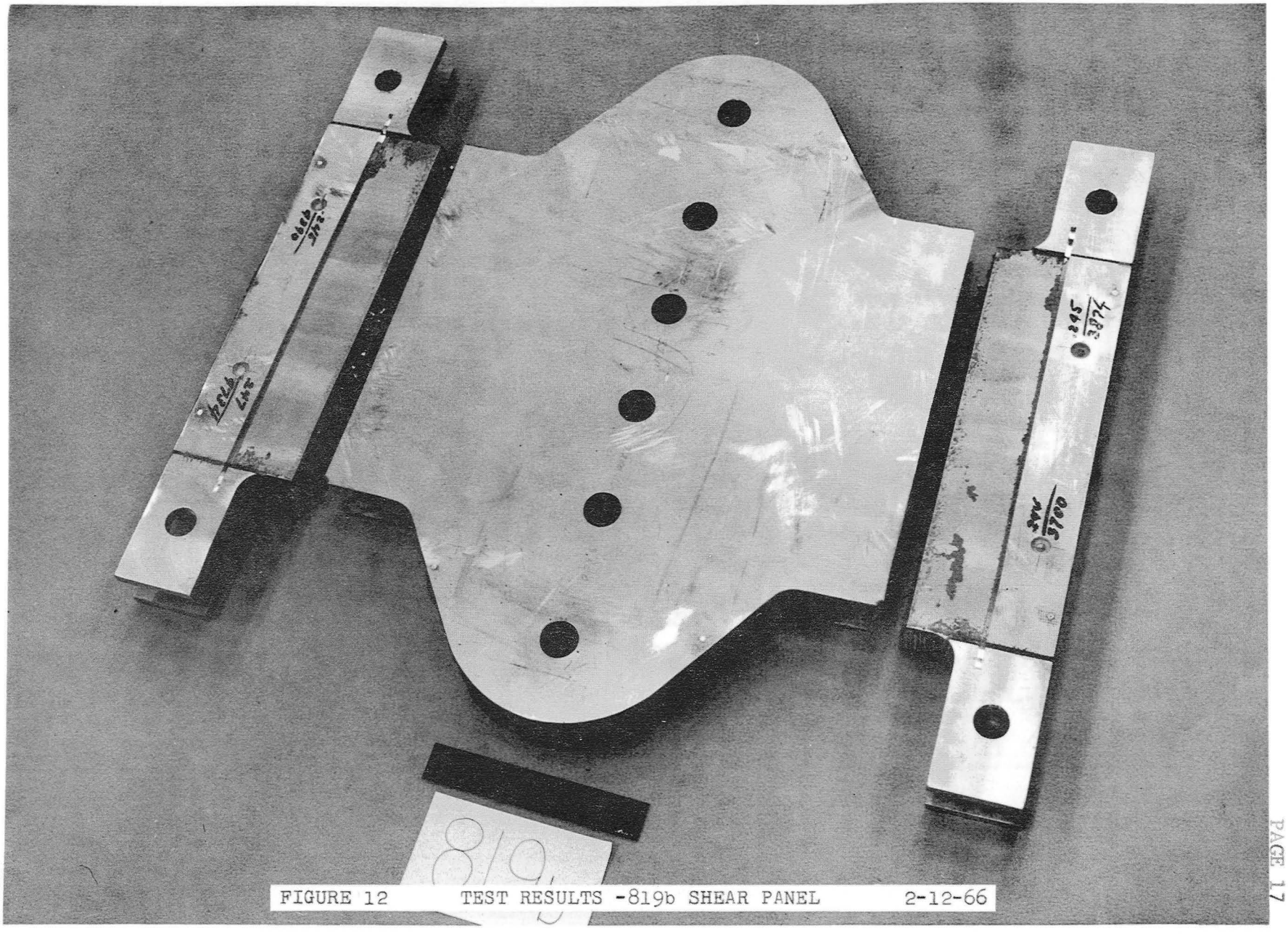

FIGURE 12 TEST RESULTS -819b SHEAR PANEL 2-12-66

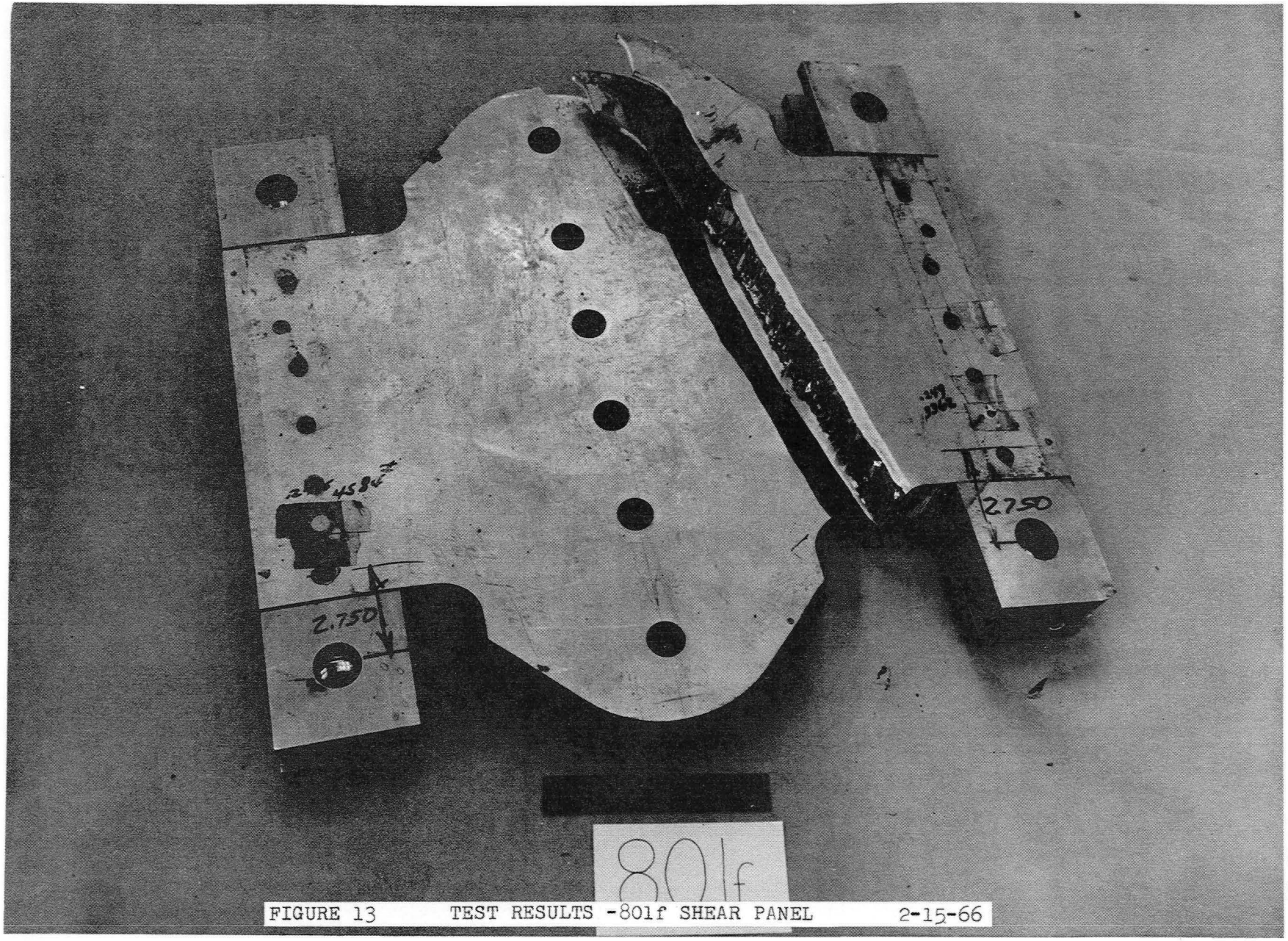

FIGURE 13 TEST RESULTS -801f SHEAR PANEL 2-15-66

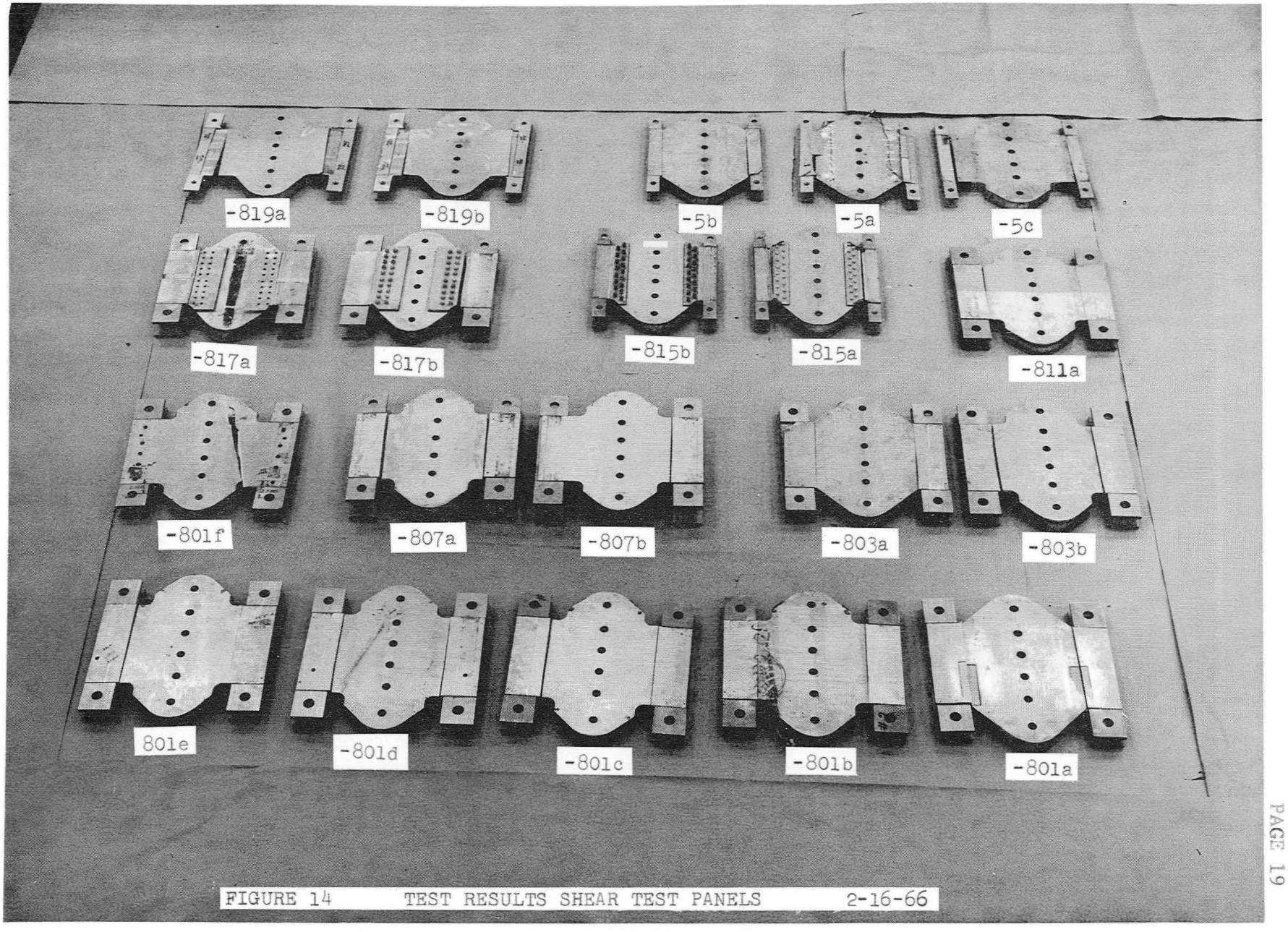

FIGURE 14 TEST RESULTS SHEAR TEST PANELS 2-16-66

TABLE I

SUMMARY OF TEST RESULTS
HEAVY GAGE BONDED HONEYCOMB PANEL TEST PROGRAM

SPECIMEN NUMBER	SPECIMEN TYPE	LOAD RATE (LBS. PER MIN.)	FAILING LOAD (POUNDS)
-57a	Comp.	41,600	86,400
b			79,600
c			94,600
d			85,200
e			97,800
f			124,600
g			125,300
h			128,000
-59a			139,800
b	Comp.		130,600
c			122,600
-61a	Comp.		91,600
b			105,400
c			92,000
d			144,000
e			139,800
f			139,500
-809a	Comp.		74,800
b			92,000
c			80,800
d			95,000
e			118,000
f			156,000
g			167,600
h	Comp.	41,600	127,800
- 5a	Shear	Strain Data	184,000
b		116,700	178,000
c		116,700	215,000
-801a		Strain Data	306,000
b		Strain Data	300,000
c		234,000	309,000
d			316,000
e			336,000
f			500,000
-803a			367,000
b			401,000
-807a			359,000
b			342,000
-811a		234,000	313,000
-815a		116,700	215,000
b		116,700	190,000
-817a		234,000	249,000
b			352,000
-819a			240,000
b	Shear	234,000	251,000

NOTE: Dash numbers refer to drawing FW6528004.

TABLE II

STRAIN GAGE DATA PANEL NUMBER FW6528004-5a
HEAVY GAGE BONDED HONEYCOMB TEST PROGRAM

LOAD GAGE NO.	0	10%	20%	30%	40%	45%	50%	60%
1A	4	- 62	-259	- 503	- 738	- 875	-1019	-1406
1B	- 1	- 60	349	555	769	879	998	1169
1C	2	-219	-319	- 410	- 479	- 526	- 576	- 649
2A	- 2	-260	-509	- 806	-1084	-1249	-1429	-1779
2B	1	206	379	569	749	849	940	1062
2C	1	-134	-208	- 271	- 319	- 359	- 389	- 469
3A	2	408	759	1119	1468	1655	1849	2199
3B	5	-198	-379	- 572	- 749	- 829	- 919	-1240
3C	- 1	96	142	189	249	292	339	505
4A	5	459	799	1169	1519	1719	1898	2249
4B	4	-149	-289	- 469	- 619	- 717	- 799	-1069
4C	7	- 37	- 13	- 5	24	49	79	185
5A	0	-469	-805	-1163	-1489	-1668	-1849	-1839
5B	- 5	210	369	542	719	805	879	1259
5C	- 3	40	44	55	80	66	52	239
6A	-10	-270	-559	- 849	-1139	-1289	-1449	-1469
6B	- 3	148	339	544	739	849	969	1389
6C	-0	-110	-149	- 202	- 244	- 273	- 319	- 589
7A	- 1	488	876	1269	1632	1827	2012	2439
7B	- 2	-174	-349	- 549	- 720	- 819	- 918	-1109
7C	-0	- 48	- 51	- 47	- 31	- 11	15	77
8A	-10	480	832	1194	1521	1699	1869	2294
8B	- 2	-254	-441	- 639	- 836	- 929	-1030	-1189
8C	- 5	71	119	189	255	306	359	504

NOTES:

1. 100% load was 270,000 pounds.
2. All strain readings in micro inches per inch.

TABLE III

STRAIN GAGE DATA PANEL NUMBER FW6528004-801b
HEAVY GAGE BONDED HONEYCOMB TEST PROGRAM

LOAD GAGE NO.	0	10%	20%	30%	40%	45%	50%
1A	5	279	511	729	919	939	879
1B	0	-439	- 769	-1106	-1442	-1619	-1849
1C	7	-701	-1310	-1907	-2449	-2650	-2819
2A	6	619	1139	1669	2219	2489	2769
2B	10	- 92	- 169	- 259	- 319	- 349	- 389
2C	8	-619	-1219	-1849	-2459	-2819	-3219
3A	8	659	1243	1842	2439	2769	3159
3B	7	- 19	- 49	- 79	- 81	- 79	- 59
3C	1	-489	- 989	-1530	-2049	-2349	-2689
4A	10	719	1329	1979	2629	2999	3390
4B	3	29	49	74	129	171	230
4C	4	-469	- 959	-1479	-1979	-2259	-2589
5A	- 3	747	1399	2091	2779	3139	3549
5B	5	101	179	279	400	490	600
5C	6	-469	- 948	-1449	-1929	-2190	-2479
6A	- 1	813	1519	2259	3017	3410	3819
6B	5	220	420	639	889	1051	1240
6C	0	-479	- 949	-1449	-1919	-2159	-2439
7A	3	886	1660	2449	3269	3659	4069
7B	- 1	339	640	952	1310	1520	1749
7C	3	-498	- 989	-1499	-1979	-2219	-2459
8A	2	789	1479	2222	2969	3249	3519
8B	- 2	410	789	1207	1630	1810	1979
8C	- 3	-319	- 612	- 919	-1189	-1299	-1399

NOTES:

1. 100% load was 540,000 pounds.
2. All strain readings in micro inches per inch.

TABLE IV

PHOTOELASTIC DATA RECORDED DURING TESTS
ON PANELS FW 6528004-5a AND -801b

Panel No. FW 6528004-5a: Test Load: 81,000 lbs.

Point No.	Isoclinic Angle (θ) * (Degrees)	Isochromatic No. (n)* (Fringes)	Point No.	Isoclinic Angle (θ) * (Degrees)	Isochromatic No. (n)* (Fringes)
1	50	3.22	16	55	3.44
2	50	3.22	17	55	3.40
3	50	3.08	18	54	3.21
4	50	2.98	19	54	3.07
5	51	2.87	20	51	2.93
6	51	2.89	21	50	2.88
7	54	2.89	22	50	2.88
8	54	2.90	23	50	2.88
9	51	2.83	24	50	2.89
10	51	2.89	25	50	2.92
11	51	2.96	26	50	3.00
12	55	3.14	27	50	3.26
13	58	3.25	28	50	3.32
14	59	3.56	29	50	3.77
15	59	3.88	30	46	3.84

Panel No. 6528004-801: Test Load: 162,000 lbs.

Point No.	Isoclinic Angle (θ) * (Degrees)	Isochromatic No. (n)* (Fringes)	Point No.	Isoclinic Angle (θ) * (Degrees)	Isochromatic No. (n)* (Fringes)
1	60	3.00	16	29	2.22
2	57	4.27	17	42	3.35
3	57	4.27	18	42	3.21
4	55	4.05	19	45	3.24
5	55	3.29	20	46	3.00
6	55	3.19	21	47	3.08
7	53	3.12	22	47	3.15
8	53	3.12	23	48	3.15
9	50	3.05	24	47	3.15
10	49	3.08	25	50	3.08
11	49	3.22	26	50	3.00
12	42	4.08	27	50	3.27
13	41	4.09	28	52	4.00
14	39	4.09	29	55	4.00
15	31	3.33	30	61	3.00

* For explanation of Isoclinics, Isochromatic, and equation for determining shear stresses, see explanation notes on following page.

EXPLANATION NOTES FOR TABLE IV

Definitions:

Isoclinic - The isoclinic is the angle between the slope of the principal stress at a point and the axis parallel to the externally applied load. All angles are measured clockwise from the vertical axis when viewed normal to the panel face.

Isochromatic - The isochromatic is a color band containing areas of equal shear stress. The number of fringes, associated with the isochromatics, indicates the magnitude of the shear stress at a point.

Determination of Shear Stress

Maximum Shear Stress = $\tau_{max} = 3,983\,n$

Where: 3,983 = conversion factor as determined by the type of photoelastic material used,

n = fringe number from Table IV

Shear Stress along Vertical Axis = $\tau_{xy} = \tau_{max} \sin 2\theta$

Where: θ = isoclinic shown in Table IV.

"I, _____, attest to the fact that the instrumentation used in obtaining the data for the test described in this report was at all times calibrated within the specified period established by standard engineering practices at the Fort Worth Division of General Dynamics."

Consider the shear test specimen and the element dx by dy as shown in Figure B-1. A typical cross section of a shear test

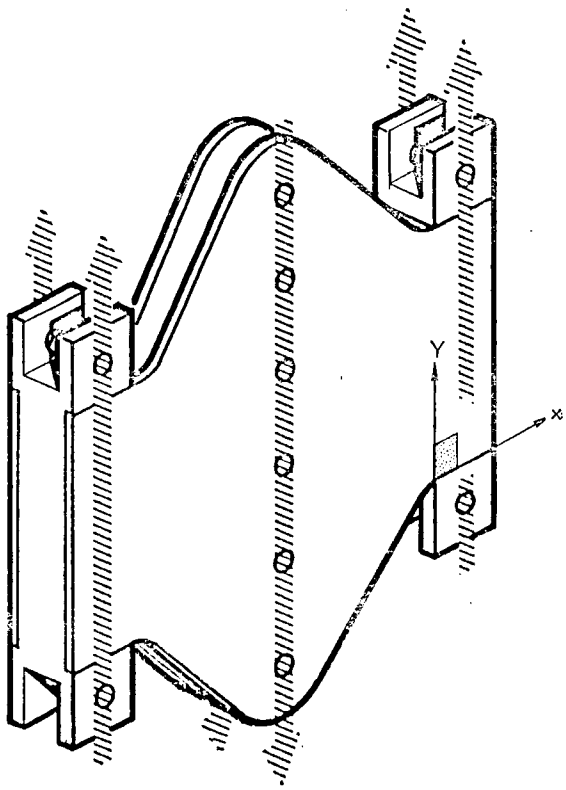

Figure B-1 SHEAR TEST SPECIMEN

specimen with solid edgemembers is shown in Figure B-2. The location of the element with respect to the solid edgemember

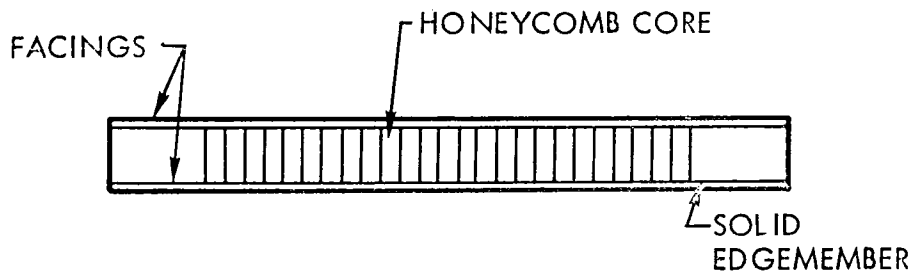

Figure B-2 CROSS SECTION OF SHEAR TEST SPECIMEN

is shown in Figure B-3. The stresses which act on the element are

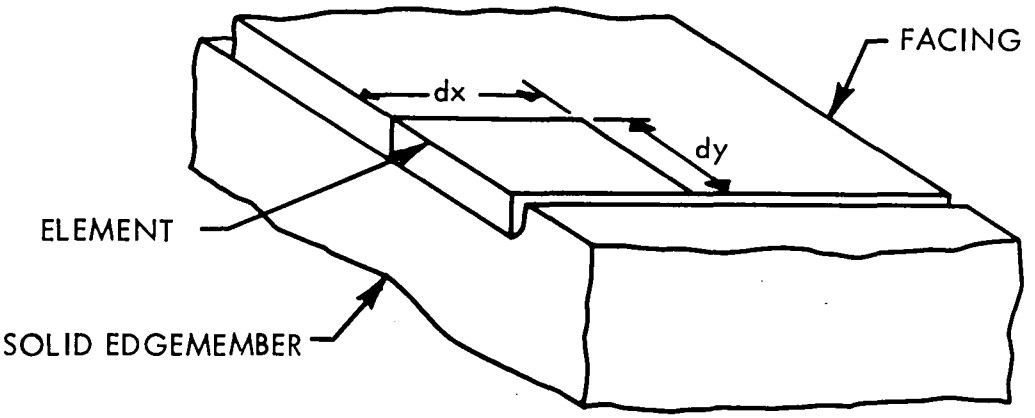

Figure B-3 ELEMENT LOCATION

shown in Figure B-4 where τ_f is the shear stress in the facing and τ_b is the shear stress in the adhesive.

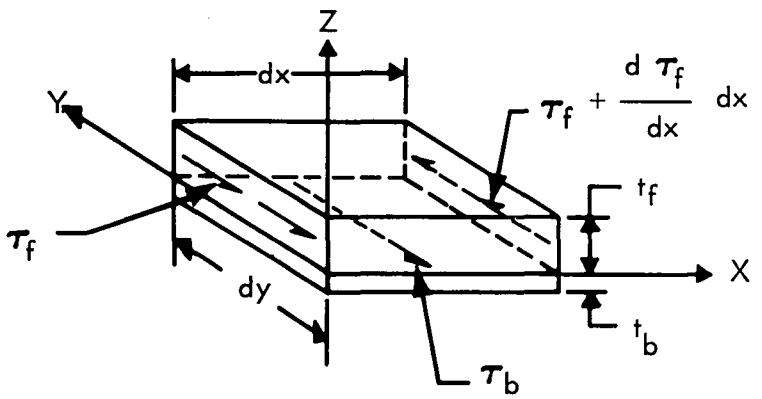

Figure B-4 ELEMENT STRESSES

Equilibrium conditions yield

$$\tau_f t_f dy + \tau_b dx dy - \left(\tau_f + \frac{d\tau_f}{dx} dx\right) t_f dy = 0$$

Then (B-1)

$$\tau_b = t_f \frac{d\tau_f}{dx}$$

Assume:

1. The edgemember is completely rigid and does not strain in the area of the bond.

2. The displacement of the facing in the Y-direction, v_f, measured relative to the edgemember, is independent of Y.

3. There is no displacement of the facing in the x-direction. ($\mu_f = 0$)

The shearing strain in the adhesive, γ_b, is given by (B-2)

$$\gamma_b = \frac{v_f}{t_b}$$

because $\mu_f = 0$ by assumption 3. Differentiating Equation (B-2) we find

$$\frac{\partial \gamma_b}{\partial x} = \frac{1}{t_b} \frac{\partial v_f}{\partial x} \quad ; \quad \frac{\partial \gamma_b}{\partial y} = \frac{1}{t_b} \frac{\partial v_f}{\partial y}$$

However

$$\frac{\partial v_f}{\partial y} = 0$$

by assumption 2. Then

$$\frac{d\gamma_b}{dx} = \frac{1}{t_b} \frac{dv_f}{dx}$$

From theory of elasticity (B-3)

$$\gamma_f = \frac{d\mu_f}{dy} + \frac{dv_f}{dx}$$

where γ_f is the shearing strain in the facing. For our case however,

$$\frac{d\mu_f}{dy} = 0$$

by Assumption 3. Then (B-4)

$$\gamma_f = \frac{dv_f}{dx}$$

Substitution of Equation (B-4) into Equation (B-3) yields (B-5)

$$\frac{d\gamma_b}{dx} = \frac{1}{t_b} \gamma_f$$

Shearing strains and stresses are related by (B-6)

$$\gamma_b = \frac{1}{G_b} \tau_b \quad ; \quad \gamma_f = \frac{1}{G_f} \tau_f$$

where G is shear modulus. Substituting Equations (B-6) into (B-5) yields (B-7)

$$\frac{d\tau_b}{dx} = \frac{G_b}{t_b G_f} \tau_f$$

Differentiating Equation (B-7) yields (B-8)

$$\frac{d^2\tau_b}{dx^2} = \frac{G_b}{t_b G_f} \frac{d\tau_f}{dx}$$

After substitution from Equation (B-1) we find (B-9)

$$\frac{d^2\tau_b}{dx^2} - \frac{G_b}{t_b t_f G_f} \tau_b = 0$$

If we let (B-10)

$$K = \sqrt{\frac{G_b}{t_b t_f G_f}}$$

then Equation (B-9) becomes (B-11)

$$\frac{d^2\tau_b}{dx^2} - K^2 \tau_b = 0$$

and the solution is (B-12)

$$\tau_b = A \sinh Kx + B \cosh Kx$$

The boundary conditions that we wish to consider are

1. $\tau_f = \tau_o$ at $x=0$ where τ_o is a known value of the shear stress in the facing
2. $\int_0^L \tau_b W dX = \tau_o W t_f$ where W is the width of the element being considered and L is the width of the edgemember.

Boundary condition 1.) yields

$$AK \cosh K(o) + BK \sinh K(o) = \frac{G_b}{t_b G_f} \tau_o$$

after substitution of Equation (B-12) into (B-7). Then

$$A = \frac{G_b}{K t_b G_f} \tau_o \quad \text{(B-13)}$$

Boundary condition 2. yields

$$\int_0^L (A \sinh kx + B \cosh Kx)\, dx = \tau_o t_f$$

which leads to

$$B = \frac{K\tau_o t_f}{\sinh KL}\left[2 - \cosh KL\right] \qquad \text{(B-14)}$$

Substituting Equations (B-13) and (B-14) into (B-12) and simplifying leads to

$$\tau_b = K\tau_o t_f \left\{\sinh KX + \left(\frac{2-\cosh KL}{\sinh KL}\right)\cosh KX\right\} \qquad \text{(B-15)}$$

Assuming the following material properties and characteristics:

1. G_b = 150,000 psi
2. t_b = 0.010 inch
3. G_f = 4.04 x 10^6 psi
4. t_f = 0.25 inch
5. τ_o = 17,500 psi
6. L = 3.75 inch

leads to

$$\tau_b = 16{,}890\left[\sinh (3.86x) - \cosh (3.86x)\right] \qquad \text{(B-16)}$$

from Equation (B-15). Assuming the identical material properties and characteristics except G_b = 50,000 psi leads to

$$\tau_b = 9.740\left[\sinh (2.23x) - \cosh (2.23x)\right]$$

Equations (B-16) and (B-17) are shown in Figure B-5. It should be noted in Figure B-5 that the adhesive shear stress, τ_b, has a negative sign which means that τ_b is acting in the opposite direction to that originally assumed in Figure B-4. Then this analytical treatment shows that the shear stresses τ_f and τ_b act in opposite directions, a fact which certainly must be true for the physical situation.

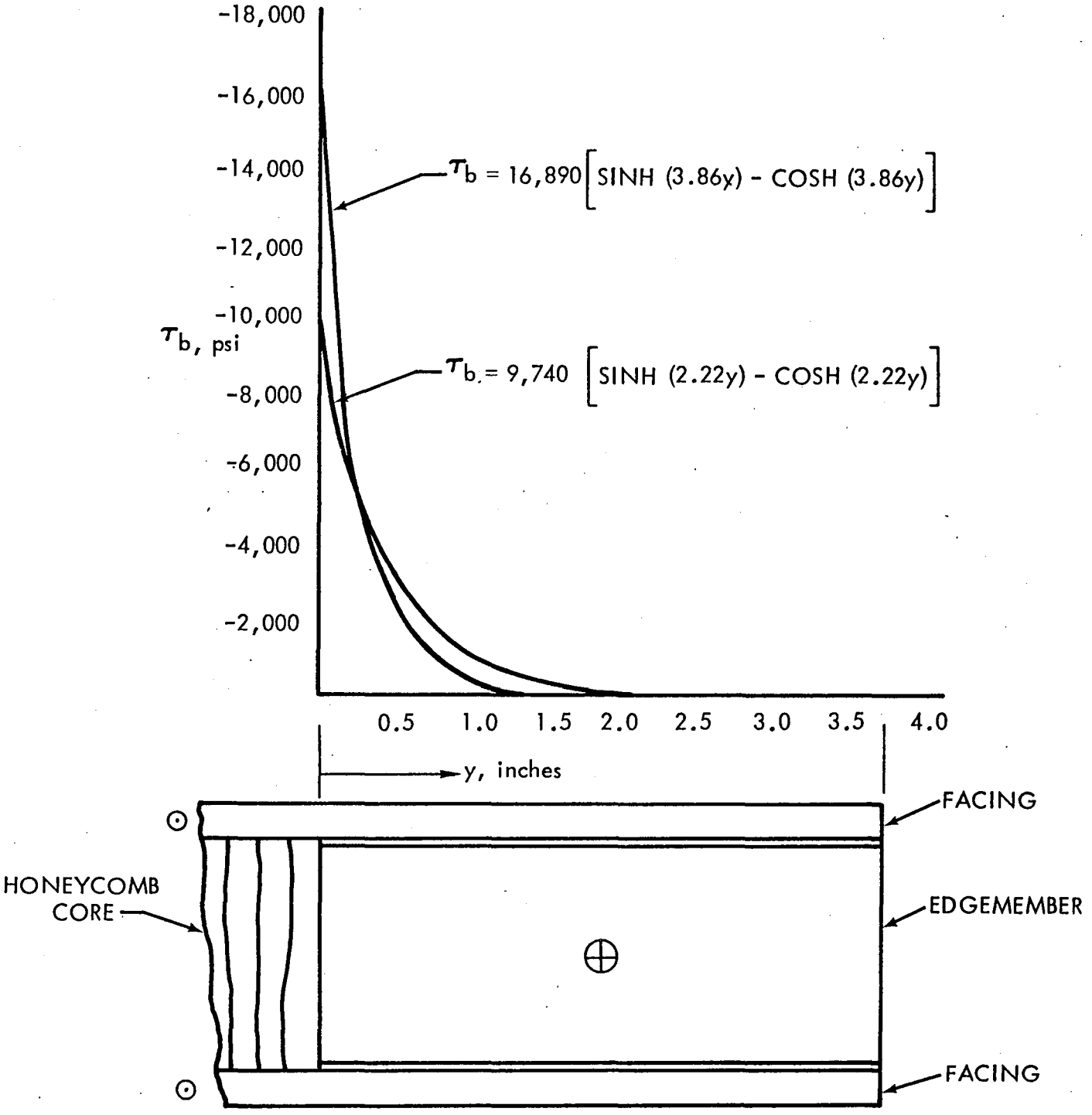

Figure B-5 ADHESIVE SHEAR STRESS DISTRIBUTION

A P P E N D I X C

This appendix contains the computer program U42 utilized in the solution for the one dimensional numerical analyses of shear lag. An example problem is included.

C U S T O M E R U T I L I Z A T I O N

P R O G R A M U 4 2

IDENTIFICATION

U42 One Dimensional Shear Lag Analysis, M. E. Waddoups 5-11-66, General Dynamics - Fort Worth Division

PURPOSE

The purpose is to provide the load distribution in a bi-directionally taper panel, with or without stringers, subjected to a concentrated load in one stringer and with a clamped boundary on the opposite edge. The analysis is presented in Section 2.1.2.

METHOD

The analysis is a one dimensional shear lag analysis based on constant area, constant thickness, and constant stress finite elements.

USAGE

A. Inputs - Card sequence

(1) KEY3, KEY4 - Format (I3, 2X, I3)

KEY3 = Optional output variable

KEY3 = 0 No output, No loads check

KEY3 = 1 All output, loads check

KEY4 = Inversion Option

KEY4 = 1 Invert

KEY4 = 0 No Inversion

(2) T(I), R(I), T(I+1), R(I + 1), T(I + 2), R(I + 2) -

Format (6E10.4),

T = Panel thickness at the node (I), (I+1), (I+2)

R = Stringer area at the node (I), (I+1), (I+2)

Thirty (30) total cards in this group.

(3) AW(I1), AH(I1) - Format (6E10.4)

AW = Distance between nodes (width)

AH = Height between nodes

Each row and column must have the same y and x coordinates respectively. There are 9 total cards in this group with the last card having a dummy width.

(4) EM, GM, P83, P56 - Format (6E10.4)

EM = Panel and longeron modulus of elasticity

GM = Panel modulus of rigidity

P83, P56 = external loads at nodes 83, 56

(5) DENS, KEY5 - Format (E10.4.2 X, 13)

DENS = Panel and longeron weight per unit volume

KEY5 = Output Option

KEY5 = 1 No weight check

KEY5 = 0 Weight check

B. Outputs

All outputs are listed in the KEY3 = 1 mode. Deleted outputs are listed as optional and may be deleted by running in the KEY3 = 0 mode.

(1) Panel thicknesses - the average thicknesses between nodes (R (I))
(2) Average equivalent longeron areas plus panel effective areas. (H (I))
(3) Optional, the stiffness matrix
(4) External loads
(5) Displacements
(6) Shear flows
(7) Axial loads
(8) Optional, panel weights
(9) Optional, equilibrium check

RUN TIME

Approximately .018 7090 hrs.

An example problem follows:

Sample Input Data

```
1    1                                                                001509P00100001U42
      .240     1.50      .240     .0       .230     .0               001509P00100002U42
      .200      .0       .170     .0       .150     .0               001509P00100003U42
      .120      .0       .100     .0       .100     .6               001509P00100004U42
      .250     2.70      .250     .0       .240     .0               001509P00100005U42
      .220      .0       .200     .0       .170     .0               001509P00100006U42
      .140      .0       .120     .0       .120     .72              001509P00100007U42
      .300     3.50      .220     .0       .270     .0               001509P00100008U42
      .250      .0       .220     .0       .185     .0               001509P00100009U42
      .145      .0       .135     .0       .135    2.20              001509P00100010U42
      .380     3.85      .365     .0       .340     .0               001509P00100011U42
      .300      .0       .250     .0       .190     .0               001509P00100012U42
      .150      .0       .150     .0       .165    2.53              001509P00100013U42
      .450     4.09      .430     .0       .395     .0               001509P00100014U42
      .340      .0       .270     .0       .200     .0               001509P00100015U42
      .180      .0       .195     .0       .210    3.28              001509P00100016U42
      .500     6.14      .480     .0       .400     .0               001509P00100017U42
      .370      .0       .275     .0       .210     .0               001509P00100018U42
      .190      .0       .225     .0       .255    3.80              001509P00100019U42
      .620     8.00      .580     .0       .500     .0               001509P00100020U42
      .390      .0       .280     .0       .195     .0               001509P00100021U42
      .195      .0       .255     .0       .310    6.79              001509P00100022U42
      .800    10.90      .700     .0       .600     .0               001509P00100023U42
      .400      .0       .270     .0       .180     .0               001509P00100024U42
      .190      .0       .290     .0       .420   10.78              001509P00100025U42
     1.000    15.40      .800     .0       .600     .0               001509P00100026U42
      .378      .0       .250     .0       .168     .0               001509P00100027U42
      .181      .0       .320     .0       .650   17.20               01509P00100028U42
     1.200    22.55      .900     .0       .650     .0               01509P00100029U42
      .335      .0       .225     .0       .106     .0               01509P00100030U42
      .107      .0       .290     .0      1.000   31.40              01509P00100031U42
     8.        48.                                                   01509P00100032U42
    10.        40.                                                   01509P00100033U42
    13.        36.                                                   01509P00100034U42
    16.        32.                                                   01509P00100035U42
    19.        26.                                                   01509P00100036U42
    23.        22.                                                   01509P00100037U42
    26.        18.                                                   01509P00100038U42
    29.        14.                                                   01509P00100039U42
     0.        10.                                                   01509P00100040U42
  10.E+06  4.35E+06 1.605E+06                                        01509P00100041U42
      .1    1                                                        01509P00100042U42
                                                                                000042
```

```
$IBFTC U42SLA                                                                  U42A0000
C      IBM 7090  HEAVY GAGE SANDWICH SHEAR LAG ANALYSIS                        U42A0010
C      CODED IN FORTRAN IV                                                     U42A0020
       CALL GSTART(3HU42,KEY1)                                                 U42A0030
       COMMON T(92),R(92),AW(10),AH(10),TA(92),AA(92),A(91,91),SV(90),U(9U42A0040
      10),UF(92),AQ(92),F(92),PIV(91),MN(92),NUM1,DENS,KEY2                    U42A0050
   10  CALL PROB                                                               U42A0060
       READ(5,20) KEY3,KEY4                                                    U42A0070
   20  FORMAT(I3,2X,I3,2X,I3,2X,I3)                                            U42A0080
       DO 40 I=2,89,3                                                          U42A0090
   40  READ(5,50)T(I),R(I),T(I+1),R(I+1),T(I+2),R(I+2)                         U42A0100
   50  FORMAT(6E10.4)                                                          U42A0110
       DO 60 I1=1,9                                                            U42A0120
   60  READ(5,50)AW(I1),AH(I1)                                                 U42A0130
       READ(5,50)EM,GM,P83,P56                                                 U42A0140
       READ(5,30) DENS,KEY5                                                    U42A0150
   30  FORMAT(E10.4,2X,I3)                                                     U42A0160
C      COMPUTE MEAN THICKNESS AND AREA PER ELEMENT                             U42A0170
       K1=0                                                                    U42A0180
       DO 70 I2=1,10                                                           U42A0190
       DO 80 I3=2,9                                                            U42A0200
       I3A=I3+K1                                                               U42A0210
       I3B=I3A+1                                                               U42A0220
       TA(I3A  )=(T(I3A  )+T(I3B    ))/2.                                      U42A0230
   80  CONTINUE                                                                U42A0240
       K1=K1+9                                                                 U42A0250
   70  CONTINUE                                                                U42A0260
       K3=9                                                                    U42A0270
       DO 90 I4=2,10                                                           U42A0280
       DO 100 I5=2,10                                                          U42A0290
       I5A=I5+K3                                                               U42A0300
       IF(I5.EQ.2)GO TO 110                                                    U42A0310
       IF(I5.EQ.10)GO TO 120                                                   U42A0320
       AA(I5A  )=(TA(I5A  -10)+TA(I5A-1)) *AW(I5-2)/4.+(TA(I5A  -9)+TA(I5U42A0330
      1A)) *AW(I5-1)/4.+(R(I5A)+R(I5A-9))/2.                                   U42A0340
       GO TO 130                                                               U42A0350
  110  AA(I5A  )=(TA(I5A  )+TA(I5A-9)) *AW(I5-1)/4.+(R(I5A)+R(I5A-9))/2.      U42A0360
       GO TO 130                                                               U42A0370
  120  AA(I5A  )=(TA(I5A-1)+TA(I5A-10))* AW(I5-2)/4.+(R(I5A)+R(I5A-9))/2.U42A0380
  130  CONTINUE                                                                U42A0390
  100  CONTINUE                                                                U42A0400
       K3=K3+9                                                                 U42A0410
   90  CONTINUE                                                                U42A0420
       IF(KEY3.NE.1)GO TO 140                                                  U42A0430
       WRITE(6,150)                                                            U42A0440
  150  FORMAT(1H ,8X,4HW(1),6X,4HW(2),6X,4HW(3),6X,4HW(4),6X,4HW(5),6X,4HU42A0450
      1W(6),6X,4HW(7),6X,4HW(8))                                               U42A0460
       K4=0                                                                    U42A0470
       DO 160 I6=1,10                                                          U42A0480
       WRITE(6,170) I6,TA(K4+2),TA(K4+3),TA(K4+4),TA(K4+5),TA(K4+6),TA(K4U42A0490
      1+7),TA(K4+8),TA(K4+9)                                                   U42A0500
  170  FORMAT(1H ,2HR(,I2,1H),   8E10.4)                                       U42A0510
       K4=K4+9                                                                 U42A0520
  160  CONTINUE                                                                U42A0530
       WRITE(6,180)                                                            U42A0540
  180  FORMAT(1H ,8X,4HC(1),6X,4HC(2),6X,4HC(3),6X,4HC(4),6X,4HC(5),6X,4HU42A0550
```

```
     1C(6),6X,4HC(7),6X,4HC(8),6X,4HC(9))                                    U42A0560
      K5=9                                                                   U42A0570
      DO 190  I7=1,9                                                         U42A0580
      WRITE(6,200) I7,AA(K5+2),AA(K5+3),AA(K5+4),AA(K5+5),AA(K5+6),AA(K5U42A0590
     1+7),AA(K5+8),AA(K5+9),AA(K5+10)                                        U42A0600
  200 FORMAT(1H ,2HH(,I1,1H),1X,9E10.4)                                      U42A0610
      K5=K5+9                                                                U42A0620
  190 CONTINUE                                                               U42A0630
  140 CONTINUE                                                               U42A0640
C     ENTER THE ELEMENTS INTO THE TOTAL STIFFNESS MATRIX  I-INTERIOR PTSU42A0650
      NA1=9                                                                  U42A0660
      DO 460 K15=1,91                                                        U42A0670
      DO 460 J15=1,91                                                        U42A0680
      A(K15,J15)=0.                                                          U42A0690
  460 CONTINUE                                                               U42A0700
      NA1=9                                                                  U42A0710
      DO 470 J16=1,8                                                         U42A0720
      DO 480 K15=3,9                                                         U42A0730
      NA2=NA1+K15                                                            U42A0740
      A(NA2,NA2-9)=AA(NA2)*EM/AH(J16)                                        U42A0750
      A(NA2,NA2-1)=TA(NA2-1)*GM/AW(K15-2)*(AH(J16)+AH(J16+1))/2.             U42A0760
      A(NA2,NA2+1)=TA(NA2)*GM/AW(K15-1)*(AH(J16)+AH(J16+1))/2.               U42A0770
      A(NA2,NA2+9)=AA(NA2+9)*EM/AH(J16+1)                                    U42A0780
      A(NA2,NA2)=-(A(NA2,NA2-9)+A(NA2,NA2-1)+A(NA2,NA2+1)+A(NA2,NA2+9))      U42A0790
  480 CONTINUE                                                               U42A0800
      NA1=NA1+9                                                              U42A0810
  470 CONTINUE                                                               U42A0820
C     II BOUNDARY POINTS 11-74, 19-82                                        U42A0830
      NB2=11                                                                 U42A0840
      DO 490 I16=1,8                                                         U42A0850
      A(NB2,NB2+1)=TA(NB2)*GM/AW(1)*(AH(I16)+AH(I16+1))/2.                   U42A0860
      A(NB2,NB2-9)=AA(NB2)*EM/AH(I16)                                        U42A0870
      A(NB2,NB2+9)=AA(NB2+9)*EM/AH(I16+1)                                    U42A0880
      A(NB2,NB2)=-(A(NB2,NB2+1)+A(NB2,NB2-9)+A(NB2,NB2+9))                   U42A0890
      NB2=NB2+9                                                              U42A0900
  490 CONTINUE                                                               U42A0910
      NB3=19                                                                 U42A0920
      DO 500 I17=1,8                                                         U42A0930
      A(NB3,NB3-9)=AA(NB3)*EM/AH(I17)                                        U42A0940
      A(NB3,NB3-1)=TA(NB3-1)*GM/AW(8)*(AH(I17)+AH(I17+1))/2.                 U42A0950
      A(NB3,NB3+9)=AA(NB3+9)*EM/AH(I17+1)                                    U42A0960
      A(NB3,NB3)=-(A(NB3,NB3-9)+A(NB3,NB3-1)+A(NB3,NB3+9))                   U42A0970
      NB3=NB3+9                                                              U42A0980
  500 CONTINUE                                                               U42A0990
C     III BOUNDARY POINTS  FORWARD EDGE -AFTEDGE                             U42A1000
      DO 510 I18=2,10                                                        U42A1010
      A(I18,I18+1)=0.                                                        U42A1020
      A(I18,I18-1)=0.                                                        U42A1030
      IF(I18.NE.2) A(I18,I18-1)=TA(I18-1)*GM/AW(I18-2)*AH(1)/2.              U42A1040
      IF(I18.NE.10)A(I18,I18+1)=TA(I18)*GM/AW(I18-1)*AH(1)/2.                U42A1050
      A(I18,I18+9)=AA(I18+9)*EM/AH(1)                                        U42A1060
      A(I18,I18)=-(A(I18,I18+1)+A(I18,I18-1)+A(I18,I18+9))                   U42A1070
  510 CONTINUE                                                               U42A1080
      DO 520 I19=83,91                                                       U42A1090
      A(I19,I19-1)=0.                                                        U42A1100
      A(I19,I19+1)=0.                                                        U42A1110
```

```
      IF(I19.NE.83)A(I19,I19-1)=TA(I19-1)*GM/AW(I19-83)*AH(9)/2.          U42A1120
      IF(I19.NE.91)A(I19,I19+1)=TA(I19)*GM/AW(I19-82)*AH(9)/2.            U42A1130
      A(I19,I19-9)=AA(I19)*EM/AH(9)                                       U42A1140
      A(I19,I19)=-(A(I19,I19-1)+A(I19,I19+1)+A(I19,I19-9))                U42A1150
  520 CONTINUE                                                            U42A1160
C     BACK SHIFT THE COEFFICIENTS                                         U42A1170
  531 DO 591 KJ1=1,90                                                     U42A1180
      DO 591 JK1=1,90                                                     U42A1190
  591 A(KJ1,JK1)=A(KJ1+1,JK1+1)                                           U42A1200
C     MATRIX COMPLETE -OUTPUT OPTION AND FINAL ANALYSIS                   U42A1210
      NUM1=90                                                             U42A1220
C     ZERO COEFFICIENTS FOR A CLAMPED FORWARD EDGE                        U42A1230
      DO 610 M1=1,9                                                       U42A1240
      DO 610 N1=1,90                                                      U42A1250
      A(M1,N1)=0.                                                         U42A1260
      A(N1,M1)=0.                                                         U42A1270
  610 CONTINUE                                                            U42A1280
      DO 620 M2=1,81                                                      U42A1290
      DO 620 N2=1,81                                                      U42A1300
      A(M2,N2)=A(M2+9 ,N2+9 )                                             U42A1310
  620 CONTINUE                                                            U42A1320
      NUM1=81                                                             U42A1330
C     OUTPUT THE TOTAL STIFFNESS MATRIX                                   U42A1340
      IF(KEY3.NE.1) GO TO  690                                            U42A1350
      WRITE(6,630)                                                        U42A1360
  630 FORMAT(1H ,29HSTIFFNESS MATRIX R-C NOTATION)                        U42A1370
      N2=1                                                                U42A1380
      N3=9                                                                U42A1390
      DO 680 IJ=1,10                                                      U42A1400
      DO 640 M1=N2,N3                                                     U42A1410
  640 MN(M1)=M1                                                           U42A1420
      WRITE(6,650)(MN(M1),M1=N2,N3)                                       U42A1430
  650 FORMAT(1H ,12X,4HCOL(,I2,1H),4X,4HCOL(,I2,1H),4X,4HCOL(,I2,1H),4X,U42A1440
     14HCOL(,I2,1H),4X,4HCOL(,I2,1H),4X,4HCOL(,I2,1H),4X,4HCOL(,I2,1H),4U42A1450
     2X,4HCOL(,I2,1H),4X,4HCOL(,I2,1H))                                   U42A1460
      DO 660 M2=1,NUM1                                                    U42A1470
  660 WRITE(6,670) M2,(A(M2,M4),M4=N2,N3)                                 U42A1480
  670 FORMAT(1H ,4HROW(,I2,1H),E10.4,2X,E10.4,2X,E10.4,2X,E10.4,2X,E10.4U42A1490
     1,2X,E10.4,2X,E10.4,2X,E10.4,2X,E10.4,2X,E10.4)                      U42A1500
      IF(N3.EQ.NUM1) GO TO 690                                            U42A1510
      N2=N2+9                                                             U42A1520
      N3=N3+9                                                             U42A1530
  680 CONTINUE                                                            U42A1540
  690 CONTINUE                                                            U42A1550
      AK64=A(64,64)                                                       U42A1560
      DO 691 KK=1,NUM1                                                    U42A1570
      DO 691 KJ=1,NUM1                                                    U42A1580
  691 A(KK,KJ)=A(KK,KJ)/AK64                                              U42A1590
C     PREPARE INVERSION AND OUTPUT LOADS                                  U42A1600
      IF(KEY4.NE.1) GO TO 700                                             U42A1610
      N=NUM1                                                              U42A1620
      K=1                                                                 U42A1630
      IER=0                                                               U42A1640
      IA=91                                                               U42A1650
      CALL INVRC(A,N,K,IER,IA,PIV)                                        U42A1660
      IF(IER.EQ.3) KER=3                                                  U42A1670
```

```
      IF(IER.EQ.3) GO TO 940                                                U42A1680
      DO 710 N5=1,90                                                        U42A1690
      SV(N5)=0.                                                             U42A1700
  710 CONTINUE                                                              U42A1710
      SV(55)=-P56/AK64                                                      U42A1720
      SV(73)=-P83/AK64                                                      U42A1730
      DO 720 II=1,NUM1                                                      U42A1740
      U(II)=0.                                                              U42A1750
      DO 720 KK=1,NUM1                                                      U42A1760
  720 U(II)=U(II)+A(II,KK)*SV(KK)                                           U42A1770
C     COMPUTE FINAL FORCE SYSTEM                                            U42A1780
      DO 730 IK1=1,81                                                       U42A1790
      UF(IK1+10)=U(IK1)                                                     U42A1800
  730 CONTINUE                                                              U42A1810
      DO 740 IK2=2,10                                                       U42A1820
      UF(IK2)=0.                                                            U42A1830
  740 CONTINUE                                                              U42A1840
      WRITE(6,731) P83,SV(73),SV(55)                                        U42A1850
  731 FORMAT(1H ,11HAXIAL LOAD=,E10.4,2X,7HSV(73)=,E10.4,2X,7HSV(55)=,E1U42A1860
     10.4)                                                                  U42A1870
      WRITE(6,732)                                                          U42A1880
  732 FORMAT(1H ,19HFINAL DISPLACEMENTS)                                    U42A1890
      DO 733 IZ=2,91                                                        U42A1900
  733 WRITE(6,734) IZ,UF(IZ)                                                U42A1910
  734 FORMAT(1H , 2HU(,I2,2H)=,E10.4)                                       U42A1920
      DO 780 IK4=2,9                                                        U42A1930
      AQ(IK4)=(UF(IK4+1)-UF(IK4))*TA(IK4)*GM/AW(IK4-1)                      U42A1940
  780 CONTINUE                                                              U42A1950
      MA=9                                                                  U42A1960
      DO 790 IK5=2,10                                                       U42A1970
      DO 800 IK6=2,10                                                       U42A1980
      MB=MA+IK6                                                             U42A1990
      IF(IK6.NE.10) AQ(MB)=(UF(MB+1)-UF(MB))*TA(MB)*GM/AW(IK6-1)            U42A2000
      F(MB)=(UF(MB-9)-UF(MB))*AA(MB)*EM/AH(IK5-1)                           U42A2010
  800 CONTINUE                                                              U42A2020
      MA=MA+9                                                               U42A2030
  790 CONTINUE                                                              U42A2040
      WRITE(6,801)                                                          U42A2050
  801 FORMAT(1H ,25HSHEAR FLOWS, R-C NOTATION)                              U42A2060
      WRITE(6,810)                                                          U42A2070
  810 FORMAT(1H ,10X,      4HW(1),8X,      4HW(2),8X,      4HW(3),8X,       U42A2080
     14HW(4),8X,      4HW(5),8X,      4HW(6),8X,      4HW(7),8X,      4HW(8)U42A2090
     2)                                                                     U42A2100
  820 FORMAT(1H ,6X,E10.4,2X,E10.4,2X,E10.4,2X,E10.4,2X,E10.4,2X,E10.4,2U42A2110
     1X,E10.4,2X,E10.4)                                                     U42A2120
      DO 830 IK=2,83,9                                                      U42A2130
      WRITE(6,820)AQ(IK),AQ(IK+1),AQ(IK+2),AQ(IK+3),AQ(IK+4),AQ(IK+5),AQU42A2140
     1(IK+6),AQ(IK+7)                                                       U42A2150
  830 CONTINUE                                                              U42A2160
      WRITE(6,880)                                                          U42A2170
  880 FORMAT(1H ,25HAXIAL LOADS, R-C NOTATION)                              U42A2180
                                                                            U42A2190
      DO 890 IJ=11,83,9                                                     U42A2200
                                                                            U42A2210
      WRITE(6,900)F(IJ),F(IJ+1),F(IJ+2),F(IJ+3),F(IJ+4),F(IJ+5),F(IJ+6),U42A2220
     1F(IJ+7),F(IJ+8)                                                       U42A2230
```

```
  900  FORMAT(1H ,E10.4,2X,E10.4,2X,E10.4,2X,E10.4,2X,E10.4,2X,E10.4,2X,EU42A2240
     110.4,2X,E10.4,2X,E10.4)                                          U42A2250
  890  CONTINUE                                                        U42A2260
       IF(KEY5.NE.1) GO TO 920                                         U42A2270
       CALL U42WTP                                                     U42A2280
  920  CONTINUE                                                        U42A2290
       GO TO 910                                                       U42A2300
  700  WRITE(6,930)                                                    U42A2310
  930  FORMAT(1H ,44HINVERSION HAS BEEN SKIPPED,CALL NEXT PROBLEM)     U42A2320
       GO TO 10                                                        U42A2330
  910  CONTINUE                                                        U42A2340
       IF(KEY3.NE.1) GO TO 959                                         U42A2350
       CALL U42LCK                                                     U42A2360
  959  CONTINUE                                                        U42A2370
       GO TO 10                                                        U42A2380
  940  CONTINUE                                                        U42A2390
       WRITE(6,950) KER                                                U42A2400
  950  FORMAT(1H ,13HMATRIX NUMBER,I1,52HIS SINGULAR FINAL SOLUTION SKIPPU42A2410
     1ED CALL NEXT PROBLEM)                                            U42A2420
       GO TO 10                                                        U42A2430
       END                                                             U42A2440
$IBFTC U42WTP                                                          U42C2450
       SUBROUTINE U42WTP                                               U42C2460
       COMMON T(92),R(92),AW(10),AH(10),TA(92),AA(92),A(91,91),SV(90),U(9U42C2470
     10),UF(92),AQ(92),F(92),PIV(91),MN(92),NUM1,DENS,KEY2             U42C2480
       VOL=0.                                                          U42C2490
       KC=9                                                            U42C2500
       DO 20 II=1,9                                                    U42C2510
       DO 10 M1=2,10                                                   U42C2520
       K2=KC+M1                                                        U42C2530
       VOL=VOL+AA(K2)*AH(II)                                           U42C2540
  10   CONTINUE                                                        U42C2550
       KC=KC+9                                                         U42C2560
  20   CONTINUE                                                        U42C2570
       WT=VOL*DENS                                                     U42C2580
       WRITE(6,30)WT,VOL                                               U42C2590
  30   FORMAT(1H ,30HPANEL WEIGHT PER 1/2 QUADRANT=,E10.4, 30HPANEL VOLUMU42C2600
     1N PER 1/2 QUADRANT=,E10.4)                                       U42C2610
       RETURN                                                          U42C2620
       END                                                             U42C2630
$IBFTC U42LCK                                                          U42D2640
       SUBROUTINE U42LCK                                               U42D2650
C      LOADS CHECK PROGRAM                                             U42D2660
       COMMON T(92),R(92),AW(10),AH(10),TA(92),AA(92),A(91,91),SV(90),U(9U42D2670
     10),UF(92),AQ(92),F(92),PIV(91),MN(92),NUM1,DENS,KEY2             U42D2680
C      SHEAR FORCES                                                    U42D2690
       N1=2                                                            U42D2700
       N2=9                                                            U42D2710
       DO  90 JJ=1,10                                                  U42D2720
       DO  100 KK=N1,N2                                                U42D2730
       IF(JJ.EQ.1)  GO TO 110                                          U42D2740
       IF(JJ.EQ.10) GO TO 120                                          U42D2750
       AQ(KK)=AQ(KK)*(AH(JJ-1)+AH(JJ))/2.                              U42D2760
       GO TO 100                                                       U42D2770
 110   AQ(KK)=AQ(KK)*AH(JJ)/2.                                         U42D2780
       GO TO 100                                                       U42D2790
```

```
  120  AQ(KK)=AQ(KK)*AH(JJ-1)/2.                                          U42D2800
  100  CONTINUE                                                           U42D2810
       N1=N1+9                                                            U42D2820
       N2=N2+9                                                            U42D2830
   90  CONTINUE                                                           U42D2840
C      PREPARE AND OUTLET THE LOADS                                       U42D2850
C      I-UPPER EDGE                                                       U42D2860
       WRITE(6,130)                                                       U42D2870
  130  FORMAT(1H ,9HPOINT( N),5X,4HFPEX,8X,4HF(N),7X,6HF(N+9),6X,5HFQ(N),U42D2880
      14X,7HFQ(N+9),7X,3HSUM)                                             U42D2890
       DO 140 N3=2,10                                                     U42D2900
       FPE=0.                                                             U42D2910
       FN=0.                                                              U42D2920
       FN9=0.                                                             U42D2930
       QN=0.                                                              U42D2940
       QN1=0.                                                             U42D2950
       IF(N3.NE.2) QN1=AQ(N3-1)                                           U42D2960
       IF(N3.NE.10)QN=AQ(N3)                                              U42D2970
       FN9=F(N3+9)                                                        U42D2980
       SUM=FPE-FN9+QN-QN1+FN                                              U42D2990
       WRITE(6,150) N3,FPE,FN,FN9,QN,QN1,SUM                              U42D3000
  150  FORMAT(1H ,6HPOINT(,I2,1H),2X,E10.4,2X,E10.4,2X,E10.4,2X,E10.4,2X,U42D3010
     1E10.4,2X,E10.4)                                                    U42D3020
  140  CONTINUE                                                           U42D3030
       FPE=0.                                                             U42D3040
       K5=1                                                               U42D3050
       DO 160 N4=1,8                                                      U42D3060
       K5=K5+9                                                            U42D3070
       DO 170 N5=1,9                                                      U42D3080
       J5=K5+N5                                                           U42D3090
       QN=0.                                                              U42D3100
       QN1=0.                                                             U42D3110
       IF(N5.NE.1)QN1=AQ(J5-1)                                            U42D3120
       IF(N5.NE.9)QN=AQ(J5)                                               U42D3130
       FN=F(J5)                                                           U42D3140
       FN9=F(J5+9)                                                        U42D3150
       SUM=FPE-FN9+QN-QN1+FN                                              U42D3160
  170  WRITE(6,150)N5,FPE,FN,FN9,QN,QN1,SUM                               U42D3170
  160  CONTINUE                                                           U42D3180
C      LOWER EDGE                                                         U42D3190
       FN9=0.                                                             U42D3200
       DO 180  M1=83,91                                                   U42D3210
       FPE=0.                                                             U42D3220
       QN=0.                                                              U42D3230
       QN1=0                                                              U42D3240
       IF(M1.NE.83)QN1=AQ(M1-1)                                           U42D3250
       IF(M1.NE.91)QN=AQ(M1)                                              U42D3260
       FN=F(M1)                                                           U42D3270
       SUM=FPE-FN9+QN-QN1+FN                                              U42D3280
  180  WRITE(6,150)M1,FPE,FN,FN9,QN,QN1,SUM                               U42D3290
       CONTINUE                                                           U42D3300
       RETURN                                                             U42D3310
       END                                                                U42D3320
                                                                             000333
```

	W(1)	W(2)	W(3)	W(4)	W(5)	W(6)	W(7)	W(8)
R(1)	0.2400-00	0.2350-00	0.2150-00	0.1850-00	0.1600-00	0.1350-00	0.1100-00	0.1000-00
R(2)	0.2500-00	0.2450-00	0.2300-00	0.2100-00	0.1850-00	0.1550-00	0.1300-00	0.1200-00
R(3)	0.2950-00	0.2800-00	0.2600-00	0.2350-00	0.2025-00	0.1650-00	0.1400-00	0.1350-00
R(4)	0.3725-00	0.3525-00	0.3200-00	0.2750-00	0.2200-00	0.1700-00	0.1550-00	0.1625-00
R(5)	0.4400-00	0.4125-00	0.3675-00	0.3050-00	0.2350-00	0.1900-00	0.1875-00	0.2025-00
R(6)	0.4900-00	0.4400-00	0.3850-00	0.3225-00	0.2425-00	0.2000-00	0.2075-00	0.2400-00
R(7)	0.6000+00	0.5400+00	0.4450-00	0.3350-00	0.2375-00	0.1950-00	0.2250-00	0.2825-00
R(8)	0.7500+00	0.6500+00	0.5000-00	0.3350-00	0.2250-00	0.1850-00	0.2400-00	0.3550-00
R(9)	0.9000+00	0.7000+00	0.4890-00	0.3140-00	0.2090-00	0.1745-00	0.2505-00	0.4850-00
R(10)	0.1050+01	0.7750+00	0.4925-00	0.2800-00	0.1655-00	0.1065-00	0.1965-00	0.6450+00

	C(1)	C(2)	C(3)	C(4)	C(5)	C(6)	C(7)	C(8)	C(9)
H(1)	0.3080+01	0.2180+01	0.2646+01	0.3026+01	0.3219+01	0.3306+01	0.3227+01	0.3155+01	0.2255+01
H(2)	0.4190+01	0.2402+01	0.2905+01	0.3372+01	0.3621+01	0.3681+01	0.3595+01	0.3604+01	0.3309+01
H(3)	0.5010+01	0.2916+01	0.3466+01	0.3925+01	0.4047+01	0.3933+01	0.3844+01	0.4074+01	0.4522+01
H(4)	0.5595+01	0.3537+01	0.4147+01	0.4554+01	0.4481+01	0.4231+01	0.4296+01	0.4872+01	0.5551+01
H(5)	0.6975+01	0.3991+01	0.4577+01	0.4956+01	0.4778+01	0.4511+01	0.4810+01	0.5776+01	0.6748+01
H(6)	0.9250+01	0.4630+01	0.5147+01	0.5327+01	0.4910+01	0.4551+01	0.5082+01	0.6599+01	0.9083+01
H(7)	0.1215+02	0.5675+01	0.6046+01	0.5751+01	0.4877+01	0.4382+01	0.5207+01	0.7644+01	0.1341+02
H(8)	0.1645+02	0.6675+01	0.6589+01	0.5810+01	0.4657+01	0.4129+01	0.5255+01	0.9278+01	0.2008+02
H(9)	0.2287+02	0.7587+01	0.6877+01	0.5566+01	0.4155+01	0.3395+01	0.4534+01	0.1111+02	0.3249+02

STIFFNESS MATRIX R-C NOTATION

	COL(1)	COL(2)	COL(3)	COL(4)	COL(5)	COL(6)	COL(7)	COL(8)	COL(9)
ROW(1)	-0.7670+07	0.5981+07	0.	0.	0.	0.	0.	0.	0.
ROW(2)	0.5981+07	-0.1173+08	0.4689+07	0.	0.	0.	0.	0.	0.
ROW(3)	0.	0.4689+07	-0.9353+07	0.3386+07	0.	0.	0.	0.	0.
ROW(4)	0.	0.	0.3386+07	-0.7372+07	0.2512+07	0.	0.	0.	0.
ROW(5)	0.	0.	0.	0.2512+07	-0.5951+07	0.1864+07	0.	0.	0.
ROW(6)	0.	0.	0.	0.	0.1864+07	-0.4762+07	0.1290+07	0.	0.
ROW(7)	0.	0.	0.	0.	0.	0.1290+07	-0.3818+07	0.9570+06	0.
ROW(8)	0.	0.	0.	0.	0.	0.	0.9570+06	-0.3307+07	0.7920+06
ROW(9)	0.	0.	0.	0.	0.	0.	0.	0.7920+06	-0.2089+07
ROW(10)	0.1047+07	0.	0.	0.	0.	0.	0.	0.	0.
ROW(11)	0.	0.6006+06	0.	0.	0.	0.	0.	0.	0.
ROW(12)	0.	0.	0.7262+06	0.	0.	0.	0.	0.	0.
ROW(13)	0.	0.	0.	0.8431+06	0.	0.	0.	0.	0.
ROW(14)	0.	0.	0.	0.	0.9052+06	0.	0.	0.	0.
ROW(15)	0.	0.	0.	0.	0.	0.9202+06	0.	0.	0.
ROW(16)	0.	0.	0.	0.	0.	0.	0.8987+06	0.	0.
ROW(17)	0.	0.	0.	0.	0.	0.	0.	0.9009+06	0.
ROW(18)	0.	0.	0.	0.	0.	0.	0.	0.	0.8272+06
ROW(19)	0.	0.	0.	0.	0.	0.	0.	0.	0.
ROW(20)	0.	0.	0.	0.	0.	0.	0.	0.	0.
ROW(21)	0.	0.	0.	0.	0.	0.	0.	0.	0.
ROW(22)	0.	0.	0.	0.	0.	0.	0.	0.	0.
ROW(23)	0.	0.	0.	0.	0.	0.	0.	0.	0.
ROW(24)	0.	0.	0.	0.	0.	0.	0.	0.	0.
ROW(25)	0.	0.	0.	0.	0.	0.	0.	0.	0.
ROW(26)	0.	0.	0.	0.	0.	0.	0.	0.	0.
ROW(27)	0.	0.	0.	0.	0.	0.	0.	0.	0.
ROW(28)	0.	0.	0.	0.	0.	0.	0.	0.	0.

ROW(29)	0.	0.	0.	0.	0.	0.	0.	0.	0.
ROW(30)	0.	0.	0.	0.	0.	0.	0.	0.	0.
ROW(31)	0.	0.	0.	0.	0.	0.	0.	0.	0.
ROW(32)	0.	0.	0.	0.	0.	0.	0.	0.	0.
ROW(33)	0.	0.	0.	0.	0.	0.	0.	0.	0.
ROW(34)	0.	0.	0.	0.	0.	0.	0.	0.	0.
ROW(35)	0.	0.	0.	0.	0.	0.	0.	0.	0.
ROW(36)	0.	0.	0.	0.	0.	0.	0.	0.	0.
ROW(37)	0.	0.	0.	0.	0.	0.	0.	0.	0.
ROW(38)	0.	0.	0.	0.	0.	0.	0.	0.	0.
ROW(39)	0.	0.	0.	0.	0.	0.	0.	0.	0.
ROW(40)	0.	0.	0.	0.	0.	0.	0.	0.	0.
ROW(41)	0.	0.	0.	0.	0.	0.	0.	0.	0.
ROW(42)	0.	0.	0.	0.	0.	0.	0.	0.	0.
ROW(43)	0.	0.	0.	0.	0.	0.	0.	0.	0.
ROW(44)	0.	0.	0.	0.	0.	0.	0.	0.	0.
ROW(45)	0.	0.	0.	0.	0.	0.	0.	0.	0.
ROW(46)	0.	0.	0.	0.	0.	0.	0.	0.	0.
ROW(47)	0.	0.	0.	0.	0.	0.	0.	0.	0.
ROW(48)	0.	0.	0.	0.	0.	0.	0.	0.	0.
ROW(49)	0.	0.	0.	0.	0.	0.	0.	0.	0.
ROW(50)	0.	0.	0.	0.	0.	0.	0.	0.	0.
ROW(51)	0.	0.	0.	0.	0.	0.	0.	0.	0.
ROW(52)	0.	0.	0.	0.	0.	0.	0.	0.	0.
ROW(53)	0.	0.	0.	0.	0.	0.	0.	0.	0.
ROW(54)	0.	0.	0.	0.	0.	0.	0.	0.	0.
ROW(55)	0.	0.	0.	0.	0.	0.	0.	0.	0.
ROW(56)	0.	0.	0.	0.	0.	0.	0.	0.	0.
ROW(57)	0.	0.	0.	0.	0.	0.	0.	0.	0.
ROW(58)	0.	0.	0.	0.	0.	0.	0.	0.	0.
ROW(59)	0.	0.	0.	0.	0.	0.	0.	0.	0.
ROW(60)	0.	0.	0.	0.	0.	0.	0.	0.	0.
ROW(61)	0.	0.	0.	0.	0.	0.	0.	0.	0.
ROW(62)	0.	0.	0.	0.	0.	0.	0.	0.	0.
ROW(63)	0.	0.	0.	0.	0.	0.	0.	0.	0.
ROW(64)	0.	0.	0.	0.	0.	0.	0.	0.	0.
ROW(65)	0.	0.	0.	0.	0.	0.	0.	0.	0.
ROW(66)	0.	0.	0.	0.	0.	0.	0.	0.	0.
ROW(67)	0.	0.	0.	0.	0.	0.	0.	0.	0.
ROW(68)	0.	0.	0.	0.	0.	0.	0.	0.	0.
ROW(69)	0.	0.	0.	0.	0.	0.	0.	0.	0.
ROW(70)	0.	0.	0.	0.	0.	0.	0.	0.	0.
ROW(71)	0.	0.	0.	0.	0.	0.	0.	0.	0.
ROW(72)	0.	0.	0.	0.	0.	0.	0.	0.	0.
ROW(73)	0.	0.	0.	0.	0.	0.	0.	0.	0.
ROW(74)	0.	0.	0.	0.	0.	0.	0.	0.	0.
ROW(75)	0.	0.	0.	0.	0.	0.	0.	0.	0.
ROW(76)	0.	0.	0.	0.	0.	0.	0.	0.	0.
ROW(77)	0.	0.	0.	0.	0.	0.	0.	0.	0.
ROW(78)	0.	0.	0.	0.	0.	0.	0.	0.	0.
ROW(79)	0.	0.	0.	0.	0.	0.	0.	0.	0.

ROW(80)	0.	0.	0.	0.	0.	0.	0.	0.	0.
ROW(81)	0.	0.	0.	0.	0.	0.	0.	0.	0.
	COL(10)	COL(11)	COL(12)	COL(13)	COL(14)	COL(15)	COL(16)	COL(17)	COL(18)
ROW(1)	0.1047+07	0.	0.	0.	0.	0.	0.	0.	0.
ROW(2)	0.	0.6006+06	0.	0.	0.	0.	0.	0.	0.
ROW(3)	0.	0.	0.7262+06	0.	0.	0.	0.	0.	0.
ROW(4)	0.	0.	0.	0.8431+06	0.	0.	0.	0.	0.
ROW(5)	0.	0.	0.	0.	0.9052+06	0.	0.	0.	0.
ROW(6)	0.	0.	0.	0.	0.	0.9202+06	0.	0.	0.
ROW(7)	0.	0.	0.	0.	0.	0.	0.8987+06	0.	0.
ROW(8)	0.	0.	0.	0.	0.	0.	0.	0.9009+06	0.
ROW(9)	0.	0.	0.	0.	0.	0.	0.	0.	0.8272+06
ROW(10)	-0.8535+07	0.6095+07	0.	0.	0.	0.	0.	0.	0.
ROW(11)	0.6095+07	-0.1213+08	0.4628+07	0.	0.	0.	0.	0.	0.
ROW(12)	0.	0.4628+07	-0.9623+07	0.3306+07	0.	0.	0.	0.	0.
ROW(13)	0.	0.	0.3306+07	-0.7667+07	0.2428+07	0.	0.	0.	0.
ROW(14)	0.	0.	0.	0.2428+07	-0.6219+07	0.1762+07	0.	0.	0.
ROW(15)	0.	0.	0.	0.	0.1762+07	-0.4960+07	0.1186+07	0.	0.
ROW(16)	0.	0.	0.	0.	0.	0.1186+07	-0.4042+07	0.8901+06	0.
ROW(17)	0.	0.	0.	0.	0.	0.	0.8901+06	-0.3692+07	0.7695+06
ROW(18)	0.	0.	0.	0.	0.	0.	0.	0.7695+06	-0.2853+07
ROW(19)	0.1392+07	0.	0.	0.	0.	0.	0.	0.	0.
ROW(20)	0.	0.8101+06	0.	0.	0.	0.	0.	0.	0.
ROW(21)	0.	0.	0.9628+06	0.	0.	0.	0.	0.	0.
ROW(22)	0.	0.	0.	0.1090+07	0.	0.	0.	0.	0.
ROW(23)	0.	0.	0.	0.	0.1124+07	0.	0.	0.	0.
ROW(24)	0.	0.	0.	0.	0.	0.1093+07	0.	0.	0.
ROW(25)	0.	0.	0.	0.	0.	0.	0.1068+07	0.	0.
ROW(26)	0.	0.	0.	0.	0.	0.	0.	0.1132+07	0.
ROW(27)	0.	0.	0.	0.	0.	0.	0.	0.	0.1256+07
ROW(28)	0.	0.	0.	0.	0.	0.	0.	0.	0.
ROW(29)	0.	0.	0.	0.	0.	0.	0.	0.	0.
ROW(30)	0.	0.	0.	0.	0.	0.	0.	0.	0.
ROW(31)	0.	0.	0.	0.	0.	0.	0.	0.	0.
ROW(32)	0.	0.	0.	0.	0.	0.	0.	0.	0.
ROW(33)	0.	0.	0.	0.	0.	0.	0.	0.	0.
ROW(34)	0.	0.	0.	0.	0.	0.	0.	0.	0.
ROW(35)	0.	0.	0.	0.	0.	0.	0.	0.	0.
ROW(36)	0.	0.	0.	0.	0.	0.	0.	0.	0.
ROW(37)	0.	0.	0.	0.	0.	0.	0.	0.	0.
ROW(38)	0.	0.	0.	0.	0.	0.	0.	0.	0.
ROW(39)	0.	0.	0.	0.	0.	0.	0.	0.	0.
ROW(40)	0.	0.	0.	0.	0.	0.	0.	0.	0.
ROW(41)	0.	0.	0.	0.	0.	0.	0.	0.	0.
ROW(42)	0.	0.	0.	0.	0.	0.	0.	0.	0.
ROW(43)	0.	0.	0.	0.	0.	0.	0.	0.	0.
ROW(44)	0.	0.	0.	0.	0.	0.	0.	0.	0.
ROW(45)	0.	0.	0.	0.	0.	0.	0.	0.	0.
ROW(46)	0.	0.	0.	0.	0.	0.	0.	0.	0.
ROW(47)	0.	0.	0.	0.	0.	0.	0.	0.	0.
ROW(48)	0.	0.	0.	0.	0.	0.	0.	0.	0.

ROW(49)	0.	0.	0.	0.	0.	0.	0.	0.	0.
ROW(50)	0.	0.	0.	0.	0.	0.	0.	0.	0.
ROW(51)	0.	0.	0.	0.	0.	0.	0.	0.	0.
ROW(52)	0.	0.	0.	0.	0.	0.	0.	0.	0.
ROW(53)	0.	0.	0.	0.	0.	0.	0.	0.	0.
ROW(54)	0.	0.	0.	0.	0.	0.	0.	0.	0.
ROW(55)	0.	0.	0.	0.	0.	0.	0.	0.	0.
ROW(56)	0.	0.	0.	0.	0.	0.	0.	0.	0.
ROW(57)	0.	0.	0.	0.	0.	0.	0.	0.	0.
ROW(58)	0.	0.	0.	0.	0.	0.	0.	0.	0.
ROW(59)	0.	0.	0.	0.	0.	0.	0.	0.	0.
ROW(60)	0.	0.	0.	0.	0.	0.	0.	0.	0.
ROW(61)	0.	0.	0.	0.	0.	0.	0.	0.	0.
ROW(62)	0.	0.	0.	0.	0.	0.	0.	0.	0.
ROW(63)	0.	0.	0.	0.	0.	0.	0.	0.	0.
ROW(64)	0.	0.	0.	0.	0.	0.	0.	0.	0.
ROW(65)	0.	0.	0.	0.	0.	0.	0.	0.	0.
ROW(66)	0.	0.	0.	0.	0.	0.	0.	0.	0.
ROW(67)	0.	0.	0.	0.	0.	0.	0.	0.	0.
ROW(68)	0.	0.	0.	0.	0.	0.	0.	0.	0.
ROW(69)	0.	0.	0.	0.	0.	0.	0.	0.	0.
ROW(70)	0.	0.	0.	0.	0.	0.	0.	0.	0.
ROW(71)	0.	0.	0.	0.	0.	0.	0.	0.	0.
ROW(72)	0.	0.	0.	0.	0.	0.	0.	0.	0.
ROW(73)	0.	0.	0.	0.	0.	0.	0.	0.	0.
ROW(74)	0.	0.	0.	0.	0.	0.	0.	0.	0.
ROW(75)	0.	0.	0.	0.	0.	0.	0.	0.	0.
ROW(76)	0.	0.	0.	0.	0.	0.	0.	0.	0.
ROW(77)	0.	0.	0.	0.	0.	0.	0.	0.	0.
ROW(78)	0.	0.	0.	0.	0.	0.	0.	0.	0.
ROW(79)	0.	0.	0.	0.	0.	0.	0.	0.	0.
ROW(80)	0.	0.	0.	0.	0.	0.	0.	0.	0.
ROW(81)	0.	0.	0.	0.	0.	0.	0.	0.	0.

	COL(19)	COL(20)	COL(21)	COL(22)	COL(23)	COL(24)	COL(25)	COL(26)	COL(27)
ROW(1)	0.	0.	0.	0.	0.	0.	0.	0.	0.
ROW(2)	0.	0.	0.	0.	0.	0.	0.	0.	0.
ROW(3)	0.	0.	0.	0.	0.	0.	0.	0.	0.
ROW(4)	0.	0.	0.	0.	0.	0.	0.	0.	0.
ROW(5)	0.	0.	0.	0.	0.	0.	0.	0.	0.
ROW(6)	0.	0.	0.	0.	0.	0.	0.	0.	0.
ROW(7)	0.	0.	0.	0.	0.	0.	0.	0.	0.
ROW(8)	0.	0.	0.	0.	0.	0.	0.	0.	0.
ROW(9)	0.	0.	0.	0.	0.	0.	0.	0.	0.
ROW(10)	0.1392+07	0.	0.	0.	0.	0.	0.	0.	0.
ROW(11)	0.	0.8101+06	0.	0.	0.	0.	0.	0.	0.
ROW(12)	0.	0.	0.9628+06	0.	0.	0.	0.	0.	0.
ROW(13)	0.	0.	0.	0.1090+07	0.	0.	0.	0.	0.
ROW(14)	0.	0.	0.	0.	0.1124+07	0.	0.	0.	0.
ROW(15)	0.	0.	0.	0.	0.	0.1093+07	0.	0.	0.
ROW(16)	0.	0.	0.	0.	0.	0.	0.1068+07	0.	0.
ROW(17)	0.	0.	0.	0.	0.	0.	0.	0.1132+07	0.

ROW(18)	0.	0.	0.	0.	0.	0.	0.	0.	0.1256+07
ROW(19)	-0.1003+08	0.6887+07	0.	0.	0.	0.	0.	0.	0.
ROW(20)	0.6887+07	-0.1402+08	0.5213+07	0.	0.	0.	0.	0.	0.
ROW(21)	0.	0.5213+07	-0.1111+08	0.3641+07	0.	0.	0.	0.	0.
ROW(22)	0.	0.	0.3641+07	-0.8696+07	0.2542+07	0.	0.	0.	0.
ROW(23)	0.	0.	0.	0.2542+07	-0.6779+07	0.1713+07	0.	0.	0.
ROW(24)	0.	0.	0.	0.	0.1713+07	-0.5221+07	0.1093+07	0.	0.
ROW(25)	0.	0.	0.	0.	0.	0.1093+07	-0.4385+07	0.8817+06	0.
ROW(26)	0.	0.	0.	0.	0.	0.	0.8817+06	-0.4365+07	0.8287+06
ROW(27)	0.	0.	0.	0.	0.	0.	0.	0.8287+06	-0.3820+07
ROW(28)	0.1748+07	0.	0.	0.	0.	0.	0.	0.	0.
ROW(29)	0.	0.1105+07	0.	0.	0.	0.	0.	0.	0.
ROW(30)	0.	0.	0.1296+07	0.	0.	0.	0.	0.	0.
ROW(31)	0.	0.	0.	0.1423+07	0.	0.	0.	0.	0.
ROW(32)	0.	0.	0.	0.	0.1400+07	0.	0.	0.	0.
ROW(33)	0.	0.	0.	0.	0.	0.1322+07	0.	0.	0.
ROW(34)	0.	0.	0.	0.	0.	0.	0.1343+07	0.	0.
ROW(35)	0.	0.	0.	0.	0.	0.	0.	0.1523+07	0.
ROW(36)	0.	0.	0.	0.	0.	0.	0.	0.	0.1735+07
ROW(37)	0.	0.	0.	0.	0.	0.	0.	0.	0.
ROW(38)	0.	0.	0.	0.	0.	0.	0.	0.	0.
ROW(39)	0.	0.	0.	0.	0.	0.	0.	0.	0.
ROW(40)	0.	0.	0.	0.	0.	0.	0.	0.	0.
ROW(41)	0.	0.	0.	0.	0.	0.	0.	0.	0.
ROW(42)	0.	0.	0.	0.	0.	0.	0.	0.	0.
ROW(43)	0.	0.	0.	0.	0.	0.	0.	0.	0.
ROW(44)	0.	0.	0.	0.	0.	0.	0.	0.	0.
ROW(45)	0.	0.	0.	0.	0.	0.	0.	0.	0.
ROW(46)	0.	0.	0.	0.	0.	0.	0.	0.	0.
ROW(47)	0.	0.	0.	0.	0.	0.	0.	0.	0.
ROW(48)	0.	0.	0.	0.	0.	0.	0.	0.	0.
ROW(49)	0.	0.	0.	0.	0.	0.	0.	0.	0.
ROW(50)	0.	0.	0.	0.	0.	0.	0.	0.	0.
ROW(51)	0.	0.	0.	0.	0.	0.	0.	0.	0.
ROW(52)	0.	0.	0.	0.	0.	0.	0.	0.	0.
ROW(53)	0.	0.	0.	0.	0.	0.	0.	0.	0.
ROW(54)	0.	0.	0.	0.	0.	0.	0.	0.	0.
ROW(55)	0.	0.	0.	0.	0.	0.	0.	0.	0.
ROW(56)	0.	0.	0.	0.	0.	0.	0.	0.	0.
ROW(57)	0.	0.	0.	0.	0.	0.	0.	0.	0.
ROW(58)	0.	0.	0.	0.	0.	0.	0.	0.	0.
ROW(59)	0.	0.	0.	0.	0.	0.	0.	0.	0.
ROW(60)	0.	0.	0.	0.	0.	0.	0.	0.	0.
ROW(61)	0.	0.	0.	0.	0.	0.	0.	0.	0.
ROW(62)	0.	0.	0.	0.	0.	0.	0.	0.	0.
ROW(63)	0.	0.	0.	0.	0.	0.	0.	0.	0.
ROW(64)	0.	0.	0.	0.	0.	0.	0.	0.	0.
ROW(65)	0.	0.	0.	0.	0.	0.	0.	0.	0.
ROW(66)	0.	0.	0.	0.	0.	0.	0.	0.	0.
ROW(67)	0.	0.	0.	0.	0.	0.	0.	0.	0.
ROW(68)	0.	0.	0.	0.	0.	0.	0.	0.	0.

ROW(69)	0.	0.	0.	0.	0.	0.	0.	0.	0.
ROW(70)	0.	0.	0.	0.	0.	0.	0.	0.	0.
ROW(71)	0.	0.	0.	0.	0.	0.	0.	0.	0.
ROW(72)	0.	0.	0.	0.	0.	0.	0.	0.	0.
ROW(73)	0.	0.	0.	0.	0.	0.	0.	0.	0.
ROW(74)	0.	0.	0.	0.	0.	0.	0.	0.	0.
ROW(75)	0.	0.	0.	0.	0.	0.	0.	0.	0.
ROW(76)	0.	0.	0.	0.	0.	0.	0.	0.	0.
ROW(77)	0.	0.	0.	0.	0.	0.	0.	0.	0.
ROW(78)	0.	0.	0.	0.	0.	0.	0.	0.	0.
ROW(79)	0.	0.	0.	0.	0.	0.	0.	0.	0.
ROW(80)	0.	0.	0.	0.	0.	0.	0.	0.	0.
ROW(81)	0.	0.	0.	0.	0.	0.	0.	0.	0.
	COL(28)	COL(29)	COL(30)	COL(31)	COL(32)	COL(33)	COL(34)	COL(35)	COL(36)
ROW(1)	0.	0.	0.	0.	0.	0.	0.	0.	0.
ROW(2)	0.	0.	0.	0.	0.	0.	0.	0.	0.
ROW(3)	0.	0.	0.	0.	0.	0.	0.	0.	0.
ROW(4)	0.	0.	0.	0.	0.	0.	0.	0.	0.
ROW(5)	0.	0.	0.	0.	0.	0.	0.	0.	0.
ROW(6)	0.	0.	0.	0.	0.	0.	0.	0.	0.
ROW(7)	0.	0.	0.	0.	0.	0.	0.	0.	0.
ROW(8)	0.	0.	0.	0.	0.	0.	0.	0.	0.
ROW(9)	0.	0.	0.	0.	0.	0.	0.	0.	0.
ROW(10)	0.	0.	0.	0.	0.	0.	0.	0.	0.
ROW(11)	0.	0.	0.	0.	0.	0.	0.	0.	0.
ROW(12)	0.	0.	0.	0.	0.	0.	0.	0.	0.
ROW(13)	0.	0.	0.	0.	0.	0.	0.	0.	0.
ROW(14)	0.	0.	0.	0.	0.	0.	0.	0.	0.
ROW(15)	0.	0.	0.	0.	0.	0.	0.	0.	0.
ROW(16)	0.	0.	0.	0.	0.	0.	0.	0.	0.
ROW(17)	0.	0.	0.	0.	0.	0.	0.	0.	0.
ROW(18)	0.	0.	0.	0.	0.	0.	0.	0.	0.
ROW(19)	0.1748+07	0.	0.	0.	0.	0.	0.	0.	0.
ROW(20)	0.	0.1105+07	0.	0.	0.	0.	0.	0.	0.
ROW(21)	0.	0.	0.1296+07	0.	0.	0.	0.	0.	0.
ROW(22)	0.	0.	0.	0.1423+07	0.	0.	0.	0.	0.
ROW(23)	0.	0.	0.	0.	0.1400+07	0.	0.	0.	0.
ROW(24)	0.	0.	0.	0.	0.	0.1322+07	0.	0.	0.
ROW(25)	0.	0.	0.	0.	0.	0.	0.1343+07	0.	0.
ROW(26)	0.	0.	0.	0.	0.	0.	0.	0.1523+07	0.
ROW(27)	0.	0.	0.	0.	0.	0.	0.	0.	0.1735+07
ROW(28)	-0.1137+08	0.6938+07	0.	0.	0.	0.	0.	0.	0.
ROW(29)	0.6938+07	-0.1478+08	0.5204+07	0.	0.	0.	0.	0.	0.
ROW(30)	0.	0.5204+07	-0.1183+08	0.3566+07	0.	0.	0.	0.	0.
ROW(31)	0.	0.	0.3566+07	-0.9300+07	0.2405+07	0.	0.	0.	0.
ROW(32)	0.	0.	0.	0.2405+07	-0.7203+07	0.1560+07	0.	0.	0.
ROW(33)	0.	0.	0.	0.	0.1560+07	-0.5660+07	0.1042+07	0.	0.
ROW(34)	0.	0.	0.	0.	0.	0.1042+07	-0.5144+07	0.9097+06	0.
ROW(35)	0.	0.	0.	0.	0.	0.	0.9097+06	-0.5535+07	0.8809+06
ROW(36)	0.	0.	0.	0.	0.	0.	0.	0.8809+06	-0.5211+07
ROW(37)	0.2683+07	0.	0.	0.	0.	0.	0.	0.	0.

ROW(38)	0.	0.1535+07	0.	0.	0.	0.	0.	0.	0.
ROW(39)	0.	0.	0.1760+07	0.	0.	0.	0.	0.	0.
ROW(40)	0.	0.	0.	0.1906+07	0.	0.	0.	0.	0.
ROW(41)	0.	0.	0.	0.	0.1838+07	0.	0.	0.	0.
ROW(42)	0.	0.	0.	0.	0.	0.1735+07	0.	0.	0.
ROW(43)	0.	0.	0.	0.	0.	0.	0.1850+07	0.	0.
ROW(44)	0.	0.	0.	0.	0.	0.	0.	0.2221+07	0.
ROW(45)	0.	0.	0.	0.	0.	0.	0.	0.	0.2595+07
ROW(46)	0.	0.	0.	0.	0.	0.	0.	0.	0.
ROW(47)	0.	0.	0.	0.	0.	0.	0.	0.	0.
ROW(48)	0.	0.	0.	0.	0.	0.	0.	0.	0.
ROW(49)	0.	0.	0.	0.	0.	0.	0.	0.	0.
ROW(50)	0.	0.	0.	0.	0.	0.	0.	0.	0.
ROW(51)	0.	0.	0.	0.	0.	0.	0.	0.	0.
ROW(52)	0.	0.	0.	0.	0.	0.	0.	0.	0.
ROW(53)	0.	0.	0.	0.	0.	0.	0.	0.	0.
ROW(54)	0.	0.	0.	0.	0.	0.	0.	0.	0.
ROW(55)	0.	0.	0.	0.	0.	0.	0.	0.	0.
ROW(56)	0.	0.	0.	0.	0.	0.	0.	0.	0.
ROW(57)	0.	0.	0.	0.	0.	0.	0.	0.	0.
ROW(58)	0.	0.	0.	0.	0.	0.	0.	0.	0.
ROW(59)	0.	0.	0.	0.	0.	0.	0.	0.	0.
ROW(60)	0.	0.	0.	0.	0.	0.	0.	0.	0.
ROW(61)	0.	0.	0.	0.	0.	0.	0.	0.	0.
ROW(62)	0.	0.	0.	0.	0.	0.	0.	0.	0.
ROW(63)	0.	0.	0.	0.	0.	0.	0.	0.	0.
ROW(64)	0.	0.	0.	0.	0.	0.	0.	0.	0.
ROW(65)	0.	0.	0.	0.	0.	0.	0.	0.	0.
ROW(66)	0.	0.	0.	0.	0.	0.	0.	0.	0.
ROW(67)	0.	0.	0.	0.	0.	0.	0.	0.	0.
ROW(68)	0.	0.	0.	0.	0.	0.	0.	0.	0.
ROW(69)	0.	0.	0.	0.	0.	0.	0.	0.	0.
ROW(70)	0.	0.	0.	0.	0.	0.	0.	0.	0.
ROW(71)	0.	0.	0.	0.	0.	0.	0.	0.	0.
ROW(72)	0.	0.	0.	0.	0.	0.	0.	0.	0.
ROW(73)	0.	0.	0.	0.	0.	0.	0.	0.	0.
ROW(74)	0.	0.	0.	0.	0.	0.	0.	0.	0.
ROW(75)	0.	0.	0.	0.	0.	0.	0.	0.	0.
ROW(76)	0.	0.	0.	0.	0.	0.	0.	0.	0.
ROW(77)	0.	0.	0.	0.	0.	0.	0.	0.	0.
ROW(78)	0.	0.	0.	0.	0.	0.	0.	0.	0.
ROW(79)	0.	0.	0.	0.	0.	0.	0.	0.	0.
ROW(80)	0.	0.	0.	0.	0.	0.	0.	0.	0.
ROW(81)	0.	0.	0.	0.	0.	0.	0.	0.	0.

	COL(37)	COL(38)	COL(39)	COL(40)	COL(41)	COL(42)	COL(43)	COL(44)	COL(45)
ROW(1)	0.	0.	0.	0.	0.	0.	0.	0.	0.
ROW(2)	0.	0.	0.	0.	0.	0.	0.	0.	0.
ROW(3)	0.	0.	0.	0.	0.	0.	0.	0.	0.
ROW(4)	0.	0.	0.	0.	0.	0.	0.	0.	0.
ROW(5)	0.	0.	0.	0.	0.	0.	0.	0.	0.
ROW(6)	0.	0.	0.	0.	0.	0.	0.	0.	0.

ROW(7)	0.	0.	0.	0.	0.	0.	0.	0.	0.
ROW(8)	0.	0.	0.	0.	0.	0.	0.	0.	0.
ROW(9)	0.	0.	0.	0.	0.	0.	0.	0.	0.
ROW(10)	0.	0.	0.	0.	0.	0.	0.	0.	0.
ROW(11)	0.	0.	0.	0.	0.	0.	0.	0.	0.
ROW(12)	0.	0.	0.	0.	0.	0.	0.	0.	0.
ROW(13)	0.	0.	0.	0.	0.	0.	0.	0.	0.
ROW(14)	0.	0.	0.	0.	0.	0.	0.	0.	0.
ROW(15)	0.	0.	0.	0.	0.	0.	0.	0.	0.
ROW(16)	0.	0.	0.	0.	0.	0.	0.	0.	0.
ROW(17)	0.	0.	0.	0.	0.	0.	0.	0.	0.
ROW(18)	0.	0.	0.	0.	0.	0.	0.	0.	0.
ROW(19)	0.	0.	0.	0.	0.	0.	0.	0.	0.
ROW(20)	0.	0.	0.	0.	0.	0.	0.	0.	0.
ROW(21)	0.	0.	0.	0.	0.	0.	0.	0.	0.
ROW(22)	0.	0.	0.	0.	0.	0.	0.	0.	0.
ROW(23)	0.	0.	0.	0.	0.	0.	0.	0.	0.
ROW(24)	0.	0.	0.	0.	0.	0.	0.	0.	0.
ROW(25)	0.	0.	0.	0.	0.	0.	0.	0.	0.
ROW(26)	0.	0.	0.	0.	0.	0.	0.	0.	0.
ROW(27)	0.	0.	0.	0.	0.	0.	0.	0.	0.
ROW(28)	0.2683+07	0.	0.	0.	0.	0.	0.	0.	0.
ROW(29)	0.	0.1535+07	0.	0.	0.	0.	0.	0.	0.
ROW(30)	0.	0.	0.1760+07	0.	0.	0.	0.	0.	0.
ROW(31)	0.	0.	0.	0.1906+07	0.	0.	0.	0.	0.
ROW(32)	0.	0.	0.	0.	0.1838+07	0.	0.	0.	0.
ROW(33)	0.	0.	0.	0.	0.	0.1735+07	0.	0.	0.
ROW(34)	0.	0.	0.	0.	0.	0.	0.1850+07	0.	0.
ROW(35)	0.	0.	0.	0.	0.	0.	0.	0.2221+07	0.
ROW(36)	0.	0.	0.	0.	0.	0.	0.	0.	0.2595+07
ROW(37)	-0.1328+08	0.6394+07	0.	0.	0.	0.	0.	0.	0.
ROW(38)	0.6394+07	-0.1463+08	0.4594+07	0.	0.	0.	0.	0.	0.
ROW(39)	0.	0.4594+07	-0.1179+08	0.3092+07	0.	0.	0.	0.	0.
ROW(40)	0.	0.	0.3092+07	-0.9524+07	0.2104+07	0.	0.	0.	0.
ROW(41)	0.	0.	0.	0.2104+07	-0.7506+07	0.1332+07	0.	0.	0.
ROW(42)	0.	0.	0.	0.	0.1332+07	-0.6044+07	0.9078+06	0.	0.
ROW(43)	0.	0.	0.	0.	0.	0.9078+06	-0.5901+07	0.8332+06	0.
ROW(44)	0.	0.	0.	0.	0.	0.	0.8332+06	-0.6918+07	0.8640+06
ROW(45)	0.	0.	0.	0.	0.	0.	0.	0.8640+06	-0.7588+07
ROW(46)	0.4205+07	0.	0.	0.	0.	0.	0.	0.	0.
ROW(47)	0.	0.2105+07	0.	0.	0.	0.	0.	0.	0.
ROW(48)	0.	0.	0.2340+07	0.	0.	0.	0.	0.	0.
ROW(49)	0.	0.	0.	0.2422+07	0.	0.	0.	0.	0.
ROW(50)	0.	0.	0.	0.	0.2232+07	0.	0.	0.	0.
ROW(51)	0.	0.	0.	0.	0.	0.2069+07	0.	0.	0.
ROW(52)	0.	0.	0.	0.	0.	0.	0.2310+07	0.	0.
ROW(53)	0.	0.	0.	0.	0.	0.	0.	0.3000+07	0.
ROW(54)	0.	0.	0.	0.	0.	0.	0.	0.	0.4129+07
ROW(55)	0.	0.	0.	0.	0.	0.	0.	0.	0.
ROW(56)	0.	0.	0.	0.	0.	0.	0.	0.	0.
ROW(57)	0.	0.	0.	0.	0.	0.	0.	0.	0.

ROW(58)	0.	0.	0.	0.	0.	0.	0.	0.	0.
ROW(59)	0.	0.	0.	0.	0.	0.	0.	0.	0.
ROW(60)	0.	0.	0.	0.	0.	0.	0.	0.	0.
ROW(61)	0.	0.	0.	0.	0.	0.	0.	0.	0.
ROW(62)	0.	0.	0.	0.	0.	0.	0.	0.	0.
ROW(63)	0.	0.	0.	0.	0.	0.	0.	0.	0.
ROW(64)	0.	0.	0.	0.	0.	0.	0.	0.	0.
ROW(65)	0.	0.	0.	0.	0.	0.	0.	0.	0.
ROW(66)	0.	0.	0.	0.	0.	0.	0.	0.	0.
ROW(67)	0.	0.	0.	0.	0.	0.	0.	0.	0.
ROW(68)	0.	0.	0.	0.	0.	0.	0.	0.	0.
ROW(69)	0.	0.	0.	0.	0.	0.	0.	0.	0.
ROW(70)	0.	0.	0.	0.	0.	0.	0.	0.	0.
ROW(71)	0.	0.	0.	0.	0.	0.	0.	0.	0.
ROW(72)	0.	0.	0.	0.	0.	0.	0.	0.	0.
ROW(73)	0.	0.	0.	0.	0.	0.	0.	0.	0.
ROW(74)	0.	0.	0.	0.	0.	0.	0.	0.	0.
ROW(75)	0.	0.	0.	0.	0.	0.	0.	0.	0.
ROW(76)	0.	0.	0.	0.	0.	0.	0.	0.	0.
ROW(77)	0.	0.	0.	0.	0.	0.	0.	0.	0.
ROW(78)	0.	0.	0.	0.	0.	0.	0.	0.	0.
ROW(79)	0.	0.	0.	0.	0.	0.	0.	0.	0.
ROW(80)	0.	0.	0.	0.	0.	0.	0.	0.	0.
ROW(81)	0.	0.	0.	0.	0.	0.	0.	0.	0.

	COL(46)	COL(47)	COL(48)	COL(49)	COL(50)	COL(51)	COL(52)	COL(53)	COL(54)
ROW(1)	0.	0.	0.	0.	0.	0.	0.	0.	0.
ROW(2)	0.	0.	0.	0.	0.	0.	0.	0.	0.
ROW(3)	0.	0.	0.	0.	0.	0.	0.	0.	0.
ROW(4)	0.	0.	0.	0.	0.	0.	0.	0.	0.
ROW(5)	0.	0.	0.	0.	0.	0.	0.	0.	0.
ROW(6)	0.	0.	0.	0.	0.	0.	0.	0.	0.
ROW(7)	0.	0.	0.	0.	0.	0.	0.	0.	0.
ROW(8)	0.	0.	0.	0.	0.	0.	0.	0.	0.
ROW(9)	0.	0.	0.	0.	0.	0.	0.	0.	0.
ROW(10)	0.	0.	0.	0.	0.	0.	0.	0.	0.
ROW(11)	0.	0.	0.	0.	0.	0.	0.	0.	0.
ROW(12)	0.	0.	0.	0.	0.	0.	0.	0.	0.
ROW(13)	0.	0.	0.	0.	0.	0.	0.	0.	0.
ROW(14)	0.	0.	0.	0.	0.	0.	0.	0.	0.
ROW(15)	0.	0.	0.	0.	0.	0.	0.	0.	0.
ROW(16)	0.	0.	0.	0.	0.	0.	0.	0.	0.
ROW(17)	0.	0.	0.	0.	0.	0.	0.	0.	0.
ROW(18)	0.	0.	0.	0.	0.	0.	0.	0.	0.
ROW(19)	0.	0.	0.	0.	0.	0.	0.	0.	0.
ROW(20)	0.	0.	0.	0.	0.	0.	0.	0.	0.
ROW(21)	0.	0.	0.	0.	0.	0.	0.	0.	0.
ROW(22)	0.	0.	0.	0.	0.	0.	0.	0.	0.
ROW(23)	0.	0.	0.	0.	0.	0.	0.	0.	0.
ROW(24)	0.	0.	0.	0.	0.	0.	0.	0.	0.
ROW(25)	0.	0.	0.	0.	0.	0.	0.	0.	0.
ROW(26)	0.	0.	0.	0.	0.	0.	0.	0.	0.

ROW(27)	0.	0.	0.	0.	0.	0.	0.	0.	0.
ROW(28)	0.	0.	0.	0.	0.	0.	0.	0.	0.
ROW(29)	0.	0.	0.	0.	0.	0.	0.	0.	0.
ROW(30)	0.	0.	0.	0.	0.	0.	0.	0.	0.
ROW(31)	0.	0.	0.	0.	0.	0.	0.	0.	0.
ROW(32)	0.	0.	0.	0.	0.	0.	0.	0.	0.
ROW(33)	0.	0.	0.	0.	0.	0.	0.	0.	0.
ROW(34)	0.	0.	0.	0.	0.	0.	0.	0.	0.
ROW(35)	0.	0.	0.	0.	0.	0.	0.	0.	0.
ROW(36)	0.	0.	0.	0.	0.	0.	0.	0.	0.
ROW(37)	0.4205+07	0.	0.	0.	0.	0.	0.	0.	0.
ROW(38)	0.	0.2105+07	0.	0.	0.	0.	0.	0.	0.
ROW(39)	0.	0.	0.2340+07	0.	0.	0.	0.	0.	0.
ROW(40)	0.	0.	0.	0.2422+07	0.	0.	0.	0.	0.
ROW(41)	0.	0.	0.	0.	0.2232+07	0.	0.	0.	0.
ROW(42)	0.	0.	0.	0.	0.	0.2069+07	0.	0.	0.
ROW(43)	0.	0.	0.	0.	0.	0.	0.2310+07	0.	0.
ROW(44)	0.	0.	0.	0.	0.	0.	0.	0.3000+07	0.
ROW(45)	0.	0.	0.	0.	0.	0.	0.	0.	0.4129+07
ROW(46)	-0.1748+08	0.6525+07	0.	0.	0.	0.	0.	0.	0.
ROW(47)	0.6525+07	-0.1648+08	0.4698+07	0.	0.	0.	0.	0.	0.
ROW(48)	0.	0.4698+07	-0.1337+08	0.2978+07	0.	0.	0.	0.	0.
ROW(49)	0.	0.	0.2978+07	-0.1042+08	0.1822+07	0.	0.	0.	0.
ROW(50)	0.	0.	0.	0.1822+07	-0.7850+07	0.1087+07	0.	0.	0.
ROW(51)	0.	0.	0.	0.	0.1087+07	-0.6328+07	0.7376+06	0.	0.
ROW(52)	0.	0.	0.	0.	0.	0.7376+06	-0.6694+07	0.7529+06	0.
ROW(53)	0.	0.	0.	0.	0.	0.	0.7529+06	-0.8847+07	0.8475+06
ROW(54)	0.	0.	0.	0.	0.	0.	0.	0.8475+06	-0.1242+08
ROW(55)	0.6750+07	0.	0.	0.	0.	0.	0.	0.	0.
ROW(56)	0.	0.3153+07	0.	0.	0.	0.	0.	0.	0.
ROW(57)	0.	0.	0.3359+07	0.	0.	0.	0.	0.	0.
ROW(58)	0.	0.	0.	0.3195+07	0.	0.	0.	0.	0.
ROW(59)	0.	0.	0.	0.	0.2709+07	0.	0.	0.	0.
ROW(60)	0.	0.	0.	0.	0.	0.2434+07	0.	0.	0.
ROW(61)	0.	0.	0.	0.	0.	0.	0.2893+07	0.	0.
ROW(62)	0.	0.	0.	0.	0.	0.	0.	0.4247+07	0.
ROW(63)	0.	0.	0.	0.	0.	0.	0.	0.	0.7448+07
ROW(64)	0.	0.	0.	0.	0.	0.	0.	0.	0.
ROW(65)	0.	0.	0.	0.	0.	0.	0.	0.	0.
ROW(66)	0.	0.	0.	0.	0.	0.	0.	0.	0.
ROW(67)	0.	0.	0.	0.	0.	0.	0.	0.	0.
ROW(68)	0.	0.	0.	0.	0.	0.	0.	0.	0.
ROW(69)	0.	0.	0.	0.	0.	0.	0.	0.	0.
ROW(70)	0.	0.	0.	0.	0.	0.	0.	0.	0.
ROW(71)	0.	0.	0.	0.	0.	0.	0.	0.	0.
ROW(72)	0.	0.	0.	0.	0.	0.	0.	0.	0.
ROW(73)	0.	0.	0.	0.	0.	0.	0.	0.	0.
ROW(74)	0.	0.	0.	0.	0.	0.	0.	0.	0.
ROW(75)	0.	0.	0.	0.	0.	0.	0.	0.	0.
ROW(76)	0.	0.	0.	0.	0.	0.	0.	0.	0.
ROW(77)	0.	0.	0.	0.	0.	0.	0.	0.	0.

ROW(78)	0.	0.	0.	0.	0.	0.	0.	0.	0.
ROW(79)	0.	0.	0.	0.	0.	0.	0.	0.	0.
ROW(80)	0.	0.	0.	0.	0.	0.	0.	0.	0.
ROW(81)	0.	0.	0.	0.	0.	0.	0.	0.	0.
	COL(55)	COL(56)	COL(57)	COL(58)	COL(59)	COL(60)	COL(61)	COL(62)	COL(63)
ROW(1)	0.	0.	0.	0.	0.	0.	0.	0.	0.
ROW(2)	0.	0.	0.	0.	0.	0.	0.	0.	0.
ROW(3)	0.	0.	0.	0.	0.	0.	0.	0.	0.
ROW(4)	0.	0.	0.	0.	0.	0.	0.	0.	0.
ROW(5)	0.	0.	0.	0.	0.	0.	0.	0.	0.
ROW(6)	0.	0.	0.	0.	0.	0.	0.	0.	0.
ROW(7)	0.	0.	0.	0.	0.	0.	0.	0.	0.
ROW(8)	0.	0.	0.	0.	0.	0.	0.	0.	0.
ROW(9)	0.	0.	0.	0.	0.	0.	0.	0.	0.
ROW(10)	0.	0.	0.	0.	0.	0.	0.	0.	0.
ROW(11)	0.	0.	0.	0.	0.	0.	0.	0.	0.
ROW(12)	0.	0.	0.	0.	0.	0.	0.	0.	0.
ROW(13)	0.	0.	0.	0.	0.	0.	0.	0.	0.
ROW(14)	0.	0.	0.	0.	0.	0.	0.	0.	0.
ROW(15)	0.	0.	0.	0.	0.	0.	0.	0.	0.
ROW(16)	0.	0.	0.	0.	0.	0.	0.	0.	0.
ROW(17)	0.	0.	0.	0.	0.	0.	0.	0.	0.
ROW(18)	0.	0.	0.	0.	0.	0.	0.	0.	0.
ROW(19)	0.	0.	0.	0.	0.	0.	0.	0.	0.
ROW(20)	0.	0.	0.	0.	0.	0.	0.	0.	0.
ROW(21)	0.	0.	0.	0.	0.	0.	0.	0.	0.
ROW(22)	0.	0.	0.	0.	0.	0.	0.	0.	0.
ROW(23)	0.	0.	0.	0.	0.	0.	0.	0.	0.
ROW(24)	0.	0.	0.	0.	0.	0.	0.	0.	0.
ROW(25)	0.	0.	0.	0.	0.	0.	0.	0.	0.
ROW(26)	0.	0.	0.	0.	0.	0.	0.	0.	0.
ROW(27)	0.	0.	0.	0.	0.	0.	0.	0.	0.
ROW(28)	0.	0.	0.	0.	0.	0.	0.	0.	0.
ROW(29)	0.	0.	0.	0.	0.	0.	0.	0.	0.
ROW(30)	0.	0.	0.	0.	0.	0.	0.	0.	0.
ROW(31)	0.	0.	0.	0.	0.	0.	0.	0.	0.
ROW(32)	0.	0.	0.	0.	0.	0.	0.	0.	0.
ROW(33)	0.	0.	0.	0.	0.	0.	0.	0.	0.
ROW(34)	0.	0.	0.	0.	0.	0.	0.	0.	0.
ROW(35)	0.	0.	0.	0.	0.	0.	0.	0.	0.
ROW(36)	0.	0.	0.	0.	0.	0.	0.	0.	0.
ROW(37)	0.	0.	0.	0.	0.	0.	0.	0.	0.
ROW(38)	0.	0.	0.	0.	0.	0.	0.	0.	0.
ROW(39)	0.	0.	0.	0.	0.	0.	0.	0.	0.
ROW(40)	0.	0.	0.	0.	0.	0.	0.	0.	0.
ROW(41)	0.	0.	0.	0.	0.	0.	0.	0.	0.
ROW(42)	0.	0.	0.	0.	0.	0.	0.	0.	0.
ROW(43)	0.	0.	0.	0.	0.	0.	0.	0.	0.
ROW(44)	0.	0.	0.	0.	0.	0.	0.	0.	0.
ROW(45)	0.	0.	0.	0.	0.	0.	0.	0.	0.
ROW(46)	0.6750+07	0.	0.	0.	0.	0.	0.	0.	0.

ROW(47)	0.	0.3153+07	0.	0.	0.	0.	0.	0.	0.
ROW(48)	0.	0.	0.3359+07	0.	0.	0.	0.	0.	0.
ROW(49)	0.	0.	0.	0.3195+07	0.	0.	0.	0.	0.
ROW(50)	0.	0.	0.	0.	0.2709+07	0.	0.	0.	0.
ROW(51)	0.	0.	0.	0.	0.	0.2434+07	0.	0.	0.
ROW(52)	0.	0.	0.	0.	0.	0.	0.2893+07	0.	0.
ROW(53)	0.	0.	0.	0.	0.	0.	0.	0.4247+07	0.
ROW(54)	0.	0.	0.	0.	0.	0.	0.	0.	0.7448+07
ROW(55)	-0.2502+08	0.6525+07	0.	0.	0.	0.	0.	0.	0.
ROW(56)	0.6525+07	-0.1897+08	0.4524+07	0.	0.	0.	0.	0.	0.
ROW(57)	0.	0.4524+07	-0.1527+08	0.2677+07	0.	0.	0.	0.	0.
ROW(58)	0.	0.	0.2677+07	-0.1148+08	0.1457+07	0.	0.	0.	0.
ROW(59)	0.	0.	0.	0.1457+07	-0.8318+07	0.8242+06	0.	0.	0.
ROW(60)	0.	0.	0.	0.	0.8242+06	-0.6767+07	0.5598+06	0.	0.
ROW(61)	0.	0.	0.	0.	0.	0.5598+06	-0.7849+07	0.6425+06	0.
ROW(62)	0.	0.	0.	0.	0.	0.	0.6425+06	-0.1237+08	0.8520+06
ROW(63)	0.	0.	0.	0.	0.	0.	0.	0.8520+06	-0.2264+08
ROW(64)	0.1175+08	0.	0.	0.	0.	0.	0.	0.	0.
ROW(65)	0.	0.4768+07	0.	0.	0.	0.	0.	0.	0.
ROW(66)	0.	0.	0.4707+07	0.	0.	0.	0.	0.	0.
ROW(67)	0.	0.	0.	0.4150+07	0.	0.	0.	0.	0.
ROW(68)	0.	0.	0.	0.	0.3327+07	0.	0.	0.	0.
ROW(69)	0.	0.	0.	0.	0.	0.2949+07	0.	0.	0.
ROW(70)	0.	0.	0.	0.	0.	0.	0.3754+07	0.	0.
ROW(71)	0.	0.	0.	0.	0.	0.	0.	0.6627+07	0.
ROW(72)	0.	0.	0.	0.	0.	0.	0.	0.	0.1434+08
ROW(73)	0.	0.	0.	0.	0.	0.	0.	0.	0.
ROW(74)	0.	0.	0.	0.	0.	0.	0.	0.	0.
ROW(75)	0.	0.	0.	0.	0.	0.	0.	0.	0.
ROW(76)	0.	0.	0.	0.	0.	0.	0.	0.	0.
ROW(77)	0.	0.	0.	0.	0.	0.	0.	0.	0.
ROW(78)	0.	0.	0.	0.	0.	0.	0.	0.	0.
ROW(79)	0.	0.	0.	0.	0.	0.	0.	0.	0.
ROW(80)	0.	0.	0.	0.	0.	0.	0.	0.	0.
ROW(81)	0.	0.	0.	0.	0.	0.	0.	0.	0.

	COL(64)	COL(65)	COL(66)	COL(67)	COL(68)	COL(69)	COL(70)	COL(71)	COL(72)
ROW(1)	0.	0.	0.	0.	0.	0.	0.	0.	0.
ROW(2)	0.	0.	0.	0.	0.	0.	0.	0.	0.
ROW(3)	0.	0.	0.	0.	0.	0.	0.	0.	0.
ROW(4)	0.	0.	0.	0.	0.	0.	0.	0.	0.
ROW(5)	0.	0.	0.	0.	0.	0.	0.	0.	0.
ROW(6)	0.	0.	0.	0.	0.	0.	0.	0.	0.
ROW(7)	0.	0.	0.	0.	0.	0.	0.	0.	0.
ROW(8)	0.	0.	0.	0.	0.	0.	0.	0.	0.
ROW(9)	0.	0.	0.	0.	0.	0.	0.	0.	0.
ROW(10)	0.	0.	0.	0.	0.	0.	0.	0.	0.
ROW(11)	0.	0.	0.	0.	0.	0.	0.	0.	0.
ROW(12)	0.	0.	0.	0.	0.	0.	0.	0.	0.
ROW(13)	0.	0.	0.	0.	0.	0.	0.	0.	0.
ROW(14)	0.	0.	0.	0.	0.	0.	0.	0.	0.
ROW(15)	0.	0.	0.	0.	0.	0.	0.	0.	0.

ROW(16)	0.	0.	0.	0.	0.	0.	0.	0.	0.
ROW(17)	0.	0.	0.	0.	0.	0.	0.	0.	0.
ROW(18)	0.	0.	0.	0.	0.	0.	0.	0.	0.
ROW(19)	0.	0.	0.	0.	0.	0.	0.	0.	0.
ROW(20)	0.	0.	0.	0.	0.	0.	0.	0.	0.
ROW(21)	0.	0.	0.	0.	0.	0.	0.	0.	0.
ROW(22)	0.	0.	0.	0.	0.	0.	0.	0.	0.
ROW(23)	0.	0.	0.	0.	0.	0.	0.	0.	0.
ROW(24)	0.	0.	0.	0.	0.	0.	0.	0.	0.
ROW(25)	0.	0.	0.	0.	0.	0.	0.	0.	0.
ROW(26)	0.	0.	0.	0.	0.	0.	0.	0.	0.
ROW(27)	0.	0.	0.	0.	0.	0.	0.	0.	0.
ROW(28)	0.	0.	0.	0.	0.	0.	0.	0.	0.
ROW(29)	0.	0.	0.	0.	0.	0.	0.	0.	0.
ROW(30)	0.	0.	0.	0.	0.	0.	0.	0.	0.
ROW(31)	0.	0.	0.	0.	0.	0.	0.	0.	0.
ROW(32)	0.	0.	0.	0.	0.	0.	0.	0.	0.
ROW(33)	0.	0.	0.	0.	0.	0.	0.	0.	0.
ROW(34)	0.	0.	0.	0.	0.	0.	0.	0.	0.
ROW(35)	0.	0.	0.	0.	0.	0.	0.	0.	0.
ROW(36)	0.	0.	0.	0.	0.	0.	0.	0.	0.
ROW(37)	0.	0.	0.	0.	0.	0.	0.	0.	0.
ROW(38)	0.	0.	0.	0.	0.	0.	0.	0.	0.
ROW(39)	0.	0.	0.	0.	0.	0.	0.	0.	0.
ROW(40)	0.	0.	0.	0.	0.	0.	0.	0.	0.
ROW(41)	0.	0.	0.	0.	0.	0.	0.	0.	0.
ROW(42)	0.	0.	0.	0.	0.	0.	0.	0.	0.
ROW(43)	0.	0.	0.	0.	0.	0.	0.	0.	0.
ROW(44)	0.	0.	0.	0.	0.	0.	0.	0.	0.
ROW(45)	0.	0.	0.	0.	0.	0.	0.	0.	0.
ROW(46)	0.	0.	0.	0.	0.	0.	0.	0.	0.
ROW(47)	0.	0.	0.	0.	0.	0.	0.	0.	0.
ROW(48)	0.	0.	0.	0.	0.	0.	0.	0.	0.
ROW(49)	0.	0.	0.	0.	0.	0.	0.	0.	0.
ROW(50)	0.	0.	0.	0.	0.	0.	0.	0.	0.
ROW(51)	0.	0.	0.	0.	0.	0.	0.	0.	0.
ROW(52)	0.	0.	0.	0.	0.	0.	0.	0.	0.
ROW(53)	0.	0.	0.	0.	0.	0.	0.	0.	0.
ROW(54)	0.	0.	0.	0.	0.	0.	0.	0.	0.
ROW(55)	0.1175+08	0.	0.	0.	0.	0.	0.	0.	0.
ROW(56)	0.	0.4768+07	0.	0.	0.	0.	0.	0.	0.
ROW(57)	0.	0.	0.4707+07	0.	0.	0.	0.	0.	0.
ROW(58)	0.	0.	0.	0.4150+07	0.	0.	0.	0.	0.
ROW(59)	0.	0.	0.	0.	0.3327+07	0.	0.	0.	0.
ROW(60)	0.	0.	0.	0.	0.	0.2949+07	0.	0.	0.
ROW(61)	0.	0.	0.	0.	0.	0.	0.3754+07	0.	0.
ROW(62)	0.	0.	0.	0.	0.	0.	0.	0.6627+07	0.
ROW(63)	0.	0.	0.	0.	0.	0.	0.	0.	0.1434+08
ROW(64)	-0.4050+08	0.5872+07	0.	0.	0.	0.	0.	0.	0.
ROW(65)	0.5872+07	-0.2188+08	0.3654+07	0.	0.	0.	0.	0.	0.
ROW(66)	0.	0.3654+07	-0.1720+08	0.1964+07	0.	0.	0.	0.	0.

ROW(67)	0.	0.	0.1964+07	-0.1270+08	0.1024+07	0.	0.	0.	0.
ROW(68)	0.	0.	0.	0.1024+07	-0.9080+07	0.5742+06	0.	0.	0.
ROW(69)	0.	0.	0.	0.	0.5742+06	-0.7314+07	0.3960+06	0.	0.
ROW(70)	0.	0.	0.	0.	0.	0.3960+06	-0.9187+07	0.5029+06	0.
ROW(71)	0.	0.	0.	0.	0.	0.	0.5029+06	-0.1911+08	0.8730+06
ROW(72)	0.	0.	0.	0.	0.	0.	0.	0.8730+06	-0.4771+08
ROW(73)	0.2287+08	0.	0.	0.	0.	0.	0.	0.	0.
ROW(74)	0.	0.7587+07	0.	0.	0.	0.	0.	0.	0.
ROW(75)	0.	0.	0.6877+07	0.	0.	0.	0.	0.	0.
ROW(76)	0.	0.	0.	0.5566+07	0.	0.	0.	0.	0.
ROW(77)	0.	0.	0.	0.	0.4155+07	0.	0.	0.	0.
ROW(78)	0.	0.	0.	0.	0.	0.3395+07	0.	0.	0.
ROW(79)	0.	0.	0.	0.	0.	0.	0.4534+07	0.	0.
ROW(80)	0.	0.	0.	0.	0.	0.	0.	0.1111+08	0.
ROW(81)	0.	0.	0.	0.	0.	0.	0.	0.	0.3249+08

	COL(73)	COL(74)	COL(75)	COL(76)	COL(77)	COL(78)	COL(79)	COL(80)	COL(81)
ROW(1)	0.	0.	0.	0.	0.	0.	0.	0.	0.
ROW(2)	0.	0.	0.	0.	0.	0.	0.	0.	0.
ROW(3)	0.	0.	0.	0.	0.	0.	0.	0.	0.
ROW(4)	0.	0.	0.	0.	0.	0.	0.	0.	0.
ROW(5)	0.	0.	0.	0.	0.	0.	0.	0.	0.
ROW(6)	0.	0.	0.	0.	0.	0.	0.	0.	0.
ROW(7)	0.	0.	0.	0.	0.	0.	0.	0.	0.
ROW(8)	0.	0.	0.	0.	0.	0.	0.	0.	0.
ROW(9)	0.	0.	0.	0.	0.	0.	0.	0.	0.
ROW(10)	0.	0.	0.	0.	0.	0.	0.	0.	0.
ROW(11)	0.	0.	0.	0.	0.	0.	0.	0.	0.
ROW(12)	0.	0.	0.	0.	0.	0.	0.	0.	0.
ROW(13)	0.	0.	0.	0.	0.	0.	0.	0.	0.
ROW(14)	0.	0.	0.	0.	0.	0.	0.	0.	0.
ROW(15)	0.	0.	0.	0.	0.	0.	0.	0.	0.
ROW(16)	0.	0.	0.	0.	0.	0.	0.	0.	0.
ROW(17)	0.	0.	0.	0.	0.	0.	0.	0.	0.
ROW(18)	0.	0.	0.	0.	0.	0.	0.	0.	0.
ROW(19)	0.	0.	0.	0.	0.	0.	0.	0.	0.
ROW(20)	0.	0.	0.	0.	0.	0.	0.	0.	0.
ROW(21)	0.	0.	0.	0.	0.	0.	0.	0.	0.
ROW(22)	0.	0.	0.	0.	0.	0.	0.	0.	0.
ROW(23)	0.	0.	0.	0.	0.	0.	0.	0.	0.
ROW(24)	0.	0.	0.	0.	0.	0.	0.	0.	0.
ROW(25)	0.	0.	0.	0.	0.	0.	0.	0.	0.
ROW(26)	0.	0.	0.	0.	0.	0.	0.	0.	0.
ROW(27)	0.	0.	0.	0.	0.	0.	0.	0.	0.
ROW(28)	0.	0.	0.	0.	0.	0.	0.	0.	0.
ROW(29)	0.	0.	0.	0.	0.	0.	0.	0.	0.
ROW(30)	0.	0.	0.	0.	0.	0.	0.	0.	0.
ROW(31)	0.	0.	0.	0.	0.	0.	0.	0.	0.
ROW(32)	0.	0.	0.	0.	0.	0.	0.	0.	0.
ROW(33)	0.	0.	0.	0.	0.	0.	0.	0.	0.
ROW(34)	0.	0.	0.	0.	0.	0.	0.	0.	0.
ROW(35)	0.	0.	0.	0.	0.	0.	0.	0.	0.

ROW(36)	0.	0.	0.	0.	0.	0.	0.	0.	0.
ROW(37)	0.	0.	0.	0.	0.	0.	0.	0.	0.
ROW(38)	0.	0.	0.	0.	0.	0.	0.	0.	0.
ROW(39)	0.	0.	0.	0.	0.	0.	0.	0.	0.
ROW(40)	0.	0.	0.	0.	0.	0.	0.	0.	0.
ROW(41)	0.	0.	0.	0.	0.	0.	0.	0.	0.
ROW(42)	0.	0.	0.	0.	0.	0.	0.	0.	0.
ROW(43)	0.	0.	0.	0.	0.	0.	0.	0.	0.
ROW(44)	0.	0.	0.	0.	0.	0.	0.	0.	0.
ROW(45)	0.	0.	0.	0.	0.	0.	0.	0.	0.
ROW(46)	0.	0.	0.	0.	0.	0.	0.	0.	0.
ROW(47)	0.	0.	0.	0.	0.	0.	0.	0.	0.
ROW(48)	0.	0.	0.	0.	0.	0.	0.	0.	0.
ROW(49)	0.	0.	0.	0.	0.	0.	0.	0.	0.
ROW(50)	0.	0.	0.	0.	0.	0.	0.	0.	0.
ROW(51)	0.	0.	0.	0.	0.	0.	0.	0.	0.
ROW(52)	0.	0.	0.	0.	0.	0.	0.	0.	0.
ROW(53)	0.	0.	0.	0.	0.	0.	0.	0.	0.
ROW(54)	0.	0.	0.	0.	0.	0.	0.	0.	0.
ROW(55)	0.	0.	0.	0.	0.	0.	0.	0.	0.
ROW(56)	0.	0.	0.	0.	0.	0.	0.	0.	0.
ROW(57)	0.	0.	0.	0.	0.	0.	0.	0.	0.
ROW(58)	0.	0.	0.	0.	0.	0.	0.	0.	0.
ROW(59)	0.	0.	0.	0.	0.	0.	0.	0.	0.
ROW(60)	0.	0.	0.	0.	0.	0.	0.	0.	0.
ROW(61)	0.	0.	0.	0.	0.	0.	0.	0.	0.
ROW(62)	0.	0.	0.	0.	0.	0.	0.	0.	0.
ROW(63)	0.	0.	0.	0.	0.	0.	0.	0.	0.
ROW(64)	0.2287+08	0.	0.	0.	0.	0.	0.	0.	0.
ROW(65)	0.	0.7587+07	0.	0.	0.	0.	0.	0.	0.
ROW(66)	0.	0.	0.6877+07	0.	0.	0.	0.	0.	0.
ROW(67)	0.	0.	0.	0.5566+07	0.	0.	0.	0.	0.
ROW(68)	0.	0.	0.	0.	0.4155+07	0.	0.	0.	0.
ROW(69)	0.	0.	0.	0.	0.	0.3395+07	0.	0.	0.
ROW(70)	0.	0.	0.	0.	0.	0.	0.4534+07	0.	0.
ROW(71)	0.	0.	0.	0.	0.	0.	0.	0.1111+08	0.
ROW(72)	0.	0.	0.	0.	0.	0.	0.	0.	0.3249+08
ROW(73)	-0.2573+08	0.2855+07	0.	0.	0.	0.	0.	0.	0.
ROW(74)	0.2855+07	-0.1213+08	0.1686+07	0.	0.	0.	0.	0.	0.
ROW(75)	0.	0.1686+07	-0.9387+07	0.8240+06	0.	0.	0.	0.	0.
ROW(76)	0.	0.	0.8240+06	-0.6770+07	0.3806+06	0.	0.	0.	0.
ROW(77)	0.	0.	0.	0.3806+06	-0.4725+07	0.1895+06	0.	0.	0.
ROW(78)	0.	0.	0.	0.	0.1895+06	-0.3685+07	0.1007+06	0.	0.
ROW(79)	0.	0.	0.	0.	0.	0.1007+06	-0.4801+07	0.1661+06	0.
ROW(80)	0.	0.	0.	0.	0.	0.	0.1661+06	-0.1176+08	0.4837+06
ROW(81)	0.	0.	0.	0.	0.	0.	0.	0.4837+06	-0.3298+08

AXIAL LOAD= 0.1605+07 SV(73)= 0.3963-01 SV(55)=-0.

FINAL DISPLACEMENTS

U(2)= 0.

U(3)= 0.

U(4)= 0.

U(5)= 0.
U(6)= 0.
U(7)= 0.
U(8)= 0.
U(9)= 0.
U(10)= 0.
U(11)= 0.3306-00
U(12)= 0.3246-00
U(13)= 0.3179-00
U(14)= 0.3094-00
U(15)= 0.2990-00
U(16)= 0.2835-00
U(17)= 0.2686-00
U(18)= 0.2614-00
U(19)= 0.2715-00
U(20)= 0.5672+00
U(21)= 0.5634+00
U(22)= 0.5553+00
U(23)= 0.5403+00
U(24)= 0.5173+00
U(25)= 0.4874-00
U(26)= 0.4557-00
U(27)= 0.4356-00
U(28)= 0.4355-00
U(29)= 0.7623+00
U(30)= 0.7577+00
U(31)= 0.7466+00
U(32)= 0.7249+00
U(33)= 0.6907+00
U(34)= 0.6454+00
U(35)= 0.5947+00
U(36)= 0.5584+00
U(37)= 0.5434+00
U(38)= 0.9355+00
U(39)= 0.9242+00
U(40)= 0.9047+00
U(41)= 0.8720+00
U(42)= 0.8235+00
U(43)= 0.7591+00
U(44)= 0.6877+00
U(45)= 0.6370+00
U(46)= 0.6143+00
U(47)= 0.1077+01
U(48)= 0.1060+01
U(49)= 0.1030+01
U(50)= 0.9818+00
U(51)= 0.9157+00
U(52)= 0.8308+00
U(53)= 0.7399+00
U(54)= 0.6790+00
U(55)= 0.6541+00

U(55)= 0.1195+01
U(57)= 0.1170+01
U(58)= 0.1128+01
U(59)= 0.1065+01
U(60)= 0.9801+00
U(61)= 0.8761+00
U(62)= 0.7680+00
U(63)= 0.7004+00
U(64)= 0.6738+00
U(65)= 0.1293+01
U(66)= 0.1252+01
U(67)= 0.1194+01
U(68)= 0.1117+01
U(69)= 0.1018+01
U(70)= 0.9008+00
U(71)= 0.7804+00
U(72)= 0.7089+00
U(73)= 0.6818+00
U(74)= 0.1372+01
U(75)= 0.1306+01
U(76)= 0.1231+01
U(77)= 0.1141+01
U(78)= 0.1035+01
U(79)= 0.9114+00
U(80)= 0.7842+00
U(81)= 0.7109+00
U(82)= 0.6843+00
U(83)= 0.1429+01
U(84)= 0.1326+01
U(85)= 0.1240+01
U(86)= 0.1148+01
U(87)= 0.1039+01
U(88)= 0.9145+00
U(89)= 0.7844+00
U(90)= 0.7109+00
U(91)= 0.6847+00

SHEAR FLOWS, R-C NOTATION

W(1)	W(2)	W(3)	W(4)	W(5)	W(6)	W(7)	W(8)
0.	0.	0.	0.	0.	0.	0.	0.
-0.8119+03	-0.7199+03	-0.6549+03	-0.6471+03	-0.6143+03	-0.4388+03	-0.1561+03	0.1827+03
-0.6199+03	-0.9892+03	-0.1300+04	-0.1473+04	-0.1384+04	-0.9903+03	-0.4709+03	-0.1544+01
-0.9241+03	-0.1709+04	-0.2318+04	-0.2555+04	-0.2285+04	-0.1631+04	-0.9394+03	-0.3667+03
-0.2688+04	-0.3505+04	-0.4023+04	-0.4024+04	-0.3463+04	-0.2566+04	-0.1591+04	-0.6876+03
-0.4746+04	-0.5734+04	-0.6159+04	-0.5796+04	-0.4717+04	-0.3438+04	-0.2113+04	-0.8981+03
-0.8309+04	-0.9774+04	-0.9428+04	-0.7703+04	-0.5658+04	-0.3987+04	-0.2542+04	-0.1127+04
-0.1658+05	-0.1636+05	-0.1301+05	-0.8982+04	-0.6040+04	-0.4215+04	-0.2869+04	-0.1445+04
-0.3205+05	-0.2309+05	-0.1461+05	-0.9080+04	-0.5908+04	-0.4197+04	-0.3072+04	-0.1937+04
-0.5884+05	-0.2889+05	-0.1530+05	-0.8255+04	-0.4722+04	-0.2620+04	-0.2442+04	-0.2534+04

AXIAL LOADS, R-C NOTATION

-0.2121+06 -0.1474+06 -0.1753+06 -0.1951+06 -0.1999+06 -0.1953+06 -0.1806+06 -0.1718+06 -0.1276+06
-0.2479+06 -0.1434+06 -0.1724+06 -0.1947+06 -0.1984+06 -0.1876+06 -0.1681+06 -0.1569+06 -0.1356+06

-0.2714+06	-0.1574+06	-0.1842+06	-0.2013+06	-0.1950+06	-0.1726+06	-0.1484+06	-0.1391+06	-0.1355+06
-0.3028+06	-0.1841+06	-0.2049+06	-0.2093+06	-0.1859+06	-0.1504+06	-0.1249+06	-0.1196+06	-0.1231+06
-0.3808+06	-0.2078+06	-0.2199+06	-0.2094+06	-0.1696+06	-0.1244+06	-0.9660+05	-0.9341+05	-0.1031+06
-0.4947+06	-0.2315+06	-0.2301+06	-0.2006+06	-0.1437+06	-0.9368+05	-0.6481+05	-0.6424+05	-0.8158+05
-0.6609+06	-0.2608+06	-0.2232+06	-0.1661+06	-0.1028+06	-0.6026+05	-0.3590+05	-0.3595+05	-0.5904+05
-0.9262+06	-0.2574+06	-0.1696+06	-0.1017+06	-0.5573+05	-0.3105+05	-0.1438+05	-0.1317+05	-0.3591+05
-0.1311+07	-0.1498+06	-0.6792+05	-0.3524+05	-0.1767+05	-0.1051+05	-0.8872+03	0.4579+03	-0.1267+05

PANEL WEIGHT PER 1/2 QUADRANT= 0.1078+04PANEL VOLUMN PER 1/2 QUADRANT= 0.1078+05

POINT(N)	FPEX	F(N)	F(N+9)	FQ(N)	FQ(N+9)	SUM
POINT(2)	0.	0.	-0.2121+06	0.	0.	0.2121+06
POINT(3)	0.	0.	-0.1474+06	0.	0.	0.1474+06
POINT(4)	0.	0.	-0.1753+06	0.	0.	0.1753+06
POINT(5)	0.	0.	-0.1951+06	0.	0.	0.1951+06
POINT(6)	0.	0.	-0.1999+06	0.	0.	0.1999+06
POINT(7)	0.	0.	-0.1953+06	0.	0.	0.1953+06
POINT(8)	0.	0.	-0.1806+06	0.	0.	0.1806+06
POINT(9)	0.	0.	-0.1718+06	0.	0.	0.1718+06
POINT(10)	0.	0.	-0.1276+06	0.	0.	0.1276+06
POINT(1)	0.	-0.2121+06	-0.2479+06	-0.3573+05	0.	-0.3105-00
POINT(2)	0.	-0.1474+06	-0.1434+06	-0.3168+05	-0.3573+05	0.1738-00
POINT(3)	0.	-0.1753+06	-0.1724+06	-0.2882+05	-0.3168+05	-0.1270-00
POINT(4)	0.	-0.1951+06	-0.1947+06	-0.2847+05	-0.2882+05	-0.1992-00
POINT(5)	0.	-0.1999+06	-0.1984+06	-0.2703+05	-0.2847+05	0.2734-01
POINT(6)	0.	-0.1953+06	-0.1876+06	-0.1931+05	-0.2703+05	-0.1563-00
POINT(7)	0.	-0.1806+06	-0.1681+06	-0.6868+04	-0.1931+05	0.4492-01
POINT(8)	0.	-0.1718+06	-0.1569+06	0.8037+04	-0.6868+04	-0.2344-01
POINT(9)	0.	-0.1276+06	-0.1356+06	0.	0.8037+04	-0.1367-01
POINT(1)	0.	-0.2479+06	-0.2714+06	-0.2356+05	0.	-0.1080+01
POINT(2)	0.	-0.1434+06	-0.1574+06	-0.3759+05	-0.2356+05	0.6895+00
POINT(3)	0.	-0.1724+06	-0.1842+06	-0.4941+05	-0.3759+05	-0.3770-00
POINT(4)	0.	-0.1947+06	-0.2013+06	-0.5598+05	-0.4941+05	-0.1367-00
POINT(5)	0.	-0.1984+06	-0.1950+06	-0.5260+05	-0.5598+05	0.3906-01
POINT(6)	0.	-0.1876+06	-0.1726+06	-0.3763+05	-0.5260+05	-0.9766-02
POINT(7)	0.	-0.1681+06	-0.1484+06	-0.1790+05	-0.3763+05	-0.1523-00
POINT(8)	0.	-0.1569+06	-0.1391+06	-0.5866+02	-0.1790+05	0.5859-02
POINT(9)	0.	-0.1356+06	-0.1355+06	0.	-0.5866+02	-0.4883-01
POINT(1)	0.	-0.2714+06	-0.3028+06	-0.3142+05	0.	-0.5781+00
POINT(2)	0.	-0.1574+06	-0.1841+06	-0.5809+05	-0.3142+05	0.7324+00
POINT(3)	0.	-0.1842+06	-0.2049+06	-0.7882+05	-0.5809+05	-0.2715-00
POINT(4)	0.	-0.2013+06	-0.2093+06	-0.8687+05	-0.7882+05	-0.4824-00
POINT(5)	0.	-0.1950+06	-0.1859+06	-0.7769+05	-0.8687+05	0.3906-01
POINT(6)	0.	-0.1726+06	-0.1504+06	-0.5545+05	-0.7769+05	-0.1777-00
POINT(7)	0.	-0.1484+06	-0.1249+06	-0.3194+05	-0.5545+05	0.8398-01
POINT(8)	0.	-0.1391+06	-0.1196+06	-0.1247+05	-0.3194+05	-0.1426-00
POINT(9)	0.	-0.1355+06	-0.1231+06	0.	-0.1247+05	0.8789-01
POINT(1)	0.	-0.3028+06	-0.3808+06	-0.7796+05	0.	-0.2285+01
POINT(2)	0.	-0.1841+06	-0.2078+06	-0.1017+06	-0.7796+05	0.1844+01
POINT(3)	0.	-0.2049+06	-0.2199+06	-0.1167+06	-0.1017+06	-0.6777+00
POINT(4)	0.	-0.2093+06	-0.2094+06	-0.1167+06	-0.1167+06	0.6836-01
POINT(5)	0.	-0.1859+06	-0.1696+06	-0.1004+06	-0.1167+06	-0.5605+00
POINT(6)	0.	-0.1504+06	-0.1244+06	-0.7443+05	-0.1004+06	0.9961-01

POINT(7)	0.	-0.1249+06	-0.9660+05	-0.4613+05	-0.7443+05	-0.3252-00
POINT(8)	0.	-0.1196+06	-0.9341+05	-0.1994+05	-0.4613+05	0.1162-00
POINT(9)	0.	-0.1231+06	-0.1031+06	0.	-0.1994+05	-0.4854-00
POINT(1)	0.	-0.3808+06	-0.4947+06	-0.1139+06	0.	0.9766-01
POINT(2)	0.	-0.2078+06	-0.2315+06	-0.1376+06	-0.1139+06	-0.1016-00
POINT(3)	0.	-0.2199+06	-0.2301+06	-0.1478+06	-0.1376+06	-0.2383-00
POINT(4)	0.	-0.2034+06	-0.2026+06	-0.1391+06	-0.1478+06	-0.6211+00
POINT(5)	0.	-0.1696+06	-0.1437+06	-0.1132+06	-0.1391+06	0.3164-00
POINT(6)	0.	-0.1244+06	-0.9368+05	-0.8251+05	-0.1132+06	-0.3916-00
POINT(7)	0.	-0.9660+05	-0.6481+05	-0.5072+05	-0.8251+05	-0.1289-00
POINT(8)	0.	-0.9341+05	-0.6424+05	-0.2155+05	-0.5072+05	-0.3877-00
POINT(9)	0.	-0.1031+06	-0.9158+05	0.	-0.2155+05	-0.1309-00
POINT(1)	0.	-0.4947+06	-0.6609+06	-0.1662+06	0.	-0.1242+01
POINT(2)	0.	-0.2315+06	-0.2608+06	-0.1955+06	-0.1662+06	0.1008+01
POINT(3)	0.	-0.2301+06	-0.2232+06	-0.1886+06	-0.1955+06	-0.8125+00
POINT(4)	0.	-0.2026+06	-0.1661+06	-0.1541+06	-0.1886+06	-0.4297-01
POINT(5)	0.	-0.1437+06	-0.1028+06	-0.1132+06	-0.1541+06	-0.2344-01
POINT(6)	0.	-0.9368+05	-0.6026+05	-0.7975+05	-0.1132+06	0.9277-01
POINT(7)	0.	-0.6481+05	-0.3590+05	-0.5083+05	-0.7975+05	0.1948-00
POINT(8)	0.	-0.6424+05	-0.3595+05	-0.2255+05	-0.5083+05	0.2637-01
POINT(9)	0.	-0.8158+05	-0.5904+05	0.	-0.2255+05	0.1299-00
POINT(1)	0.	-0.6609+06	-0.9262+06	-0.2653+06	0.	0.2891-00
POINT(2)	0.	-0.2608+06	-0.2574+06	-0.2618+06	-0.2653+06	-0.4063-00
POINT(3)	0.	-0.2232+06	-0.1696+06	-0.2082+06	-0.2618+06	0.1738-00
POINT(4)	0.	-0.1661+06	-0.1017+06	-0.1437+06	-0.2042+06	-0.7617+00
POINT(5)	0.	-0.1028+06	-0.5573+05	-0.9664+05	-0.1437+06	-0.1062+01
POINT(6)	0.	-0.6026+05	-0.3105+05	-0.6743+05	-0.9664+05	-0.3697-00
POINT(7)	0.	-0.3590+05	-0.1438+05	-0.4591+05	-0.6743+05	-0.4556-00
POINT(8)	0.	-0.3595+05	-0.1317+05	-0.2312+05	-0.4591+05	-0.8350-01
POINT(9)	0.	-0.5904+05	-0.3591+05	0.	-0.2312+05	-0.3071-00
POINT(1)	0.	-0.9262+06	-0.1311+07	-0.3846+06	0.	0.6820+01
POINT(2)	0.	-0.2574+06	-0.1498+06	-0.2770+06	-0.3846+06	-0.3516-01
POINT(3)	0.	-0.1696+06	-0.6792+05	-0.1754+06	-0.2770+06	0.9688+00
POINT(4)	0.	-0.1017+06	-0.3524+05	-0.1090+06	-0.1754+06	0.1069+01
POINT(5)	0.	-0.5573+05	-0.1767+05	-0.7090+05	-0.1090+06	0.9180+00
POINT(6)	0.	-0.3105+05	-0.1051+05	-0.5036+05	-0.7090+05	0.1909-00
POINT(7)	0.	-0.1438+05	-0.8872+03	-0.3687+05	-0.5036+05	0.5964+00
POINT(8)	0.	-0.1317+05	0.4579+03	-0.2324+05	-0.3687+05	0.1032+01
POINT(9)	0.	-0.3591+05	-0.1267+05	0.	-0.2324+05	0.2904+01
POINT(83)	0.	-0.1311+07	0.	-0.2942+06	0.	-0.1605+07
POINT(84)	0.	-0.1498+06	0.	-0.1444+06	-0.2942+06	0.5098+00
POINT(85)	0.	-0.6792+05	0.	-0.7651+05	-0.1444+06	-0.1991+01
POINT(86)	0.	-0.3524+05	0.	-0.4128+05	-0.7651+05	-0.1516+01
POINT(87)	0.	-0.1767+05	0.	-0.2361+05	-0.4128+05	-0.9551+00
POINT(88)	0.	-0.1051+05	0.	-0.1310+05	-0.2361+05	-0.5410+00
POINT(89)	0.	-0.8872+03	0.	-0.1221+05	-0.1310+05	-0.7238+00
POINT(90)	0.	0.4579+03	0.	-0.1267+05	-0.1221+05	-0.1038+01
POINT(91)	0.	-0.1267+05	0.	0.	-0.1267+05	-0.3255+01

A P P E N D I X D

This appendix contains the descriptions for development of the finite element stiffness matrix of the Tapered Beam, and the theoretical basis for the finite element stiffness matrix of the quadrilateral complex plate.

TAPERED BEAM THEORY

1.0 GENERAL

This appendix describes development of the finite element stiffness matrix of the Tapered Beam. The beam forces include bending moments, end torques, side shear and uniformly distributed transverse shears. These forces, fifteen in all, are placed on the element as shown in Figure D-1.

2.0 THEORETICAL BASIS OF MATRIX

The bending, side shear, and torque portions of the theory are independent of each other, hence the corresponding stiffness matrices are developed separately and combined subsequently into an overall stiffness matrix by means of transformation matrices.

The equation for the total stiffness matrix is

$$S_{15 \times 15} = SX + SY + SZ + SQ \qquad (B1)$$

where SX = Stiffness matrix for bending about the ξ axis
SY = Stiffness matrix for bending about the η axis
SZ = Stiffness matrix for torsion
SQ = Stiffness matrix for the shear and axial loads

3.0 THEORETICAL BASIS OF STIFFNESS MATRIX FOR TAPERED TORQUE TUBE

The dummy unit load method is employed to determine the influence coefficients for the supported structure shown in Figure D-2. The following equations which assume a linearly varying torsional stiffness, are used:

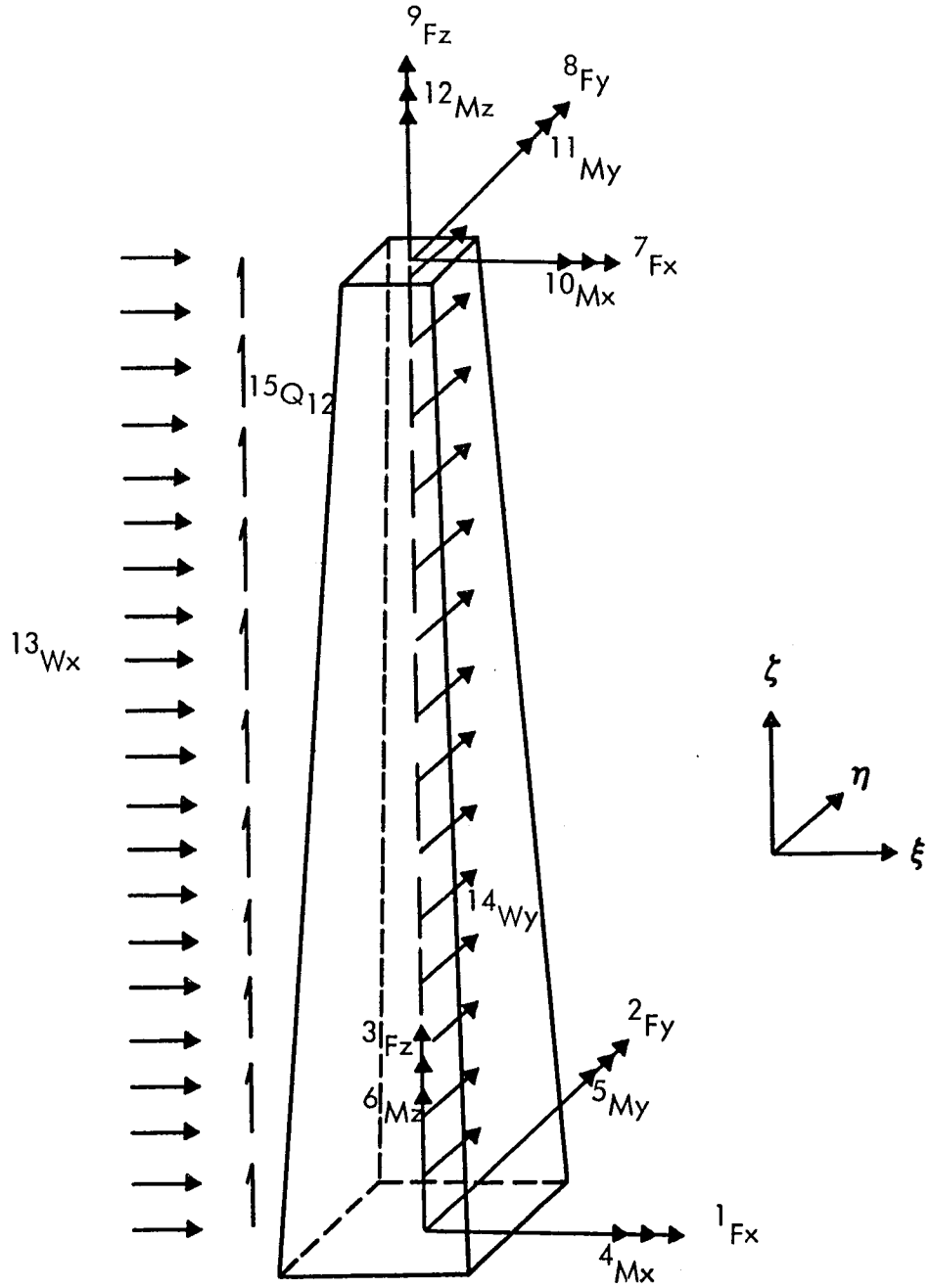

Figure D-1 TAPERED BEAM WITH BENDING, TORQUE AND SHEAR

$$J_x = J_1 \left(1 + \frac{wx}{L}\right) \qquad w = \frac{J_2 - J_1}{J_1} \tag{B2}$$

$$F_{11} = \int_0^L \frac{dx}{GJx} = \frac{1}{GJ_1} \int_0^L \frac{dx}{\left(1 + \frac{wx}{L}\right)} \tag{B3}$$

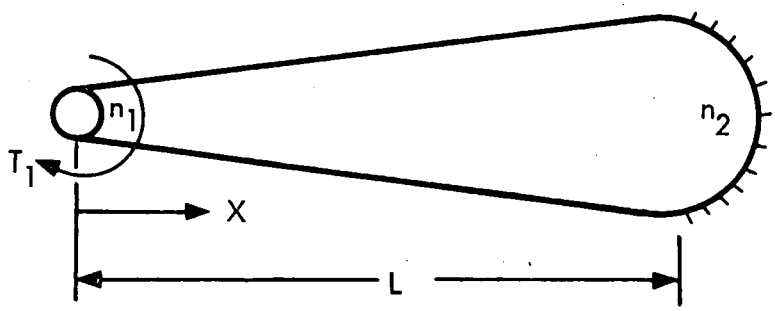

Figure D-2 COORDINATE SYSTEM FOR TAPERED BEAM THEORY

Be inversion of Equation (B3) one obtains the 1 x 1 stiffness matrix of the support element

$$\bar{S} = F_{11}^{-1} \tag{B4}$$

To obtain the unsupported 2 x 2 stiffness matrix SZ of the torque tube we define the load transformation matrix H to satisfy the equations of static equilibrium

$$\begin{Bmatrix} T_1 \\ T_2 \end{Bmatrix} = [H] \; T_1 \tag{B5}$$

so that

$$SZ = H \, \bar{S} \, H^T \tag{B6}$$

This is then transformed into its proper position in the $S_{15 \times 15}$ stiffness matrix by Equation (B1).

The developments for the tapered beam with bending and for the tapered beam with shear follow the same steps as that shown for the torque therefore they will not be included in this appendix.

The final resulting matrix expression is

$$\begin{Bmatrix} {}^{1}F_X \\ {}^{2}F_Y \\ {}^{3}F_Z \\ {}^{4}M_X \\ {}^{5}M_Y \\ {}^{6}M_Z \\ {}^{7}F_X \\ {}^{8}F_Y \\ {}^{9}F_Z \\ {}^{10}M_X \\ {}^{11}M_Y \\ {}^{12}M_Z \\ {}^{13}W_X \\ {}^{14}W_Y \\ {}^{15}Q_Z \end{Bmatrix} = \begin{bmatrix} S_{15 \times 15} \end{bmatrix} \begin{Bmatrix} {}^{1}\delta_X \\ {}^{2}\delta_Y \\ {}^{3}\delta_Z \\ {}^{4}\theta_X \\ {}^{5}\theta_Y \\ {}^{6}\theta_Z \\ {}^{7}\delta_X \\ {}^{8}\delta_Y \\ {}^{9}\delta_Z \\ {}^{10}\theta_X \\ {}^{11}\theta_Y \\ {}^{12}\theta_Z \\ {}^{13}d_X \\ {}^{14}d_Y \\ {}^{15}\gamma_{12} \end{Bmatrix}$$

QUADRILATERAL COMPLEX PLATE THEORY

1.0 GENERAL

This appendix describes the theoretical basis for the finite element stiffness matrix of the quadrilateral complex plate. The plate forces are restricted to be in-plane and are represented by the twelve (12) resultant forces as shown on the element in Figure D-3. The resulting internal stresses are distributed according to a quadratic stress assumption.

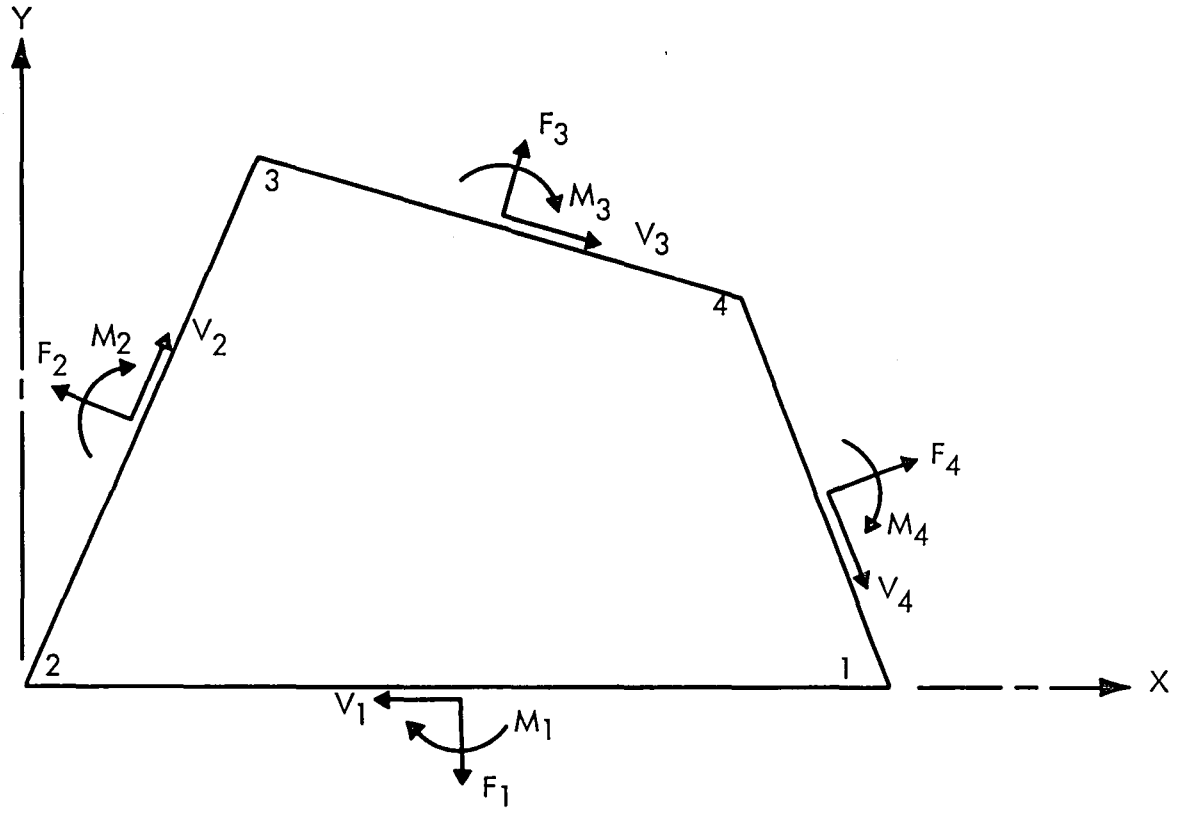

Figure D-3 COORDINATE SYSTEM FOR QUADRILATERAL PLATE

2.0 THEORETICAL BASIS OF MATRIX

The stress assumption is:

$$\sigma_x = a + bx + cy + dxy$$

$$\sigma_y = e + fx + gy + hxy \qquad \text{(A1)}$$

$$\tau_{xy} = k - gx - by - \frac{hx^2}{2} - \frac{dy^2}{2}$$

These equations satisfy the equations of equilibrium and compatibility. They can be written in matrix notation as:

$$\sigma = Uk \qquad \text{(A2)}$$

where $\sigma = \text{col}\ (\sigma_x, \sigma_y, \tau_{xy})$

$k = \text{col}\ (a, b, c, d, e, f, g, h, k)$

and U contains the remaining terms from Equation (A1).

Now, the stress and strain vectors are related by an equation of the form

$$\epsilon = N\sigma$$

where $\epsilon = \text{col}\ (\epsilon_x, \epsilon_y, \gamma_{xy})$ (A3)

and N is a nonsingular symmetric matrix involving Poisson's ratio and Young's modulus.

The stresses are integrated along each edge of the element giving a relation between the applied forces p, the resultants of these stresses, and the vector k.

$$p = Vk$$

where $p = \text{col}\ (F_1, V_1, M_1, \ldots\ldots, F_4, V_4, M_4)$ (A4)

Since the stresses satisfy the conditions of equilibrium the element is also in equilibrium under the forces p. Note that the number of constants in the stress assumption is numerically equal to the number of applied forces, hence the rank of V is the same as that of k.

Now, the first nine (9) rows of V are assumed linearly independent, hence a partitioning of equation (A4) gives

$$\left[\frac{p_1}{p_2}\right] = \left[\frac{V_1}{V_2}\right] \left[\ k\ \right] \tag{A5}$$

where V_1 is nonsingular. From this one obtains

$$p_1 = V_1\ k \qquad p_2 = V_2\ k \tag{A6}$$

giving

$$k = V_1^{-1}\ p_1 \tag{A7}$$

Hence p_1 alone determines k and the components of p_1 may be taken as independent variables. Fixing the displacements corresponding to p_2 the element becomes supported.

Now consider the flexibility matrix of the supported element. The following formula* is given:

$$f_{ij} = \int_V \epsilon_i^T\ \sigma_j\ dV \tag{A8}$$

where ϵ_i = the column strain vector at points in the element of volume V due to a unit load at coordinate i, σ_j = the column stress vector at points in the element due to a unit load at j.

Combining Eq. (A2) and (A7) and letting e_j = a column vector with unity in the jth place and zeros elsewhere gives

$$\sigma_j = U V_1^{-1}\ e_j \tag{A9}$$

*See Argylis, J. H., and Kelsey, S., Energy Theories and Structural Analysis, Butterworth, London, 1960, Equation (84), Page 18.

from which by use of Eq. (A3) one obtains

$$\epsilon_i^T = (N\,\sigma_i)^T = \sigma_i^T N = e_i^T \quad V_1^{-1T} \quad U^T N \tag{A10}$$

Inserting in Eq. (A8) and noting that only the components of the U matrix are affected by the integration gives

$$f_{ij} = e_i^T \; V_1^{-1T} \; G V_1^{-1} \; e_j \tag{A11}$$

where

$$G = \int_V U^T \, NU dV \tag{A12}$$

But (A11) amounts to the matrix equation

$$F = [f_{ij}] = V_1^{-1T} \; G \; V_1^{-1} \tag{A13}$$

By the inversion of Eq. (A13) one obtains the 9 x 9 stiffness matrix of the support element

$$\bar{S} = V_1 \; G^{-1} \; V_1^T \tag{A14}$$

To obtain the unsupported 12 x 12 stiffness matrix S we define the load transformation matrix H to satisfy the equations of static equilibrium

$$\begin{pmatrix} p_1 \\ \hline p_2 \end{pmatrix} = Hp1 \tag{A15}$$

so that

$$S = H \; \bar{S} \; H^T \tag{A16}$$

where S is the 12 x 12 unsupported finite element stiffness matrix of the complex quadrilateral plate.

The resulting expression is

$$\begin{Bmatrix} F_1 \\ V_1 \\ M_1 \\ F_2 \\ V_2 \\ M_2 \\ F_3 \\ V_3 \\ M_3 \\ F_4 \\ V_4 \\ M_4 \end{Bmatrix} = \left[S_{12 \times 12} \right] \begin{Bmatrix} \delta_1 \\ \gamma_1 \\ \theta_1 \\ \delta_2 \\ \gamma_2 \\ \theta_2 \\ \delta_3 \\ \gamma_3 \\ \theta_3 \\ \delta_4 \\ \gamma_4 \\ \theta_4 \end{Bmatrix}$$

A P P E N D I X E

This appendix contains a sample Manufacturing Plan for the fabrication and assembly of a heavy gage bonded honey comb thrust structure.

FOREWORD

Outlined in this document is the concept of planning, design, and manufacture of tools.

The object of this plan is to describe operational sequences and provide illustrations for the structural fabrication of the details and sub-assemblies for the thrust skirt, longeron-fittings, the aft ring and the final assembly of all components.

The plan is prepared to serve as a guide for the preparation of the manufacturing and process specifications appropriate for the full scale thrust skirt structure.

CONTENTS

Foreword	E-2
General Description	E-4
Thrust Skirt Assembly	E-5
Plant Layout	E-6
Major Tools	E-7
Manufacturing Sequence	E-11
Assemblies	E-20

GENERAL DESCRIPTION

The 396 inch diameter thrust skirt assembly is of bonded construction consisting of sixteen panels. Each panel is a bonded sandwich design, composed of outer and inner skins, machined edgemembers, and aluminum core. The panels are assembled into eight sub-assemblies either by splice plates or joined by welding. The eight sub-assemblies are attached by bolts to eight vertical longerons and a bonded honeycomb aft ring assembly to complete the thrust skirt assembly.

Figures E-1 through E-7 illustrate required detail parts.

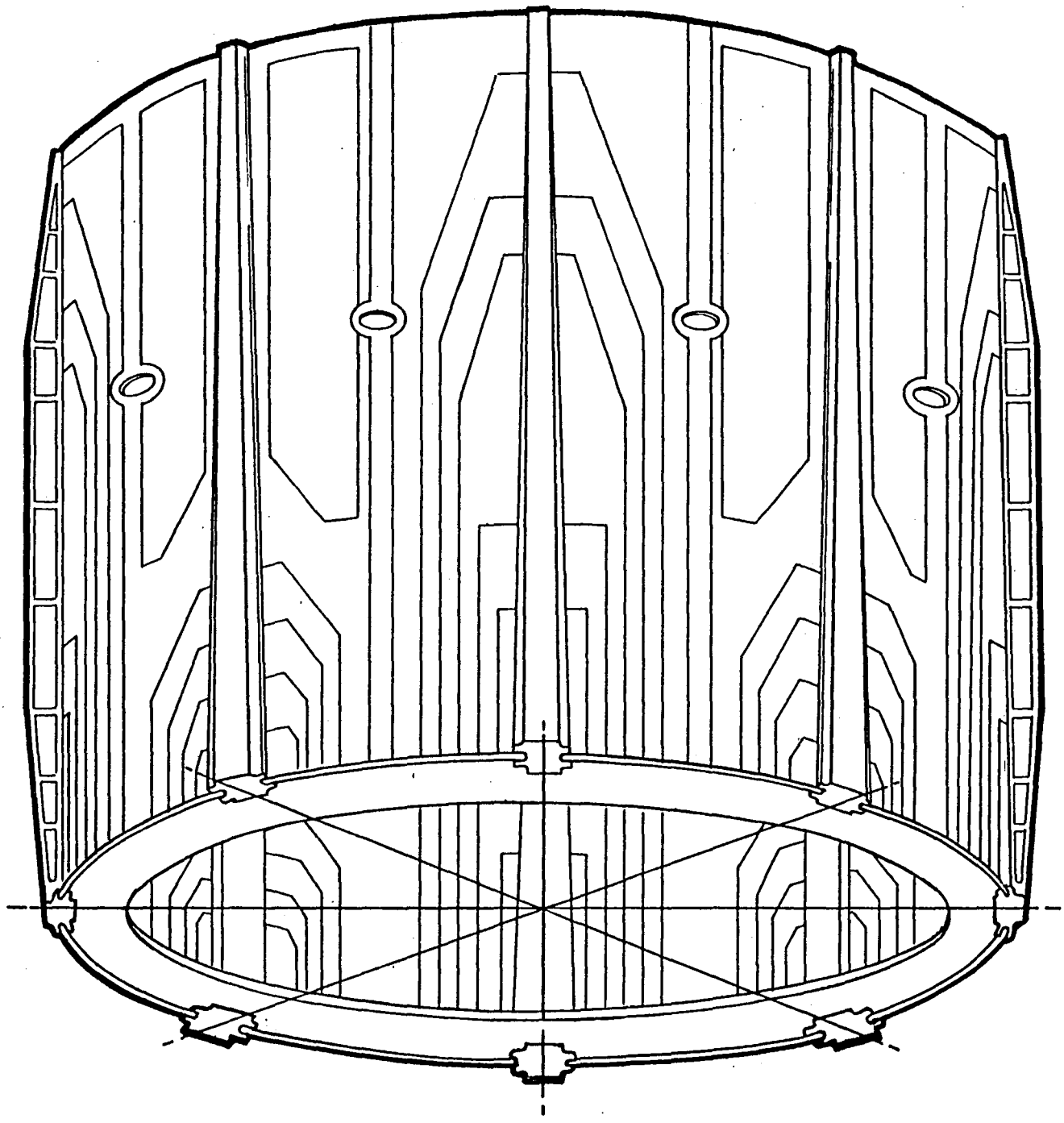

Figure E-1 THRUST SKIRT ASSEMBLY

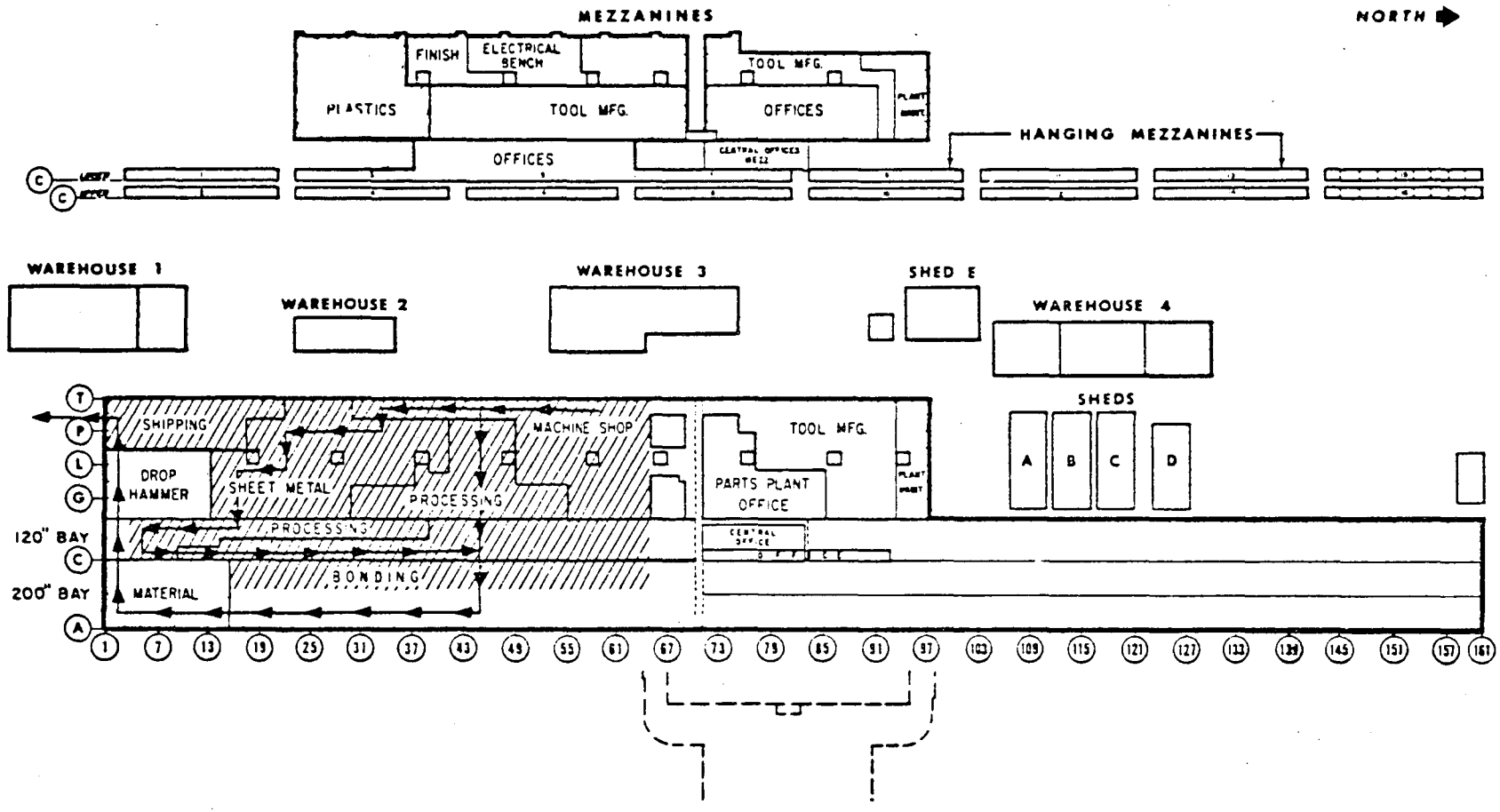

Figure E-2 PLANT LAYOUT

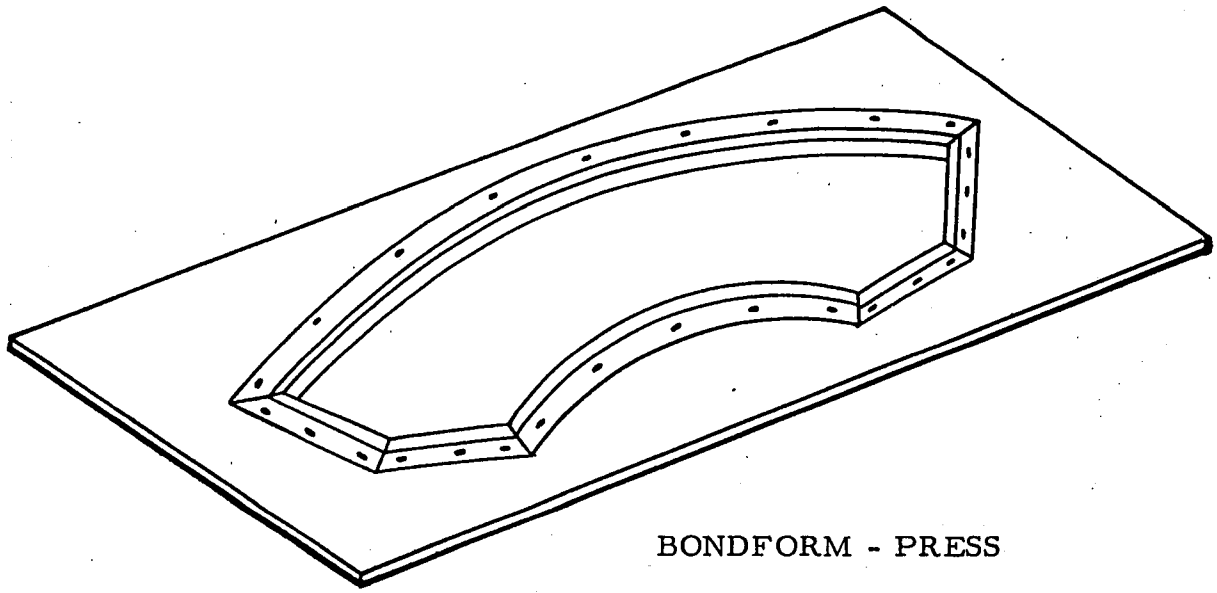

BONDFORM - PRESS

Figure E-3 AFT RING - ASSEMBLY

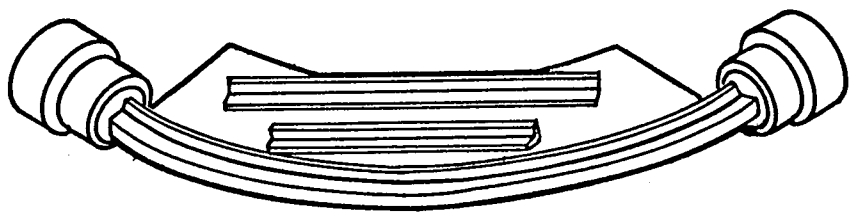

STRETCHER FORM

Figure E-4 MAJOR TOOLS

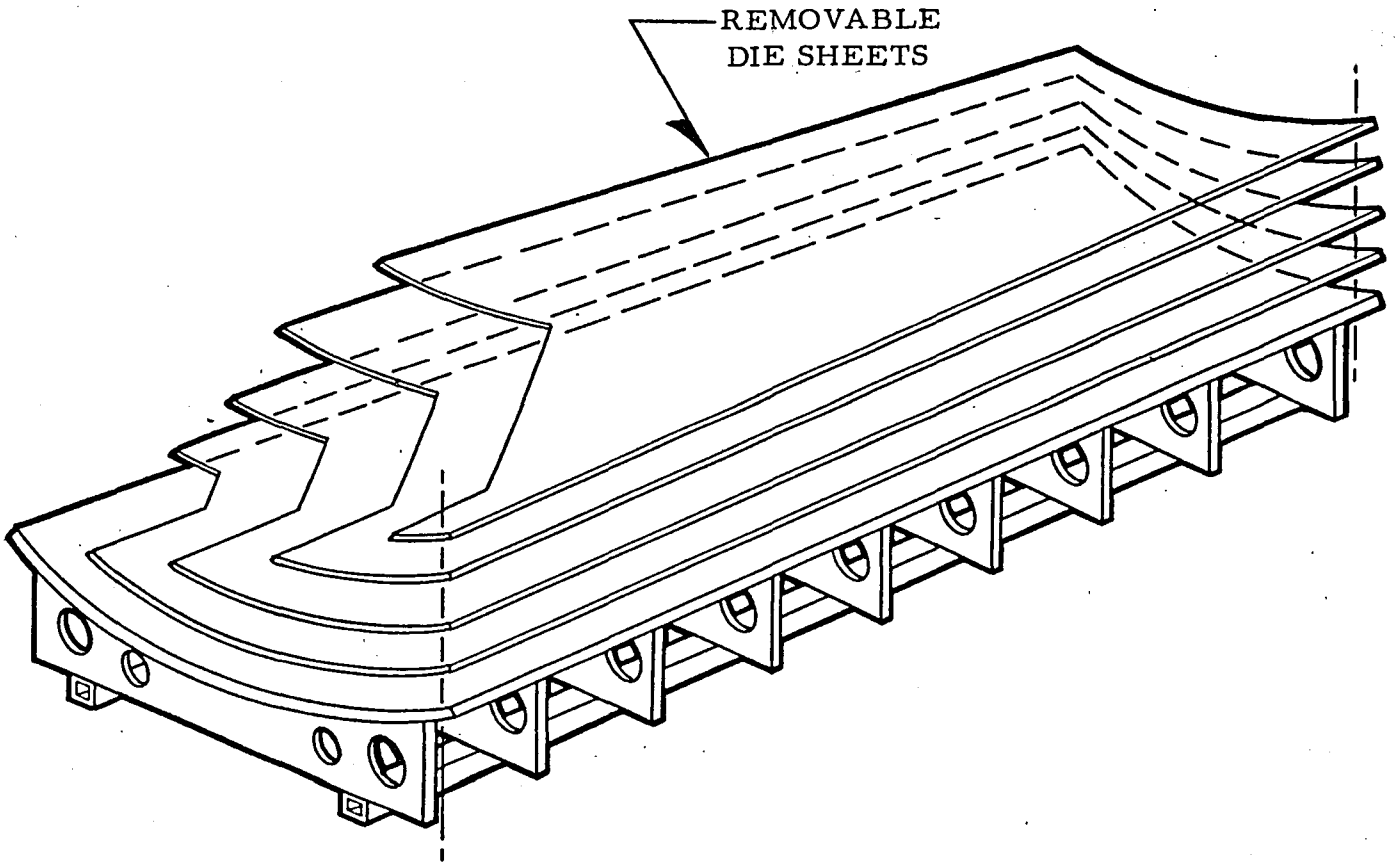

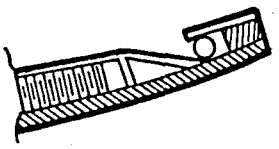

EDGE SEAL METHOD
(Not Shown on Assembly)

Figure E-5 BONDFORM - AUTOCLAVE

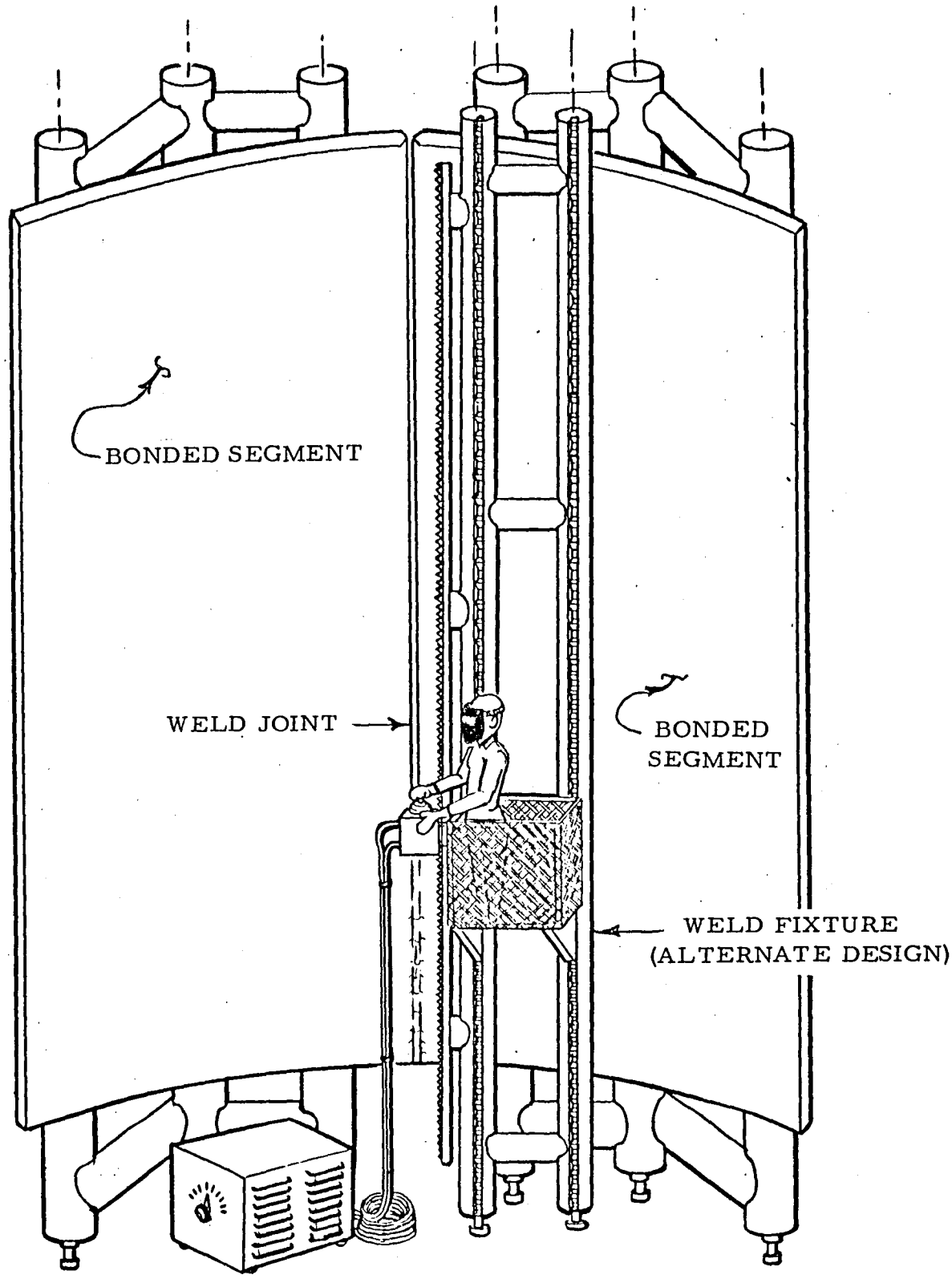

Figure E-6 THRUST SKIRT BONDED SEGMENT ASSEMBLY

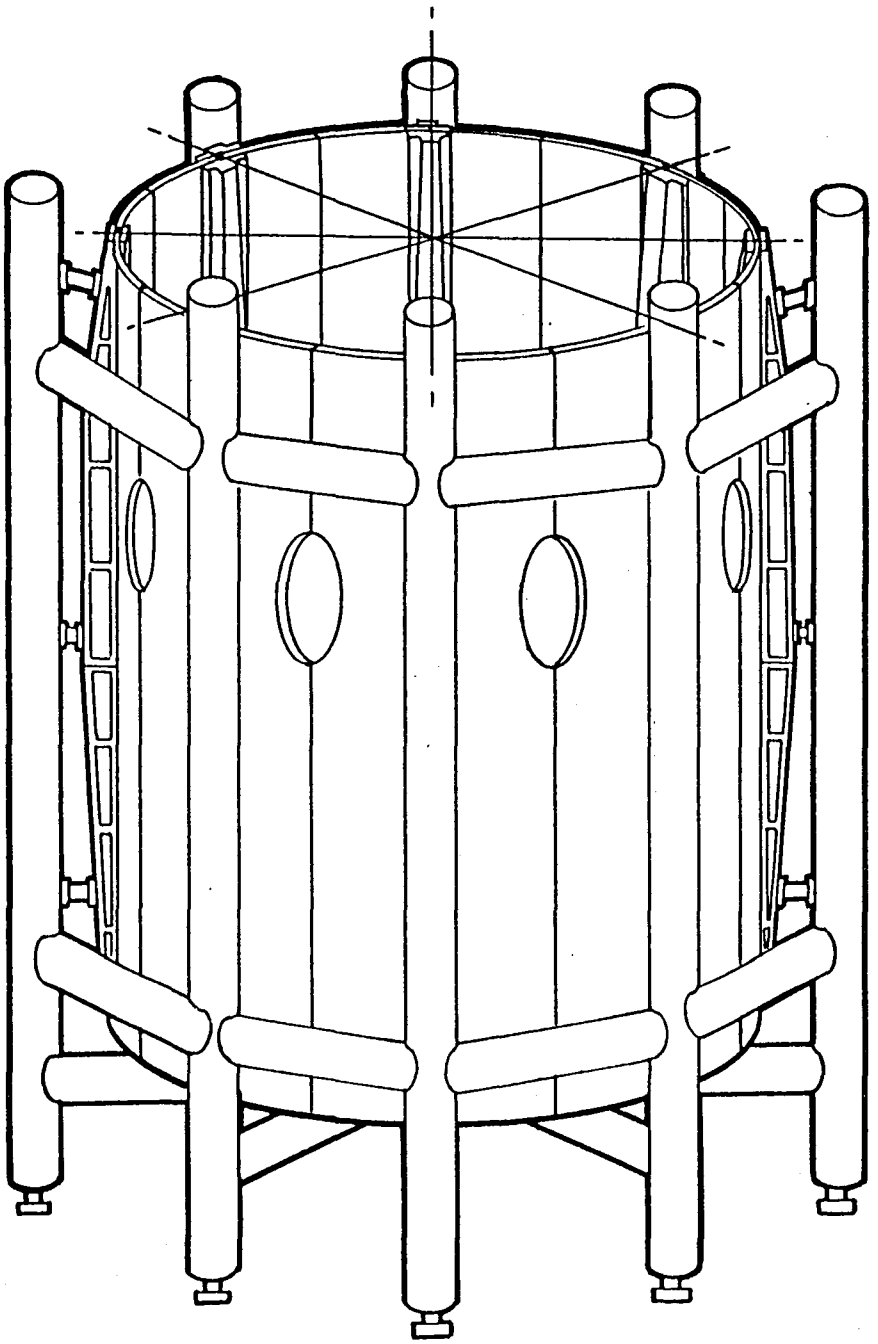

Figure E-7 SEGMENT ASSEMBLY FIXTURE

MANUFACTURING SEQUENCES FOR DETAILS AND SUB-ASSEMBLIES

DETAILS

Figures E-8 through E-15 depict the significant steps required to manufacture details for producing the thrust skirt assembly.

1. Inspect Forging
2. Rough Machine
3. Deburr
4. Heat Treat
5. Finish Machine to B/P
6. Straighten and Deburr
7. Penetrant Inspect
8. Number Tag
9. Heat Treat
10. AGE
11. Inspect
12. Forward to Stock

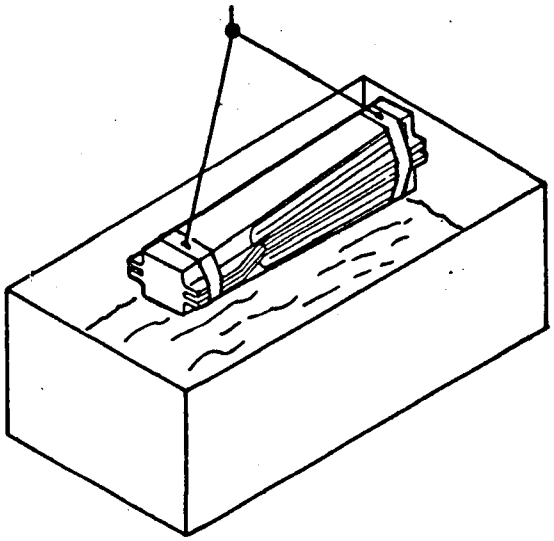

HEAT TREAT

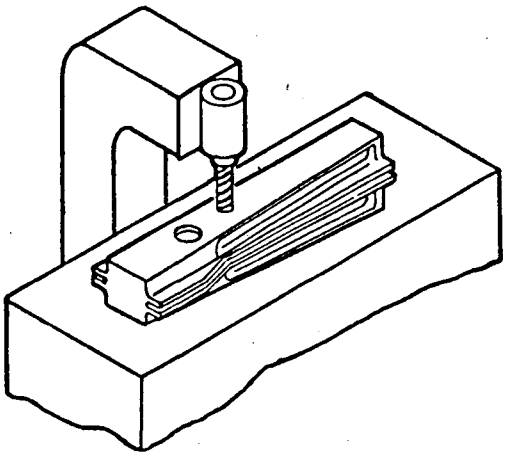

ROUGH MACHINE

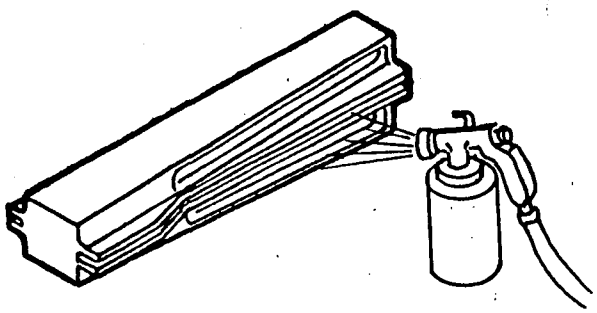

SPRAY PENETRANT
INSPECT

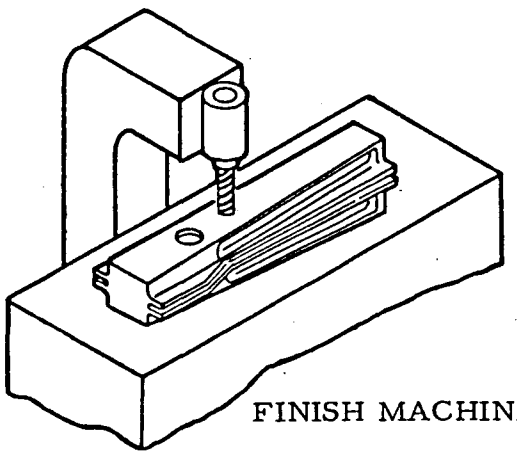

FINISH MACHINE

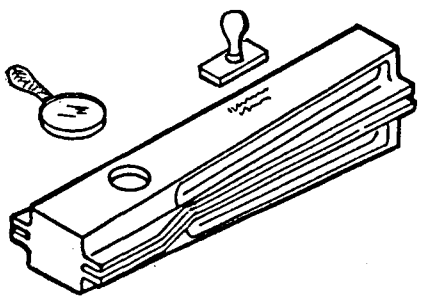

IDENTIFY AND INSPECT

Figure E-8 REBOUND AND THRUST LONGERON FITTING - LOWER
FW 6528005
FW 6528008

1. Inspect Forging
2. Rough Machine
3. Deburr
4. Heat Treat
5. Finish Machine to B/P
6. Straighten and Deburr
7. Penetrant Inspect
8. Number Tag
9. Heat Treat
10. AGE
11. Inspect
12. Forward to Stock

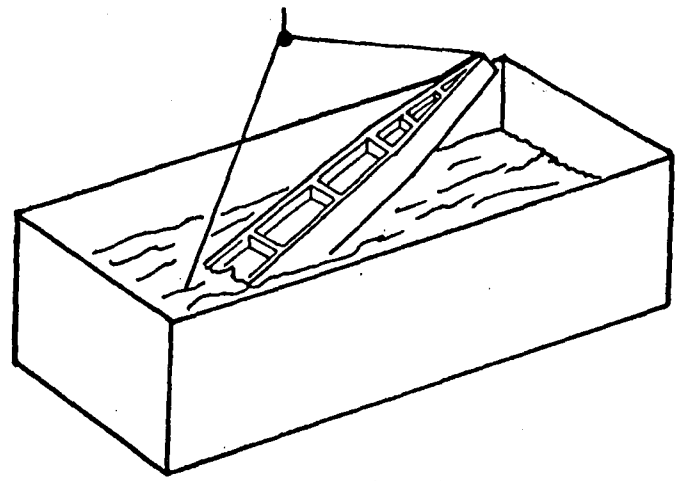

HEAT TREAT

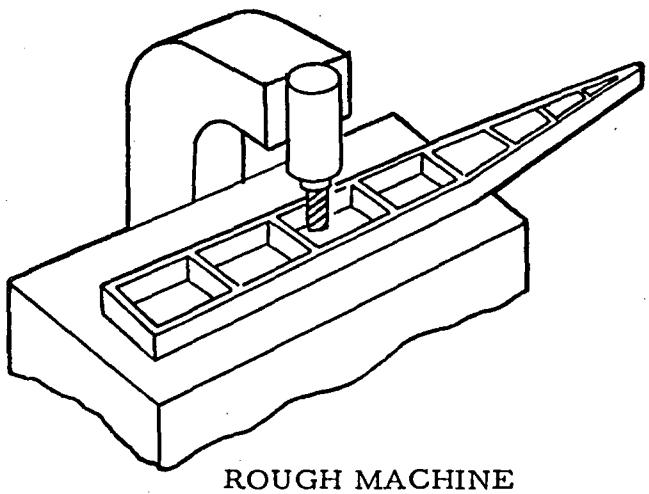

ROUGH MACHINE

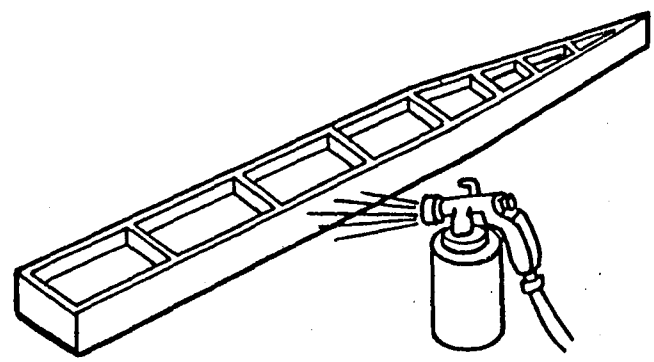

SPRAY PENETRANT INSPECT

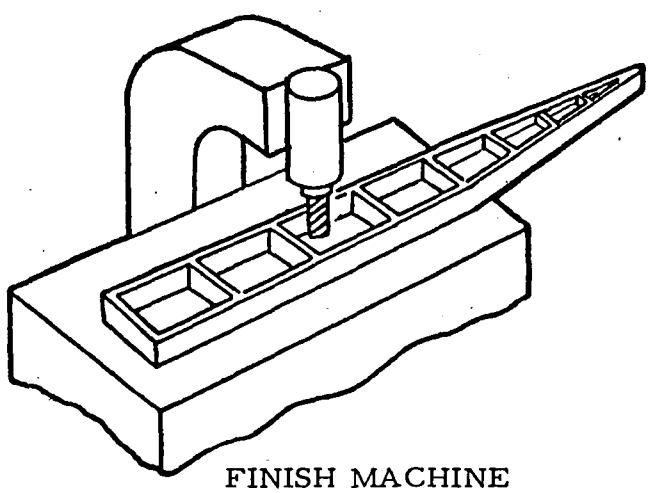

FINISH MACHINE

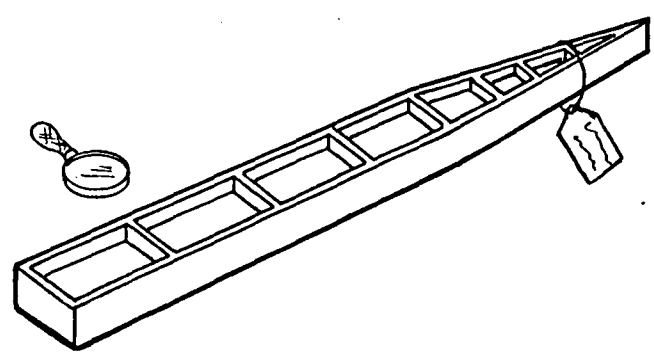

IDENTIFY AND INSPECT

Figure E-9 REBOUND AND THRUST LONGERON FITTING - UPPER

1. Inspect Material
2. Saw to Width, Length, (Allow Excess for Forming)
3. Roll or Brake Form
4. Inspect
5. Mask for Etching
6. Etch
7. Inspect
8. Trim
9. Deburr
10. Identify
11. Inspect
12. Forward to Stock

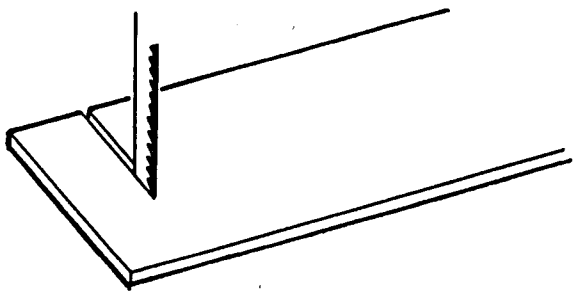

SAW TO LENGTH

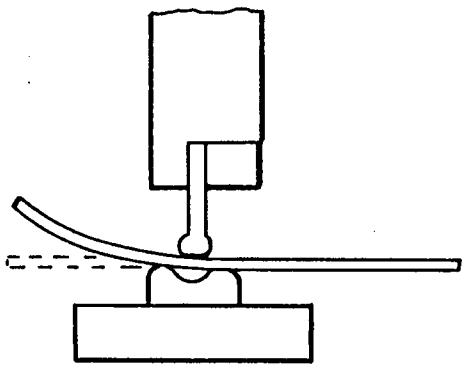

BRAKE FORM

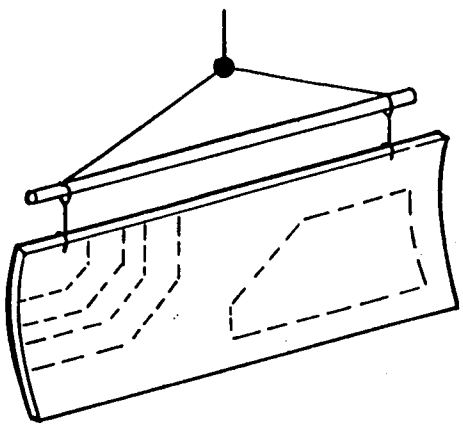

MASK AND LAYOUT FOR ETCHING

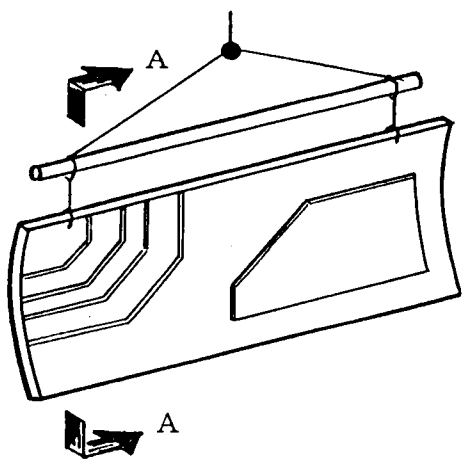

*ETCH STEPS

*SECTION A-A NEXT PAGE

Figure E-10 INNER AND OUTER SKINS

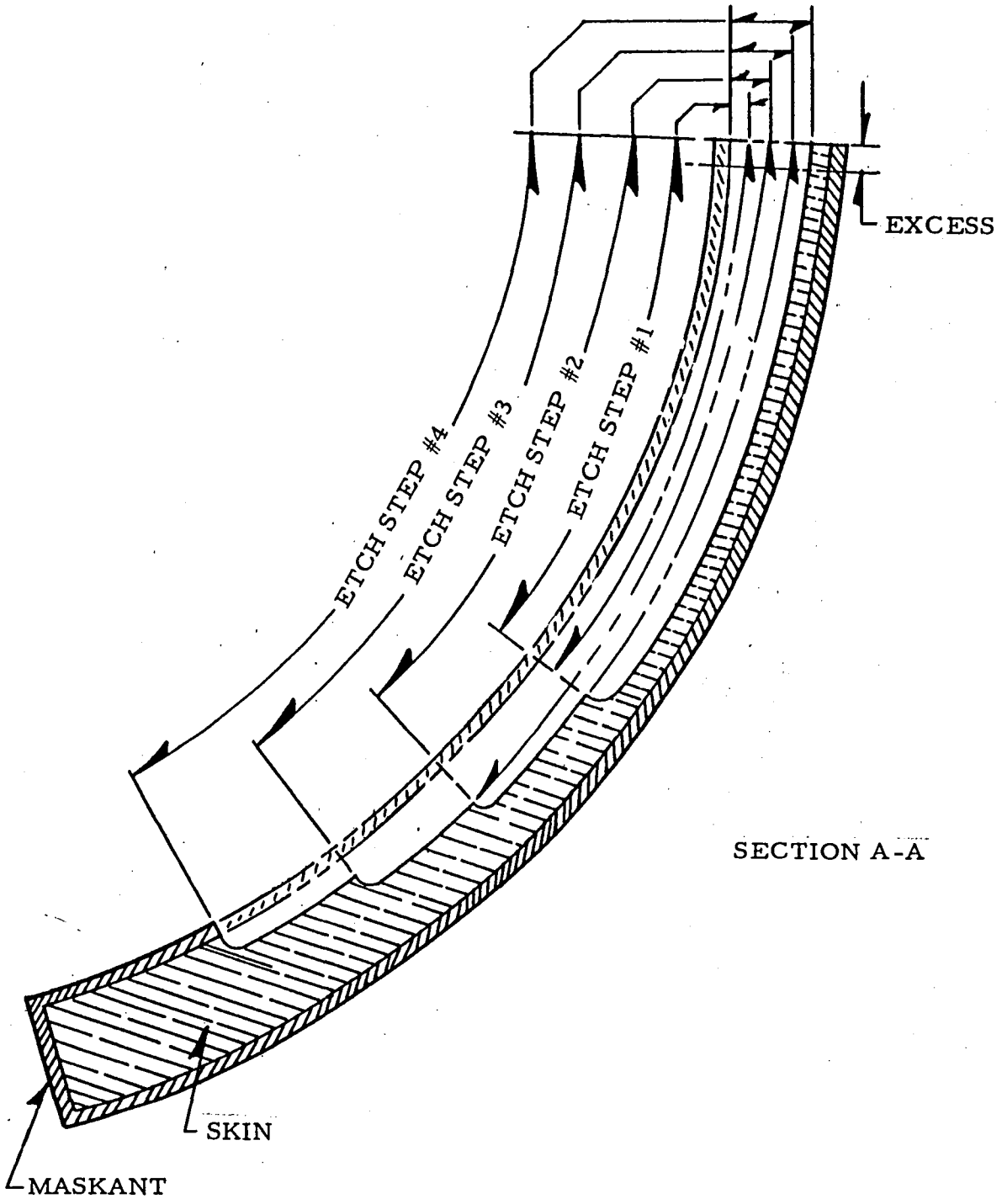

Figure E-11 ETCH STEP SEQUENCES

1. Inspect Material
2. Saw Extrusion to Length (Allow 4" Excess Each End)
3. Machine to B/P Dimensions
4. Deburr and Number
5. Penetrant Inspect
6. Heat Treat
7. Stretch Form
8. Heat Treat
9. Finish Form
10. Inspect
11. AGE
12. Inspect
13. Forward to Stock

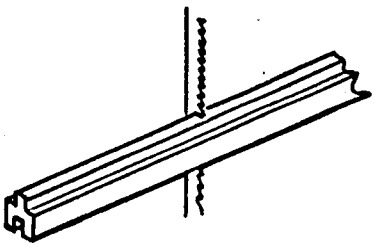

SAW TO LENGTH

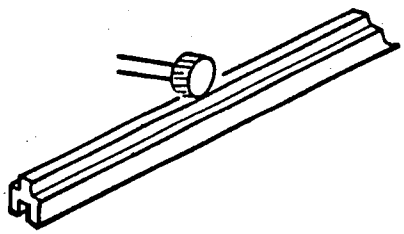

MACHINE

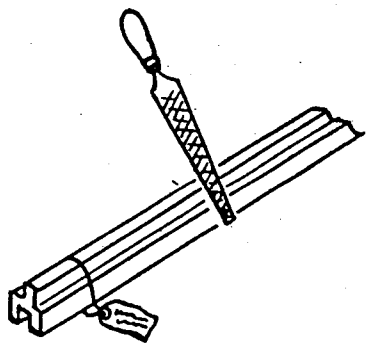

DEBURR, IDENTIFY

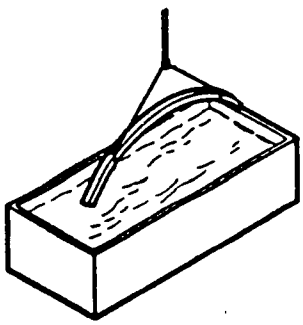

HEAT TREAT

STRETCH FORM,
CONTOUR

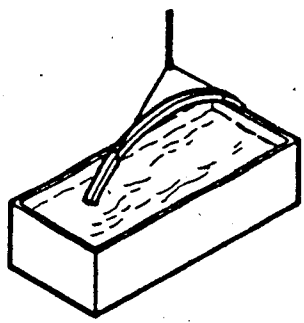

REPEAT HEAT TREAT

FINISH STRETCH FORM,
AND STRETCH CONTOUR

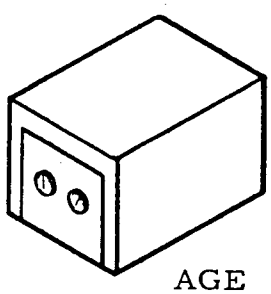

AGE

Figure E-12 EDGEMEMBER UPPER

1. Inspect Material
2. Saw to Length (Allow Excess for Forming)
3. Machine to B/P
4. Deburr and Identify
5. Inspect
6. Form
7. Heat Treat
8. AGE
9. Inspect
10. Forward to Stock

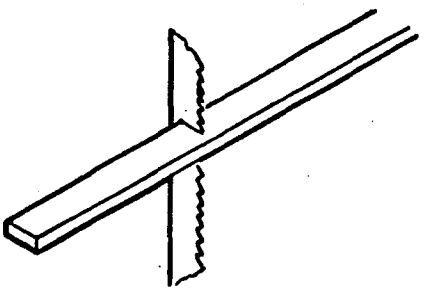

SAW

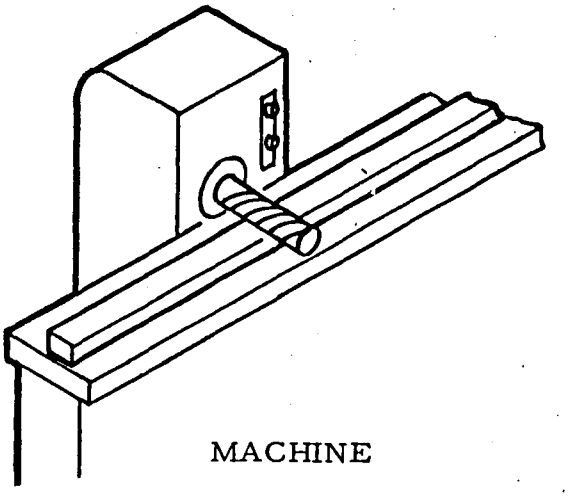

MACHINE

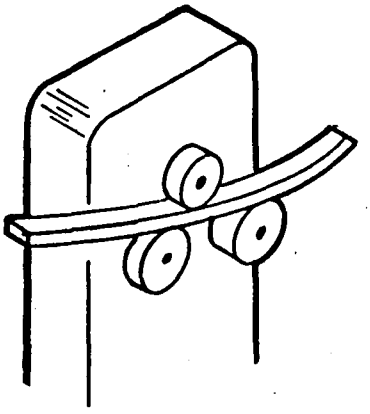

FORM

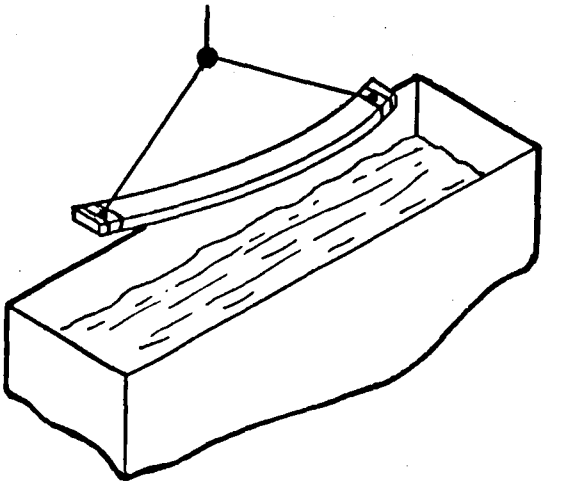

HEAT TREAT

Figure E-13 EDGEMEMBERS - LOWER

1. Inspect Material
2. Saw to Thickness
3. Expand Core or Expanding Machine
4. Cut to Size
5. Identify and Inspect
6. Forward to Stock

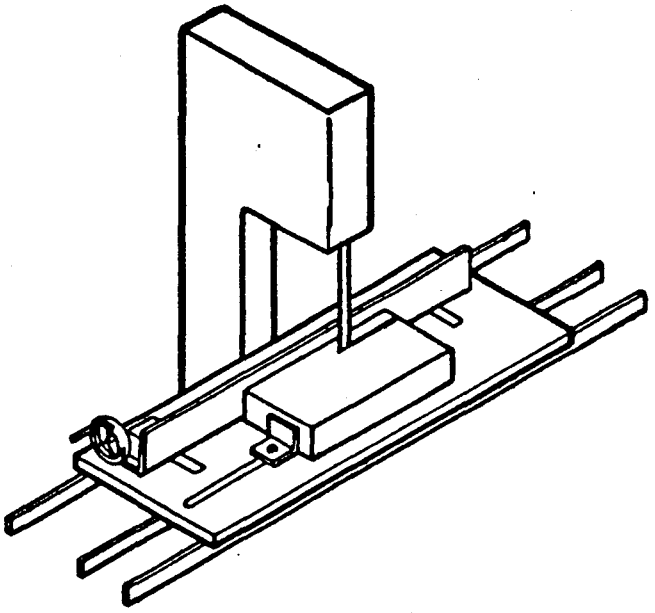

SAW

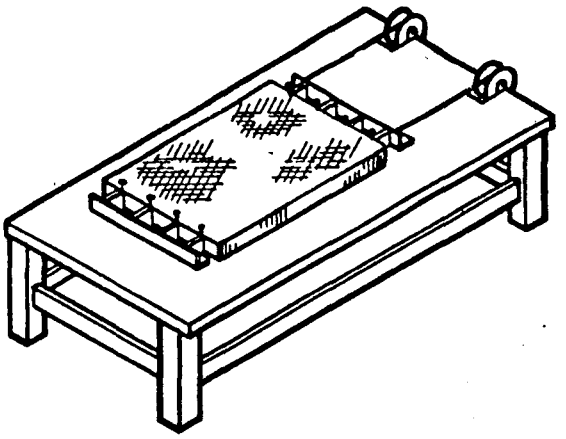

EXPAND

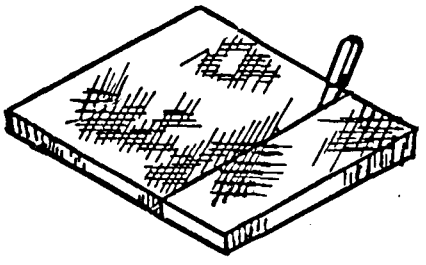

TRIM TO SIZE

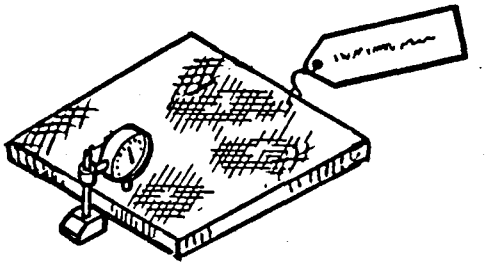

INSPECT AND IDENTIFY

Figure E-14 CORE FABRICATION

1. Inspect Material
2. Shear to Size
3. Deburr and Number
4. Drill Hole Pattern

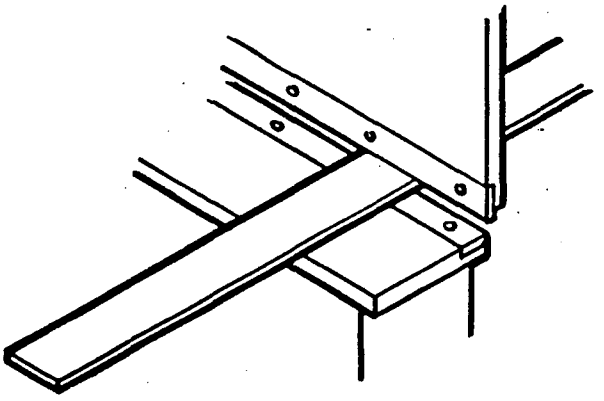

SHEAR

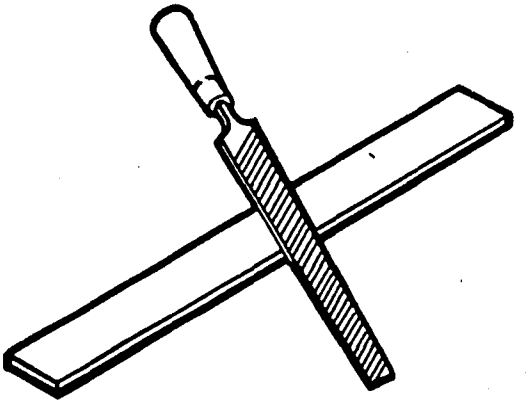

DEBURR

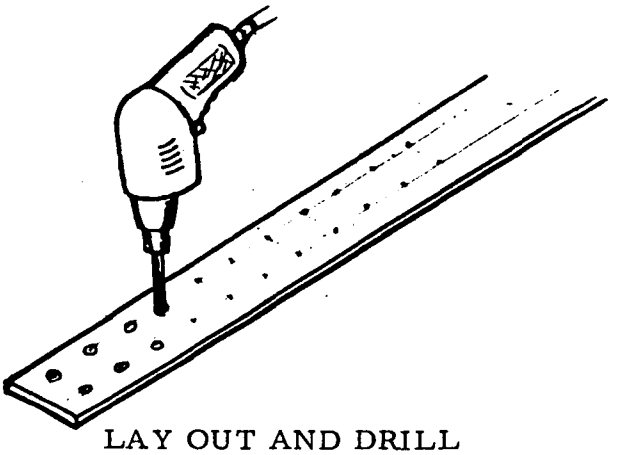

LAY OUT AND DRILL

Figure E-15 SPLICEPLATE

ASSEMBLIES

Significant steps in manufacturing the assemblies are illustrated in Figures E-16 through E-18.

1. Apply Adhesive to Inside of Outer Skin
2. Install Core
3. Apply Core Splice Material
4. Apply Adhesive to Inside of Inner Skin
5. Locate Edgemembers
6. Locate Inner Skin to Edgemembers Using Cherry Rivets
7. Inspect
8. Forward to Autoclave for Bonding

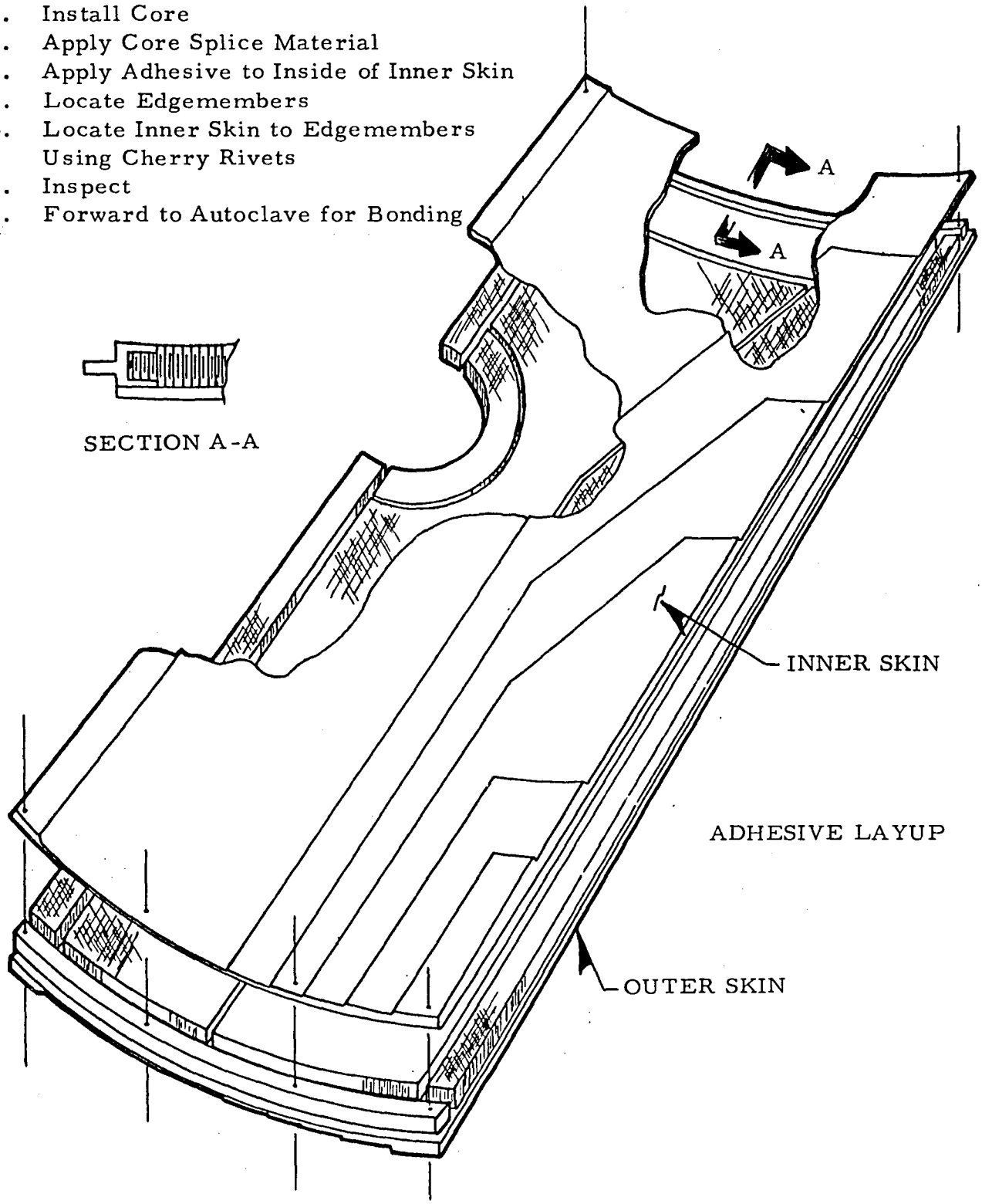

Figure E-16 THRUST SKIRT PANEL ASSEMBLY - BONDED

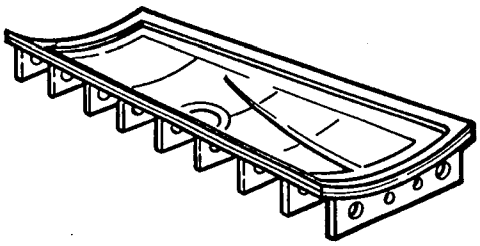

PREFIT

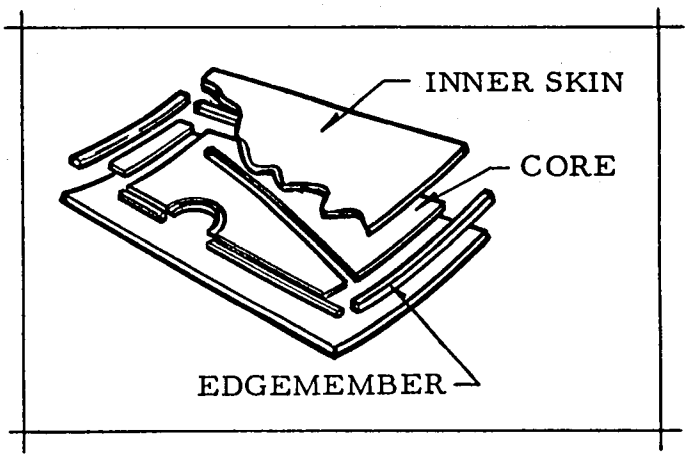

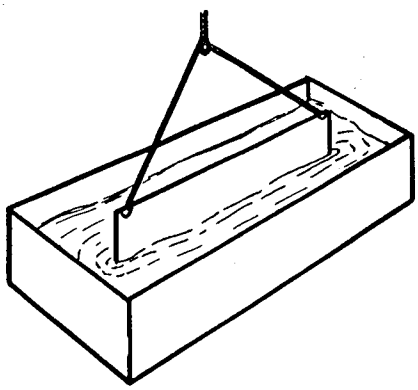

CLEAN DETAILS

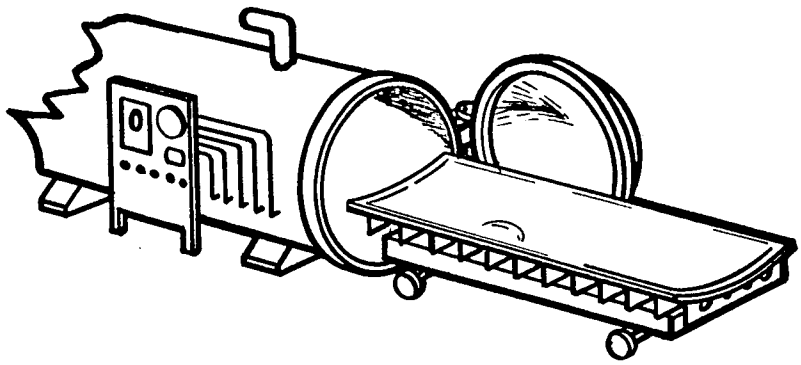

BOND - AUTOCLAVE

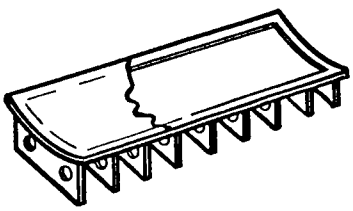

PREPARE PANEL FOR
AUTOCLAVE BONDING

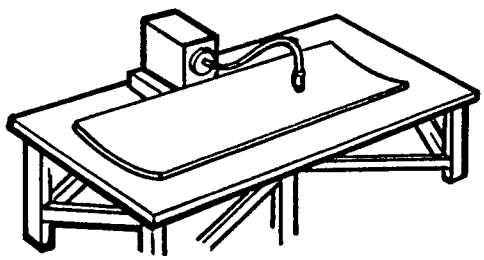

INSPECT - STUBCHECK

Figure E-17 THRUST SKIRT PANEL

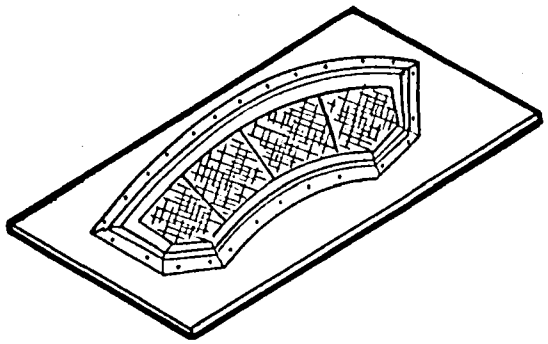

PREFIT

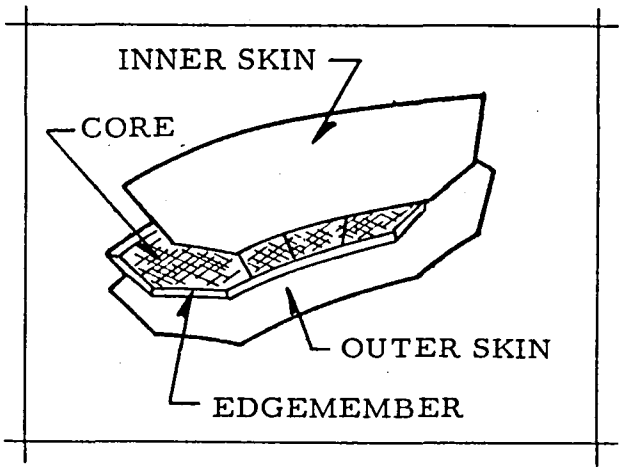

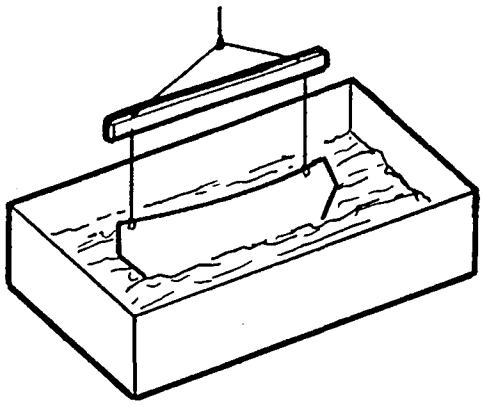

CLEAN DETAILS

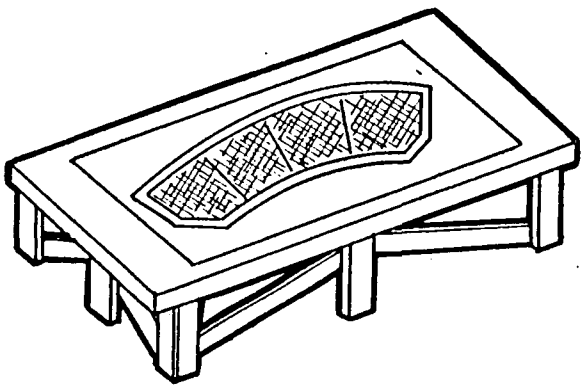

APPLY ADHESIVE

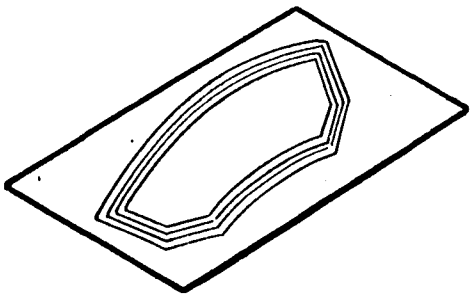

PREPARE FOR BONDING

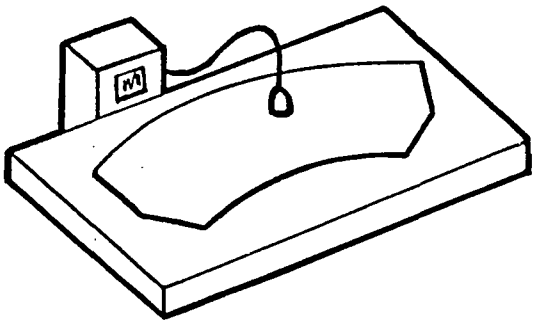

INSPECT - STUBCHECK

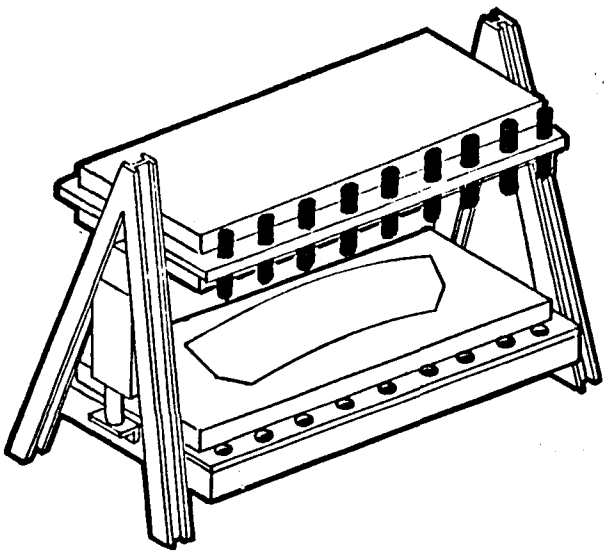

BOND - PRESS

Figure E-18 AFT RING PANEL

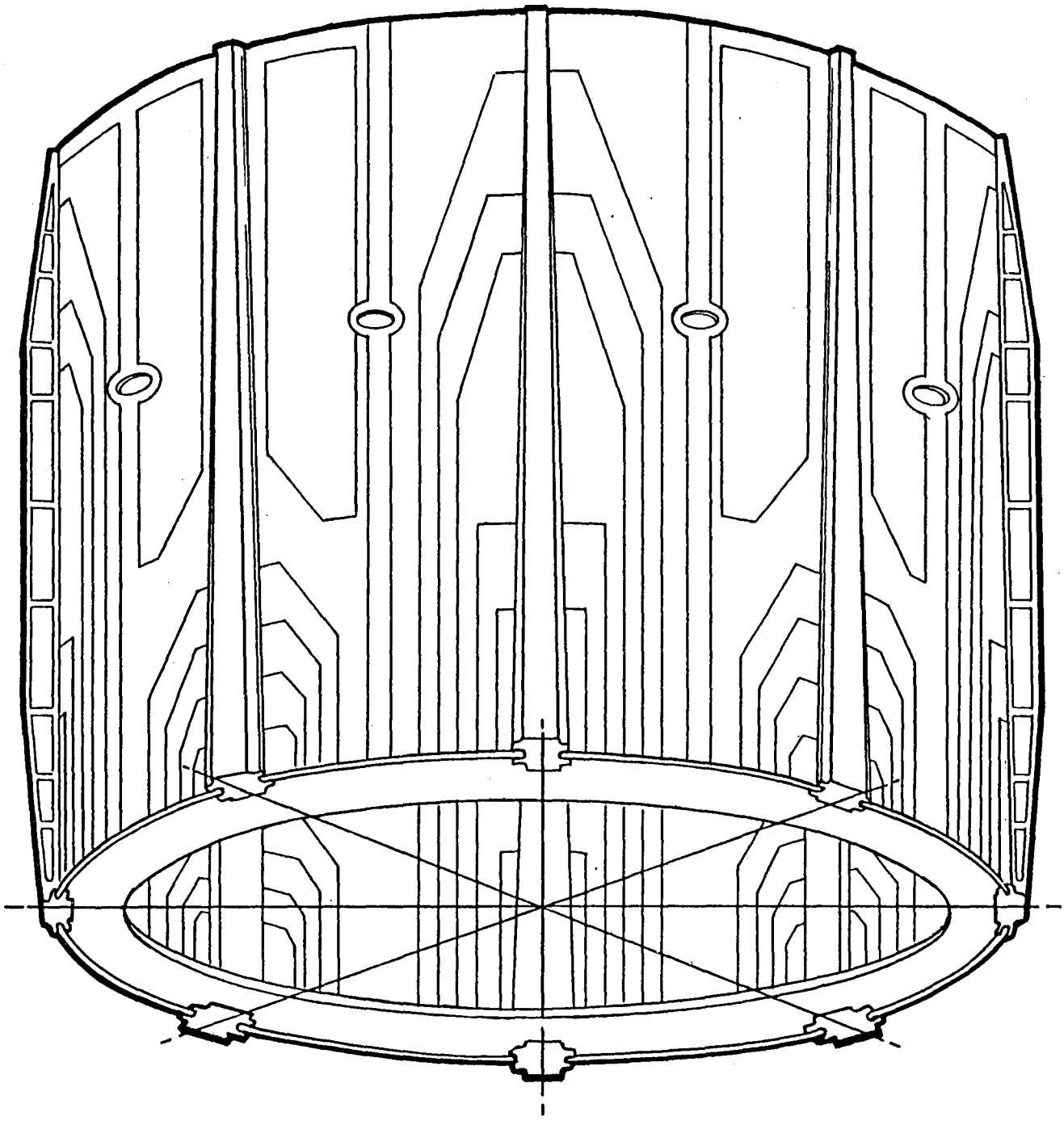

Figure E-19 THRUST SKIRT FINAL ASSEMBLY

A P P E N D I X F

This appendix contains a Quality Control Plan outline for the manufacture of a heavy gage bonded honeycomb thrust structure.

QUALITY CONTROL REQUIREMENTS FOR MANUFACTURE OF THE HEAVY GAGE BONDED PANEL ASSEMBLIES

I. PURPOSE

This document outlines the policy to be used in establishing procedures for use in controlling the incoming materials to assure they comply with specifications, and in controlling and monitoring the manufacturing processes.

II. APPLICABILITY

The provisions herein shall apply to the manufacture of the Heavy Gage Bonded Panel assemblies and shall be implemented by the contractor's written procedures.

III. DETAIL REQUIREMENTS

A. Control of Incoming Raw Material:

1. Receiving Inspection shall inspect raw materials for conformance to applicable Engineering drawings and specifications.

2. Assure material is received with adequate test reports or certificates when required by the purchase order.

3. Submit samples of material or parts to Process Control Laboratory when verification tests are required.

4. Inspect material for proper identification, special process or inspection stamps (ultrasonic, fluorescent, penetrant, magnetic, etc.) per blueprint/specification.

5. Forward acceptable material to stock. Reject all nonconforming material.

B. Identification, Handling and Storage of Material:

1. Aluminum Sheet Stock and Detail Parts:

Aluminum sheet stock and detail parts shall be protected at all times to avoid scratches, bowing, warping, dings, dents and abrasions.

Critical surfaces shall be protected by one of the following methods:

a. Adhesive backed sandblast paper.
b. Sprayed-on strippable plastic film.
c. Loose sheets of paper.

Detail parts shall not be stacked unless such details are of the same configuration and are separated by one of the methods described above. Use care and assure contour is not affected when stacking contoured parts.

Large contour detail parts shall be stored in a rack, in a vertical position, with plastic covered pipe separators between each detail part.

2. Core Materials:

Aluminum core logs and hobes shall be stored in the original shipping container until they are cut into slices or detail parts. If logs or hobes are removed from the original container, they shall be separated by a layer of cardboard, plywood or other suitable material.

Core slices shall be protected with cardboard, plywood or other suitable material.

After prefit, details, shall be wrapped with clean, wax-free, oil-free brown paper.

Core materials and detail parts shall be transported between clean pieces of cardboard taped together with general purpose masking tape.

3. Adhesives and Resins:

Storage shall be in roll form with the layers of adhesive separated from mutual contact with a plastic separator film (liner). Each roll shall be wrapped with heavy wrapping paper or an equivalent material and sealed with general purpose masking tape.

Each roll shall be stored on its side. Do not stack or stand rolls of adhesive on ends.

Liquid adhesives shall be stored in air-tight and light-tight containers at a temperature of 25°F to 80°F.

4. Identification:

Parts requiring markings for identification purposes shall be marked in accordance with applicable Engineering drawings, specifications and/or operation sheets.

C. Inspection and Test:

1. Sheet Metal and Machined Parts:

a. Inspect material
b. Inspect thickness, holes and dimensions per blueprint
c. Hardness test when applicable
d. Inspect finish
e. Inspect identification

2. Welded Assemblies:

a. Preweld inspection

(1) Inspect tools, jigs and fixtures
(2) Inspect preparation of joints and fit-up.
(3) Inspect filler metal
(4) Inspect pre-heat methods and temperature.

b. In-process inspection:

(1) Monitor temperature control during welding.
(2) Inspect for proper cleaning and removal of visible defective weld deposits.
(3) Inspect for proper stress-relieving, straightening and cleaning after welding.

c. Post Weld Inspection:

(1) Visual inspection
(2) Magnetic particle inspection (Class II welds)
(3) Penetrant inspection (Class II welds)
(4) Radiographic inspection (Class I welds)

3. Bonded Panel Assemblies:

a. Inspect pre-fit of details to bond form.
b. Inspect details and core for proper cleaning.
c. Inspect application of adhesives.

d. Inspect preparation of panel for bonding in autoclave or press.
e. Perform mechanical impedance check (stubcheck) of glue lines for voids or unbonded areas.
f. Inspect dimensions and contour per blueprint and bond form.
g. Inspect finish
h. Inspect identification

4. Quality Control Tests:

a. Non-integral test tabs bonded with assemblies.
b. Portashear tests of bonded structures.
c. Stubmeter tests.
d. Acceptance testing of adhesives and core materials.

D. Process Control

1. Process Control personnel shall:

a. Monitor all manufacturing processes directly related to the development and production of adhesive bonded assemblies to assure compliance with applicable specifications, instructions and/or approved methods.

E. Control of Inspection, Measuring and Test Equipment:

1. Survey, calibration, and/or checks on bonding equipment shall be conducted at intervals as specified:

a. Temperature uniformity survey on autoclaves - every 6 months.

b. Recording instrument accuracy check - once each week.

c. Recording instrument check - daily.

d. Pressure gauge check - every 60 days.

F. Records of Inspection and Tests

1. Quality Control shall maintain records of:

a. Acceptable "in-process" inspection operations connected with bonding, drying and storage of cleaned parts through their assembly for final bonding.

b. Surveys, calibration, and checks of bonding equipment.
c. Test results of acceptance testing of adhesives and core materials. Records shall include lot numbers and date of manufacture of adhesives.

LIST OF FIGURES

Figure	Title	Page
1-1	Test Specimen Configuration	1-3
1-2	Typical Failed Single Lap Test Specimens	1-5
1-3	Typical Failed Double Lap Test Specimens	1-6
2-1	Assumed Panel and Longeron Geometry	2-3
2-2	Superposition of Loads	2-4
2-3	$f_1(x,y)$ vs Y	2-10
2-4	$f_2(x,y)$ vs Y	2-11
2-5	$f_4(x,y)$ vs Y	2-12
2-6	ϕ vs t - Rebound Longeron	2-13
2-7	Initial Structure Requirements	2-15
2-8	Half Quadrant Geometry	2-14
2-9	Coordinate System	2-17
2-10	Interior Point Equilibrium	2-19
2-11	Skirt Structure Simulation for Digital Analysis	2-24
2-12	Laterally Deflected Bar in Compression	2-25
2-13	General Quadrilateral Plate Layout	2-27
2-14	Linear Single-Degree-of-Freedom System	2-30
2-15	Response of Structure to Random Noise	2-33
2-16	Idealized σ -n Curve	2-40
3-1	Stringer Axial Load vs y	3-5
3-2	Shear Flow vs y	3-6

LIST OF FIGURES (Con't)

Figure	Title	Page
3-3	Axial Stress Resultant vs x	3-7
3-4	Axial Stress Resultant vs Distance from Fitting	3-9a
3-5	Typical Core Shear Instability Failure	3-10
3-6	Core Shear Instability vs Core Modulus	3-12
3-7	Core Shear Instability vs Core Thickness	3-13
3-8	Thickness Parameter - Core in "L" Direction	3-15
3-9	Thickness Parameter - Core in "W" Direction	3-16
3-10	Face Wrinkling vs Effective Modulus & A_o (Thick Core)	3-17
3-11	Face Wrinkling vs Effective Modulus & A_o (Thin Core)	3-18
3-12	Face Wrinkling vs Effective Modulus & F_c (Thick Core)	3-19
3-13	Face Wrinkling vs Effective Modulus & F_c (Thin Core)	3-20
3-14	Initial Imperfection	3-21
3-15	Critical Half Wave Length (Thick Core)	3-22
3-16	Critical Half Wave Length (Thin Core)	3-23
3-17	Cylinder Buckling vs Core Thickness	3-25
3-18	Critical Buckling Stress vs Imperfection Amplitude (Small Deflection Theory)	3-28
3-19	Preliminary Structural Configuration Heavy Gage Honeycomb Sandwich (FW6528003A)	3-30
3-20	Phase II Test Specimens - Heavy Gage Bonded Honeycomb (FW6528002A)	3-32

LIST OF FIGURES (Cont.)

Figure	Title	Page
3-21	Typical Overlap Test Specimens	3-35
3-22	Typical Welded Test Specimens	3-36
3-23	Typical Bonded-Bolted Test Specimens	3-37
3-24	Typical Face Wrinkling Test Specimens	3-38
3-25	Cutter Form Configuration	3-40
3-26	Sandwich Butt-Welding in Process	3-42
3-27	Vacuum Chuck Fixture	3-43
3-28	Welding Pass Sequence	3-49
3-29	Weld Distortion on .500 Inch 2219 Plate	3-50
3-30	Welded Sandwich Specimens	3-51
3-31	Post-Weld Peen Tool and Peen Tool Set Up	3-52
4-1	Phase III Test Specimens Heavy Gage Bonded Honeycomb (FW 6528004A)	4-2
4-2	Test Specimens and Loading Conditions	4-5
4-3	Bonded Edgemember Compression Test Specimens (1.50 Inch Core)	4-10
4-4	Bonded Edgemember Compression Test Specimens (3.00 Inch Core)	4-11
4-5	Mode of Failure for 4.4 lb/ft^3 Core Specimens	4-12
4-6	Mode of Failure for Basic 1.50 Inch Core Specimens	4-12
4-7	Failed Edgemember Test Specimens, 1.50 Inch Core, .125 Skins	4-13

LIST OF FIGURES (Cont.)

Figure	Title	Page
4-8	Failed EdgememberTest Specimens, 3.00 Inch Core, .125 Skin	4-15
4-9	Failed Edgemember Test Specimens, 1.50 Inch Heavy Core, Thick Adhesive	5-16
4-10	Bonded Edgemember Compression Test Data	4-17
4-11	Bolted Splice Joint Specimen	4-14
4-12	Shear Test Specimen	4-21
4-13	Bonded-Bolted Specimen Configuration	4-22
4-14	Specimen Configuration - Channel Edgemembers	4-23
4-15	Specimen Configuration - Flange Edgemembers	4-24
4-16	Shear Test Specimens After Testing	4-25
4-17	Typical Shear Test Specimen - .250 Facings	4-26
4-18	Bonded - Bolted Shear Test Specimen	4-27
4-19	Modified Shear Test Specimen - .25 Facings, 3.0 Inch Sandwich, Channel Edgemembers	4-28
4-20	Welded Shear Test Specimen - .250 - .375 Facings	4-29
4-21	Modified Shear Test Specimen - .125 Facings, Flange Edgemembers	4-30
4-22	Shear Test Specimen with Instrumentation	4-31
4-23	Stress Concentrations in Shear Specimens	4-32
4-24	Modification of Corners of Shear Specimens	4-32

LIST OF FIGURES (Cont.)

Figure	Title	Page
4-25	Skin Stress Distributions on Shear Specimens	4-34
4-26	Adhesive Shear Stress Distribution	4-35
4-27	Prefit of Skin to Slug and Core	4-36
4-28	Shear Specimen Cure Cycles	4-40
4-29	Core Insert Installation Procedure	4-39
4-30	Core Insert with Loose Fit	4-41
4-31	Proposed Modification to the Shear Tip Insert for Portashear	4-42
4-32	Schematism of Portashear Testing Component	4-43
4-33	Schematism of Portashear Shear Mechanism	4-44
5-1	Regular Node Coordinate Location Data	5-3
5-2	Dual Node Coordinate Location Data	5-4
5-3	Typical Section of Sandwich Shell Simulation	5-5
5-4	Simulation of Sandwich Shell and Elastic Foundation	5-6
5-5	Typical P-42 Substructure	5-8
5-6	Rebound Load Distribution	5-9
5-7	Hold-Down Load Distribution	5-10
5-8	Thrust Load Distribution	5-11
5-9	Prebuckling Shape for Rebound Load	5-12
5-10	Heavy Gage Bonded Honeycomb - Thrust Panel Assembly (FW 6528011)	5-14

LIST OF FIGURES (Cont.)

Figure	Title	Page
5-11	Heavy Gage Bonded Honeycomb - Thrust Longeron Fitting, Lower (FW 6528008A)	5-15
5-12	Heavy Gage Bonded Honeycomb - Thrust Longeron (FW 6528009)	5-16
5-13	Heavy Gage Bonded Honeycomb - Rebound Longeron Fitting, Lower (FW 6528005A)	5-17
5-14	Heavy Gage Bonded Honeycomb - Rebound Longeron (FW 6528007)	5-18
5-15	Thrust Longeron Area Profile	5-19
5-16	Rebound Longeron Area Profile	5-20
5-17	Thrust Longeron Applied Streee Profile	5-22
5-18	Rebound Longeron Applied Stress Profile	5-23
5-19	Skin Stresses, Thrust Condition	5-28
5-20	Skin Stresses, Rebound Condition	5-29
5-21	Skin Stresses, Hold-Down Condition	5-30
5-22	Skin Panel Axial Stress Zones	5-31
5-23	Skin Panel Shear Stress Zones	5-32
5-24	Panel Upper Edge Joint Loading and Strength	5-34
5-25	Panel Lower Edge Joint Loading and Strength	5-35
5-26	Thrust Longeron Attachment Loading and Strength	5-36
5-27	Rebound Longeron Attachment Loading and Strength	5-37

LIST OF FIGURES (Cont.)

Figure	Title	Page
5-28	Panel Splice Attachment Loading and Strength	5-38
5-29	Heavy Gage Bonded Honeycomb - Aft Ring Installation (FW 6528010)	5-40
5-30	Access Hole - Heavy Gage Bonded Honeycomb (FW 6528006A)	5-43
5-31	Panel Flutter Prediction	5-56
6-1	Relative Weights of Major Structural Categories	6-2

LIST OF TABLES

Table	Title	Page
1-1	Preliminary Test Results	1-7
3-1	Welding Parameters Data on 2219, .188 Gage, Flat Position	3-44
3-2	Welding Parameters Data on 2219, .375 Gage, Flat Position	3-45
3-3	Welding Parameters Data on 2219, .500 Gage, Flat Position	3-46
3-4	Skin Temperatures Adjacent to Weld Zone	3-47
4-1	Bonded Edgemember Test Data	4-9
4-2	Bolted Splice Joint Test Data	4-18
4-3	Shear Test Results	4-20
6-1	Total Weights of Major Structural Categories	6-1
6-2	Detailed Weight Tabulation for Sandwich Cylinder	6-2
6-3	Detailed Weight Tabulation for Auxiliary Structure	6-3
6-4	Weight Comparison - Sandwich Versus Plate Stringer	6-5

GENERAL DYNAMICS

Fort Worth Division